NATIONAL AERONAUTICS AND SPACE ADMINISTRATION

APOLLO 6 MISSION REPORT

DISTRIBUTION AND REFERENCING

This paper is not suitable for general distribution or referencing. It may be referenced only in other working correspondence and documents by participating organizations.

MANNED SPACECRAFT CENTER
HOUSTON, TEXAS
MAY 1968

APOLLO SPACECRAFT FLIGHT HISTORY

Mission	Spacecraft	Description	Launch date	Launch site
PA-1	BP-6	First pad abort	Nov. 7, 1963	White Sands Missile Range, N. Mex.
A-001	BP-12	Transonic abort	May 13, 1964	White Sands Missile Range, N. Mex.
AS-101	BP-13	Nominal launch and exit environment	May 28, 1964	Cape Kennedy, Fla.
AS-102	BP-15	Nominal launch and exit environment	Sept. 18, 1964	Cape Kennedy, Fla.
A-002	BP-23	Maximum dynamic pressure abort	Dec. 8, 1964	White Sands Missile Range, N. Mex.
AS-103	BP-16	Micrometeoroid experiment	Feb. 16, 1965	Cape Kennedy, Fla.
A-003	BP-22	Low-altitude abort (planned high-altitude abort)	May 19, 1965	White Sands Missile Range, N. Mex.
AS-104	BP-26	Micrometeoroid experiment and service module RCS launch environment	May 25, 1965	Cape Kennedy, Fla.
PA-2	BP-23A	Second pad abort	June 29, 1965	White Sands Missile Range, N. Mex.
AS-105	BP-9A	Micrometeoroid experiment and service module RCS launch environment	July 30, 1965	Cape Kennedy, Fla.
A-004	SC-002	Power-on tumbling boundary abort	Jan. 20, 1966	White Sands Missile Range, N. Mex.
AS-201	SC-009	Supercircular entry with high heat rate	Feb. 26, 1966	Cape Kennedy, Fla.
AS-202	SC-011	Supercircular entry with high heat load	Aug. 25, 1966	Cape Kennedy, Fla.

(Continued inside back cover)

MSC-PA-R-68-9

APOLLO 6 MISSION REPORT

Prepared by: Apollo 6 Mission Evaluation Team

Approved by: George M Low

George M. Low
Manager
Apollo Spacecraft Program

NATIONAL AERONAUTICS AND SPACE ADMINISTRATION
MANNED SPACECRAFT CENTER
HOUSTON, TEXAS
June 1968

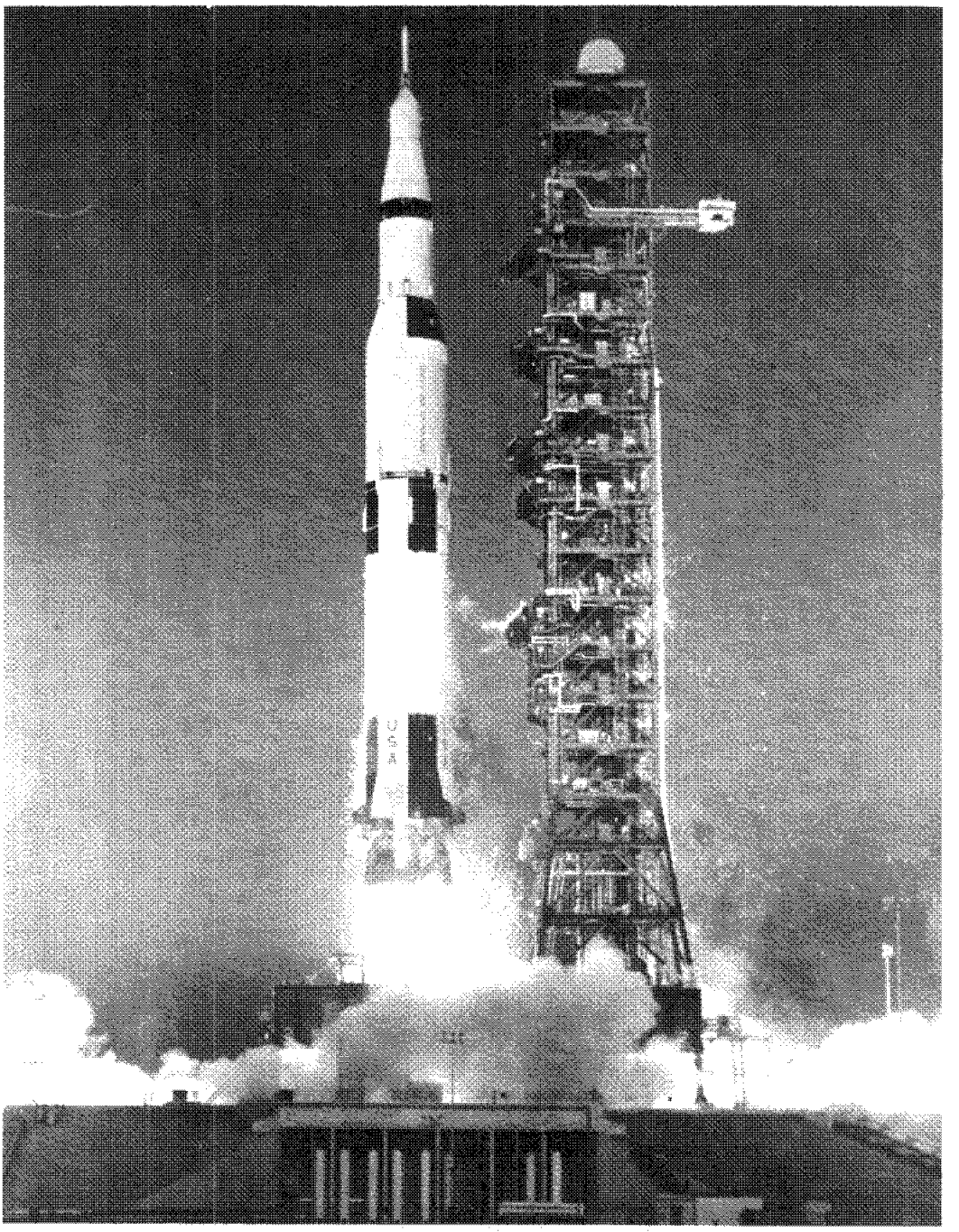

Apollo 6 space vehicle at lift-off.

CONTENTS

TABLES

FIGURES

1.0 SUMMARY

The Apollo 6 mission was accomplished on April 4, 1968. This was the second mission to use a Saturn V launch vehicle with an unmanned block I command and service module (CSM 020) and a lunar module test article (LTA-2R). The single primary spacecraft objective — demonstration of the performance of the emergency detection system operating in a closed-loop mode — was achieved. The secondary spacecraft objectives that were satisfied include demonstration of: (a) effective operation of mission-support facilities during the launch, orbital, and recovery phases of the mission; (b) successful operation of the service propulsion system (including a no-ullage start); and (c) proper operation of selected spacecraft systems (electrical power, primary guidance, guidance and control, environmental control, and communications). The secondary spacecraft objectives that were partially satisfied include: (a) demonstration of the adequacy of the block II command module heat shield for entry at lunar-return conditions (not fully satisfied because of failure to achieve the high velocity planned for entry); (b) demonstration of the structural and thermal integrity and compatibility of launch vehicle and spacecraft; and (c) confirmation of launch loads and dynamic characteristics. A major structural anomaly occurred during first-stage boost, although the launch vehicle satisfactorily inserted the spacecraft into orbit. Valid data were obtained to determine some structural loads during the launch phase. The anomaly has not been resolved at the time of publication of this report but will be explained in detail in a separate report.

The space vehicle was launched from complex 39A, Kennedy Space Center, Florida. The lift-off was normal. During the S-IC boost phase, 5-Hz (approximately) oscillations and abrupt measurement changes were observed. After second-stage ignition, the boost was nominal until two engines in the S-II stage shut down early. In an attempt to attain the desired velocity, the firing time of the remaining three S-II stage engines was extended approximately 1 minute. The S-IVB firing was also longer than planned. At termination of the S-IVB thrust, the orbit had a 198-n. mi. apogee and a 96-n. mi. perigee, instead of being 100-n. mi. near-circular as planned. An attempt to reignite the S-IVB engine for the translunar injection firing was unsuccessful. A ground command to the command and service module implemented a preplanned alternate mission that consisted of a long-duration firing (442 seconds) of the service propulsion system engine. This firing was under onboard guidance computer control, and the onboard programmed apogee (12 000 n. mi.) was attained. After the service propulsion system engine firing, the command and service module was aligned to a preset cold-soak attitude. The preflight-planned second firing of the service propulsion system engine was inhibited by ground command. Atmospheric entry (400 000) feet occurred at an inertial velocity of 32 830 ft/sec and a flight-path angle of

minus 5.85 degrees. These entry parameters were lower than had been predicted as a result of the S-IVB failure to reignite. The command module landed approximately 49.2 n. mi. uprange of the targeted landing point, also as a result of the abnormal launch and insertion trajectory.

The overall performance of the command and service module was excellent. None of the system anomalies precluded satisfactory completion of the mission.

The electrical power distribution system functioned normally throughout the mission. Event data established that an ac essential load transfer occurred at approximately the time the command and service module was separated from the S-IVB. This transfer was a normal function of the distribution system in response to an anomalous load condition. The performance of the fuel cells and the electrical power system radiators was excellent throughout the mission. Fuel cell outputs and temperatures agreed favorably with prelaunch prediction. Water production estimates were based upon power generation, reactant consumption, and potable water tank quantity, and all agreed favorably.

Performance of the communication system was satisfactory except for an intermittent timing/telemetry problem that was most prevalent from 00:01:28 through 00:08:20.

Performance of the guidance and control system was excellent. The monitoring functions and navigation during the ascent and earth-orbital phases were nominal. Guidance during the service propulsion system engine firing was excellent, and all attitude maneuvers were performed correctly. Numerous computer update alarms were generated, but these appeared to have been caused by a source external to the computer. Sequencing of the mission control programmer was satisfactory throughout the mission.

All maneuvers requiring use of the reaction control system were completed satisfactorily.

The thermal protection system survived the entry environment satisfactorily. Although the desired entry conditions were not obtained, the entry velocity (32 830) provided additional data points for the total spectrum of Apollo entry conditions between the 28 512 ft/sec achieved during the AS-202 mission and the 36 537 ft/sec achieved during the Apollo 4 mission. All components of the earth landing system performed satisfactorily. Parachute loads were commensurate with values expected for a normal entry. The main-parachute disconnect system functioned correctly. This was the first mission in which the command module assumed the stable II (inverted) flotation attitude after landing. The command module was returned to the stable I (upright) attitude by the uprighting system.

The unified side hatch of the block II configuration was flown for the first time and performed satisfactorily.

The most significant spacecraft anomaly occurred at approximately 00:02:13 (2 minutes 13 seconds after lift-off) when abrupt changes were indicated by strain, vibration, and acceleration measurements in the S-IVB, instrument unit, adapter, lunar module test article, and command and service module. The apparent cause of the structural anomaly was the 5-Hz oscillations induced by the launch vehicle; these oscillations exceeded the spacecraft design criteria. Photographic coverage from ground and aircraft cameras revealed material coming from the area of the adapter.

Abnormal occurrences during the boost phase subjected the command and service modules to adverse environments that would normally not be seen during a flight test program. The alternate mission flown was the more difficult to accomplish of the two alternatives, which were to attempt to complete the planned trajectory and obtain new evaluation data points or to abort the mission and recover the spacecraft. The manner in which the command and service modules performed during this alternate mission, after the adverse initial conditions, demonstrated the versatility of the systems.

2.0 MISSION DESCRIPTION

The actual Apollo 6 mission sequence is compared with the planned mission sequence in figure 2-1 and table 2-I. The planned and actual orbital elements are listed in table 2-II. Major events during the mission are shown in figure 2-2.

2.1 PLANNED MISSION

The planned Saturn V boost sequence consisted of nominal firings of the S-IC, S-II, and S-IVB stages, resulting in a near-circular 100 n. mi. orbit.

Two revolutions in earth parking orbit were to have been completed, followed by a second S-IVB firing to inject the vehicle into a typical translunar conic trajectory. Targeting to attain terminal conditions near the moon were not included.

The next planned maneuver of significance was separation of the command and service modules (CSM) from the adapter and a 280-second service propulsion system engine retrograde firing to achieve an elliptical orbit of 11 984 by 19 n. mi., resulting in a free-return earth-intersecting trajectory. Service propulsion engine cutoff was scheduled to occur 3 hours 24 minutes after lift-off; immediately following cutoff, the command and service module was to be oriented to a cold-soak attitude.

Approximately 6 hours after the first service propulsion system engine firing, and following a computer update from Carnarvon, a second service propulsion system engine firing was to occur. This firing was to provide a velocity of 36 500 ft/sec and a flight-path angle of minus 6.5 degrees at entry interface (400 000 feet). Atmospheric entry was planned for approximately 09:29:00, with the command module following an entry under guidance and navigation control. The planned landing point was 157 degrees 11 minutes West longitude and 27 degrees 19 minutes North latitude.

2.2 ACTUAL MISSION

Lift-off occurred at 12:00:01 G.m.t. (7:00 a.m. e.s.t.) on April 4, 1968, from launch complex 39A, Kennedy Space Center, Florida. During first-stage boost, low-frequency oscillations of ±0.6g, which exceed the design criteria, were measured in the command module. The launch phase profile was nominal until two engines in the S-II stage shut down early.

This required the remaining three S-II stage engines and the S-IVB to fire longer than planned to obtain the desired velocity. During the S-IVB firing, a substantial amount of steering was required in an attempt to remove the S-II generated error in the trajectory plane. At thrust termination, the orbit was 198 by 96 n. mi. instead of 100 n. mi. circular that had been planned.

The vehicle remained in an earth parking orbit for the next 3 hours of flight. During this period, systems were checked, operational tests such as the S-band evaluation were performed, and several attitude maneuvers were made.

The second S-IVB firing was scheduled to occur during the Cape Kennedy pass at the end of the second revolution, but this firing could not be accomplished. Therefore, the command and service module was separated from the S-IVB, and a service propulsion system engine firing sequence was initiated. This was a long-duration firing of 442 seconds and provided a 12 019.5 by 18 n. mi. free-return orbit.

After service propulsion system engine cutoff, the command and service module was maneuvered to a cold-soak attitude with the minus X axis oriented toward the sun, thus allowing the desired shading on the command module. The cold-soak attitude was maintained for about 6 hours.

Since the service propulsion system was used to insert the spacecraft into the desired high apogee, insufficient propellant remained to gain the high velocity desired from the second service propulsion system engine firing. Specifically, the total propellant remaining would allow only 22 percent of the desired velocity increase. For this reason, a decision was made to inhibit the second firing. A complete firing sequence was performed, including all nominal events except that thrust was inhibited.

After the service propulsion engine cutoff signal, the command and service module was maneuvered to separation attitude, and the service module was separated at 09:36:57. This was followed by command module entry attitude orientation and coast to 400 000 feet.

At 09:38:29, the entry interface was reached with a velocity of 32 830 ft/sec and a flight-path angle of minus 5.85 degrees. These interface conditions were less than planned; as a result, the heating rates and loads during entry were lower than desired.

The parachute deployment sequence was normal, beginning with drogue deployment at 09:51:27. Landing occurred at approximately 09:57:20 and was about 49 n. mi. uprange of the targeted landing point of 157 degrees 11 minutes West longitude and 27 degrees 19 minutes North latitude.

TABLE 2-I.- SEQUENCE OF EVENTS

Event	Time, hr:min:sec	
	Planned[a]	Actual
Launch Phase		
Range zero (12:00:01 G.m.t.)		
Lift-off	00:00:00.0	00:00:00.5
Maximum dynamic pressure	00:01:19.8	00:01:15.2
S-IC inboard engine cutoff	00:02:24.4	00:02:24.9
S-IC outboard engine cutoff	00:02:27.3	00:02:28.4
S-IC/S-II separation	00:02:28.0	00:02:29.1
S-II engine ignition (command)	00:02:28.7	00:02:29.8
Interstage jettison	00:02:58.0	00:02:59.1
Launch escape tower jettison	00:03:03.7	00:03:04.8
S-II engine 2 cutoff	--	00:06:52.9
S-II engine 3 cutoff	--	00:06:54.2
S-II engine cutoff	00:08:37.5	00:09:36.3
S-II/S-IVB separation	00:08:38.3	00:09:37.1
S-IVB engine ignition (command)	00:08:38.5	00:09:37.3
S-IVB engine cutoff	00:10:59.0	00:12:27.0
Orbital Phase		
S-IVB engine ignition (command)	03:10:11.2	03:13:34.7
S-IVB engine cutoff (command)	03:15:27.9	[b]03:13:50.3
Spacecraft/S-IVB separation	03:14:26	03:14:27.8
Service propulsion engine ignition	03:16:16	03:16:06.2
Service propulsion engine cutoff	03:23:27	03:23:27.9
Apogee	06:28:24	06:28:58
Plus X translation ON	09:29:24	09:29:19.1
Plus X translation OFF	09:29:54	09:30:09.2
Entry Phase		
Command module/service module separation	09:37:01	09:36:56.6
400 000-foot altitude	09:38:27	09:38:29
Begin blackout	09:38:52	09:38:53.2
End blackout	09:48:18	[c]09:48:18
Drogue deployment	09:51:00	09:51:27.4
Main parachute deployment	09:51:49	09:52:13.4
Landing	09:57:14	09:57:19.9

[a]Planned times after S-IVB cutoff command at 03:13:50.3 are those updated in real time for the alternate mission.

[b]Cutoff was commanded by the guidance system.

[c]Estimated from best known trajectory.

TABLE 2-II.- ORBITAL ELEMENTS

Phase	Condition	Planned	Actual
Initial parking orbit	Apogee, n. mi.	106	198
	Perigee, n. mi.	101	96
	Period, min	88.28	89.92
	Inclination, deg	32.56	32.63
Parking orbit at second S-IVB ignition (after S-IVB venting)	Apogee, n. mi.	111	200
	Perigee, n. mi.	106	99
	Period, min	88.47	90.01
	Inclination, deg	32.56	32.63
Coast ellipse	Apogee, n. mi.	11 984	12 019.5
	Perigee, n. mi.	19	18
	Period, min	383.6	384.8
	Inclination, deg	32.57	32.58

NASA-S-68-3500

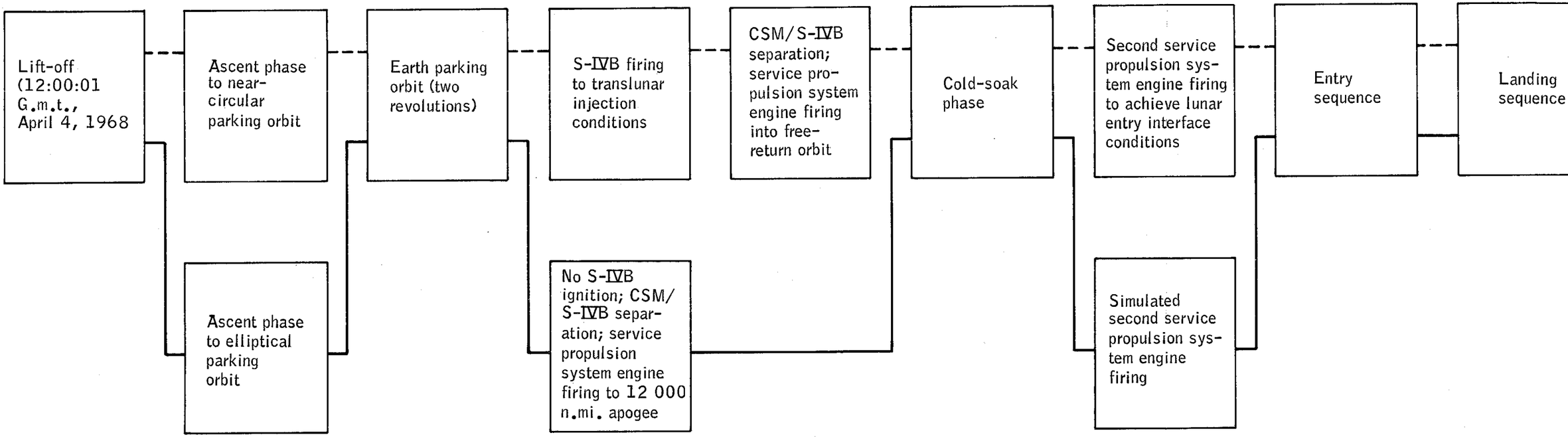

Figure 2-1.- Comparison of planned and actual mission.

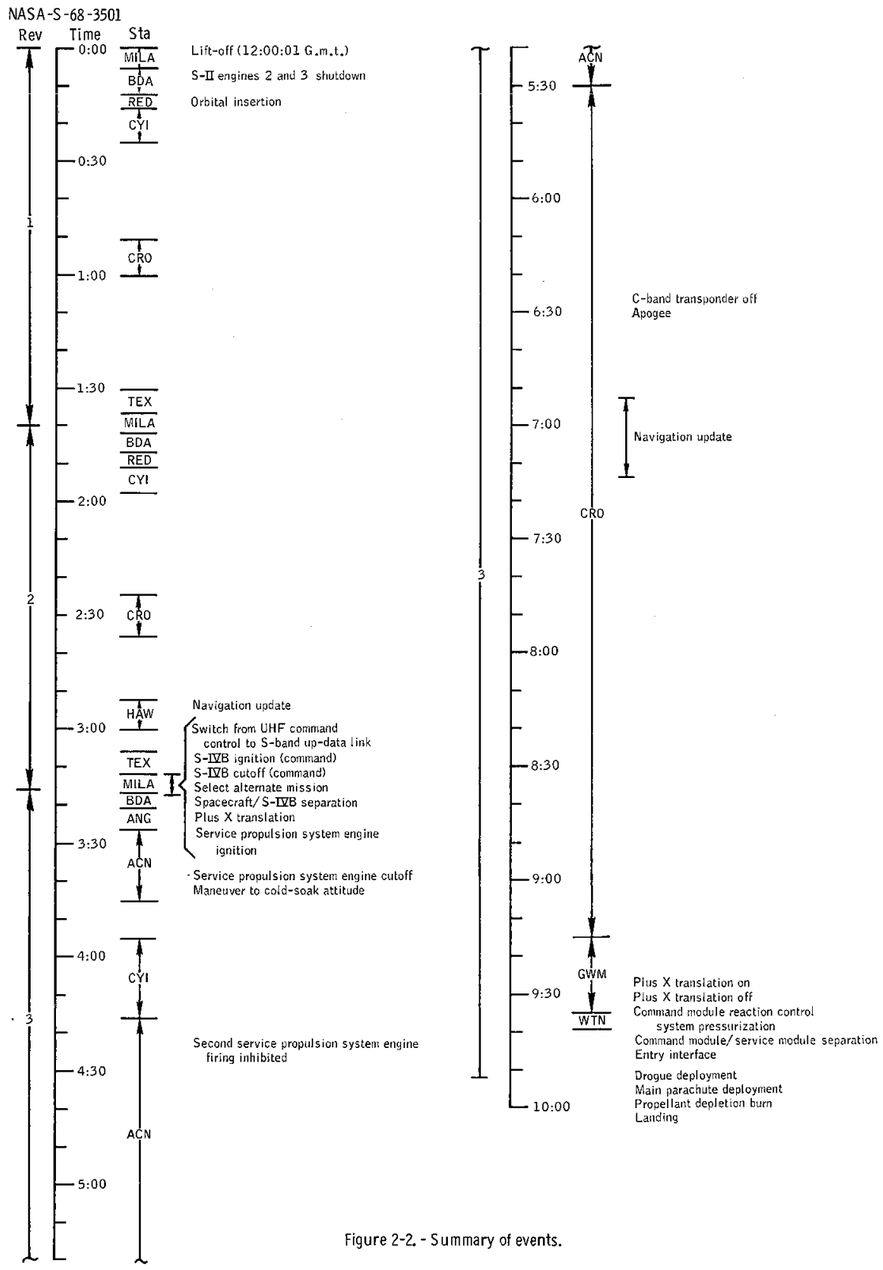

Figure 2-2. - Summary of events.

3.0 TRAJECTORY DATA

A comparison of the planned and actual trajectories of the Apollo 6 mission is presented in this section. The launch and parking orbit trajectories referred to as planned are preflight-calculated trajectories obtained from reference 1. The coast ellipse and entry trajectories referred to as planned are based on real-time predictions utilizing the navigation update state vectors. The actual trajectories are based on tracking data from the Manned Space Flight Network and on flight data. The Marshall Space Flight Center has supplied the trajectory data for the launch and parking orbit phase, up to the time of separation of the command and service modules (CSM) and the S-IVB, and a detailed analysis is presented in reference 2. The orbital analysis in this section is based on the preliminary best-estimate trajectory data generated 21 days after the end of the mission; the final trajectory data will be published as supplement 1 to this report.

The earth model for all trajectories and analysis of the trackers contained geodetic and gravitational constants representing the Fischer ellipsoid. The state vectors for the events during the coast ellipse are based on results from the orbital analysis in section 3.3. These vectors are in the geographic coordinate system defined in table 3-I. The ground track of the orbit and the location of the tracking network sites are shown in figure 3-1.

3.1 LAUNCH

The launch phase trajectory for the S-IC stage was nominal as shown in figure 3-2. Mach 1 occurred at 00:01:00.5 at an altitude of 23 435 feet and was approximately 0.6 second earlier and 779 feet lower in altitude than expected. The maximum dynamic pressure of 784 lb/ft^2 occurred at 00:01:15.2 and was 4.5 seconds earlier and 5330 feet lower in altitude than planned. The actual cutoff times for the inboard and outboard engines were within 1.1 second of the planned times. The conditions at outboard engine cutoff (table 3-II) were high in velocity and altitude by 24 ft/sec and 3648 feet, respectively, and low in flight-path angle by 0.17 degree. Launch escape tower jettison occurred in a normal manner at 00:03:04.8. The predicted time of tower jettison was 00:03:03.4.

As shown in figure 3-2, the trajectory for the S-II stage began diverging from the planned trajectory at 00:06:52.9. This was caused by the premature shutdown of S-II stage engines 2 and 3. The remaining

engines continued to thrust until the cutoff signal at 00:09:36.3. As compared with the planned conditions in table 3-II, this was an increased firing time of almost 59 seconds. The altitude and flight-path angle were high by 20 979 feet and 0.81 degree, respectively, and velocity was low by 336 ft/sec.

The premature shutdown of the two engines in the S-II stage caused the trajectory of the space vehicle to be perturbed prior to S-IVB ignition in such a manner that the S-IVB flight program could not converge on the altitude and velocity requirements for a nominal insertion. The S-IVB performance was satisfactory; however, the S-IVB had to thrust an additional 29 seconds to achieve a guidance cutoff command. At S-IVB cutoff, the launch phase was 88 seconds longer than planned. Velocity was high by 160 ft/sec, and altitude and flight-path angle were low by 2577 feet and 0.40 degree, respectively. At insertion, velocity was high by 158 ft/sec, and altitude and flight-path angle were low by 4333 feet and 0.38 degree, respectively.

3.2 PARKING ORBIT

The trajectory for the parking-orbit phase was calculated from C-band radar data (Merritt Island, Carnarvon, Hawaii, and White Sands) and from venting acceleration data from the S-IVB. No S-band data were used.

Polynomials for the venting were developed from the S-IVB guidance data and were used with the tracking data to calculate the best-estimate trajectory. The CSM/S-IVB parking orbit was elliptical, as shown in figure 3-3; the S-IVB venting increased the altitude by approximately 6 n. mi. between insertion and restart preparations. The trajectory parameters for discrete events during this phase are presented in table 3-III.

During the second revolution, a Bermuda state vector (25) was used to generate the navigation update. This vector was propagated approximately 83 minutes and included 12.4 pounds of predicted S-IVB venting thrust. A comparison was made between the navigation update solution from the Real Time Computer Complex and the best-estimate trajectory to determine the accuracy of the initial state vector and of the update

solution. The comparison also indicated the major contributing error sources in the update solution. The results of this comparison are as follows:

Solution	Time, hr:min:sec	Position, ft	Velocity, ft/sec
Bermuda 25 initial state vector	01:41:05	1 800	1.78
Navigation update propagation error	03:05:00.8	10 367	12.28
Navigation update venting error	03:05:00.8	9 008	8.55
Total navigation update error	03:05:00.8	19 375	20.82

The position and velocity errors caused by propagation accounted for more than half the navigation update error. The predicted venting model was apparently satisfactory for this mission; however, an investigation is being performed at the Marshall Space Flight Center to determine the effect for a nominal S-IVB mass configuration.

At the termination of the parking orbit, the S-IVB failed to restart for the translunar injection firing. The command and service modules were then separated from the S-IVB, and an alternate mission plan was used for the coast ellipse. The trajectory parameters for the restart attempt and the separation are presented in table 3-III.

3.3 TRAJECTORY ANALYSIS

The preliminary C-band and S-band evaluations were based upon the individual station performance for each tracker. In addition, vectors obtained by fitting C-band data were compared with those obtained by fitting S-band data.

A performance summary in the form of residual statistics for the individual stations is shown in table 3-IV. The magnitude of the bias was taken as the mean value of the residuals. The noise value was

obtained by calculating the root mean square of the residuals. To obtain the residuals, the computed value was based on the orbit obtained from the data fit, and it was subtracted from the observed value for each data type. As shown in table 3-IV, the tracker residuals were within the theoretical limits, with the exception of noise for the Ascension S-band ranging data. The noise (rms values) appeared to be a timing error or station location error; however, it affected the fit very slightly because the bias was within the theoretical limits.

The agreement between the orbit determinations from C-band data and from S-band data was considerably better than for the Apollo 5 mission. The following table compares the results of the C-band and S-band orbit determinations:

Event	Time, hr:min:sec	Difference between C-band and S-band	
		Position, ft	Velocity, ft/sec
Service propulsion system engine cutoff	03:23:28	560	1.20
Apogee	06:28:58	363	0.30
Plus X translation	09:29:19	1936	1.62

Several difficulties were encountered during the coast ellipse phase, particularly with the tracking data from the Ascension TPQ-18 radar at approximately the time of the second navigation update computation. The range residual plots for Ascension and Carnarvon (fig. 3-4) show biases in two segments of the Ascension data. This is a recurring phenomenon that has appeared on three consecutive missions.

The second navigation update was based on an Ascension state vector, which used the Ascension biased range data, and on the Carnarvon C-band and S-band data. This state vector was propagated over a 3-hour period to the navigation update time, then to the time of entry interface. The navigation update solution was then compared with the propagated best-estimate trajectory vector, which contained the C-band data, the S-band

data, and the Ascension data with the bias removed. The effect of the bias was as follows:

Event	Time, hr:min:sec	Position, ft	Velocity, ft/sec
Ascension state vector	05:45:35	5601	0.13
Navigation update	09:15:33	3761	1.66
Entry interface	09:38:29	6178	13.56

The velocity was out of plane at entry interface, thus having negligible effect on the dynamic condition during entry; however, an out-of-plane position error resulted.

A run, similar to the procedures at the Real Time Computer Complex, was made to determine the amount of possible error in the navigation update. All available C-band data, which included the biased Ascension data, were used; all S-band data from Carnarvon were deleted. The following comparisons were then made with the propagated best-estimate trajectory vector:

Event	Time, hr:min:sec	Position, ft	Velocity, ft/sec
Navigation update	09:15:33	13 000	8
Entry interface	09:38:29	18 000	18

As a result of these comparisons, it was concluded that the S-band data from Carnarvon after the C-band transponder was turned off assisted in minimizing the errors caused by the TPQ-18 bias at Ascension.

Other difficulties were encountered in the orbit determination during the coast ellipse phase. The C-band data, which stopped when the C-band transponder was turned off, appeared to fit well. The S-band data, which covered the entire 6-hour free-flight span, were usable but did not

fit with the C-band data as well as expected. When the C-band vector was compared with the S-band Doppler data, the residual pattern shown in figure 3-4 was apparent. This pattern was characteristic of an unmodeled thrust, and the Doppler shift of 17 Hz represented a total radial velocity of approximately 4 ft/sec. Water boil-off from the environmental control system was probably the cause for this velocity perturbation. Preliminary figures indicate that the water boil-off could have accounted for as much as 12 ft/sec change in velocity.

A comparison of the planned and actual conditions for discrete events in the coast ellipse phase is presented in table 3-V. The velocity, flight-path angle, and altitude are shown in figure 3-5.

3.4 SERVICE PROPULSION SYSTEM MANEUVER AND TARGETING ANALYSIS

The planned service propulsion system engine firing was to have been posigrade, inplane, guided, and targeted to an earth-intersecting ellipse characterized by a semilatus rectum of 34 340 227 feet, an orbit eccentricity of 0.63429326, and an apogee altitude of 11 984 n. mi. The resulting ellipse, established from tracking results, was chracterized by a semilatus rectum of 34 355 117 feet, an orbit eccentricity of 0.63498723, and an apogee altitude of 12 019.5 n. mi. The primary reasons for differences between the planned ellipse and the actual ellipse can be attributed to the following:

a. The disagreement between the onboard computer state vector and the actual state vector of the vehicle at the time of service propulsion system engine ignition.

b. The difference between the actual tailoff impulse and the onboard predicted tailoff, as discussed in section 5.16.

c. Minor differences resulting from water boiler venting effects.

The errors in the computer state vector at the time of service propulsion system engine ignition were a result of the navigation update which reflected venting and propagation effects, as presented in section 3.2. Based on simulated results, these errors had no appreciable effect on firing time or the total velocity change. The 36.6-n. mi. difference between planned and actual apogee conditions was less than a one sigma deviation from the predicted navigational accuracy.

The times for service propulsion system engine ignition and guidance cutoff established from the chamber pressure data were 03:16:06.5 at

initial buildup of chamber pressure and 03:23:28.2 when the chamber pressure indicated a decrease from the steady-state value. The actual time designated for tailoff was 1.1 second; however, only 0.8 second was indicated for the chamber pressure measurement to attain 0.0 psi. The remaining 0.3 second corresponded to a chamber pressure bias of 1 to 2 psi, which would indicate no effective velocity change. The effective service propulsion firing time resulted in a total velocity change of 7848.0 ft/sec. The best estimates of spacecraft state vector conditions at the time of service propulsion ignition and cutoff are presented in table 3-V. The planned and actual service propulsion time history profiles for space-fixed velocity, flight-path angle, and altitude are presented in figure 3-6.

The service propulsion maneuver profile was reconstructed from two independent postflight trajectory programs — the guidance and navigation trajectory reconstruction program and an operational trajectory simulation program. The guidance and navigation trajectory reconstruction program, which processes accelerometer data to generate the best estimate of the actual firing profile, did not include a finalized set of inertial measurement unit performance errors. Engine and chamber pressure performance data are used in the operational trajectory simulation program to model service propulsion buildup, steady state, and tailoff characteristics of the firing. The simulation program models the onboard guidance equations. It was established that guidance cutoff was indicated for the times when the onboard targeting quantities (semilatus rectum and orbit eccentricity) were satisfied and when the simulated firing time agreed very closely with the computer telemetry value. No inertial measurement unit error effects were included in the simulation. Agreement between the two reconstruction programs was very good, and the finalized set of inertial measurement unit errors is not expected to change the guidance and navigation results significantly.

Five simulations of the service propulsion system engine firing were made using the actual thrust characteristics and actual inertial measurement unit gimbal angles at the time of ignition. The postflight performance data indicated a thrust of 20 840 pounds before crossover and 21 360 pounds after crossover, with an average specific impulse of 310.2 seconds. The tailoff impulse was 11 905 lb-sec buildup and steady-state propulsion characteristics were well within the expected tolerances. However, the tailoff impulse was 2608 lb-sec greater than the expected nominal value of 9297 lb-sec. The total CSM weight at ignition was 55 468 pounds. The inertial measurement unit gimbal angles at time of ignition were as follows: inner angle 214.37 degrees, middle angle 2.74 degrees, and outer angle 182.62 degrees. A summary of the results obtained from these simulations, and the best estimation of firing conditions, established from guidance and navigation data, and the best-estimate trajectory are presented in table 3-VI.

The first simulation, case 1, represented the onboard computer solution at time of service propulsion system engine ignition, integrated through a firing designed to achieve the onboard targets. This simulation represented actual computer performance during the firing. The firing time and change in velocity from this simulation compared closely with the guidance and navigation best-estimate trajectory results presented as case 6, differing only by 0.3 second in firing time and 1.3 ft/sec in change in velocity. The resulting apogee altitude of 11 995.6 n. mi. was 12.6 n. mi. higher than that defined by the onboard computer targets. This difference resulted from the tailoff impulse being higher than expected.

The second simulation, case 2, is identical to case 1 except that a nominal tailoff impulse was used. As shown in table 3-VI, the apogee altitude was reduced to 11 982.9 n. mi. and the total change in velocity to 7845.9 ft/sec. These results indicate that the computer performed nominally and the higher tailoff impulse added approximately 3.4 ft/sec to the trajectory, raising the apogee 12.7 n. mi.

The third simulation, case 3, again integrated the computer vector through the firing; however, the onboard guidance was designed to achieve best-estimate trajectory targets that reflected the actual ellipse obtained and a time-to-go calculation bias (0.558) based on actual performance data. The actual targets represented the best-estimate trajectory conditions attained at cutoff. The firing time differed from the first simulation by 0.1 second; this indicated that the actual ellipse was very close to the ellipse achieved by the onboard guidance.

The fourth simulation, case 4, integrated a best-estimate trajectory vector, which reflected the actual condition of the spacecraft at time of ignition, through the service propulsion firing using best-estimate trajectory targets. The resulting firing time was 0.9 second longer than the actual firing time, indicating the best-estimate trajectory vector accurately reflected the actual condition at time of ignition.

The fifth simulation, case 5, integrated the best-estimate trajectory vector through the firing, using onboard targets. This simulation indicated that, if the computer vector had been equal to the actual vector, the firing would have been 0.4 second longer. This indicated good agreement between the computer state vector and the best-estimate trajectory vector; as stated previously, no appreciable differences in cutoff conditions resulted.

3.5 ENTRY ANALYSIS

The planned and actual entry trajectories are shown in figure 3-7. The planned entry trajectory was based on the Ascension (76) navigation update state vector. The entry was simulated by flying the guidance and navigation equations with the preflight nominal lift-to-drag ratio of 0.343 and the 1962 standard atmosphere. Because of a difference in the entry interface vectors, the planned trajectory landing point differed from the landing point predicted by the Real Time Computer Complex during the mission (see section 9.1). The real-time solution did not include the plus X translation and resulted in entry interface conditions of 32 813 ft/sec in velocity and a flight-path angle of -5.94 degrees. The landing point predicted with this vector was approximately 296 n. mi. short of the target. By including the planned plus X translation, the entry conditions were 32 823 ft/sec in velocity and -5.84 degrees in flight-path angle. With these conditions, the predicted landing point was 85 n. mi. short of the target. This large difference in predicted landing points was due to the variations in the predicted time that the onboard computer would command a reversal in the direction of the command module lift vector. If this reversal occurred late in the UPCONTROL phase and was flown through negative lift, the command module would land 100 to 380 n. mi. short of the target. This sensitivity to roll reversals was caused by the marginal reference trajectory which the onboard computer set up for this entry. The marginal reference trajectory is discussed in section 5.16. The small differences in the entry conditions were sufficient to change the roll reversal time from the critical region in the real-time solution to the noncritical region in the plus X translation maneuver case. This sensitivity to roll reversals was known before the flight and was a factor in the procedures used by the flight controllers in compensating for the entry guidance problem. These procedures are discussed in section 9.1.

The actual trajectory was based on the best-estimate entry vector and was generated by using the corrected telemetry accelerometer counts. The actual trajectory did not have the critical roll reversal problem. The planned and actual conditions at entry interface are shown in table 3-VII. Table 3-VIII presents a summary of the planned and actual entry dynamic parameters.

The aerodynamics for entry is discussed in section 5.2. The analysis of the guidance and navigation system has shown no inflight anomalies and is discussed in detail in section 5.16. The guidance and navigation system indicated a 36.4 n. mi. undershoot at drogue deployment. The postflight reconstruction best-estimate trajectory indicated a 49.2 n. mi. undershoot.

TABLE 3-I.- DEFINITION OF TRAJECTORY AND ORBITAL PARAMETERS

Trajectory parameters	Definition
Geodetic latitude	Spacecraft position measured North or South from the equator to the local vertical vector, deg
Longitude	Spacecraft position measured East or West from the Greenwich meridian to the local vertical vector, deg
Altitude	Perpendicular distance from the reference ellipsoid to the point of orbit intersect, ft
Space-fixed velocity	Magnitude of the inertial velocity vector referenced to the earth-centered, inertial reference coordinate system, ft/sec
Space-fixed flight-path angle	Flight-path angle measured positive upward from the geocentric local horizontal plane to the inertial velocity vector, deg
Space-fixed heading	Angle of the projection of the inertial velocity vector onto the local geocentric horizontal plane, measured positive eastward from north, deg
Apogee	Predicted maximum altitude above the oblate earth model, n. mi.
Perigee	Predicted minimum altitude above the oblate earth model, n. mi.
Period	Time required for spacecraft to complete 360 degrees of orbit rotation (perigee to perigee, for example), min
Inclination	Angle between the orbit plane and the equator, deg

TABLE 3-II.- PLANNED AND ACTUAL TRAJECTORY

FOR THE LAUNCH PHASE

Condition	Planned[a]	Actual
S-IC Inboard Engine Cutoff		
Time from range zero, min:sec	02:24.4	02:24.7
Geodetic latitude, deg North	28.81	28.82
Longitude, deg West	79.87	79.87
Altitude, ft	182 421	183 946
Altitude, n. mi	30.0	30.3
Space-fixed velocity, ft/sec	8657	8598
Space-fixed flight-path angle, deg	20.25	20.14
Space-fixed heading angle, deg E of N	75.58	75.13
S-IC Outboard Engine Cutoff		
Time from range zero, min:sec	02:27.3	02:28.4
Geodetic latitude, deg North	28.83	28.84
Longitude, deg West	79.80	79.78
Altitude, ft	191 380	195 028
Altitude, n. mi.	31.5	32.1
Space-fixed velocity, ft/sec	9007	9031
Space-fixed flight-path angle, deg	19.84	19.67
Space-fixed heading angle, deg E of N	75.50	75.00

[a]Based on alternate mission plan.

TABLE 3-II.- PLANNED AND ACTUAL TRAJECTORY

FOR THE LAUNCH PHASE - Concluded

Condition	Planned[a]	Actual
S-II Engine Cutoff		
Time from range zero, min:sec	08:37.5	09:36.3
Geodetic latitude, deg North	31.74	32.14
Longitude, deg West	65.43	62.18
Altitude, ft	619 091	640 070
Altitude, n. mi.	101.9	105.3
Space-fixed velocity, ft/sec	22 402	22 066
Space-fixed flight-path angle, deg	0.79	1.60
Space-fixed heading angle, deg E of N	81.61	83.39
S-IVB Engine Cutoff		
Time from range zero, min:sec	10:59.0	12:27
Geodetic latitude, deg North	32.62	32.74
Longitude, deg West	55.47	50.16
Altitude, ft	628 274	625 697
Altitude, n. mi.	103.4	103.0
Space-fixed velocity, ft/sec	25 561	257 21
Space-fixed flight-path angle, deg	0.00	-0.40
Space-fixed heading angle, deg E of N	87.19	90.24

[a]Based on alternate mission plan.

TABLE 3-III.- PLANNED AND ACTUAL TRAJECTORY PARAMETERS

FOR THE PARKING ORBIT PHASE

Condition	Planned[a]	Actual
Insertion (S-IVB Cutoff +10 seconds)		
Time from range zero, min:sec	11:09.0	12:37.0
Geodetic latitude, deg North	32.65	32.73
Longitude, deg West	54.71	49.39
Altitude, ft	628 314	623 981
Altitude, n. mi.	103.4	102.7
Space-fixed velocity, ft/sec	25 571	25 729
Space-fixed flight-path angle, deg	0.00	-0.38
Space-fixed heading angle, deg E of N	87.62	90.67
S-IVB Restart Command		
Time from range zero, hr:min:sec	03:10:11	03:13:35
Geodetic latitude, deg North	32.48	32.50
Longitude, deg West	88.11	89.13
Altitude, ft	671 296	651 464
Altitude, n. mi.	110.5	107.2
Space-fixed velocity, ft/sec	25 556	25 724
Space-fixed flight-path angle, deg	-0.02	-0.33
Space-fixed heading angle, deg E of N	94.31	94.16

[a]Based on alternate mission plan.

TABLE 3-III.- PLANNED AND ACTUAL TRAJECTORY PARAMETERS

FOR THE PARKING ORBIT PHASE - Concluded

Condition	Planned	Actual
S-IVB Cutoff Command		
Time from range zero, hr:min:sec	03:15:28	03:13:50
Geodetic latitude, deg North	27.39	32.41
Longitude, deg West	61.14	87.98
Altitude, ft	1 021 793	649 078
Altitude, n. mi.	168.2	106.8
Space-fixed velocity, ft/sec	35 588	25 736
Space-fixed flight-path angle, deg	6.51	-0.32
Space-fixed heading angle, deg E of N	108.42	94.83
Command Module/S-IVB Separation[a]		
Time from range zero, hr:min:sec	03:14:26	03:14:28
Geodetic latitude, deg North	32.16	32.16
Longitude, deg West	85.12	85.11
Altitude, ft	642 544	643 752
Altitude, n. mi.	105.7	105.9
Space-fixed velocity, ft/sec	25 728	25 743
Space-fixed flight-path angle, deg	-0.29	-0.28
Space-fixed heading angle, deg E of N	96.45	96.45

[a]Based on alternate mission plan.

TABLE 3-IV.- STATISTICAL SUMMARY OF TRACKER RESIDUALS

Station	Radar	Condition	Bias		Noise	
			Theoretical	Actual	Theoretical	Actual
Ascension	C-band	Range, ft	±40	0.8	20	16.1
		Azimuth, deg	±0.018	0.010	0.009	0.010
		Elevation, deg	±0.018	-0.003	0.009	0.012
Carnarvon	C-band	Range, ft	±40	0.5	20	17.0
		Azimuth, deg	±0.018	-0.004	0.009	0.006
		Elevation, deg	±0.018	0.005	0.009	0.007
Ascension	S-band	Range, ft	±60	1.4	30	75.6
		X, deg	±0.090	0.015	0.045	0.010
		Y, deg	±0.090	0.021	0.045	0.007
		Doppler ($\dot{R}$), Hz	±0.150	-0.143	0.100	0.084
Carnarvon	S-band	Range, ft	±60	2.5	30	9.1
		X, deg	±0.090	-0.054	0.045	0.014
		Y, deg	±0.090	0.028	0.045	0.010
		Doppler ($\dot{R}$), Hz	±0.150	-0.001	0.100	0.239

TABLE 3-V.- PLANNED AND ACTUAL TRAJECTORY PARAMETERS

FOR THE COAST ELLIPSE PHASE

Condition	Planned[a]	Actual
Service Propulsion System Engine Ignition		
Time from range zero, hr:min:sec	03:16:06	03:16:06
Geodetic latitude, deg North	31.15	31.16
Longitude, deg West	77.67	77.71
Altitude, ft	630 468	632 242
Altitude, n. mi.	103.8	104.0
Space-fixed velocity, ft/sec	25 744	25 757
Space-fixed flight-path angle, deg	-0.20	-0.19
Space-fixed heading angle, deg E of N	100.57	100.55
Service Propulsion System Engine Cutoff		
Time from range zero, hr:min:sec	03:23:27	03:23:28
Geodetic latitude, deg North	20.39	20.39
Longitude, deg West	44.76	44.72
Altitude, ft	1 693 224	1 696 889
Altitude, n. mi.	278.9	279.3
Space-fixed velocity, ft/sec	31 630	31 629
Space-fixed flight-path angle, deg	13.52	13.53
Space-fixed heading angle, deg E of N	116.05	116.07

[a]Based on alternate mission plan.

TABLE 3-V.- PLANNED AND ACTUAL TRAJECTORY PARAMETERS

FOR THE COAST ELLIPSE PHASE - Concluded

Condition	Planned[a]	Actual
Apogee		
Time from range zero, hr:min:sec	06:28:24	06:28:58
Geodetic latitude, deg South	31.39	31.40
Longitude, deg East	51.65	51.54
Altitude, ft	72 817 217	73 032 036
Altitude, n. mi.	11 984.2	12 019.5
Space-fixed velocity, ft/sec	7418	7403
Space-fixed flight-path angle, deg	0.00	0.00
Space-fixed heading angle, deg E of N . . .	80.69	80.65

[a]Based on alternate mission plan.

TABLE 3-VI.- SERVICE PROPULSION SYSTEM SUMMARY

Case	Targets		Firing parameters		Characteristics of resulting ellipse		
	Semilatus rectum, ft	Eccentricity	Firing time, sec	Total change in velocity, ft/sec	Semilatus rectum, ft	Eccentricity	Apogee altitude, n. mi.
Computer vector							
1. Onboard targets	34 340 227	0.63429326	442.8	7849.3	34 344 510	0.63453910	11 995.6
2. Onboard targets and nominal tailoff	34 340 227	0.63429326	442.8	7845.9	34 339 945	0.63428575	11 982.9
3. Best-estimate trajectory targets	34 355 117	0.63498273	442.9	7852.6	34 355 560	0.63499648	12 019.9
Best-estimate trajectory vector							
4. Best-estimate trajectory targets	34 355 117	0.63498273	443.4	7864.3	34 355 567	0.63499791	12 020.2
5. Onboard targets	34 340 227	0.63429326	443.2	7861.1	34 345 000	0.63455424	11 997.2
6. Tracking (guidance and navigation best-estimate trajectory results)	34 340 227	0.63429326	442.5	7848.0	34 355 117	0.63498273	12 019.5

TABLE 3-VII.- PLANNED AND ACTUAL TRAJECTORY

PARAMETERS FOR THE ENTRY PHASE

Condition	Planned[a]	Actual
Plus X Translation Ignition		
Time from range zero, hr:min:sec	09:29:24	09:29:19
Geodetic latitude, deg North	23.93	23.80
Longitude, deg East	122.49	122.15
Altitude, ft	4 492 745	4 564 056
Altitude, n. mi.	739.4	751.1
Space-fixed velocity, ft/sec	29 384	29 331
Space-fixed flight-path angle, deg	-21.34	-21.45
Space-fixed heading angle, deg E of N	67.10	66.97
Plus X Translation Cutoff		
Time from range zero, hr:min:sec	09:29:54	09:30:09
Geodetic latitude, deg North	24.66	25.00
Longitude, deg East	124.27	125.13
Altitude, ft	4 176 271	4 038 098
Altitude, n. mi.	687.3	664.6
Space-fixed velocity, ft/sec	29 633	29 746
Space-fixed flight-path angle, deg	-20.65	-20.35
Space-fixed heading angle, deg E of N	67.88	68.27

[a]Based on alternate mission plan.

TABLE 3-VII.- PLANNED AND ACTUAL TRAJECTORY

PARAMETERS FOR THE ENTRY PHASE - Continued

Condition	Planned[a]	Actual
Command Module/Service Module Separation		
Time from range zero, hr:min:sec	09:37:01	09:36:57
Geodetic latitude, deg North	32.40	32.36
Longitude, deg East	157.79	157.33
Altitude, ft	757 658	783 792
Altitude, n. mi.	124.7	128.9
Space-fixed velocity, ft/sec	32 489	32 472
Space-fixed flight-path angle, deg	-8.72	-8.90
Space-fixed heading angle, deg E of N	85.15	84.90
Entry Interface		
Time from range zero, hr:min:sec	09:38:27	09:38:29
Geodetic latitude, deg North	32.73	32.73
Longitude, deg East	166.27	166.29
Altitude, ft	400 000	400 000
Altitude, n. mi.	65.8	65.8
Space-fixed velocity, ft/sec	32 823	32 830
Space-fixed flight-path angle, deg	-5.84	-5.85
Space-fixed heading angle, deg E of N	89.90	89.92

[a]Based on alternate mission plan.

TABLE 3-VII.- PLANNED AND ACTUAL TRAJECTORY

PARAMETERS FOR THE ENTRY PHASE - Concluded

Condition	Planned[a]	Actual
Drogue Deployment		
Time from range zero, hr:min:sec	09:51:00	09:51:27
Geodetic latitude, deg North	27.80	27.57
Longitude, deg West	158.69	158.00
Altitude, ft	23 500	21 512
Altitude, n. mi.	3.9	3.5
Space-fixed velocity, ft/sec	1585	1582
Space-fixed flight-path angle, deg	-14.25	-14.72
Space-fixed heading angle, deg E of N . . .	90.98	93.07

[a]Based on alternate mission plan.

TABLE 3-VIII.- MAXIMUM ENTRY CONDITIONS

Condition	Planned[a]	Actual
Space-fixed velocity, ft/sec	32 918	32 923
Earth-fixed velocity, ft/sec	31 619	31 625
Deceleration 1, g	4.57	4.65
Deceleration 2, g	2.11	2.04
Dynamic pressure 1, lb/ft^2	335	349
Dynamic pressure 2, lb/ft^2	152	181
Skip altitude, ft	225 909	218 232

[a]Based on alternate mission plan.

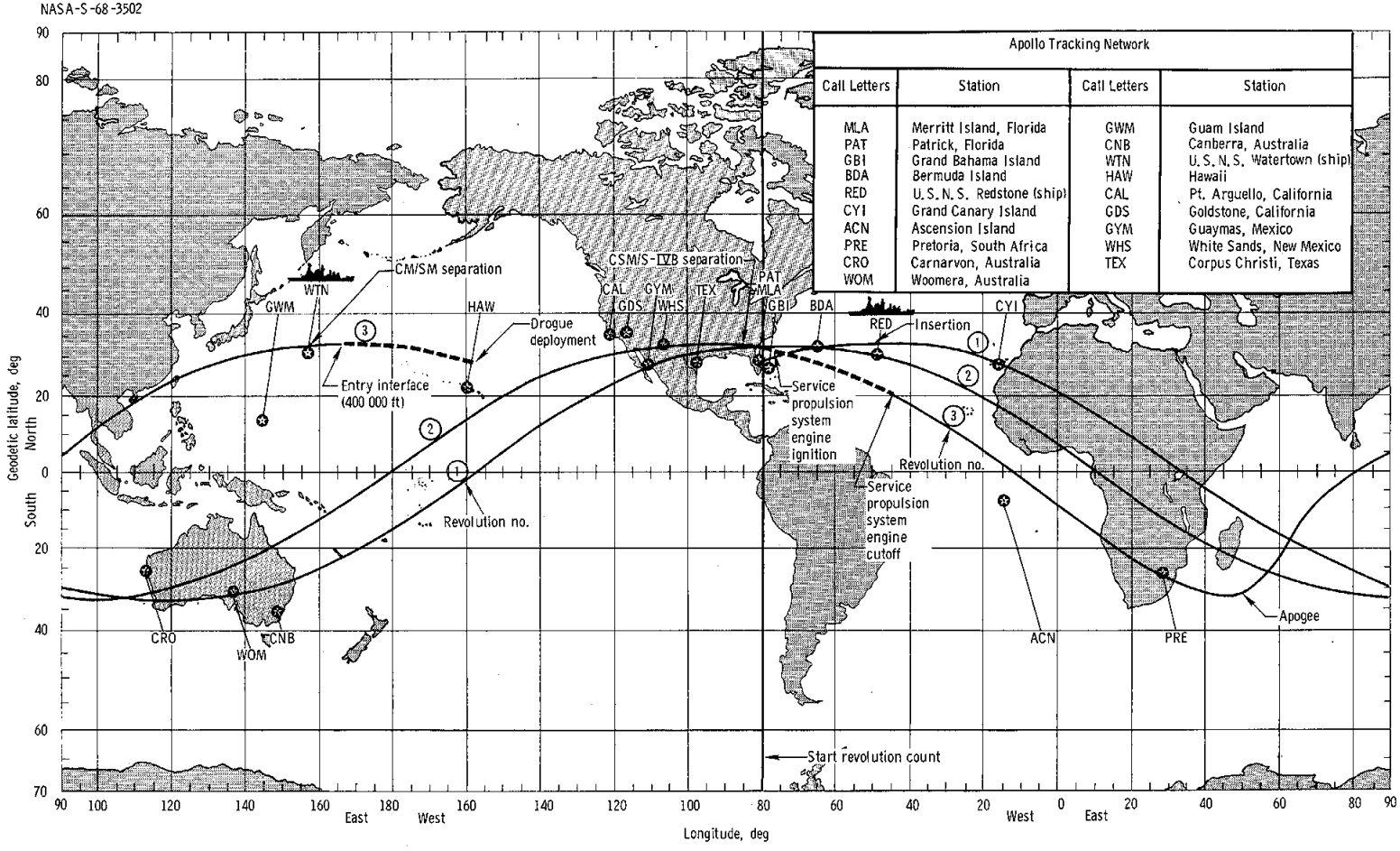

Figure 3-1. - Apollo 6 mission ground track.

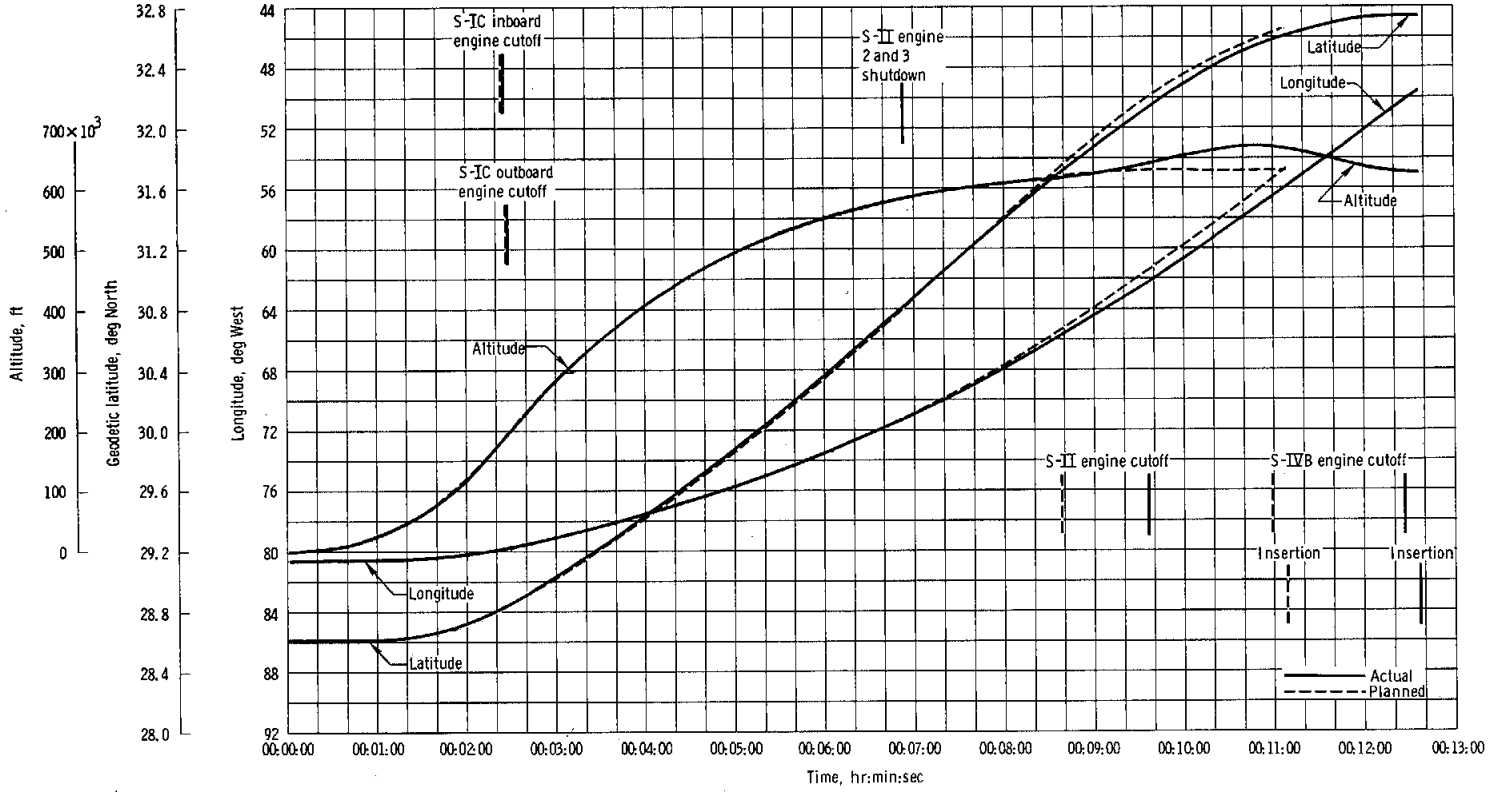

(a) Latitude, longitude, and altitude.

Figure 3-2. - Trajectory parameters during the launch phase.

NASA-S-68-3504

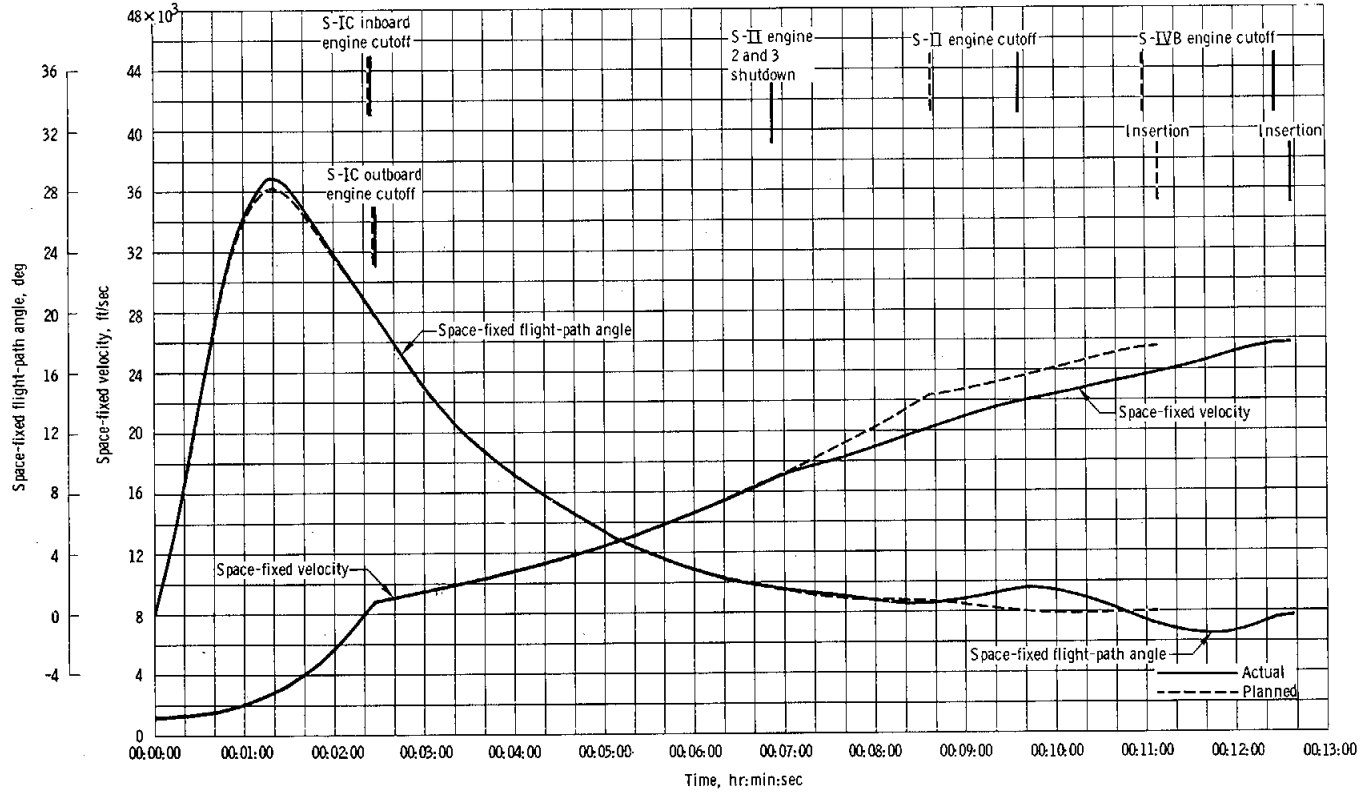

(b) Space-fixed flight-path angle and velocity.

Figure 3-2. - Continued.

NASA-S-68-3505

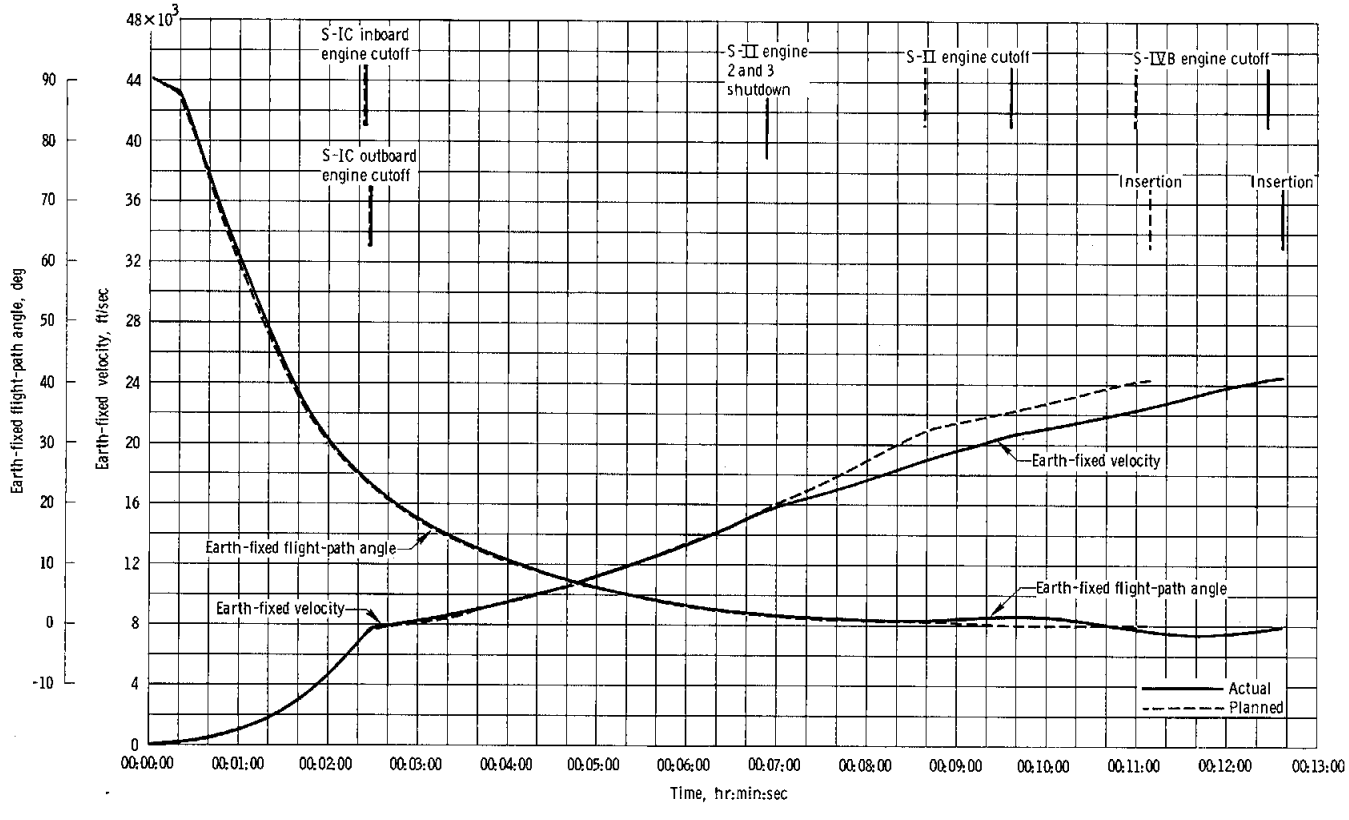

(c) Earth-fixed flight-path angle and velocity.

Figure 3-2. - Continued.

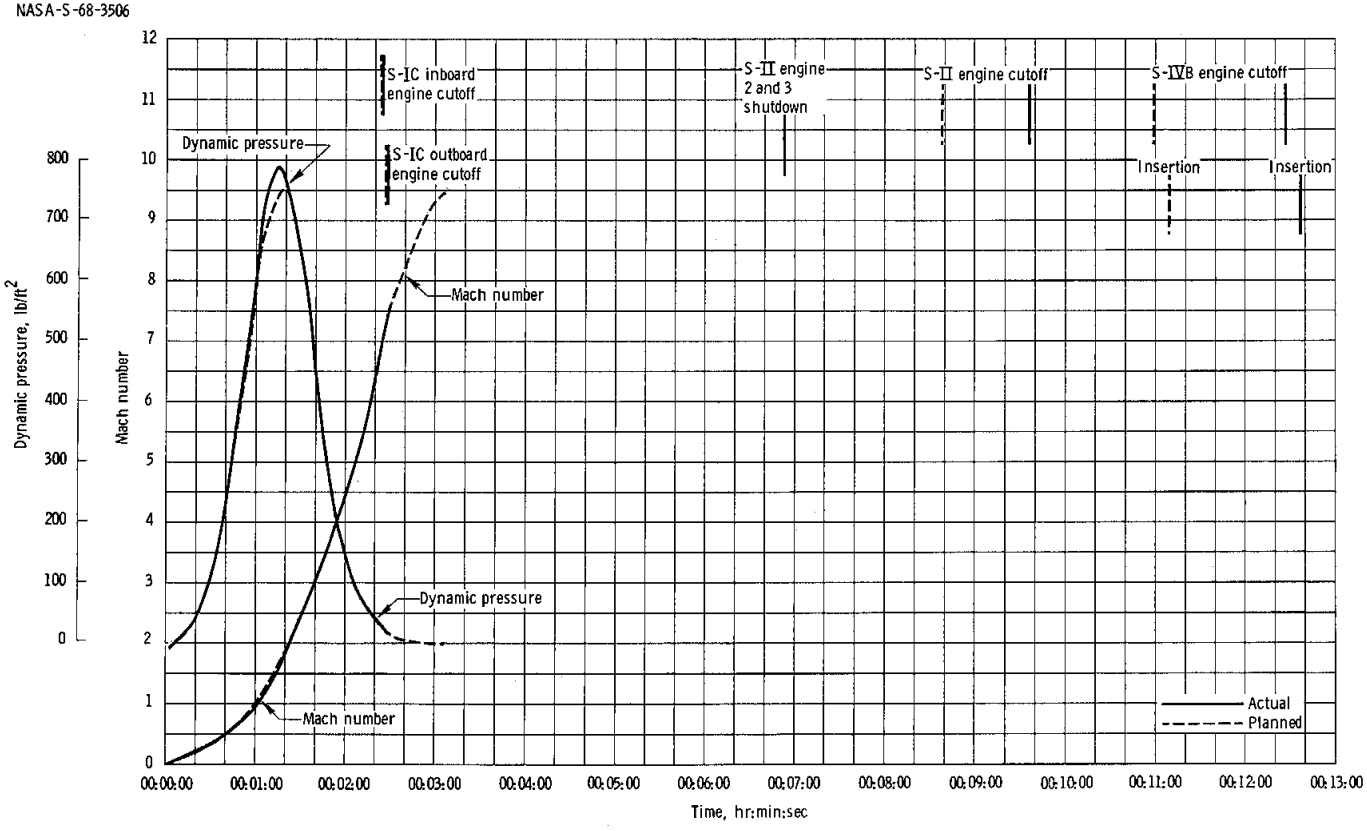

(d) Mach number and dynamic pressure.

Figure 3-2. - Concluded.

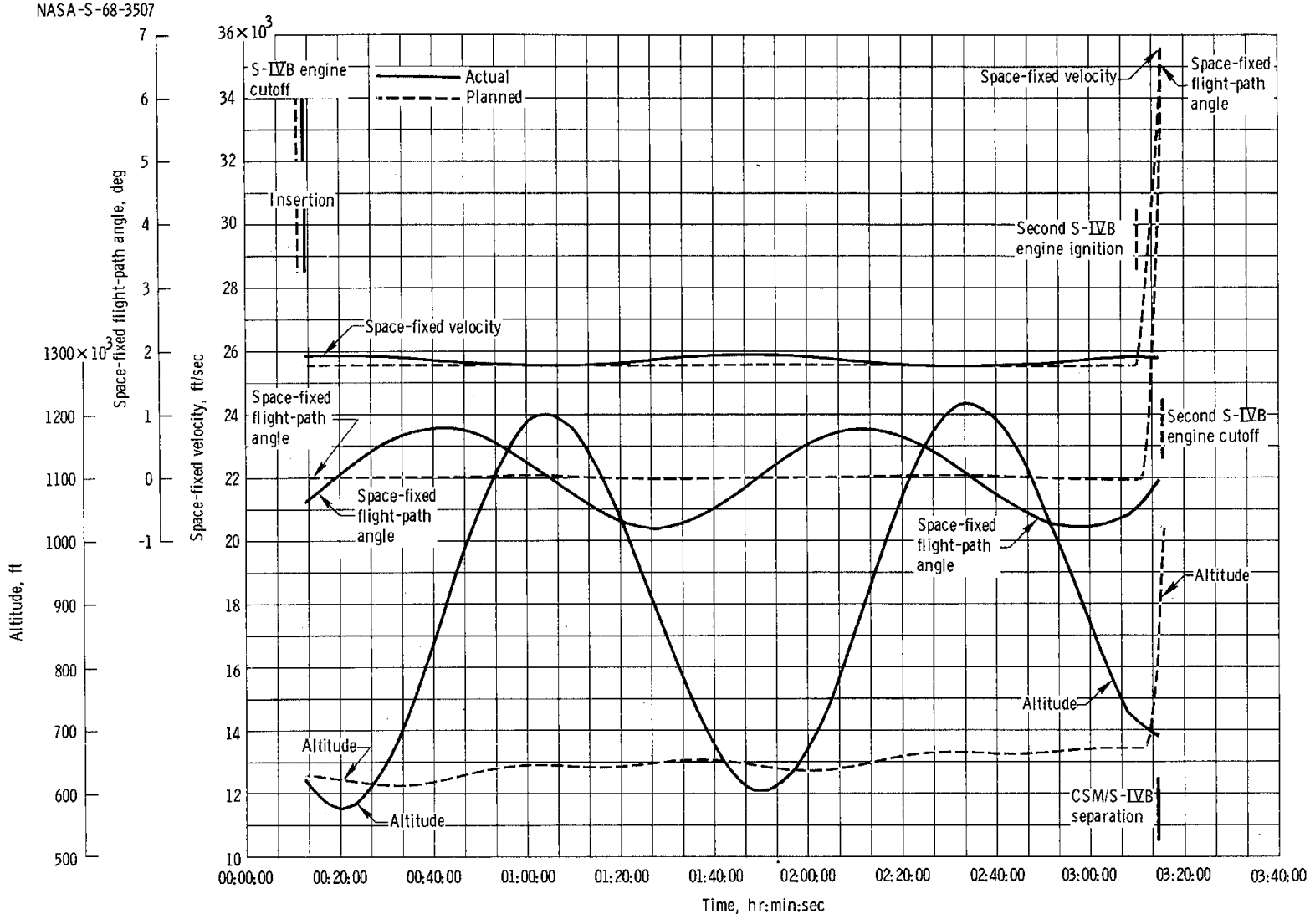

Figure 3-3. - Space-fixed velocity, flight-path angle, and altitude during the parking orbit.

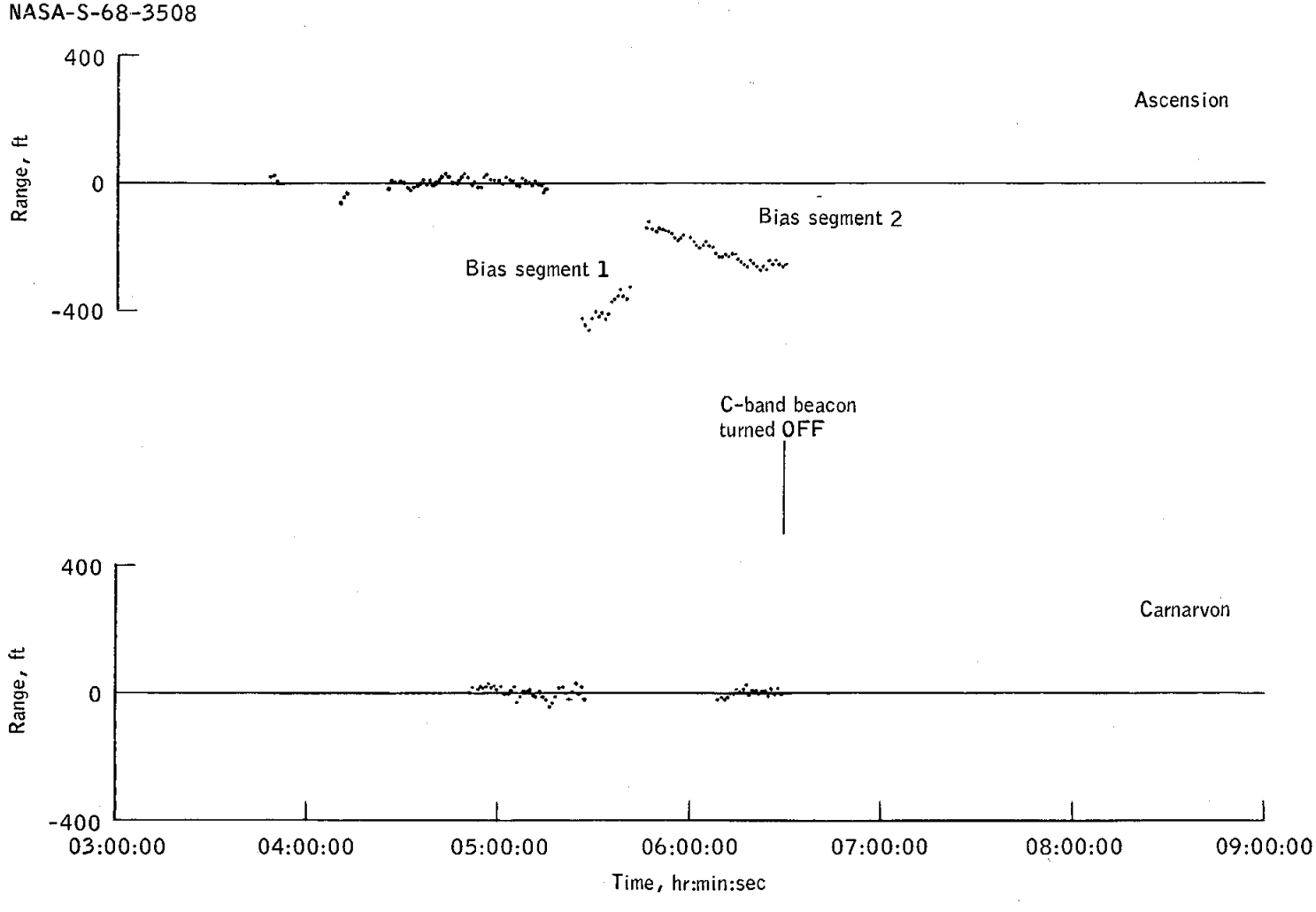

(a) C-band range residuals.

Figure 3-4.- Ascension and Carnarvon tracker residuals.

NASA-S-68-3509

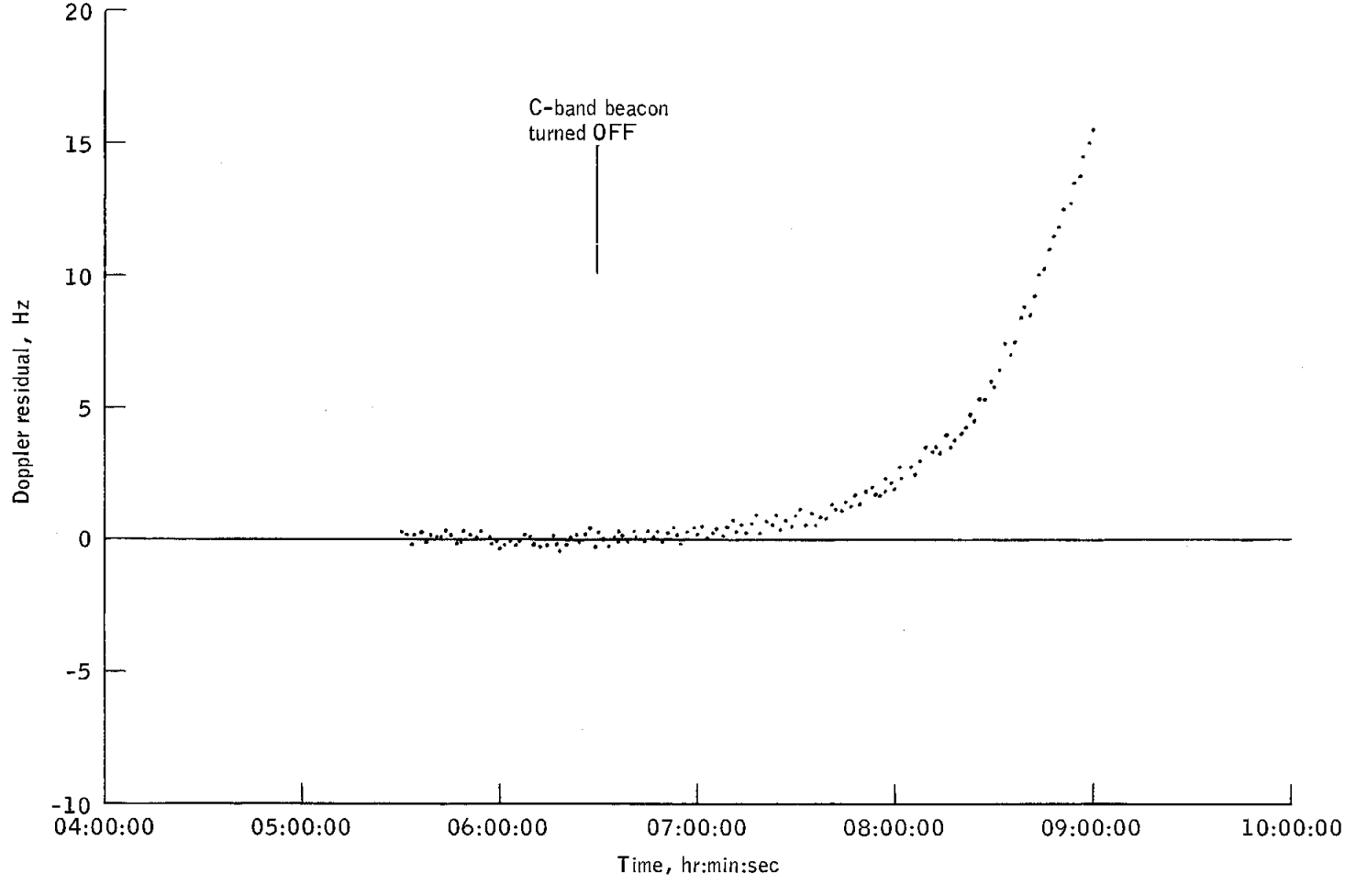

(b) Carnarvon S-band Doppler residuals.

Figure 3-4.- Concluded.

NASA-S-68-3510

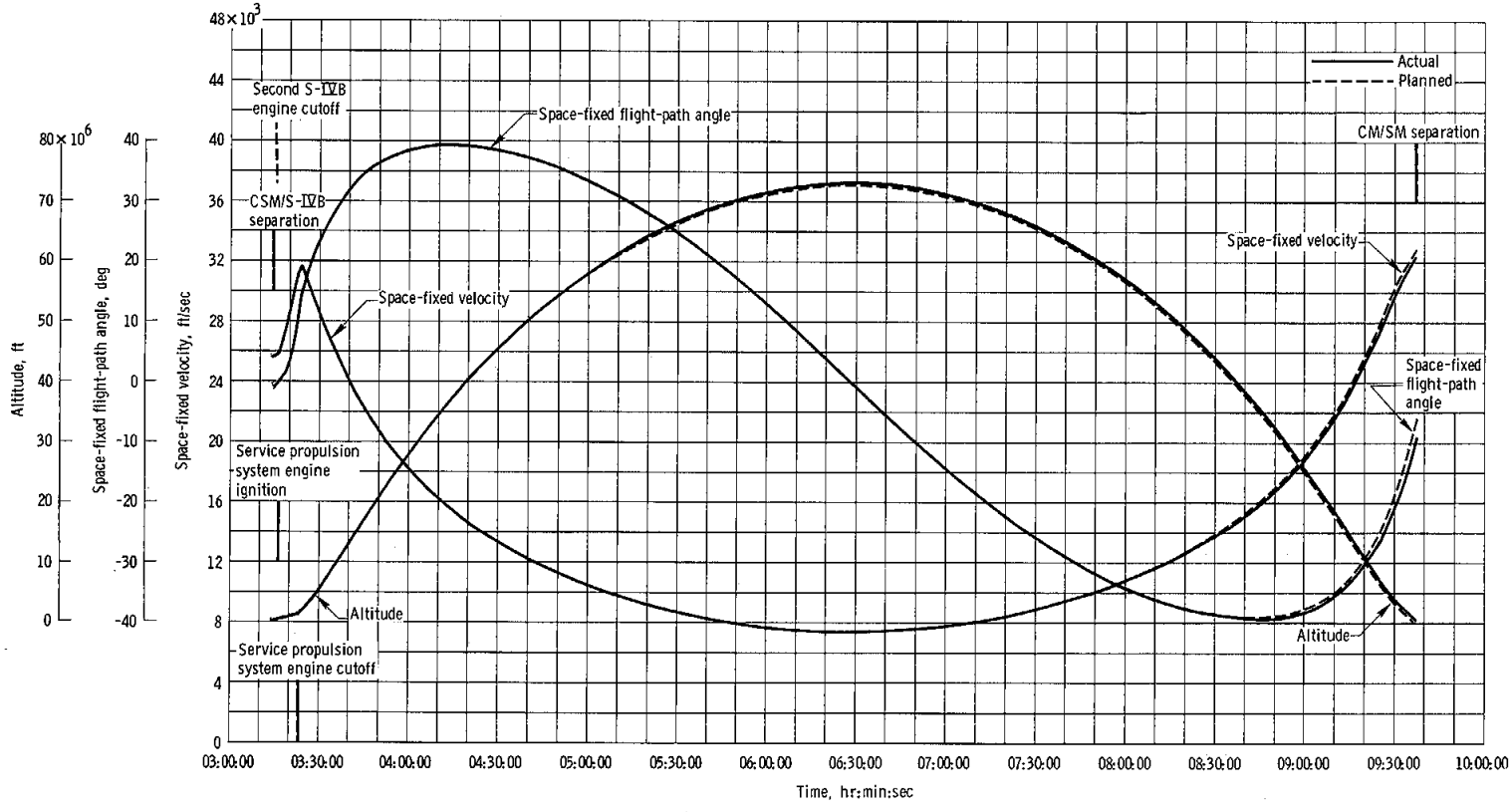

Figure 3-5. - Space-fixed velocity, flight-path angle, and altitude during the coast ellipse.

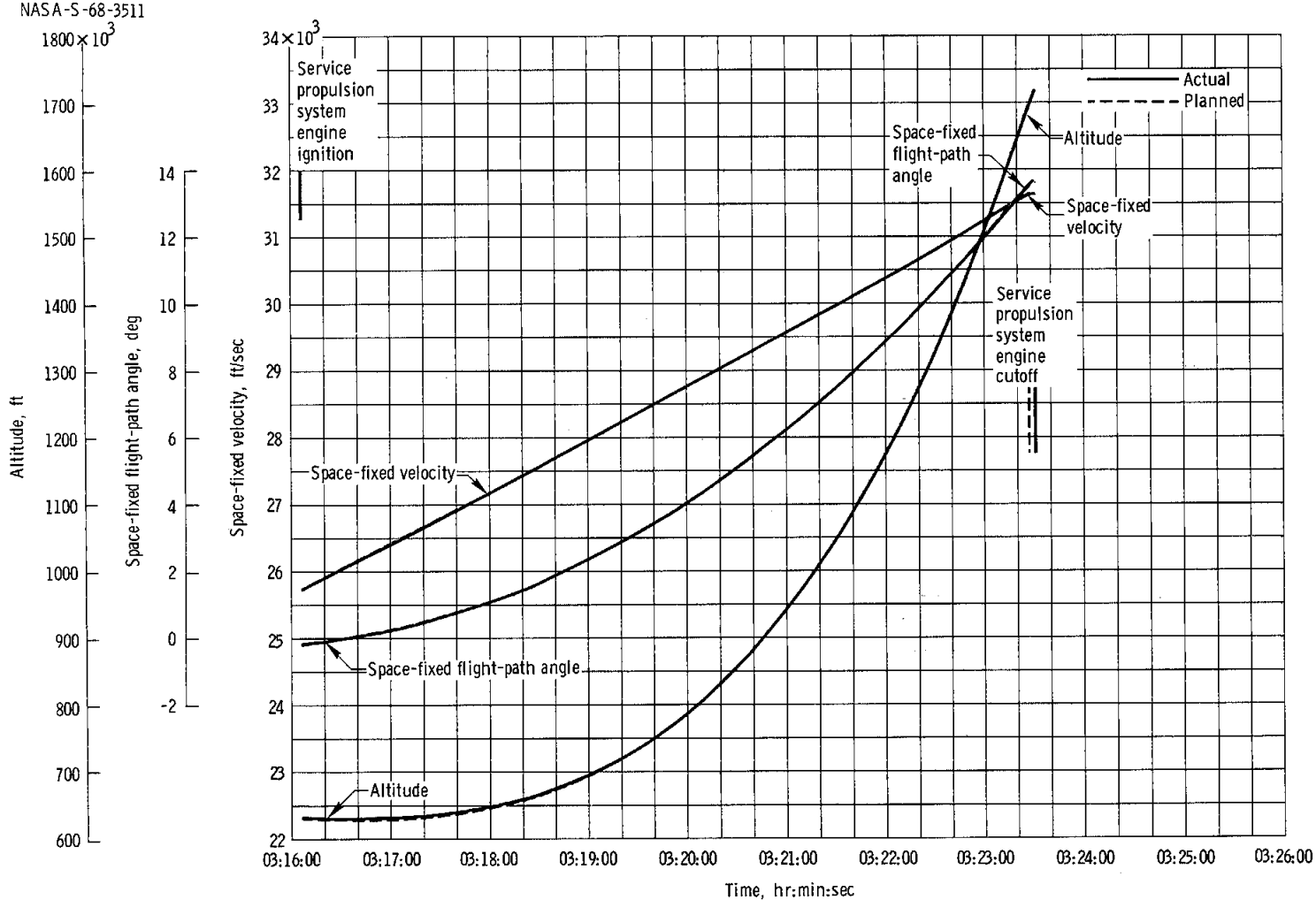

Figure 3-6. - Space-fixed velocity, flight-path angle, and altitude during the service propulsion system engine firing.

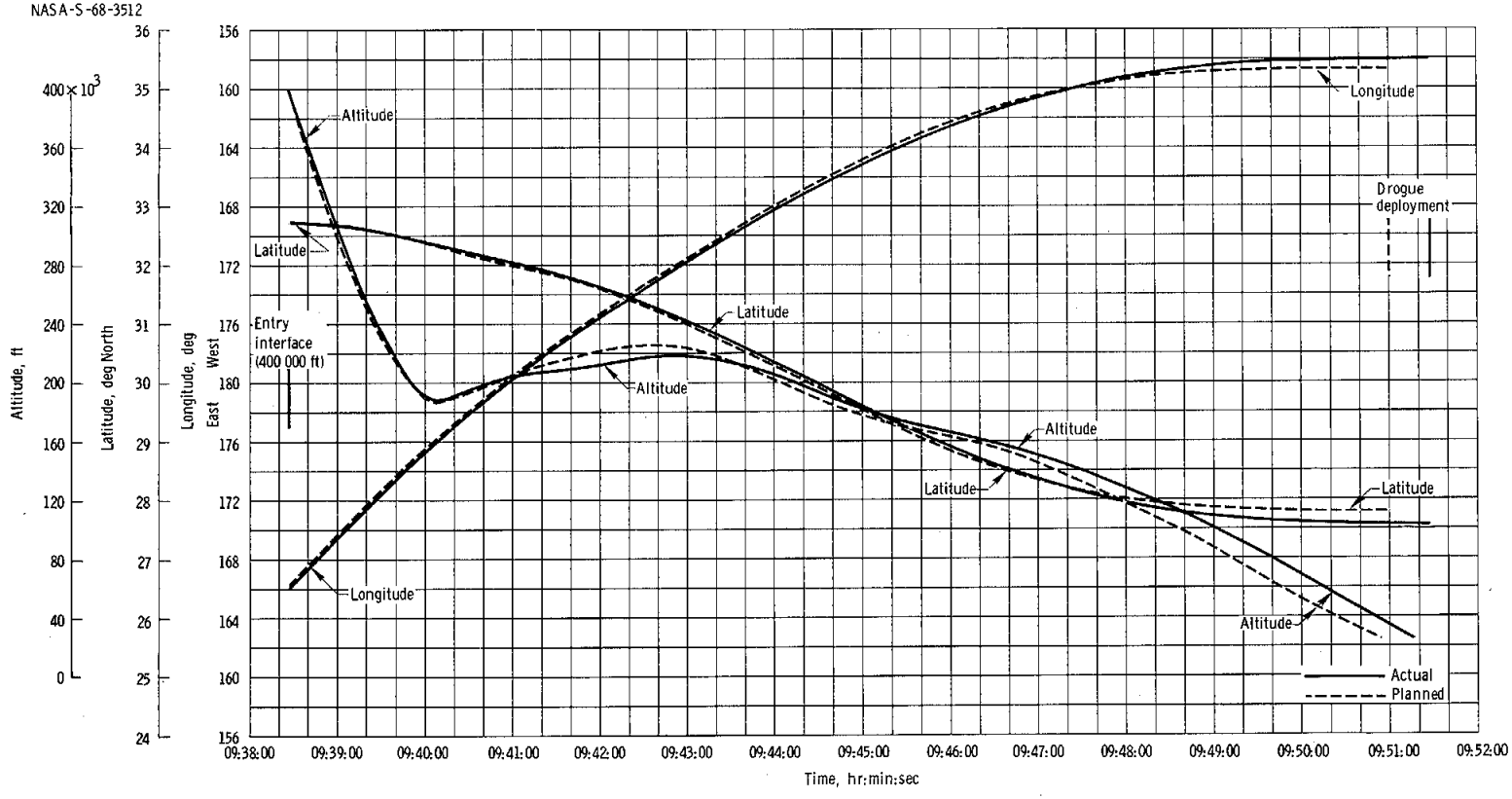

(a) Latitude, longitude, and altitude.

Figure 3-7. - Trajectory parameters during the entry phase.

NASA-S-68-3513

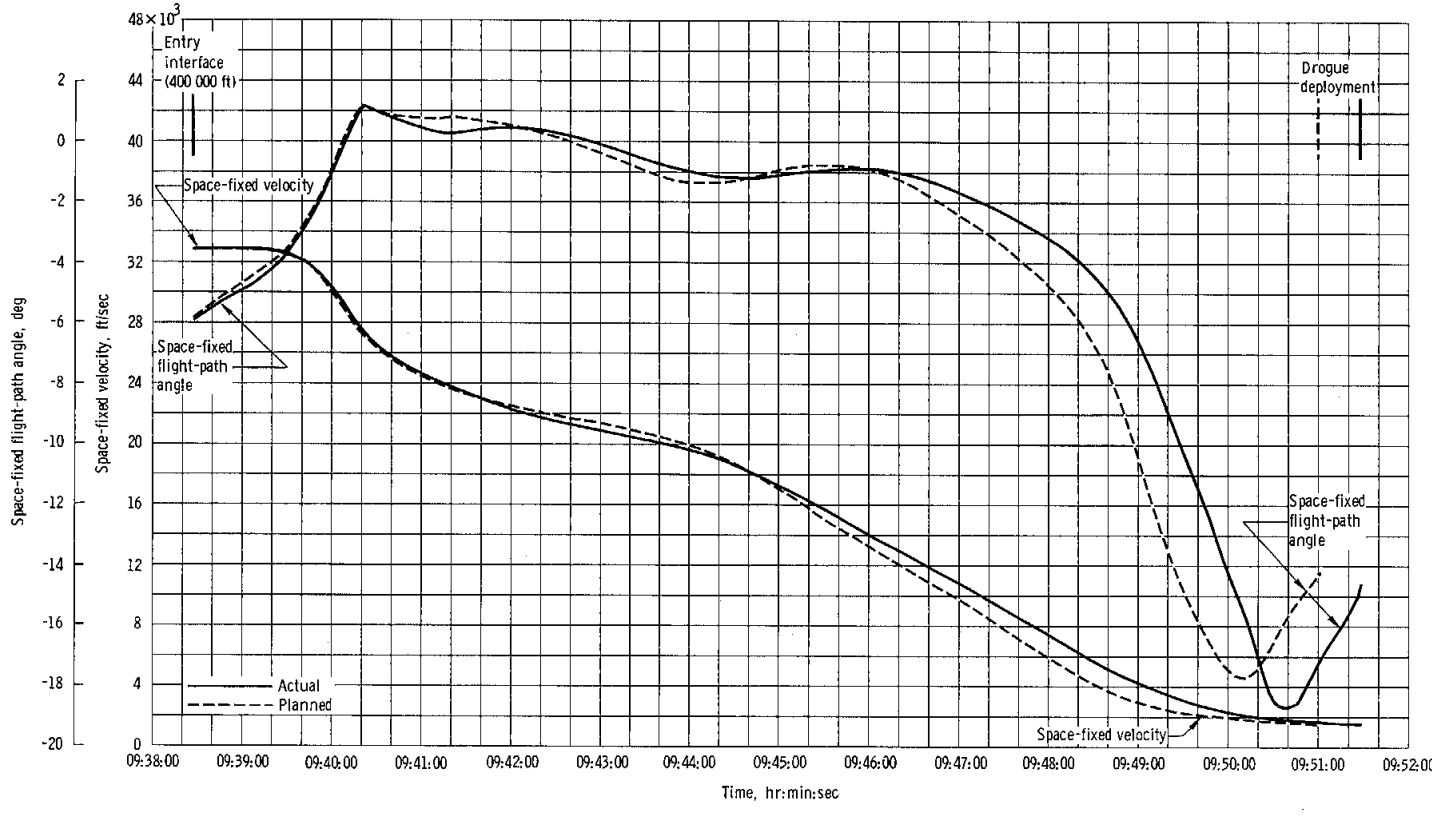

(b) Space-fixed velocity and flight-path angle.

Figure 3-7. - Continued.

NASA-S-68-3514

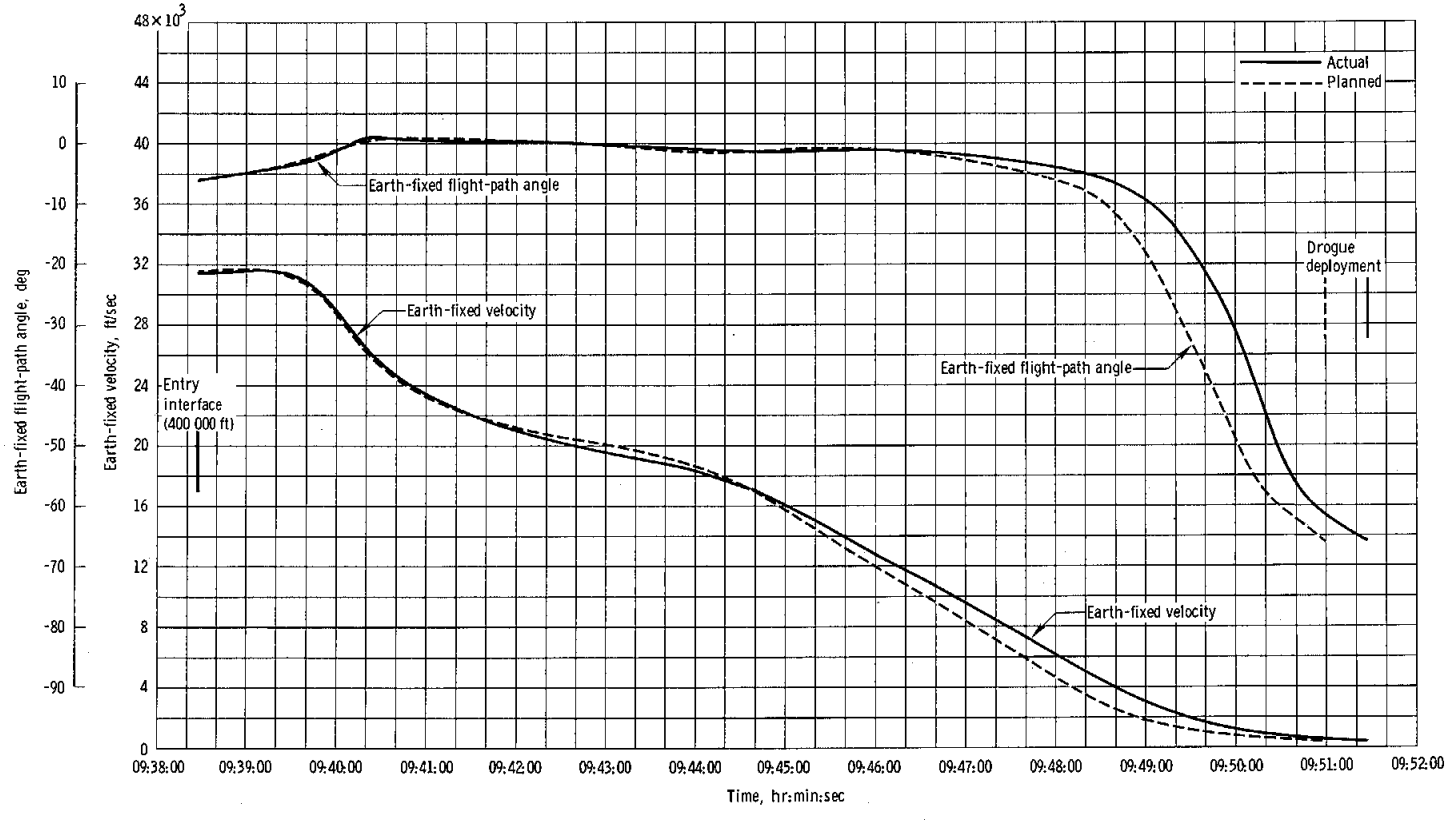

(c) Earth-fixed flight-path angle and velocity.

Figure 3-7. - Continued.

NASA-S-68-3515

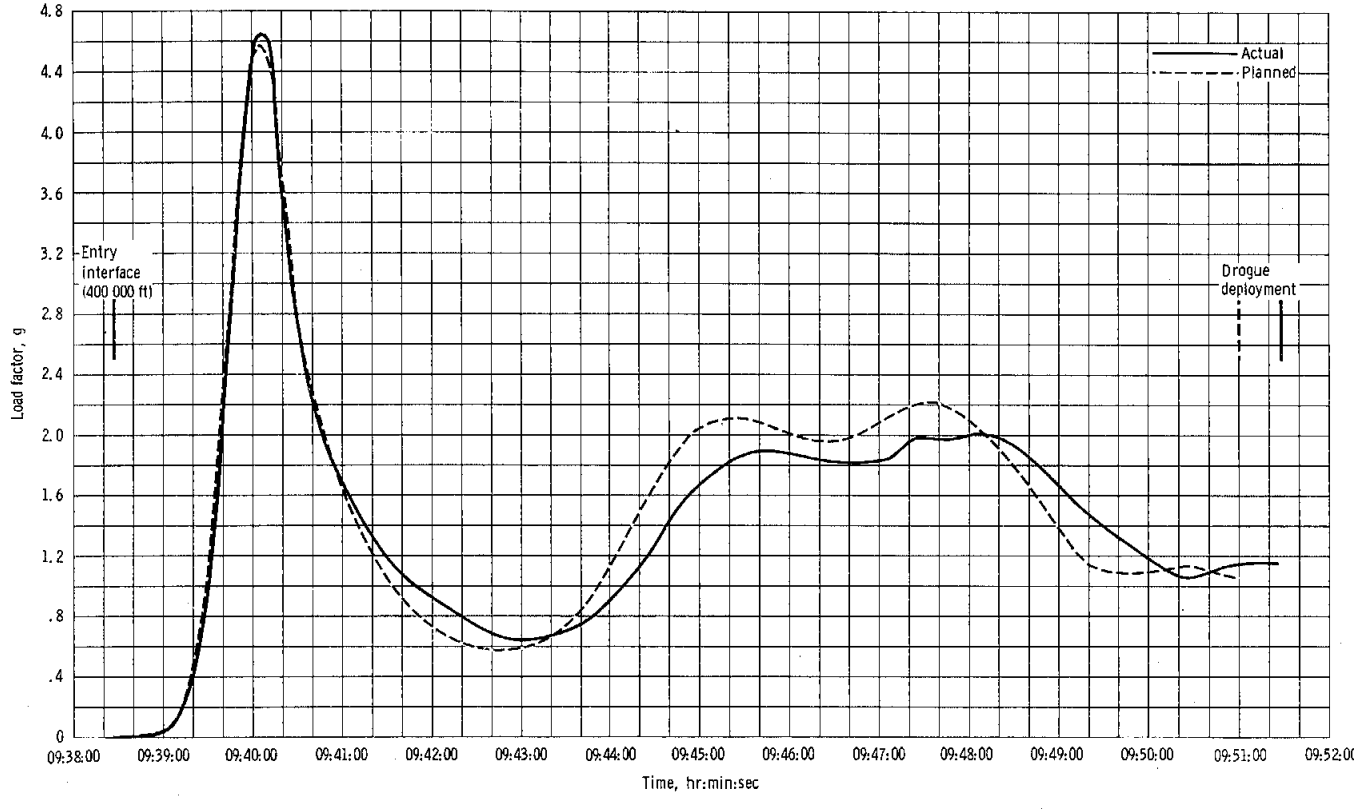

(d) Load factor.

Figure 3-7. - Concluded.

4.0 LAUNCH VEHICLE PERFORMANCE

Lift-off of the launch vehicle was near nominal and within predicted limits. A yaw bias was accomplished as programmed and tower clearance was maintained. The maximum angle of attack was 3.0 degrees. The maximum bending moment occurred at 00:01:06.5 and was considerably below the design bending moment. The longitudinal structural response peaked at about 00:02:06, when the first longitudinal mode frequency became coincident with 5.3-Hz thrust oscillations. The thrust oscillations showed a general increase from 00:01:40 to 00:02:00 with all engines appearing to be in phase. The amplitude of the structural response diminished after 00:02:06, but was still present at S-IC/S-II separation.

The second stage (S-II) propulsion system remained within nominal limits during the S-IC boost phase, S-II ignition, and through the early portion of the firing. Engine 2 prematurely shut down at 00:06:52.9 and engine 3 subsequently shut down at 00:06:54.2 because of electrical crosswiring. The cutoff signal to the remaining engines (1, 4, and 5) occurred approximately 58.5 seconds later than predicted based upon nominal operation of all engines. The S-II hydraulic system performance was nominal until approximately 00:04:43 when deviations in the engine 2 yaw and pitch actuators were noted.

The flight program performed nominally until loss of S-II engines 2 and 3, when the program shifted to the guidance logic for a single-engine failure (a two-engines-out mode had not been programmed).

The third stage (S-IVB) propulsion system remained within nominal limits during the S-IC stage and S-II powered flight and for approximately 100 seconds of the S-IVB firing; however, the S-IVB scheduled restart during parking orbit could not be achieved.

A pronounced transient in many vehicle measurements was seen at approximately 00:02:13. The transient was observed on most of the instrument unit accelerometers and a current peak was observed in the 6D11 battery bus. A small current increase was noted on the S-IVB aft battery 2 and some S-IVB accelerometer data contained this transient as well as two S-IVB forward skirt strain gages.

Overall ground and airborne camera coverage was good; approximately 92 percent of the film data was usable. Three of the four onboard S-IC cameras failed to eject and only one of the two S-II cameras was recovered. The two onboard television cameras provided good data.

A detailed description of the launch vehicle performance is contained in reference 2.

5.0 COMMAND AND SERVICE MODULE PERFORMANCE

5.1 SPACECRAFT STRUCTURE

5.1.1 Spacecraft Interface Loads

Of primary interest for the Apollo 6 mission were (1) demonstration of the structural compatibility of the command and service module (CSM), spacecraft/lunar module adapter, and launch vehicle in the Saturn V launch environment and (2) determination of launch loads.

A major anomaly occurred at 2 minutes 13 seconds after lift-off. This was apparent from large structural and electrical transients throughout the vehicle as well as photographs that reveal objects separating from the adapter area. This anomaly was preceded by unexplained measured load shifts in the LTA-2R and the S-IVB forward skirt and by large amplitude axial and pitch plane oscillations. This anomaly will be discussed in detail in Anomaly Report number 6 and is mentioned briefly in section 12.

Spacecraft structural loads have been evaluated for the critical load conditions that occurred during portions of the boost phase. The critical load conditions dictate the design of the spacecraft structure. The critical load portions of the boost phase were as follows.

a. Launch release

b. Maximum dynamic pressure region

c. End of first-stage boost

d. First-stage separation

e. Two engines out on S-II stage.

Structural loads have been determined for the following interfaces during the boost periods of concern.

a. Launch release

   (1) Launch escape system/command module

   (2) Command module/service module

   (3) Lunar module/adapter.

b. Maximum dynamic pressure region (max q)

(1) Launch escape system/command module

(2) Command module/service module

(3) Service module/adapter

(4) Adapter/lunar module

(5) Adapter/instrument unit.

c. End of first-stage (S-IC) boost

(1) Launch escape system/command module

(2) Command module/service module

(3) Service module/adapter

(4) Adapter/lunar module

(5) Adapter/instrument unit.

d. First-stage separation — Torsional loads at command module/service module interface

e. Two engines out on S-II stage

(1) Command module/service module

(2) Service module/adapter

(3) Adapter/instrument unit

All spacecraft structural loads were based on aerodynamic data and accelerations measured at the locations shown in figure 5.1-1.

5.1.2 Mission Phase Loads

Lift-off.- Normally, spacecraft lateral loads before launch release result from steady-state winds, gusts, vortex shedding, and S-IC unsymmetric thrust buildup. These external forces also cause a large constraining moment and shear at the base of the launch vehicle. Spacecraft lateral loads immediately after lift-off are caused primarily by sudden release of this constraining moment and shear.

Only moderate ground winds and gusts were measured before S-IC ignition. The average steady-state wind at the 60-foot level was 10.5 knots with an average peak of 18.1 knots. No vehicle responses could be attributed to vortex shedding; however, vortex shedding was not expected at the measured ground wind velocities. The spacecraft lateral loads and accelerations before and after launch release were of about the same magnitude, although the sources of excitation were different. Lateral accelerations measured in the spacecraft before launch release were caused primarily by the unsymmetric thrust buildup of the S-IC engines (fig. 5.1-2). Spacecraft accelerations during launch are shown in figure 5.1-3. Except for the anomaly, the maximum torsion at the command module/service module interface was excited during launch release. Torsional loads were also of about the same magnitude before and after launch release. Launch escape system/command module and command module/service module interface loads are compared to design limit loads in table 5.1-I. All launch release load conditions were compared with design loads and had factors of safety greater than the design factor of safety.

Maximum dynamic pressure region.- Large spacecraft interface loads normally occur in the region of flight where the product of dynamic pressure and angle of attack are maximum (max $q\alpha$). ←

The shears and magnitude of the winds aloft were moderate in the region of maximum dynamic pressure (fig. 5.1-4). The maximum angle of attack measured by the q-ball during the max q region of flight was 3.0 degrees. However, a 2.5-Hz lateral oscillation was recorded throughout the first-stage flight and added significantly to the calculated lateral loads in the spacecraft. Although the 2.5-Hz oscillation is included in the design analysis, the magnitude of this oscillation had not been included in any analysis for spacecraft design loads.

The spacecraft loads presented in table 5.1-II were derived by three methods:

a. Predicted loads from a Marshall Space Flight Center preflight trajectory simulation based on lift-off winds (used for the go/no-go determination)

b. Predicted loads from a Manned Spacecraft Center trajectory simulation based on winds of lift-off

c. Calculated loads based on measured aerodynamic and acceleration data.

Values obtained by these three methods were compared with the max $q\alpha$ design loads (table 5.1-II). The predicted and calculated loads compared

favorably and were well below the design values. The 2.5-Hz lateral oscillation caused a difference between the predicted and calculated loads. The command module/service module, service module/adapter, adapter/lunar module, and adapter/instrument unit interface loads were also compared with the structural capability of each interface (figs. 5.1-5 through 5.1-8). The typical 2.5-Hz lateral acceleration is shown by the tower Z-axis accelerometer in figure 5.1-9.

Command and service module axial and lateral accelerations of approximately 5 Hz were measured from 00:01:50 seconds through the remainder of first-stage boost. The greatest magnitude of axial oscillations occurred at 00:02:05 seconds. Oscillations of this magnitude were not considered in the prediction of design loads and caused increased loads in the command and service module during boost. The accelerations for this period of the flight are shown in figure 5.1-10.

End of first-stage boost.- The maximum axial acceleration and compression loads in the spacecraft are normally experienced immediately prior to inboard engine cutoff. The 2-Hz lateral acceleration of the command and service module and the 5-Hz axial acceleration were both present at the end of first-stage boost. These effects had not been included in the analysis for the determination of the design loads. The bending moment at the command module/service module interface was lower than the value used for design. Interface loads at the end of first-stage boost are shown in table 5.1-III, and spacecraft accelerations are shown in figure 5.1-11.

Staging.- S-IC/S-II staging causes maximum tension and minimum acceleration for the command and service module design. The maximum torsion calculated was 75 000 in-lb and was well below the torsional capability of the interface. The accelerations during staging are shown in figure 5.1-11.

S-II stage operation.- The only significant spacecraft loading experienced while the S-II stage was firing occurred at 00:07:41 (at which time two adjacent S-II engines were out). The resulting command and service module loads were small and are shown on the spacecraft capability curves (figs. 5.1-5 through 5.1-8) and in table 5.1-IV.

S-IVB stage operation.- There are no design conditions for the S-IVB stage boost phase. However, telemetered data indicated that all command and service module acceleration levels were at a minimum during the S-IVB stage operation, and no significant command and service module loads were experienced.

5.1.3 Internal Loads

The three command module tension ties were instrumented with strain gages (fig. 5.1-12) to measure the forces in the axial direction of the tension tie. The data indicated a 5-Hz oscillation throughout first-stage boost. The forces obtained during significant launch phases are shown in the following table.

Phase	Beam 2, lb	Beam 4, lb	Beam 6, lb
Pre-ignition	9 000	8 300	11 500
Lift-off	13 500	12 300	13 900
Max qα (00:01:12)	3 000	1 400	7 800
End of first-stage boost	0	0	6 100
Staging (S-IC/S-II)	11 600	12 300	16 300

Peak loads occurred, as expected, during the launch phase and again during S-IC/S-II staging. These loads were well within the 40 000 pounds allowable for the structure.

The adapter was instrumented with 16 strain gages (fig. 5.1-13) to obtain launch loads. Two of these gages were inoperative prior to launch. Strains measured during the boost phase were converted to stresses and are presented in table 5.1-V, for lift-off and maximum qα. The 14 adapter strain measurements became inoperative because of a commutator malfunction at about 00:01:29. All 14 were recovered for approximately 3 seconds at 00:02:10. Four continued to provide data for an additional 17 seconds (00:02:13 to 00:02:30). Therefore, no stresses were available after that time. All stresses were well within the allowable stress levels during the period of good data.

5.1.4 Low-Frequency Vibrations

Low-frequency vibrations of significant magnitude were observed during most of the first-stage launch phase. During launch release, the longitudinal and lateral oscillations occurred from lift-off minus 3 seconds to approximately lift-off plus 3 seconds (fig. 5.1-3). These oscillations contained frequencies of 2.5, 4.5, and 12.0 Hz. A tabulation of

the peak values which occurred in the 2.5, 4.5, and 12.0 Hz frequencies during launch release is presented in table 5.1-VI. The values in table 5.1-VI were derived from a combination of oscillographs and power spectral density analyses. The effects of accelerations on structural loads are evaluated for all launch phases in section 5.1.1.

Longitudinal oscillations at approximately 5 Hz were predominant in the command module during all phases of first-stage boost and during the first few seconds of second-stage boost. This oscillation is shown in figure 5.1-10. The actual frequency at launch release was 4.5 Hz which corresponds with the second longitudinal mode of the Saturn V vehicle at launch-release weights. The 2.5-Hz oscillation is the second lateral bending mode, and its effects are discussed in the mission loads section.

At approximately 00:01:50, a significant 5-Hz axial and lateral oscillation began in the spacecraft (fig. 5.1-10). This oscillation is discussed briefly in section 12.0 and in detail in Anomaly Report number 6.

At first-stage inboard engine cutoff, the only significant oscillation was the axial response of the command module (fig. 5.1-11) resulting from engine thrust decay. The value of the oscillation is given in table 5.1-VI. Oscillations from first-stage outboard engine cutoff are shown in figure 5.1-11). After separation, 5.7-Hz oscillations continued for approximately 3 seconds after engine cutoff. The peak values are given in table 5.1-VI. There were no significant low-frequency vibrations subsequent to those discussed.

5.1.5 Command and Service Module

Vibration and Acoustics

Table 5.1-VII lists the vibration measurements and their locations on the Apollo 6 command and service module (CSM). The table also presents ranges and frequency response of each vibration measurement.

Power spectral density analyses of all vibration measurements were performed on time slices from lift-off minus 7.0 to minus 5.0 seconds in order to establish instrumentation system noise. Data from all instrumentation showed energy concentrations in the vicinity of 30 Hz and 90 Hz prior to engine ignition. Oscillograph records from all CSM vibration data channels show oscillations at a frequency of approximately 90 Hz. These oscillations were apparent on tape-recorded data channels and on the tape-recorded time code. Postflight bench tests performed on the tape recorder showed high-noise levels on all channels at approximately

90 Hz. Based on the preceding, vibration and acoustic data in the vicinity of 30 Hz and 90 Hz are not considered valid and comparisons of measured vibrations to vibration criteria cannot be made at these frequencies.

A comparison of measured vibrations on the command module lower equipment bay bulkhead with the block I and block II criteria is shown on figure 5.1-14. The comparison shows the measured vibrations to be below the criteria and below the mission level (mission level = $\frac{\text{criteria level}}{(1.5)^2}$).

Figure 5.1-15 compares measured vibrations on the fuel cell aft bulkhead X axis and radial plane, at the base of the fuel cell, with block I and block II criteria and the mission level. At lift-off, the measured X axis vibration exceeded the mission level by an insignificant margin at a frequency of 112 Hz. Radial vibrations at frequencies above 1000 Hz exceeded the mission level at transonic Mach numbers and at maximum dynamic pressure. The fuel cell system was mounted on vibration isolators which attenuated the high-frequency vibration, and the fuel cells operated satisfactorily.

Data from the helium pressurization panel tangential measurement on the service module exhibited a poor signal-to-noise ratio throughout atmospheric flight as a result of the high amplitude range of the instrument (±500g). Data show a peak of $0.55g^2/Hz$ at 140 Hz, which is above the criteria by a significant margin. Power spectral density analysis of data from this measurement at times prior to first-stage engine ignition shows a maximum value of $0.04g^2/Hz$ at 140 Hz. Comparison of the power spectral density analysis taken prior to engine ignition with the transonic levels taken inflight are shown on figure 5.1-16 and show the data to be unusable below 150 Hz with the exception of the peak at 145 Hz. The peak at 145 Hz is considered valid. Qualification test amplitudes for the helium pressurization panel components will be compared to this peak for final evaluations.

The electrical power system radiator panel radial vibration measurement was slightly overdriven between 00:00:58 and 00:01:00. Data from this measurement exceeded mission levels. The peaks are within 1.5 dB of the mission level and below the criteria.

The root mean square time histories of command module internal sound pressure levels are presented in figure 5.1-17. The measured sound pressure levels were well below CSM systems criteria.

All vibration measurements showed a change in character beginning at approximately 00:01:28 at which time all PCM and onboard-recorded vibration data became erratic, as discussed in section 12. Therefore, no analysis of vibrations after 00:01:28 can be made.

TABLE 5.1-I.- LATERAL LOADS AT LIFT-OFF

Interface	Condition	Lift-off	Design limit load[a]
Launch escape system/ command module	Bending moment, in-lb Axial force, lb	840 000 [b]-11 100	2 380 000 [b]-11 000
Command module/ service module	Bending moment, in-lb Axial force, lb Torsion, in-lb	880 000 [b]-26 700 185 000	3 150 000 [b]-27 000 [c]118 000
Adapter/ lunar module	Bending moment, in-lb Axial force, lb	7 140 000 [b]-114 800	26 000 000 [b]-124 500

[a]Design limit load is defined as the maximum predicted load for this condition and is normally less than the capability of the structure.

[b]Negative sign indicates compression.

[c]Torsion capability exceeds 300 000 in-lb.

TABLE 5.1-II.- SPACECRAFT LOADS AT MAXIMUM qα

Interface	Condition	Predicted from MSFC simulation using lift-off winds	Predicted from MSC simulation using lift-off winds	Calculated from flight data	Design[a]
	Flight time, sec	68	68.7	68	69.6
	Mach no.	1.31	1.33	1.3	1.3
	Dynamic pressure, psf	734	755	741	713
	Angle of attack, deg	3.40	2.9	3.0	9.0
	Max qα, psf-deg	2590	2189	2223	6417.0
Launch escape system/ command module	Bending moment, in-lb	330 000	380 000	496 000	1 100 000
	Axial force, lb	[b]-21 000	[b]-18 000	[b]-21 300	[b]-29 200
Command module/ service module	Bending moment, in-lb	690 000	620 000	900 000	2 100 000
	Axial force, lb	[b]-88 000	[b]-82 800	[b]-90 500	[b]-90 600
Service module/ adapter	Bending moment, in-lb	2 300 000	2 480 000	2 260 000	11 000 000
	Axial force, lb	[b]-170 000	[b]-168 200	[b]-179 000	[b]-193 000
Adapter/ lunar module	Bending moment, in-lb	--	6 160 000	4 850 000	24 682 000
	Axial force, lb	--	[b]-248 600	[b]-255 700	[b]-278 400
Adapter/ instru-ment unit	Bending moment, in-lb	8 000 000	8 340 000	6 000 000	26 000 000
	Axial force, lb	[b]-250 000	[b]-257 600	[b]-268 000	[b]-272 000

[a]Derived from preliminary postflight trajectory data.

[b]Negative sign indicates compression.

TABLE 5.1-III.- MAXIMUM SPACECRAFT LOADS

AT END OF FIRST-STAGE BOOST

Interface	Condition	Calculated from flight	Design limit load[a]
	Axial acceleration, g	4.9	4.9
Launch escape system/command module	Bending moment, in-lb	140 000	182 000
	Axial force, lb	[b]-44 400	[b]-44 000
Command module/ service module	Bending moment, in-lb	355 000	550 000
	Axial force, lb	[b]-105 000	[b]-97 600
Service module/ adapter	Bending moment, in-lb	2 035 000	3 000 000
	Axial force, lb	[b]-312 000	[b]-332 000
Adapter/lunar module	Bending moment, in-lb	2 129 000	5 008 000
	Axial force, lb	-459 000	-518 000
Adapter/instrument unit	Bending moment, in-lb	2 159 000	4 700 000
	Axial force, lb	[b]-462 000	[b]-482 000

[a]Same as on page 8.

[b]Negative sign indicates compression.

TABLE 5.1-IV.- SPACECRAFT LOADS AT S-II TWO ENGINE OUT

Interface	Condition	Predicted from MSC simulation
Command module/ service module	Bending moment, in-lb	153 000
	Axial force, lb	[a]-13 900
Service module/ adapter	Bending moment, in-lb	1 646 000
	Axial force, lb	[a]-61 200
Adapter/instrument unit	Bending moment, in-lb	7 130 000
	Axial force, lb	[a]-94 300

[a]Negative sign indicates compression.

TABLE 5.1-V.- SPACECRAFT/LUNAR MODULE ADAPTER

STRAIN GAGE MEASUREMENTS

Gage location	Lift-off, psi	Max qα, psi
Outer shell, longitudinal, 34 deg	(a)	(a)
Outer shell, circumferential, 34 deg	(a)	(a)
Inner shell, longitudinal, 34 deg	-1630	-5000
Inner shell, circumferential, 34 deg	+760	-550
Outer shell, longitudinal, 124 deg	(a)	(a)
Outer shell, circumferential, 124 deg	(a)	(a)
Inner shell, longitudinal, 124 deg	-2000	-5840
Inner shell, circumferential, 124 deg	+350	-170
Outer shell, longitudinal, 214 deg	-1810	-4680
Outer shell, circumferential, 214 deg	-1490	-2980
Inner shell, longitudinal, 214 deg	-380	-4080
Inner shell, circumferential, 214 deg	+810	-280
Outer shell, longitudinal, 304 deg	-2710	-4550
Outer shell, circumferential, 304 deg	-290	-1150
Inner shell, longitudinal, 304 deg	-2530	-3810
Inner shell, circumferential, 304 deg	-1070	-2200

[a]Stresses cannot be determined because of loss of longitudinal strain measurements AA8120S and AA8124S.

TABLE 5.1-VI.- MAXIMUM VALUES OF LAUNCH ESCAPE SYSTEM AND COMMAND MODULE

LOW-FREQUENCY VIBRATION DURING FIRST-STAGE BOOST

	Lift-off		Mid-boost[a]		Inboard engine cutoff		Outboard engine cutoff	
	Frequency, Hz	Amplitude, g	Frequency, Hz	Amplitude, g	Frequency, Hz	Amplitude, g	Frequency, Hz	Amplitude, g
Launch escape system								
Axial	2.5	±0.6	2.5	0.25	9.0	±0.2	1.2	±0.25
Lateral	12.0	±0.2					9.0	±0.5
Command module								
Lateral	2.5	±0.1	not significant		not significant		5.0	±0.15
Command module								
Axial	4.5	±0.35	not significant		5.7	±0.35	5.7	0.7

[a]Mid-boost is the time period from approximately 00:00:50 to 00:01:40.

TABLE 5.1-VII.- CSM VIBRATION AND SOUND MEASUREMENTS

Number	Title	Channel number/ IRIG number	Response, Hz	Range, g
CA2530D	Y axis, lower equipment bay kick ring	FR5/Direct	0 to 2500	±50
CA2531D	Z axis, lower equipment bay kick ring	FR6/Direct	0 to 2500	±50
CA2532D	X axis, honeycomb, bulkhead	FR2/15	0 to 450	±50
CA2533D	Z axis, honeycomb, bulkhead	FR2/16	0 to 600	±50
CK0032Y	Sound, command module interior	FR13/Direct	0 to 2500	
SA2210D	X axis, aft bulkhead/fuel cell	FR11/Direct	0 to 2500	±75
SA2211D	Radial, aft bulkhead/fuel cell	FR12/Direct	0 to 2500	±75
SA2213D	Tangential, helium pressure panel	FR14/Direct	0 to 2500	±500
SA2214D	Y axis, oxygen tank mount	FR2/14	0 to 330	±20
SA2215D	Z axis, oxygen tank mount	FR7, 8/11	0 to 110	±20
SA2216D	Radial beam 4/shell	FR7, 8/12	0 to 160	±50
SA2218D	Radial, electrical power radiator panel	FR7,8/15	0 to 450	±75

NASA-S-68-3516

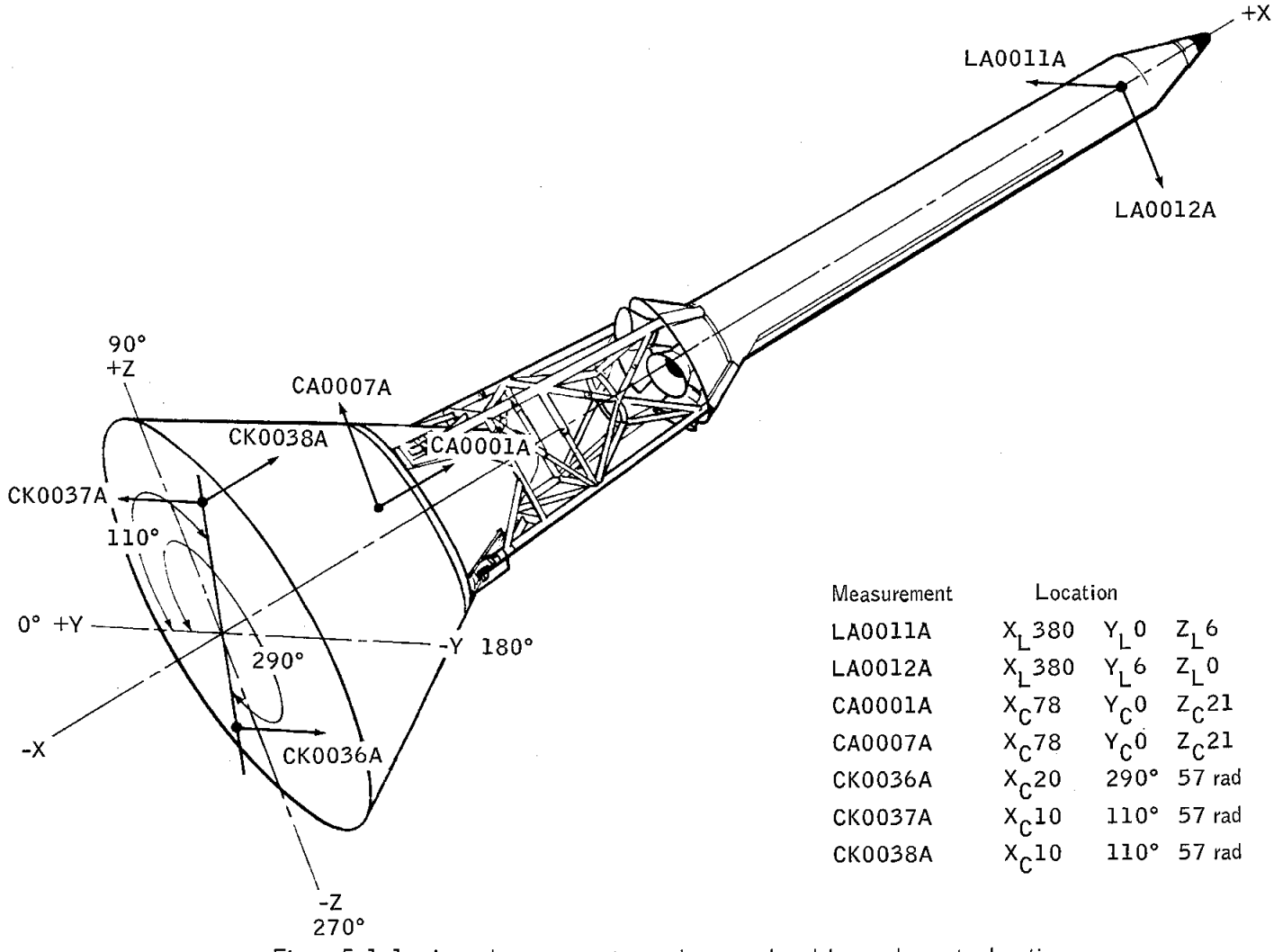

Measurement	Location		
LA0011A	X_L 380	Y_L 0	Z_L 6
LA0012A	X_L 380	Y_L 6	Z_L 0
CA0001A	X_C 78	Y_C 0	Z_C 21
CA0007A	X_C 78	Y_C 0	Z_C 21
CK0036A	X_C 20	290°	57 rad
CK0037A	X_C 10	110°	57 rad
CK0038A	X_C 10	110°	57 rad

Figure 5.1-1.- Launch escape system and command module accelerometer locations.

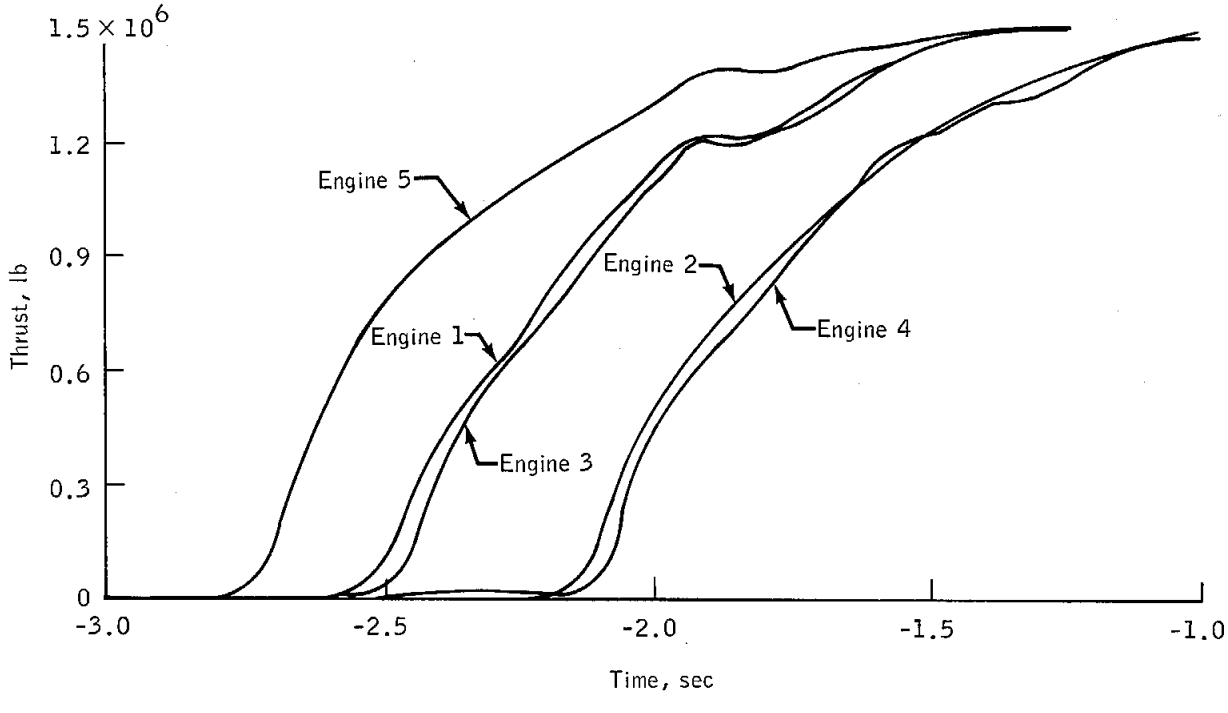

Figure 5.1-2.- S-IC thrust buildup.

NASA-S-68-3518

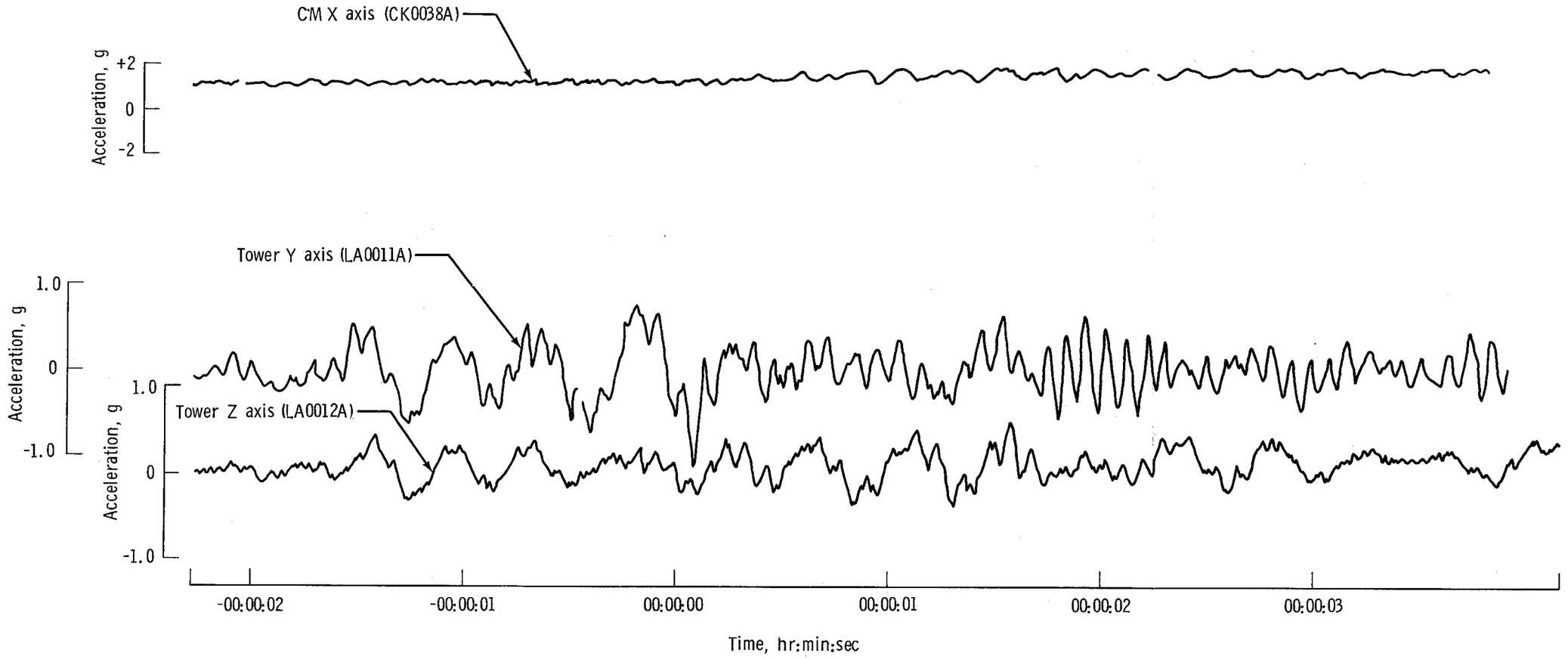

(a) Command module X axis, tower Y and Z axes.

Figure 5.1-3. - Spacecraft acceleration time histories during lift-off.

NASA-S-68-3519

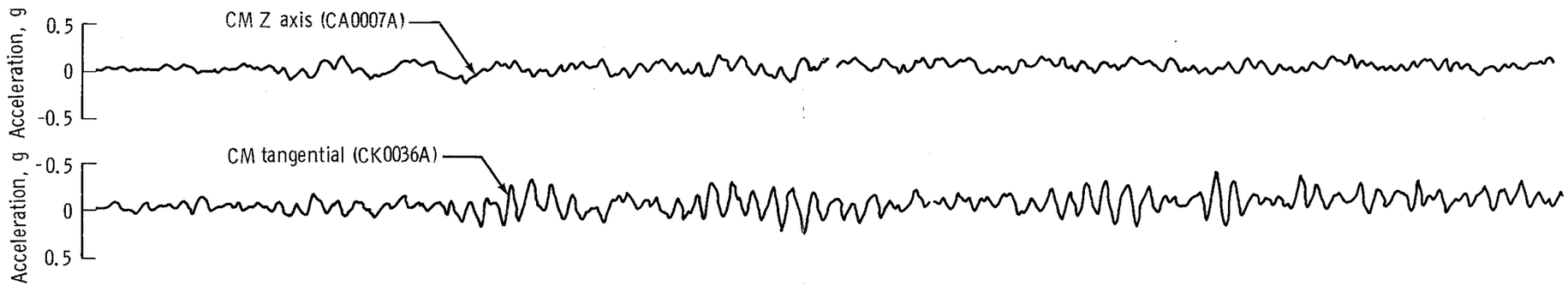

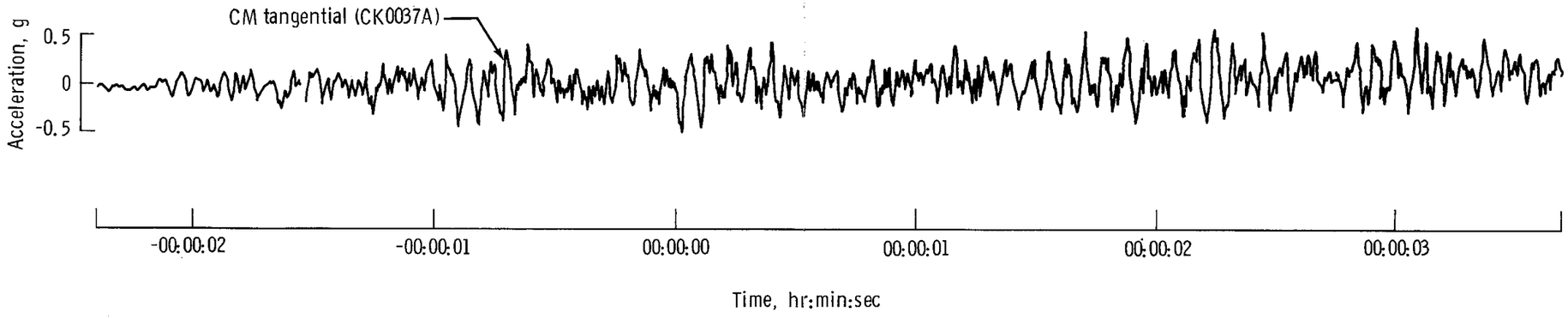

(b) Command module Z axis and tangential.

Figure 5.1-3. - Concluded.

NASA-S-68-3520

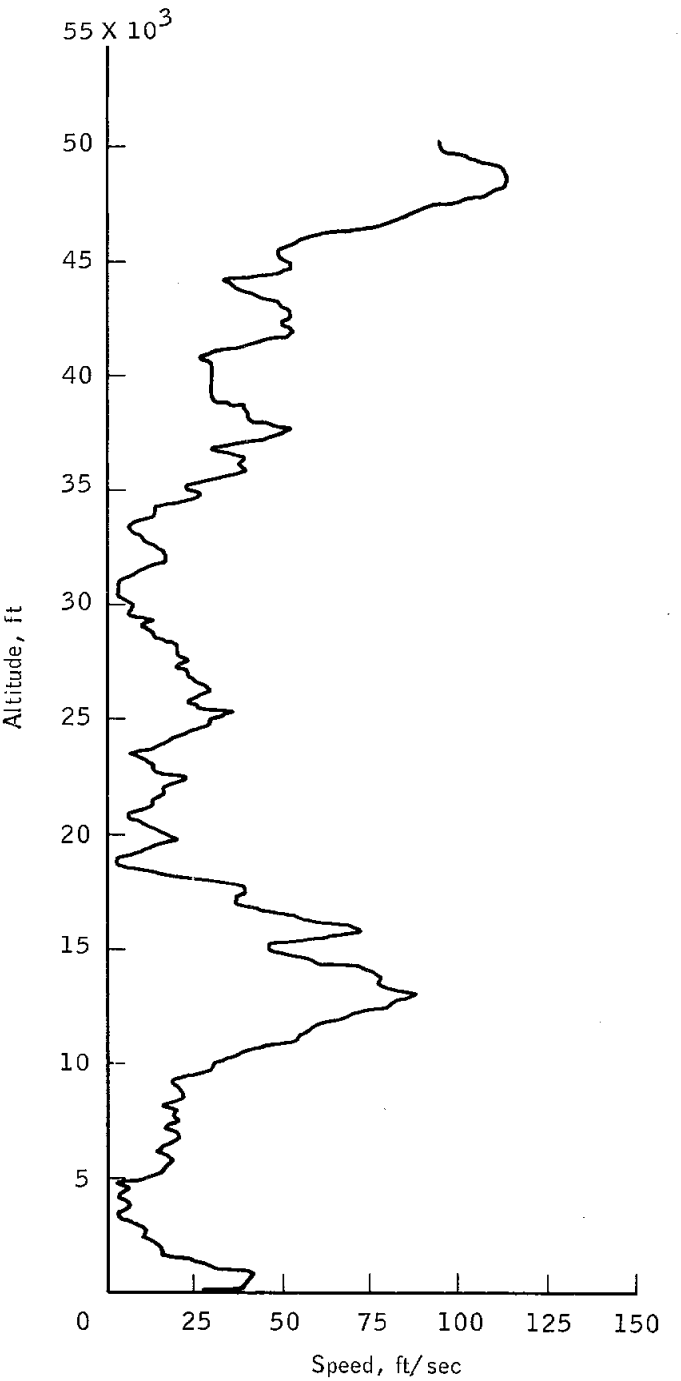

(a) Wind speed.

Figure 5.1-4.- Launch time scalar winds.

NASA-S-68-3521

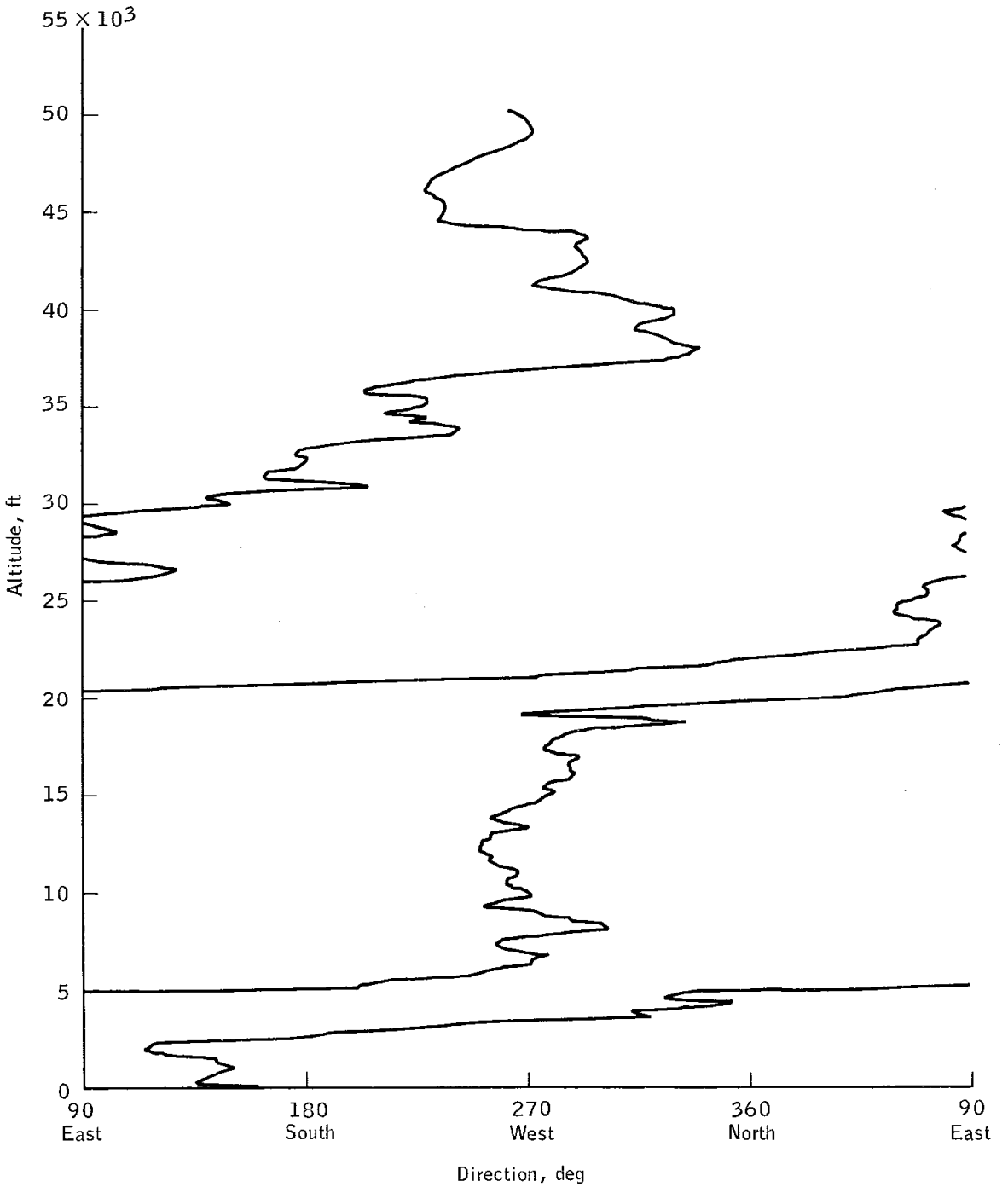

(b) Wind direction.

Figure 5.1-4.- Concluded.

NASA-S-68-3522

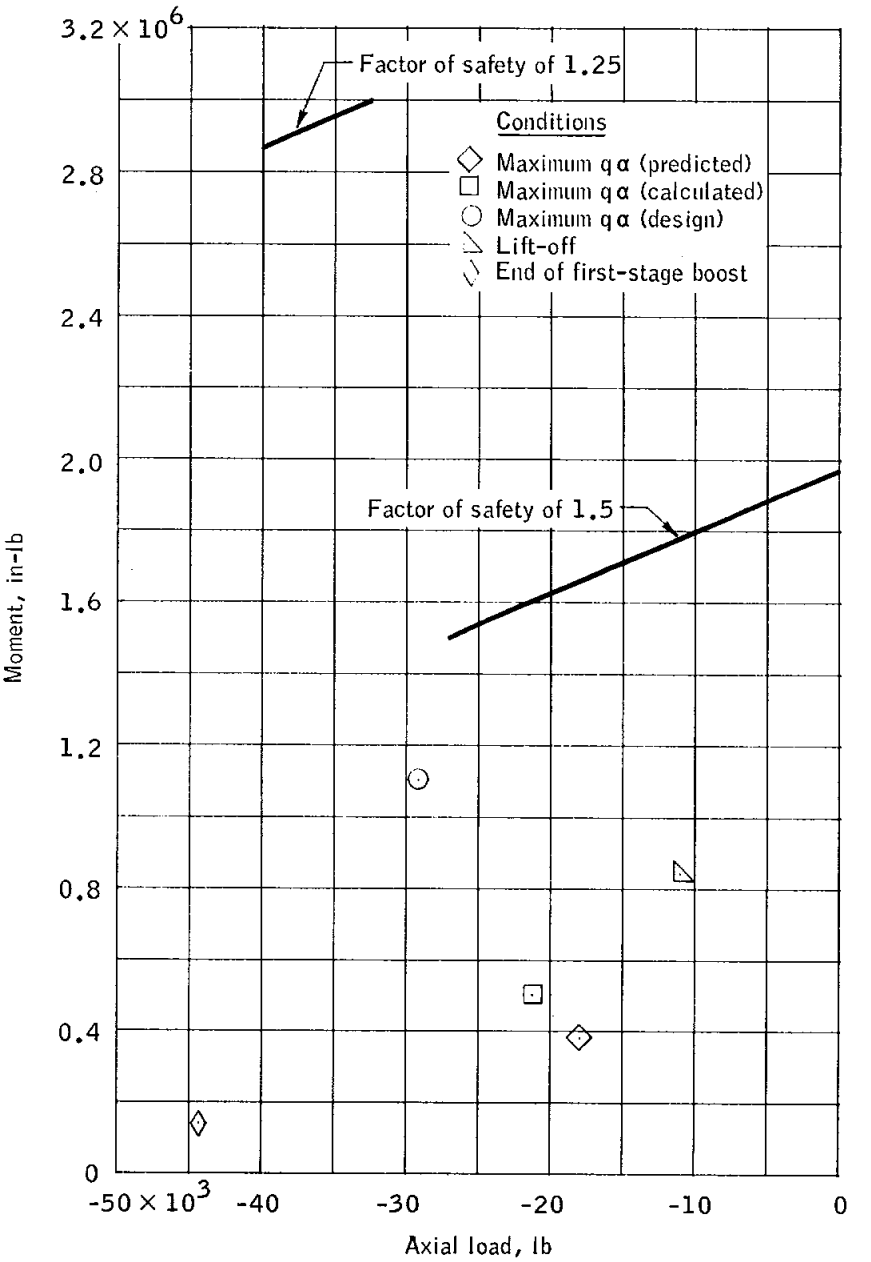

Figure 5.1-5.- Comparison of launch escape system/command module interface loads with structural capabilities.

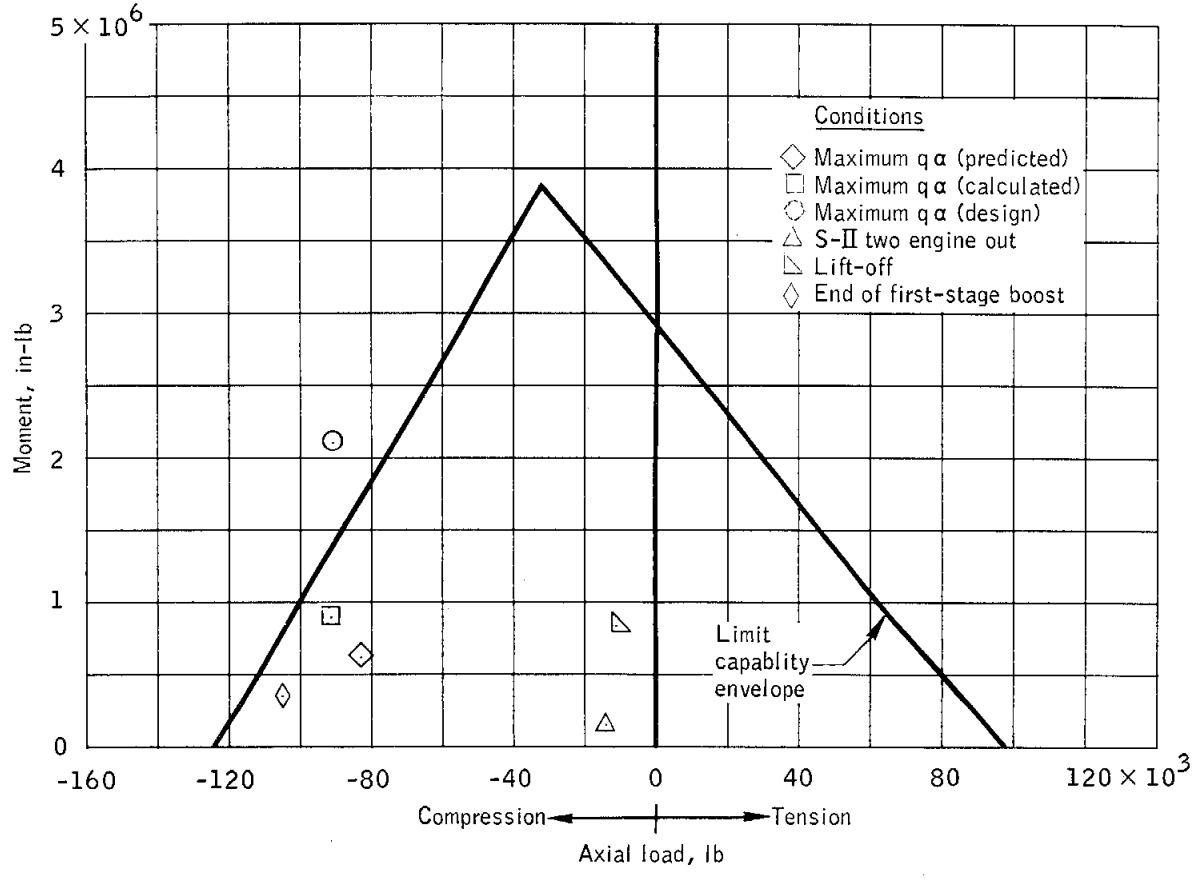

Figure 5.1-6.- Comparison of command module/service module interface loads with structural capabilities.

NASA-S-68-3524

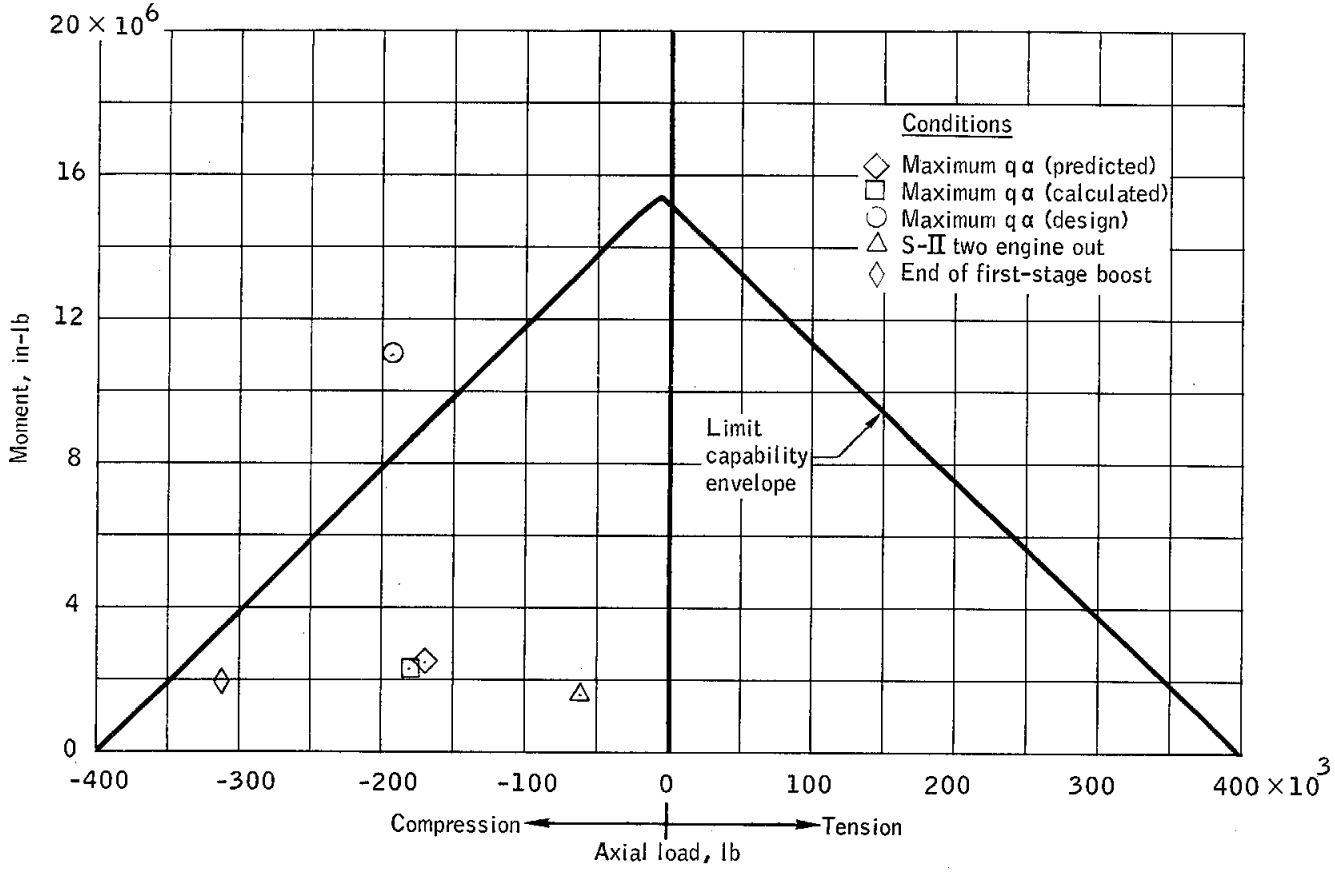

Figure 5.1-7.- Comparison of service module/spacecraft lunar module adapter interface loads with structural capabilities.

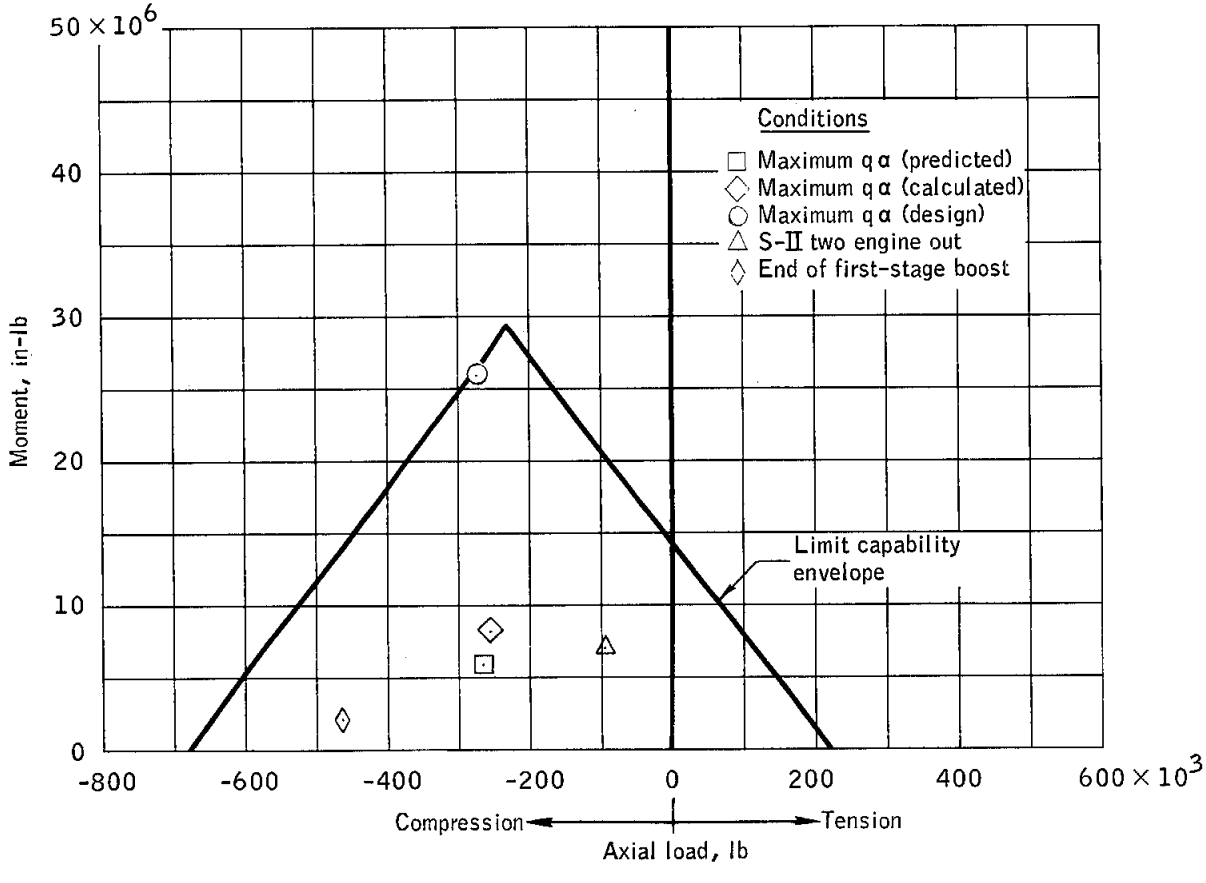

Figure 5.1-8.- Comparison of spacecraft lunar module adapter/instrument unit interface loads with structural capabilities.

NASA-S-68-3526

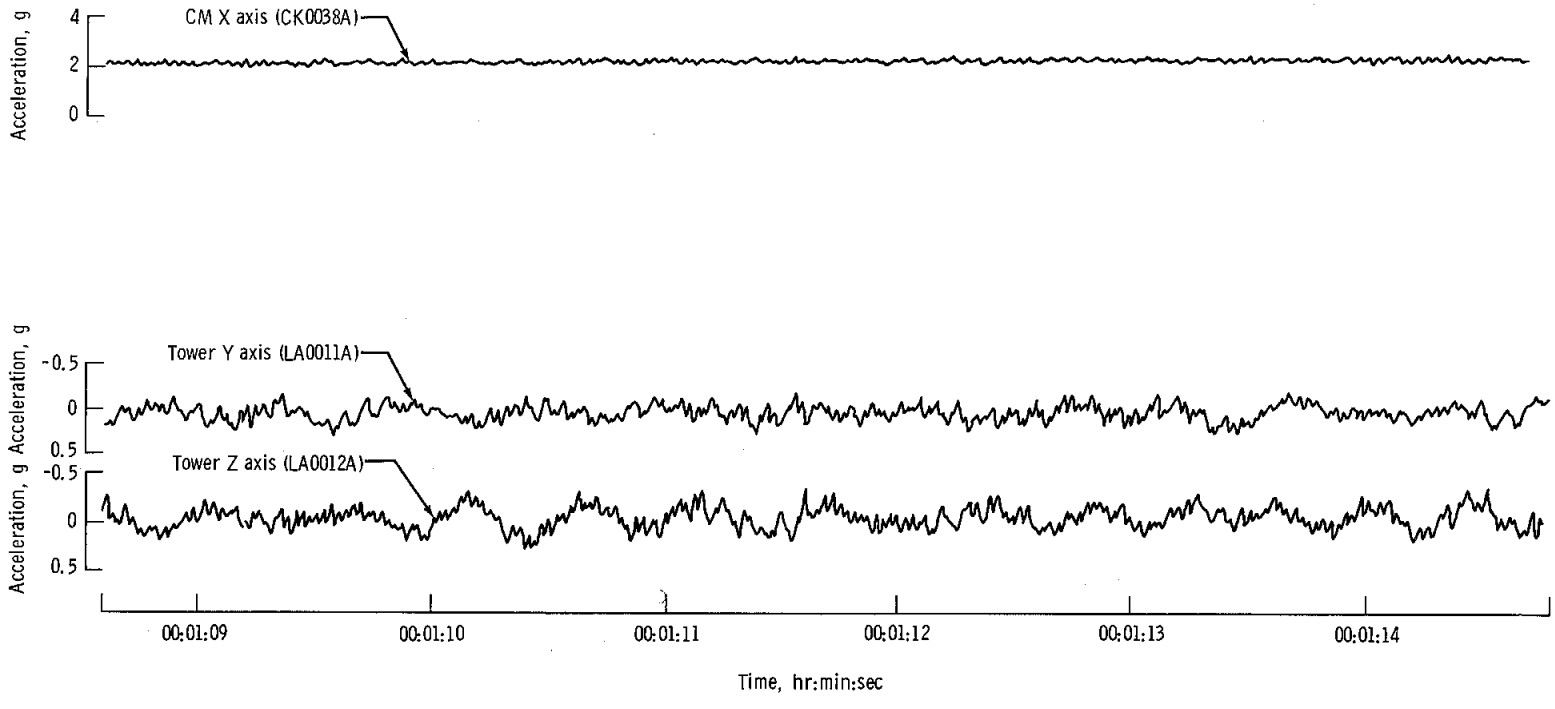

(a) Command module X axis and tower Y and Z axes.

Figure 5.1-9. - Spacecraft accelerations during maximum dynamic pressure region of flight.

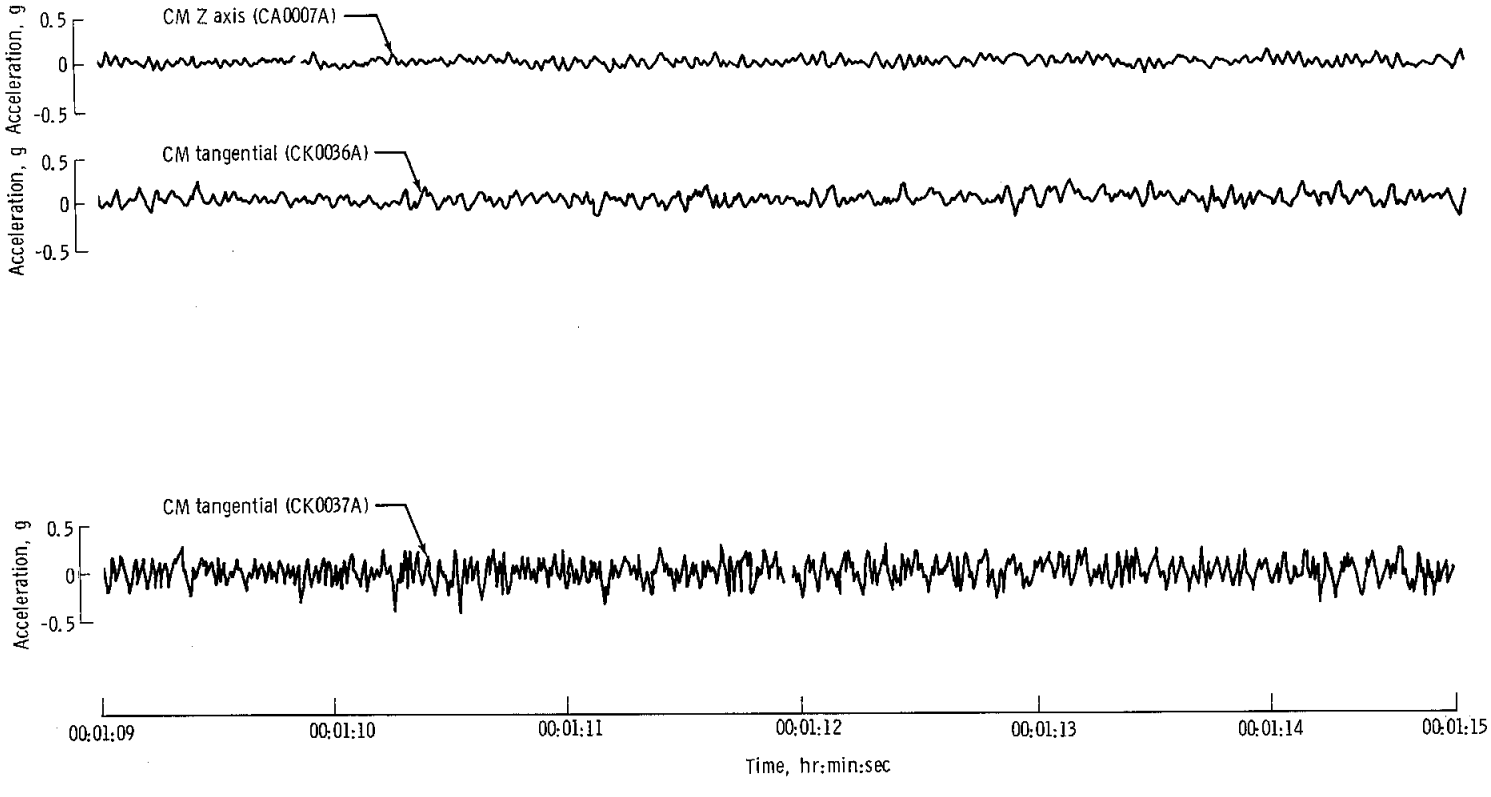

(b) Command module Z axis and tangential.

Figure 5.1-9. - Concluded.

NASA-S-68-3528

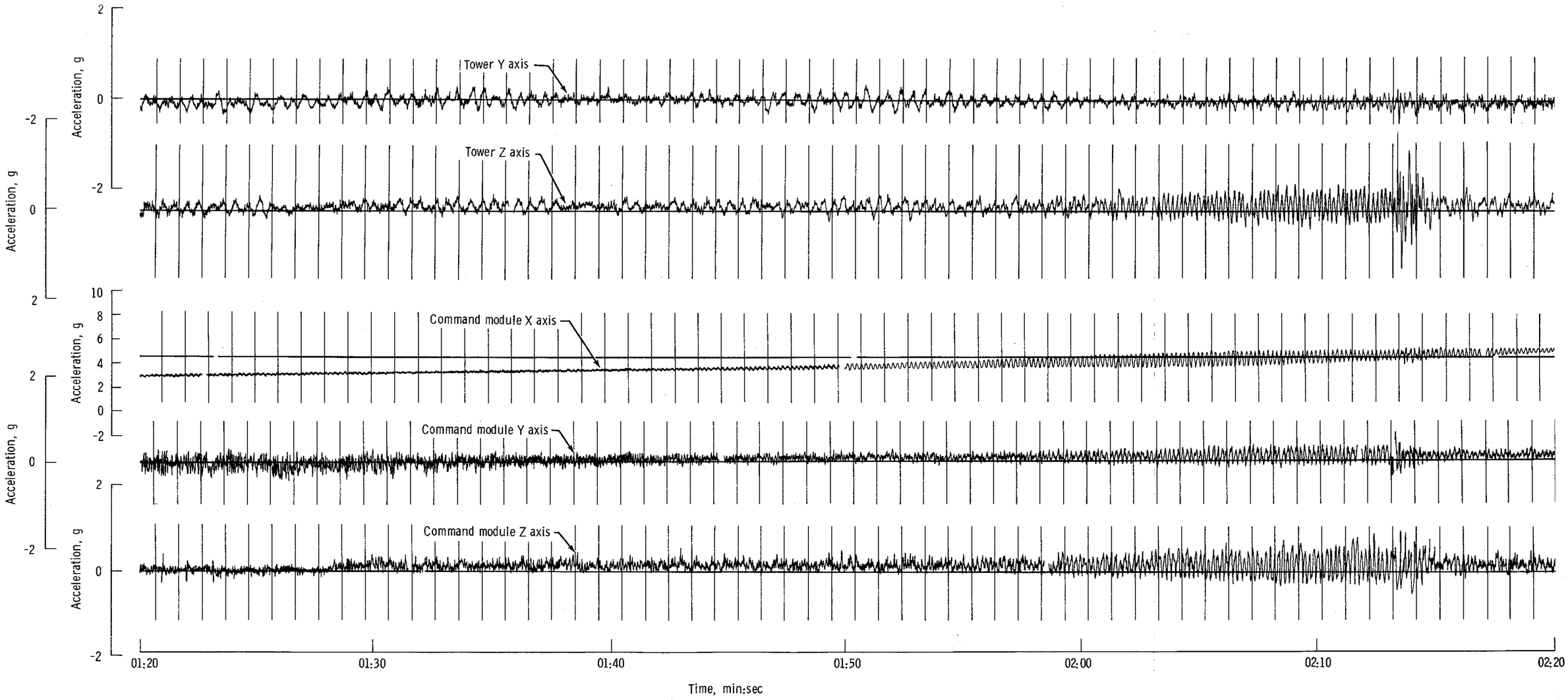

Figure 5.1-10. - Spacecraft accelerations during period of high axial acceleration.

NASA-S-68-3529

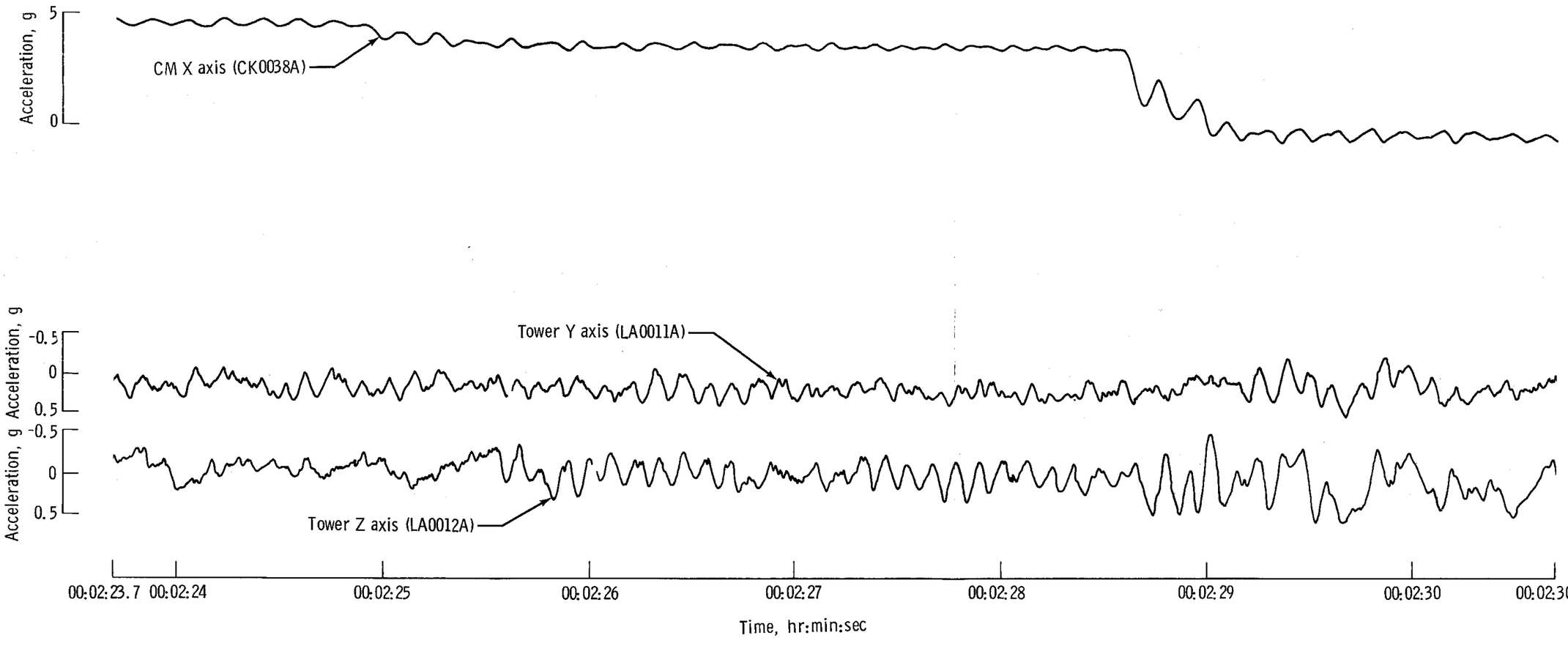

(a) Command module X axis, tower Y and Z axes.

Figure 5.1-11. - Spacecraft accelerations at end of first stage boost.

NASA-S-68-3530

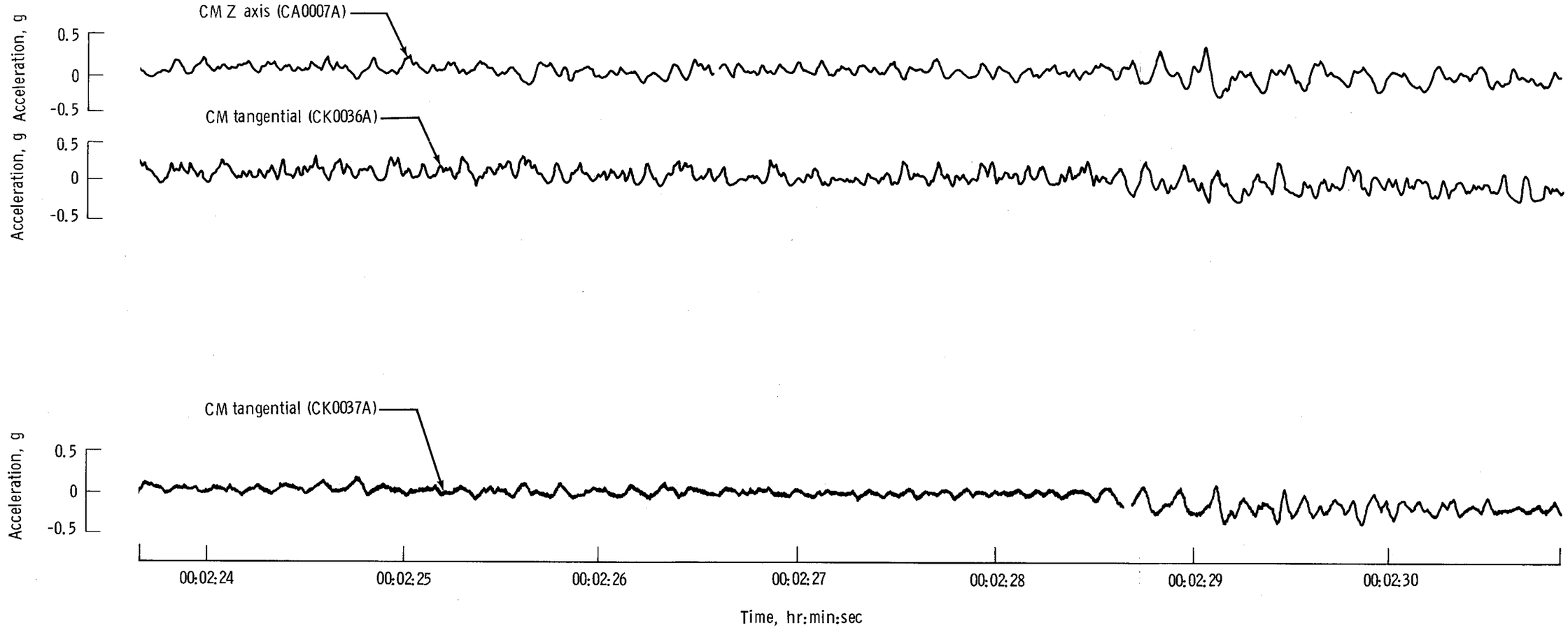

(b) Command module Z axis and tangential.

Figure 5.1-11. - Concluded.

NASA-S-68-3531

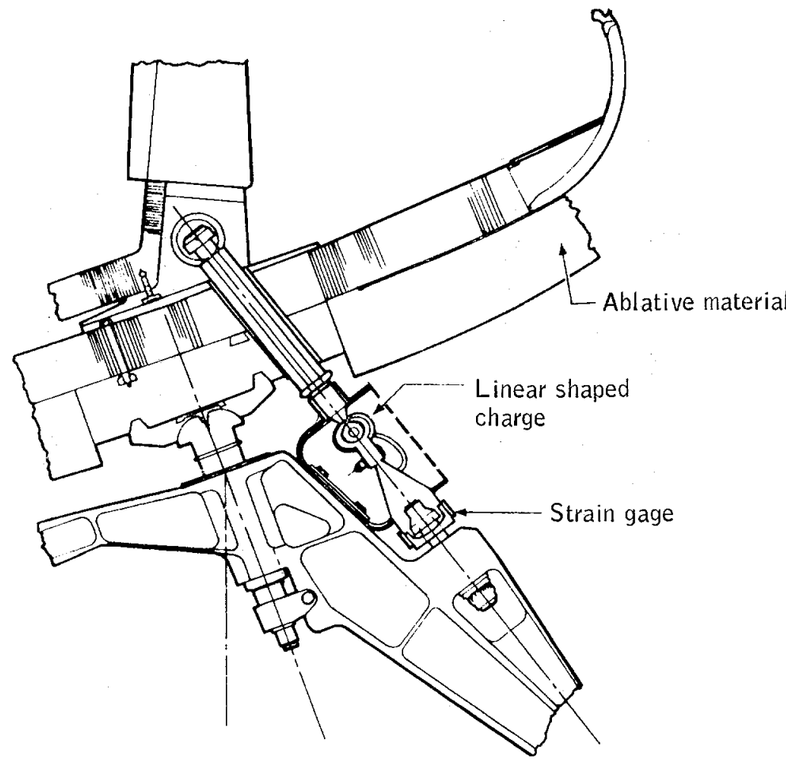

Figure 5.1-12.- Typical command module/service module tension tie strain gage location.

NASA-S-68-3532

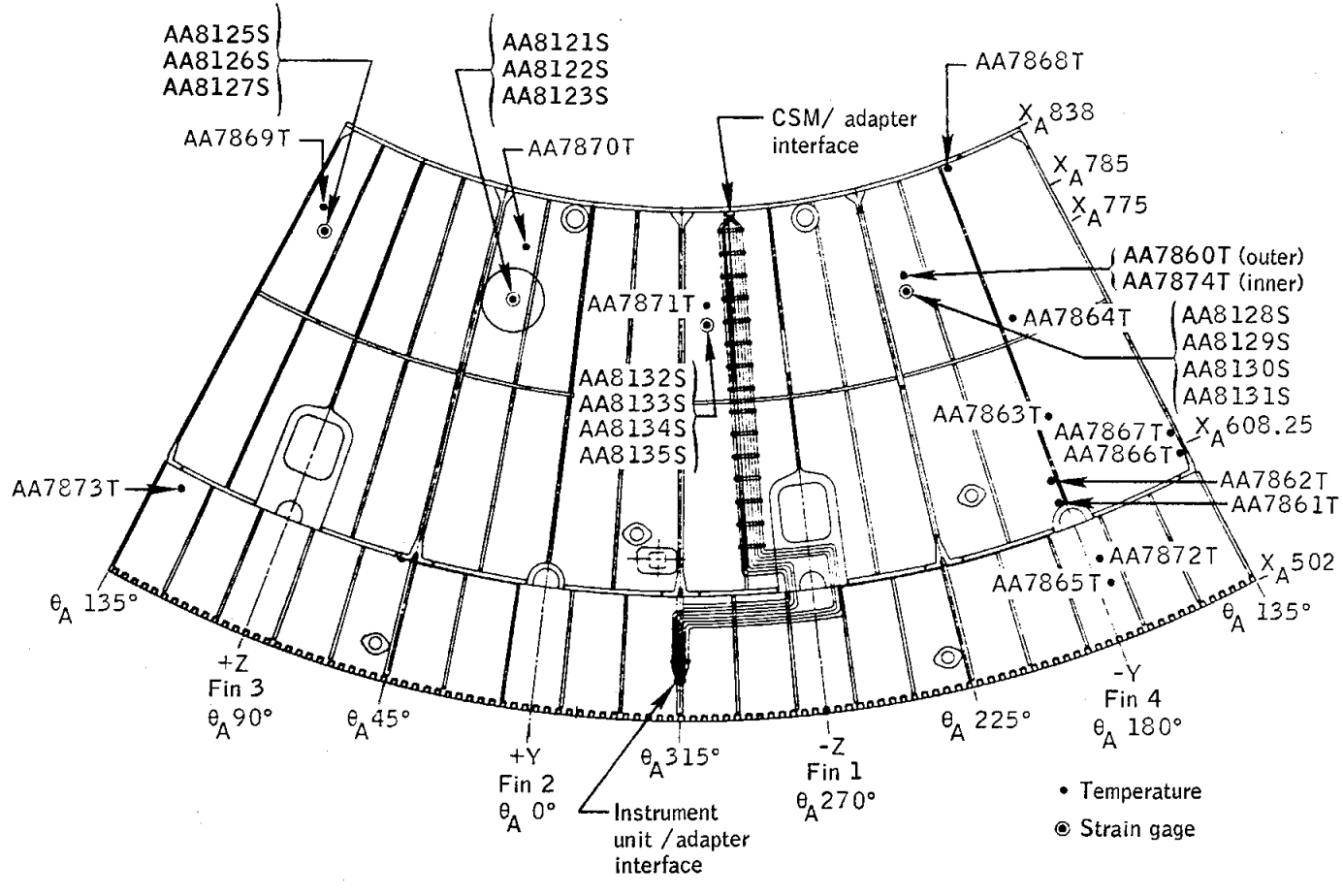

Figure 5.1-13.- Adapter structural measurement locations.

NASA-S-68-3533

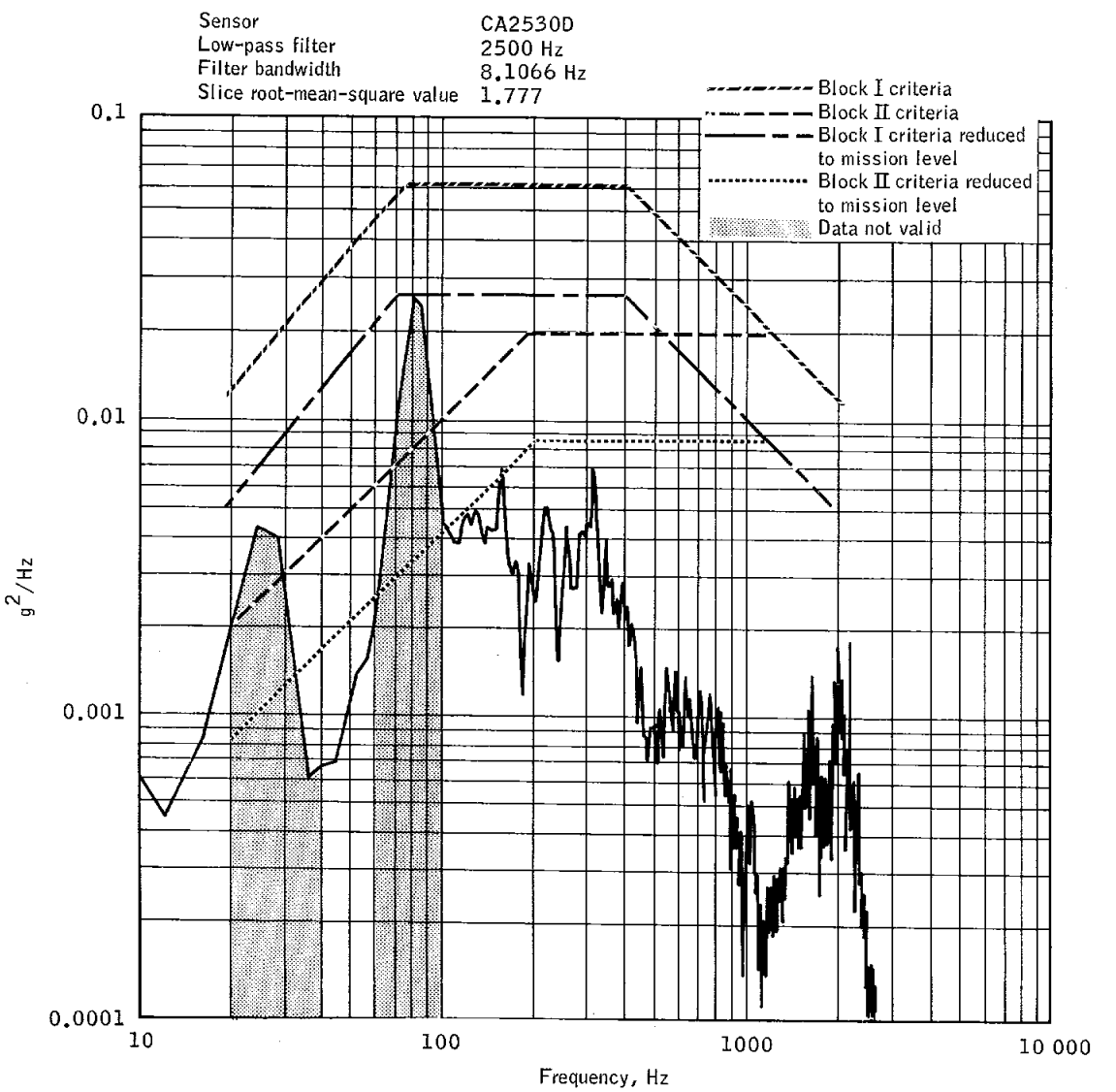

Figure 5.1-14.- Comparison of lower equipment bay vibration to criteria.

NASA-S-68-3534

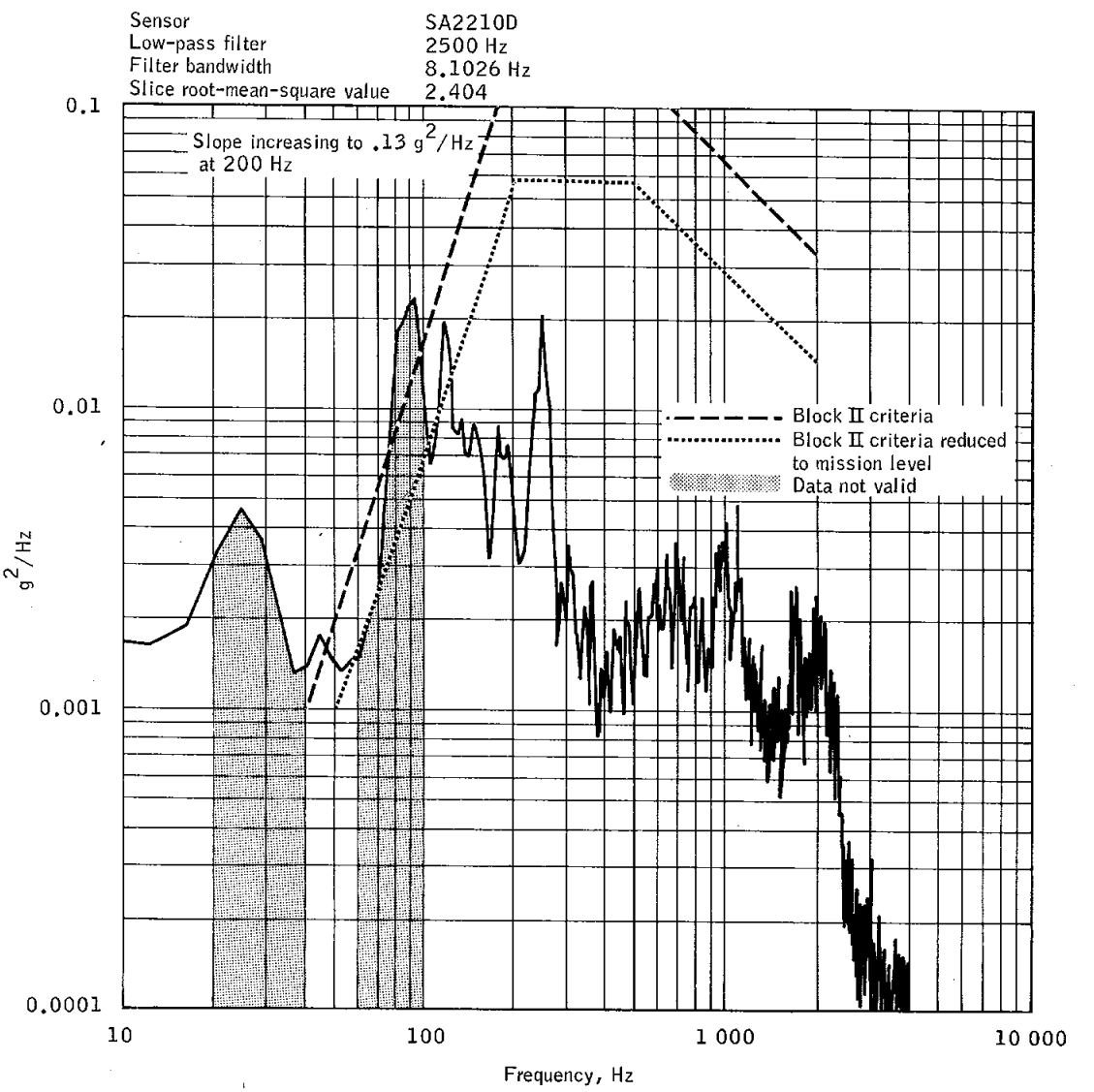

(a) -1 to 1 sec.

Figure 5.1-15.- Comparison of aft bulkhead vibration to criteria.

NASA-S-68-3535

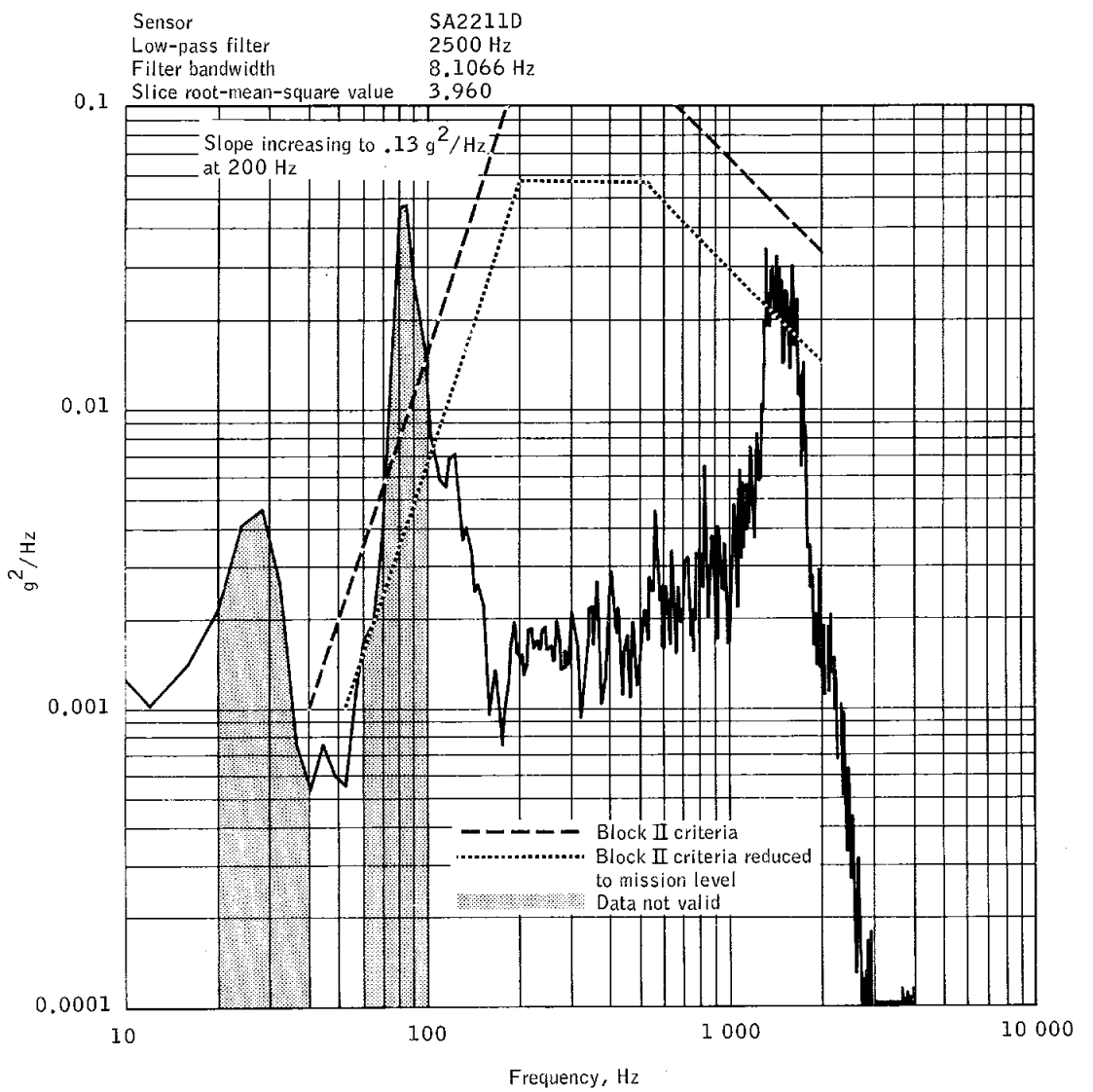

(b) 58 to 60 sec.

Figure 5.1-15.- Continued.

NASA-S-68-3536

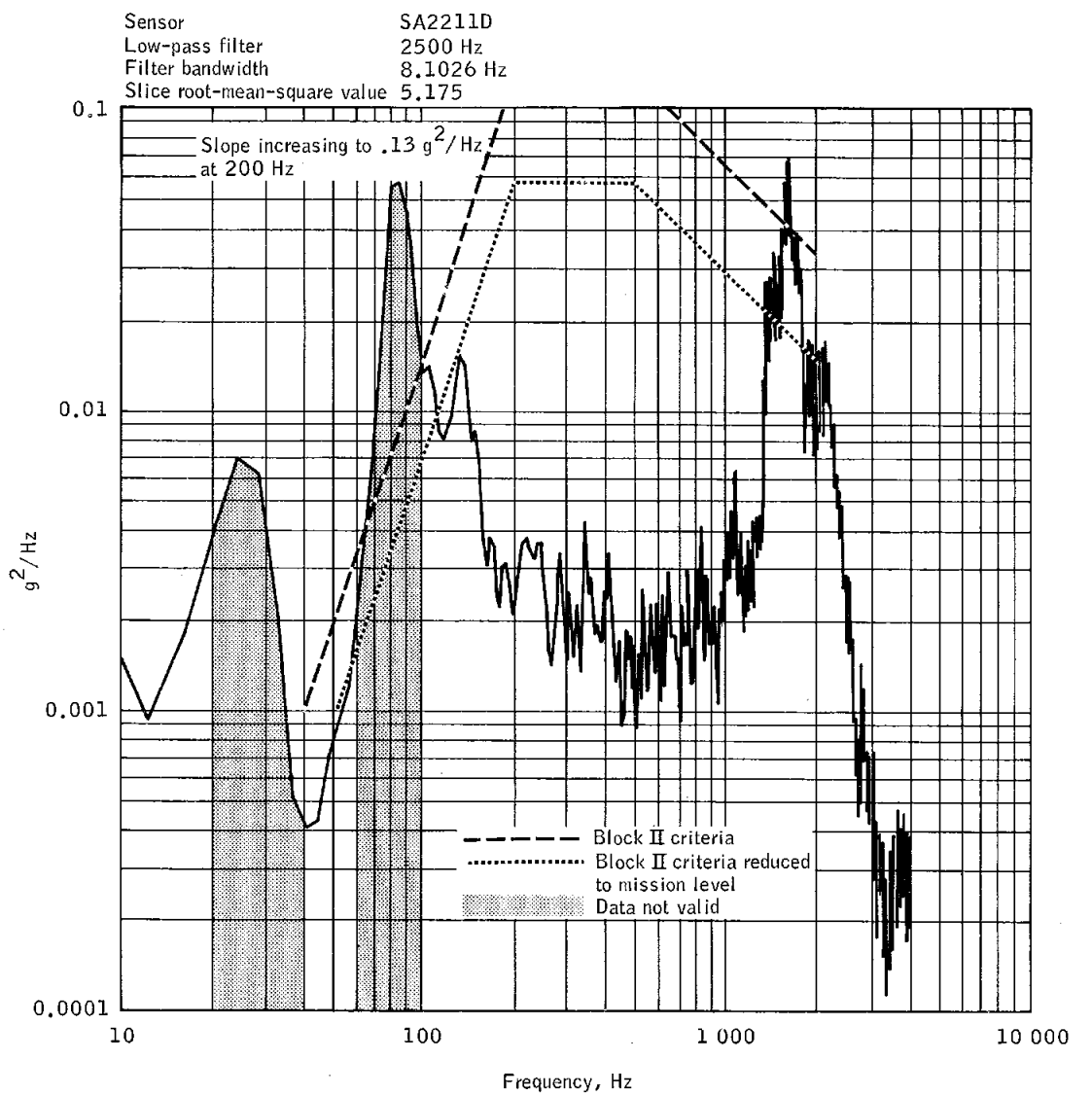

(c) 74 to 76 sec.

Figure 5.1-15.- Concluded.

NASA-S-68-3537

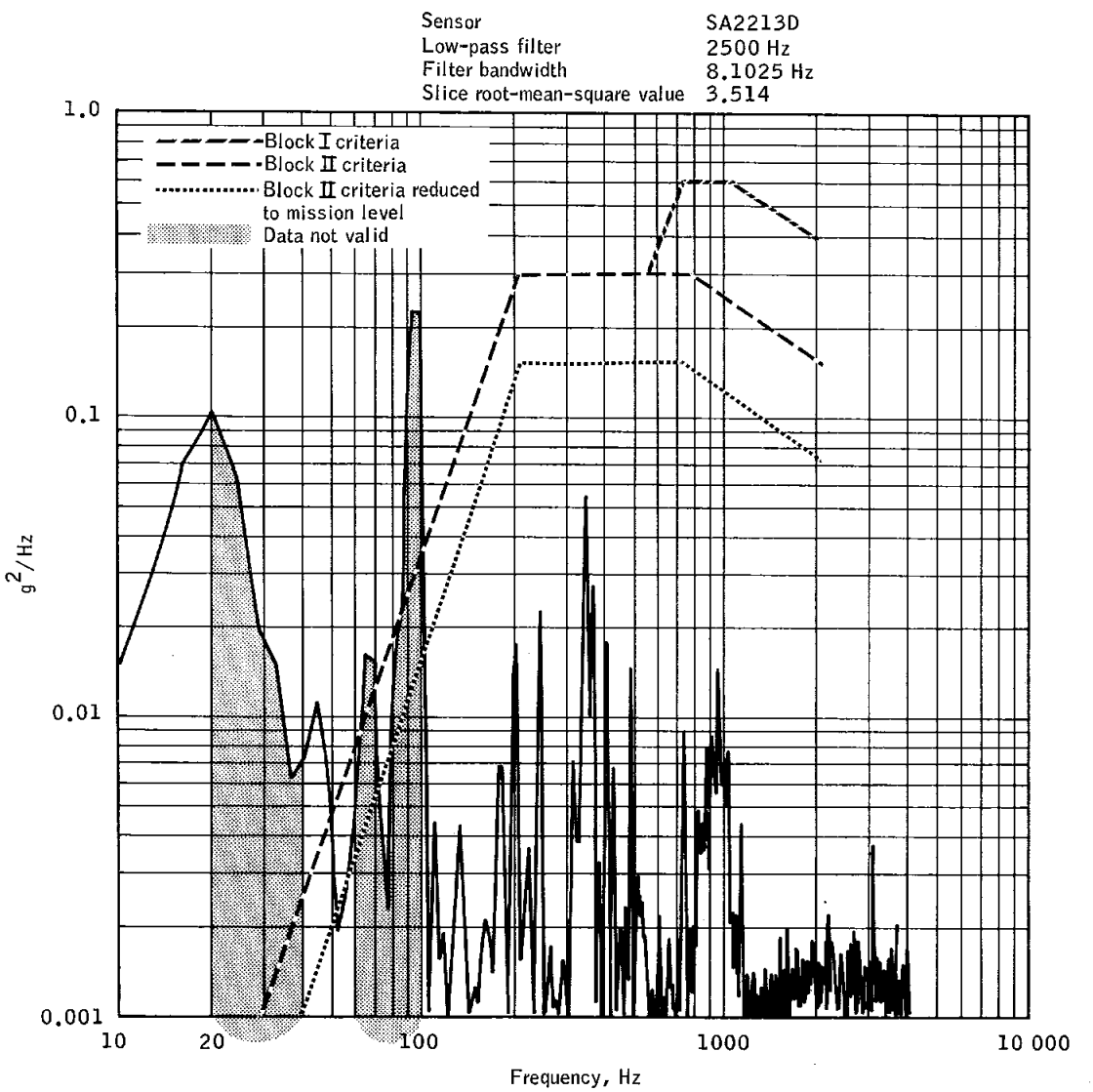

(a) -7 to -5 sec.

Figure 5.1-16.- Comparison of helium pressurization panel vibration to criteria.

NASA-S-68-3538

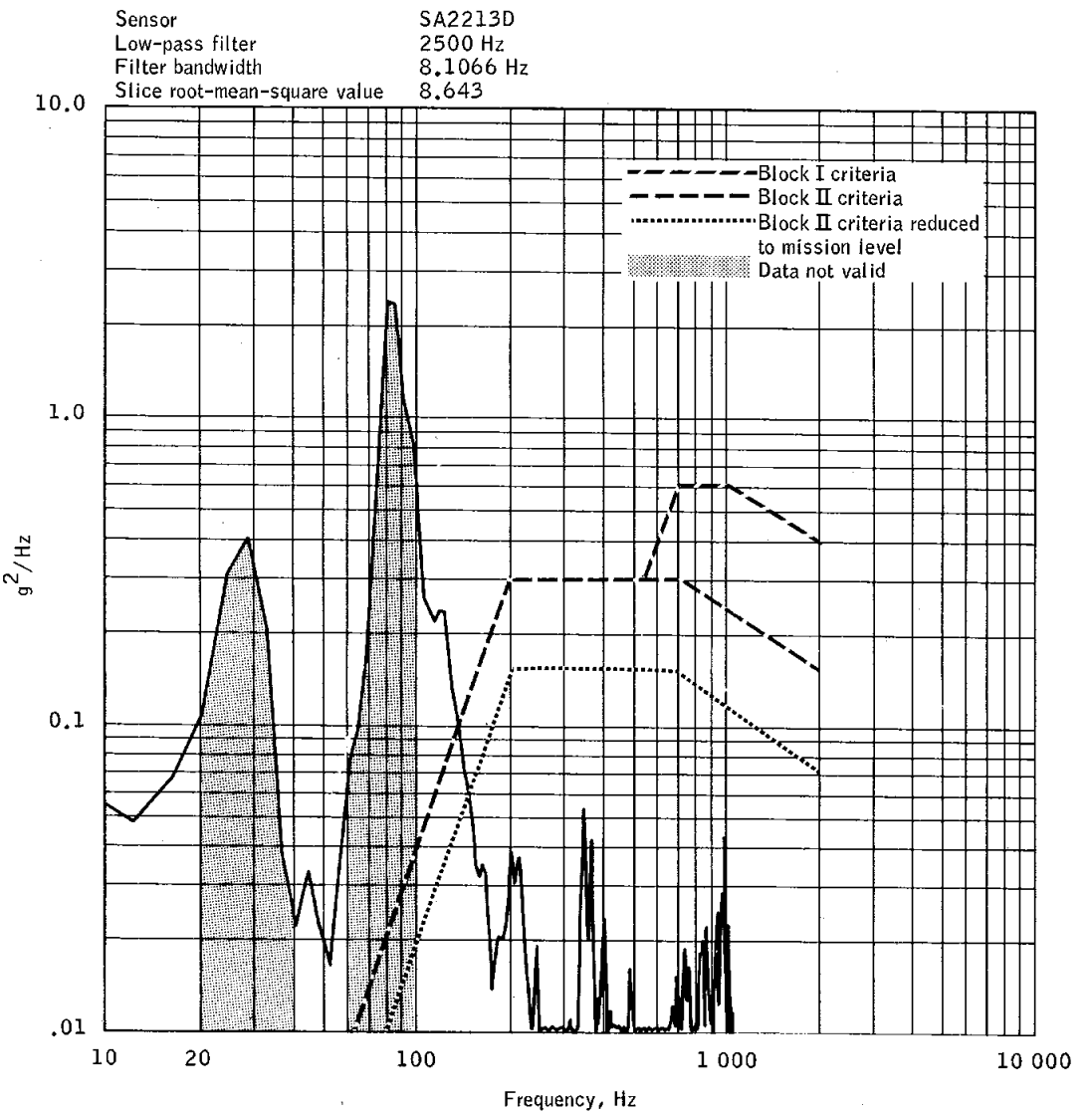

(b) 58 to 60 sec.

Figure 5.1-16.- Continued.

NASA-S-68-3539

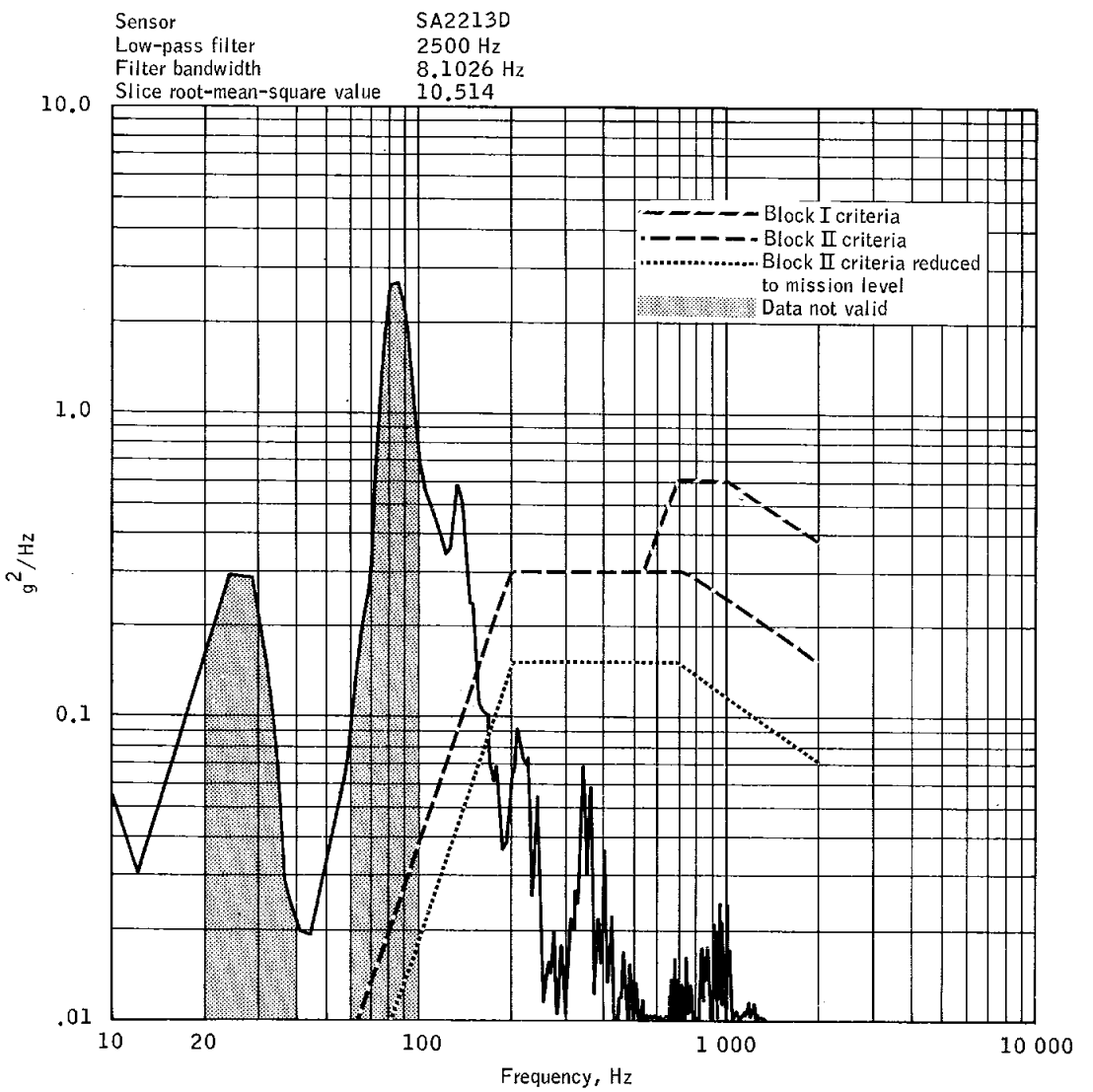

(c) 74 to 76 sec.

Figure 5.1-16.- Concluded.

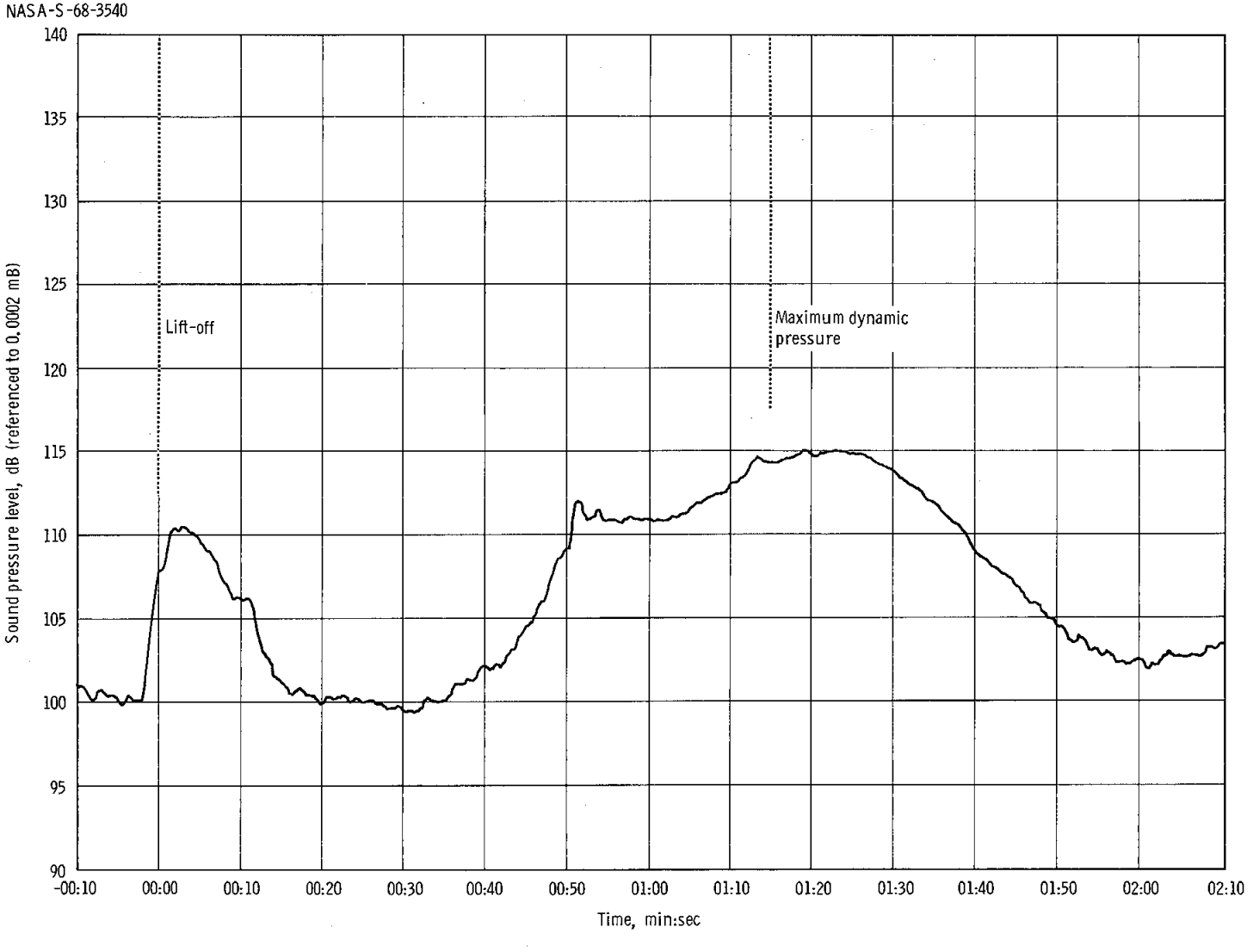

(a) -00:10 to 02:10

Figure 5.1-17. - Root-mean-square time history of internal command module sound pressure.

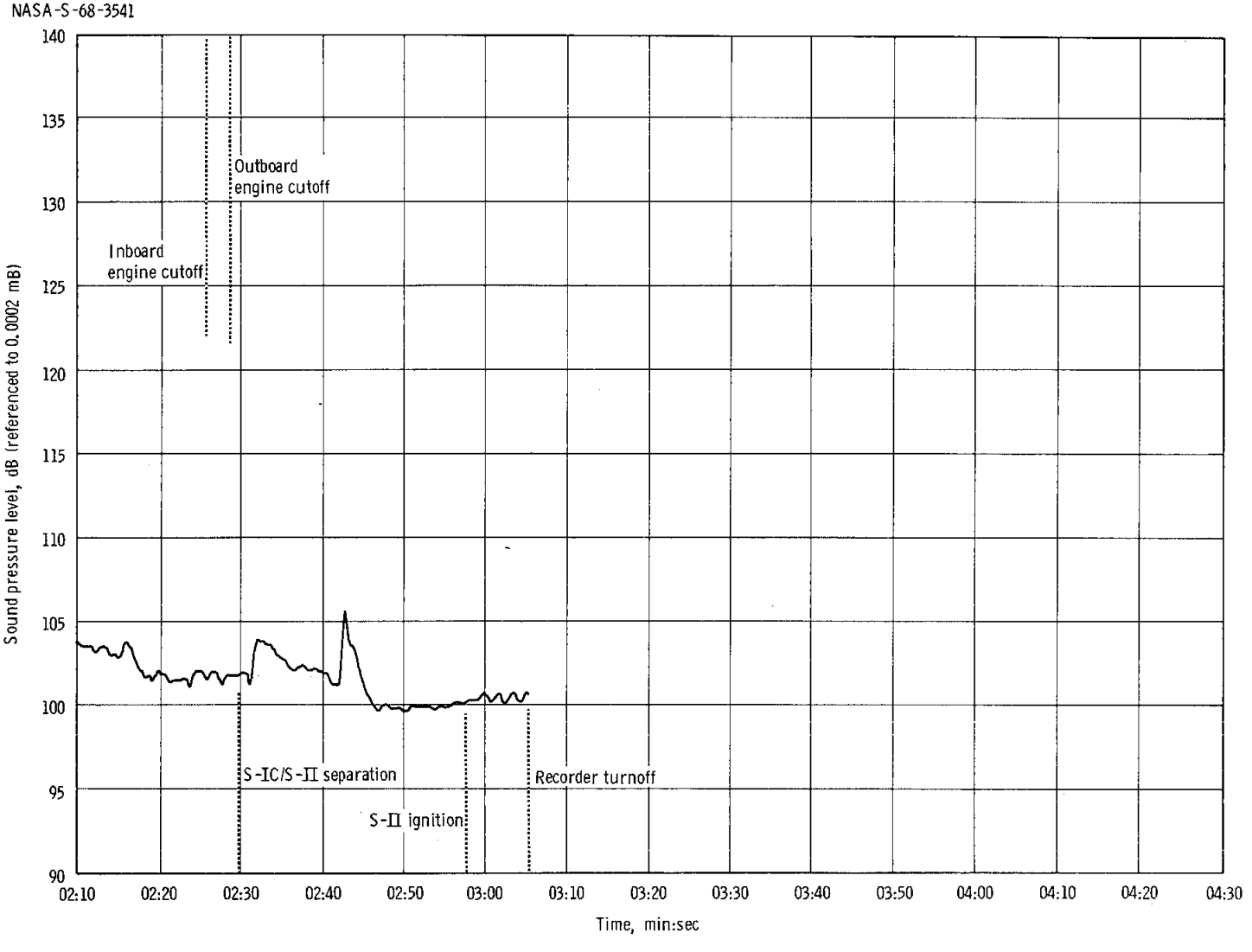

(b) 02:10 to 04:30.

Figure 5.1-17. - Concluded.

5.2 AERODYNAMICS

The flight-derived trim lift-to-drag ratio was approximately 0.350 at the entry interface (400 000 ft), and increased to 0.365 at the first peak g point and 0.415 at the second peak g point (corresponding to trim angles of attack α_T of 156.7 degrees, 155.7 degrees, and 152.2 degrees, respectively). This lifting capability was adequate to reach the preflight-targeted landing point despite the reduced initial velocity conditions at the entry interface. The flight-derived lift-to-drag ratio was within the predicted uncertainty limits for most of the hypersonic flight regime (down to Mach 10). The trim lift-to-drag ratio increased during entry, and the trend was very similar to the trends obtained from previous Apollo flights.

5.2.1 Predicted Aerodynamics

The prediction of the command module aerodynamics represented a combination of modified wind tunnel data and previous Apollo flight-derived aerodynamic data. The wind tunnel data, consisting of ground facility data for a symmetrical command module, were then analytically modified to compensate for the canting of the aft heat shield with respect to the structural centerline of the conical section. The effects of the umbilical housing and umbilical housing ramp were also incorporated.

Flight-derived aerodynamics from previous Apollo flights, compared with the modified wind tunnel data for those flights, have indicated a trim several degrees higher in angle of attack, and resulting lower lift-to-drag ratio, at the entry interface. To compensate for this difference, the modified wind tunnel data for the hypersonic flight regime were shifted by approximately 3 degrees. The predicted trim aerodynamics were then calculated for an entry phase based on the latest predicted center of gravity (cg) at entry interface, of X_{cg} = 1039.2, Y_{cg} = 0.3, and Z_{cg} = 6.4, when the X_{cg} had an origin 1000 inches below the tangency line of the command module substructure mold line. The resulting values were a lift-to-drag ratio of 0.343 and an angle of attack of 157.2 degrees at the entry interface.

The effect of reaction control fuel usage during entry was considered. Ablative material loss was estimated to have had no significant effect on the center of gravity.

The final set of predicted trim aerodynamic data had an unsymmetrical uncertainty band of plus 0.066 and minus 0.028 compared with the

nominal. This band accounts for unknown aerodynamic flow effects, uncertainties in the nominal center of gravity, aft-heat-shield/conical-after-body mating misalignment, and aft heat shield cant-determination uncertainty.

5.2.2 Flight-Derived Aerodynamics

The flight-derived total lift-to-drag ratio was obtained from the corrected accelerations sensed by the inertial measurement unit. These acceleration data were transformed from the inertial platform frame to the stability axis frame by processing through the earth-centered inertial and geodetic axis systems. Data inputs for this calculation were obtained from the reconstructed entry trajectory (section 3.5).

Estimates of the flight-derived angle of attack were obtained using the wind tunnel data variation of angle of attack with lift-to-drag ratio, and with the flight-derived lift-to-drag ratio.

5.2.3 Performance

A comparison of the flight-derived total lift-to-drag ratio and the predicted trim values is presented in figure 5.2-1 (the onboard-computer control phases and the Mach-number/deceleration-load-factor time histories are also shown). The initial entry velocity was approximately 3700 ft/sec below that originally planned for a nominal mission. Shortly after the 0.05g point, the command module was in a steady-state trim attitude with a flight-derived lift-to-drag ratio of approximately 0.350 (α_T of 156.7 degrees), which is 0.007 above the predicted nominal value of 0.343 (α_T of 157.2 degrees). This ratio then increased, reaching approximate values of 0.365 (α_T of 155.7 degrees), 0.380 (α_T of 154.7 degrees), and 0.415 (α_T of 152.2 degrees) at the first peak g point, initiation of ballistic phase, and second peak g point, respectively. The flight-derived lift-to-drag ratio was within the predicted uncertainty bands for most of the hypersonic flight regime, down to Mach 10, and reached the closest correlation with predicted values during the initial entry phases of the flight when most of the ranging was done (that is, before the ballistic phase was reached). Use of the available lifting capability is shown in figure 5.2-2 in the form of a vertical lift-to-drag ratio referenced to the ground. This ratio was a function of the roll attitude of the command module relative to the ground, or bank angle. The figure shows that the command module entered the atmosphere in a lift-up attitude, which was maintained until the first peak g point was reached (coincident with the start of UPCONTROL). At that time, a negative lift trajectory was flown for approximately 50 seconds. After this, period, a vertical lift-to-drag between 0.25 and 0.30 was maintained for

2 minutes 40 seconds. The dynamic pressure in this region did not go below 55 psf; therefore, the aerodynamic forces would still have been considerable. The bank angle used during the portion of the flight from UPCONTROL to the final phase obviously reduced the entry-ranging capability of the command module.

During the second (final) entry phase, the command module could not compensate for the loss of range, even though the lift-to-drag ratio was higher than predicted because the two previous control phases had resulted in reduced velocity and altitude.

The flight-derived lift-to-drag ratio was compared with those obtained during the AS-202 and Apollo 4 flights (fig. 5.2-3). A consistent trend existed in that the lift-to-drag ratio decreased with higher Mach numbers.

The data have been presented with Mach numbers for clarity, but this correlation parameter is not necessarily the most definitive.

NASA-S-68-3542

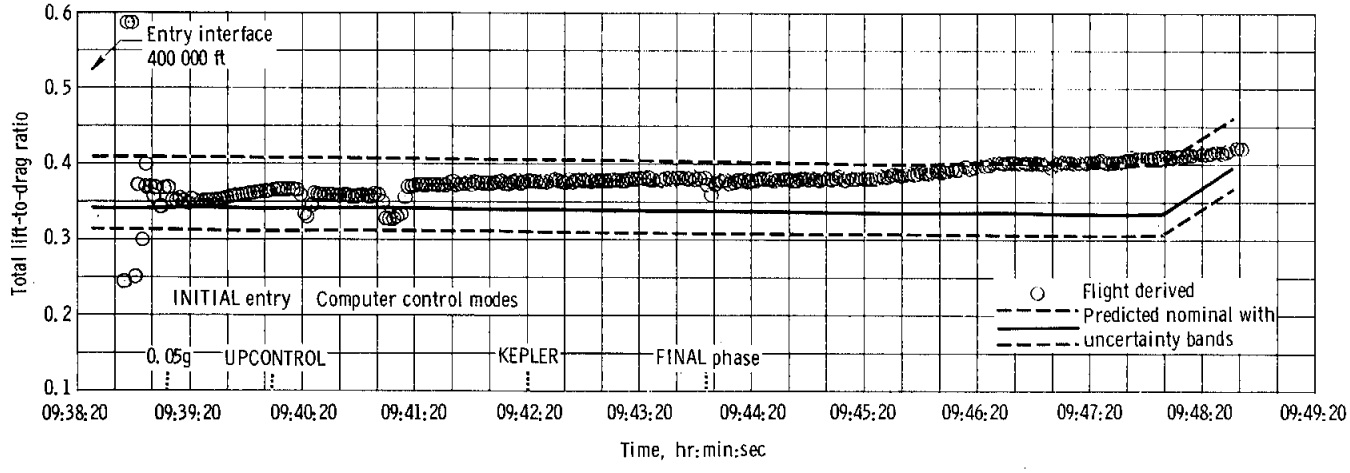

(a) Lift-to-drag ratio time history.

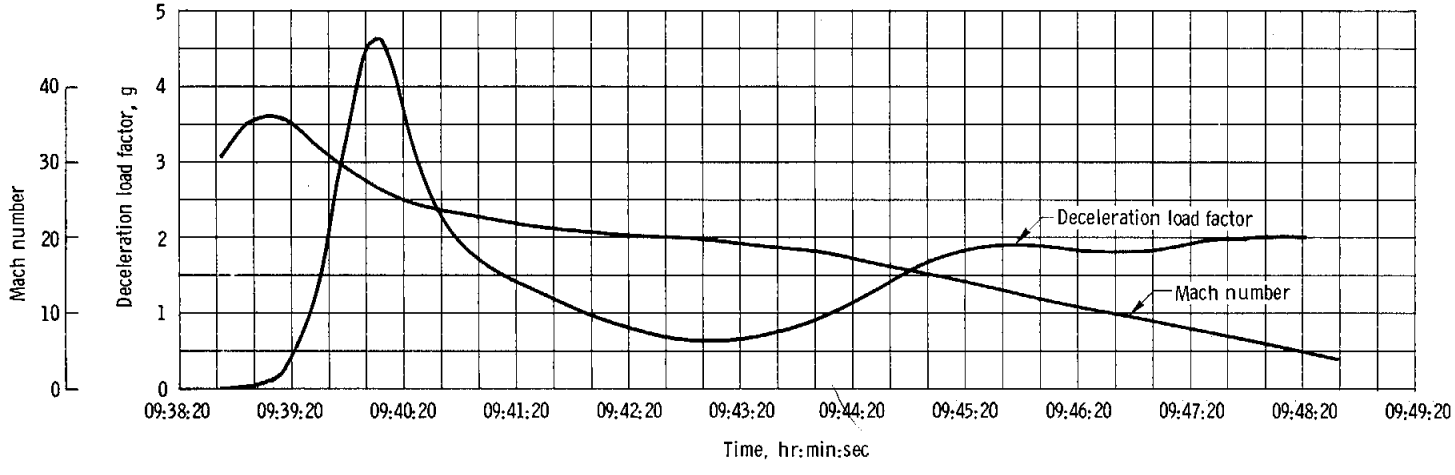

(b) Mach number and deceleration load factor time histories.

Figure 5.2-1. - Aerodynamic data comparison.

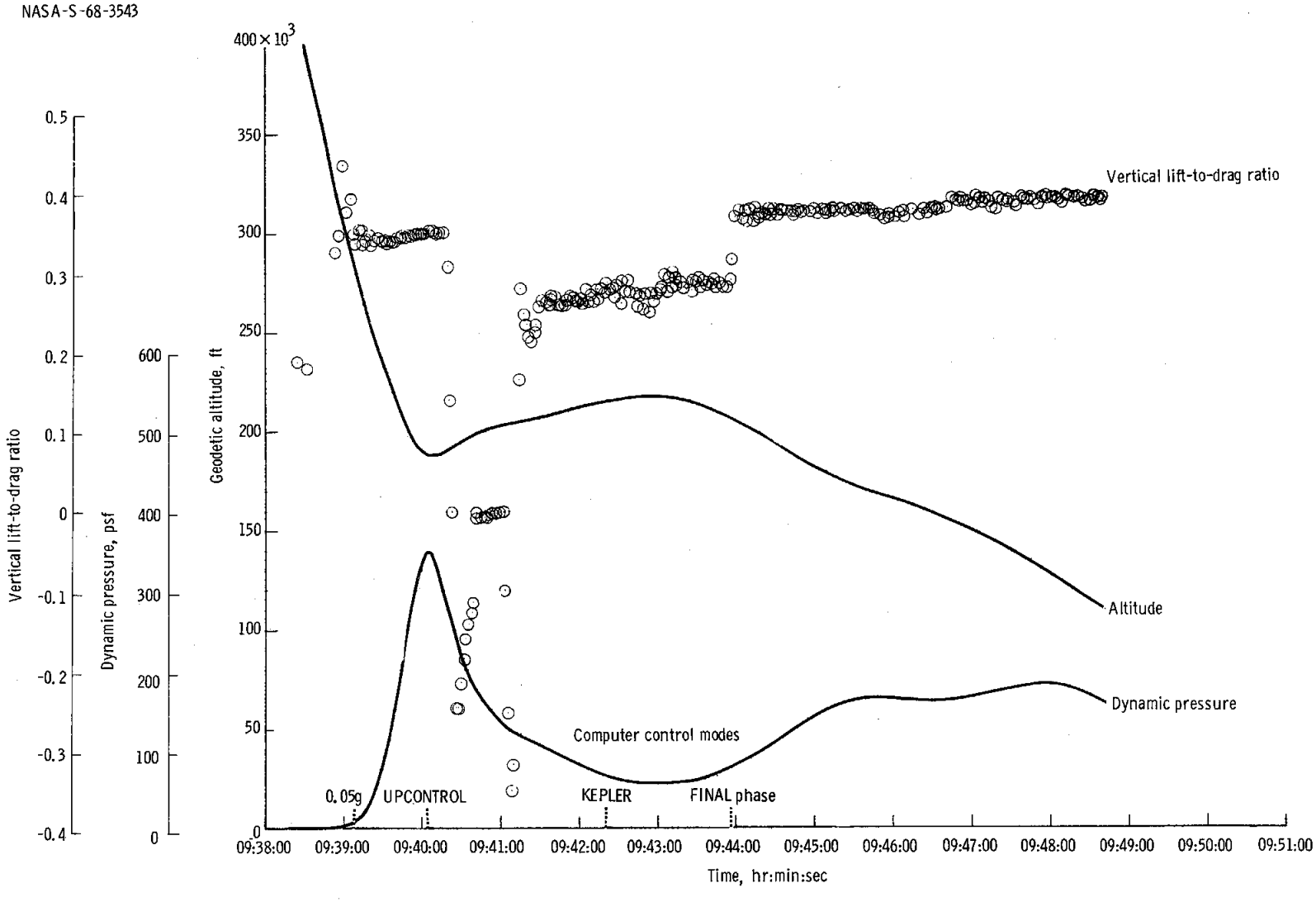

Figure 5.2-2. - Utilization of lifting capabilities.

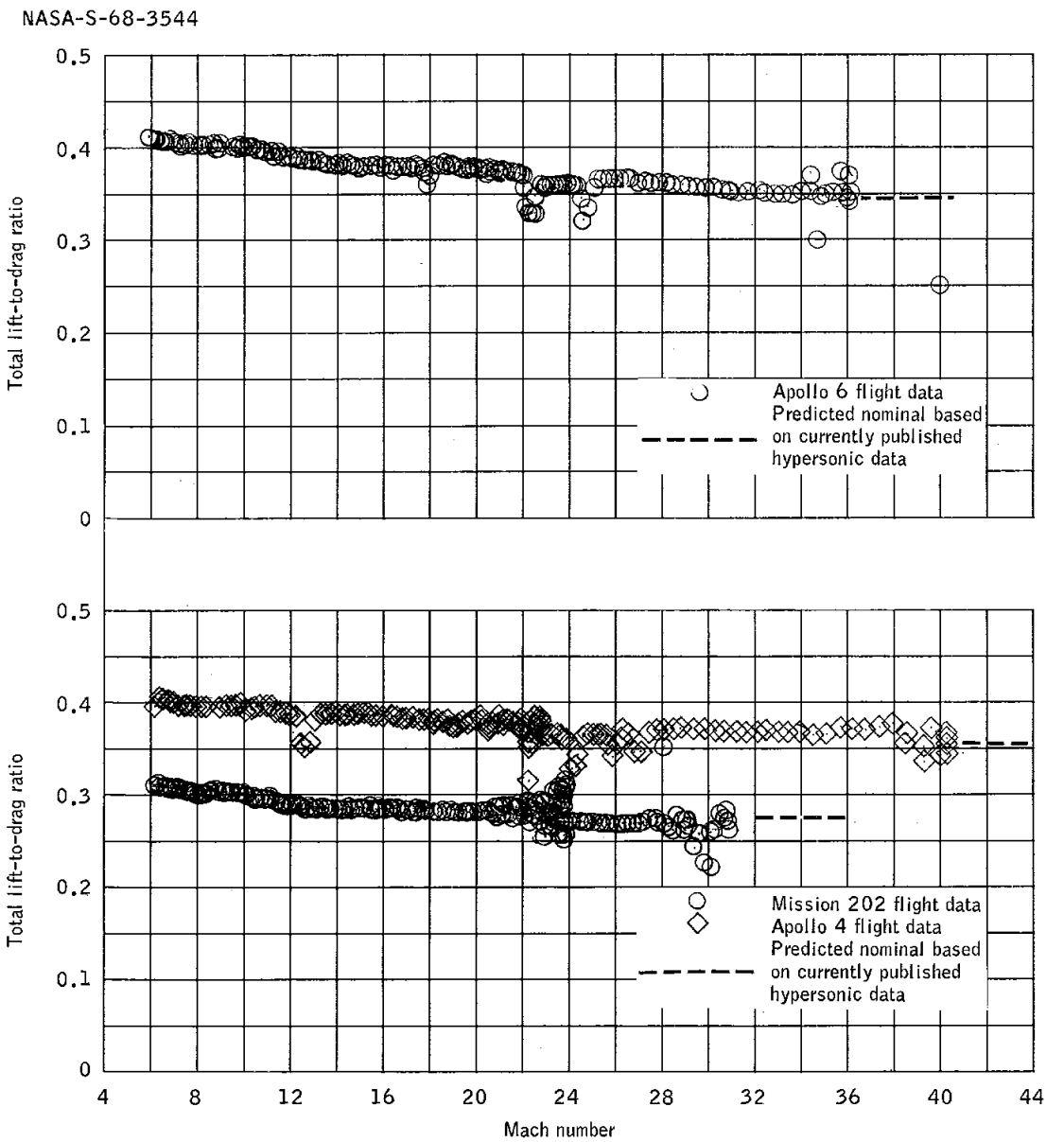

Figure 5.2-3.- Comparison of flight-derived data trend in the hypersonic flight region.

5.3 THERMAL STRUCTURES

5.3.1 Launch Phase

Heat transfer (boost).- The thermal environment of the Apollo 6 ascent trajectory has been evaluated for the service module and the adapter. All thermocouple data were lost at 00:01:28 (section 12.0), and only the correlation between the analytical predictions based on actual trajectory data and the similar Apollo 4 predictions (and thermocouple data) is discussed in this section.

Service module temperatures.- The peak analytical cold wall heating rate for service module location X_S 280 inches was 14.6 percent higher than the Apollo 4 analytical maximum. Based on the measured Apollo 4 peak inner-skin temperatures of 90° F, it was estimated that the Apollo 6 peak inner-skin temperature was less than 100° F. The relatively low temperature levels resulted from the cork protection on the outer skin of the service module.

Adapter temperatures.- The data bands and the maximum predicted thermal response for adapter sensor AA7864T for the boost phase of the Apollo 4 and 6 missions are shown in figure 5.3-1. Sensor AA7864T was located on the outer skin at longitudinal station X_A 730 inches and 174 degrees from the plus Y axis. The maximum predicted response was based on adapter radiation interchange with the sun and the earth, and the increase over the predicted Apollo 4 adapter response was the result of a slightly hotter launch trajectory. The peak predicted cold wall heating rate at X_A 730 was 14.2 percent higher than the corresponding for the Apollo 4 adapter peak. As shown in figure 5.3-1, the Apollo 6 adapter data band was just beginning to increase at the time the data were lost. Based on corrected Apollo 4 predictions, the predicted Apollo 6 adapter thermal response should be similar to the response actually experienced by the Apollo 6 adapter at that particular location. The analytical predictions were that the Apollo 6 adapter temperatures would be slightly greater than the Apollo 4 adapter temperatures; this was substantiated by temperature data from the launch vehicle instrument units on both the Apollo 4 and 6 missions. At 00:02:30, instrument unit sensor C43-603 measured 132° F during Apollo 4 and 145° F during Apollo 6. This sensor was located on the instrument unit inner honeycomb skin at station 3247.0 (11.55 inches from the bottom of the adapter on the 36-inch instrument unit). The Apollo 6 peak estimated temperatures at the 14 adapter sensor locations are shown in figure 5.3-2. These estimates were obtained using

the Apollo 4 data for each sensor and the ratio between the Apollo 6 and Apollo 4 maximum predicted changes in temperature for location X_A 730 inches.

5.3.2 Orbital Flight

The command module heat shield thermal response during the orbital phase of the mission was determined by three operational ablator bondline temperature measurements. Four temperature measurements of the service module aluminum honeycomb inner skin and two service module fuel tank skin temperature measurements were also recorded during this period. The period of interest was from orbital insertion to the end of the cold-soak phase (approximately 00:12:37 to 09:15:29).

The entire conic heat shield was painted with a carbon-black-pigmented white paint, which appeared gray. The undegraded thermal control properties of this paint were solar absorptance of 0.52 to 0.56 and infrared emittance of 0.87 to 0.91. A paint with a high infrared emittance was chosen, because such a paint allowed a faster cool-down response; in addition, if the expected cold-soak solar orientation could not be achieved, the bondline temperature would not exceed 150° F.

The location of the command module sensors (CA1502T, CA1505T, and CA1509T) for which data were available during portions of the orbital phase of the mission and for which predictions were made are shown in figure 5.3-3. Predicted and measured temperatures for each of the three sensors are shown in figures 5.3-4, 5.3-5, and 5.3-6. Excellent correlation was obtained between measured data and predicted responses. The bondline temperature increased when the command and service module was reoriented for the simulated second service propulsion system engine firing. The increased ablator bondline temperatures indicated that a large portion of the command module conic surface was subjected to solar heating.

The skin temperature on the block I service module (which has total cork insulation) was measured by four sensors and fuel tank temperatures were measured by two sensors (fig. 5.3-7). The temperature responses are shown in figure 5.3-8. These responses indicate that the spacecraft attitude was such that, during the coast ellipse phase (03:16:06 to 09:15:29), the minus Z to minus Y quadrant of the service module was oriented toward the sun. The temperature of sensor SA2360T, which was in a total cold-soak condition, exceeded the instrumentation data range (minus 100° F to plus 200° F) at 05:46:00. The temperature data from sensor SA2367T, which received a small solar incidence, did not reach -100° F. Sensor SA2366T received heat from the fuel cells located in

bay IV of the service module; thus, the temperature measured by this sensor ranged from 25° to 29° F during the cold-soak phase. The data from sensor SA2361T, which was in the quadrant of maximum solar incidence, increased from approximately -8° F at the beginning of the cold-soak period and leveled out at 45° to 47° F during the cold-soak ellipse phase. Tank temperature responses were as expected.

One of the flight objectives was to thermally cold-condition the entire conic ablator before entry so as to induce thermal stresses and distortions on the command module; this was achieved. Available measurements indicate that the command module surface was in the required cold-soak attitude; the ablator surface, which was subjected to a sun angle of approximately 7 degrees, was almost completely shadowed.

NASA-S-68-3545

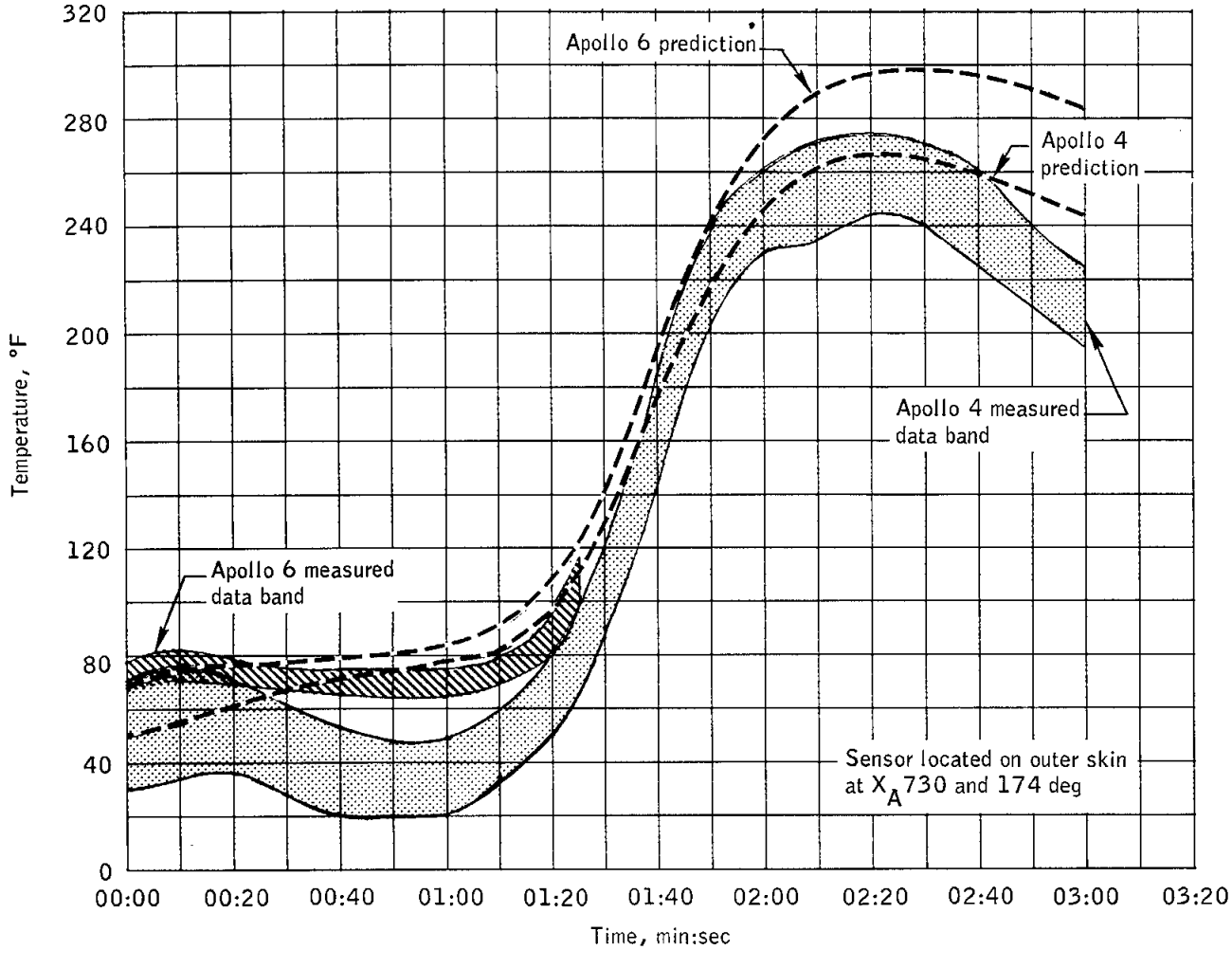

Figure 5.3-1.- Temperature measured by spacecraft/lunar module adapter sensor AA7864, Apollo 4 and 6 missions.

NASA-S-68-3546

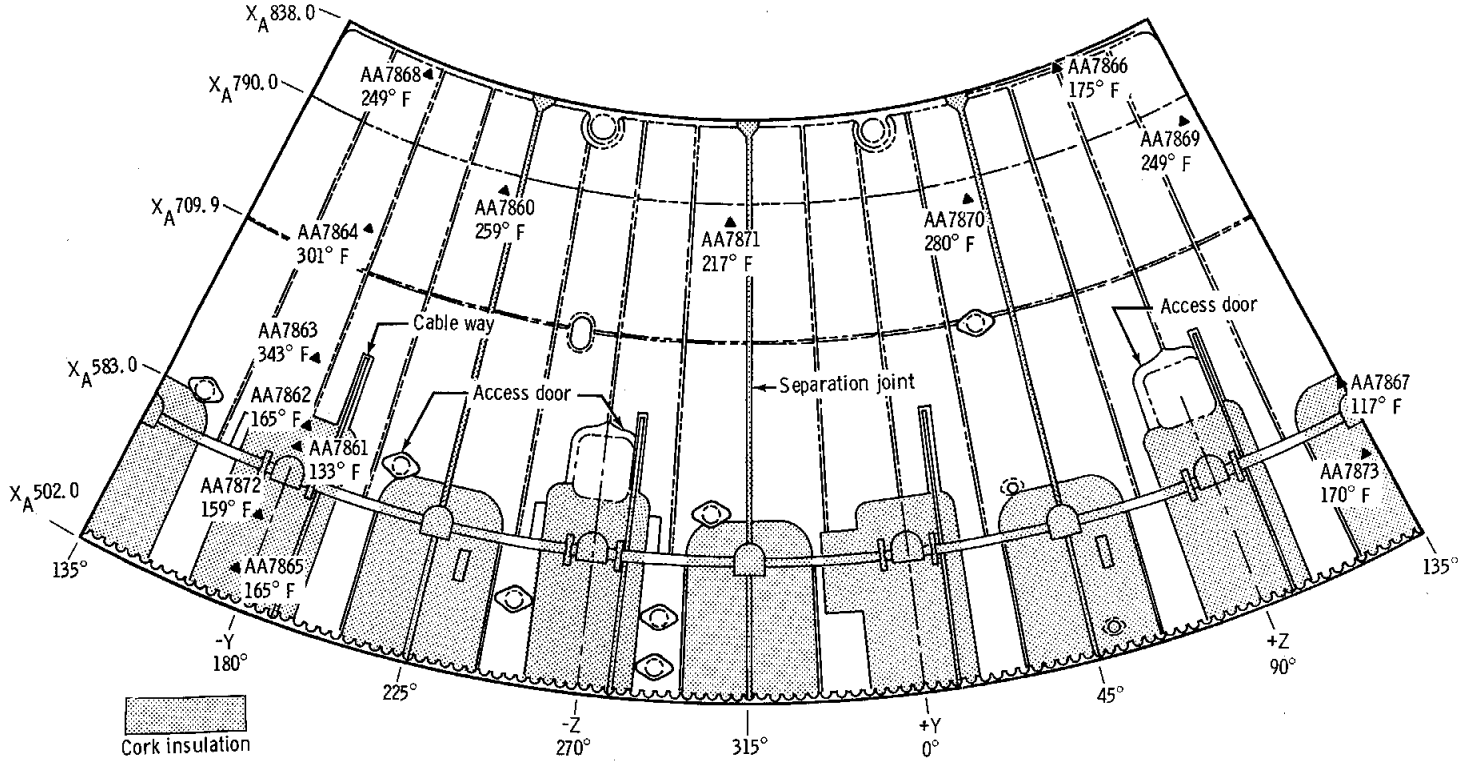

Figure 5.3-2. - Estimated temperatures on spacecraft/lunar module adapter outer surface during the launch phase.

NASA-S-68-3547

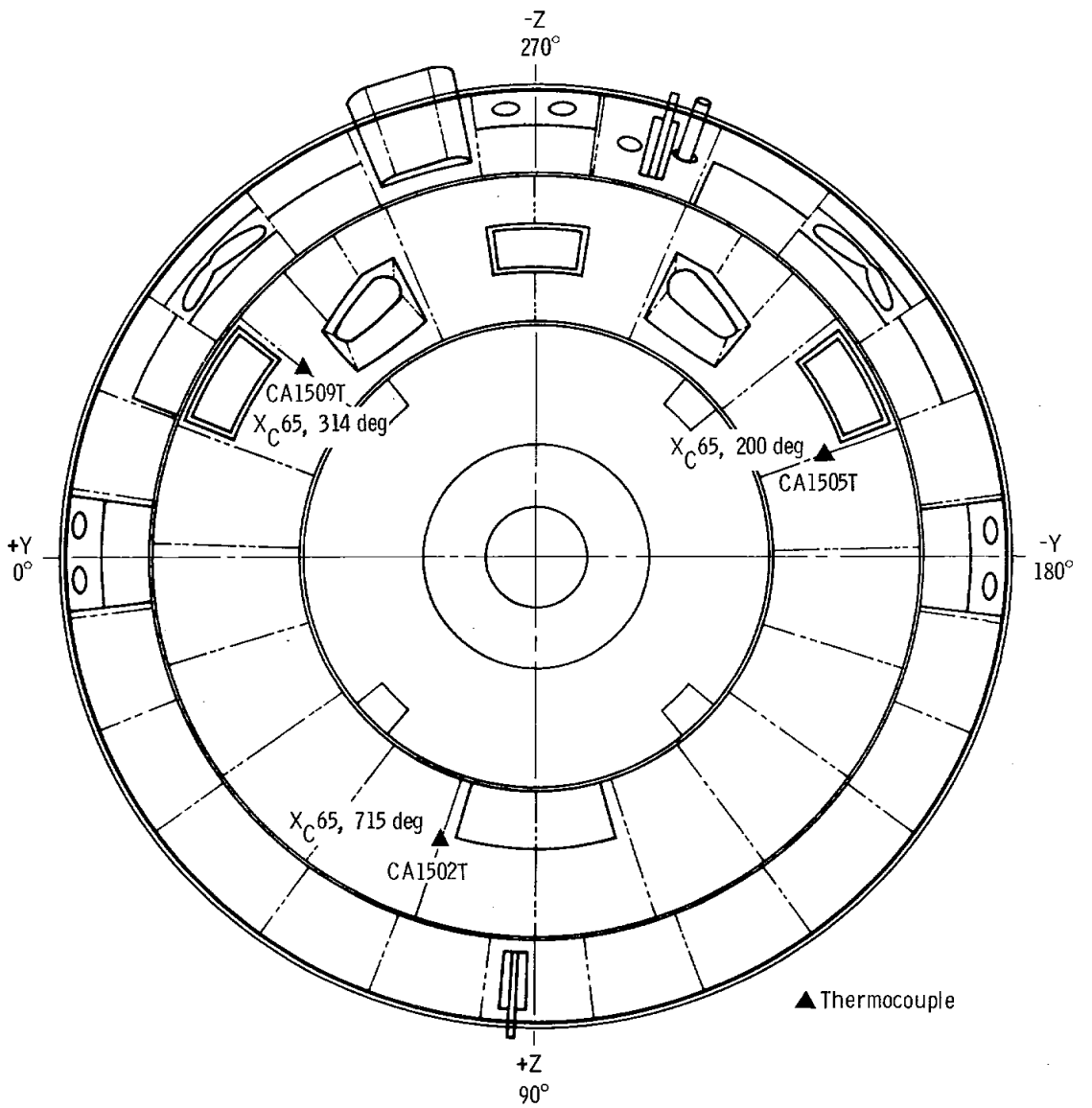

Figure 5.3-3. - Operational command module ablator bondline temperature sensor locations.

NASA-S-68-3548

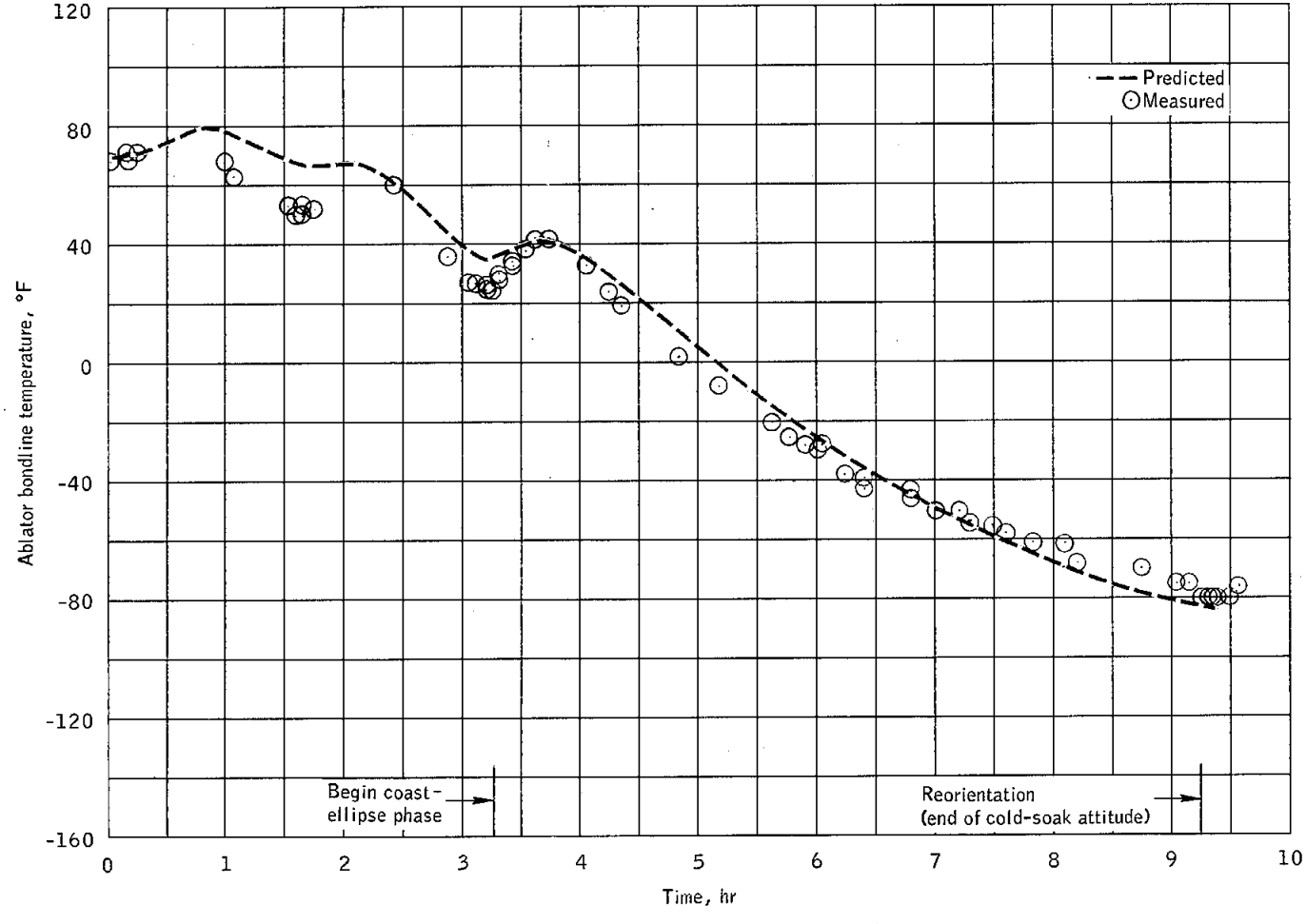

Figure 5.3-4.- Temperature measured by command module sensor CA1502T.

NASA-S-68-3549

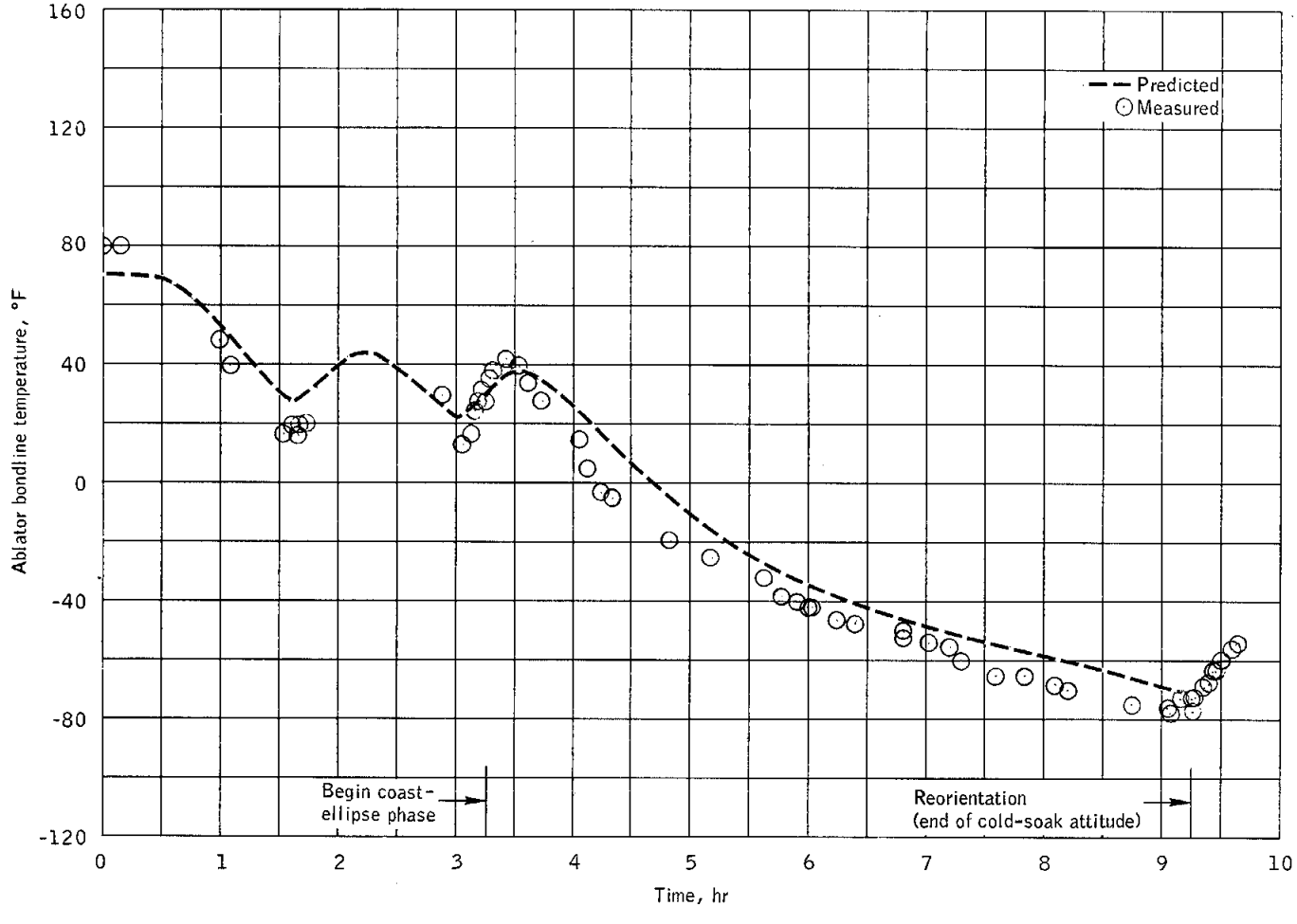

Figure 5.3-5.- Temperature measured by command module sensor CA1505T.

NASA-S-68-3550

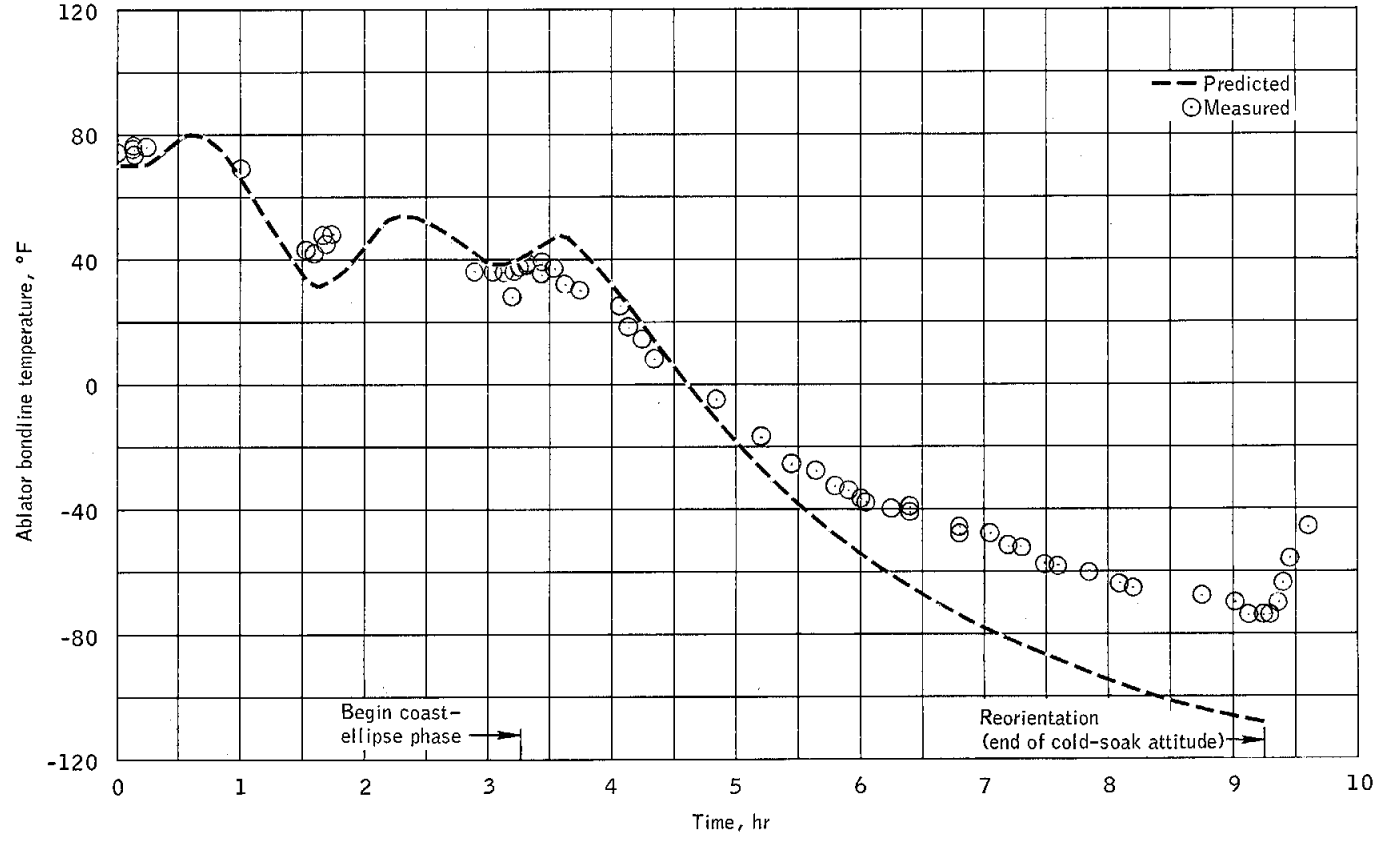

Figure 5.3-6.- Temperature measured by command module sensor CA1509T.

NASA-S-68-3551

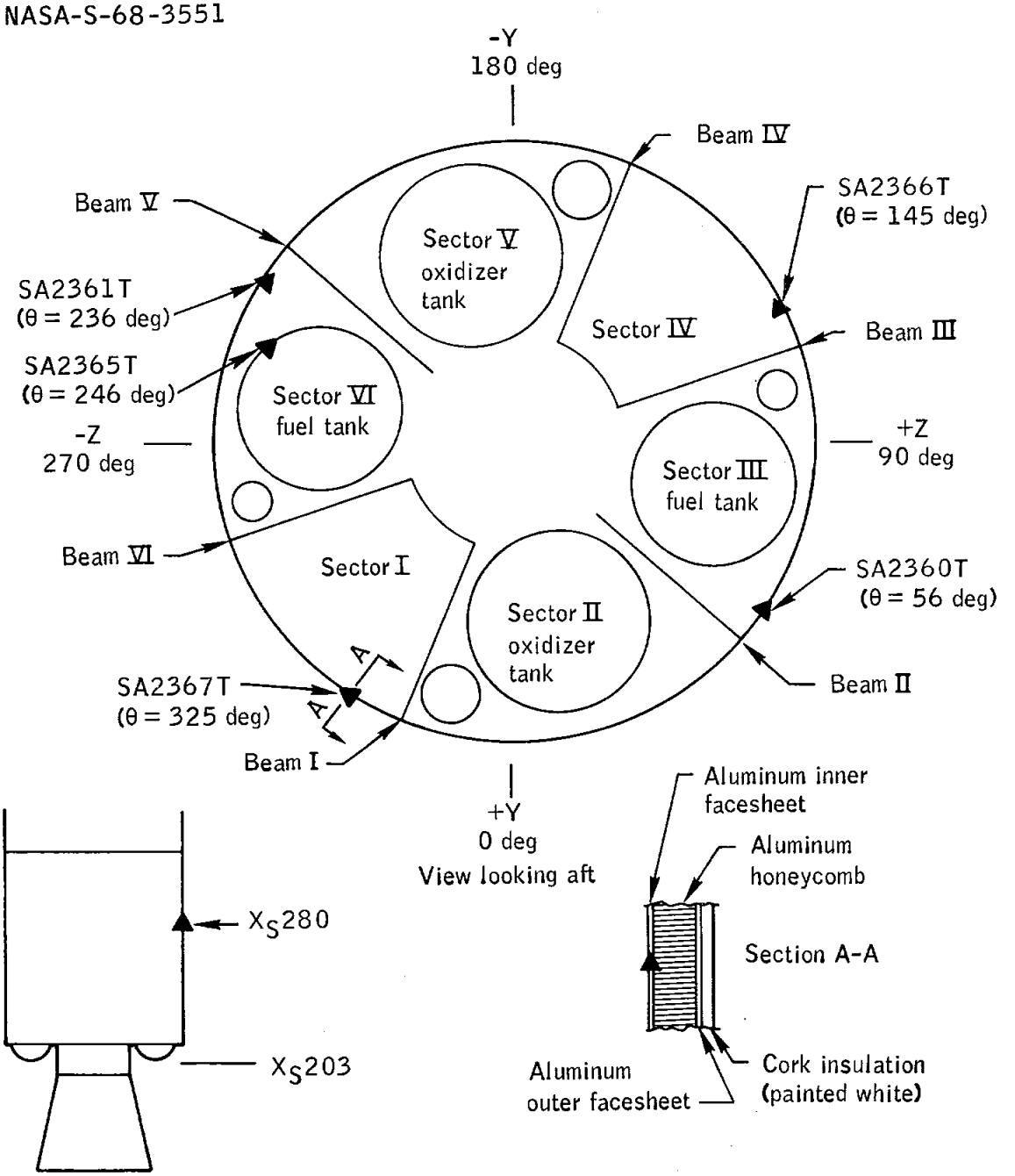

Figure 5.3-7.- Location of service module skin and fuel tank sensors.

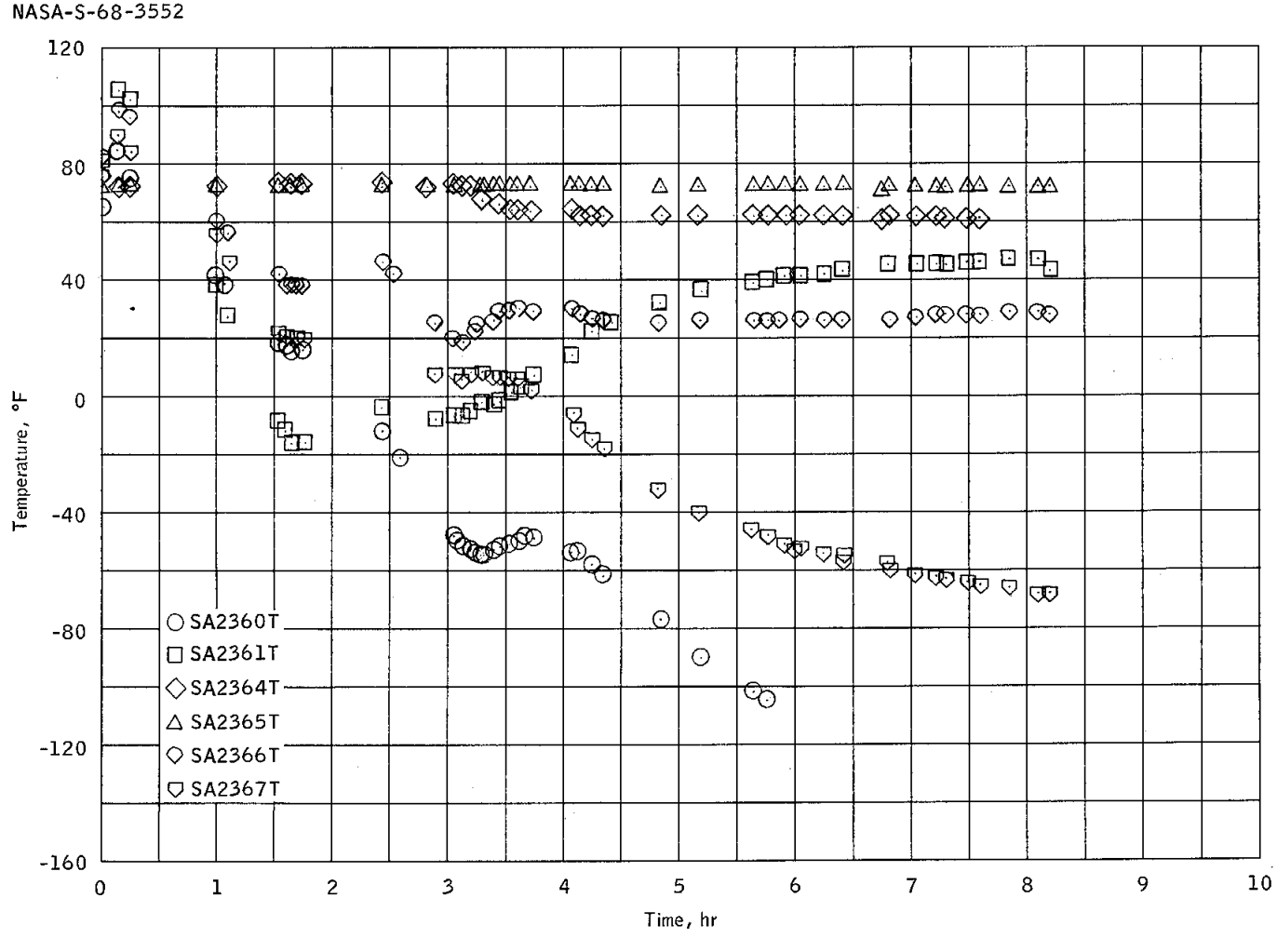

Figure 5.3-8.- Service module skin and fuel tank temperature.

5.4 AEROTHERMODYNAMICS AND HEAT PROTECTION

5.4.1 Aerothermodynamics

Measurements of local pressure and heating rates on the Apollo 6 command module were obtained from pressure transducers, surface-mounted calorimeters, and radiometers (fig. 5.4-1 and table 5.4-I). The instrumentation for defining the entry environment was identical to that of the Apollo 4 command module, except the hatch gap calorimeters were omitted. The pressure measurements at all aft heat shield locations showed good agreement with predictions based on wind tunnel data. A number of conical section pressure measurements were considerably lower than the predictions during the time of peak measurement.

The low entry velocity resulted in radiative predictions an order of magnitude lower than for a lunar-return velocity. The postflight predictions were in essential agreement with the radiometer measurements, although the low level of the data resulted in a questionable quantitative comparison. The molecular and non-equilibrium radiations were dominant in the radiative heating but will be of minor importance in the lunar-return environment.

The convective cold-wall heating rates used for predicting flight performance were found to be adequate when local mass injection from ablator pyrolysis was taken into account. Local mass injection significantly influenced the heating rates to the calorimeters on the aft heat shield and the windward conical section.

The wafer calorimeter temperatures were valid for approximately 80 seconds of initial entry time. These data were used to calculate the aft compartment heating rates, which were in good agreement with heating rate predictions adjusted for local mass injection.

The heating rates measured on the conical section were in agreement with heating rate predictions adjusted for local mass injection, and with predictions for both the windward region where local blowing was significant and the leeward portion which experienced little or no mass injection. Measurement values on the toroid, however, were considerably higher than the predictions.

5.4.2 Heat Protection

The block II thermal protection system, previously qualified by the Apollo 4 mission, was tested on Apollo 6 at a velocity approximately

3600 ft/sec less than the Apollo 4 velocity. Although the reference heating rate was about half that of Apollo 4 and the heat load was about 10 000 Btu/ft^2 less, the temperature responses on the Apollo 6 conical section and on the aft heat shield leeward side were equal to or greater than those on Apollo 4. This paradoxical situation may be attributed to three causes: the Apollo 6 command module flew faster at lower altitudes, did not skip out to as great an altitude to allow an ablator cool-down phase (only one blackout period), and flew approximately 80 seconds longer to reach the required target. Because the ablator response was very similar to that of Apollo 4, the data provided a test point between the near-earth entry of the AS-202 mission, and the simulated lunar return of the Apollo 4 mission.

Postflight inspection of the command module indicated that the block II heat shield performed satisfactorily during entry. Sufficient flight data were obtained to permit a thorough evaluation of the performance of the block II thermal protection system. The temperature data were within design limits for the flight, although the ablator temperature rises were higher than for the Apollo 4.

The instrumentation used to measure the performance of the ablative heat shield and the singular components was identical to that used on the Apollo 4 command module except in the area of the unified side hatch. The locations of the thermocouples and char sensors on the aft heat shield and conical heat shield are shown in figures 5.4-2 and 5.4-3, respectively. Temperature measurements for these components are presented in table 5.4-II.

Aft heat shield.- The aft ablative heat shield was heavily charred over the entire surface (fig. 5.4-4a). Extrapolated temperature data indicated that surface temperatures exceeded 4000° F, which resulted in the formation of a strong carbonaceous char. No visible streamlines emanated from the stagnation area; however, flow patterns downstream of the compression and shear compression pads (fig. 5.4-4b) indicated aerodynamic flow away from the stagnation area on the aft heat shield. There were no areas of excessive erosion caused by heating, although pieces of charred ablator were broken off locally.

Some ablator was missing from the gap splice, as shown in figure 5.4-4c. Visual inspection showed that most of the gap was intact; there was no evidence of erosion at the cavity edges where ablator was missing. These findings indicated that the ablator was lost after entry; the ablator could have been broken at landing or have been washed out by wave action. This phenomenon did not occur on the Apollo 4 command module (which remained in the water only briefly during recovery) but did occur on the AS-202 (which, like the Apollo 6 command module, was in the water for a longer period). Improved manufacturing processes eliminated the ablator splice between honeycomb segments on all block II heat shields.

No ablator core measurements are available for inclusion in this report; consequently, ablator recession and char thickness were estimated at aft heat shield locations corresponding to instrument locations (table 5.4-III).

Block I umbilical and ramp.- Recession of the ablative ramp was less than that on the Apollo 4 command module; the ramp adequately performed the function of limiting the entry environment to the umbilical. The umbilical bundle had melted approximately flush on the right-hand side but protruded about 1 inch on the left-hand side. The umbilical ablator was rounded at the aft edges and was charred about 40 percent of the way up the sides (fig. 5.4-4a).

Shear compression and compression pads.- The tension tie bolts extended 1/4 to 5/8 inch outboard of the shear pad surfaces. The pads (fig. 5.4-4b) remained recessed below the ablator moldline (7/8 to 1-1/8 inches) and were slightly eroded on the downstream sides (as much as 1/4 inch at pad 1).

The temperatures measured in depth at three locations on the aft heat shield are shown in figure 5.4-5. By crossplotting the 1000° F isotherm as a function of time at two locations on the pitch plane (R_c = 71.8 in., θ = 90 deg, and R_c = 50 in., θ = 2.72 deg), reasonable correlation with char sensor data was obtained (fig. 5.4-6). The char sensor data were indicative of the progression rate of the 1000° F isotherm through the ablative material.

The maximum temperatures measured in depth for the same two locations, as functions of depth, are shown in figure 5.4-7. The depth of the 1000° F isotherm, obtained by interpolating these data, closely agreed with the preliminary char interface measurements.

The third thermocouple plug (fig. 5.4-5c) was located on the umbilical ramp downstream of the shear compression pad. The region downstream of the pad experienced considerable erosion, which affected the thermocouple plug. The area eroded was not critical to the performance of the heat shield; however, the temperature data cannot be correlated in depth.

Thermocouples were located at the bondline (interface of the ablator and stainless steel honeycomb substructure) at various other aft heat shield locations. The minimum and maximum temperatures and the temperature rise for each location are shown in table 5.4-IV. During entry, all of the bondline temperatures, except the toroidal bondline measurement, dropped below the initial-temperature values. Some temperatures decreased during the entire entry period, whereas others temporarily decreased, then reversed and increased to the initial-temperature value. This may have been caused by reversal of the polarity of the thermocouples, and the data are unrecoverable (see section 5.15).

Toroidal heat shield.- The aft heat shield toroidal area, located at the maximum heat shield diameter, had a radius of 5.5 inches at the ablator bondline where the aft heat shield interfaced with the crew compartment heat shield. Three thermocouple plugs were located in this area: at θ = 182 deg (-Y), θ = 222 deg, and θ = 268 deg (-Z). The in-depth temperature response of the thermocouples (fig. 5.4-8) was very similar to the temperatures measured on the Apollo 4 mission. Because of the rapidly changing contour of the heat shield in the toroidal section and the resultant changes in the aerodynamic flow field, heating for the exact location of the plug was difficult to assess. The correlation of the measured and predicted temperatures on Apollo 4 was considered acceptable for evaluation of the toroidal heat shield performance.

Conical heat shield.- The postflight appearance of the Apollo 6 crew compartment heat shield was similar to that of Apollo 4. The windward side (+Z) was lightly charred from approximately θ = 45 deg to θ = 135 deg (fig. 5.4-9a). The remainder of the heat shield showed only minor effects of entry heating, except near the reaction control engines where the ablator was charred in patterns similar to Apollo 4 (fig. 5.4-9b and c). The maximum surface recession upstream of the roll engine nozzles was estimated to be 0.25 inch.

Astrosextant and telescope.- The astrosextant and telescope performed satisfactorily (fig. 5.4-10). The downstream side of the outer ablator was charred around the sextant and telescope. The inner ablator and primary thermal seal on the downstream side were discolored. The downstream side of the RTV coating on the inboard side of the telescope and sextant cans was swollen approximately 1/16 inch.

Unified side hatch.- The unified hatch was generally in preflight condition, except for paint discoloration. Associated components, such as the ingress mechanism, dump plug, extravehicular activity handles, et cetera, showed no evidence of damage. The primary thermal seal (fig. 5.4-11) was blackened on the outer edge along the top of the hatch and at the inner valley of the seal along the top and right-hand side of the hatch. However, the area did not appear to be blackened as the result of entry heating, but rather as the result of liquid leaking from the pitch engine port.

Extravehicular activity handholds.- The surfaces of the handholds were discolored, but no structural distortion or melting had occurred.

Air and stream vents.- A visual inspection could detect no debris inside the air and steam vents and little or no discoloration of the fiberglass interiors was evident.

Sea anchor.- The sea anchor attachment ring and adjancent ablator appeared to have experienced only minor heating during entry (fig. 5.4-12). Some ablator damage was incurred after landing.

Windows.- The outer panes of the windows showed no evidence of excessive heating. The hatch window showed some brown stains on the exterior surface.

Forward bulkhead.- Maximum temperatures indicated by the temperature indicator plates (temp-plates) on the forward bulkhead (-Z side) were 120° F. The temp-plates on the tunnel did not respond.

Heat shield bondline.- At the time of command module/service module separation, the heat shield bondline thermocouples indicated cold temperatures as a result of the cold-soak orientation. The minimum bondline temperature measured was - 105° F on the forward compartment at X_c = 104 in., θ = 85.2 deg. Other measurements on the command module were 10° to 20° F warmer, depending on the ablator thickness and the spacecraft orientation. There was no evidence of heat flow in the gasket areas (X_c = 23.3 in. and X_c = 81.0 in.) caused by distortions of the heat shields prior to entry. The cold temperatures to which the command module was subjected did not cause any cracks in the ablator such as those experienced by CSM 008 during the thermal vacuum test.

Bondline temperatures measured on the conical section of the heat shield are summarized in table 5.4-IV. The temperatures measured in depth in the ablator on the crew compartment and forward compartment heat shields are shown in figure 5.4-13. Except for the forward heat shield area downstream of the astrosextant, all temperatures responded equal to or higher on the Apollo 6 mission than those for the same locations on the Apollo 4 mission.

Low-density ablator experiment.- A low-density ablator experiment, developed for flight evaluation on the Apollo 6 mission, was successfully recovered intact. The three low-density materials selected for the experiment were urethane foam 5I, which has a density of 2.2 lb/ft^3; balsa wood, which has a density of 8.3 lb/ft^3; and the Apollo ablator, which, because of the 5/16-in.-diameter holes drilled through three-fourths of the local ablator thickness in each honeycomb cell, had an effective density of 20 lb/ft^3.

The flight hardware consisted of three panels. The postflight appearance of the panel in the leeward micrometeoroid window location (which contained samples of the three ablation materials) is shown in figure 5.4-14(a). The postflight conditions of the urethane foam panel and the Apollo ablator panel in the simulated umbilical region are shown in figure 5.4-14(b).

Postflight inspection of the window panel showed that entry heating had very little effect on the materials. A slight swelling of approximately 0.10 inch on the foam material was observed; the balsa wood and Apollo ablator with holes showed no significant thermal effects.

Recession of the Apollo ablator panel in the umbilical area varied from 0.030 to 0.040 inch and the char penetration varied from 0.15 to 0.20 inch. The urethane foam panel from this area had approximately 0.45 to 0.50 inch of virgin material remaining; the entire char layer was missing from the urethane foam panel, probably as a result of landing impact or wave action prior to recovery; the loss can be attributed to the weakness and fragility of the char formed during heating. Temp-plate temperature indicators (which change color at designated temperatures) attached to the stainless steel backup plate of each test panel indicated that the backface temperature did not exceed 200° F.

In summary, satisfactory thermal performance of all materials used in the experiment was demonstrated. However, the usefulness of the urethane foam material in the present form is considered to be limited because of the fragility and poor structural integrity of the material.

TABLE 5.4-I.- LOCATIONS AND RANGES OF PRESSURE SENSORS, CALORIMETERS, AND RADIOMETERS

Aft compartment										Conical section									
Pressure sensor				Wafer calorimeter			Radiometer			Pressure sensor				Calorimeter			Radiometer		
Body Point	Y_c, in.	Z_c, in.	Range, psia	Y_c, in.	Z_c, in.	Range, °F	Y_c, in.	Z_c, in.	Range, Btu/ft^2/sec	Body Point	X_c, in.	θ, deg.	Range, psia	X_c, in.	θ, deg.	Range, Btu/ft^2/sec	X_c, in.	θ, deg.	Range, Btu/ft^2/sec
701	-2.0	-2.0	10	-0.5	0.5	5000				709	26.5	91.6	2	26.5	93.7	150			
702	2.7	39.1	10	0	39.0	5000				710	50.0	88.5	2	50.0	85.3	100	52.3	88.5	50
703	1.5	55.0	10	4.2	55.2	5000	-0.5	55.0	1200	711	83.4	86.9	2	83.4	82.6	100			
704	1.8	65.0	10	0	65.0	5000				712	104.0	94.8	2	104.0	101.5	75			
705	1.5	71.8	10	4.0	71.7	5000				713	26.3	135.8	2	26.3	137.9	100			
706	-1.2	75.0	5	1.3	75.0	5000				714				78.9	137.0	75			
707	-10.6	-48.9	5	-4.7	-50.0	5000	1.0	-48.8	1200	715	18.2	176.6	2	18.2	179.4	75			
719A				12.7	-49.5	5000				716	18.5	229.5	2	18.5	225.1	75			
719				13.2	-65.2	5000				717	18.5	272.3	2	18.5	264.0	75			
708				50.0	-1.5	5000				721A				52.5	179.0	50			
720				-59.6	31.9	5000				721B	78.9	185.0	2	78.9	189.0	50			
										721C				104.0	191.5	50			
										721D				50.0	228.8	50			
										721E				78.9	226.2	50			
										721F				50.0	272.0	50	45.0	270.1	50
										721G	78.9	263.9	2	78.9	267.8	50			
										721H				104.0	274.8	50			
										Umbilical cavity				35.0	90	150			
										Umbilical frame				43.0	90	150			

TABLE 5.4-II.- HEAT SHIELD COMPONENT AND EQUIPMENT THERMAL RESPONSE

Component	Measurement no.	Location/description	Measured temperature, °F		ΔT
			Minimum	Maximum	
Aft heat shield and bulkhead	CA7608T	R_c = 58, θ_c = 290; outer mold line (OML) near bolt no. 48 and pad 5	60	60	0
	CA7609T	R_c = 58, θ_c = 228; OML near bolt no. 38 and pad 4	60	60	0
	CA7610T	R_c = 58, θ_c = 184; OML near bolt no. 31	60	33	-27
	CA7800T	Center of aluminum aft bulkhead	58	62	4
Shear/compression and compression pads	CA1478T	Y_c = -60, Z_c = 29; bondline near pad 3	55	55	0
	CA1479T	Y_c = 12, Z_c = -50; bondline near pad 5	65	58	-7
	CA1480T	Y_c = -59, Z_c = 31; bondline near pad 3	50	50	0
	CA1481T	Y_c = 11, Z_c = -50; bondline near pad 5	65	65	0
	CA5090T	Y_c = -2, Z_c = 55; bondline vicinity pad 2	68	68	0
	CA5114T	Y_c = 2, Z_c = -50; bondline vicinity pad 5	63	55	-8
Tension ties	CA1461T	Aft heat shield OML near tension tie no. 1	60	60	0
	CA1464T	Longeron, tension tie no. 1	68	72	4
	CA1465T	Tension tie no. 1 barrel nut	70	95	25
	CA7801T	Aluminum aft bulkhead near longeron no. 1	69	71	2
Block II simulated CSM umbilical	CA1441T	On Bondline: Forward slot, depth ≈1.5 in.	30	70	40
	CA1442T	On Bondline: Inside bundle	40	40	0
	CA1443T	On Bondline: Near inboard end of bundle	55	55	0
	CA1446T	Side forward slot, depth ≈1.5 in.	35	70	35
	CA1447T	Inside bundle	55	50	-5
	CA1448T	Inside bundle	45	55	10
	CA1449T	Near inboard end of bundle	55	55	0
	CA1450T	Near inboard end of bundle	55	55	0
	CA1451T	In fully simulated side heat sink	55	55	0
	CA1452T	In partially simulated side sink	60	60	0
	CA1453T	Aft compartment, housing exterior	53	55	2
	CA1454T	Aft compartment, bundle exterior	53	53	0
	CA1455T	IML at fully simulated heat sink	55	55	0
Astro-sextant	CA1502T	X_c = 65, θ_c = 71.5; heat shield OML near panel	-75	81	156
	CA5812T	θ_c ≈98; heat shield downstream of astro-sextant on Z-member	-27	167	194
	CA5813T	Aluminum honeycomb (IFIS) downstream of astro-sextant	48	58	10
	CA5814T	Aluminum optical case mount downstream of astro-sextant	53	53	0

IFIS - Inner facesheet inner surface

TABLE 5.4-II.- HEAT SHIELD COMPONENT AND EQUIPMENT THERMAL RESPONSE - Concluded

Component	Measurement no.	Location/description	Measured temperature, °F		ΔT
			Minimum	Maximum	
Astro-sextant (Concluded)	CA5815T	$\theta_c \approx 72$; aluminum honeycomb (IFIS)	53	58	5
	CA5816T	$\theta_c \approx 108$; aluminum honeycomb (IFIS)	53	58	5
	CA5817T	Aluminum optical case mount on beam	48	53	5
	CA5818T	Aluminum optical case mount downstream of astro-sextant	48	53	5
Air and steam vents	CA7603T	Leading edge air vent heat exchanger	50	100	50
	CA7875T	Aluminum steam vent tube inboard of fiberglass	62	62	0
	CA7876T	Near OML in fiberglass mount, steam vent	8	60	52
C-band antennas	CA7446T	$\theta_c = 270$, near heat sink	-3	27	30
	CA7447T	$\theta_c = 76$, $X_c = 59$; near heat sink	-48	120	168
S-band antennas	CA8520T	$\theta_c = 135$; ablator/quartz interface	-20	230	250
	CA8521T	$\theta_c = 225$; 0.7 in. from quartz surface	20	185	165
	CA8522T	$\theta_c = 135$; near heat sink	-2	20	22
	CA8523T	$\theta_c = 225$; near heat sink	18	30	12
Launch escape tower leg wells	CA0210T	$X_c = 87$, $\theta_c = 135$; well wall	-52	-37	15
	CA0211T	$X_c = 87$, $\theta_c = 225$; well backwall	-32	-5	27
	CA0212T	$\theta_c = 135$; leg stud nut in longeron	40	45	5
Stringers and attach ring	CA1509T	$X_c = 65$, $\theta_c = 321$; OML near stringer no. 13	-35	58	93
	CA3600T	$X_c = 42$, $\theta_c = 90$; on attach ring	60	60	0
	CA3601T	$X_c = 42$, $\theta_c = 270$; on attach ring	35	45	10
	CA3640T	$X_c = 50$, $\theta_c = 90$; on stringer no. 5	25	30	5
	CA3641T	$X_c = 50$, $\theta_c = 182$; on stringer no. 10	20	42	22
	CA3642T	$X_c = 50$, $\theta_c = 247$; on hatch stringer no. 120	0	38	38
Windows	CA7820T	Left side window at OML	4	70	66
	CA7821T	Left side heat shield window frame	0	35	35
	CA7822T	Left side pressure vessel frame	53	63	10
Forward compartment and equipment	CA7674T	Forward cylinder ring, forward of main parachute pack	40	40	0
	CA7675T	Forward bulkhead aft of main parachute pack	45	45	0
	CA7760T	Pilot parachute mortar can	50	50	0
	CA7761T	Main parachute riser	35	37	2
	CA7762T	Main parachute pack	-21	-27	-6

IFIS - Inner facesheet inner surface

TABLE 5.4-III.- PRELIMINARY ABLATOR RECESSION AND CHAR DEPTH MEASUREMENTS AT INSTRUMENT LOCATIONS ON AFT HEAT SHIELD

Location		Surface loss, in.	Char thickness, in.
R_c, in.	θ, deg		
2.0	350.6	Unknown	0.55
39.1	92.2	Unknown	0.65
55.1	92.1	Unknown	0.65
65.1	92.4	Unknown	0.65
71.8	90.0	0.1	0.65
50.0	272.3	0.05	0.5
66.7	154.1	Unknown	0.55
51.1	283.6	Unknown	0.55

TABLE 5.4-IV.- HEAT SHIELD BONDLINE TEMPERATURES

Component	Thermocouple number	Body location		Temperature at 400 000 ft, °F	Maximum temperature, °F	ΔT
		R_c, in.	θ, deg.			
Aft heat shield	CA5080T	2.0	350.6	43	43	a
	CA5090T	55.1	92.1	68	68	a
	CA5095T	65.1	92.4	60	60	a
	CA5100T	71.8	90.0	75	30	a
	CA5105T	74.9	92.0	33	155	122
	CA5114T	50.0	272.3	63	55	a
	CA5115T	50.0	1.7	74	74	a
	CA1478T	66.7	154.1	55	55	a
	CA1480T	66.6	152.7	50	50	a
	CA1481T	51.1	282.9	65	65	a
		X_c, in.	θ, deg.			
Conic heat shield (windward)	CA5703T	25.2	90.0	-38	40	78
	CA5708T	50.0	92.0	-23	53	76
	CA5713T	83.4	93.1	-60	73	133
	CA5717T	104.0	85.2	-105	-52	53
	CA5723T	26.1	134.6	-43	70	113
	CA5725T	78.9	135.2	-90	150	240
	CA5738T	50.0	177.5	-80	83	163
	CA5742T	78.9	176.8	-80	78	158
	CA1502T	65.0	71.5	-75	81	156
Conic heat shield (leeward)	CA5733T	18.2	182.3	30	130	100
	CA5747T	104.0	184.8	-80	20	100
	CA5752T	18.5	221.6	30	45	15
	CA5755T	50.0	226.9	-20	90	110
	CA5760T	78.9	230.5	-33	53	86
	CA5767T	18.5	267.7	27	35	8
	CA5790T	45.0	270.0	20	63	43
	CA5777T	78.9	272.2	10	100	90
	CA5782T	104.0	281.5	-45	110	155
	CA1505T	65.0	200.0	-51	73	124
	CA1509T	65.0	321.0	-35	58	93

[a]Data not valid.

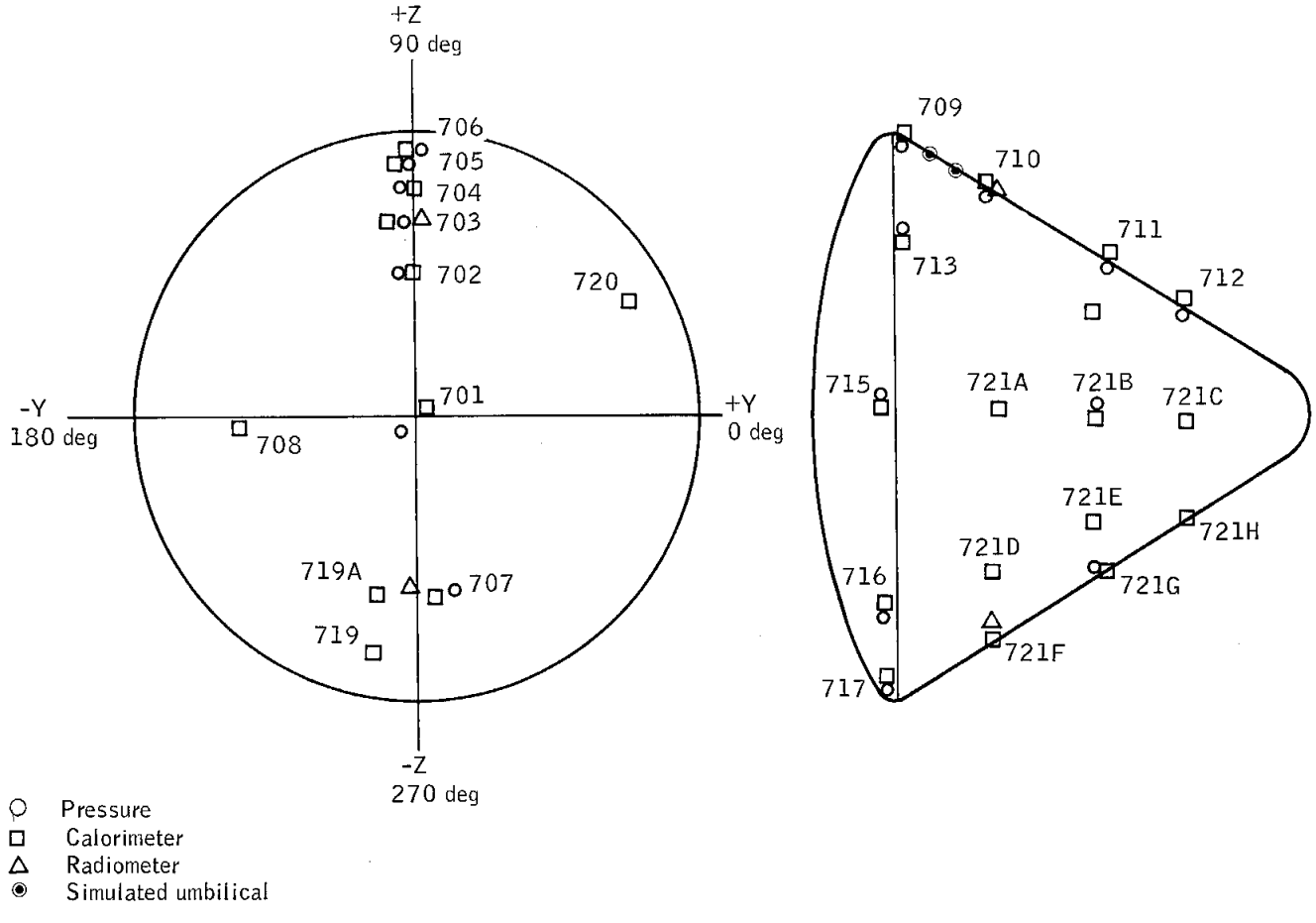

Figure 5.4-1.- Sketch of command module showing locations of aerothermodynamic sensors.

NASA-S-68-3660

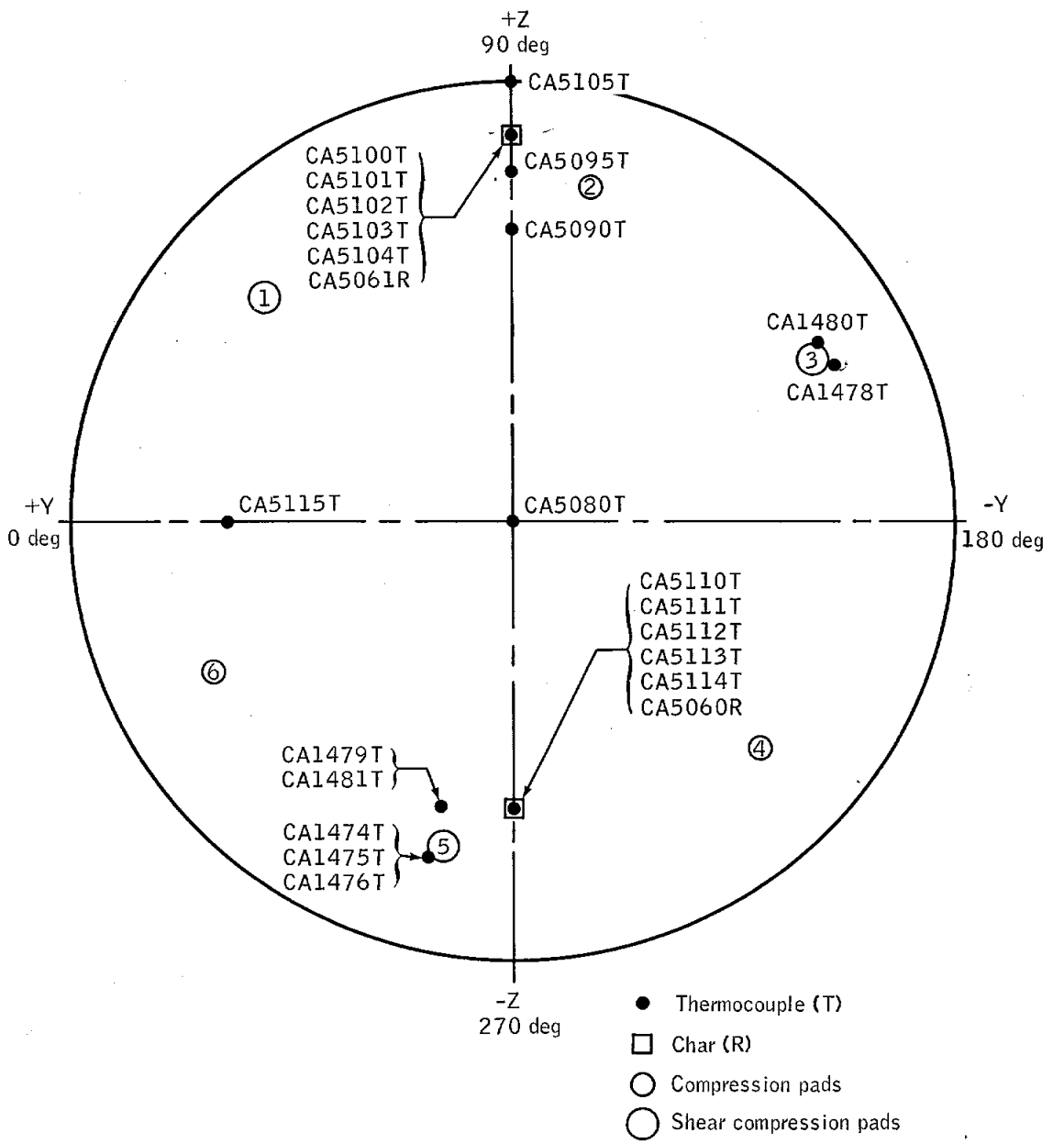

Figure 5.4-2.- Aft heat shield thermocouple and char sensor measurements.

NASA-S-68-3661

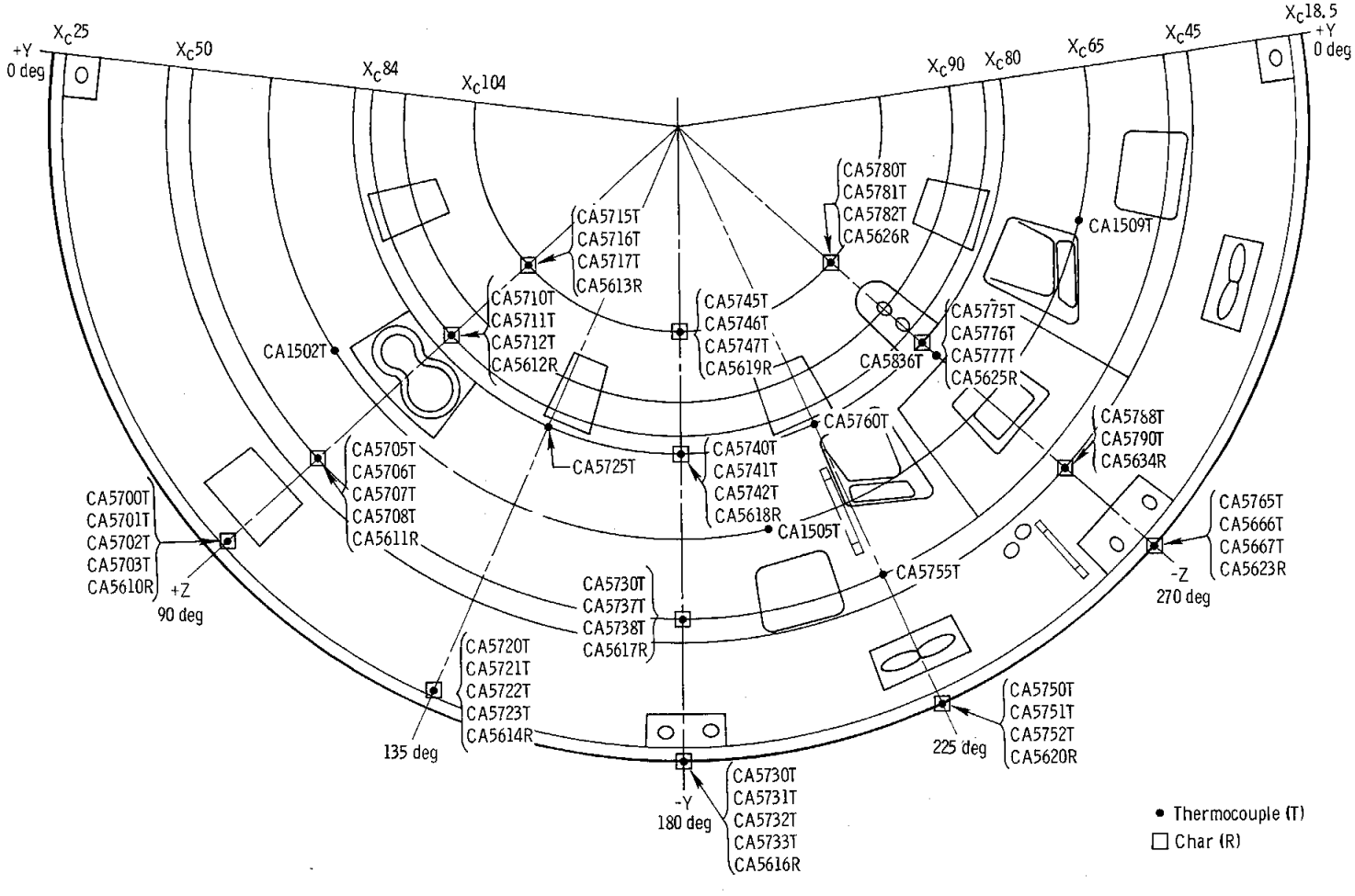

Figure 5.4-3. - Conical heat shield ablator and astro-sextant area temperature and char measurements.

NASA-S-68-3662

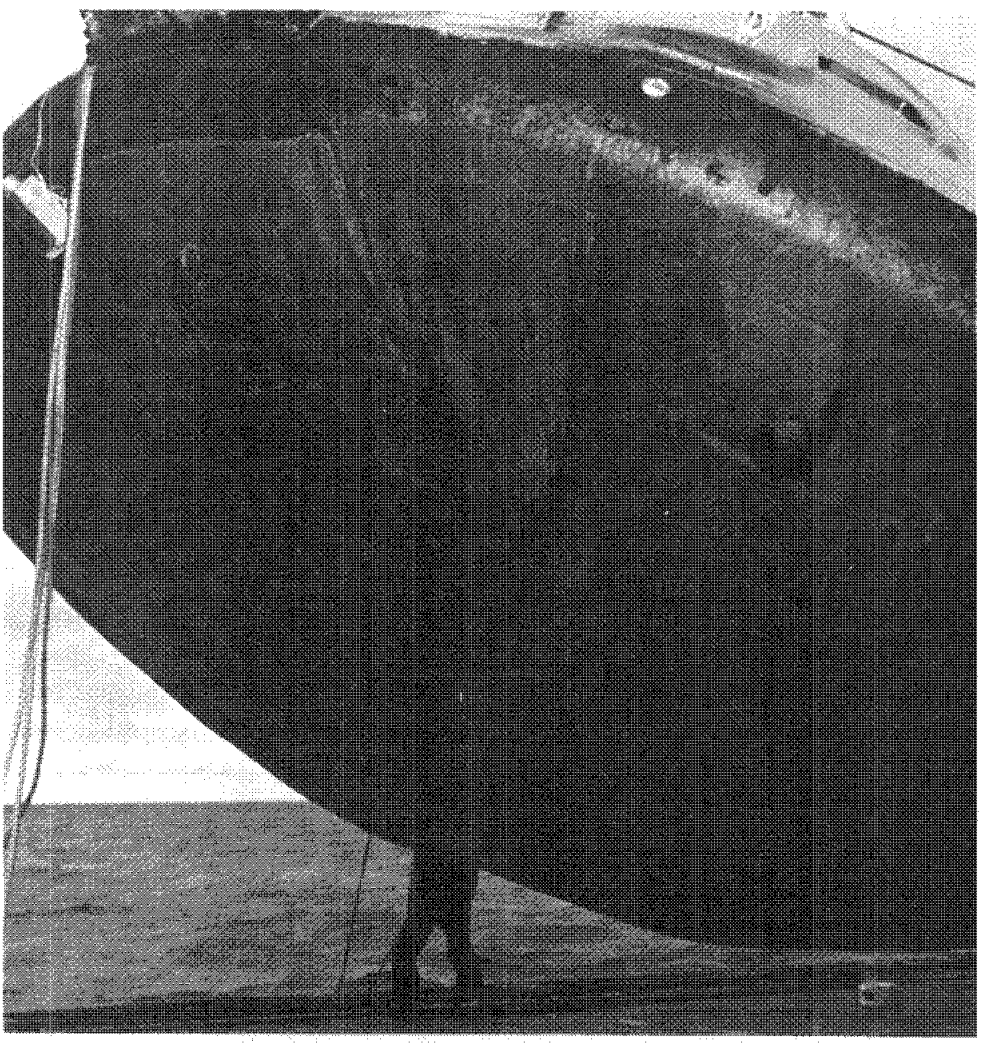

(a) Overall view.

Figure 5.4-4.- Char condition of aft heat shield.

NASA-S-68-3663

(b) Typical shear compression pad showing tension-tie rod.

Figure 5.4-4.- Continued.

NASA-S-68-3664

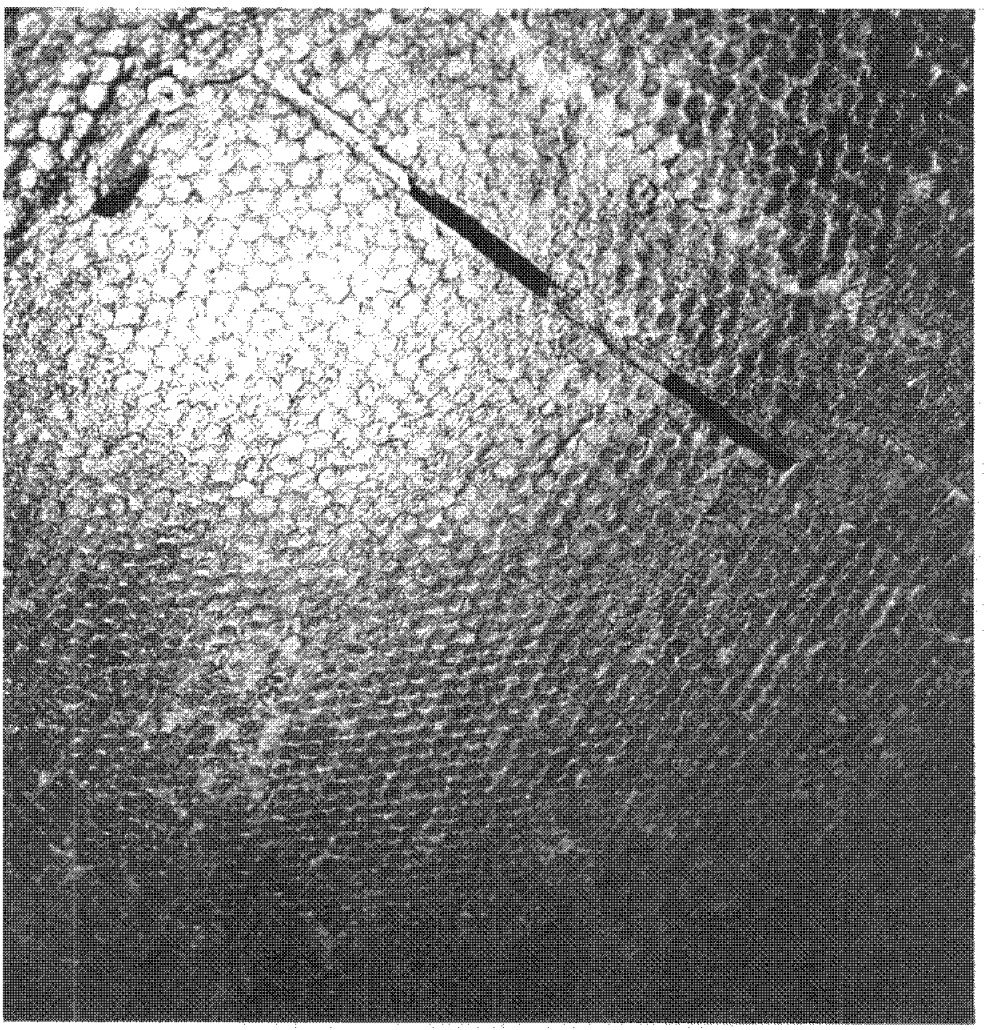

(c) Closeup view of splice area.

Figure 5.4-4.- Concluded.

NASA-S-68-3673

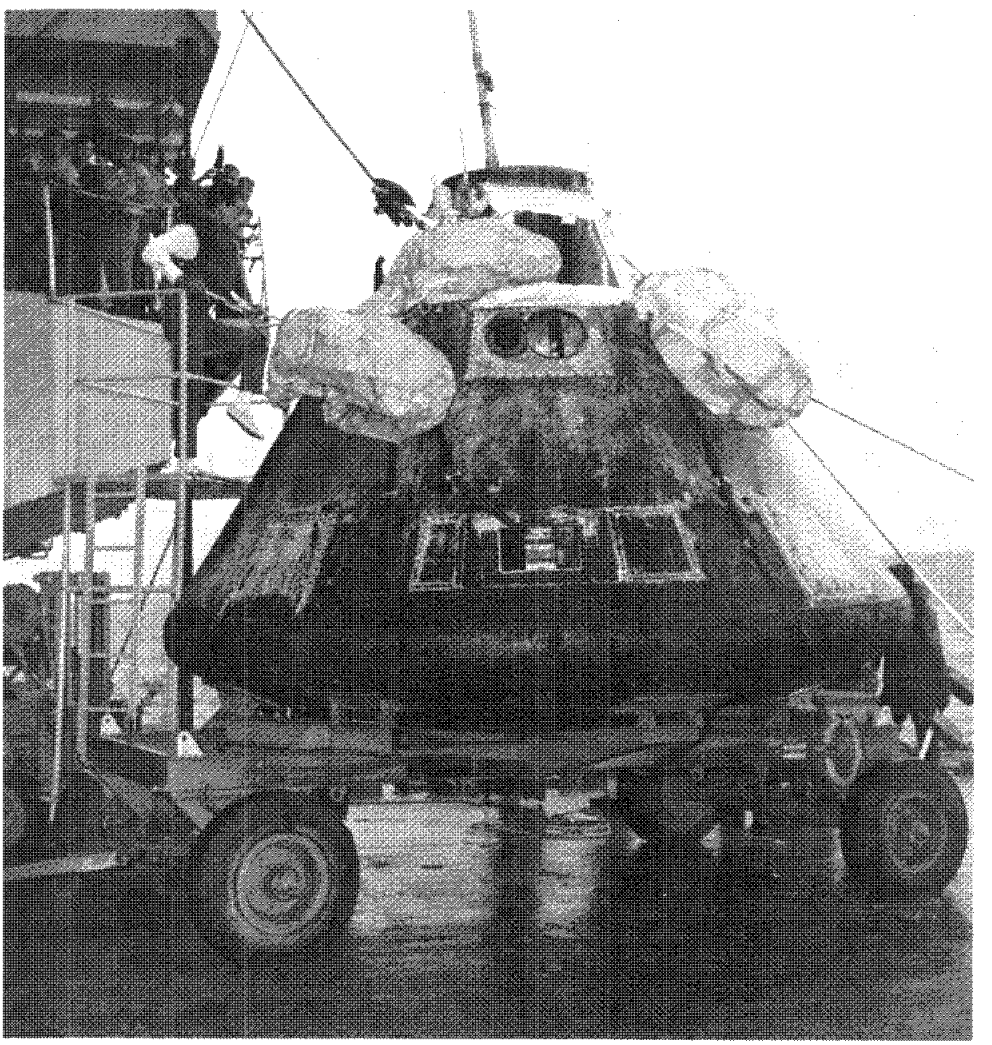

(a) +Z windward side of spacecraft.

Figure 5.4-9.- Conical heat shield.

NASA-S-68-3666

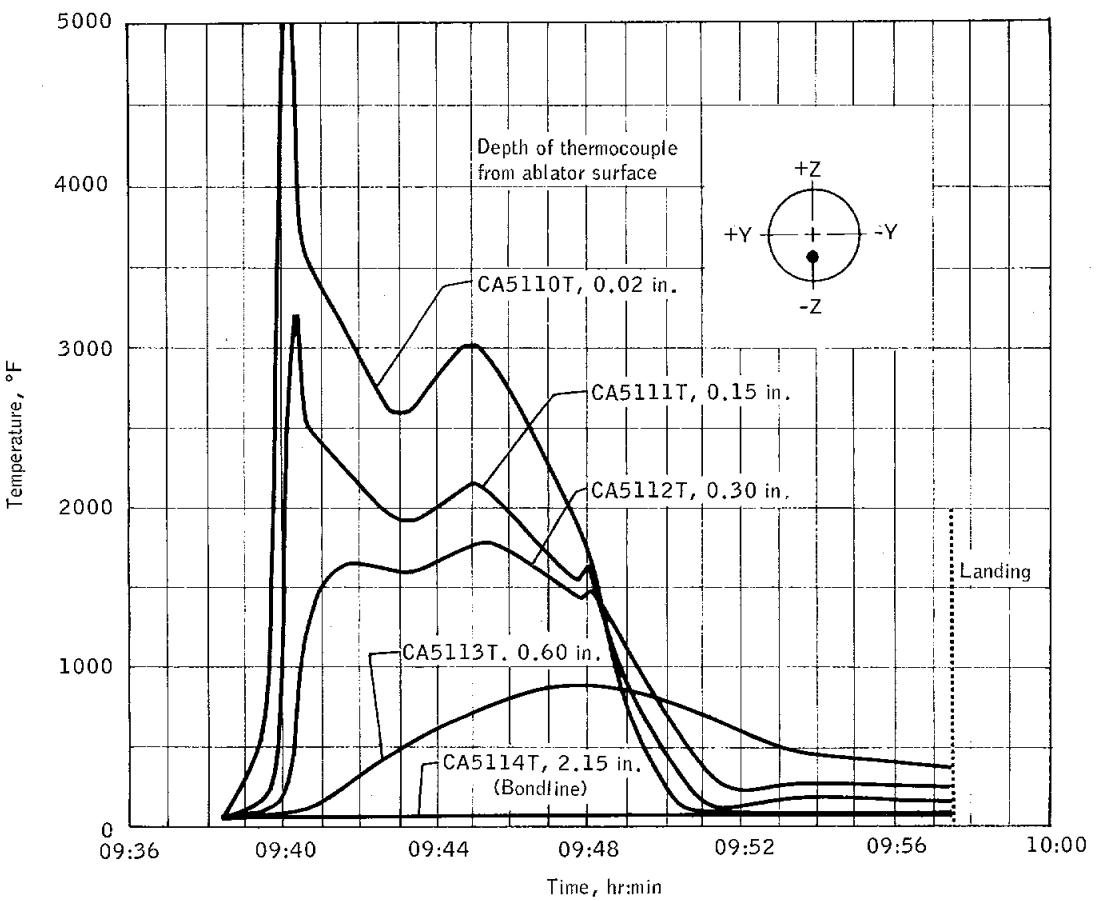

(b) R_c = 50 in.; θ = 272 deg.

Figure 5.4-5.- Continued.

NASA-S-68-3667

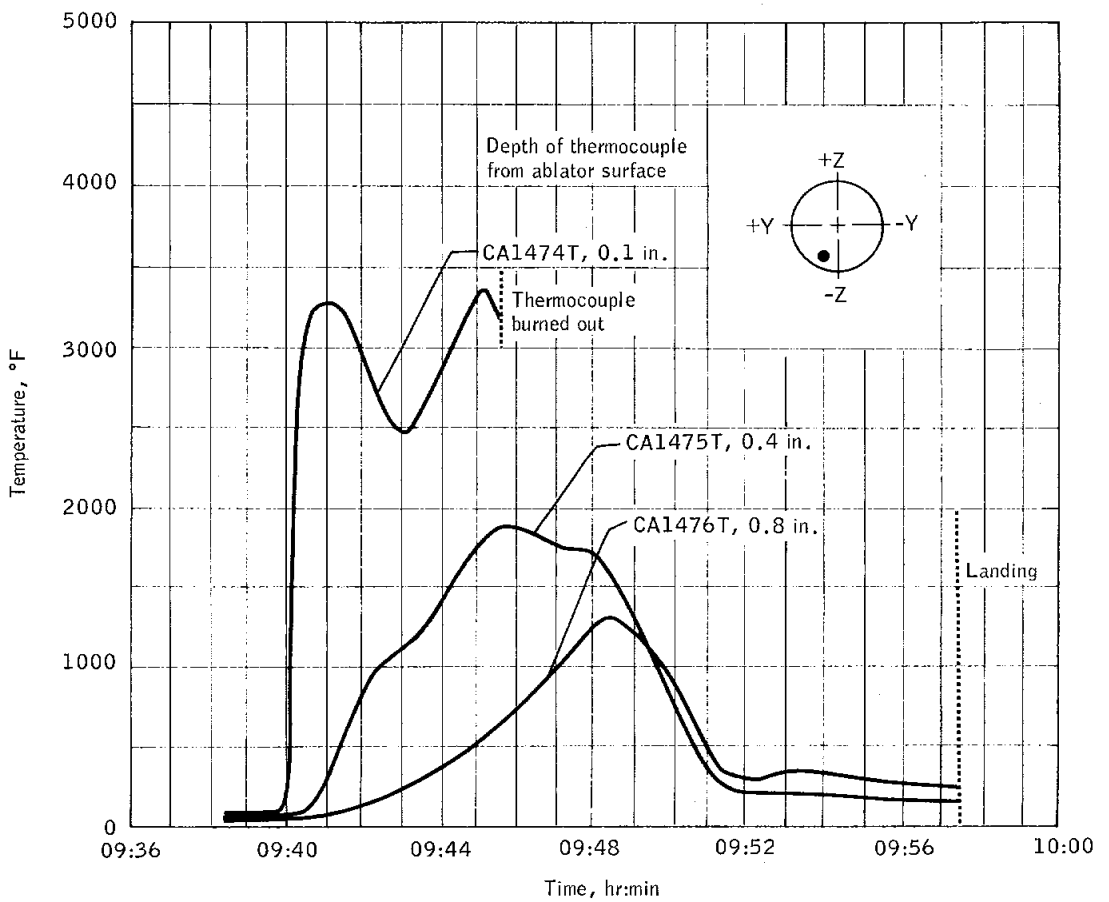

(c) R_c = 65 in.; θ = 283 deg.

Figure 5.4-5.- Concluded.

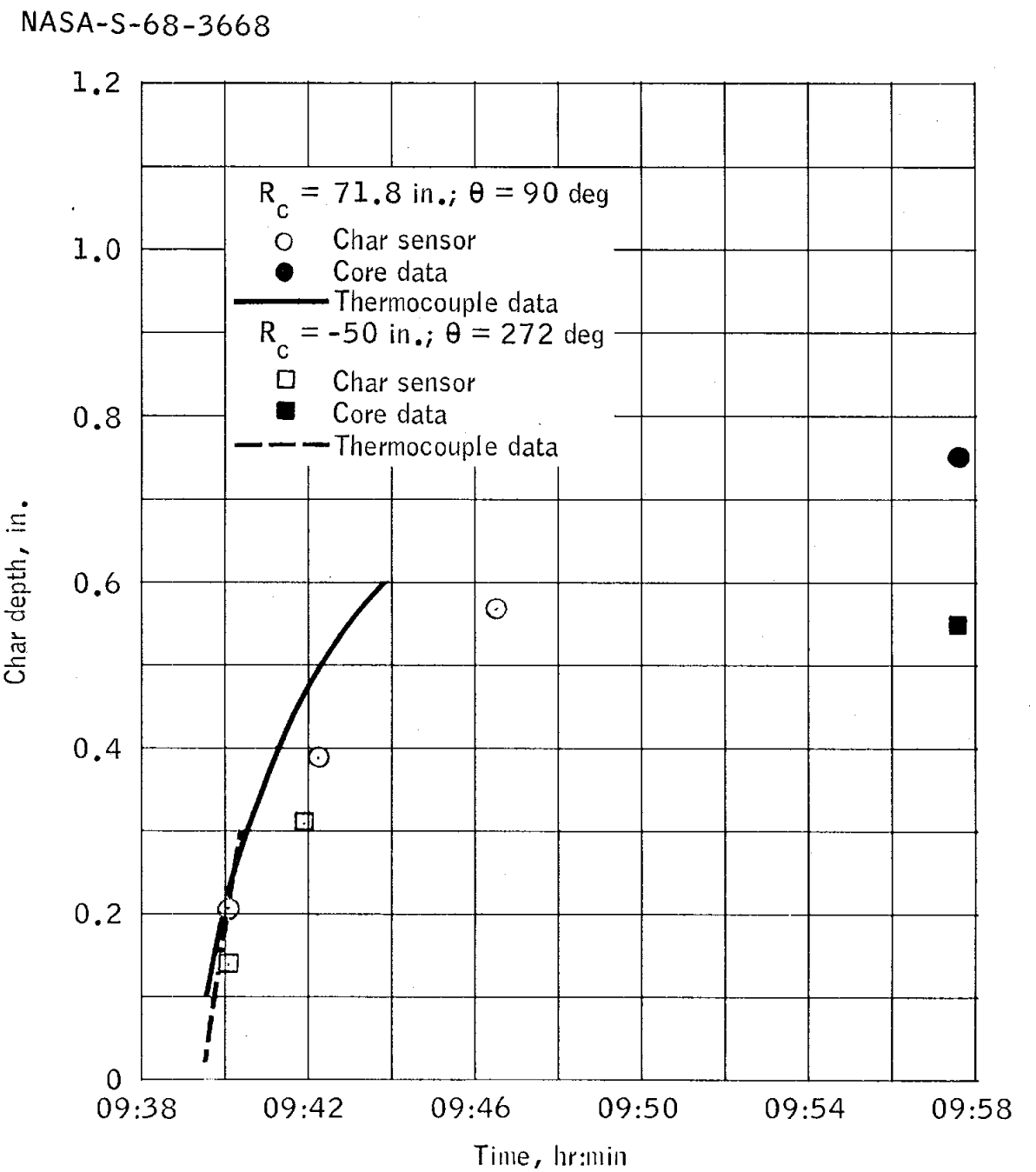

Figure 5.4-6.- Aft heat shield 1000 °F isotherm comparison with char sensor and char core measurements.

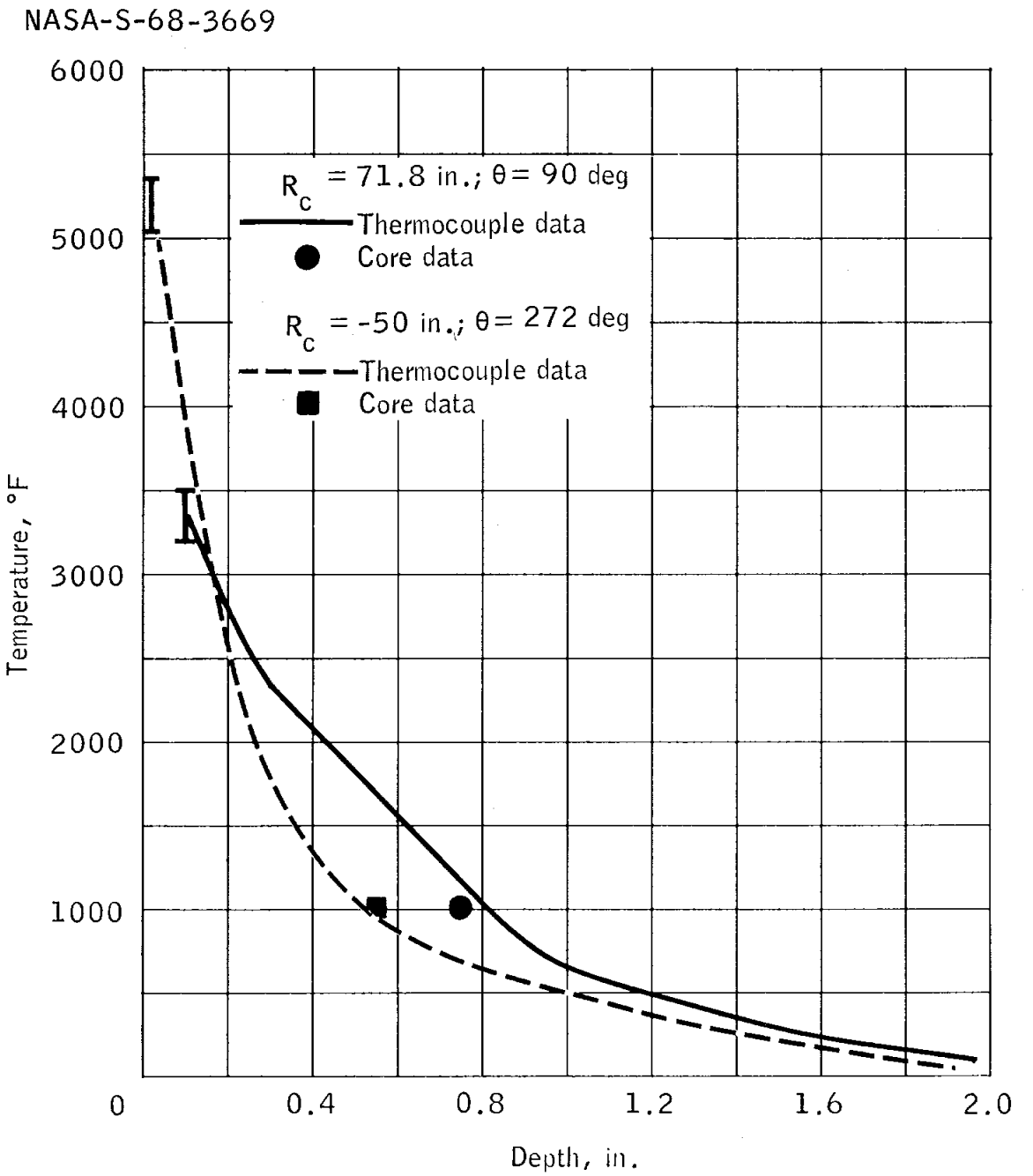

Figure 5.4-7.- Maximum temperatures measured in depth and comparison of char interface with 1000 °F isotherm.

NASA-S-68-3670

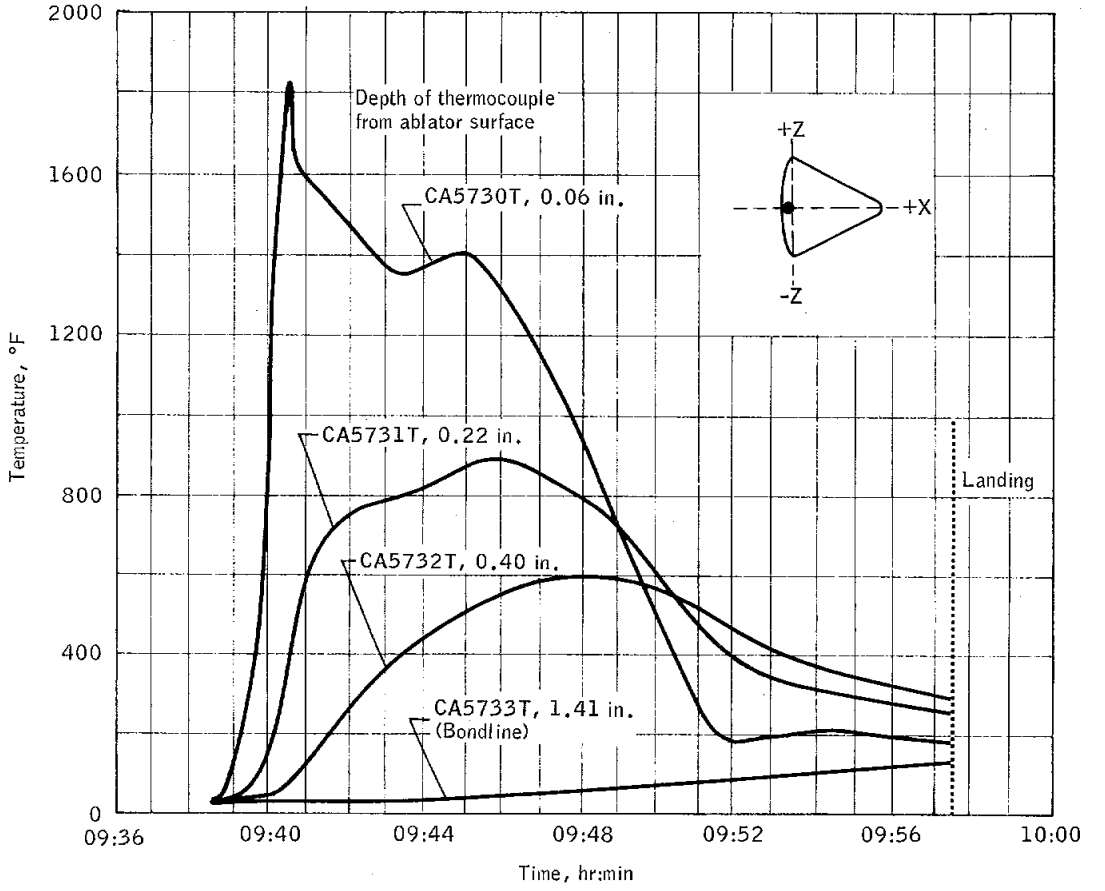

(a) X_c = 18.2 in.; θ= 182 deg.

Figure 5.4-8.- Torroidal heat shield temperature measurements at depths indicated.

NASA-S-68-3671

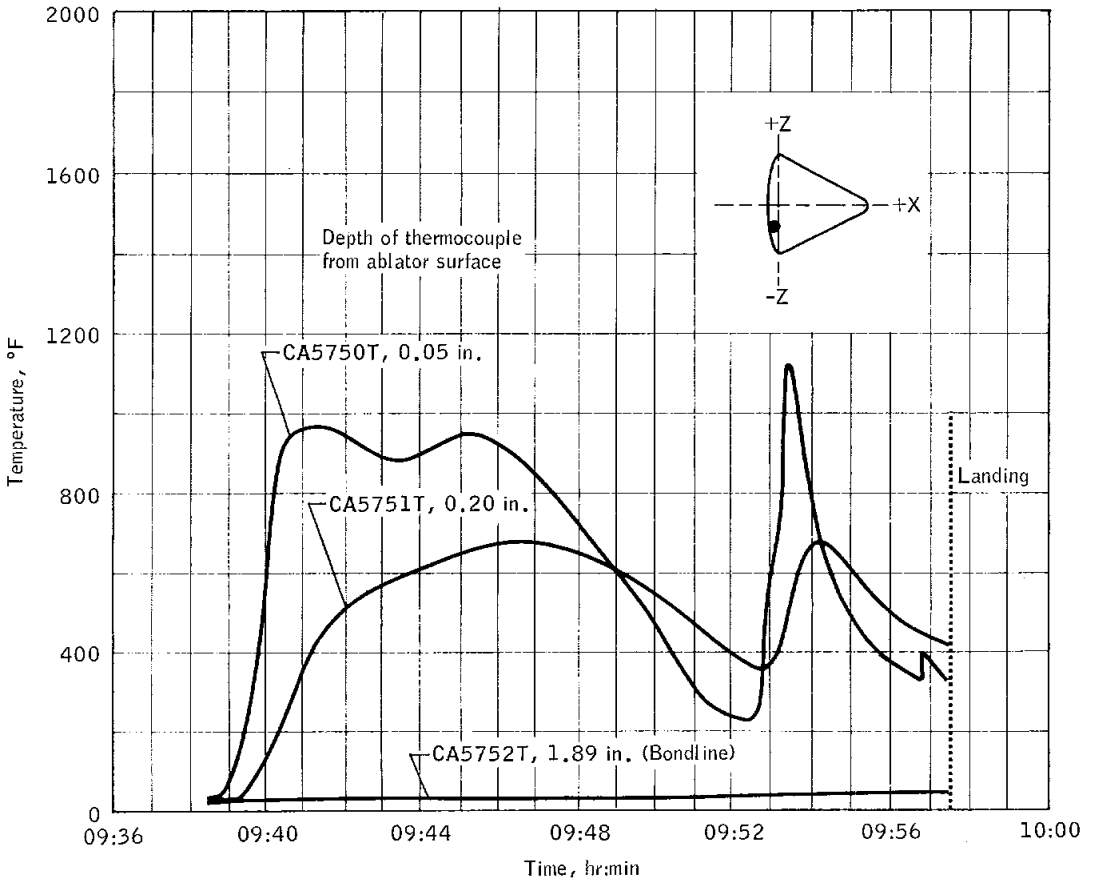

(b) X_c = 18.5 in.; θ = 221 deg.

Figure 5.4-8.- Continued.

NASA-S-68-3672

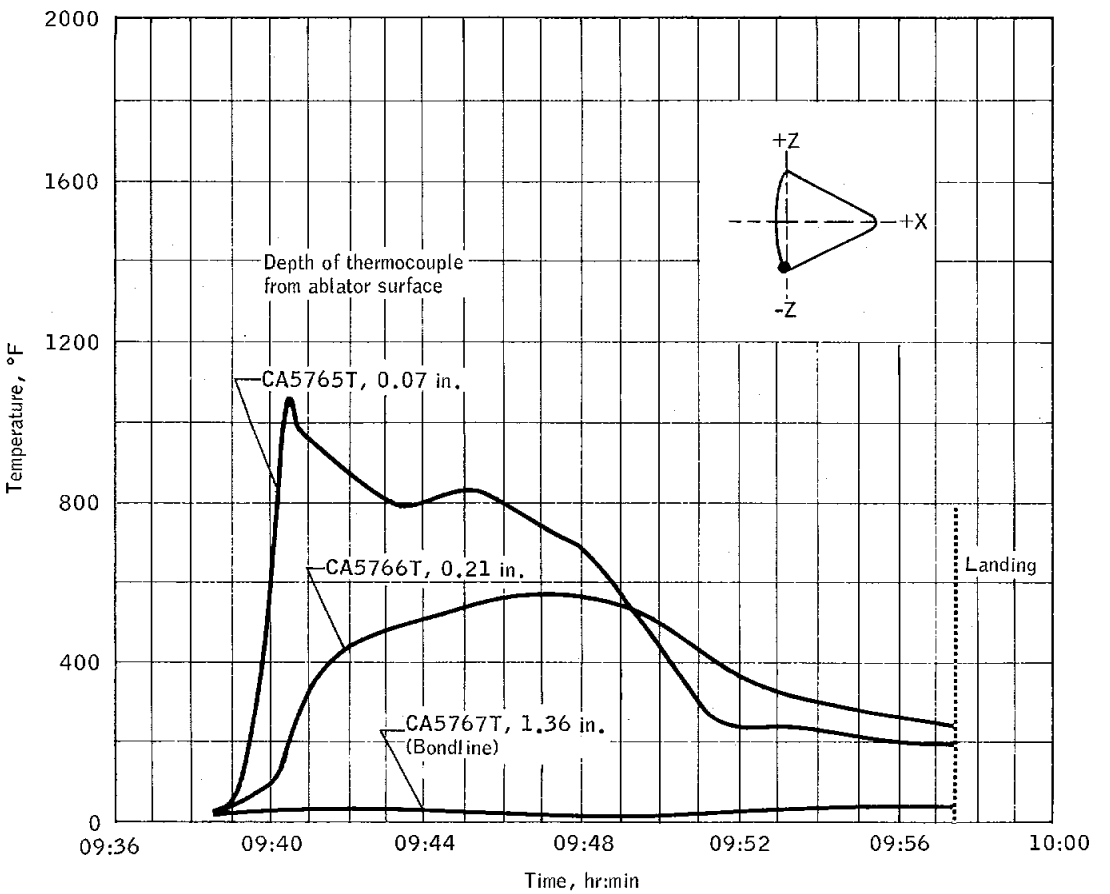

(c) X_c = 18.5 in.; θ = 268 deg.

Figure 5.4-8.- Concluded.

NASA-S-68-3673

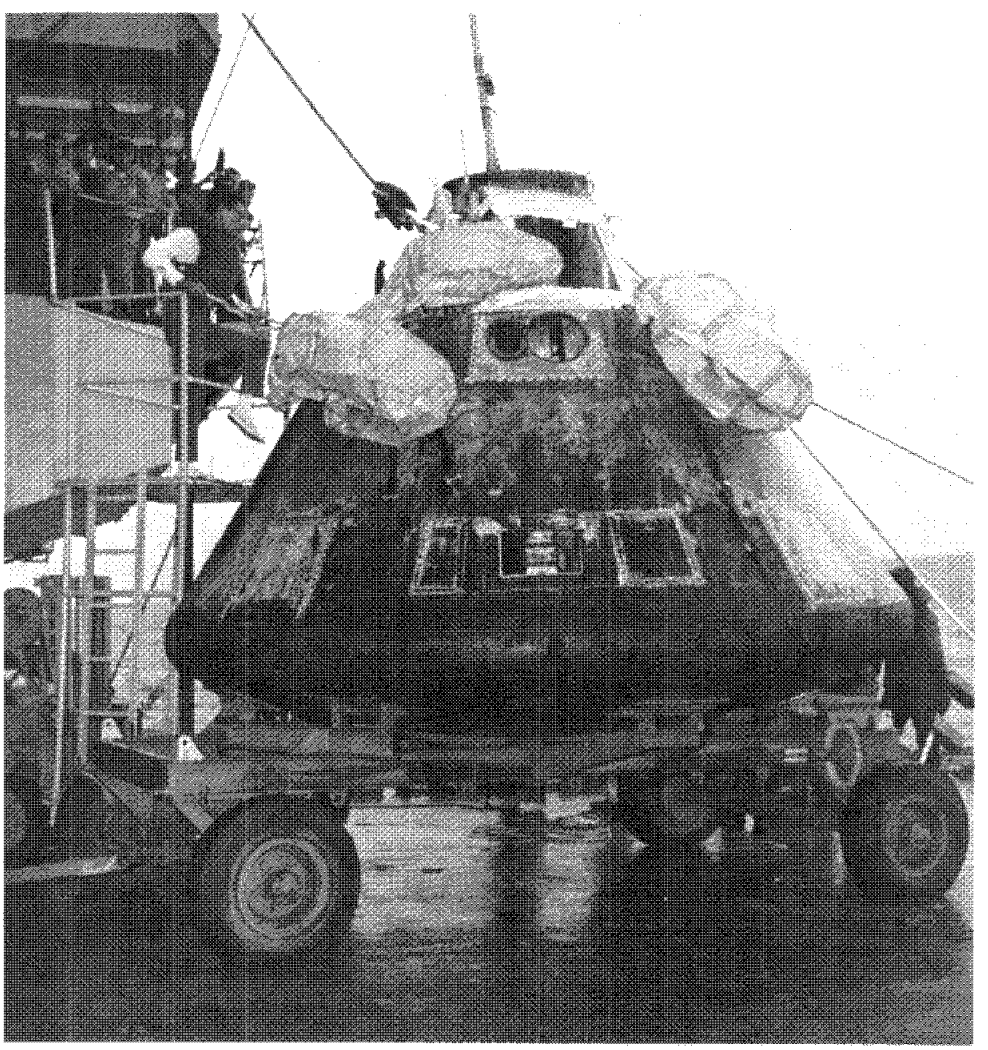

(a) +Z windward side of spacecraft.

Figure 5.4-9.- Conical heat shield.

NASA-S-68-3674

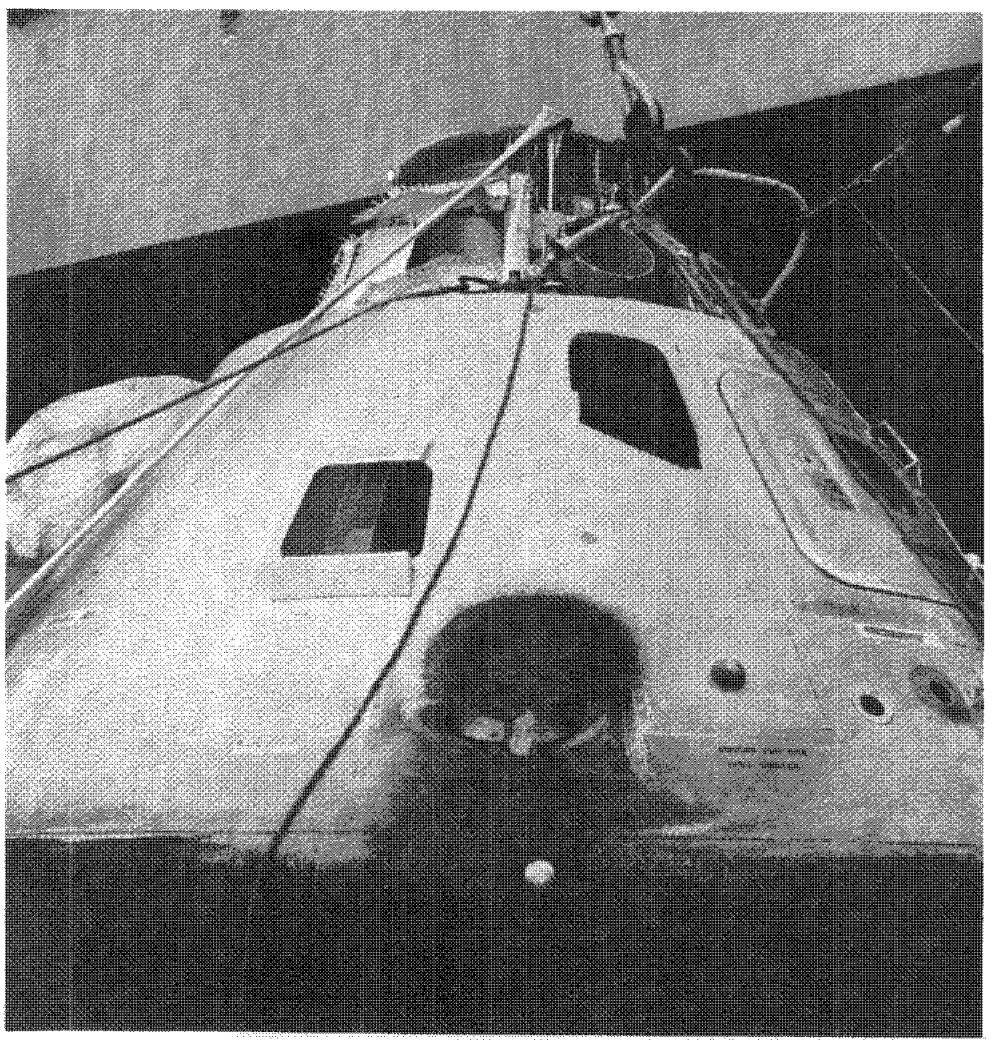

(b) -Y axis to -Z axis.

Figure 5.4-9.- Continued.

NASA-S-68-3675

(c) -Z axis to +Y axis.

Figure 5.4-9.- Concluded.

NASA-S-68-3676

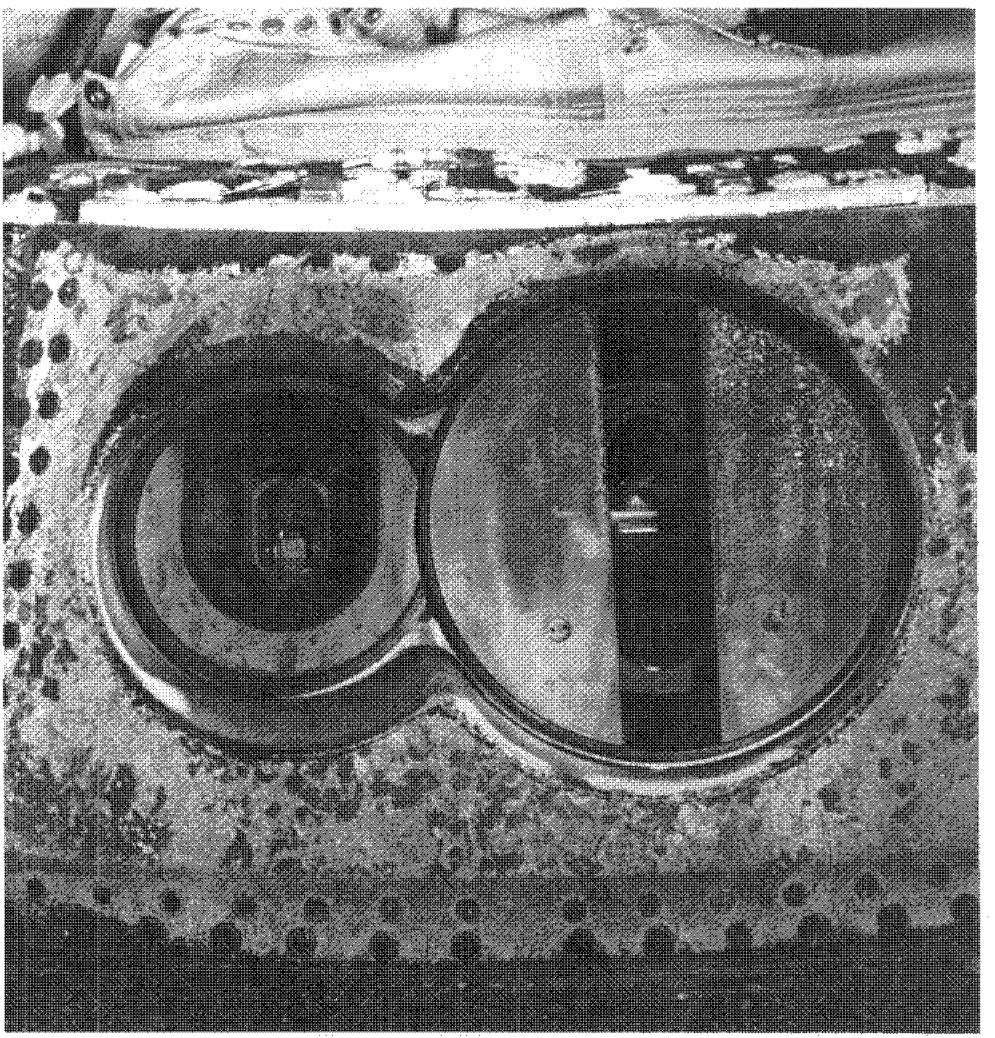

Figure 5.4-10.- Astro-sextant and telescope area.

NASA-S-68-3677

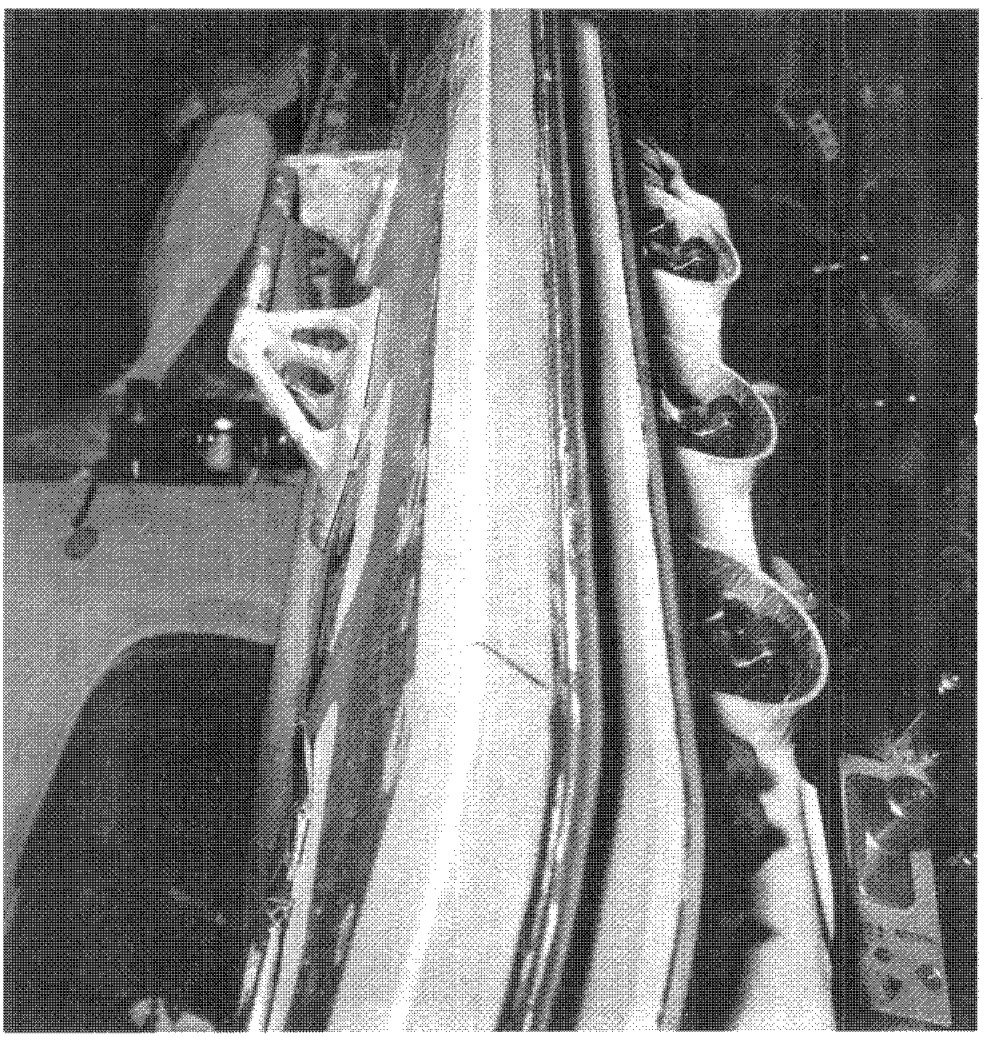

Figure 5.4-11.- Thermal seal of unified hatch.

NASA-S-68-3678

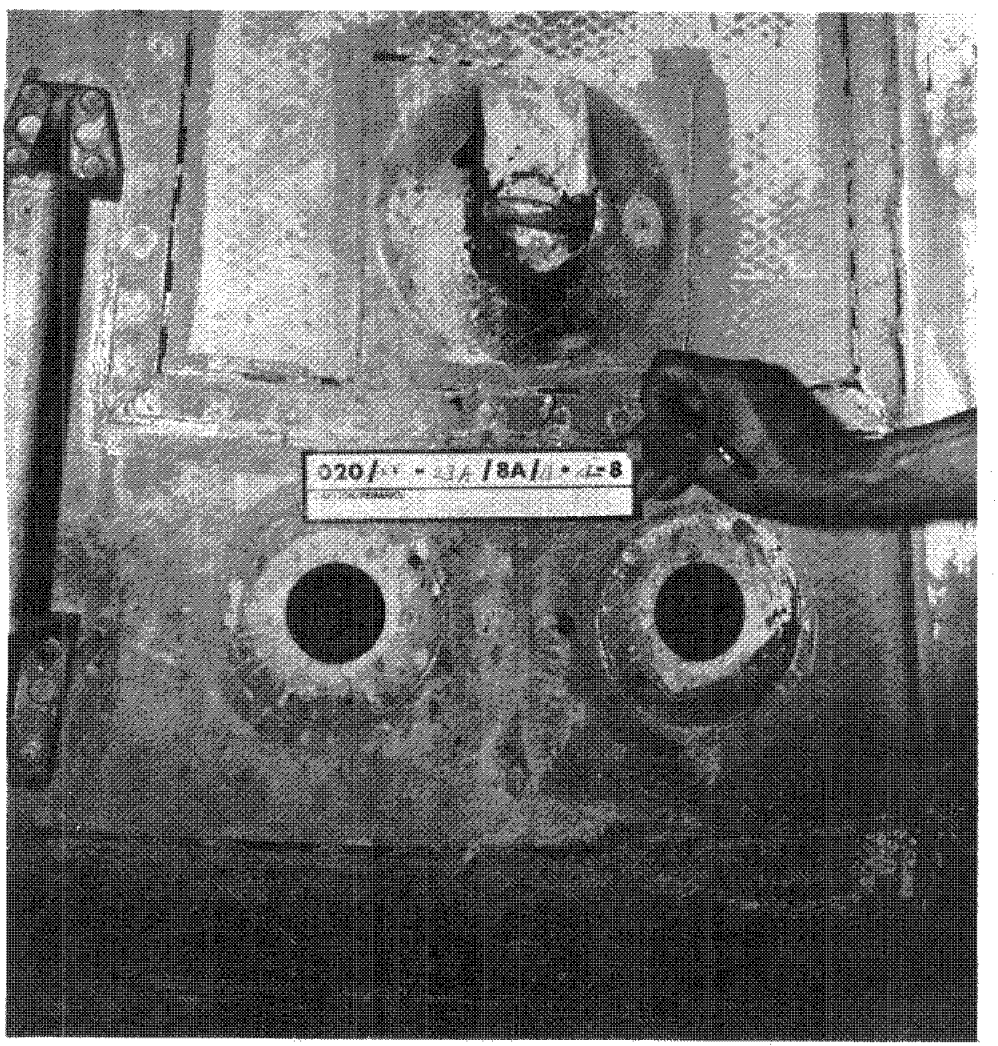

Figure 5.4-12.- Sea anchor attach ring.

NASA-S-68-3679

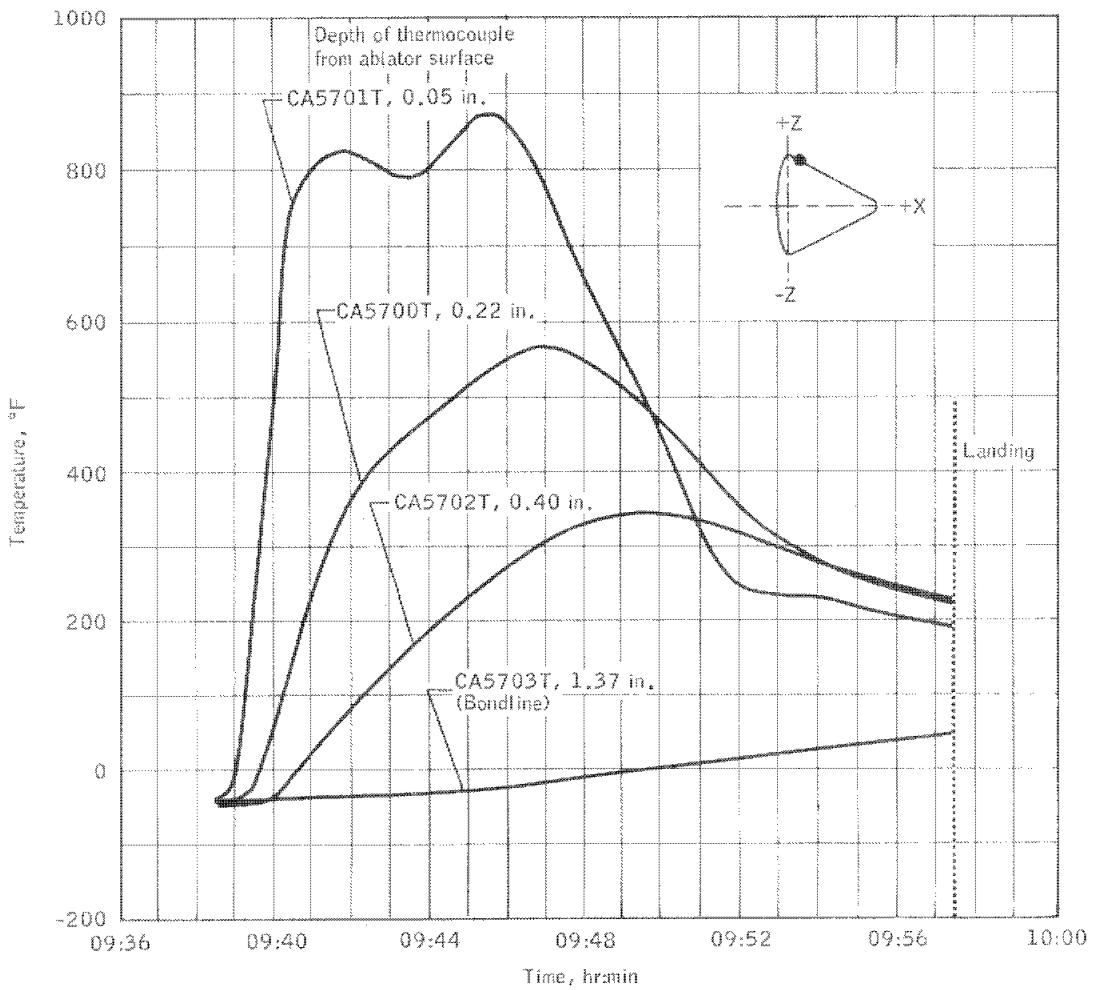

(a) X_c = 25.7 in.; θ = 89 deg.

Figure 5.4-13.- Conical heat shield temperature measurements at depths indicated.

NASA-S-68-3680

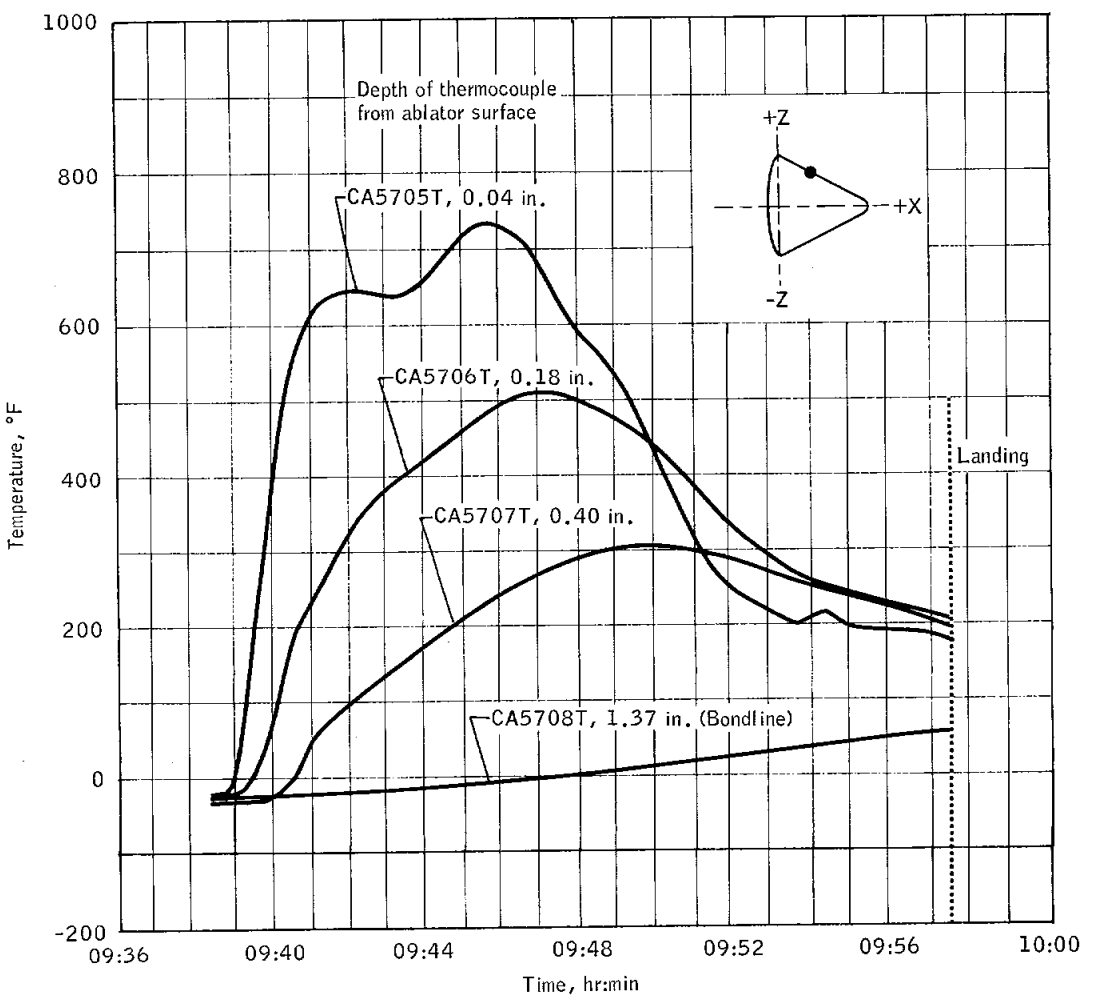

(b) X_c = 50 in.; θ = 93 deg.

Figure 5.4-13.- Continued.

NASA-S-68-3681

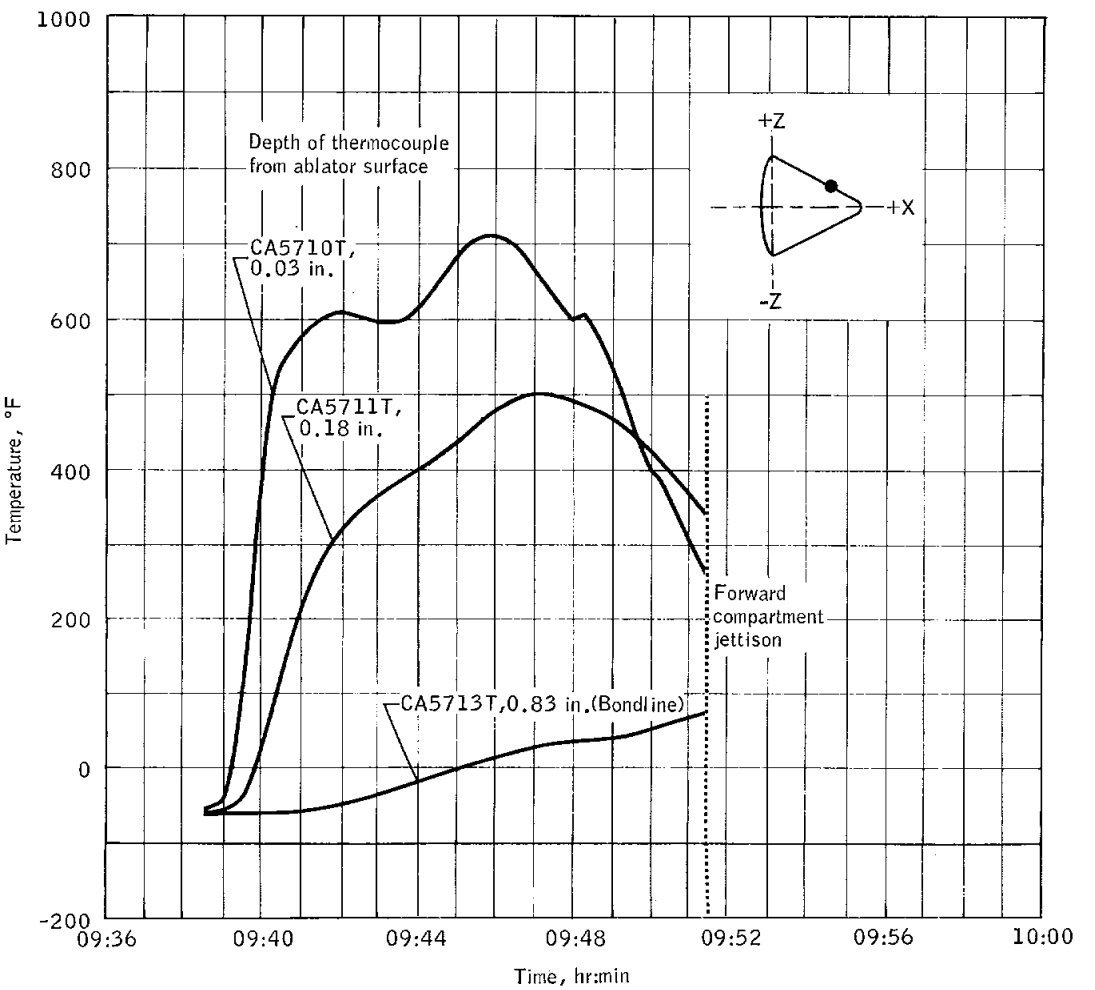

(c) X_c = 83.4 in.; θ = 95 deg.

Figure 5.4-13.- Continued.

NASA-S-68-3682

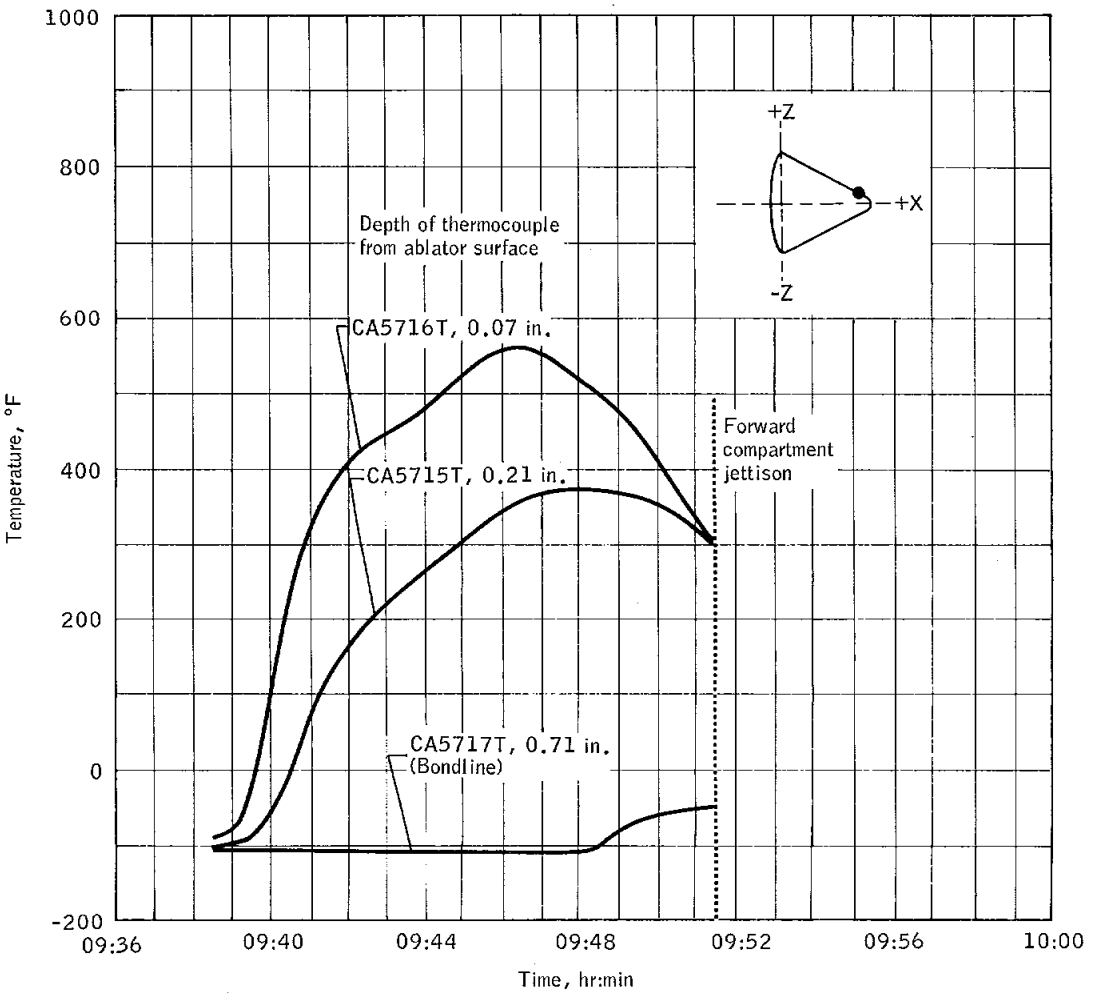

(d) X_c = 104 in.; θ = 81 deg.

Figure 5.4-13.- Continued.

NASA-S-68-3683

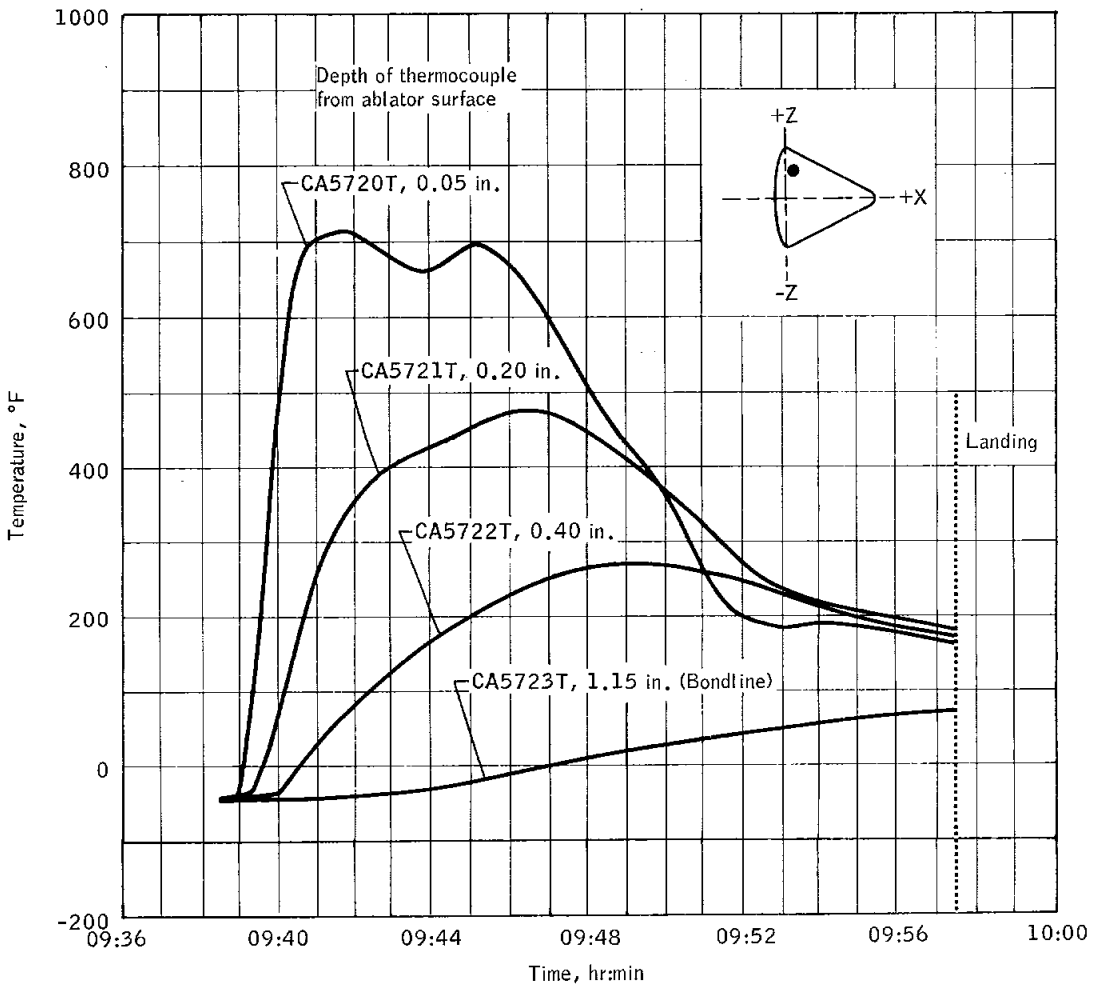

(e) X_c = 26.1 in. ; θ= 133 deg.

Figure 5.4-13.- Continued.

NASA-S-68-3684

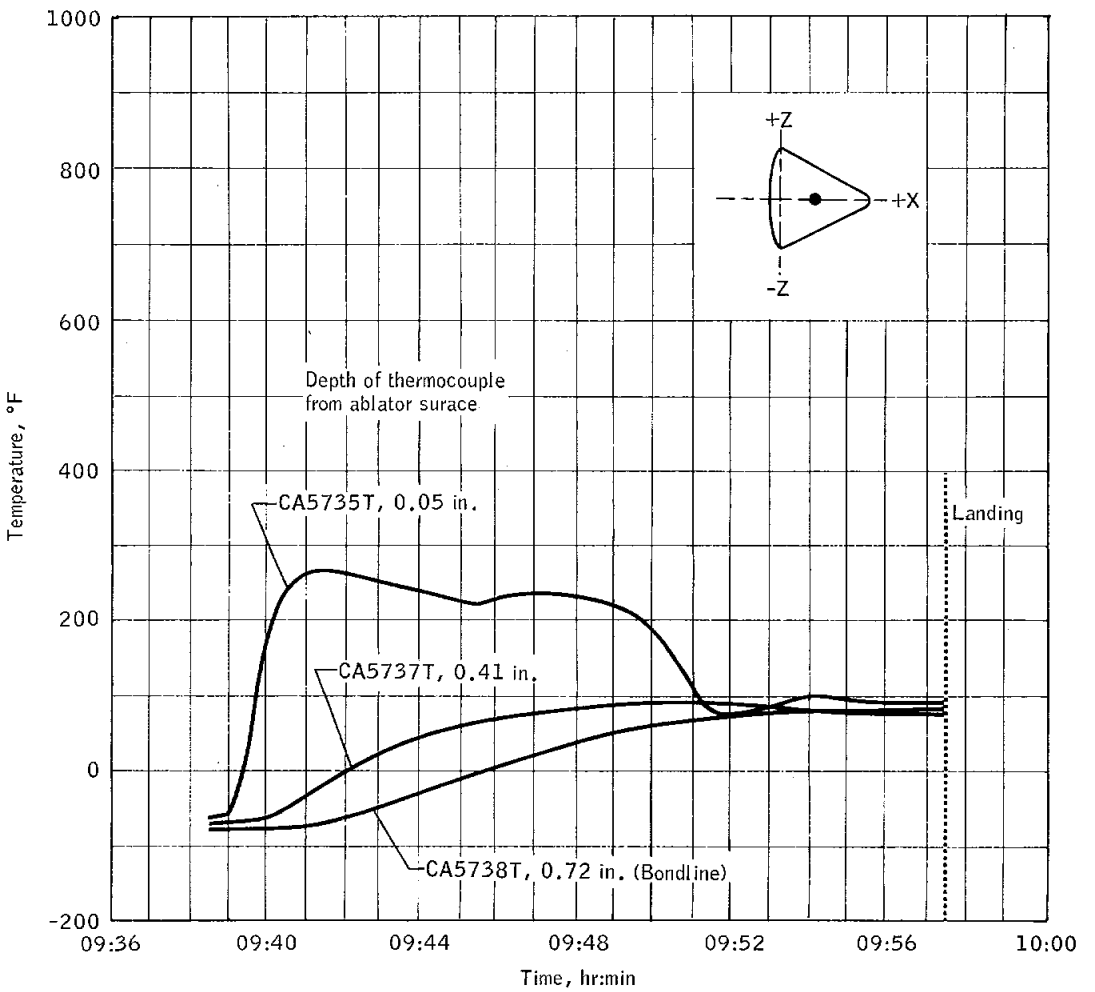

(f) X_c = 50 in. ; θ = 179 deg.

Figure 5.4-13.- Continued.

NASA-S-68-3685

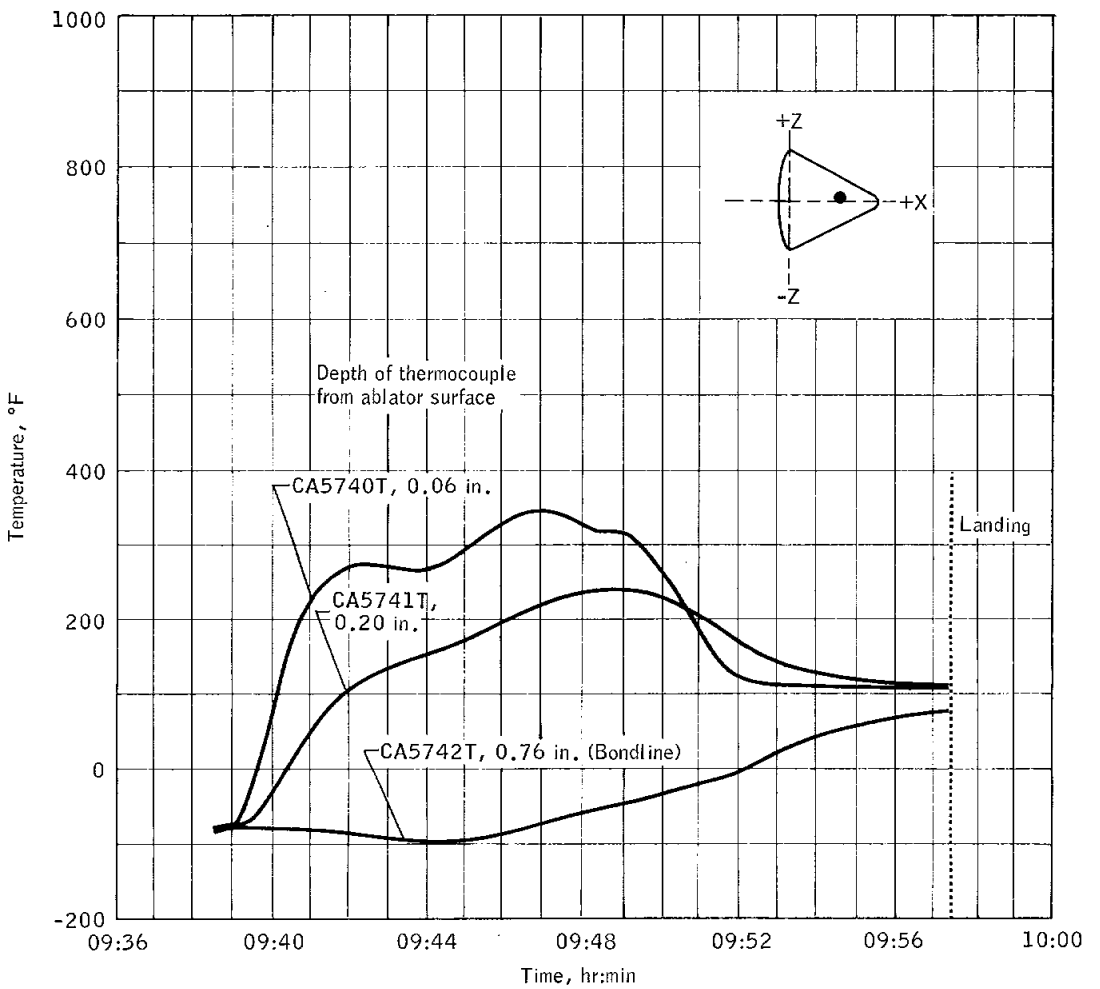

(g) X_c = 78.9 in.; θ = 175 deg.

Figure 5.4-13.- Continued.

NASA-S-68-3686

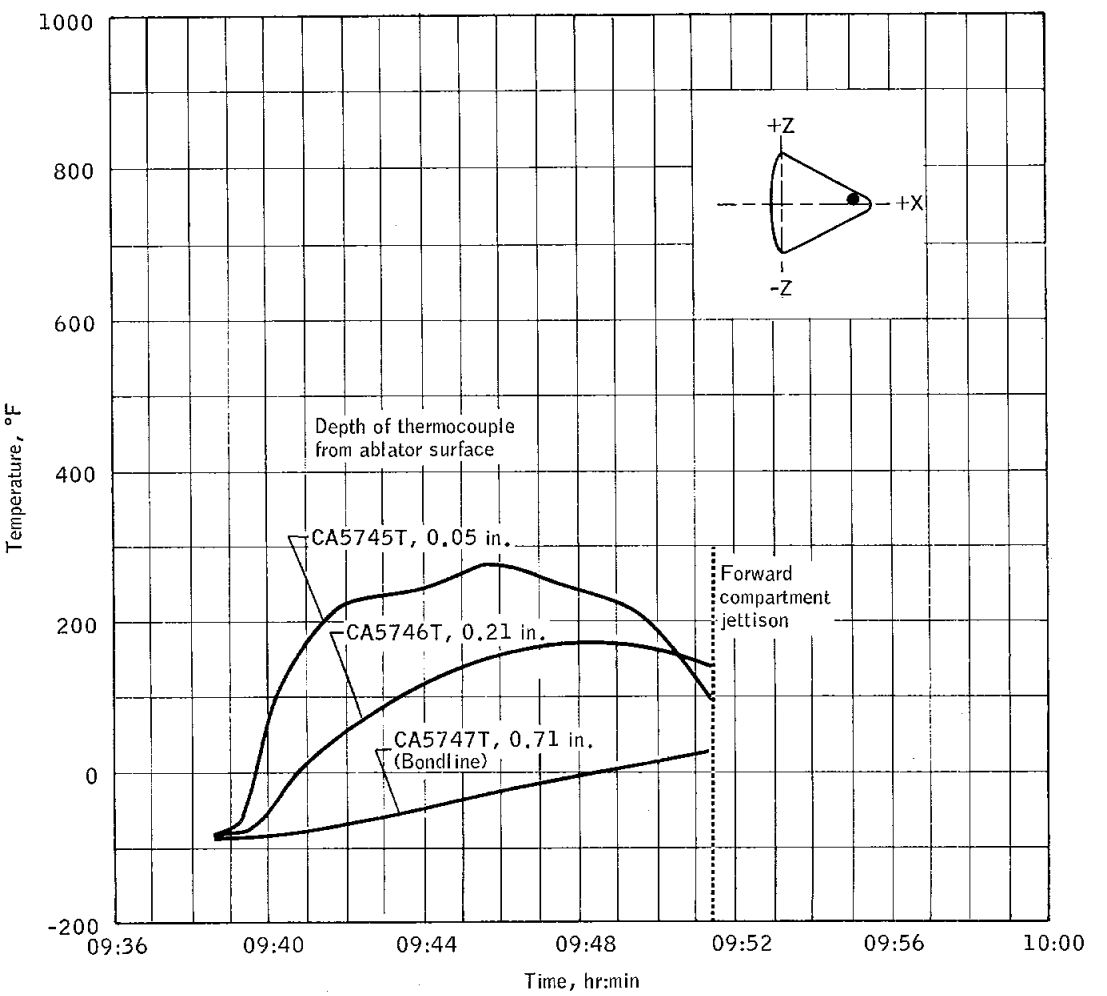

(h) X_c = 104 in.; θ = 170 deg.

Figure 5.4-13.- Continued.

NASA-S-68-3687

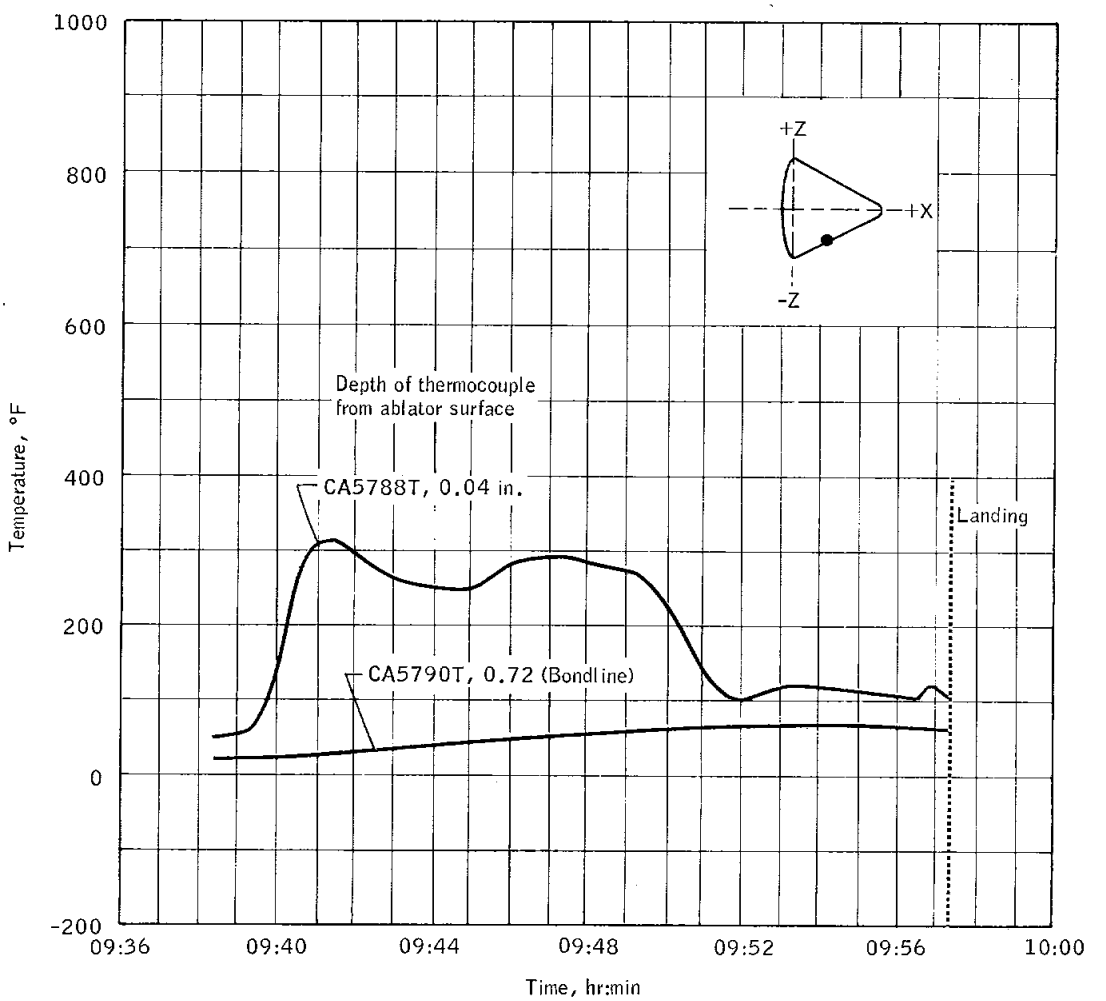

(i) X_c = 45 in.; θ = 270 deg.

Figure 5.4-13.- Continued.

NASA-S-68-3688

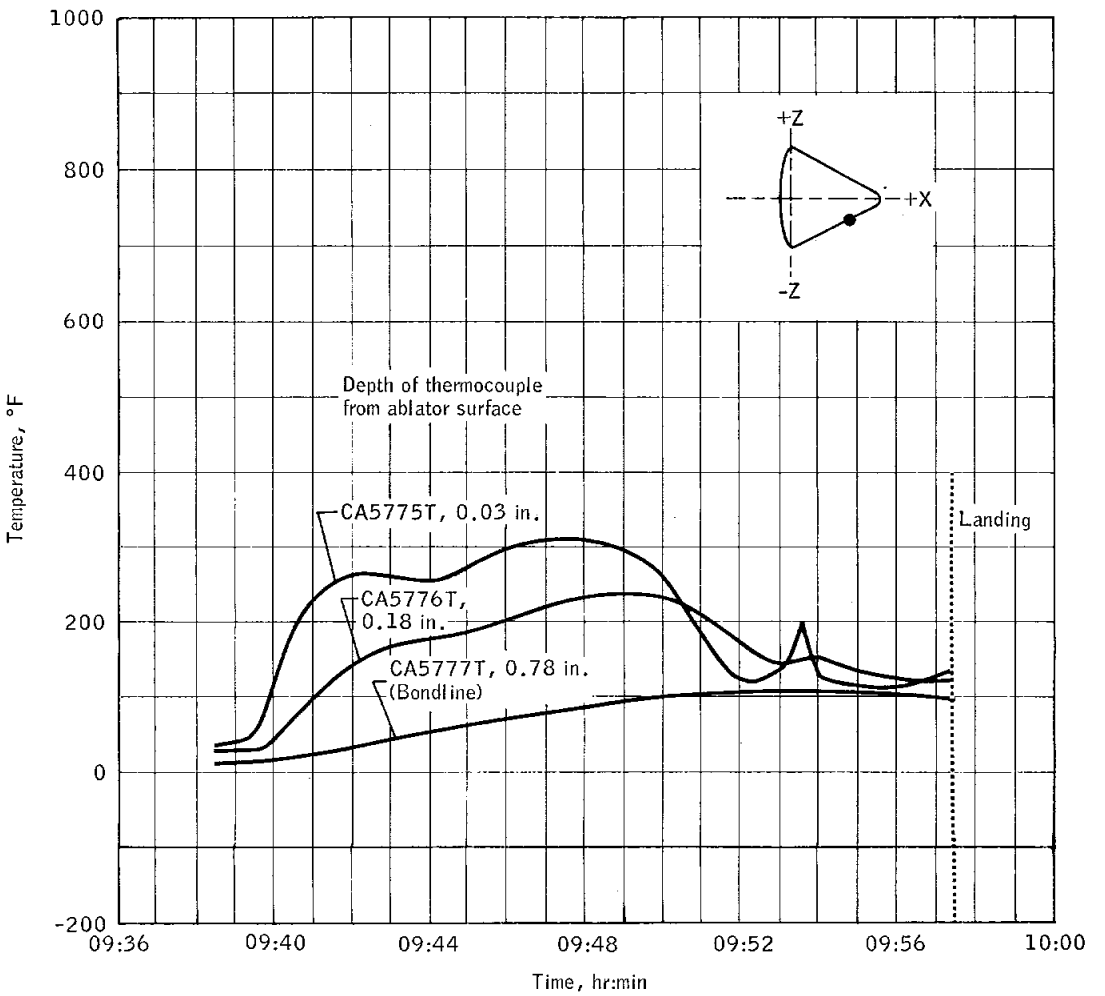

(j) X_c = 78.9 in.; θ= 274 deg.

Figure 5.4-13.- Continued.

NASA-S-68-3689

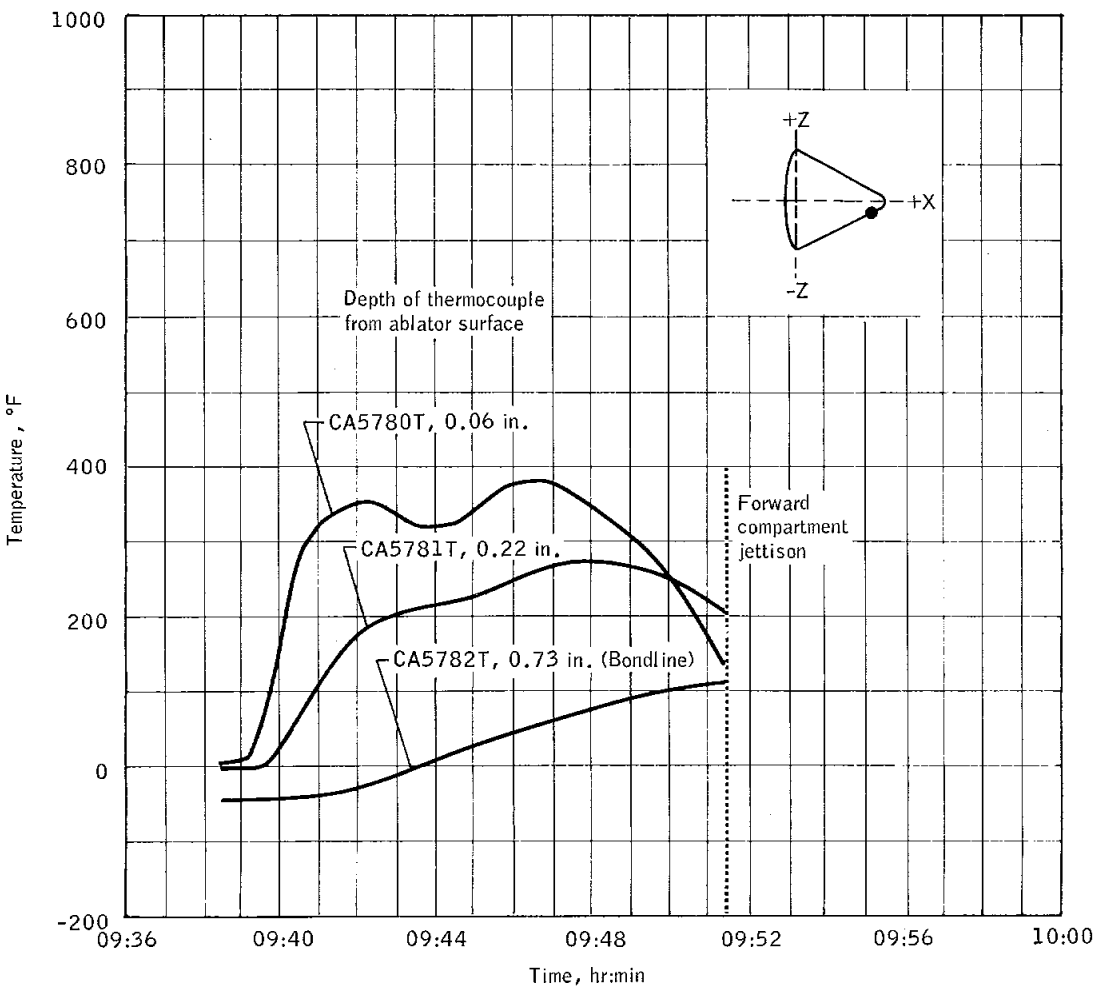

(k) X_c = 104 in.; θ = 260 deg.

Figure 5.4-13.- Concluded.

NASA-S-68-3690

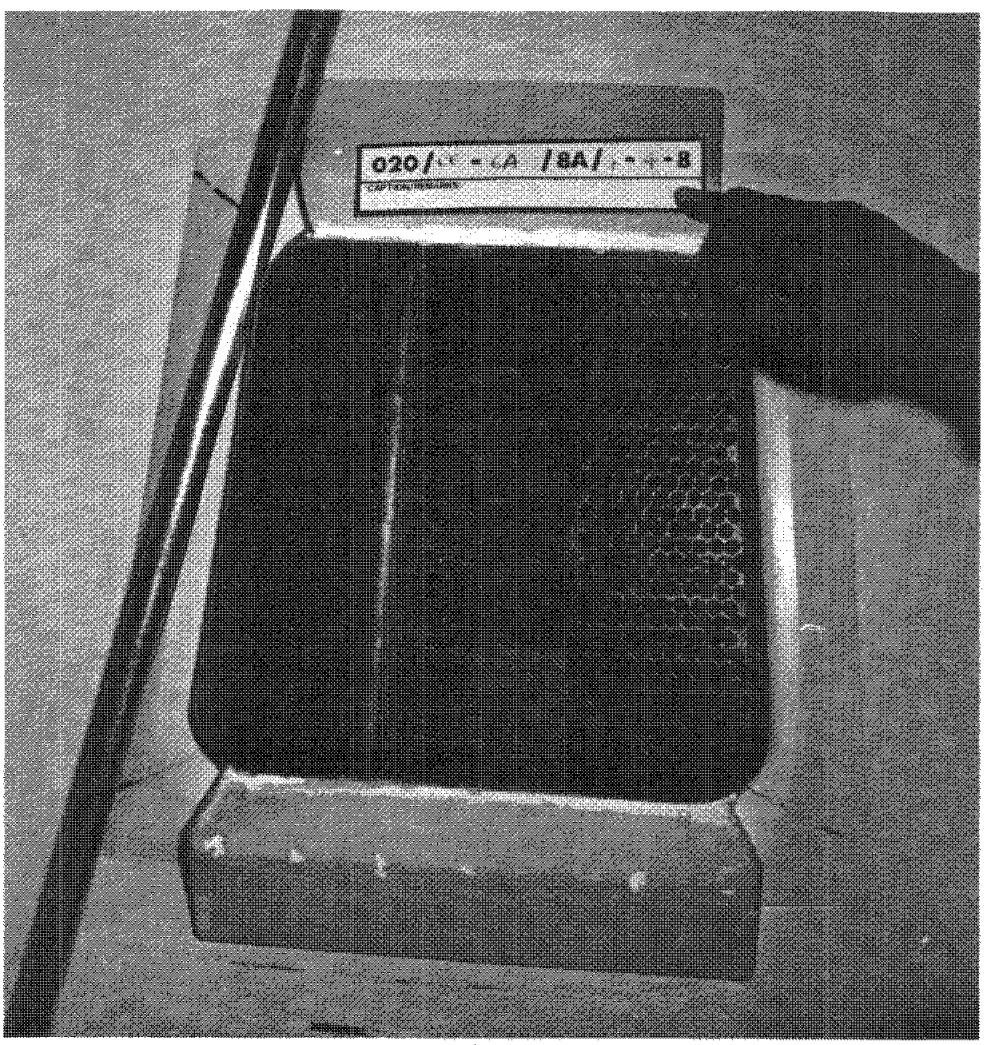

(a) Urethane foam, balsa wood, and holed Apollo ablative material over side window; $X_c = 72$ in.; $\theta = 238$ deg.

Figure 5.4-14.- Ablator test panels.

NASA-S-68-3691

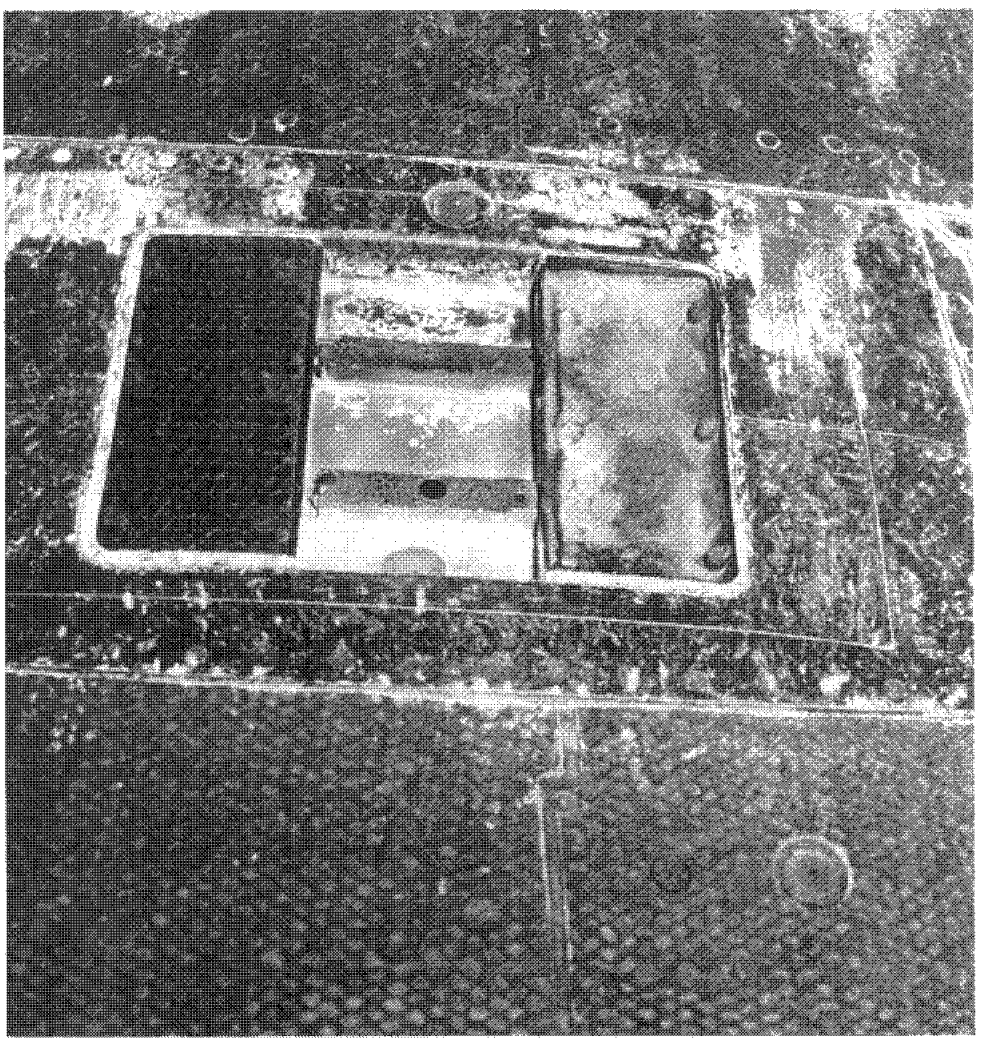

(b) Holed Apollo ablative material and urethane foam over windward umbilical cavity; $X_c = 40$ in.; $\theta = 90$ deg.

Figure 5.4-14.- Concluded.

5.5 EARTH LANDING

The earth landing sequence was initiated by closure of the high-altitude baroswitches, lasted approximately 352.5 seconds, and culminated in a successful landing.

At 09:51:27.4 drogue mortar fire was initiated at an altitude of 24 900 feet. The two drogues were satisfactorily deployed and inflated into their reefed condition. They were disreefed by mechanically initiated reefing-line cutters approximately 8.3 seconds after line stretch. Peak total drogue loads were estimated to be 10 430 pounds for the reefed condition and 7760 pounds for the disreefed condition. These loads were commensurate with the expected loading conditions. Rotational rates at drogue deployment were within ±2.5 deg/sec in pitch, ±5.0 deg/sec in yaw, and ±1.0 deg/sec in roll. After deployment, the initial inflation of the drogues induced command module rotational rates up to ±25 deg/sec in pitch, ±13 deg/sec in yaw, and ±15 deg/sec in roll, all of which were acceptable.

At 09:52:13.4, drogue release and pilot parachute deployment initiation occurred at an altitude of 11 300 feet. The pilot parachute deployed as planned, and all three main parachutes were deployed. The first main parachute was disreefed approximately 9.2 seconds after the line stretch. As determined from accelerometer data, peak total main parachute loads were approximately 21 850 pounds for the reefed condition and 8740 pounds for the disreefed condition. These loads were commensurate with loads expected for a normal entry. Command module oscillations were damped within 20 seconds after main parachute deployment, and the command module stabilized at a descent hang-angle of approximately 28 degrees from vertical.

The average rate of descent from 5000 feet to sea level was 29.75 ft/sec. A comparison of pressure altitude with events is shown in figure 5.5-1.

The command module landed at 09:57:19.9. The main-parachute disconnect system functioned correctly, separating the parachutes from the command module after landing. None of the parachutes were recovered.

There was no evidence of contact of the steel cable risers for the drogues with the airlock upper lip, which shows that the command module was in a favorable attitude at drogue deployment. Other than the minimal contact of the main parachute harness legs with the drogue mortar tubes, there was no evidence that any other earth landing system components contacted the command module upper deck.

The performance of the earth landing system was satisfactory, with all components operating as planned.

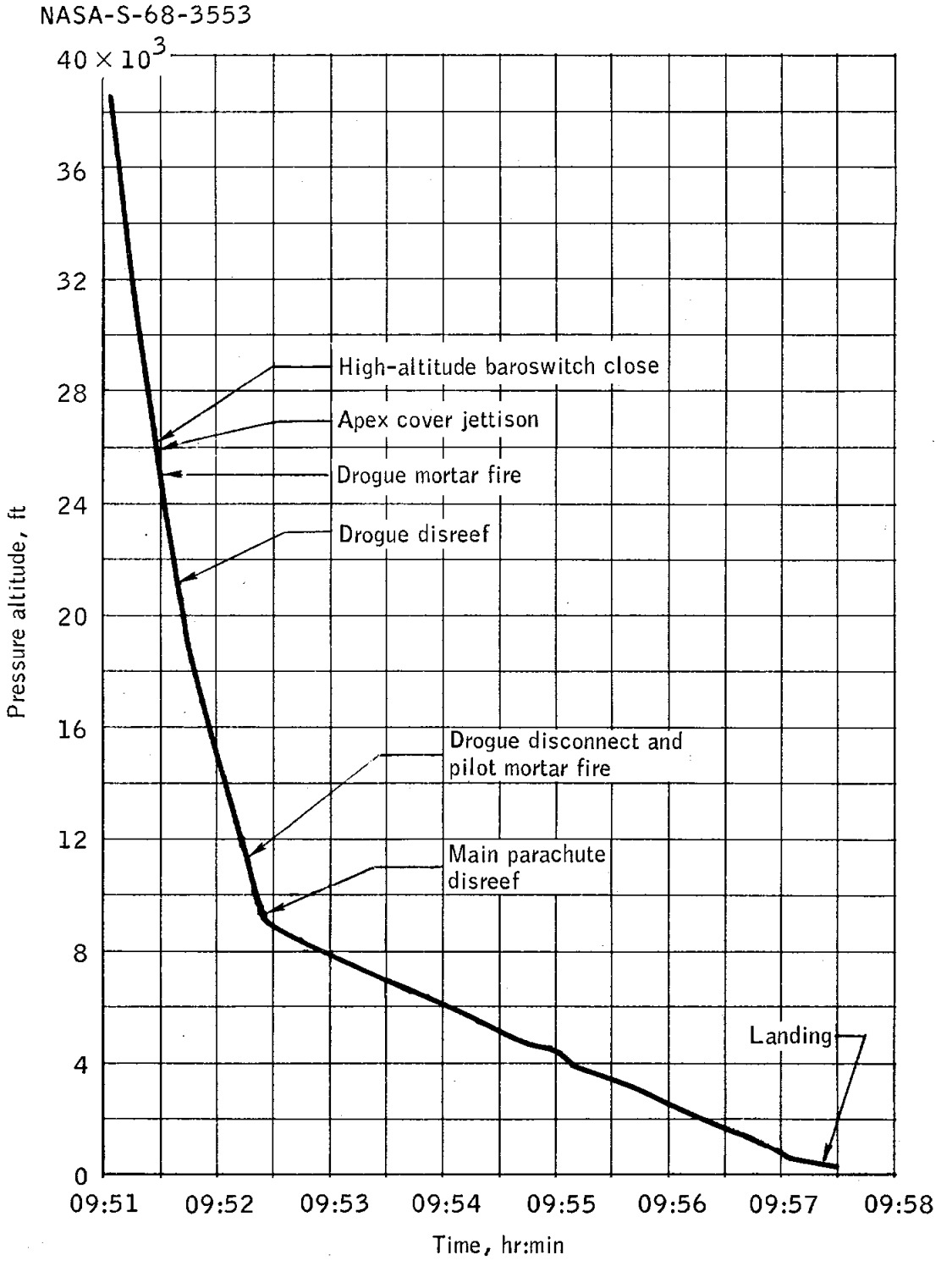

Figure 5.5-1.- Pressure altitude during descent.

5.6 MECHANICAL

The mechanical systems performed satisfactorily throughout the flight.

The unified side hatch of the block II configuration was flown for the first time and performed satisfactorily. The boost protective cover hatch was retained in position by the latching mechanism during boost. Available photographic coverage of the boost indicated that the hatch cover stayed with the boost protective cover until tower jettison.

After recovery, the hatch-latching mechanism was operated with an extension tool inserted into a socket that had been provided on the command module. This socket was not damaged or obscured in any way by entry heating. The maximum torque required to latch the hatch prior to the flight was 90 in-lb. This compares to the 110 in-lb maximum torque after the mission; the design limit torque is 860 in-lb.

With the hatch in the full-open position, the pressure in the hatch counterbalance was 750 psi compared with a prelaunch pressure of 1000 psi. The counterbalance leak rate was approximately 1.5 cc/min; the specification allowable leak rate is 3 cc/min. The mechanism on the hatch interior showed no signs of damage. Flight data indicated good sealing of the hatch during the mission.

This was the first mission in which the command module assumed the stable II (inverted) flotation attitude after landing. The command module was returned to the stable I (normal) attitude by the uprighting system. The uprighting system bag inflation was controlled by an attitude sensing switch that functioned after landing. The attitude switch normally functions when the X-axis of the command module rotates 75 degrees in the plus Z direction or 55 degrees in the minus Z direction from the vertical position (apex up). One minute after the switch has sensed and continues to sense the requirement for uprighting, the two uprighting system air compressors are turned on to inflate all three uprighting bags simultaneously. The attitude switch shuts off the compressors after uprighting.

The amount of bag inflation required to right the command module from the stable II to the stable I position is governed by the location of the command module center of gravity at the time of landing. The center of gravity at the time of landing was estimated to be very near the "no stable II" (self-righting) region; therefore, wave dynamics and/or little or no air in the bags would have uprighted the command module. At the time of recovery, the three uprighting bags contained an estimated total

of 6 cubic feet of air. This volume of air compares closely with the estimated 7.5 cubic feet of air that would have been provided to the bags for an operating time of 1 minute. This is significant in that it was reported by the recovery forces that the VHF recovery beacon was not heard for 2 minutes after landing. The VHF transmission would not be received when the command module was in the stable II attitude. Therefore it is concluded that the command module assumed a stable II attitude for approximately 2 minutes.

A visual examination indicates that the recovery aids functioned properly. Both VHF antennas were deployed and locked in the up position. The HF recovery antenna boom was buckled approximately 1-1/2 feet above the antenna storage can and the root clamp failed to engage. Although the sea conditions were well within the antenna design limits, sea tests on hardware of identical configuration produced failures of the antenna boom when the root clamp failed to engage. This command module was the last to use the HF recovery system, and further investigation of this problem is not considered necessary.

The flashing light deployed and locked in the up position and performed satisfactorily, with a flash rate of 17 to 18 flashes per minute. The dye marker and swimmer umbilical performed as required.

5.7 ELECTRICAL POWER DISTRIBUTION

The electrical power distribution system functioned normally throughout the mission.

At lift-off, the three fuel cells were providing 106 amps to the main dc buses. In addition, the two pairs of entry batteries (A/A1 and B/B1) were supplying 2 amps per pair of batteries to the emergency detection system and sequential events control system. Entry battery C was supplying 0.35 amps to the emergency detection system. During the service propulsion system engine firing, the entry batteries were providing 14 amps each (batteries A/A1 and B/B1 were considered as two single batteries). The main dc bus voltage, entry battery voltage, and pyrotechnic battery voltage were all within tolerance for the entire flight.

Based on inverter temperatures and event data, ac buses 1 and 2 were powered by inverters 1 and 2, respectively, throughout the flight. Event data and inverter temperatures verified that an essential load transfer occurred at 03:14:31.4. This transfer did not represent an anomaly in the electrical power distribution system but was a normal function in response to an anomalous load condition. Additional information concerning this essential load transfer is contained in section 12.0.

The calculated ac bus loading was as follows:

	ac bus 1	ac bus 2
Flight (prior to essential load transfer)	616 V-amp at 0.93 power factor lag	203 V-amp at 0.86 power factor lag
Flight (after essential load transfer)	292 V-amp at 0.91 power factor lag	525 V-amp at 0.92 power factor lag
Entry	495 V-amp at 0.14 power factor lead	390 V-amp at 0.97 power factor lead

The effective decrease of ac loads after service module/command module separation accounted for a slight decrease in inverter temperatures, during the entry period, of 5° and 6° F for inverters 1 and 2, respectively. The ac buses 1 and 2 were stable at 113 to 117 V ac throughout the flight, except during entry when bus 2 phase B increased to 120.26 V rms 1.8 seconds prior to service module/command module separation. The voltage did not return to a nominal 117.3 V rms until

approximately 15 minutes later. Although this increased voltage level was within the specification limits for the inverter output, it did represent a distinct departure from the output characteristics of the five remaining ac phases. There was no indication of a similar voltage overshoot during the Apollo 4 mission. Further investigation, including tests on the inverter, signal conditioner, and PCM equipment, is in progress to determine the cause.

The batteries performed well when in parallel with the fuel cells, absorbing approximately 30 percent of the total main bus loads. The entry and postlanding batteries maintained the main buses at 27 V dc throughout entry.

Entry battery case temperature varied between 74° and 84° F from lift-off through service module/command module separation. Battery B case temperature measurements were not operative after 00:01:28. During the entry phase, the indicated battery A case temperature increased 10° F; this was caused by a current drain of approximately 12.5 amps. This increase in current was normal.

The two pyrotechnic batteries initiated all required ordnance during the mission.

At landing, the mission control programmer initiated the command to connect the four entry and three auxiliary batteries to the postlanding bus. The postlanding battery (battery C) was connected to the postlanding bus by means of a baroswitch prior to landing. In addition, at 11 seconds after landing, the batteries were removed from the main and auxiliary buses. The postlanding bus provided power for the uprighting system, recovery aids, HF transceiver, and VHF recovery beacon during retrieval operations.

Postflight examination of the command module control and display panels verified that the only circuit breaker that had tripped was circuit breaker 100. This circuit breaker was associated with the essential ac bus transfer anomaly that is discussed in section 12.0.

5.8 FUEL CELLS

The performance of the fuel cells and of the electrical power system radiators was excellent throughout the prelaunch operations and during the mission. All flight data compared favorably with preflight predictions and with Apollo 4 flight data.

Fuel cell activation procedures were completed at T minus 35 hours 30 minutes (04:30:00 G.m.t. on March 28) in the countdown demonstration test. During the remainder of this test and during the launch countdown, the fuel cells shared the spacecraft electrical loads with the ground support equipment power supplies. However, because of ground support equipment malfunction and a resultant inability to top off the cryogenic hydrogen tanks, the fuel cell loads were varied to minimize hydrogen consumption during the latter portion of the countdown demonstration test and during the launch countdown.

Fuel cell performance during the prelaunch operation was normal and closely approximated the anticipated performance for sea-level operation. Prelaunch fuel cell operations at low power levels and with open circuits resulted in a high water content in the electrolyte. This is a normal occurrence when the fuel cells stabilize at low temperatures. Preheating the fuel cells before launch did not improve performance as much as anticipated because the fuel cells did not have sufficient time to stabilize at a lower water content. During the first hours of the mission, the electrolyte concentration difference between fuel cell 2 and either fuel cell 1 or 3 caused slight deviations in the nominal load-sharing performance. By the end of the mission all fuel cells had stabilized at essentially identical electrolyte concentrations and were sharing the spacecraft loads within 1 ampere.

At launch, each fuel cell was operating at approximately 36 amperes. The corresponding service module bus voltage was 29.3 V dc, and the command module bus voltage was 28.0 V dc. At launch, 3020 watts of electrical power was being provided to the command module (excluding a line loss of 140 watts). During the flight, the fuel cells provided approximately 230 kWh of energy to the command and service modules at an average current of 29 amperes per fuel cell and an average command module bus voltage of 28.4 V dc. Command module bus voltage was maintained between 27.5 and 29.3 V dc during the flight. The load profile, plotted from selected mission data, and the mission performance of fuel cell 3 are shown in figures 5.8-1 and 5.8-2, respectively. The observed performances of fuel cells 1 and 2 were almost identical to that of fuel cell 3 and are not shown.

During the first service propulsion system engine firing, the peak current was 127 amperes (70 amperes were provided by the three fuel cells and 57 amperes by the three primary batteries). During the flight, the maximum deviation from equal load sharing between individual fuel cells was 4 amperes.

Fuel cell skin temperatures during the flight agreed favorably with prelaunch predictions. All fuel cell skin temperatures at launch were approximately 443° F and stabilized at normal vacuum environment values within 1 hour after lift-off. Fuel cell skin temperatures at service module/command module separation were 434°, 435°, and 437° F for fuel cells 1, 2, and 3, respectively. Condenser exit temperatures for all fuel cells were controlled at nominal values between 162° F and 166° F during the mission.

The electric power radiator outlet temperatures for fuel cells 1 and 3 (the fuel cell 2 measurement was inoperative after lift-off) varied from 50° F during the dark segment of the orbital cycle to 114° F during the high-heat boost phase of the launch. These temperatures compared favorably with preflight predictions and with Apollo 4 flight data. During the coast ellipse phase of the mission, radiator outlet temperatures ranged from 50° to 75° F, varying in response to orientation.

Water production estimates, based upon power generation, reactant consumption, and potable water tank quantity measurement, agreed favorably and indicated a water production rate of approximately 2.1 lb/hr.

NASA-S-68-3554

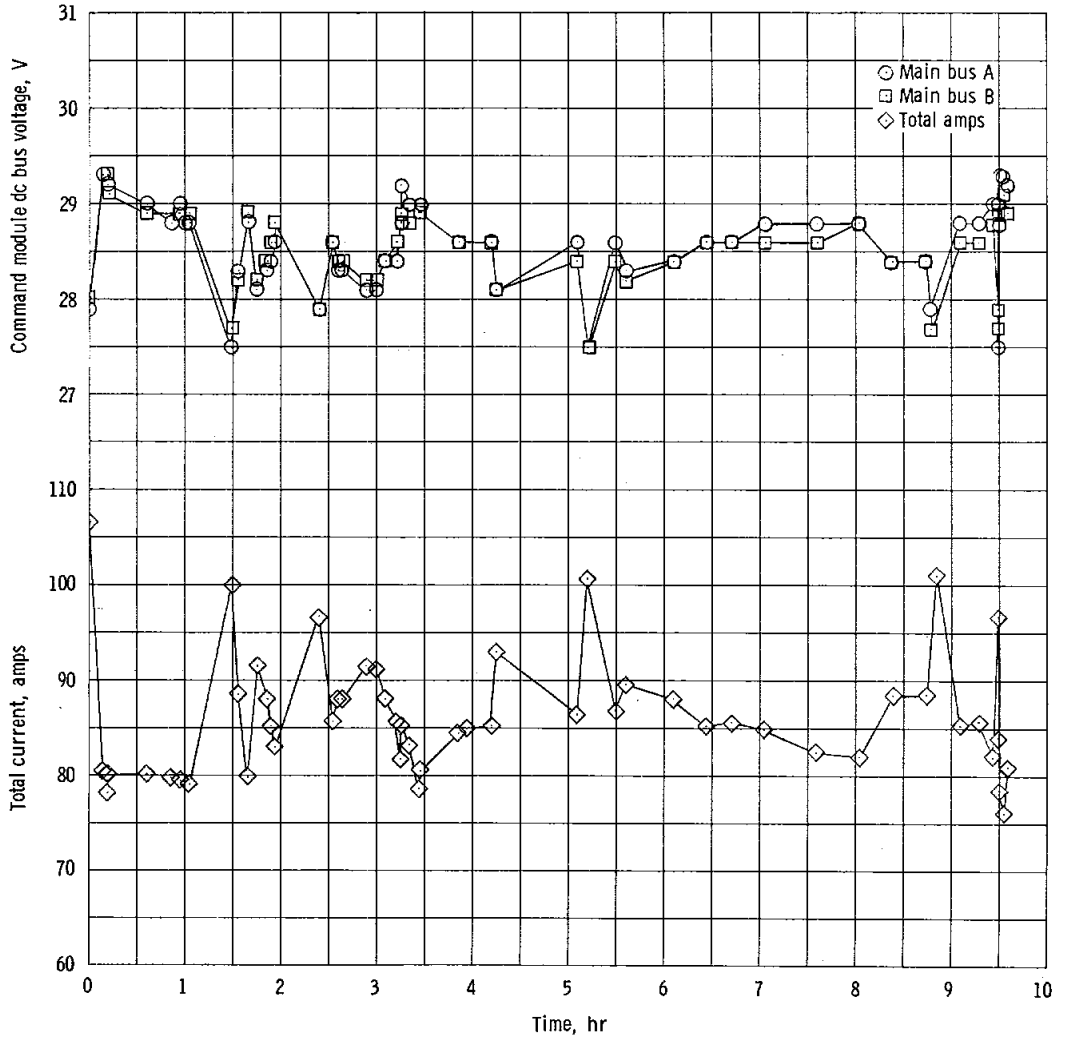

Figure 5.8-1. - Total current and dc bus voltage.

NASA-S-68-3555

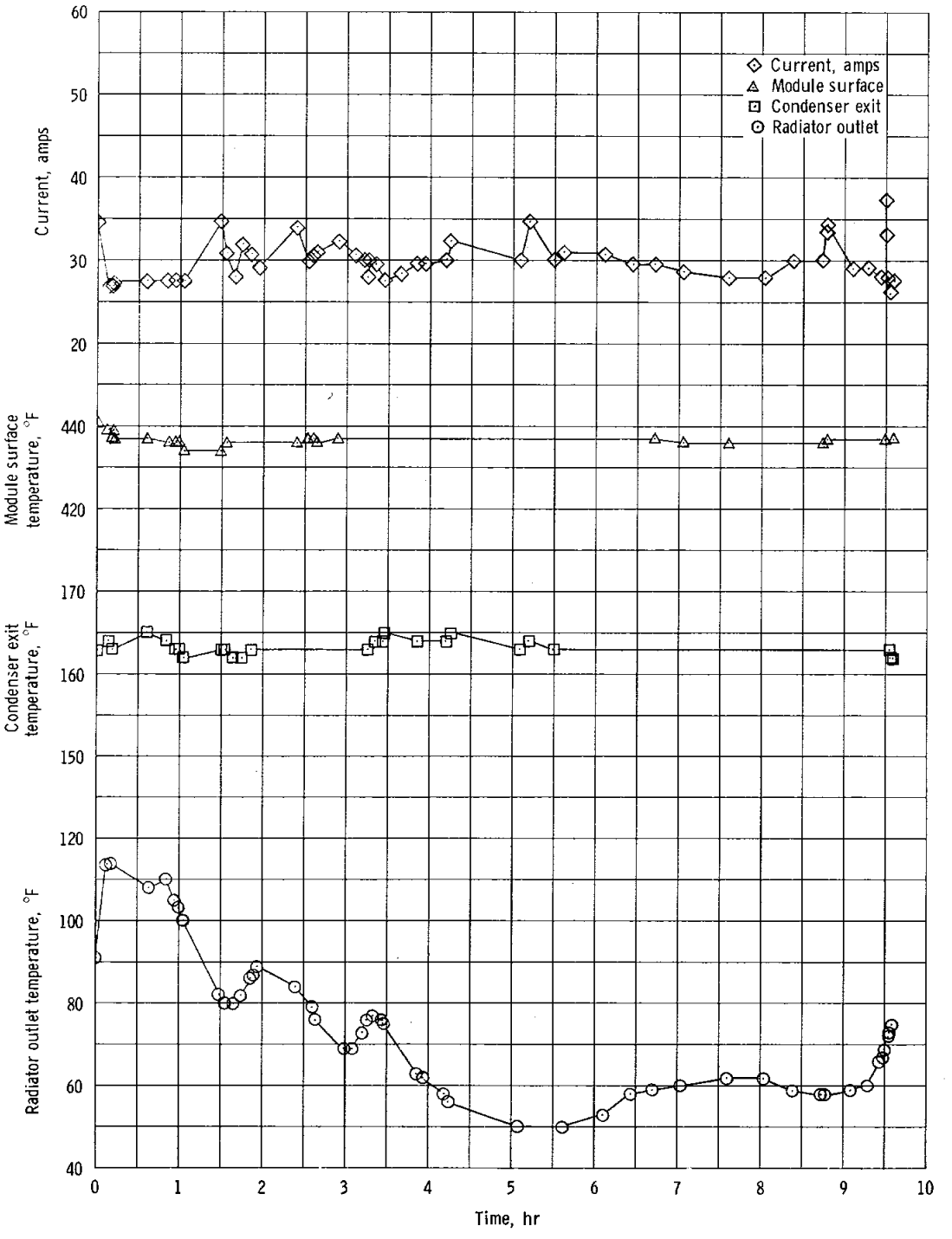

Figure 5.8-2. - Fuel cell 3 performance.

5.9 CRYOGENICS

The performance of the cryogenic gas storage system was satisfactory throughout the prelaunch operations and the mission. The flight data agreed with preflight predictions and compared favorably with Apollo 4 flight data.

5.9.1 Prelaunch Operations

Oxygen system.- The oxygen tanks were serviced at T minus 85 hours during the countdown demonstration test. The initial fill quantities were 330 pounds in tank 1 and 324 pounds in tank 2. The oxygen system remained in the vented standby mode for 60 hours. After chilldown completion, no oxygen tank topoff was performed. The tanks were pressurized with 295 pounds of oxygen remaining in tank 1 and 298 pounds in tank 2. For the remainder of the countdown demonstration test and the countdown until hatch closeout, the tank heaters and fans automatically maintained system pressures while supplying oxygen to the fuel cells. At hatch closeout, the oxygen system switches were in the following positions: tank 1 heaters in OFF and fans in AUTO, and tank 2 heaters and fans in AUTO.

Hydrogen system.- The hydrogen tanks were serviced at T minus 82 hours during the countdown demonstration test. The initial fill quantities were 28.8 pounds in tank 1 and 29.4 pounds in tank 2. After a 57-hour vented standby period, 20.5 pounds of hydrogen remained in tank 1 and 21.0 pounds in tank 2.

As programmed, an attempt was made to top off the hydrogen tanks, but malfunctions in the ground equipment prevented successful completion. After the topoff sequence was aborted, the hydrogen tanks were pressurized with a final quantity of 20.8 pounds remaining in tank 1 and 23.5 pounds in tank 2.

After tank pressurization, the fuel cells were purged periodically to maintain tank pressures below the relief valve settings. The hydrogen tank heat leaks for this mode of operation were approximately twice the normal value for a hydrogen tank having effective vapor shield cooling. With such a high boil-off rate, the system standby capability was greatly reduced. Therefore, the mode of tank pressure control was changed so that pressure was maintained only by fuel cell hydrogen consumption. This resulted in the optimum (constant) flow rate through the vapor shields to minimize tank boil-off (heat leak) and to maintain a constant system pressure. This method of hydrogen system management reduced the heat leak to a minimum and assured that hydrogen would be available in

sufficient quantity to accommodate a 2-day slip in the launch date, if required, without topoff.

5.9.2 Performance

Oxygen system.- At launch, the oxygen tank 1 heaters were OFF; consequently, oxygen tank 2 had to supply approximately 80 percent of the oxygen consumed during the flight. Although the tank 2 quantity measurement was inoperative during the flight, the tank pressure cycles, the water generated by the fuel cells, and the quantity change of oxygen in tank 1 (3 pounds) indicated that the system performed as predicted.

The pressure cycling agreed favorably with predicted system performance. During the flight, oxygen tank 2 heaters and all oxygen fans cycled automatically nine times (fig. 5.9-1). Prior to the plus X translation maneuver, the oxygen tank pressures were increased to approximately 960 psia during a 15-minute heaters ON cycle controlled by ground command. This cycle was performed to preclude an automatic heater ON cycle that could have caused a low bus voltage during the high power demand period of the translation maneuver should one fuel cell be lost.

At approximately 03:14:31, an ac bus transfer occurred. After the mission, circuit breaker 100, which controlled the power supply to phase A fans for both hydrogen tank 1 and oxygen tank 1, was found to be open. This problem is further discussed in section 12.0.

Hydrogen system.- The performance of the hydrogen system was satisfactory and agreed with the preflight predictions except that the hydrogen tank 1 pressure readout was erratic, and the readings were 22 psi below the expected values during prelaunch operations and throughout the mission. However, this problem was noted before flight and was determined to be acceptable. Block II hydrogen systems will use a different type pressure transducer, and the problem should be eliminated.

Tank quantity data indicated a consumption of 2.1 pounds of hydrogen during the flight; this agreed with the preflight prediction. Three methods were used to verify hydrogen usage and fuel cell water production and agreed within instrumentation accuracies, as follows:

Data source	Hydrogen usage, lb	Water produced, lb
Indicated quantity change	2.1	18.8
Fuel cell total amp-hr during the mission (839 amp-hr)	2.15	19.2
Indicated potable water tank quantity change	2.24	20.0

Prelaunch operation indicated a system heat leak of 11.2 Btu/hr in an average environmental temperature of 80° F; this compared favorably with acceptance test data of 13.4 Btu/hr in a 140° F environment. Calculations based on hydrogen flow rates derived from fuel cell currents indicated a combined system heat leak of 6.0 Btu/hr in flight; this represented a considerable performance improvement. During the flight, the flow rate through the hydrogen tank vapor shield was higher than the normal heat-leak flow rate, resulting in a pressure decrease during flight. This flow rate provided refrigeration to the tank insulation and resulted in a reduced system heat leak. This was a typical tank performance characteristic for periods when demand rates exceeded normal heat-leak flow rates.

NASA-S-68-3556

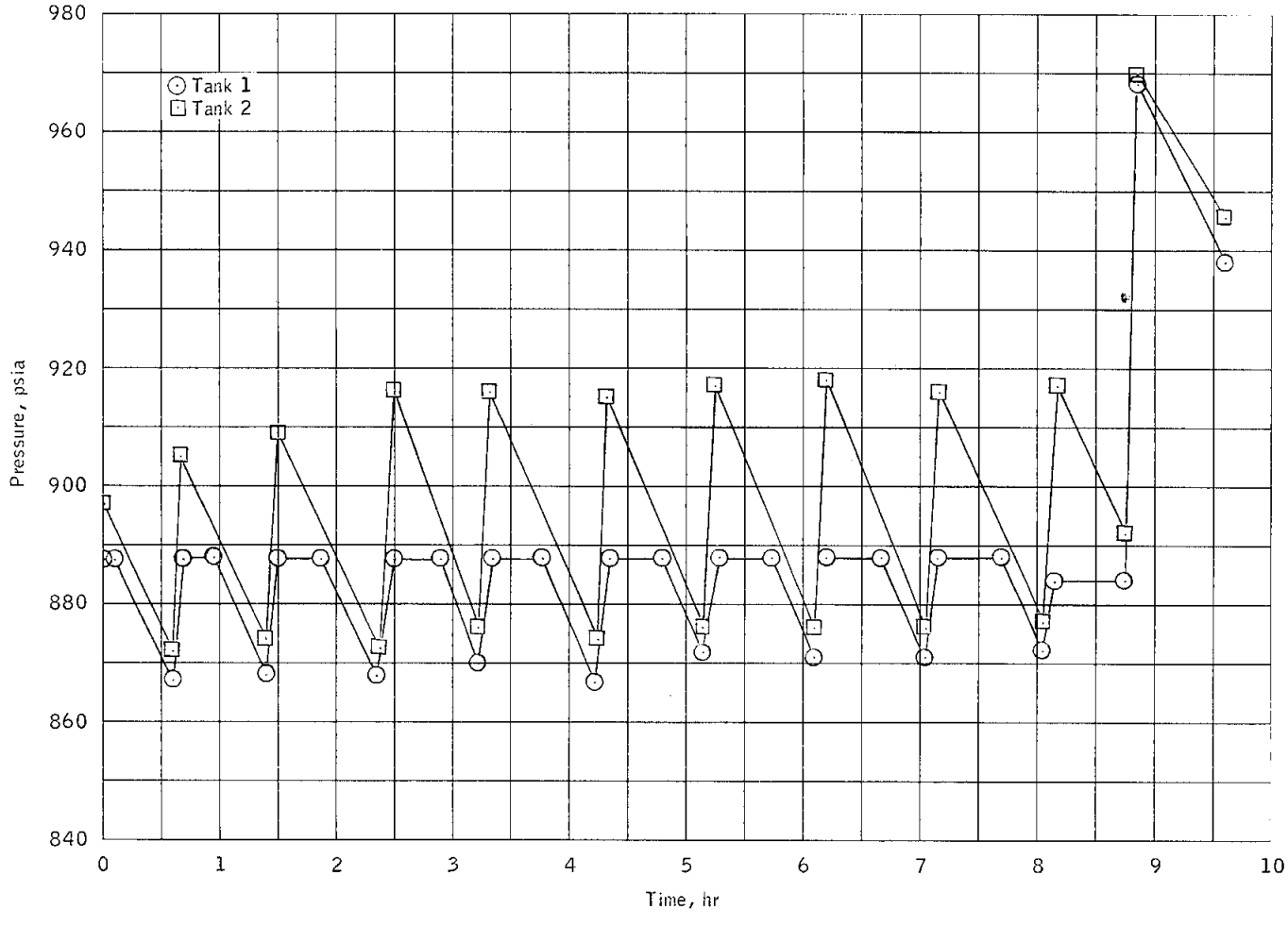

Figure 5.9-1.- Cryogenic oxygen tank pressure.

5.10 SEQUENTIAL

The sequential events control system functioned satisfactorily throughout the flight. The master events sequence controller satisfactorily enabled the emergency detection system and commanded escape tower jettison, CSM/S-IVB separation, command module/service module separation, and apex cover jettison. The service module jettison controller performed the function of commanding separation of the service module from the command module in the prescribed manner. The reaction control system controller satisfactorily commanded dumping of the remaining command module propellants and purging of the command module reaction control system. The controller also transferred the reaction control engine logic from service module to command module at command module/service module separation. The earth landing sequence controller, in conjunction with the pyrotechnic continuity verification box, commanded drogue and main parachute deployment and disconnect. The baroswitches operated within specified tolerances, as discussed in section 5.5.

5.11 PYROTECHNIC DEVICES

All pyrotechnics apparently functioned as planned. However, at physical separation of the command and service module from the adapter, a pitch body rate transient equivalent to a disturbance torque of 9000 ft-lb was observed. This torque is well above the level that could have been accrued from any combination of reaction control engine firings. The most likely cause appears to be a momentary physical hangup at the minus Z interface between the adapter and the service module. Further, if there had been a hangup, the forces introduced into the adapter panel by the deployment thrusters would have been of sufficient magnitude to cause the rate transient in the command and service module. Further discussion is included in section 12.

5.12 LAUNCH ESCAPE

Performance of the launch escape system was satisfactory. The tower jettison motor fired as programmed to separate the launch escape system, including the boost protective cover, from the command module.

5.13 EMERGENCY DETECTION

A primary objective of the Apollo 6 mission was to demonstrate the performance of the emergency detection system in the closed-loop mode (automatic abort capability enabled). The system performed satisfactorily and accomplished this objective.

The system properly responded to prelaunch thrust signals from the S-IC engines, indicating that all engines were at normal thrust 1.9 seconds prior to lift-off. Lift-off signals that enabled the automatic abort circuitry in the command module master events sequence controllers were received from the launch vehicle instrument unit at umbilical separation. The enabling commands were removed 5 seconds after lift-off, leaving the circuits enabled through the tower jettison relays. This sequence was nominal.

Data from the angle-of-attack dynamic pressure sensing system were first received at 00:00:20. The data indicated that the differential pressure reached a maximum of 1.00 psid at 00:01:07, then decayed to essentially zero at 00:01:28 as the vehicle exited the high dynamic pressure regime. These data indications correlate with redundant measurements obtained by the Marshall Space Flight Center and are well within the tentative abort limit of 3.20 psid.

The period of noisy PCM telemetry from 00:01:28 to 00:08:20 hindered evaluation of emergency detection system events. During this interval, bilevel measurements were intermittent.

At 00:02:13, the emergency detection system logic input 1 measurement (fig. 5.13-1) changed from ON to OFF and remained in that condition for the duration of the mission. This input represents one of the three normally energized automatic abort signals from the instrument unit to the command module sequential events control system. The OFF condition of any two of the three emergency detection logic inputs to the command module is sufficient to initiate automatic abort when the automatic abort circuits are enabled. During the Apollo 6 mission, these circuits were enabled from lift-off until launch escape tower jettison (00:03:04.8).

Each of the three abort signals is powered from a separate command module power source and is controlled in the instrument unit by a separate two-out-of-three voting gate. All three of the voting gates are controlled by a single automatic abort bus, which in turn is energized in the event of excessive angular rates or thrust loss on two or more first-stage engines. The automatic abort bus was not energized, and the

command module power supplied to the instrument unit was not interrupted. An OPEN failure of the voting gate in the instrument unit would require at least two relay failures. It is therefore concluded that the OFF conditions of emergency detection system logic input 1 resulted from a discontinuity in the wire between the emergency detection system distributor in the instrument unit and the master events sequence controller in the command module. This wire was in a bundle that passed close to and between the adapter access hatch and the lunar module test article attach point on the adapter minus Z axis.

The three emergency detection logic input wires are isolated from each other in their routing from the launch vehicle instrument unit into the command module. This separation ensures that damage to a wire bundle will possibly cause the loss of only one of the "hot wires," which is not sufficient to command an automatic abort. However, if structural damage or breakup is sufficient to cause the loss of two of the three "hot wires," an automatic abort would be initiated if the emergency detection system is enabled. The booster engine cutoff commands from the command module to the launch vehicle are similarly routed to ensure that engine cutoff capability is not impaired. If structural damage did occur in the adapter area on the Apollo 6 mission, the loss of one emergency detection system logic input was not contrary to the design guidelines of the system.

The S-IC/S-II staging sequence began with inboard engine cutoff at 00:02:24.9 and outboard engine cutoff at 00:02:28.4. The remainder of the sequence was confused by erratic PCM data.

Separation of the S-II aft insterstage was properly signalled to the command module at 00:02:59.1. Tower jettison commands from the instrument unit resulted in escape tower jettison at 00:03:04.8. Deactivation of the automatic abort capability in the command module occurred when planned.

Premature cutoffs of the S-II stage engines 2 and 3 were observed through telemetry of engine status signals to the command module at 00:06:52.9 and 00:06:54.2, respectively. The S-II stage cutoff (engines 1, 4, and 5), S-II stage separation, and S-IVB first start sequence were observed normally; separation occurred at 00:09:37.1. S-IVB cutoff was indicated at 00:12:27.

Ignition command for the second S-IVB firing was indicated by ON condition of the engine status signal at 03:13:34.7. Attainment of 60 percent of normal thrust by the J-2 engine would have extinguished this signal. The signal remained ON until subsequent vehicle separation, indicating that operating chamber pressure was not achieved.

Separation of the command and service module from the S-IVB was initiated by a ground command from the Mission Control Center - Houston at 03:14:26.1, as indicated by input signals to the emergency detection system from the mission control programmer. (These signals are equivalent in the emergency detection system logic to manual service propulsion system abort commands from the translational hand controller in a manned mission.) The ground command caused an emergency detection system cutoff command to the S-IVB at 03:14:26.1. Receipt of this command was confirmed by an abort request signal output from the S-IVB to the command module. Separation, the last event monitored by the emergency detection system, occurred correctly 1.7 seconds after command, as indicated by termination of all signals from the instrument unit to the command module.

NASA-S-68-3557

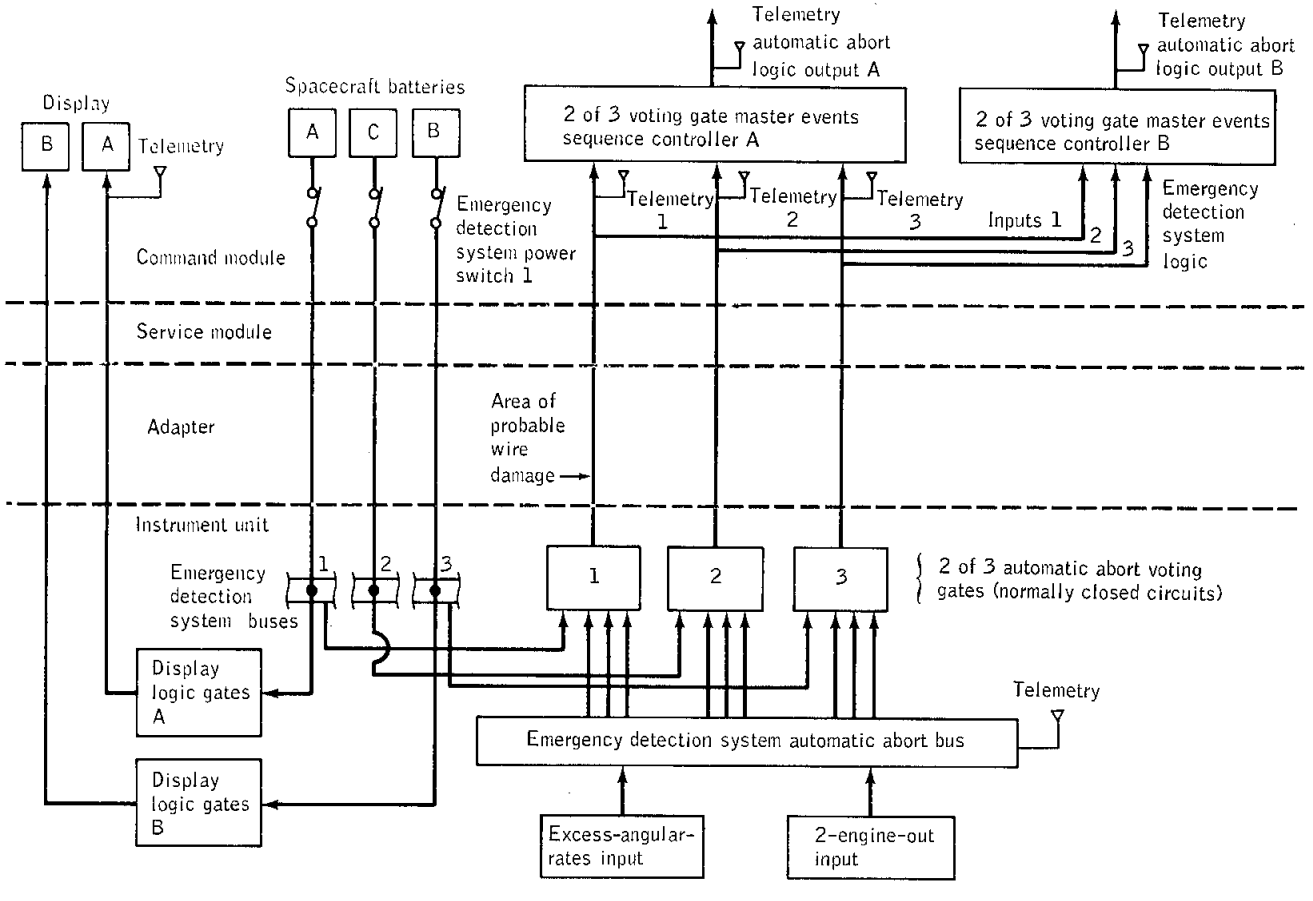

Figure 5.13-1.- Emergency detection system automatic abort interface, showing probable location of wire damage.

5.14 COMMUNICATIONS

The communications system performance was evaluated by analyzing the command module communications as an entity and by analyzing the operation of the command module communications system and the Manned Space Flight Network (MSFN) communications equipment as an integrated system. A diagram of communications capabilities during the mission is presented in figure 5.14-1. The overall performance of the communication system was satisfactory. A comparison of received carrier power levels with predictions resulted in reasonable correlation except during Bermuda (launch), Redstone (revolution 2), Ascension (coast ellipse), Carnarvon (coast ellipse), and Watertown (entry) coverage. The data indicate that the MSFN antenna polarization selected at these five sites may have been left-circular in place of the specified right-circular Computed pulse code modulation (PCM) synchronization word bit errors were derived from the S-band and VHF/PCM telemetry channels. Good telemetry performance was evident except during launch (00:01:28 to 00:08:20) and during the Ascension, Carnarvon, and Guam revolution 3 passes. Tests of the turned-around S-band up-voice, and the S-band and VHF down-voice were conducted and the data verified adequate voice communications capability. Each command and guidance computer update transmitted was accepted by the spacecraft updata link equipment.

5.14.1 Command Module Communications

The data indicate that the spacecraft communications system performed satisfactorily except for an intermittent timing/telemetry problem that was particularly evident from 00:01:28 through 00:08:20. A discussion of this problem is contained in sections 5.15 and 12.0.

The communications requirements for the mission included uplink command capability, downlink real-time telemetry, onboard transponders for ground tracking and ranging, and recovery communications equipment. In addition, audio tones were used to simulate up-voice and down-voice for evaluation of the voice link.

The description of the communication equipment is contained in section 13.0 of this report. The only operational difference between the two spacecraft was in the selection of pair-B S-band omnidirectional antennas for this mission, whereas pair A was used for Apollo 4. The selection of a given pair is based on trajectory/look-angle analysis with the criterion being optimization of coverage during the coast ellipse. The data indicate nominal performance of the pair-B antennas. With the exception of the HF recovery antenna, the other antennas

(the four C-band antennas on the command module, the two VHF scimitar antennas on the service module, and the two VHF recovery antennas on the top deck) also performed satisfactorily. The HF recovery antenna, which deployed from the top deck of the command module after uprighting, failed structurally during or after deployment and did not achieve the erect configuration required for optimum transmission. This antenna, which is known to be of marginal design will not be used for block II vehicles.

Unified S-band equipment.- The discrete communications equipment performed as follows. The S-band equipment provided telemetry, up-data (after CSM/launch vehicle separation), pseudo-random noise ranging, and two-way Doppler tracking from prelaunch until turn-off after spacecraft landing. In addition, down-voice was simulated by modulating the 1.25-MHz subcarrier with a 400-Hz audio tone. Up-voice was simulated by modulating the 30-kHz up-voice subcarrier with a 1000-Hz audio tone. There was no indication of an S-band malfunction during the mission. The data problem that occurred primarily during a portion of the launch phase was not due to S-band equipment malfunction. The S-band power amplifier switched internally from high power to bypass at 03:14:32 because of an ac power transient caused by a bus transfer. This condition corrected itself in the expected minute and a half and was not an S-band anomaly.

Very high frequency/amplitude modulation.- The VHF/AM transceiver was modulated with a 400-Hz audio tone to simulate downlink voice communications and transmitted continuously in the Simplex A mode from prelaunch until command module/service module separation. Available data indicate nominal performance of the transmitter throughout the mission.

Very high frequency/frequency modulation.- The VHF/FM telemetry transmitter operated continuously from prelaunch until command module/service module separation, providing real-time high-bit-rate (51.2 kB/sec) PCM data. These data were erratic (from 00:01:28 to 00:08:20) on the VHF/FM as well as on the S-band link and the onboard recorder (data storage equipment). However, there was no indication of other-than-nominal transmitter performance at any point in the mission, and the data problem was not caused by transmission difficulties.

Pulse code modulation telemetry.- Despite periods of erratic operation, the PCM functioned normally during most of the mission. A majority of the total expected telemetry data from the mission is of excellent quality. A summary of the general spacecraft anomaly that resulted in repeated PCM dropouts starting at 00:01:28 and lasting approximately 7 minutes is contained in section 12.0.

During the launch phase, five measurements were lost. These five measurements were common to, and could be affected by, the failure of one five-input analog gate in the PCM. Postflight testing and analysis will be required to determine the failure mode, if one occurred.

Premodulation processor.- The premodulation processor contained the subcarrier oscillators for downline S-band voice and telemetry, the data driver for the VHF/FM transmitter, and the 70-kHz S-band up-data link subcarrier discriminator. Analysis of data and preliminary postflight testing indicated nominal performance of the premodulation processor.

C-band transponder.- All data show normal C-band operation. Successful tracking by ground C-band radars was accomplished from launch through transponder turn-off by ground command at 06:29:38. No anomaly was indicated.

Up-data link.- The up-data link was utilized throughout the mission for transmission of guidance computer update information, timing updating, and real-time ground commands. In the early portion of the mission, up-data were received by the 450-MHz UHF receiver, which is part of the up-data link. Prior to CSM/S-IVB separation and initiation of the service propulsion system engine firing, the UHF receiver was programmed OFF. For the remainder of the mission, the up-data were received by S-band on the 70-kHz up-data subcarrier. Data evaluation and postflight testing indicated nominal performance of the up-data link.

Very high frequency recovery beacon.- There are conflicting reports from the recovery forces regarding receipt of both the VHF recovery beacon and the VHF survival beacon; it is not known at this time whether one or both beacons were received (section 12.0). Postflight tests have shown that both beacons are operable.

High frequency transceiver.- The HF transceiver was successfully activated in the beacon mode after landing. The transmissions were received by the recovery forces on the proper frequency but at reduced signal strength. The reports of reduced signal strength correlate the fact that the HF antenna was not properly deployed. No anomaly was indicated in the operation of the HF transceiver. This equipment will not be used on block II vehicles.

5.14.2 Command Module/Network Communications

S-band radio frequency system.- The evaluation of the S-band RF system was principally directed to the launch phase, selected near-earth orbit passes, and the coast ellipse phase. Selected postflight carrier

power level predictions have been compared with actual received carrier power levels. The postmission predictions were based on measured spacecraft attitudes, full-scale antenna patterns, and slant range. The predictions represent selected points and cannot be utilized as continuous data. The S-band RF system adequately supported the mission. However, the received carrier power level recorded at the spacecraft and MSFN sites was weaker than predicted for five station passes. The data indicate that the antenna polarization selected at these five sites may have been left-circular in place of the desired right-circular. Highlights of the performance of the S-band RF systems are presented in table 5.14-I and figures 5.4-2 through 5.4-15. The uplink combinations used during the mission are shown in table 5.14-II.

S-band telemetry channel.- The S-band telemetry performance analysis indicated an intermittent problem from 00:01:28 to 00:08:20 and during the coast ellipse phase (section 12.0).

The S-band telemetry performance was evaluated from telemetry frame synchronization bit errors and postmission data processor in-synchronization/out-of-synchronization conditions. These data were correlated with received carrier power levels for selected station passes. Frame synchronization bit errors (obtained from bit error rate bandpass tabulations) were averaged over 3-second intervals, before plotting, to approximate the average frame synchronization bit errors per second.

During the Merritt Island coverage at launch (fig. 5.14-2), the downlink received carrier power level was below the threshold for usable data for a total of 15 seconds during the period from S-IC/S-II stage separation to launch escape tower jettison. Frame synchronization was maintained from 00:08:15 until 00:09:02. However, a large number of frame synchronization bit errors caused by the weak received downlink carrier power level were recorded.

Grand Bahama Island coverage of the launch phase (fig. 5-14-3), was affected by the intermittent telemetry problem. The received carrier power level indicated that if the problem had not occurred, this station could have provided continuous telemetry support during the time of two-way lock.

Telemetry performance for the Bermuda coverage during launch phase is shown in figure 5.14-4. From 00:08:20 until 00:13:02, frame synchronization was maintained; however, the observed bit errors are not consistent with the received carrier power level.

Telemetry performance during the Ascension coverage of revolution 3 is shown in figure 5.14-12. Because the station coverage was graphically plotted over a 20-minute interval, it was necessary to average the frame

synchronization bit errors over 6-second intervals to approximate the average error per second. The average bit error rate during this interval (apogee ±10 minutes) was approximately 6.0×10^{-5} (total frame synchronization bits during this period were approximately 1.5×10^{6}). The telemetry problem observed during the launch phase recurred after this interval.

The S-band telemetry channel performance during the Carnarvon coverage of the coast ellipse was evaluated for the time period from 08:45:20 to 09:23:51 (fig. 5.14-13). During this evaluation, 2 536 300 frame synchronization bits were sampled and 820 were determined to be in error. Thus, the bit error rate was 3.2×10^{-4}. Frame synchronization was interrupted for 2 minutes 26 seconds during the evaluation period.

Telemetry performance during the Guam coverage of revolution 3 is illustrated in figure 5.14-14. The frame synchronization bit errors were averaged over 6-second intervals because of the length of the pass. The intermittent telemetry problem observed during the launch phase recurred during this interval.

The S-band telemetry channel performance during U.S.N.S. Watertown coverage of the entry phase was nominal. Frame synchronization bit errors were associated with abrupt changes in the received carrier power levels (fig. 5.14-15).

S-band ranging channel.- S-band ranging capability existed throughout the mission. The command module transponder was configured for range-code turn-around prior to launch and remained in this configuration throughout the mission. The range-code acquisition sequences for 19 station passes were examined. Typically, range-code acquisition was initiated as soon as the exciter was locked to the synthesizer and the ranging receiver acquired lock. Range receiver lock times are included in table 5.14-I. A typical range-code acquisition sequence is shown in figure 5.14-16. No S-band ranging acquisition problems were evident from the data.

S-band and ultra high frequency.- Message acceptance patterns were received at the ground station in response to each command transmitted to the spacecraft by the S-band and UHF command systems. During the mission, numerous computer update alarms were experienced (section 12.0). These occurred with and without update activity. The alarms necessitated several retransmissions of the procedural navigation update from Carnarvon. The commands transmitted by the ground were verified to be properly encoded. This, and the fact that all real-time commands were received

and executed without difficulty, substantiate the earlier evidence that the requirement for retransmission was associated with the interface between the command receiver and the guidance computer.

With the exception of U.S.N.S. Redstone coverage of revolution 2 and Antigua coverage of revolution 3, the received S-band carrier power levels were adequate to support the up-data channel (see table 5.14-I).

S-band up-voice channel.- In the command module S-band transponder, the up-voice subcarrier is turned around in the ranging channel and remodulated on the downlink carrier. Therefore, up-voice tests were performed by transmitting uplink signal combinations that included this subcarrier and recording the downlink carrier modulation at selected sites. The performance of this channel was evaluated by measuring the postdetection signal-to-noise ratio of the turned-around simulated up-voice modulation (1 kHz tone). Because the measured data were dependent on the received uplink and downlink carrier power levels, the signal-to-noise ratio that would have been received by the command module would be better than the measured data indicate. The measured signal-to-noise ratio was correlated with the results of word intelligibility tests performed at the Manned Spacecraft Center to predict channel performance.

Up-voice test coverage (fig. 5.14-17) by Merritt Island included the period from lift-off to 00:02:00 (when Merritt Island transmitted the uplink S-band signal), from 00:02:06 to 00:05:30 (when Grand Bahama transmitted the uplink signal) and from 00:05:36 to 00:07:32 (when Bermuda transmitted the uplink signal). The postdetection signal-to-noise ratio of the turned-around up-voice signal, while Merritt Island transmitted the uplink signal, was approximately 20 dB. The uplink carrier power level was steady at this time. Good up-voice communication would have been achieved during this pass with a predicted word intelligibility greater than 90 percent (18.7 dB required).

A good signal-to-noise ratio was observed by the Merritt Island station while Grand Bahama and Bermuda transmitted the uplink signal. The fluctuations observed in the signal-to-noise ratio measured at the Merritt Island station during the period from 00:02:00 to 00:03:09 were caused by handover operations and loss of downlink lock at S-IC/S-II stage separation and tower jettison. The uplink carrier power levels observed at the Grand Bahama station during that same time indicated good up-voice channel performance (fig. 5.14-3). The observed drop in signal-to-noise ratio measured at Merritt Island during the period from 00:05:30 to 00:05:36 was caused by the Grand Bahama to Bermuda handover. The turned-around signal-to-noise ratio observed at Merritt Island while the spacecraft was over Bermuda was slightly below that required. Because the uplink carrier power levels were satisfactory, the up-voice

capability over Bermuda would have been nominal. A predicted word intelligibility of 90 percent or better would have been achieved on the up-voice channel at Grand Bahama and Bermuda during the time that Merritt Island had a satisfactory downlink signal.

S-band and very-high-frequency down-voice channel.- The capability of the S-band and VHF down-voice channel was demonstrated by modulating the S-band 1.25-MHz voice subcarrier and VHF 296.8-MHz carrier with a peak clipped 400-Hz tone derived from the spacecraft ac power. The performance of these channels was evaluated by measuring the postdetection signal-to-noise ratios of the down-voice modulation. The measured signal-to-noise ratios were then correlated with the results of the word intelligibility tests performed at the Manned Spacecraft Center to predict channel performance.

Downlink voice coverage at Merritt Island was evaluated for the period from launch to 00:04:00. Except for the momentary drop at 00:01:58 (fig. 5.14-18) the postdetection signal-to-noise ratio of the down-voice subcarrier averaged better than 19 dB while Merritt Island had two-way lock. The observed fluctuations in the signal-to-noise ratio during the period from 00:02:29 to 00:03:09 were caused by intermittent receiver phase lock at the Merritt Island station.

Although the down-voice channel was not evaluated for the Grand Bahama coverage of the launch phase, the received carrier power level was indicative of good down-voice channel performance (fig. 5.14-3).

Downlink voice coverage at Bermuda included the period from 00:04:00 to 00:13:00 (fig. 5.14-19). Except for the time periods associated with handover operations, the postdetection signal-to-noise ratio of the down-voice tone averaged better than 16 dB during Bermuda coverage of the launch phase. Satisfactory voice communication would have been achieved with a predicted word intelligibility greater than 90 percent.

Downlink S-band voice coverage at Carnarvon was evaluated for the period from 05:30:00 to 07:30:39. The postdetection signal-to-noise ratio of the down-voice subcarrier averaged better than 16 dB during this time (fig. 5.14-20). Satisfactory voice communication would have been achieved with a predicted word intelligibility greater than 90 percent.

Nominal downlink S-band voice coverage would have been achieved by Guam during the period from 09:16:12 to 09:35:33. The postdetection signal-to-noise ratio of the down-voice subcarrier averaged better than 15 dB.

As expected, nominal down-voice VHF voice coverage would not have been achieved by Carnarvon from 05:27:09 to 07:30:39. The postdetection signal-to-noise ratio of the down-voice channel varied from 0 to 8 dB and was less than that required for a predicted word intelligibility of 90 percent.

From 09:15:57 to 09:35:33, nominal down-voice VHF coverage would not have been achieved by Guam. The postdetection signal-to-noise ratio of the down-voice channel varied from 0 to 6 dB and was less than that required for a predicted word intelligibility of 90 percent.

Very-high-frequency telemetry link.- The VHF telemetry link performed satisfactorily. Two command switchable omnidirectional antennas mounted on the service module were used for VHF communications. The VHF telemetry link was intended for prime support use during the launch phase and the near-earth parking orbits. As anticipated, the total received power level dropped below the telemetry threshold during the coast-ellipse phase of the mission.

The intermittent telemetry problem which was evidenced in the performance of the S-band telemetry channel, was also present in the VHF/PCM telemetry channel performance. Telemetry performance during the Merritt Island and Bermuda launch phase coverage is shown in figures 5.14-21 and 5.14-22, respectively. Performance of the VHF telemetry channel was comparable to the S-band telemetry performance during this interval. The VHF telemetry performance was nominal during the remainder of the near-earth parking orbit coverage.

TABLE 5.14-I.- S-BAND RADIO FREQUENCY SYSTEMS PERFORMANCE

Station	Revolution	Mission phase	Uplink combination[a]	Time of two-way lock, hr:min:sec	Time of range receiver lock, hr:min:sec	Location of received carrier power and telemetry performance, figure	Comments
Merritt Island	Launch	Launch	6	Prior to launch	Prior to launch	5.14-2	The Merritt Island site provided two-way S-band communications with the spacecraft from before launch to 00:02:00. The transfer of the uplink from Merritt Island to Grand Bahama was initiated at 00:02:00 and completed 6 seconds later. This transfer was scheduled so that the loss of communications which occurred on the Apollo 4 mission during critical events would be alleviated. During passive tracking following the uplink transfer, downlink phase lock was lost at S-IC/S-II stage separation and tower jettison. The difference between the received carrier power level and the predictions was caused by booster shadowing effects. The correspondence of received carrier power levels and the predictions at 00:07:00 was a result of the change in vehicle-to-Merritt Island look-angles associated with the cutoff of two S-II stage engines.
Grand Bahama	1	Launch	6	00:02:06	00:02:14	5.14-3	The communications between the Grand Bahama site and the vehicle were not adversely affected by launch phase events as shown in figure 5.14-3. The step increase in received carrier power levels (receiver 2) at tower jettison is attributed to the change in vehicle antenna patterns resulting from removal of the boost protective cover. The increase in received carrier power levels at 00:04:15 resulted from the nominal transfer of receiver 2 from the acquisition antenna to the main antenna. Close agreement between the received carrier power levels and predictions was achieved.

[a]See table 5.14-II.

TABLE 5.14-I.- S-BAND RADIO FREQUENCY SYSTEMS PERFORMANCE - Continued

Station	Revolution	Mission phase	Uplink combination[a]	Time of two-way lock, hr:min:sec	Time of range receiver lock, hr:min:sec	Location of received carrier power and telemetry performance, figure	Comments
Bermuda	1	Launch	6	00:05:31	No data because of inoperative station recorder	5.14-4	The received downlink carrier power levels at Bermuda was approximately 10 to 14 dB lower than the predictions based on right-circular polarization of the Bermuda antenna. Closer agreement exists between the received carrier power levels and predictions based on left-circular polarization as shown in figure 5.14-4. Thus, the data indicate that left-circular polarization of the Bermuda antenna was selected in place of the desired right-circular polarization. Handover to the Redstone was completed at 00:11:42.
Merritt Island	1/2	Near-earth parking orbit	5	01:37:01	01:37:29	5.14-5	The maximum difference between received downlink carrier power levels and predictions during this station pass was approximately 7 dB. Larger differences between received uplink carrier power levels and predictions were observed. At least part of these differences can be attributed to the fact that the spacecraft receiver was operating near automatic gain control saturation which significantly reduced the resolution of the telemetry measurements.
Redstone	2	Near-earth parking orbit	5	01:47:24	01:47:27	5.14-6	The Redstone made several attempts to acquire two-way lock during handover from Bermuda before successful completion at 01:47:24. At 01:47:50, the received uplink carrier power level began to decrease and continued until the received uplink carrier power level was less than the received downlink carrier power level. This decrease is being investigated. Comparison of the received downlink carrier power level with predictions presented in figure 5.14-6 indicates that the Redstone antenna may have been left-circular polarized in place of the desired right-circular polarization.

[a]See table 5.14-II.

TABLE 5.14-I.- S-BAND RADIO FREQUENCY SYSTEMS PERFORMANCE - Continued

Station	Revolution	Mission phase	Uplink combination[a]	Time of two-way lock, hr:min:sec	Time of range receiver lock, hr:min:sec	Location of received carrier power and telemetry performance, figure	Comments
Hawaii	2	Near-earth parking orbit	5	02:55:36	02:55:42	5.14-7	Hawaii acquired the S-band downlink carrier at 02:52:46. Attempts to achieve two-way lock were unsuccessful until approximately 02:55:36. The data indicate the delay may have been caused by reversal of the displayed vehicle received carrier power level telemetry data. The data show the effect of the vehicle passing through the Hawaii antenna keyhole. Measured received carrier power levels and predictions agree to within 5 dB for the downlink. The received uplink carrier power level was near the receiver automatic gain control threshold.
Merritt Island	2/3	Translunar injection	5	03:12:10	03:12:29	5.14-8	The essential ac-load power transfer occurred at 03:14:32 and resulted in an interruption of two-way lock and a momentary loss of downlink carrier. The transient produced during the ac-load power transfer caused the S-band power amplifier to recycle to the bypass mode for approximately 97 seconds (nominal recycle time). The absence of the power amplifier is evidenced by the 18 dBm reduction in the received carrier power level. A change in received carrier power level of this magnitude is an excellent indication of proper operation of the power amplifier. The up-data link was transferred from the UHF system to the S-band system at 03:13:23.7.
Bermuda	3	Translunar injection	5	03:16:31	03:16:49	5.14-9	The radio frequency system performance during the Bermuda pass was satisfactory. Bermuda transferred uplink to Antigua at 03:20:30. The attempted handover resulted in Bermuda losing downlink phase lock prematurely.
Antigua	3	Translunar injection	5				Antigua was unsuccessful in completing the handover from Bermuda. The difficulty may have been caused by antenna pointing errors.

[a]See table 5.14-II.

TABLE 5.14-I.- S-BAND RADIO FREQUENCY SYSTEMS PERFORMANCE - Concluded

Station	Revolution	Mission phase	Uplink combination[a]	Time of two-way lock, hr:min:sec	Time of range receiver lock, hr:min:sec	Location of received carrier power and telemetry performance, figure	Comments
Canary Island	3	Coast ellipse	5	03:55:05	03:55:41	5.14-10	The maximum difference between received downlink carrier power level and predictions was approximately 7 dB. Received uplink carrier power levels differed from predictions by approximately 15 dB at one point. Because of the poor received-carrier power levels at Ascension, Canary Island provided unscheduled two-way communications from 03:55:05 until 04:15:48.
Ascension	3	Coast ellipse	5	03:26:39 04:16:18	03:27:14 04:16:36	5.14-11 5.14-12	At approximately 03:45:00, Ascension experienced weak received carrier power levels and intermittent loss of both uplink and downlink S-band carrier lock. At 04:15:04, Ascension-received carrier power levels became suitable to reestablish communications. Handover from Canary Island was completed at 04:16:18. Comparison of the received carrier power levels with predictions indicates the polarization of the Ascension antenna may have been left-circular instead of the desired right-circular.
Carnarvon	3	Coast ellipse	5	05:30:01	05:30:23	5.14-13	The radio frequency system data indicate acceptable communication performance for the Carnarvon pass. Comparison of the received uplink and downlink carrier power levels with predictions indicates that the Carnarvon antenna polarization may have been left-circular in place of the desired right-circular.
Guam	3	Coast ellipse	5	09:15:46	09:16:20	5.14-14	The radio frequency system performance was satisfactory throughout the Guam pass.
Watertown	3	Entry	5	09:35:35	09:35:54	5.14-15	U.S.N.S. Watertown provided communication support for approximately 3 minutes 18 seconds. The information presented in figure 5.14-15 indicates that predictions based on left-circular polarization of the Watertown antenna more closely agree with the received carrier power levels than the predictions based on right-circular polarization.

[a]See table 5.14-II.

TABLE 5.14-II.- NETWORK/COMMAND AND SERVICE MODULE S-BAND TRANSMISSION COMBINATION SUMMARY

Combination	Information	Modulation technique	Subcarrier frequency, kHz	Subcarrier modulation	Subcarrier deviation, kHz	Carrier phase deviation, radian
5	Carrier					
	Pseudo-random noise ranging	Phase modulation (PM) on carrier	--			0.3
	Up-data	FM/PM	70	Commands	±5	0.61
6	Carrier					
	Pseudo-random noise ranging	PM on carrier	--			0.3
	Voice	FM/PM	30	1-kHz tone	±7.5	0.61
	Up-data	FM/PM	70	Commands	±5	0.61

NASA-S-68-3558

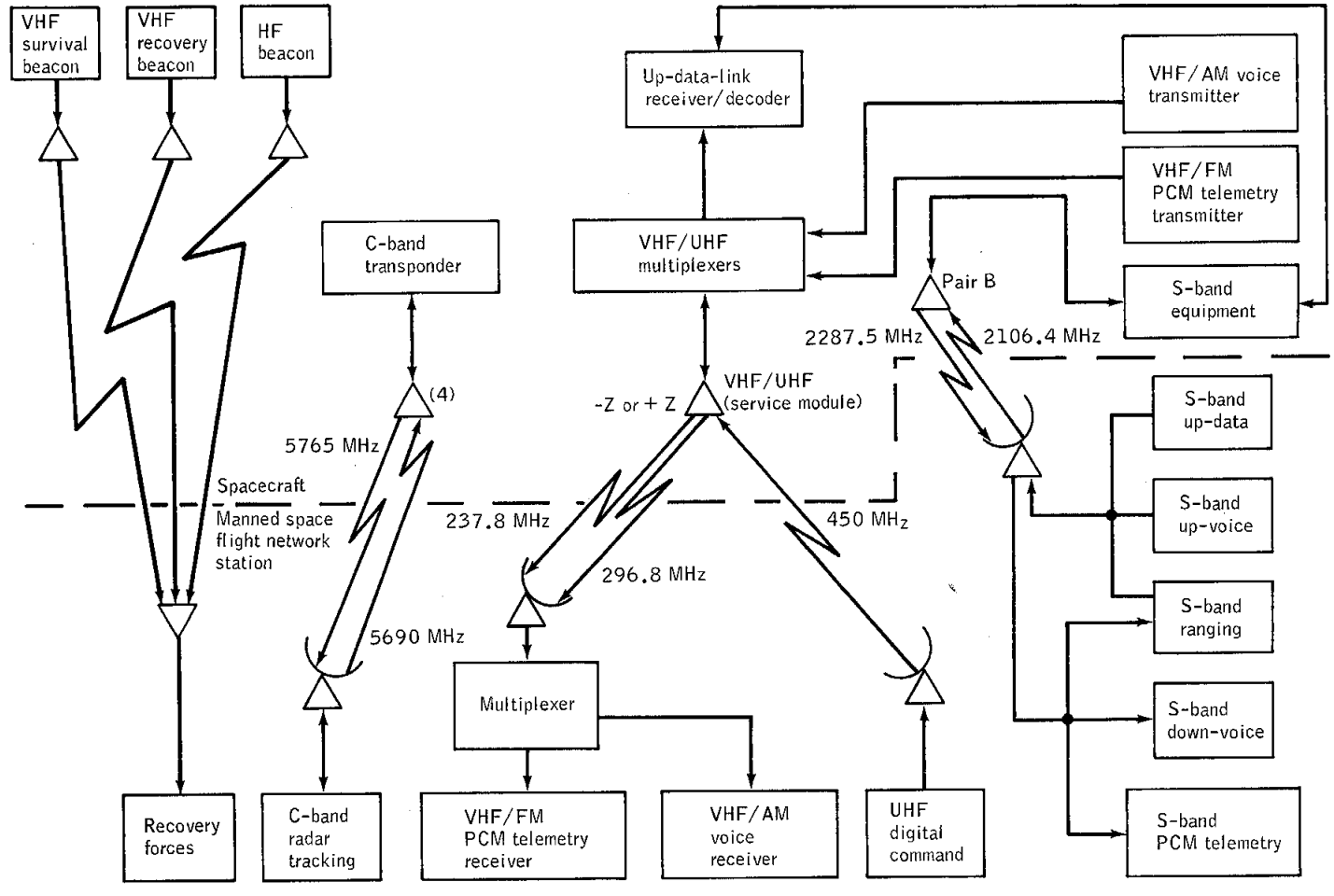

Figure 5.14-1.- Communication system configuration.

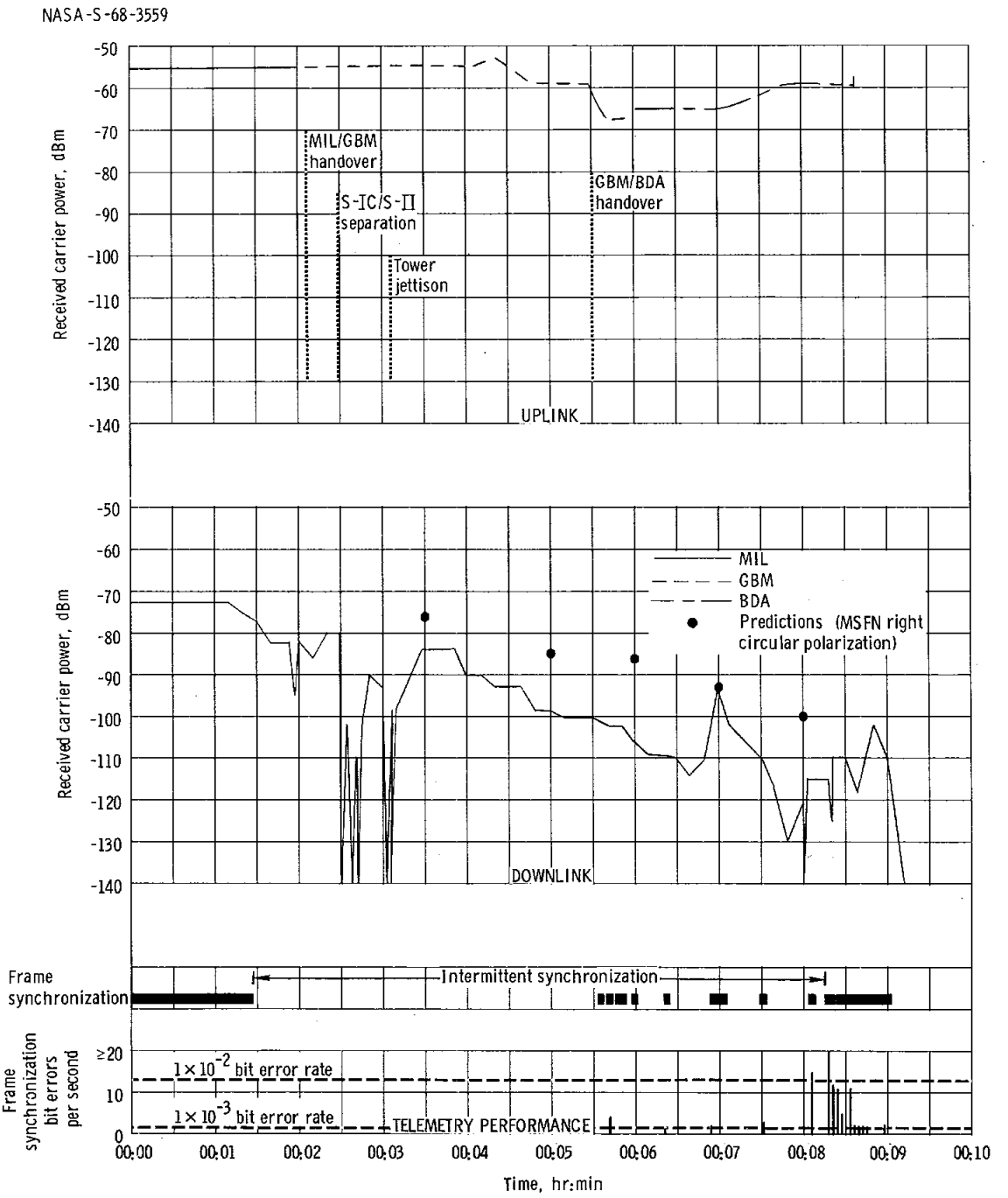

Figure 5.14-2. - Received S-band carrier power and telemetry performance, Merritt Island, launch.

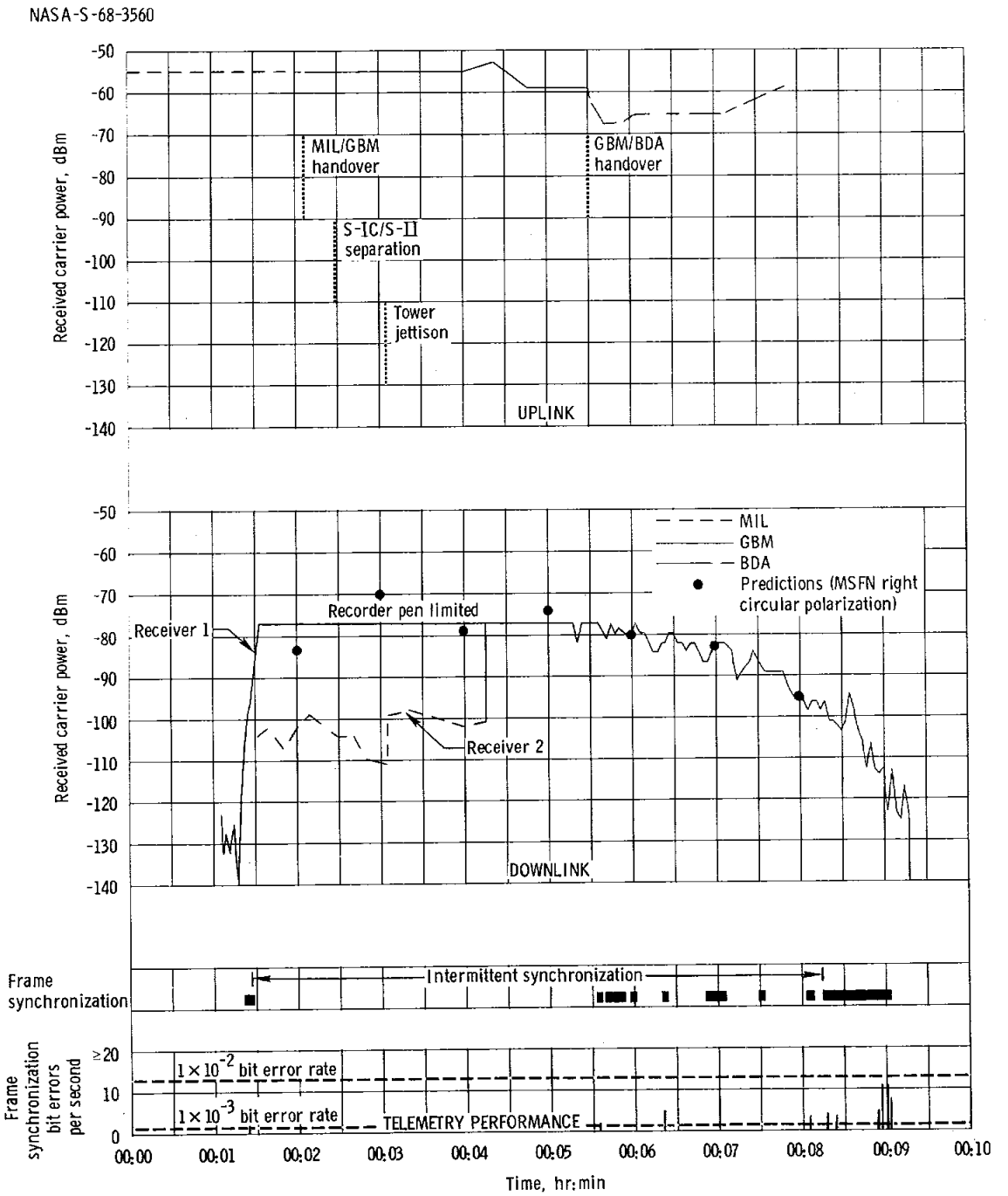

Figure 5.14-3. - Received S-band carrier power and telemetry performance, Grand Bahama, revolution 1.

NASA-S-68-3561

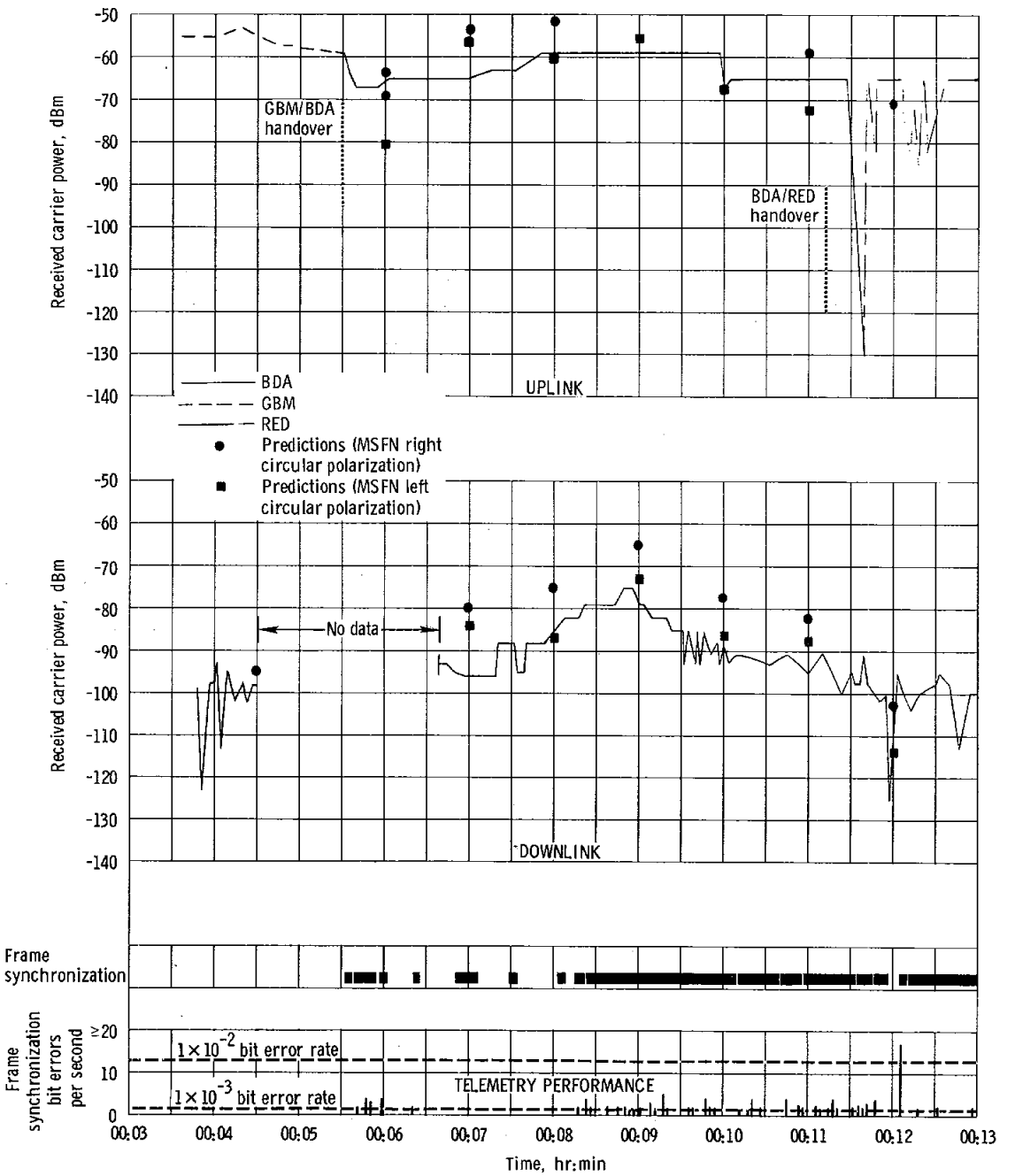

Figure 5.14-4. - Received S-band carrier power and telemetry performance, Bermuda, revolution 1.

NASA-S-68-3562

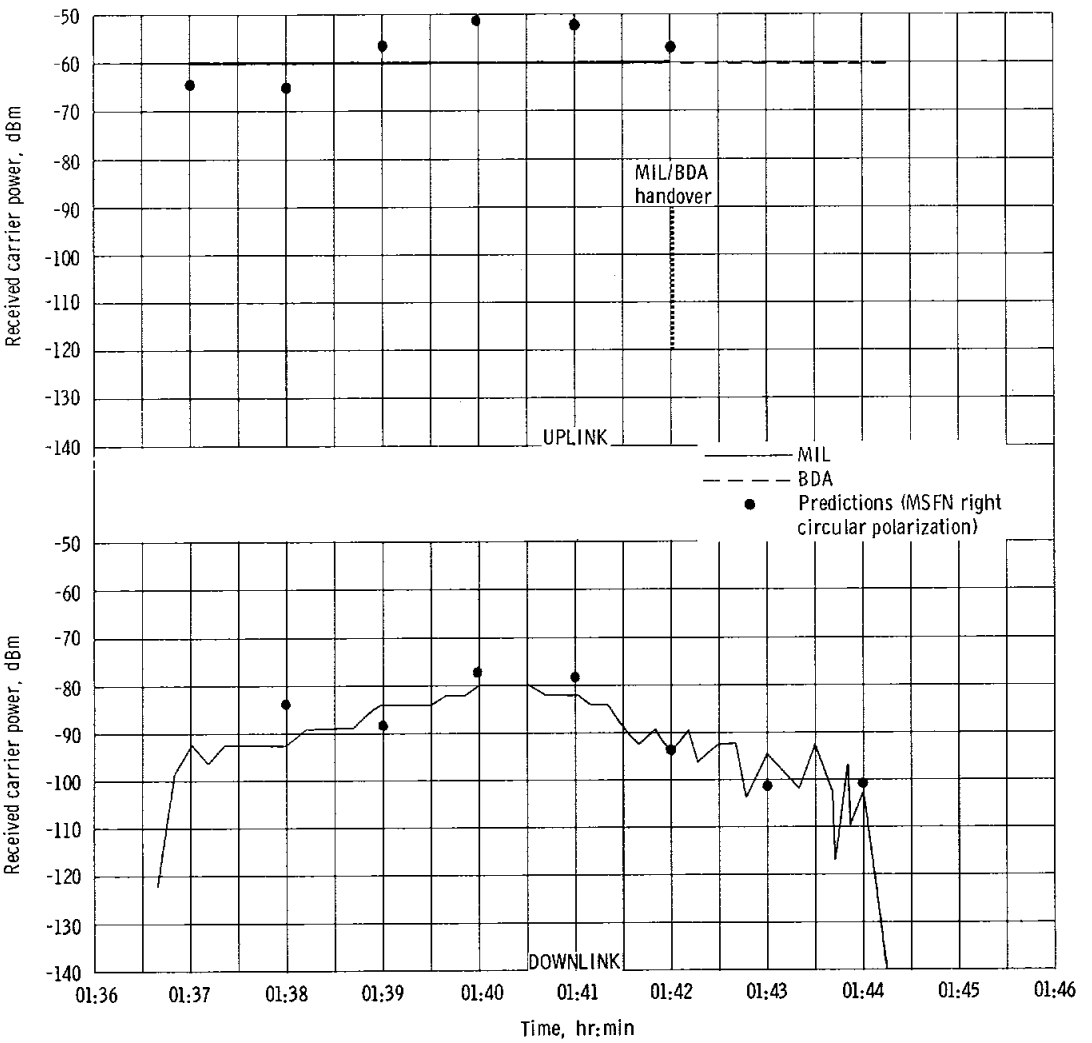

Figure 5.14-5. - Received S-band carrier power, Merritt Island, revolution 1-2.

NASA-S-68-3563

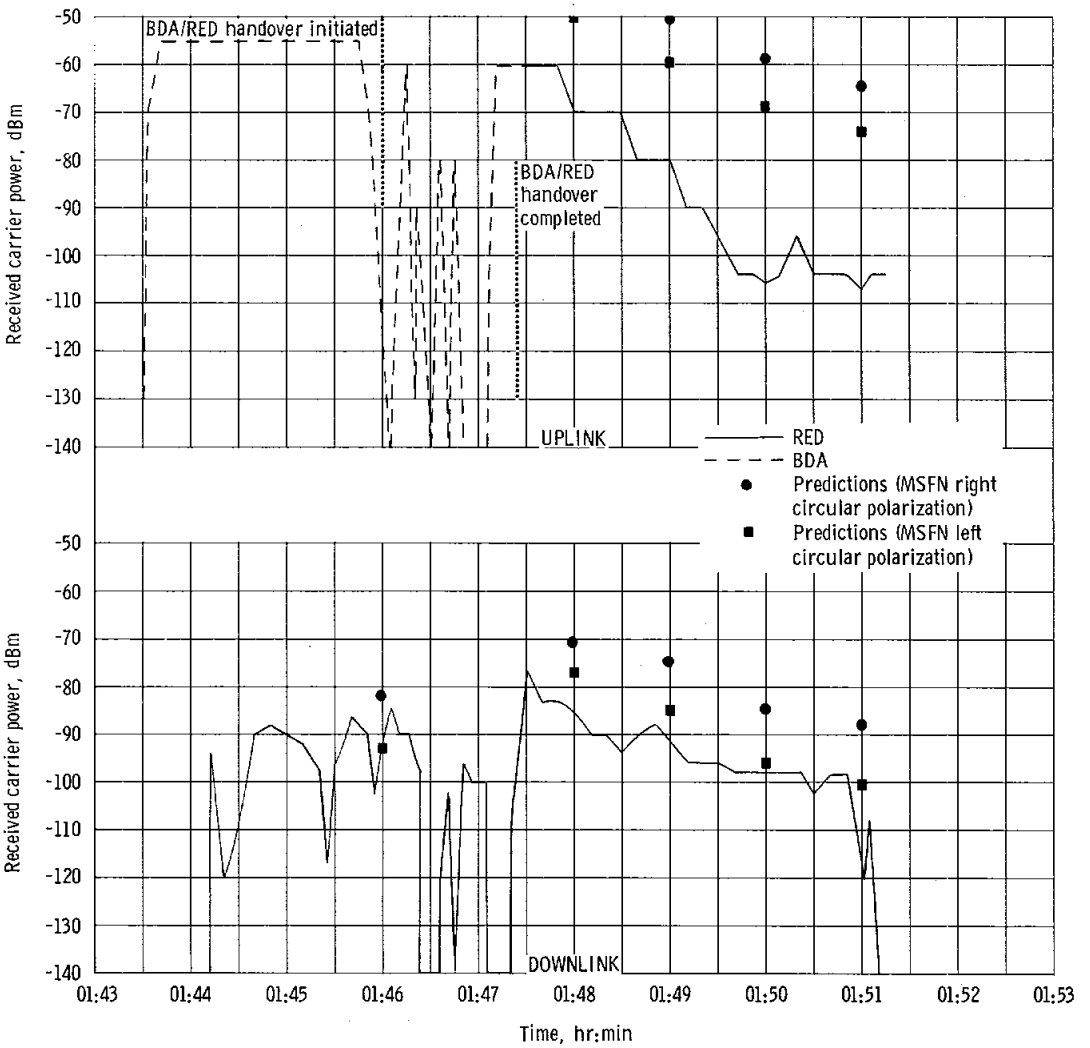

Figure 5.14-6. - Received S-band carrier power, Redstone, revolution 2.

NASA-S-68-3564

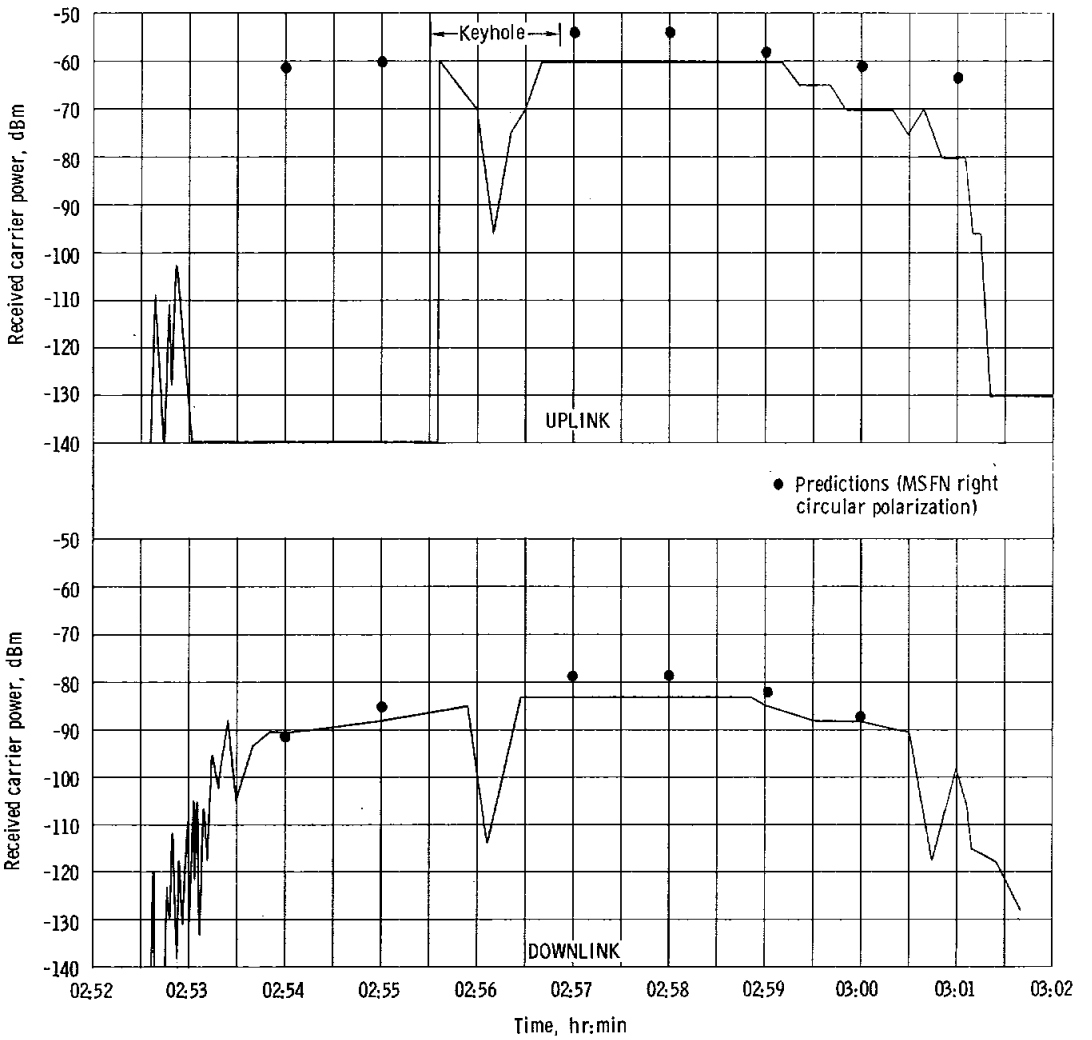

Figure 5.14-7. - Received S-band carrier power, Hawaii, revolution 2.

NASA-S-68-3565

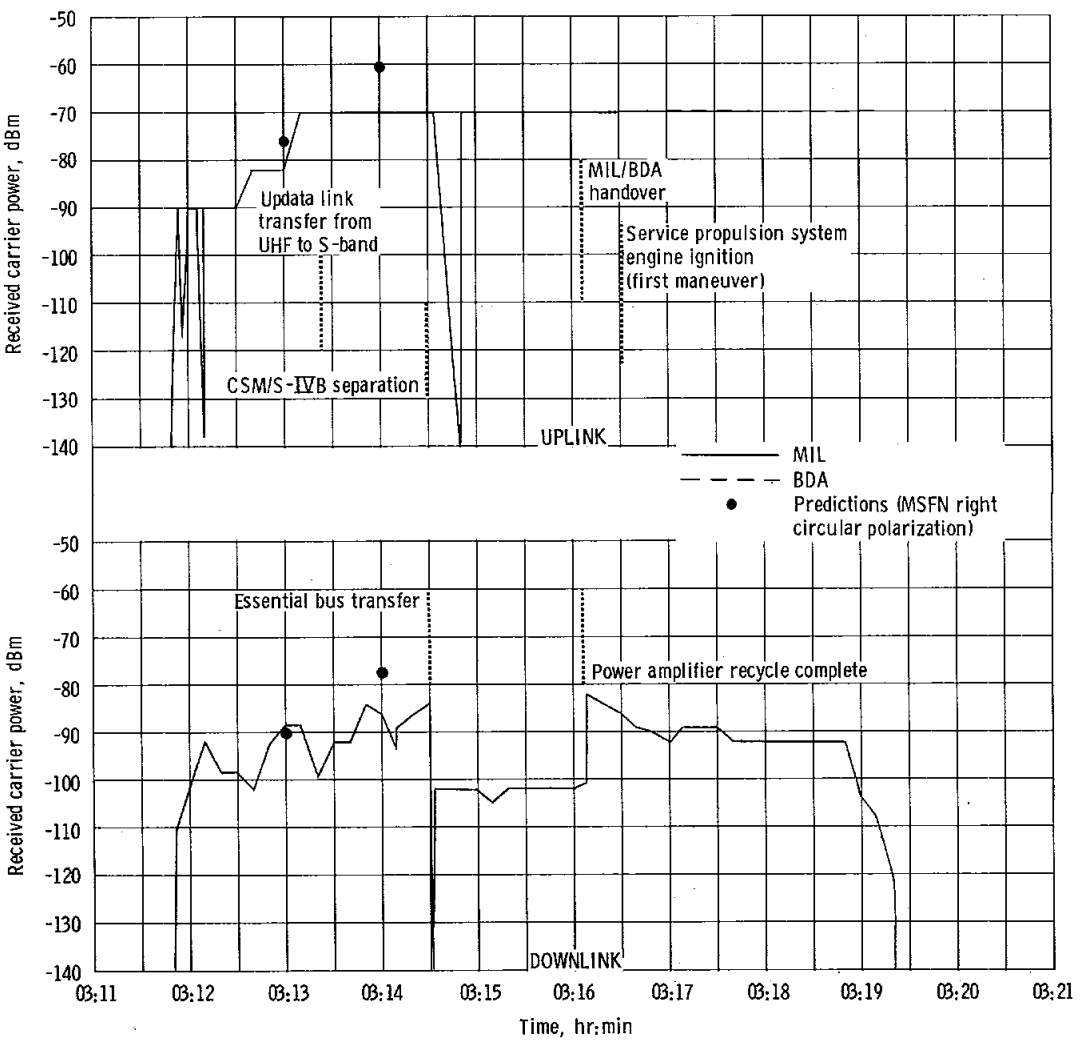

Figure 5.14-8. - Received S-band carrier power, Merritt Island, revolution 2-3.

NASA-S-68-3566

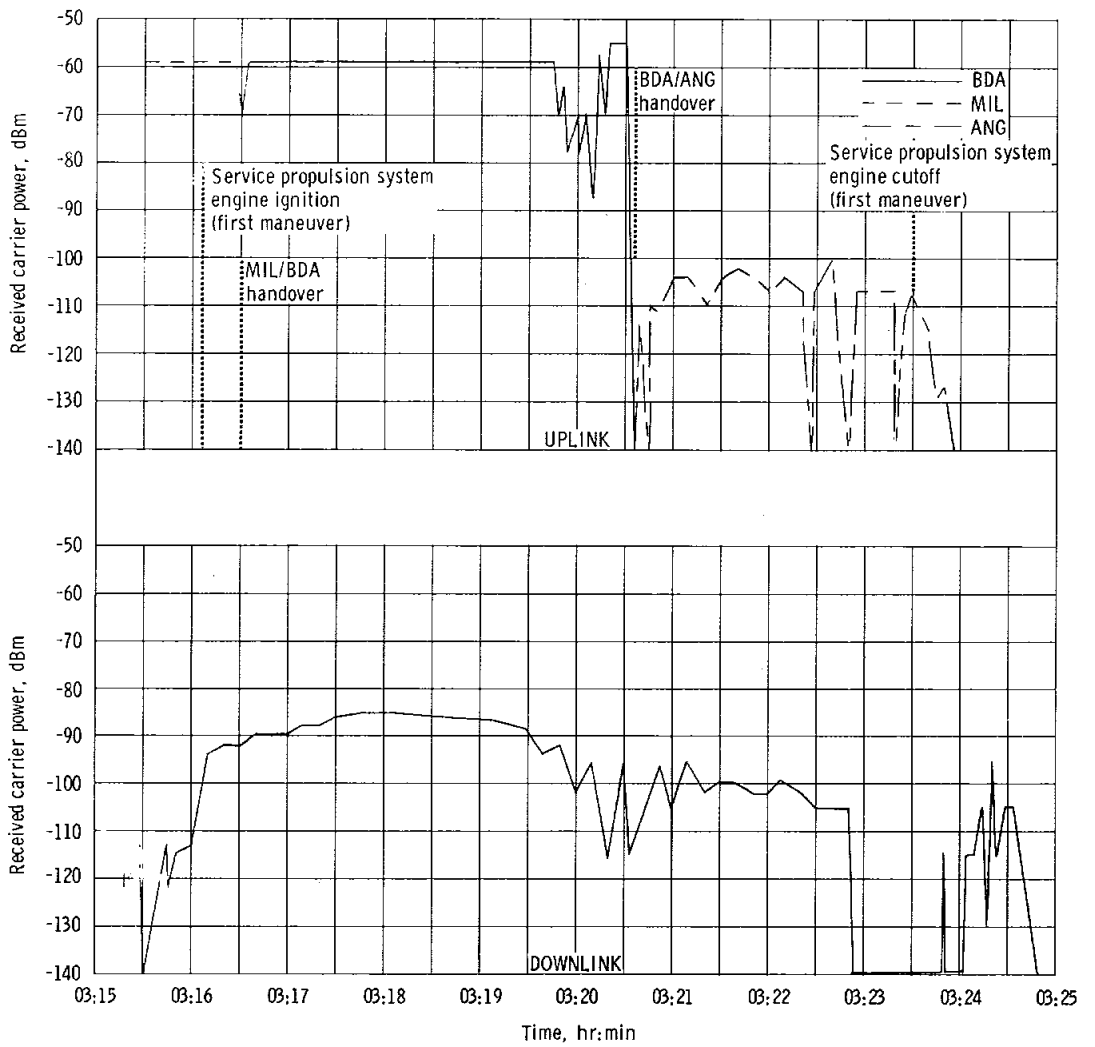

Figure 5.14-9. - Received S-band carrier power, Bermuda, revolution 3.

NASA-S-68-3567

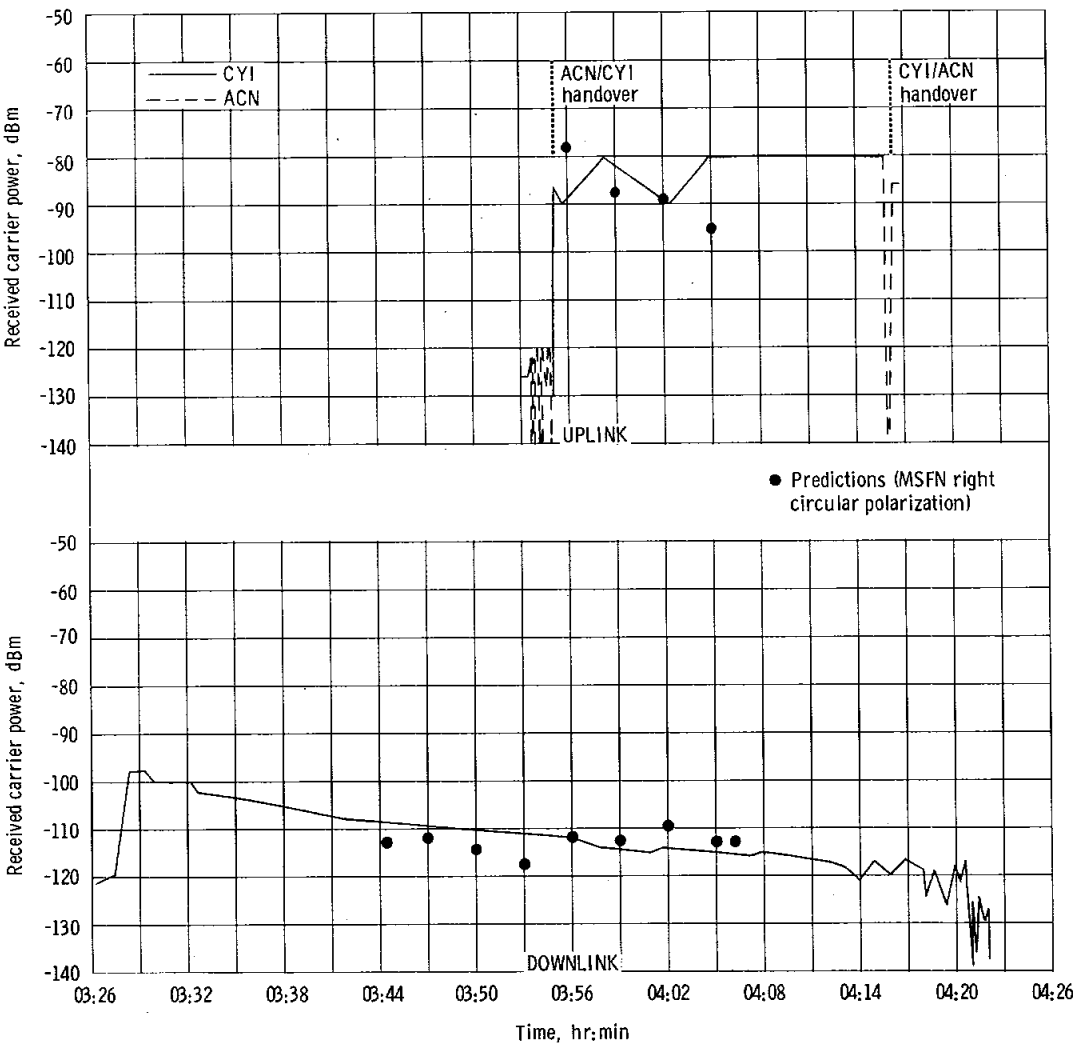

Figure 5.14-10. - Received S-band carrier power, Canary Island, revolution 3.

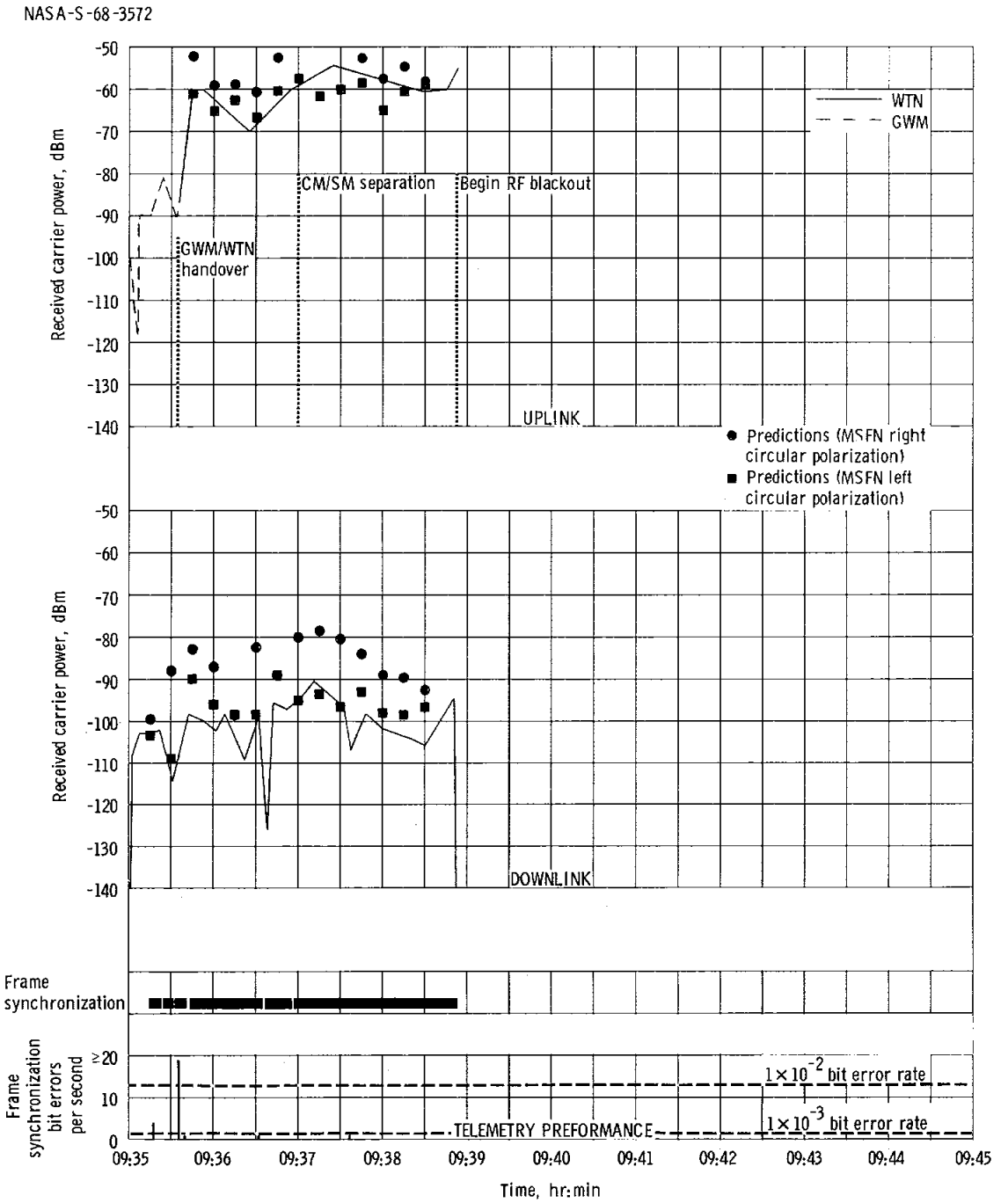

Figure 5.14-15. - Received S-band carrier power, Watertown, revolution 3.

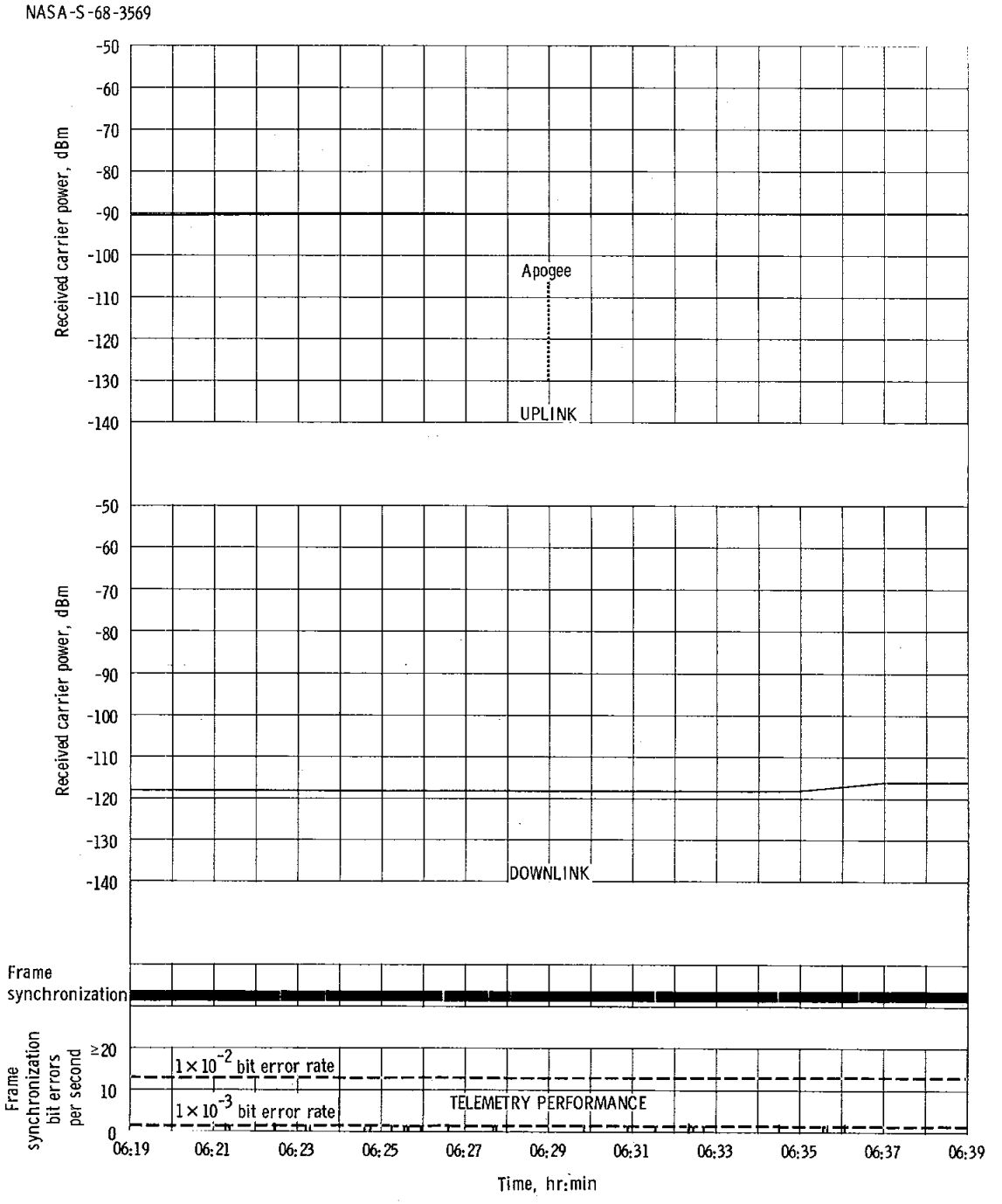

Figure 5.14-12. - Received S-band carrier power and telemetry performance, Ascension, revolution 3, apogee ± 10-minutes.

NASA-S-68-3570

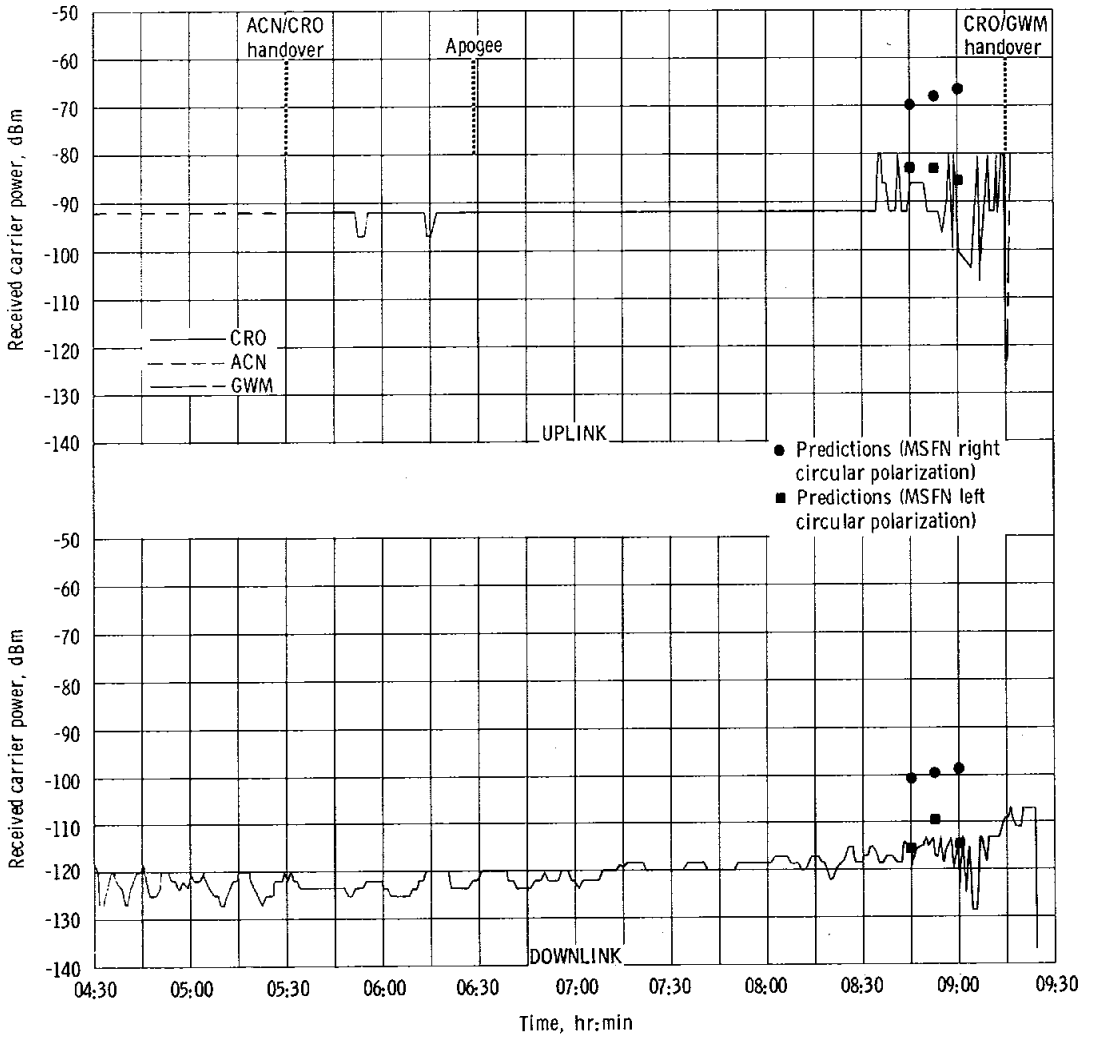

Figure 5.14-13. - Received S-band carrier power, Carnarvon, revolution 3.

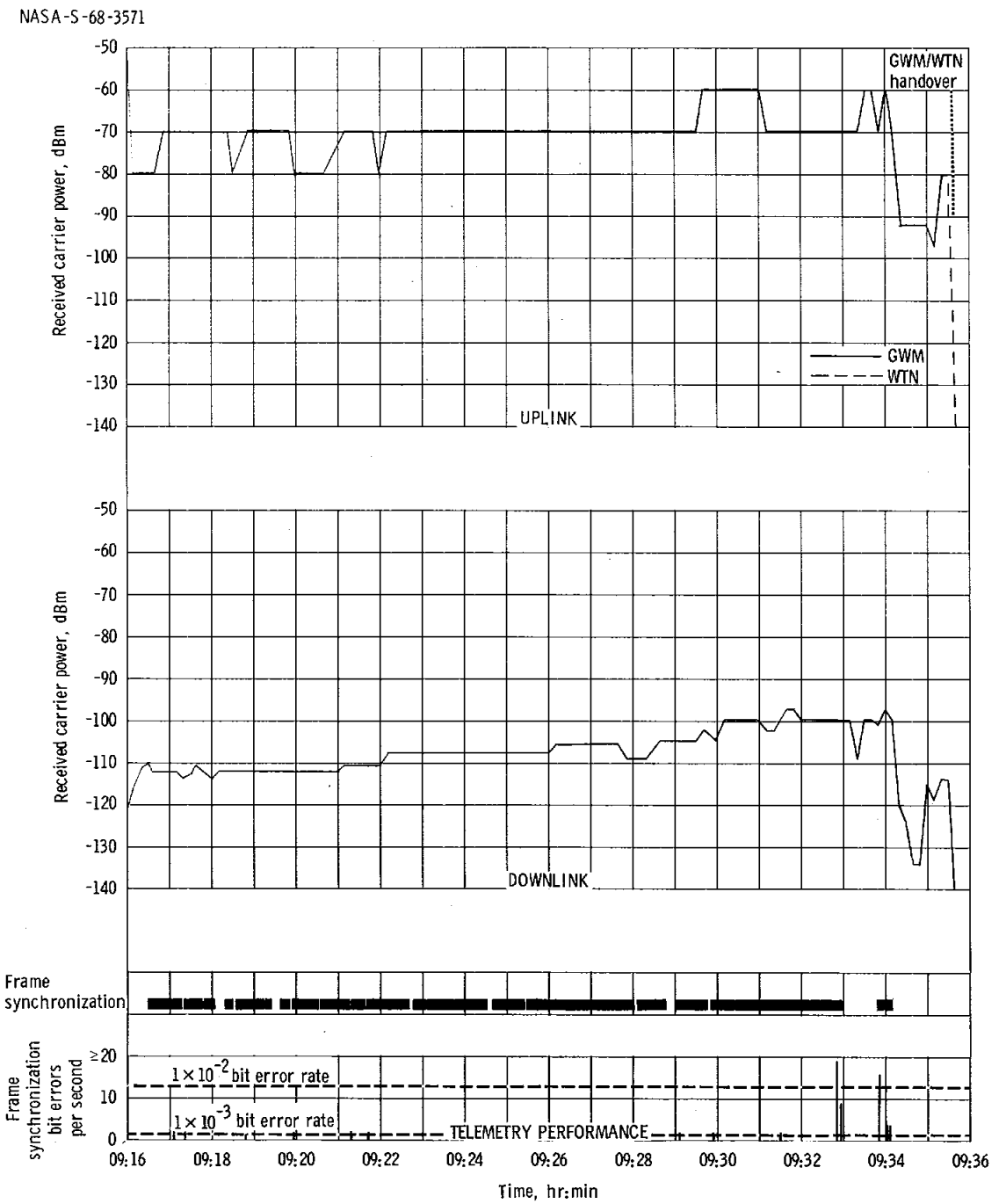

Figure 5.14-14. - Received S-band carrier power and telemetry performance, Guam, revolution 3.

NASA-S-68-3568

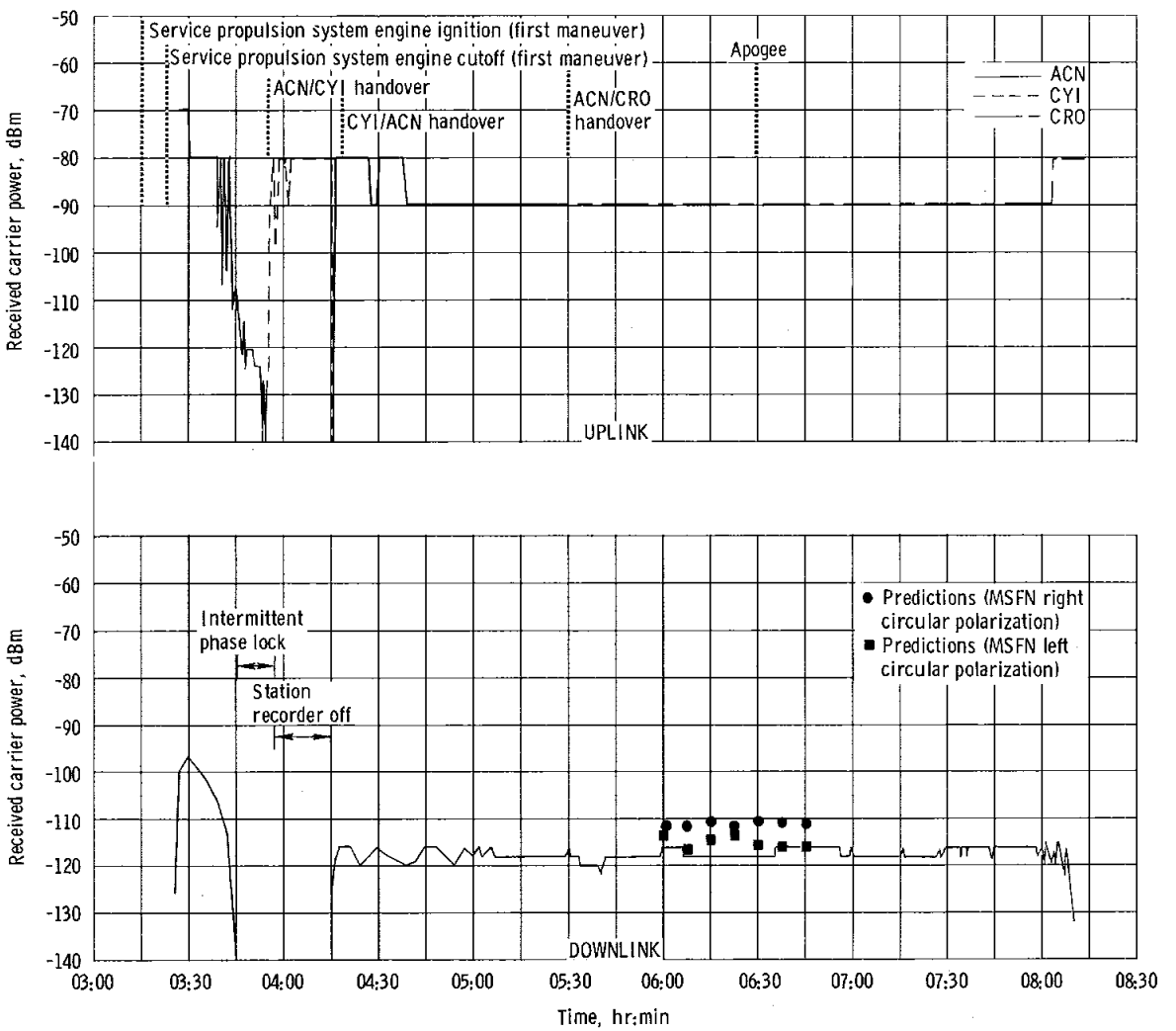

Figure 5.14-11. - Received S-band carrier power, Ascension, revolution 3.

NASA-S-68-3573

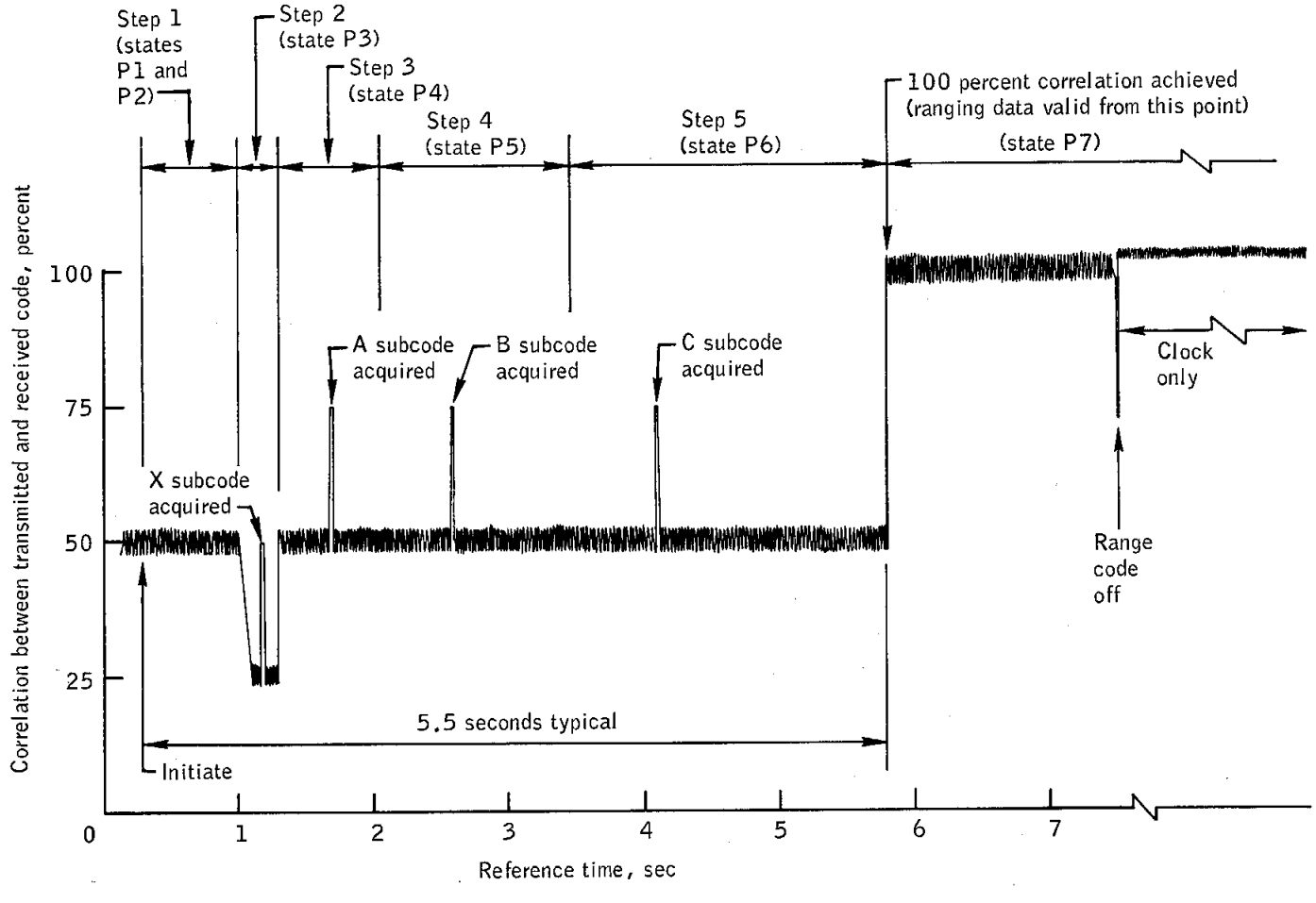

Figure 5.14-16.- Typical range code acquisition sequence (128 integrations per step).

NASA-S-68-3574

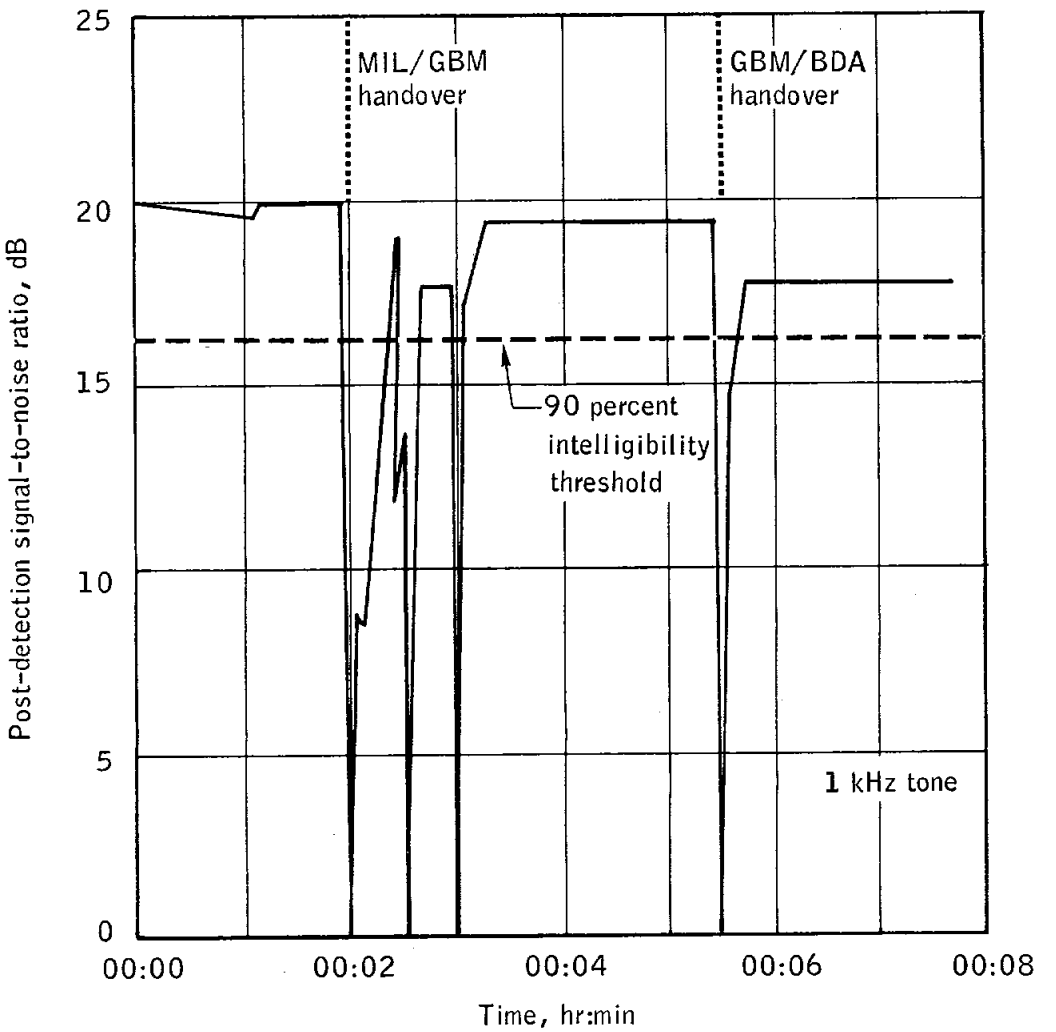

Figure 5.14-17.- Turned-around S-band up-voice signal-to-noise ratio, Merritt Island, launch.

NASA-S-68-3575

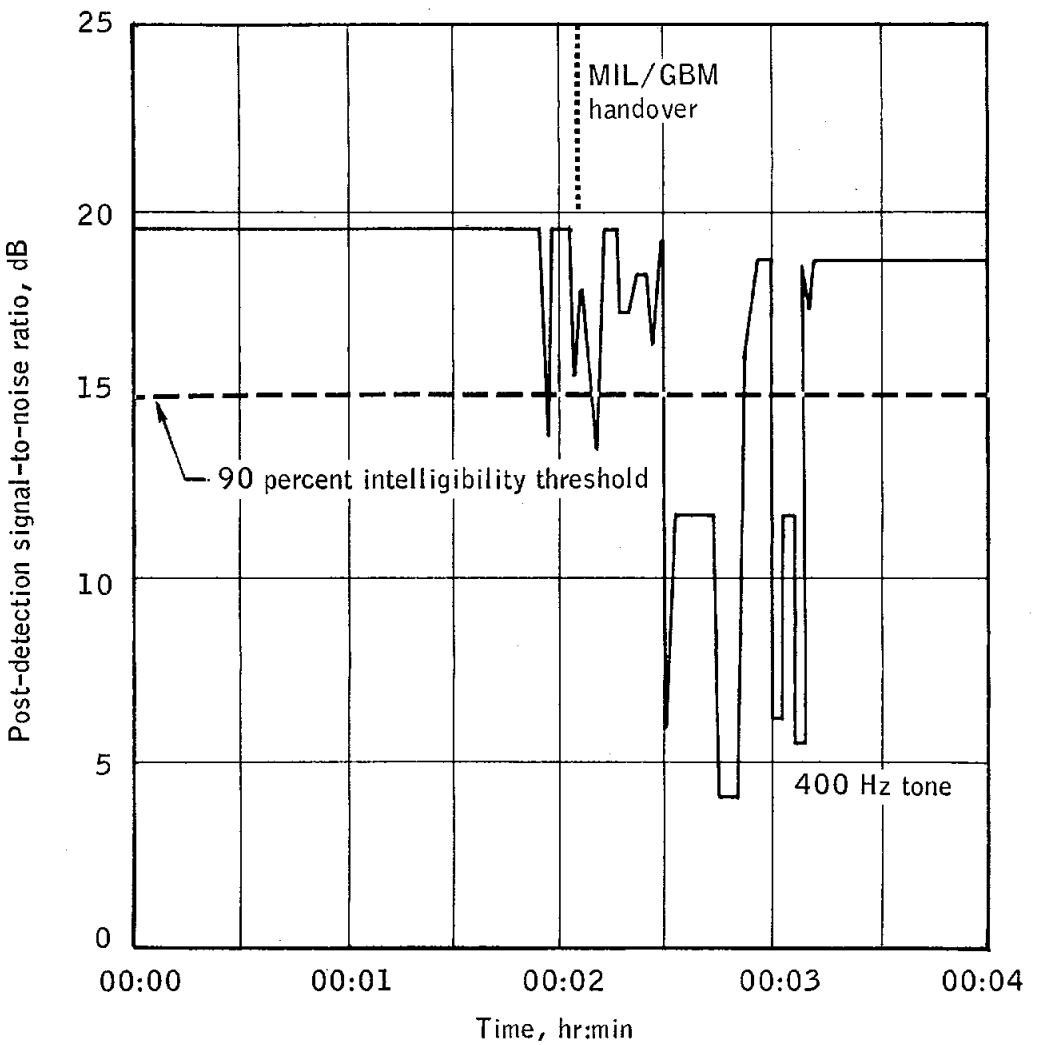

Figure 5.14-18.- S-band down-voice signal-to-noise ratio, Merritt Island, launch.

NASA-S-68-3576

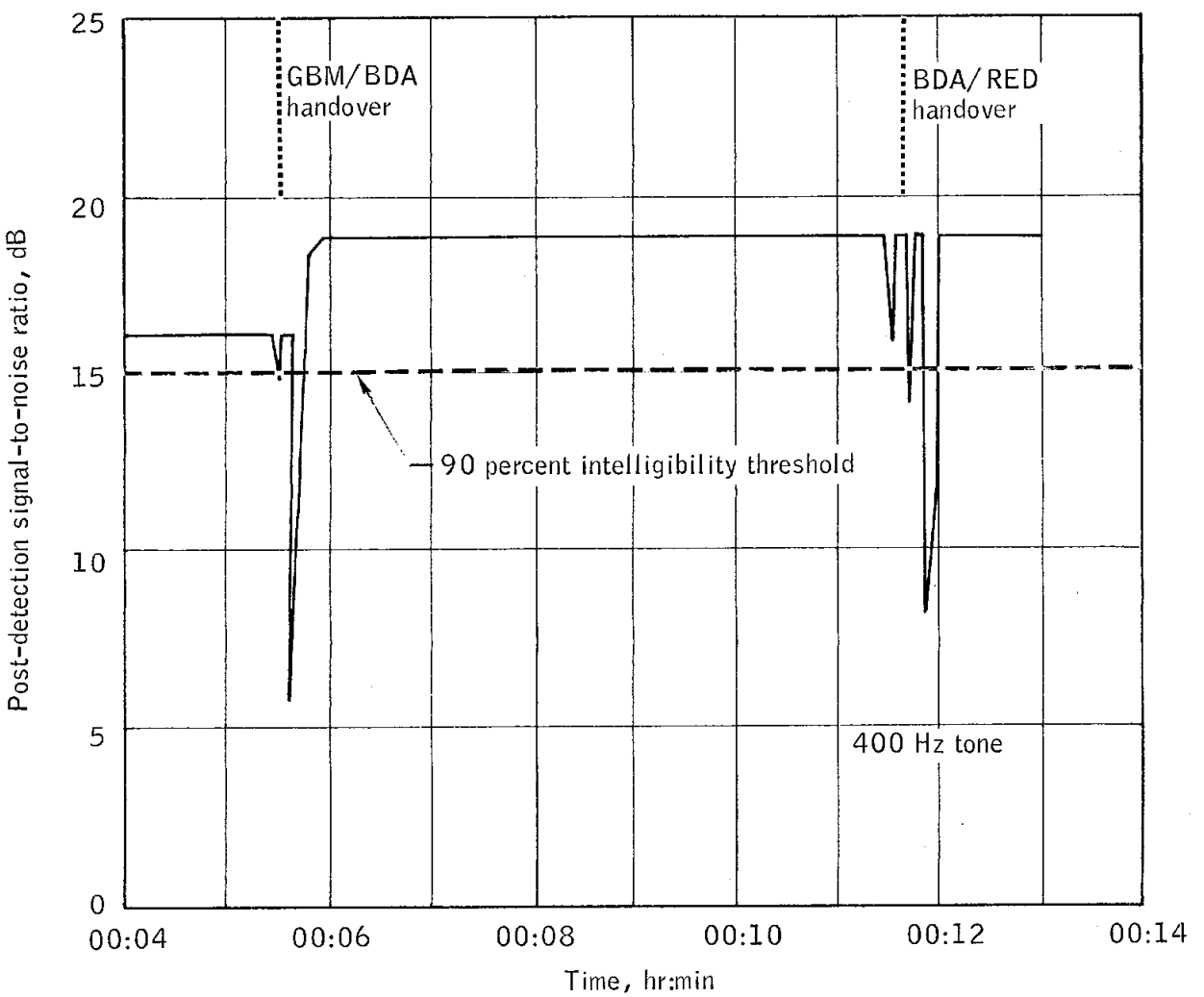

Figure 5.14-19.- S-band down-voice signal-to-noise ratio, Bermuda, revolution 1.

NASA-S-68-3577

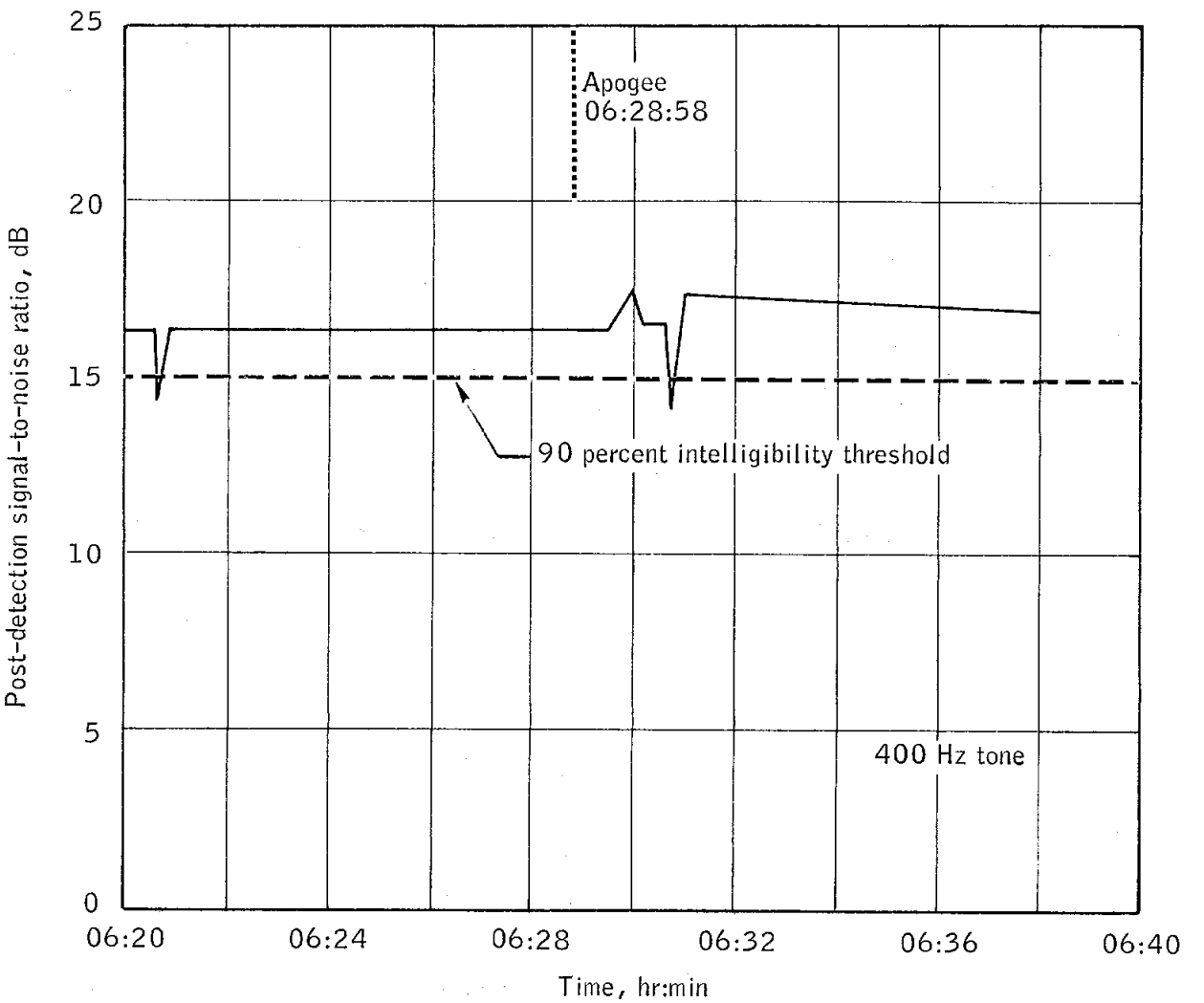

Figure 5.14-20.- S-band down-voice signal-to-noise ratio, Carnarvon, revolution 3.

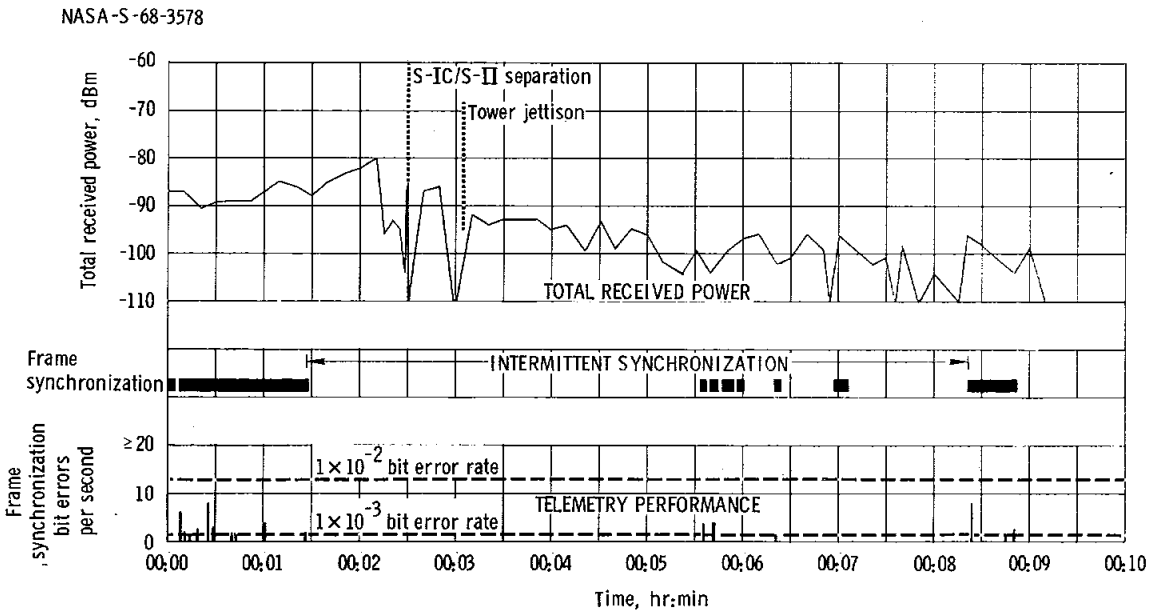

Figure 5.14-21. - Total received VHF power and telemetry performance, Merritt Island, launch.

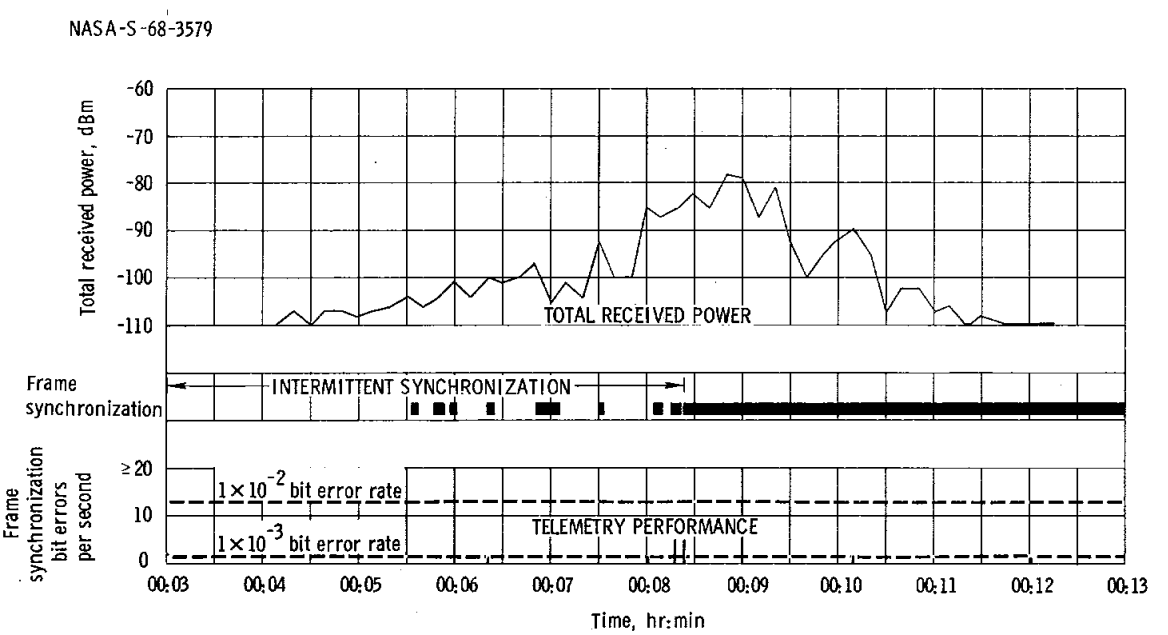

Figure 5.14-22. - Total received VHF power and telemetry performance, Bermuda, revolution 1.

5.15 INSTRUMENTATION

The spacecraft instrumentation system adequately supported the flight control of the mission and provided satisfactory data for analysis of the postflight mission evaluation, except for the data lost during the launch phase. Instrumentation equipment problems are summarized in table 5.15-I. Measurement problems are summarized in table 5.15-II.

The instrumentation system provided for the monitoring of 348 operational and 300 flight qualification measurement parameters.

In addition to this active instrumentation, 185 passive temperature (temp-plate) indicators (that change colors at specified temperatures) were attached to the command module structure and equipment. Postflight inspection of accessible indicators have indicated that temperatures did not exceed the lowest range of individual indicators.

5.15.1 Operational Instrumentation

A loss of both telemetered and onboard-recorded pulse code modulation (PCM) data during the launch phase was experienced from approximately 00:01:28 to 00:08:20. Additional PCM data losses were also experienced for short periods during the second and third revolutions. The cause of these losses is unknown at present. The central timing equipment initially jumped 2 minutes ahead at 00:02:24.7 and performed erratically until 00:55:12.7 (810 seconds ahead) and also from 03:29:35.7 until 03:29:35.7 and from 09:29:43.5 until landing. The central timing equipment was 141 956 seconds ahead at 09:29:43.5, after jumping 19 times. Additional discussion concerning these anomalies is contained in section 12.0. Postflight testing and analyses are continuing and the results will be included in an anomaly report.

The data storage equipment recorder operated satisfactorily for the two programmed periods of operation during the launch and entry phases. The recorder wow and flutter characteristics, as shown by the discriminated output of the 25-kHz reference signal, were satisfactory, except for a brief period at the time of maximum dynamic pressure (approximately 00:01:08 to 00:01:20). The flutter showed three noise spikes in the order of 3 to 4 percent during this period, although during the remainder of the flight, the value was less than 1 percent peak to peak.

The general operation of the 348 operational measurements (consisting of 221 analog and 127 bilevel event and digital words) and their associated equipment was good. Only three measurements of the anticipated instrumentation measurement complement required waivers prior to the mission. During the mission, two measurements failed, five measurements common to a single PCM signal gate provided no data, three measurements were questionable because of off-nominal data values, and one measurement provided a premature event indication. The operational instrumentation measurements were telemetered continuously by VHF and S-band communications prior to service module/command module separation and by S-band communications through entry.

The environmental control system glycol pump outlet pressure failed during the flight. During the launch phase, this measurement did not indicate the anticipated decrease which should have reflected the change in the absolute cabin pressure. Proper operation of the glycol loop was confirmed by related temperature indications. Before the mission, the system checkout at the contractor's facility and also at the launch facility had been conducted at standard atmospheric conditions which would preclude the recognition of a failure such as the one occurring during the mission. The present indications are that either a measurement failed or a gage-type (differential-type) sensing element was inadvertently installed in the transducer assembly and then the subsequent adjustment, calibration, and installation were performed as though an absolute pressure transducer had been used. A gage-type transducer will be used on block II vehicles. A postflight test has been initiated to recalibrate this transducer and to determine the exact configuration.

The cryogenic hydrogen tank 1 pressure measurement also failed. This measurement had exhibited erratic behavior during the prelaunch countdown phase as well as during the flight. This measurement had a history of failures and the corollary measurement (hydrogen tank 2 pressure) was replaced during vehicle checkout. A different model transducer for this measurement will be installed on block II vehicles.

The apparently simultaneous failure of five measurement systems (table 5.15-II) common to a single switching component within the PCM multiplex equipment was of major concern. A postflight analysis indicated the failure occurred during the period of intermittent PCM operation during the launch phase. The recovered PCM telemetry data indicated that all five affected measurements had similar characteristics that were independent of individual input stimuli. The exact nature of the equipment problem permitting this type of failure is not known; however, postflight testing is being conducted to resolve the problem.

The service propulsion system fuel tank pressure measurement did not recover from the initial pressure drop at the start of the service propulsion system engine firing and the data were considered to be questionable. The oxidizer and fuel inlet pressures and the oxidizer tank pressure were nominal for the firing conditions; however, a continuous decay in fuel tank pressure throughout the firing was observed. The resulting fuel tank pressure indicated a lower value than the engine inlet pressure. This condition was systematically impossible and indicated a malfunction of the measurement system. This transducer is located in a gaseous helium line which pressurizes the fuel tank. This line was cooled to approximately -114° F during the engine firing. Temperature compensation is normally employed to preclude erroneous pressure data resulting from these temperature extremes. The low pressure data exhibited during the extended engine firing is attributed to improper transducer temperature compensation. This measurement did provide correlated data both before and after the engine firing. Therefore, the performance of this instrumentation through the firing of the service propulsion system engine was considered questionable.

The Van Allen belt dosimeter operated satisfactorily during the ascent to apogee, except for a few isolated periods. During the descent from apogee, questionable data were caused by erratic low/high range switching of the two radiation measurements. Postflight testing of the dosimeter equipment with other spacecraft systems revealed electrical noise present on the output signal of the dosimeter measurement with sufficient amplitude to cause the switching anomaly. This noise was not observed on the output of the other dosimeter measurement. The source of this noise was indicated to be a crosscoupling effect between the inertial measurement unit sine angle measurement and the dosimeter measurement, which are sampled by the same PCM data system sequencer gate. This noise was observed on the engine valve actuation tank pressure measurement SP0601P but was not observed on the measurement inputs to the PCM data system. Additional postflight testing is being conducted to resolve this noise problem and to determine its relationship to the dosimeter switching anomaly. Additional discussion of this anomaly is contained in sections 10.2 and 12.1.

During the launch phase, a premature and erroneous indication of actual CSM/S-IVB separation was noted from one of the physical separation monitors at 00:02:13. This monitor was located in the plus Y and minus Z quadrant of the adapter and was one of two redundant measurements located 180 degrees apart. An indication of this event occurs when the measurement physical separation tape (approximately 28 feet) attached to the base of the adapter unreels approximately 3 inches. An additional 13 feet unreels during actual separation, providing distance indications of 5, 6.5, 10, and 13 feet. During actual separation, both monitors gave correct separation and measurement performance.

5.15.2 PCM Data Quality

A new synchronization and data quality program was used to measure the quality of the PCM data on this mission. Because of the erratic PCM operation (section 12.0), it was necessary to edit the synchronization and data quality outputs manually and then subtract the invalid subcommutated data (the computer could not determine whether these data were invalid) to obtain accurate usable PCM data percentages. A summary of the usable PCM data for the entire mission is presented in table 5.15-III.

The data were very poor from 00:01:28.1 until 00:08:19.9. The data quality before and after this period was excellent. Recurrence of the PCM problem was evident from 03:15:25.8 to 09:34:15.8. The launch-phase PCM data obtained from the data storage equipment indicated that, from 00:01:06.8 until 00:01:27.5 (immediately prior to the PCM problem), 13.75 percent of the data were not recoverable. This loss was caused by bit jitter in the PCM bit stream as a result of tape flutter during the maximum aerodynamic vibrations.

Although low signal strength caused the Bermuda and Antigua revolution 3 data to be only 82.14 percent and 71.25 percent usable, respectively, all data required for evaluation of the service propulsion system engine firing and attitude maneuvering were obtained.

Lower-than-normal data qualities after the launch phase were attributable to either recurrence of the PCM problem or to low signal strengths.

5.15.3 Flight Qualification Instrumentation

Flight qualification instrumentation provided data for evaluating vehicle system performance during the launch and entry phases of the mission.

The commutators mounted on the command module were used primarily to process heat shield and command module reaction control system data. The zero-scale and full-scale reference voltages for high-level commutator 1 and the corresponding commutated measurement data shifted twice during the mission. The correct levels were maintained through the launch phase until the tape recorder was turned off at 00:03:06.55. During entry, after the tape recorders were turned on at 09:36:56.13, the levels had shifted to 1 (±1) percent for the zero-scale and 95 (±2) percent for the full-scale reference level. These references shifted again at 09:52:42.44 to a level of 3 to 4 percent for the zero-scale and 87 to 88 percent for the full-scale reference levels. The zero-scale and full-scale reference voltages used by this commutator, as well as by high-level commutator 2, were derived from the operational

instrumentation 5-volt excitation reference supply. This reference supply was monitored by the operational instrumentation 5-volt sensor excitation measurement, which indicated a constant supply voltage throughout the mission. The cause of this reference shift and of all associated commutator measurement data shifts is unknown. The apparent data shift can be compensated for, and the data are considered valid. A postflight test has been initiated to establish the cause of this problem.

High-level commutator 2, which was mounted on the service module, processed 16 strain measurements, 15 temperature measurements, and 3 service propulsion system temperature measurements. This commutator exhibited erratic performance during the launch phase. The data from 00:01:28.68 until the tape recorder was turned off at 00:03:06.55 were unrecoverable by normal data processing methods. Indications were that the internal clock of the commutator lost synchronization and the wave train became less than the nominal 88 data pulses and a master pulse train. This problem was coincident with the problem of the flight qualification tape recorder time-code generator, as well as with the loss of PCM data. A review of the commutator wave train for this period indicated that realistic indications of gross measurement operation can be determined. The review also indicated a simultaneous failure of 19 measurements, all common to the same primary power source. This apparent failure was at approximately 00:02:13. The commutator performed satisfactorily when the flight qualification recorder was turned on prior to service module/command module separation. Data for the three remaining service propulsion system measurements were recovered for 640 milliseconds (from 09:36:56.13 until separation at 09:36:56.77). The service module/command module separation terminated the operation of this commutator.

The proportional bandwidth modulation package performed satisfactorily during the mission, processing 11 continuous CSM measurements.

During the launch phase, the time-code generator (4-second timer) for the flight qualification tape recorder experienced two anomalies. The first anomaly occurred at 00:01:04.5; for 0.6 second, the expected timing pulses did not occur. The following exhibited time displayed a gain of 10 minutes 25.85 seconds. The time-code generator performed normally thereafter until 00:01:26.4 when an extraneous pulse occurred. False counts were generated by the timer for the next 2.23 seconds. The timer output was unusable from 00:01:28.5 until the tape recorder was turned off at 00:03:04.84. These anomalies were not detrimental to the recovery of the data on the flight qualification recorder. During entry, the time-code generator performed nominally from the time the tape recorder was turned on at 09:36:55 until the tape recorder was turned off at 09:57:32 after command module landing.

The flight qualification tape recorder recorded data for each of the programmed periods of operation during the launch and entry phases. The recorder wow and flutter characteristics, as shown by the discriminated output of the 50-kHz reference signal, was satisfactory except that for a brief period during maximum dynamic pressure, the exhibited flutter noise was 3 to 6 percent peak to peak; the data storage equipment recorder experienced excessive flutter characteristics during this same period. The noise levels during the remainder of the flight were less than 2 percent peak to peak.

In general, satisfactory operation was provided by the 300 flight qualification measurements (23 continuous, 245 commutated, and 32 multiplexed (PCM) analog measurements) and the associated equipment. Only six measurements from the anticipated instrumentation measurement complement required waivers prior to the mission. One of the waived measurements, the tower Z-axis accelerometer, performed satisfactorily during the mission. Two measurements failed just prior to lift-off, two measurements failed during the mission, 19 measurements were questionable because of off-nominal data values, and five measurements exhibited data that indicated an instrumentation wiring transposition and a polarity reversal had occurred.

The adapter outer shell strain measurements 1 and 2 failed prior to launch. These measurements were observed to be functioning during the recorder checkout approximately 15 hours prior to launch. However, data appeared at a lower band edge at the beginning of the flight qualification tape record. The asymptotic calorimeter located on the conical heat shield at location 7 failed during entry at 09:42:12. This calorimeter was noted missing from the heat shield during entry. These plug calorimeters (0.75 inch deep and 1.35 inches in diameter) have had a history of failures resulting from heating at the weakened bond on the heat shield. Bondline temperature shear pad 5 dropped from a nominal reading of 60° F to the lower band edge of 105° F at 09:48:09. The trace remained at this level for 110 seconds and then stepped to minus 5° F. The data after the initial decrease were considered invalid.

Three aft heat shield heat flux (wafer calorimeter) measurements exhibited questionable data during entry. The measurement at location 6 was erratic and noisy after the initial heating indication. The measurements at locations 3 and 5 indicated that the initial temperatures were related to the second or third thermocouple wafer output level (when compared to relative measurements). Both these latter measurements provided a similar indication during the Apollo 4 mission.

The aft heat shield radiometer at location 3 was inconsistent with relative heat shield measurements and is considered questionable. Postflight inspection immediately after recovery revealed an obstruction of the quartz window measurement. Postflight testing and analysis are being conducted to establish the cause of questionable performance.

Several bondline heat shield temperature measurements exhibited questionable data during entry. Those which are considered suspect are listed in table 5.15-IV.

Responses to quasi-static temperature changes as encountered on the pad and during launch and the cold-soak phases were as anticipated. During entry, the majority of the bondline heat shield temperature measurements reflected the transient temperatures of entry. The measurements in question, however, indicated a negative temperature trend during a portion of entry. This problem is attributed in part to a group of defectively manufactured thermocouples together with inadequate installation and checkout procedures. These installations and checkout procedures will be reviewed and revised to prevent similar occurrences on future missions. It is also known that several defectively manufactured thermocouples have been installed on CSM 101 and will have to be considered in future analysis.

The aft heat shield boundary static pressure 4 measurement was questionable. The data exhibited the characteristic of a set diaphragm, abruptly dropping from a correct indication of 2 psia to 0 psia during the launch and entry phases (stepping up from 0 to 2 psia, then returning to 0 psia). The pressure indications higher than 2 psia appeared to be valid.

The aft heat shield boundary static pressure 6 measurement exhibited erratic bleed-down characteristics during the launch phase, possibly because of separation flow characteristics. This measurement was considered questionable, although subsequent data characteristics were nominal.

The vibration measurements were affected in varying degrees by electrical interference and noise spikes. Power spectral density plots of the vibration data isolated two frequency bands of electrical interference. These were at 20 to 26 Hz and at 85 to 95 Hz. This interference was also observed on the flight qualification tape recorder 4-second timing signal. Postflight testing is being conducted to establish whether the flight qualification tape recorder is generating the electrical interference noted.

Transient noise spikes were exhibited on four vibration measurements prior to lift-off and until approximately 00:00:45. These were the X axis aft service module bulkhead (near the fuel cell), radial service module aft bulkhead, and Y axis and Z axis command module lower equipment bay kick ring. This interference was also present on the command module acoustic microphone during the same period. All the vibration measurements exhibited electrical interference concurrently with the time code generator anomaly in the flight qualification tape recorder.

The acceleration data were also affected in varying degrees by the electrical interference and spiking shown in the vibration measurements. With the exception of the questionable data from the X axis accelerometer, all acceleration data were recoverable. The X axis accelerometer exhibited erratic peak-to-peak characteristics during the period 00:01:27 to 00:03:05, and the steady-state mean acceleration did not agree with the data obtained from the command module axial sway brace accelerometer.

All of the 17 heat shield static pressure measurements provided data during the entry period. Three pressure measurements, however, did not indicate a significant pressure increase as anticipated during the initial entry period. Two of these measurements were located on the side heat shield at locations 1 and 3. The other measurement was located on the forward heat shield at location 16. These measurements responded normally during the later phase of entry. Significant calibration offsets, caused by the constant deflection of the transducer diaphragms against the mechanical stops when at standard atmospheric pressure, were also exhibited by eight of the measurements. Compensation for these bias offsets was required in the heat shield data analysis. This condition had been experienced on previous missions, but the data were corrected for the offset. The offsets in percent of full scale were as follows:

Zero Shift of Less than a Nominal Tolerance of 10 Percent

Parameters	Shift, percent
Side heat shield pressure, location 7	3
Side heat shield pressure, location 9	3
Side heat shield pressure, location 11	2
Side heat shield pressure, location 14	2
Forward heat shield pressure, location 4	4
Forward heat shield pressure, location 16	2

Zero Shift Equal to, or Greater than,

a Nominal Tolerance of 10 Percent

Parameters	Shift, percent
Aft heat shield boundary static pressure 3	10
Side heat shield pressure, location 3	28

Four measurements were apparently not identified properly during the review of the data. Measurements of the side heat shield temperatures at locations 1-A and 1-B appeared to be interchanged, as did those of the forward heat shield temperature locations 4-A and 4-B. The tower Z axis accelerometer also indicated a polarity reversal. A review of the measurements installation drawing indicated the accelerometer was oriented 180 degrees from the designated axis. After allowance was made for these transpositions, the data were satisfactory.

5.15.4 Camera Systems

The camera systems performed satisfactorily. The photographic results are discussed in section 10.1. The camera system had no timing source; therefore, timing was determined from photographed events and camera frame speed and was accurate to within ±10 seconds. The camera installation and control logic are shown in figure 5.15-1.

The 70-mm sequence camera, supporting the earth photographs requirements, exposed a total of 754 frames through the hatch window; 370 photographs of the earth were exposed during daylight hours. The camera used a 76-mm f/2.8 lens and was loaded with 175 feet of 70-mm thin-base film. The camera was operated from approximately 01:29:55 to 03:27:38 and exposed a photograph every 8.6 seconds, allowing at least 50-percent overlap of adjacent frames.

The 16-mm movie camera operated through the left rendezvous window during the launch and entry phases. The camera used a 10-mm f/1.9 lens and was loaded with 775 feet of 16-mm thin-base film. The camera shutter was set at a speed of 1/360 second at an aperture of f/8. This camera photographed the departure of the boost protective cover and the launch phase until insertion, and then command module turnaround and plasma flow during the entry phase. The camera was operated at 10 frames per second during the two programmed periods of operation, 00:01:56 to 00:12:55 and 09:11:26 to 09:49:17.

The camera system activation was programmed during launch by onboard camera control boxes referenced to a 2.25g switch actuation which was calculated to have occurred at 00:00:46. The camera began operating at 00:01:56, after the programmed 70-second time delay.

Parachute deployment and landing sequences were not photographed because the duration of the mission was extended by approximately 10 minutes. The film in both cameras was exposed before the programmed cutoff.

TABLE 5.15-I.- INSTRUMENTATION EQUIPMENT ANOMALIES

System	Equipment	Remarks
Operational	Onboard pulse code modulation telemetry	A loss of both telemetered and onboard-recorded data during ascent (00:01:28 to 00:08:20) as well as other short periods throughout the flight was experienced.
	Central timing equipment	Erratic time information was provided during the entire flight.
Flight qualification	High level commutator 1	A data shift was noted in all measurements (not reading 0 or 100 percent full scale) during entry phase of mission.
	High level commutator 2	A partial loss of all data processed by this commutator during ascent after 00:01:28 was noted.
	Flight qualification tape recorder	There was excessive wow and flutter during maximum dynamic pressure during ascent.
	Time code generator	Time information was erratic during ascent.

TABLE 5.15-II.- APOLLO 6 CSM INSTRUMENTATION MEASUREMENT ANOMALIES

CSM system	Measurement number	Title	Category
		Operational	
Electrical power	CC0179T	Battery B case temperature	Failed[a]
Electrical power	SC2088T	Radiator 2 outlet temperature	Failed[a]
Cryogenics	SF0033Q	Oxygen tank 2 quantity	Failed[a]
Cryogenics	SF0039P	Hydrogen tank 1 pressure	Failed
Environmental control	CF0009Q	Waste water quantity	Failed[a]
Environmental control	CF0016P	Glycol pump output pressure	Failed
Flight technology	CK1051K	Radiation dosimeter rate	Questionable
Flight technology	CK1052K	Radiation dosimeter rate	Questionable
Service propulsion	SP0006P	Fuel tank pressures	Questionable
Sequential	SS0121X	SM/adapter physical separation monitor B	Questionable
		Flight Qualification	
Structures	CA0001A	X-axis spacecraft accelerometer	Questionable
Structures	LA0012A	Z-axis tower accelerometer	Reversed
Structures	CA1477T	Temperature shear pad 5 bondline	Failed
Structures	CA3363K	Radiation aft heat shield location 3	Questionable
Structures	CA5015R	Flux aft heat shield location 6	Questionable
Structures	CA5018R	Flux aft heat shield shear pad 3	Questionable
Structures	CA5019R	Flux aft heat shield shear pad 5	Questionable
Structures	CA5043P	Aft heat shield boundary static pressure 4	Questionable

[a]Measurement failures common to a PCM gate problem.

TABLE 5.15-II.- APOLLO 6 CSM INSTRUMENTATION MEASUREMENT ANOMALIES - Concluded

CSM system	Measurement number	Title	Category
Flight Qualification			
Structures	CA5045P	Aft heat shield boundary static pressure 6	Questionable
Structures	CA5556R	Flux side heat shield location 7	Failed
Structures	CA5700T	Temperature side heat shield location 1-A	Reversed
Structures	CA5701T	Temperature side heat shield location 1-B	Reversed
Structures	CA5715T	Temperature forward heat shield location 4-A	Reversed
Structures	CA5716T	Temperature forward heat shield location 4-B	Reversed
Structures	AA8120S	Adapter outer shell longeron strain 1	Failed
Structures	AA8124S	Adapter outer shell longeron strain 2	Failed
Structures	CA5834T	Temperature window frame aluminum	Failed[a]

[a]Measurement failures common to a PCM gate problem.

TABLE 5.15-III.- USABLE PULSE CODE MODULATION DATA

Station	Revolution number	Tape number	Usable data, percent
Merritt Island	Launch	Not applicable	(a)
TEL IV			(a)
Bermuda			(a)
Data storage equipment	Launch		(a)
Canary Island	1		99.72
Carnarvon	1		99.35
Canberra	1		95.69
Guaymas	1		99.49
Texas	1		99.90
Merritt Island	1/2		99.65
Bermuda	2		99.39
U.S.N.S. Redstone	2		79.33
Canary Island	2		73.99
Canberra	2		97.16
Hawaii	2		99.25
Goldstone	2		99.71
Guaymas	2		99.74
Texas	2		99.70
Merritt Island	2/3		99.05
Bermuda	3		82.14
Antigua	3	Not applicable	71.25
Canary Island	3	1	99.35
		2	99.70
		3	(b)
Ascension	3	1	99.81
		2	97.69
		3	98.67
		4	97.75
		5	(b)
		6	98.41
		7	99.39
		8	98.86
		9	99.55
		10	98.07
Carnarvon	3	4	97.06
		10	95.08
		11	(b)
		12	(a)
		13	(a)
Guaymas	3	Not applicable	97.75
U.S.N.S. Watertown	3		94.85
Data storage equipment	Entry	Not applicable	99.996

[a]Pulse code modulation prevents accurate assessment.

[b]Unable to process.

TABLE 5.15-IV.- APOLLO 6 COMMAND MODULE BONDLINE

HEAT SHIELD THERMOCOUPLE MEASUREMENTS

Measurement No.	Title
CA1479T	Temperature near shear pad 5
CA1480T	Shear pad 3 (fiberglass bondline)
CA5080T	Aft heat shield location 1
CA5085T	Aft heat shield location 2
CA5090T	Aft heat shield location 3
CA5095T	Aft heat shield location 4
CA5100T	Aft heat shield location 5
CA5114T	Aft heat shield location 7
CA5115T	Aft heat shield location 8
CA5713T	Side heat shield location 3
CA5742T	Side heat shield location 9
CA5767T	Side heat shield location 14

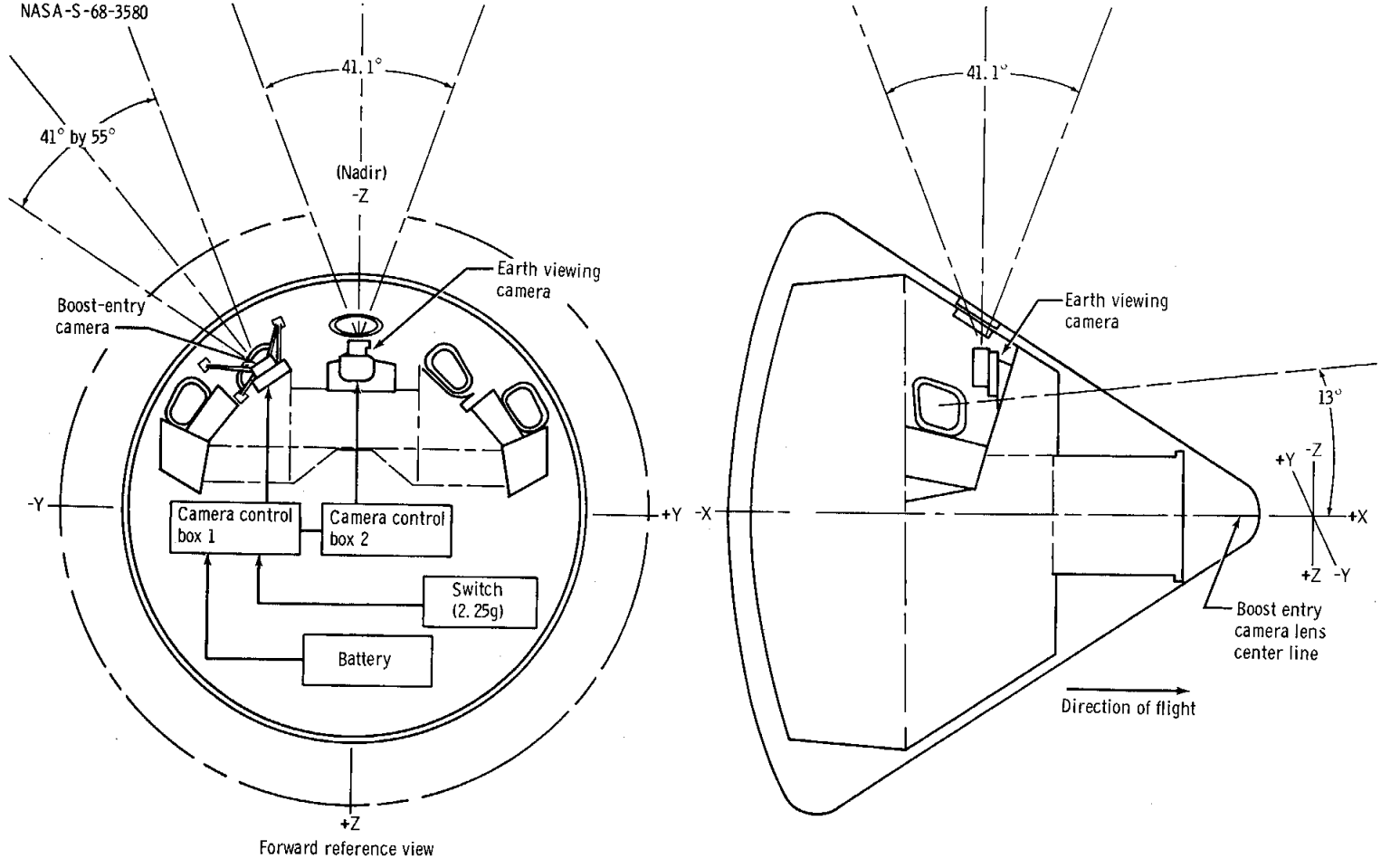

Figure 5.15-1. - Camera system look angles.

5.16 GUIDANCE AND CONTROL

Performance of the guidance and navigation system, stabilization system, stabilization and control system, and mission control programmer was excellent throughout the mission. Monitoring functions and navigation during the ascent and earth-orbital phases were nominal. Guidance during the service propulsion system engine firing was excellent and all attitude maneuvers were performed correctly. Attitude limit cycles during the coast phase were commensurate with the disturbance torques present. All sequencing performed in the computer and in the mission control programmer was correct. Numerous computer update alarms were generated, but these appeared to have been caused by a source external to the computer. The attitude reference drift in the stabilization and control system was greater than on previous flights. This condition was expected from preflight observations of sensitivity to noise generated when the C-band transponder was interrogated. Guidance, navigation, and attitude control during entry were excellent.

5.16.1 Integrated System Performance

Ascent and earth orbit.- The inertial measurement unit was released from gyrocompassing and was inertially fixed at 00:00:01.15, after receipt of the lift-off command from the instrument unit. From lift-off until launch escape tower jettison, the computer drove the coupling display units in accordance with a prestored roll program and pitch polynomial which was intended to match the launch vehicle maneuver program. As on Apollo 4, a late change was made in the launch vehicle pitch trajectory which was not reflected in the spacecraft computer program. Therefore, the pitch error shown in figure 5.16-1 was predicted. The actual error, also shown on the figure, is the difference between the computer-driven coupling display unit and the inertial measurement unit gimbal angle. The actual error would have been displayed to the crew on the flight director attitude indicator attitude error needles, if this had been a manned flight. The difference between the predicted and actual errors is attributed to initial misalignment of the two platforms, to coupling display unit lags, and to flexure of the vehicle. (Further discussion of gimbal angle behavior during ascent will be included in Anomaly Report 6.) After tower jettison, the system switched to the TUMBLE MONITOR mode in which the computer examined the gimbal angles for excessive attitude changes. No tumble alarms were indicated.

State-vector comparisons at the time of insertion and other selected events during the mission are shown in table 5.16-I. In all cases the errors were well within expected tolerances.

CSM/S-IVB separation.- The separation sequence, initiated by ground command, began at 03:14:26.2. A time history of command and service module control system parameters for this period is presented in figure 5.16-2. The S-IVB was performing a three-axis maneuver when separation occurred, as indicated by the body rates shown in the figure. The pitch rate transient after separation (minus 1.7 deg/sec) was larger than had been noted on previous missions and is unexplained at the time of this report. All sequencing was correct and the disturbance torques caused by the center of gravity offset during the plus X translation were comparable to preflight predictions. The net change in velocity accumulated during the sequence was 1.8 ft/sec.

First service propulsion system engine firing.- The attitude maneuver prior to the service propulsion system engine firing is shown in figure 5.16-2. The response of the CSM to attitude commands was correct throughout the maneuver. The firing attitude calculated by the computer was correct for the state vector and for the loaded targeting conditions.

Dynamic response during the firing is shown in figure 5.16-3. Body rate transients at ignition were plus 1.8 and plus 2.7 deg/sec in pitch and yaw, respectively; these were caused by a combination of engine gimbal trim errors (table 5.16-II) and propellant slosh from the no-ullage start. The high-frequency oscillation noted on the start transient is attributed to body bending. Although the start transients were damped out within 3 seconds, a low-grade oscillation with a 2-second period continued for approximately 1 minute. This oscillation, which had been predicted preflight, was attributed primarily to propellant slosh and was larger than experienced on the Apollo 4 flight. Differential clutch currents during the firing indicated thrust misalignment torques well within tolerances; disturbances during tailoff were low. Sequencing of the computer, stabilization and control system, and mission control programmer was correct throughout the maneuver. The initial guidance command caused a plus 2.1 deg/sec pitch rate excursion 4 seconds after ignition. Although this excursion was greater than experienced for previous missions, it was correct for the initial conditions and the system software mechanization. For this mission, the calculation of firing attitude was based on ignition immediately after the calculation. For a nominal mission with a translunar injection firing, the orbital rate prior to service propulsion system engine ignition would have been very low and the velocity vector required to meet the targeted conditions would have rotated very slowly. Therefore, no appreciable attitude error would have accumulated in the 90-second period between the firing attitude calculation and the firing. During the Apollo 6 mission, the orbital rate exceeded 4 deg/min; therefore, approximately 7 degrees of pitch attitude error accrued in the 90 seconds before ignition. The large initial guidance command was necessary to remove this error.

The steering commands and velocity-to-be-gained histories for the firing are shown in figure 5.16-4. The initial increase in X-axis velocity to be gained and the pitch steering activity were primarily caused by the firing attitude calculation previously discussed. As shown in figure 5.16-4, the guidance system drove the velocities to be gained in each axis through zero, verifying system performance. Evidence of a 3.2-ft/sec overfiring is also presented in figure 5.16-4. The computer was programmed to anticipate a thrust decay impulse equivalent to 0.44 second of full thrust and to adjust the engine OFF command accordingly. The actual tailoff impulse calculated from the inertial measurement unit accelerometers was 0.54 second of equivalent full thrust. The system was targeted for the eccentricity and semilatus rectum shown in table 5.16-III. The difference between the targeted and achieved conditions was caused by the variation in tailoff impulse.

Cold-soak phase.- The beginning of the maneuver to achieve the cold-soak attitude is shown in figure 5.16-5. Although data were not available for the entire maneuver, indications are that system performance was nominal, and the programmed attitude was achieved. Attitude limit cycles followed a consistent pattern throughout this period, but the frequency of thruster firings varied. The pattern of firings in roll and yaw was similar to that of the Apollo 4 mission; however, the ratio of plus-to-minus pitch firings decreased from as much as 20:1 to 2:1. This indicated that the pitch disturbance torque decreased significantly. The disturbance is attributed to steam venting as on the Apollo 4 mission; therefore, the magnitude or direction must have changed accordingly. The value of this disturbance at different times during the cold-soak phase is shown in table 5.16-IV.

Second service propulsion system engine firing.- The maneuver to attain the second service propulsion system engine firing attitude is shown in figure 5.16-6. System performance was nominal and the attitude commanded was correct. Although ignition had been inhibited by ground command, the computer proceeded through the sequence as programmed, initiating plus X translation and issuing the engine ON command. During the plus X translation, excessive roll rate oscillations and thruster activity occurred (fig. 5.16-7). Similar activity occurred on the AS-202 mission and was attributed to the combination of light-weight vehicle and overcontrol with four-engine authority. Two-engine or four-engine roll authority can be selected in a manned mission.

The plus X translation continued 50.15 seconds. Normally, pitch and yaw thruster activity is inhibited within the stabilization and control system 1 second after receipt of the engine ON command. Because ground control inhibited this command, the plus X translation continued until commanded OFF by the computer. After issuing the service propulsion system engine ON command, the computer monitors the velocity

accumulated during 10 successive 2-second periods in the change-of-velocity monitor routine (which is set at 2 ft/sec per 2-second period). Because the required conditions were not achieved, the computer commanded the shutdown sequence that included terminating the plus X translation.

Command module/service module separation.- Command and service module dynamic response during the separation sequence is shown in figure 5.16-8. At the time of physical separation, the CSM was rolling at minus 1.2 deg/sec in response to a guidance and navigation attitude command. The command was generated as a result of the preseparation transfer of the roll coupling display unit from the 1:1 to the 16:1 resolver. (This transfer is made to obtain greater sensitivity and faster response in the roll axis during entry. In the process of transferring, the 16:1 resolver is driven to the nearest correctly phased null. When the attitude control is resumed, any residual attitude error is effectively magnified 16 times.) On the Apollo 6 mission, the attitude error was sufficient to generate the roll rate noted. Despite the roll activity, the pattern of disturbance torques after separation was similar to that on previous missions and was consistent with plume impingement from the service module minus X control engines.

Entry.- The guidance and navigation system operated properly throughout the entry phase. The 49.2-n. mi. miss distance resulted from a known error in the guidance equations programmed in the computer. The guidance logic used on the Apollo 4 and 6 missions was a preliminary version of the logic that will be used on the lunar mission and was divided into five basic phases — INITIAL ROLL, HUNTEST, UPCONTROL, KEPLER, and FINAL. The problem in the Apollo 6 logic involved the HUNTEST and UPCONTROL phases.

During the HUNTEST phase, the guidance logic predicts the reference trajectory that will be flown during the critical UPCONTROL phase. This is accomplished by predicting the velocity and drag level at pull-out. If the velocity and drag level at pull-out are known, it is possible to predict analytically the velocity and the flight-path angle at skip-out by assuming a lift-to-drag ratio for the UPCONTROL phase and an exponential atmospheric density model. For this first prediction, skip is defined as a drag level of 6 ft/sec/sec. If the value of the skip-out flight-path angle is negative, it is assumed that skip-out cannot be achieved with the reference lift-to-drag ratio for the UPCONTROL phase. In this case the value of the drag level is recomputed to a higher value (the minimum predicted drag level), and the velocity and flight-path angle at skip-out are recomputed based on the higher value of the drag level. In addition to these parameters, the computer predicts the entry range associated with these pull-out and skip-out conditions. The computer also predicts the range for the other guidance phases and, if the total predicted entry range is within 25 n. mi. of the present range to

the target, the reference trajectory is accepted; then, the command module attempts to fly this reference trajectory in the UPCONTROL phase. If the predicted range is short of the actual target range, a new reference trajectory is established by changing the value of the pull-out velocity and thus, of velocity and flight-path angle at skip-out, without recomputing the drag level. This iteration process is continued until an acceptable reference trajectory is calculated.

For the actual Apollo 6 entry conditions, a problem (identified in preflight simulations) with the reference trajectory affected the performance of the guidance logic. On the first pass through the HUNTEST phase, a negative value of skip-out flight-path angle was computed. This caused the drag level to be recalculated to a higher value of approximately 26 ft/sec/sec. The predicted range was also short of the target; therefore, the pull-out velocity was adjusted to a higher value which caused the new skip-out flight-path angle to be positive. Because the skip-out flight-path angle was positive, the drag level should have been reinitialized. The Apollo 6 entry guidance logic did not allow reinitialization of the drag level; therefore, a non-optimum reference trajectory was established because the reference trajectory for the UPCONTROL phase was depressed below that desired. This caused the command module to fly approximately 46 seconds of negative lift in UPCONTROL in an attempt to satisfy the reference trajectory conditions. Thus, the command module was placed in a large target undershoot condition at the start of FINAL phase. This large undershoot was partially compensated for by flying with lift vector up during the second entry guidance phase.

The sequence of events as determined from telemetry is shown in figure 5.16-9. The command module reached the entry interface at 09:38:29; the computer program mode was 63. The computed inertial range to target was 2038.68 n. mi. At 09:39:09, an acceleration of 0.05g was sensed, and the computer entered the INITIAL ROLL phase (program mode 64). At 09:40:04, the computer transferred to the HUNTEST phase. The inertial velocity was 29 855.5 ft/sec, and the computed inertial range to the target was 1533.5 n. mi. The difference in the actual minus the predicted range to go was positive and was greater than 25 n. mi. on the initial pass through the HUNTEST computer phase, so the pull-out velocity was incremented until the difference was less than 25 n. mi. The final value for the difference was minus 14.3 n. mi. The computer remained in the HUNTEST phase for one 2-second cycle and then transferred to the UPCONTROL phase (program mode 65). At the beginning of the UPCONTROL phase, the inertial range to target was 1524 n. mi., and the inertial velocity was 29 576.87 ft/sec. The KEPLER phase (program mode 66) was entered at 09:42:20. The range to target at this time was 976 n. mi., and the inertial velocity was 29 733.39 ft/sec. The FINAL phase, program mode 67, began at 09:43:58 with an inertial velocity of 19 718.158 ft/sec and an inertial range to target of 655.21 n. mi.

The FINAL phase guidance was terminated at 09:50:10, when the relative velocity dropped to 1000 ft/sec and the computed range to target was 40.9 n. mi. At the time of drogue deployment, the computed range to target was 36.36 n. mi.

The maximum load factor, computed from the inertial measurement unit accelerometers, was 4.67g; this occurred at 09:40:06. A second peak load factor of 1.912g occurred at 09:45:40. The minimum altitude reached on the first entry was 185 937 feet at 09:40:10; the maximum altitude for the skip-out was 218 365 feet at 09:42:58.

The commanded bank angle (roll command) and the actual bank angle as a function of the entry time are shown in figure 5.16-10. The very good agreement between the two indicated that the command module closely followed the commanded bank angle. The navigation state vector from telemetry is compared with a trajectory reconstructed from inertial measurement unit accelerometer outputs in table 5.16-V. For the reconstruction, the guidance commands were computed from the accelerometer data. At several points along the trajectory, the comparison indicated that the computer correctly interpreted data from the accelerometers throughout the entry phase.

The planned and actual landing points are shown in figure 5.16-11. The landing point computed by the guidance and navigation system was 36.36 n. mi. short of the planned landing point, 12.01 n. mi. from the aircraft-estimated landing point, and 13.45 n. mi. from the carrier pickup point. These differences between the guidance and navigation landing point, the aircraft-estimated landing point, and the carrier pickup point were due to the initial condition errors and inertial measurement unit errors. A trajectory reconstructed from corrected accelerometer data yielded a landing at 158 degrees 4 minutes West longitude, 27 degrees 34 minutes North latitude. This trajectory indicated a navigation error of 12.9 n. mi. A comparison of the navigation data from the telemetry tape and this reconstructed trajectory is presented in table 5.16-VI. The differences shown in the table are well within the one sigma navigation accuracy that had been predicted preflight.

Command module dynamics during entry are shown in figure 5.16-12. The response to bank angle commands was nominal, and the oscillations in pitch and yaw were normal, remaining within the rate deadbands for long periods.

5.16.2 Guidance and Navigation Performance

Inertial system.- Performance of the inertial system was excellent and well within preflight predictions. The preflight history of performance data for the inertial instruments is shown in figure 5.16-13. The initial flight compensations were in reasonable agreement with the data mean during the denoted period. However, because of a procedural error in applying dc power to the system, the accelerometers were gaussed during the countdown demonstration test. As a result, the accelerometer terms had to be adjusted from the initial flight-load values, based on data previously obtained, to values determined from subsequent test data. The flight-load values indicated on figure 5.16-13 include these corrections. It should be noted that the X-axis accelerometer scale factor and the Y-axis accelerometer bias consistently exceeded the compensation range of the computer. The flight load, therefore, was set at the maximum values of 488 ppm and 2.28 cm/sec^2, respectively, for the two parameters.

Launch-phase velocity comparisons between the CSM guidance and navigation system and the launch vehicle guidance system are shown in figure 5.16-14. The data loss occurred at a critical period with respect to evaluation, and it has been as yet impossible to postulate a set of inertial measurement unit errors that match the residuals. An attempt to retrieve additional data manually is in progress. The results of this effort will be included in supplement 3 to this report. The accelerometer biases obtained from accumulated outputs during the coast phase are listed in table 5.16-VII. All instruments were within specification. Although specific gyro error coefficients have not yet been isolated, both the performance during the service propulsion system engine firing and the small landing error indicate that the various drift terms were small. All system temperatures, voltages, and the inertial measurement unit pressure were normal.

Computer system.- The computer programs used during the mission are listed in table 5.16-VIII. Operation was nominal throughout. Eleven alarms associated with the ground-update interface and several indications of incorrect interrogation of the computer by the PCM system occurred (section 12.0). As on previous missions, CDUFAIL alarms were noted during attitude maneuvers when the difference between actual and desired coupling display unit values exceeded the allowable threshold. These alarms, normal for the block I mechanization, had no effect on system operation. No computer restarts occurred.

5.16.3 Stabilization and Control Performance

The command and service module control and sequencing functions of the stabilization and control system were correct throughout the mission.

System gains and deadbands calculated in flight compared with those measured preflight as shown in table 5.16-IX. Correct rotational control priority over translation was demonstrated during plus X translation maneuvers. The pseudo rate capability, operative during attitude hold phases, correctly provided minimum impulse limit cycle operation. Performance of the service propulsion system thrust vector control loop was as predicted.

The Euler angles generated by the attitude gyro coupling unit diverged from the inertial measurement unit gimbal angles at a higher rate than had been noted on previous missions. The body-mounted attitude gyros were shown preflight to be sensitive to C-band transponder operation in that noise generated, during interrogations, on the outputs that drive the attitude gyro coupling unit caused an increase in coupling unit drift. The difference between the attitudes indicated by the inertial measurement unit and the attitude gyro coupling unit during the coast phase is shown in figure 5.16-15. The change in drift rate at approximately 06:30:00 was coincident with the C-band transponder power down and indicated that the preflight sensitivity was present in flight. The drift rates before and after the break, transferred to equivalent body coordinates, are shown in table 5.16-X. The roll-axis specification limit was slightly exceeded when the transponder was operating.

5.16.4 Mission Control Programmer Performance

The mission control programmer supplied control function inputs to various systems during the flight. No specific instrumentation was designated to analyze programmer performance; however, verification of continuity at the proper time showed proper programmer performance throughout the mission.

TABLE 5.16-I.- COMPARISON OF GUIDANCE AND NAVIGATION, AND GROUND-TRACKING STATE VECTORS

Event	Time, hr:min:sec	Axes	Guidance and navigation		Ground tracking		Difference	
			Position, ft	Velocity, ft/sec	Position, ft	Velocity, ft/sec	Position, ft	Velocity, ft/sec
S-IVB cutoff +7 sec	00:12:34	X	18 706 250.7	-12 882.32	18 720 589.0	-12 852.64	14 338.3	-29.68
		Y	303 179.1	236.76	311 192.2	248.38	-8 013.0	-11.62
		Z	10 629 037.9	22 279.95	10 628 649.9	22 286.57	388.0	-6.61
Prior to CSM/S-IVB separation	03:14:19	X	17 087 943.2	-15 790.27	17 100 224.0	-15 769.50	-12 280.8	-20.77
		Y	369 201.1	424.63	367 217.7	417.50	1 983.4	7.13
		Z	13 122 979.4	20 325.69	13 110 558.1	20 341.01	12 421.3	-15.32
First service propulsion system engine cutoff +10 sec	03:23:38	X	4 434 510.7	-28 576.83	4 454 662.0	-28 563.36	-20 111.3	-13.47
		Y	543 155.3	216.49	539 244.5	233.15	3 910.8	-16.66
		Z	22 247 276.7	13 386.31	22 247 366.1	13 417.59	89.4	-31.28
Prior to entry	09:37:02	X	20 333 909.7	-15 701.36	20 336 151.7	-15 704.82	-2 242.0	3.46
		Y	247 382.3	644.74	247 018.9	647.19	363.4	-2.45
		Z	7 448 173.4	28 450.04	7 464 633.6	28 440.75	-16 460.2	9.29

TABLE 5.16-II.- ENGINE GIMBAL TRIM VALUES DURING THE FIRST SERVICE PROPULSION SYSTEM ENGINE FIRING

Condition	Pitch, deg	Yaw, deg
Initial position	0.22	2.76
Maximum excursion	2.00	5.75
Steady state	1.54	4.11

TABLE 5.16-III.- COMPARISON OF ACHIEVED ORBIT WITH TARGET ORBIT

	Semilatus rectum, ft	Eccentricity	Radius, ft[a]	
			Apogee	Perigee
Target[b]	34 340 227	0.6342932599	93 900 995.6	21 012 279.6
Flight data[c]	34 345 717	0.634566798	93 986 306.0	22 676 373.4

[a]Apogee and perigee radius data were derived from semilatus recta and eccentricities assuming a conic trajectory.

[b]Target data for eccentricity and semilatus rectum are from eraseable memory prelaunch load.

[c]Flight data for eccentricity and semilatus rectum were derived from onboard guidance system position and velocity measurements.

TABLE 5.16-IV.- TYPICAL EXTERNAL DISTURBANCE TORQUES

DURING COLD-SOAK PHASE

Period of disturbance, hr:min		Disturbance torque, ft-lb
From	To	
03:28	03:42	-0.25
04:50	05:05	-0.21
06:01	06:20	-0.20
07:13	07:30	-0.21

TABLE 5.16-V.- APOLLO GUIDANCE COMPUTED ENTRY GUIDANCE AND NAVIGATION RECONSTRUCTION

Event	Time	Parameter	Apollo guidance computer	Reconstruction
400 000 feet	09:38:28	Position, ft		
		X	18 843 666	18 843 665
		Y	302 884.68	302 884.61
		Z	9 906 464.4	9 906 464.2
		Velocity, ft/sec		
		$\dot{X}$	-18 158.11	-18 158.11
		$\dot{Y}$	615.21	615.21
		$\dot{Z}$	27 359.9	27 359.9
		Lift-to-drag ratio command	0.2895	0.2895
		Range to target, n. mi.	2038.68	2038.68
Start of the UP-CONTROL phase	09:40:04	Position, ft		
		X	17 024 862	17 025 235
		Y	354 355.31	354 451.43
		Z	12 426 828	12 426 767
		Velocity, ft/sec		
		$\dot{X}$	-17 667.79	-17 663.02
		$\dot{Y}$	212.91	216.64
		$\dot{Z}$	23 719.9	23 720.0
		Lift-to-drag ratio command	0.2895	0.2895
		Range to target, n. mi.	1523.66	1523.69
Start of the second entry phase	09:43:56	Position, ft		
		X	13 400 299	13 401 193
		Y	273 684.4	276 580.5
		Z	16 297 994	16 299 998
		Velocity, ft/sec		
		$\dot{X}$	-15 453.21	-15 453.24
		$\dot{Y}$	140.62	161.37
		$\dot{Z}$	12 246.8	12 264.0
		Lift-to-drag ratio command	0.3000	0.3000
		Range to target, n. mi.	655.21	655.08
Guidance termination	09:50:10	Position, ft		
		X	10 024 504	10 025 914
		Y	183 007.3	199 153.7
		Z	18 387 419	18 400 638
		Velocity, ft/sec		
		$\dot{X}$	-2083.78	-2072.86
		$\dot{Y}$	-426.17	-366.44
		$\dot{Z}$	394.925	435.93
		Lift-to-drag ratio command	0.2895	0.2895
		Range to target, n. mi.	40.92	40.15

TABLE 5.16-VI.- APOLLO GUIDANCE COMPUTER ENTRY NAVIGATION ACCURACY

Event	Time, hr:min:sec	Parameter	Apollo guidance computer	Reconstructed trajectory[a]
400 000 ft	09:38:28	Position, ft		
		X	18 879 927	18 881 984
		Y	301 653.5	301 443
		Z	9 851 715.9	9 867 358
		Velocity, ft/sec		
		$\dot{X}$	-18 103.2	-18 103.7
		$\dot{Y}$	615.9	617.3
		$\dot{Z}$	27 388.6	27 379.2
		Earth-relative range to target, n. mi.	1926.9	1924.9
Start of the UP-CONTROL phase	09:40:03	Position, ft		
		X	17 060 392.7	17 068 424
		Y	353 899.7	353 089.3
		Z	12 379 187.5	12 390 012
		Velocity, ft/sec		
		$\dot{X}$	-17 862.3	-17 613.7
		$\dot{Y}$	242.8	215.3
		$\dot{Z}$	23 921.4	23 746.9
		Earth-relative range to target, n. mi.	1441.8	1441.2
Start of the second entry phase	09:43:55	Position, ft		
		X	13 431 215	13 455 598
		Y	273 413.7	273 120.2
		Z	16 273 430	16 269 927
		Velocity, ft/sec		
		$\dot{X}$	-15 463.1	-15 406.8
		$\dot{Y}$	140.6	143.5
		$\dot{Z}$	12 246.8	12 294.9
		Earth-relative range to target, n. mi.	619.6	623.1
Guidance termination	09:50:09	Position, ft		
		X	10 028 703	10 094 029
		Y	183 862	184 127.6
		Z	18 386 611	18 383 387
		Velocity, ft/sec		
		$\dot{X}$	-2114.7	-2053.5
		$\dot{Y}$	-428.7	-420.1
		$\dot{Z}$	412.7	477.6
		Earth-relative range to target, n. mi.	41.9	51.5

[a]Based on corrected onboard computer accelerometer counts.

TABLE 5.16-VII.- INFLIGHT ACCELEROMETER BIAS DETERMINATION

	Bias		
	X	Y	Z
Calculated bias, cm/sec^2	-0.83	2.77	1.93
Preflight compensation, cm/sec^2	-0.64	[a]2.94	2.10
Bias error, cm/sec^2	-0.19	-0.17	-0.17

[a]Value measured preflight. Because the maximum allowable compensation was 2.28, the effective bias error was 0.49.

TABLE 5.16-VIII.- GUIDANCE COMPUTER MAJOR MODES

Mode	Mode description
P-04	Inertial reference
P-11	First stage boost monitoring
P-14	S-IVB boost monitor with tumble monitor ON
P-27	Ground-commanded update (R, V, T)
P-14	S-IVB boost monitor with tumble monitor ON
P-31	Pre-service propulsion system engine firing
P-41	First service propulsion system engine firing
P-21	Maneuver to cold-soak attitude
P-22	Hold attitude during orbital integration
P-24	Hold attitude with state vector update allowed
P-27	Ground-commanded update (R, V, T)
P-24	Hold attitude with state vector update allowed
P-22	Hold attitude during orbital integration
P-23	Hold attitude
P-26	Hold second service propulsion system engine firing attitude and wait for time to free fall
P-32	Pre-service propulsion system engine firing
P-42	Second service propulsion system engine firing
P-61	Command module/service module separation maneuver
P-62	Pre-entry maneuver
P-63	Initiate entry steering
P-64	0.05g interface
P-65	Entry UPCONTROL phase
P-66	Entry KEPLER phase
P-67	Entry FINAL phase

TABLE 5.16-IX.- STABILIZATION AND CONTROL SYSTEM PERFORMANCE PARAMETERS

	Guidance and navigation mode	Axis	Preflight test value	Flight value
Rate loop gain	Attitude control	Pitch, V dc/deg/sec	10.1	11.2
		Yaw, V dc/deg/sec	10.4	11.0
		Roll, V dc/deg/sec	9.7	10.0
	Change in velocity	Pitch, deg gimbal/deg/sec	0.68	0.64
		Yaw, deg gimbal/deg/sec	0.66	0.62
Attitude error gain	Attitude control	Pitch, V dc/deg	11.2	9.2
		Yaw, V dc/deg	10.2	8.7
		Roll, V dc/deg	11.0	9.5
	Change in velocity	Pitch, deg gimbal/deg error	1.5	1.49
		Yaw, deg gimbal/deg error	1.4	1.36
Attitude error deadband	Attitude control	Pitch, deg	±0.18	±0.22
		Yaw, deg	±0.20	±0.23
		Roll, deg	±0.18	±0.21
	Entry	Pitch, deg	±4.9	±5.5
		Yaw, deg	±4.9	±5.5
		Roll, deg	±5.0	±4.9

TABLE 5.16-X.- BODY AXIS DRIFT RATES

Time, hr:min	Pitch drift, deg/hr	Yaw drift, deg/hr	Roll drift, deg/hr
03:30	2.29	6.77	-10.47
04:00	0.786	5.96	-10.97
05:00	1.03	6.17	-10.84
06:00	2.47	4.45	-11.42
07:00	2.55	2.75	-10.59
08:00	3.12	3.22	-10.38

NASA-S-68-3581

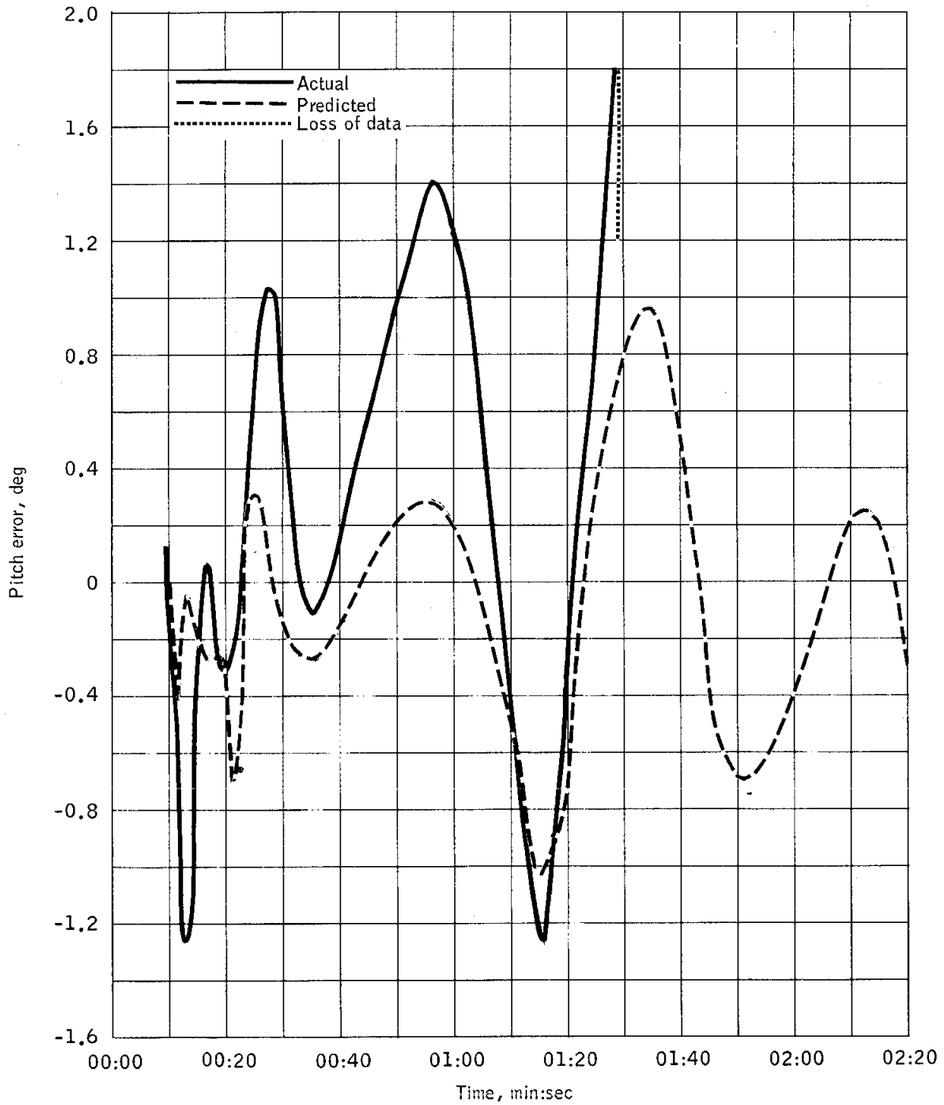

Figure 5.16-1.- Pitch polynomial comparison.

NASA-S-68-3582

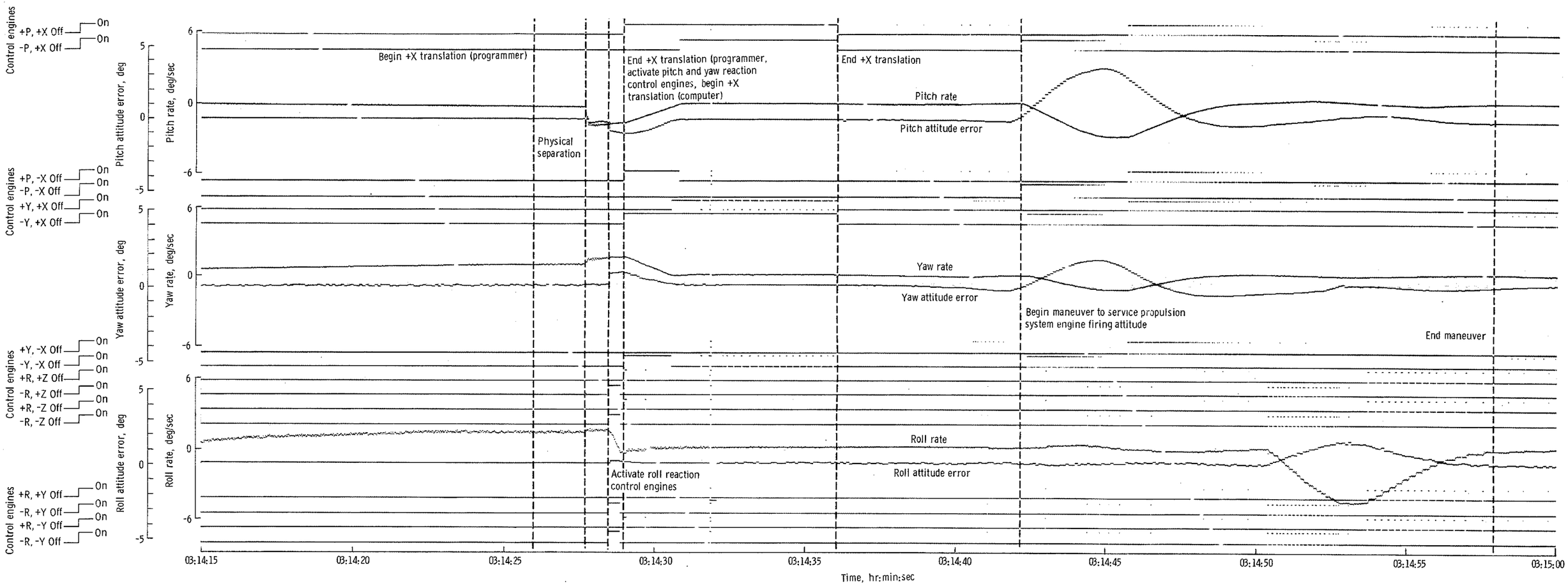

Figure 5.16-2. - Dynamics during CSM/S-IVB separation and maneuver to attitude for service propulsion system engine firing.

NASA-S-68-3583

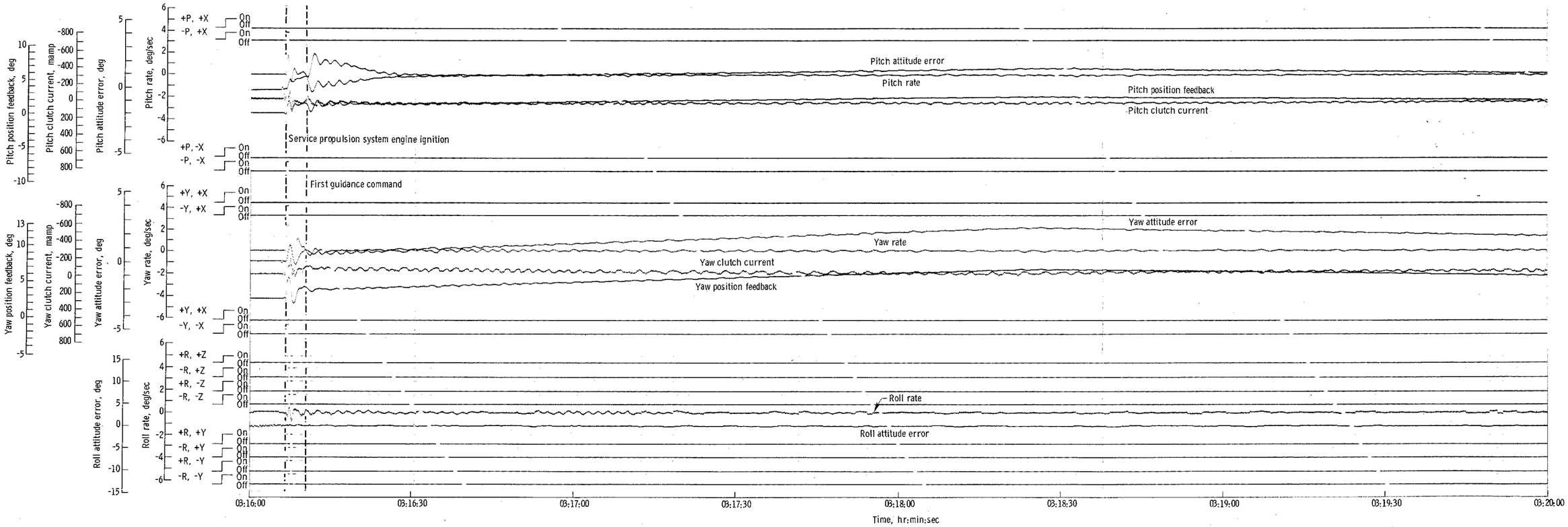

(a) Ignition.

Figure 5.16-3. - Dynamics during first service propulsion system engine firing.

NASA-S-68-3584

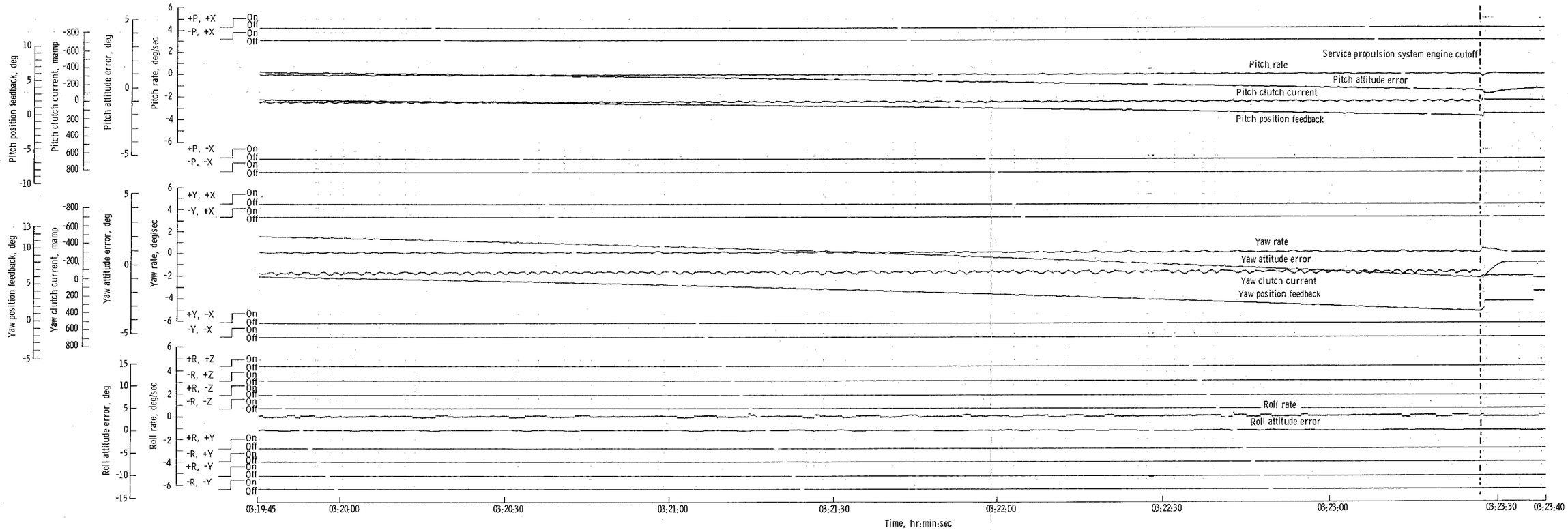

(b) Cutoff.

Figure 5.16-3. - Concluded.

NASA-S-68-3585

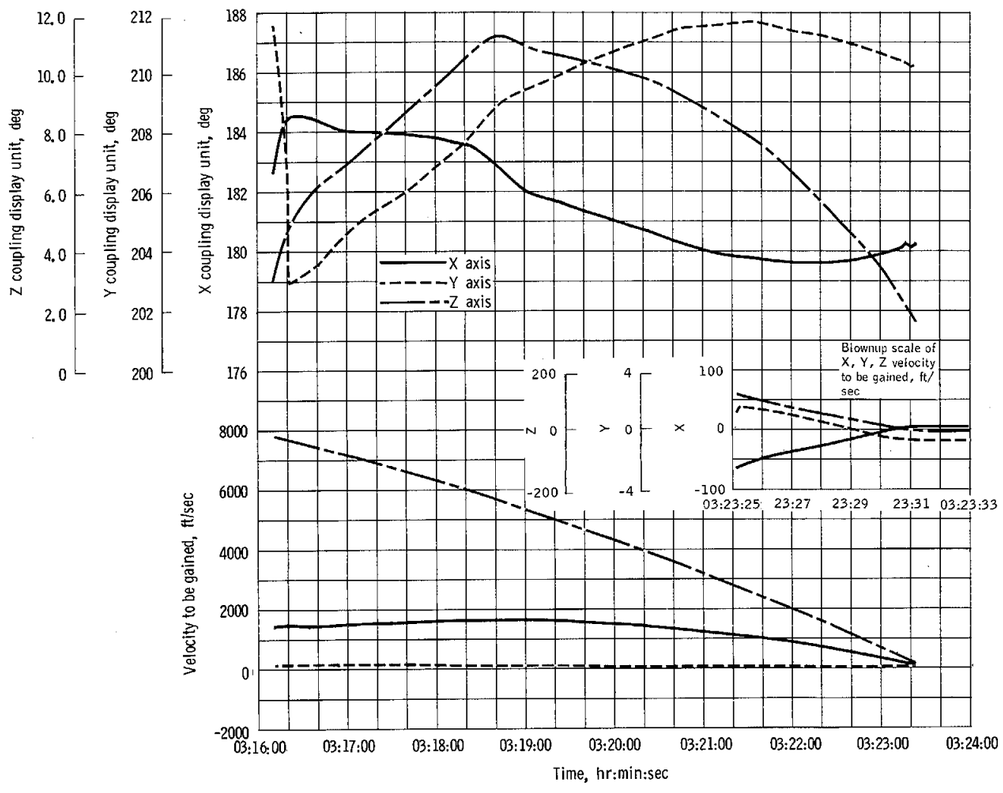

Figure 5.16-4. - Velocity to be gained during service propulsion system engine firing.

NASA-S-68-3586

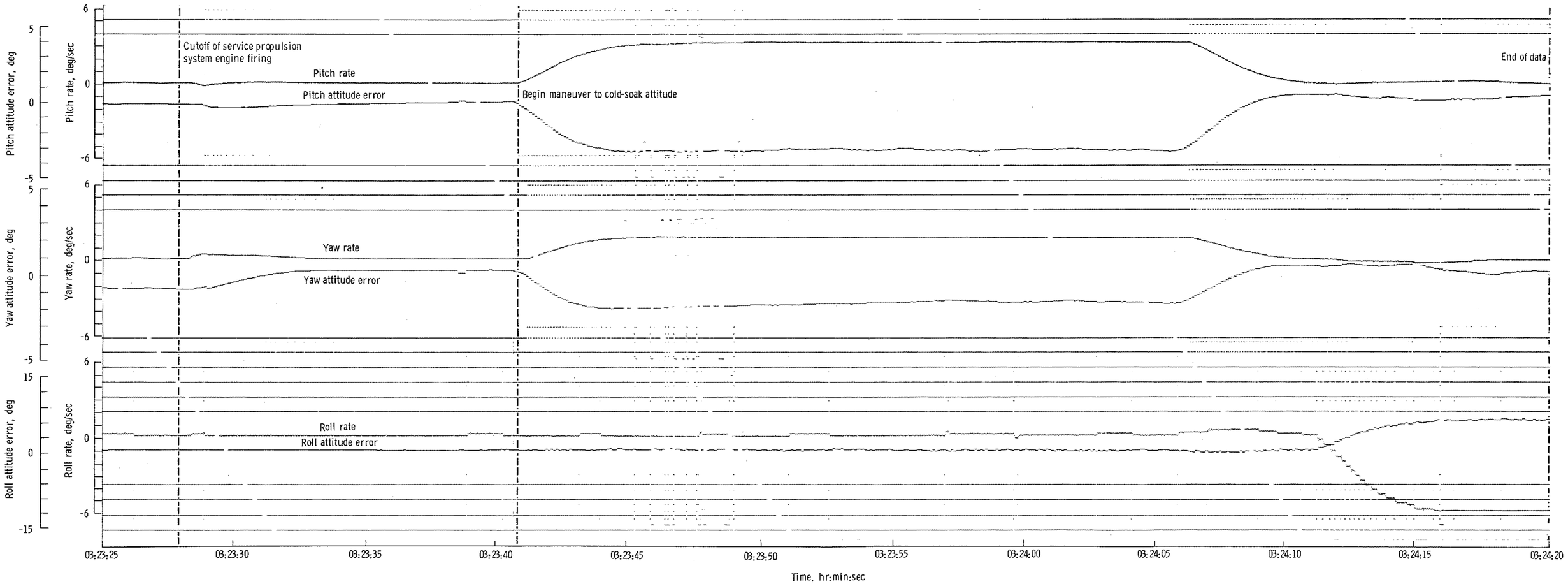

Figure 5.16-5. - Dynamics during maneuver to cold-soak attitude.

NASA-S-68-3587

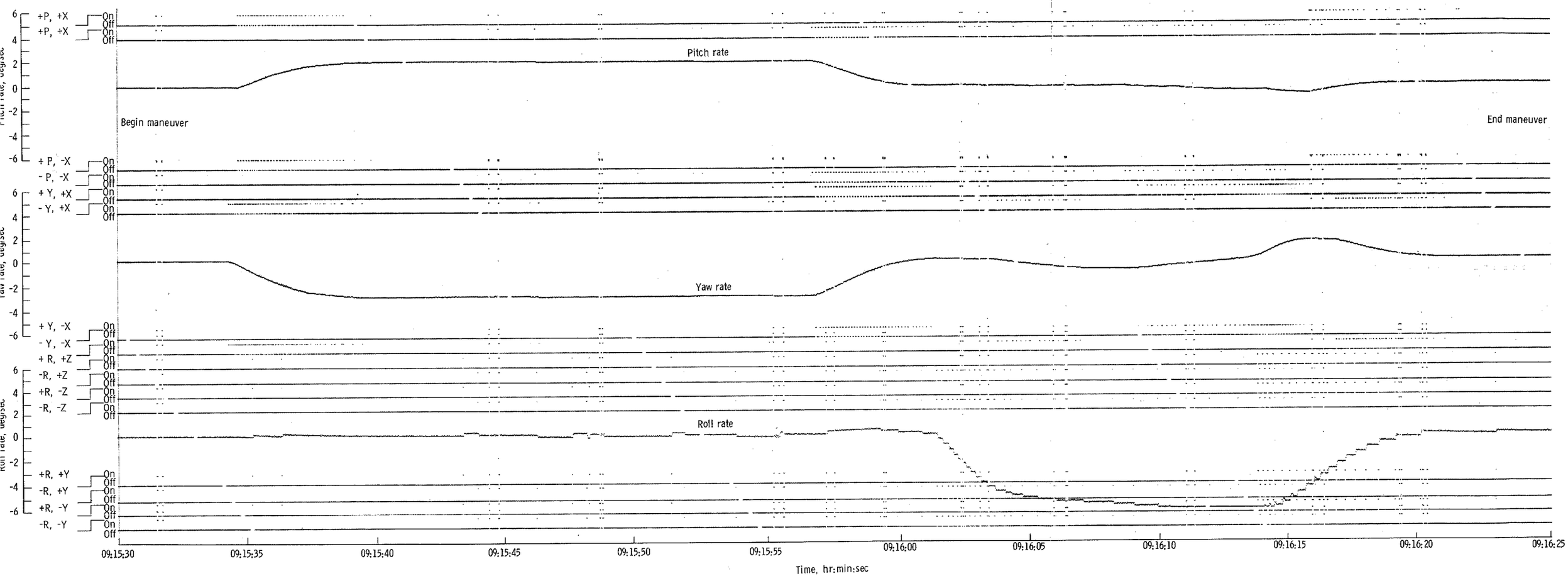

Figure 5.16-6. - Dynamics during maneuver to attitude for second service propulsion system engine firing.

NASA-S-68-3588

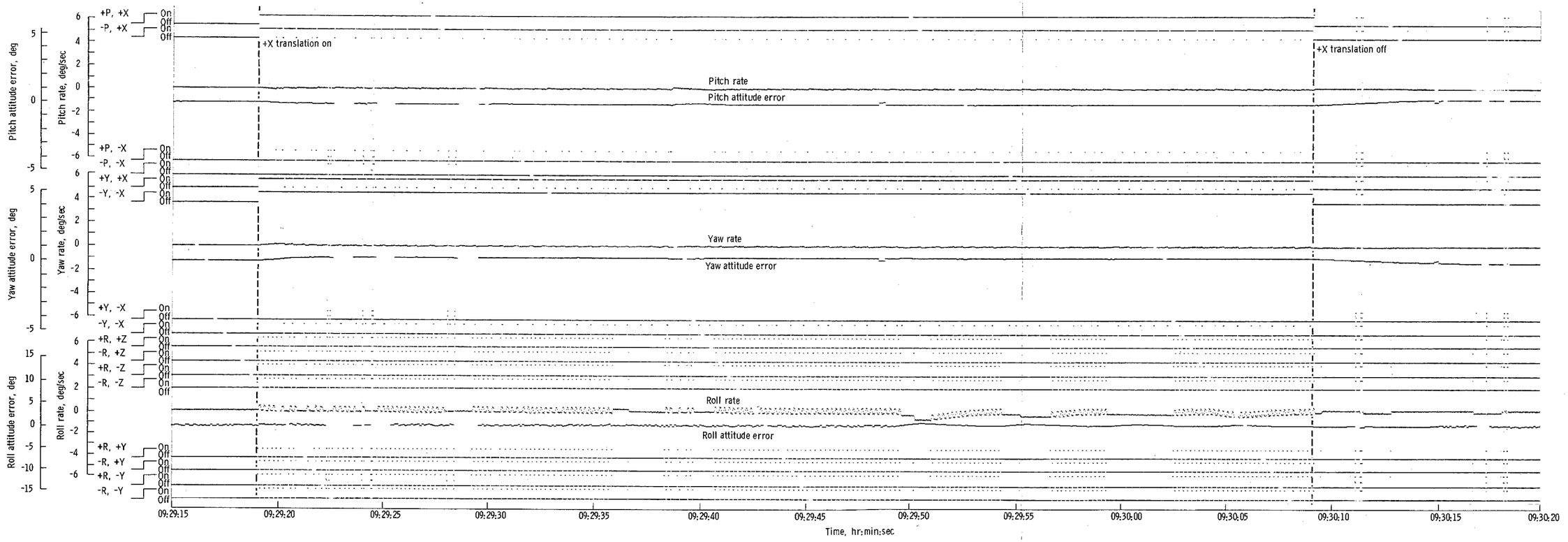

Figure 5.16-7. - Dynamics during plus X translation for second service propulsion system engine firing.

NASA-S-68-3589

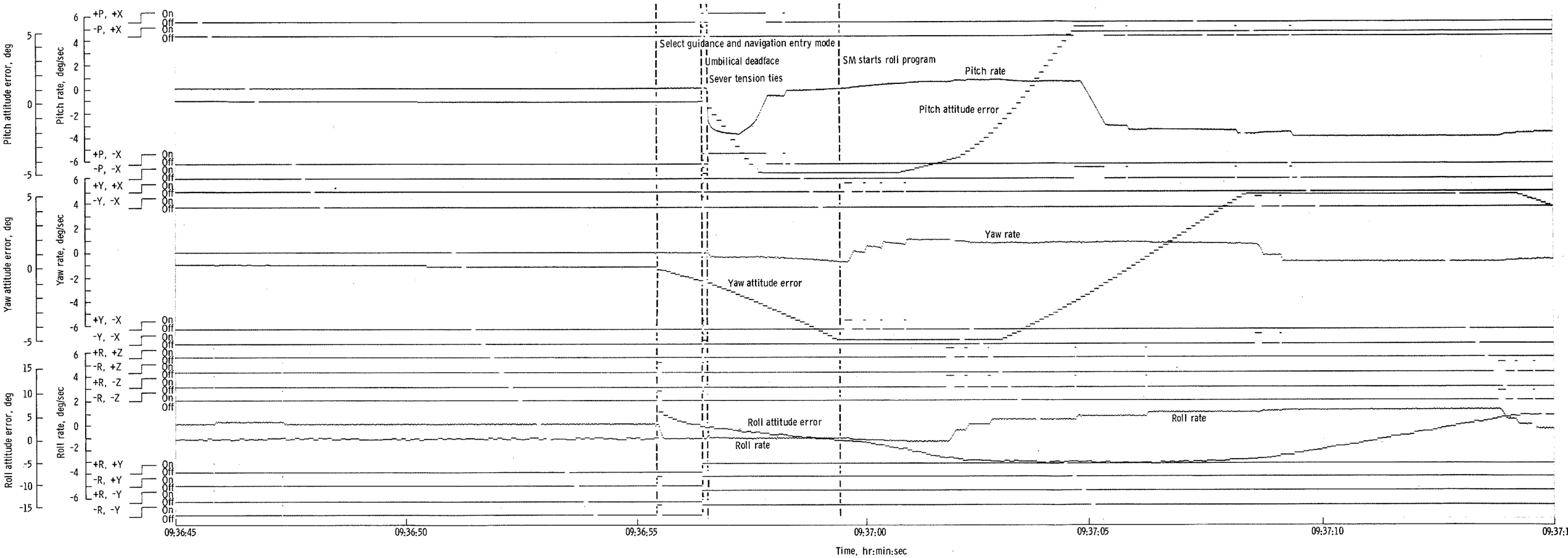

Figure 5.16-8. - CM/SM separation dynamics.

NASA-S-68-3590

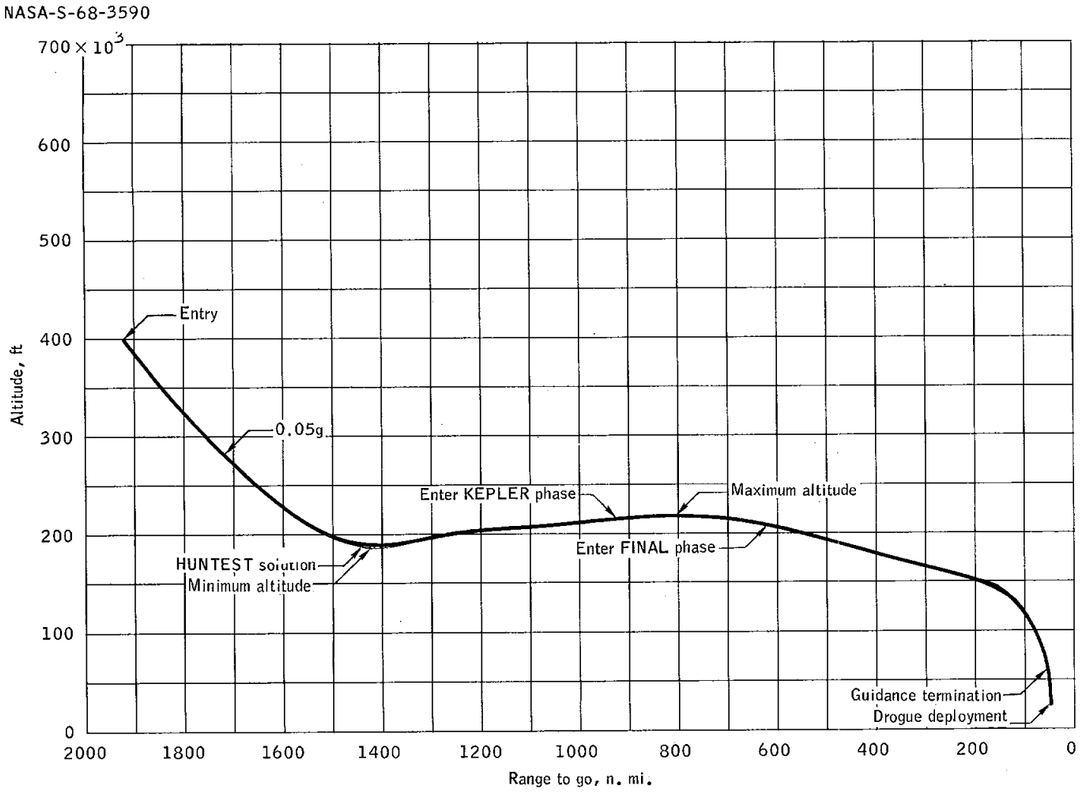

Figure 5.16-9.- Altitude and range during entry sequence.

NASA-S-68-3591

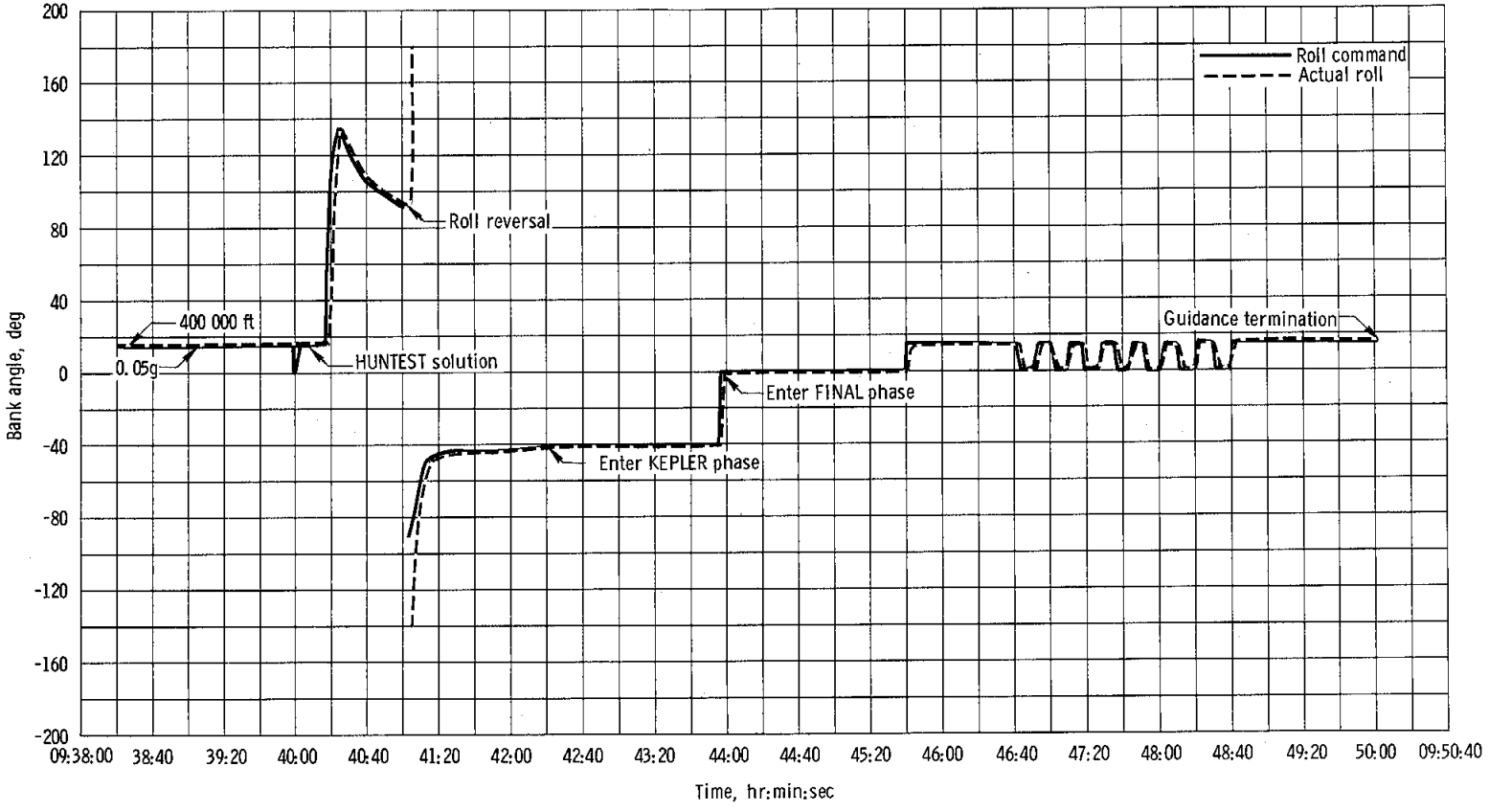

Figure 5.16-10. - Roll command plotted against actual roll.

NASA-S-68-3592

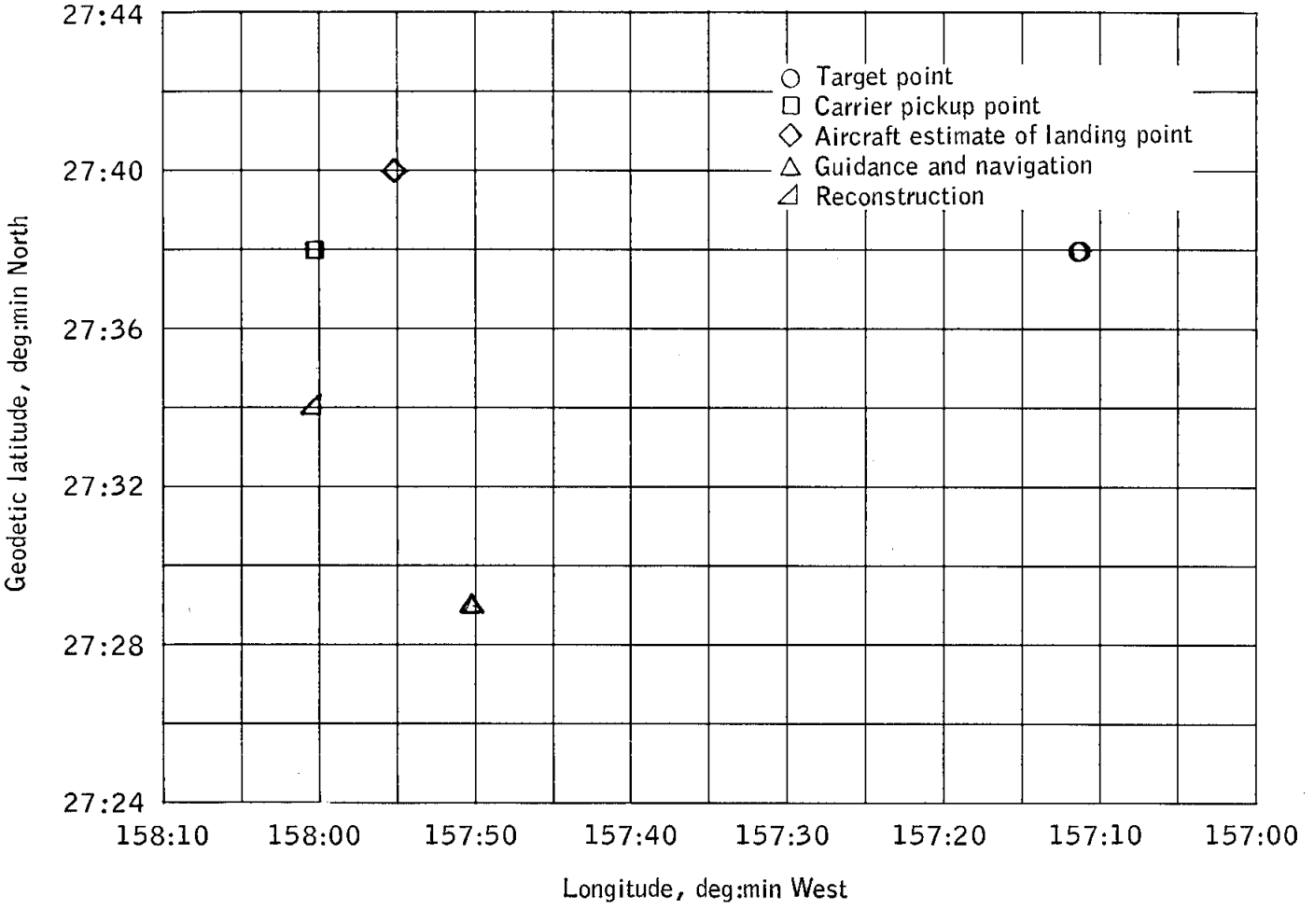

Figure 5.16-11.- Landing point data.

NASA-S-68-3593

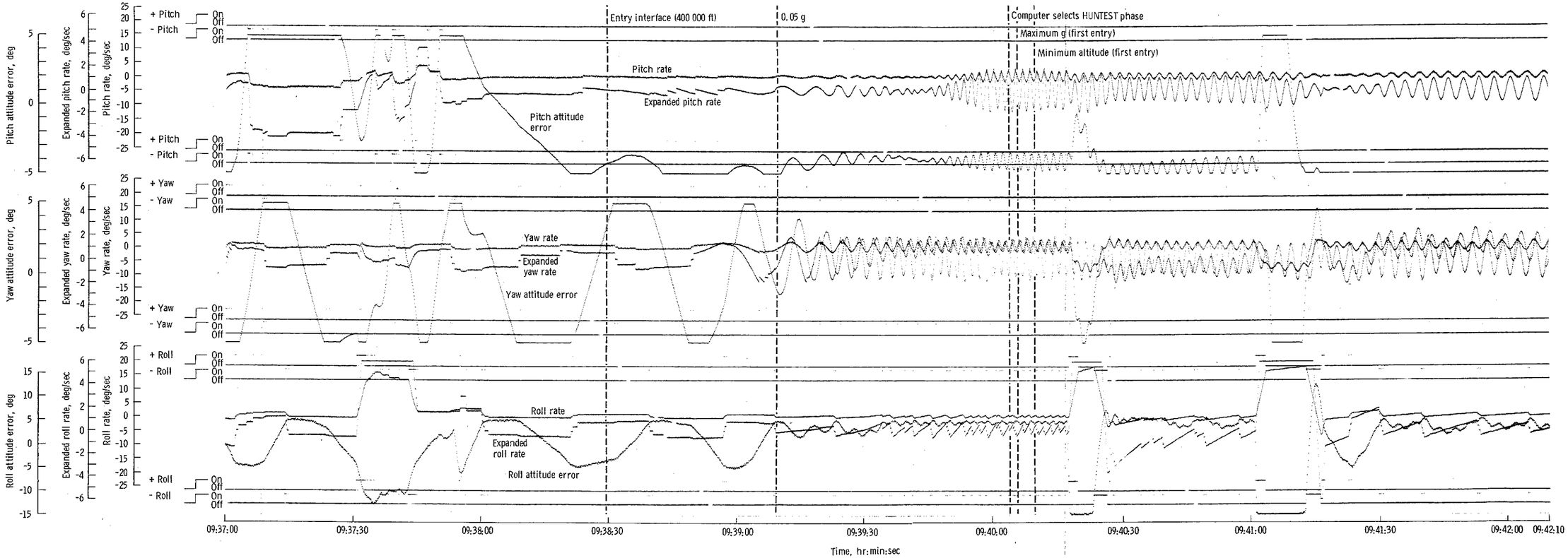

(a) 09:37:00 to 09:42:10.

Figure 5.16-12. - Dynamics during entry.

NASA-S-68-3594

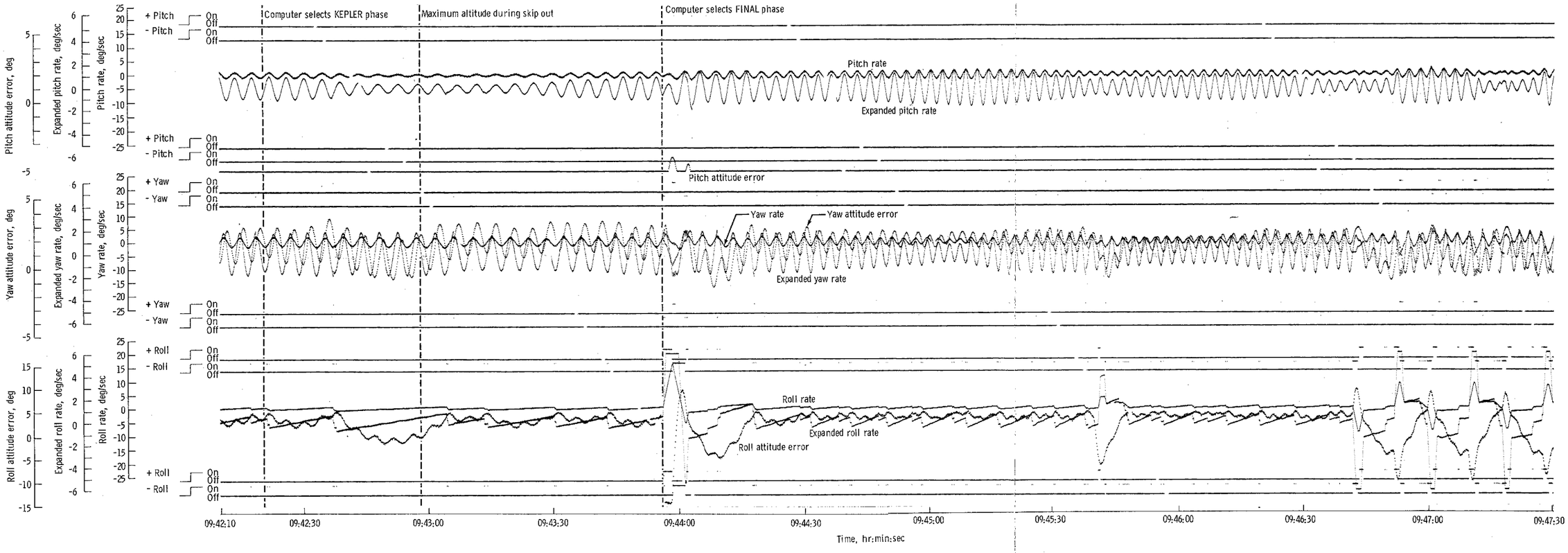

(b) 09:42:10 to 09:47:30

Figure 5.16-12. - Continued

NASA-S-68-3595

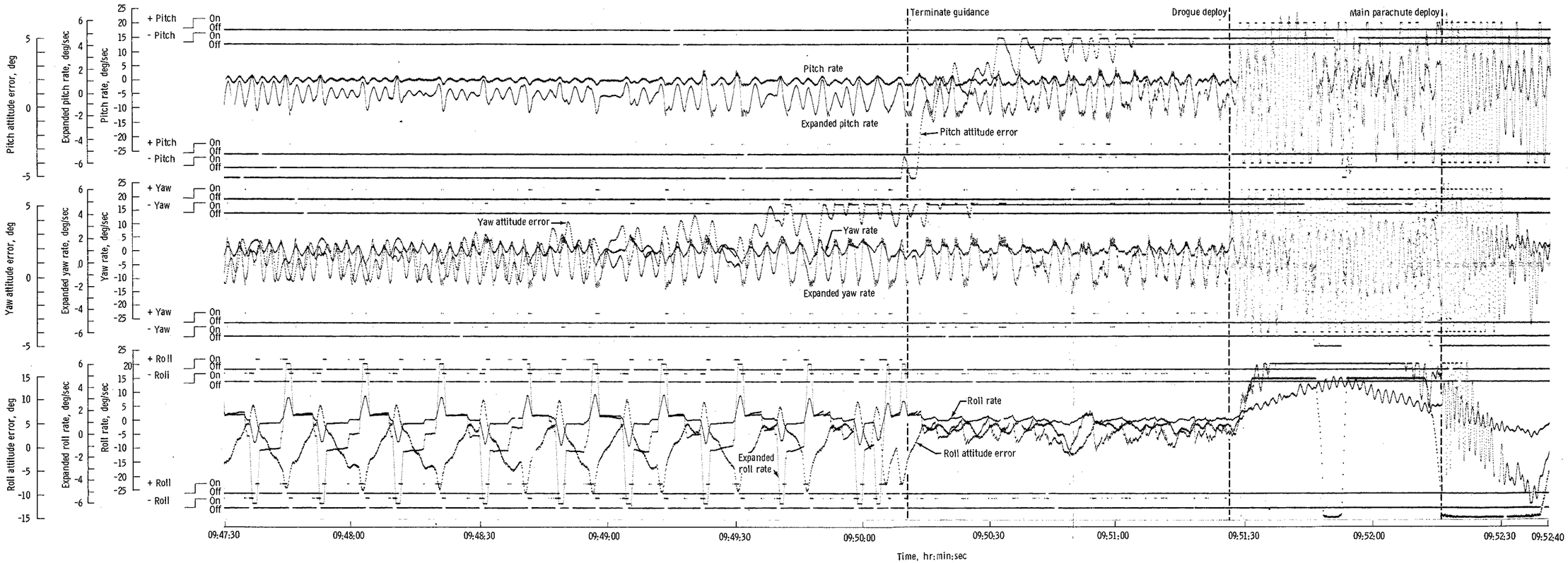

(c) 09:47:30 to 09:52:40.

Figure 5.16-12. - Continued.

NASA-S-68-3596

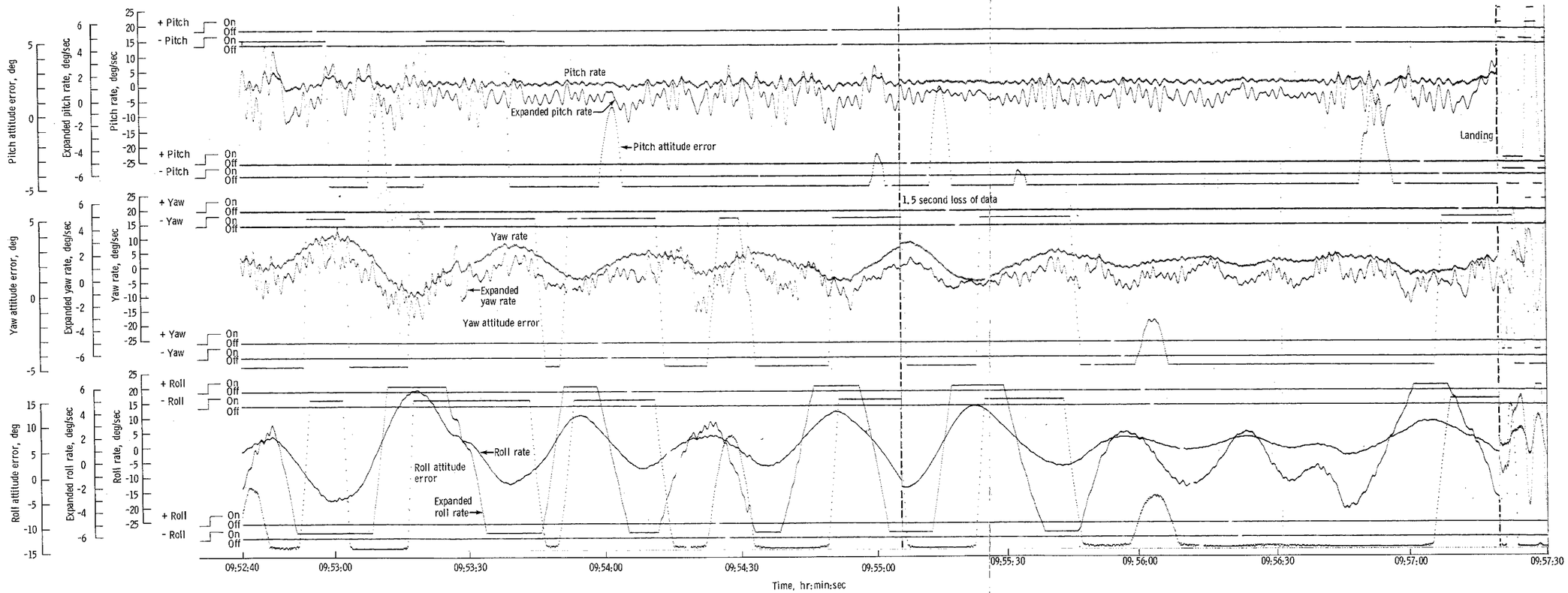

(d) 09:52:40 to 09:57:30.

Figure 5.16-12. - Concluded.

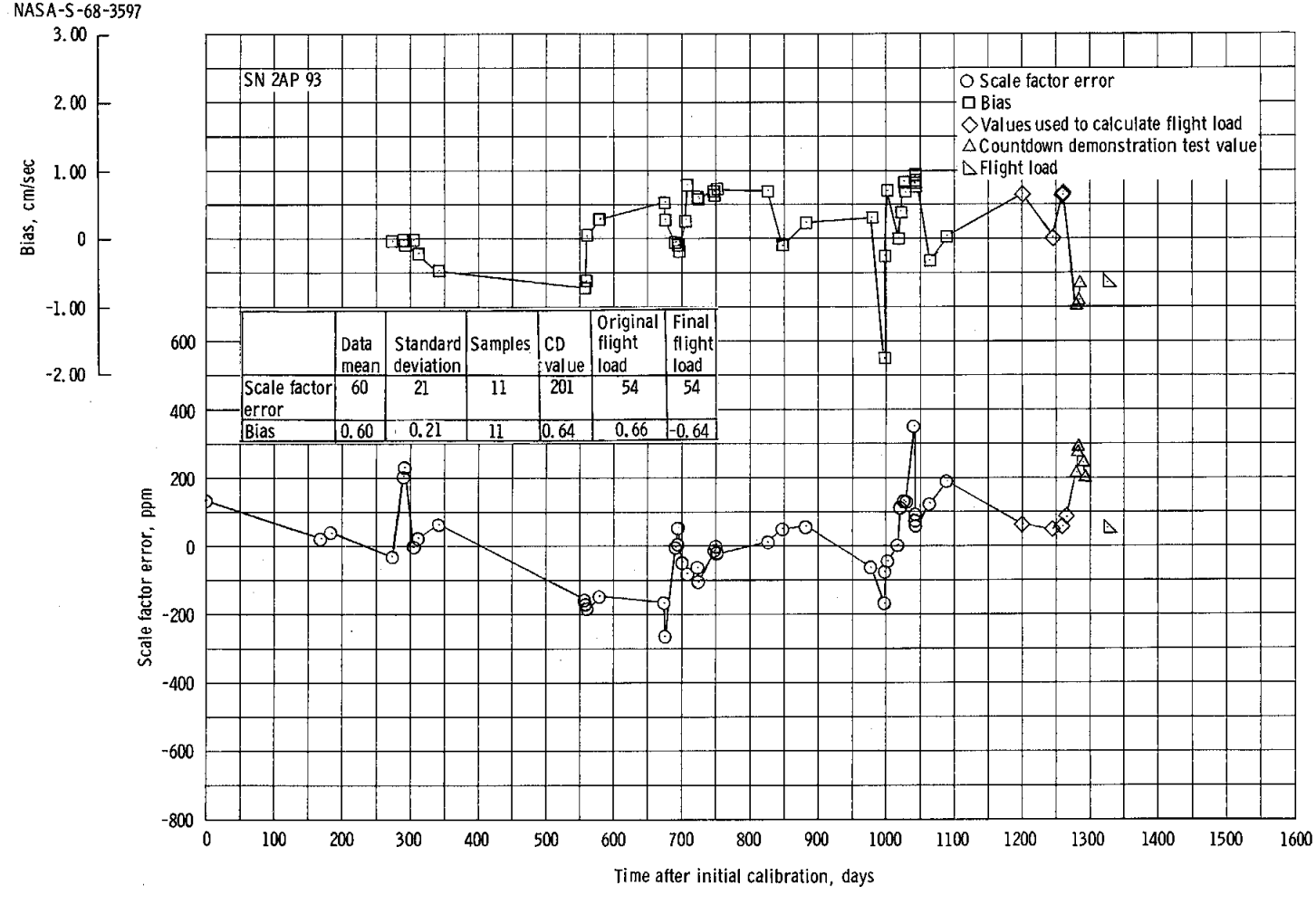

	Data mean	Standard deviation	Samples	CD value	Original flight load	Final flight load
Scale factor error	60	21	11	201	54	54
Bias	0.60	0.21	11	0.64	0.66	-0.64

(a) X-axis accelerometer.

Figure 5.16-13. - Inertial measurement unit coefficient history.

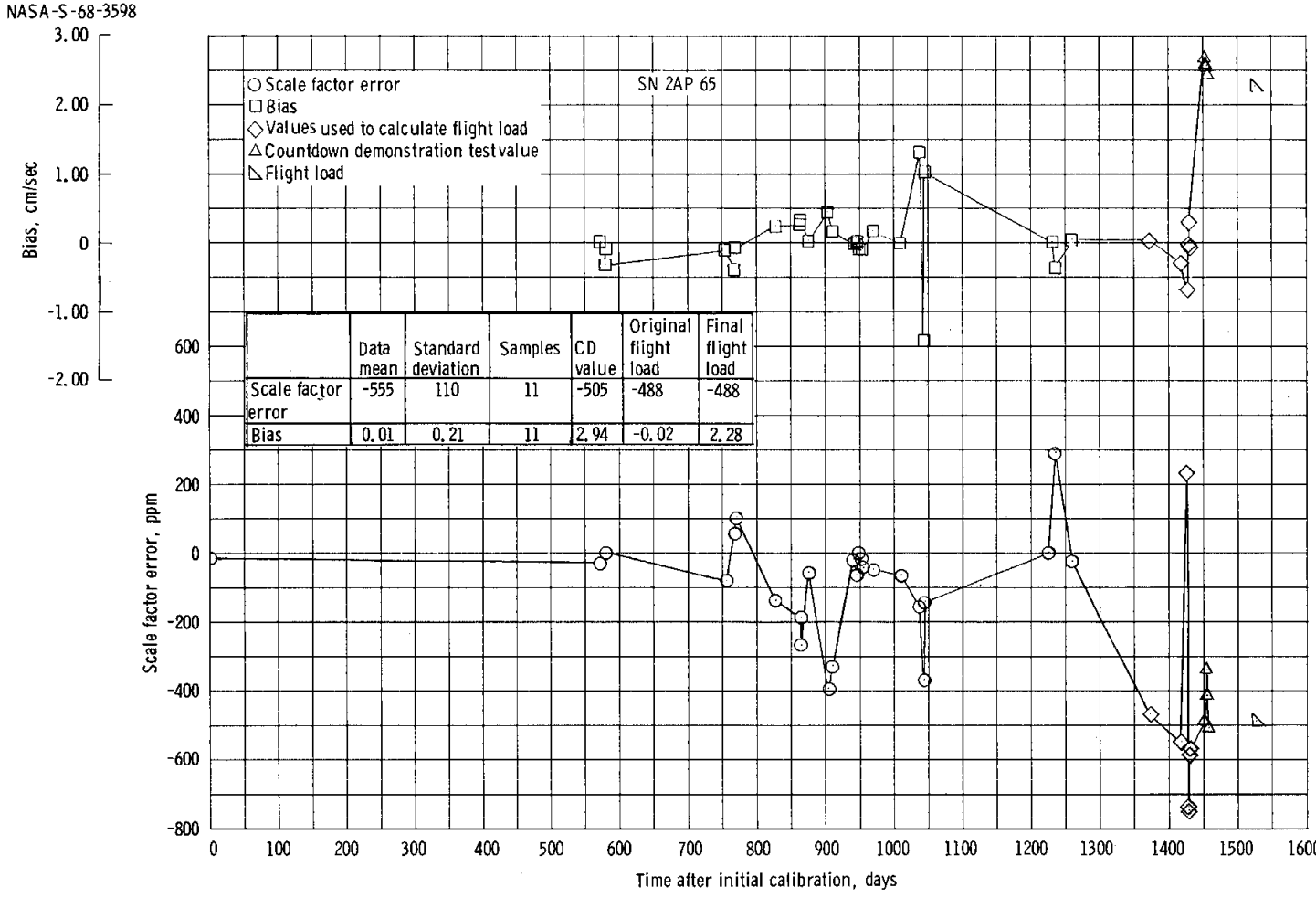

(b) Y-axis accelerometer.

Figure 5.16-13. - Continued.

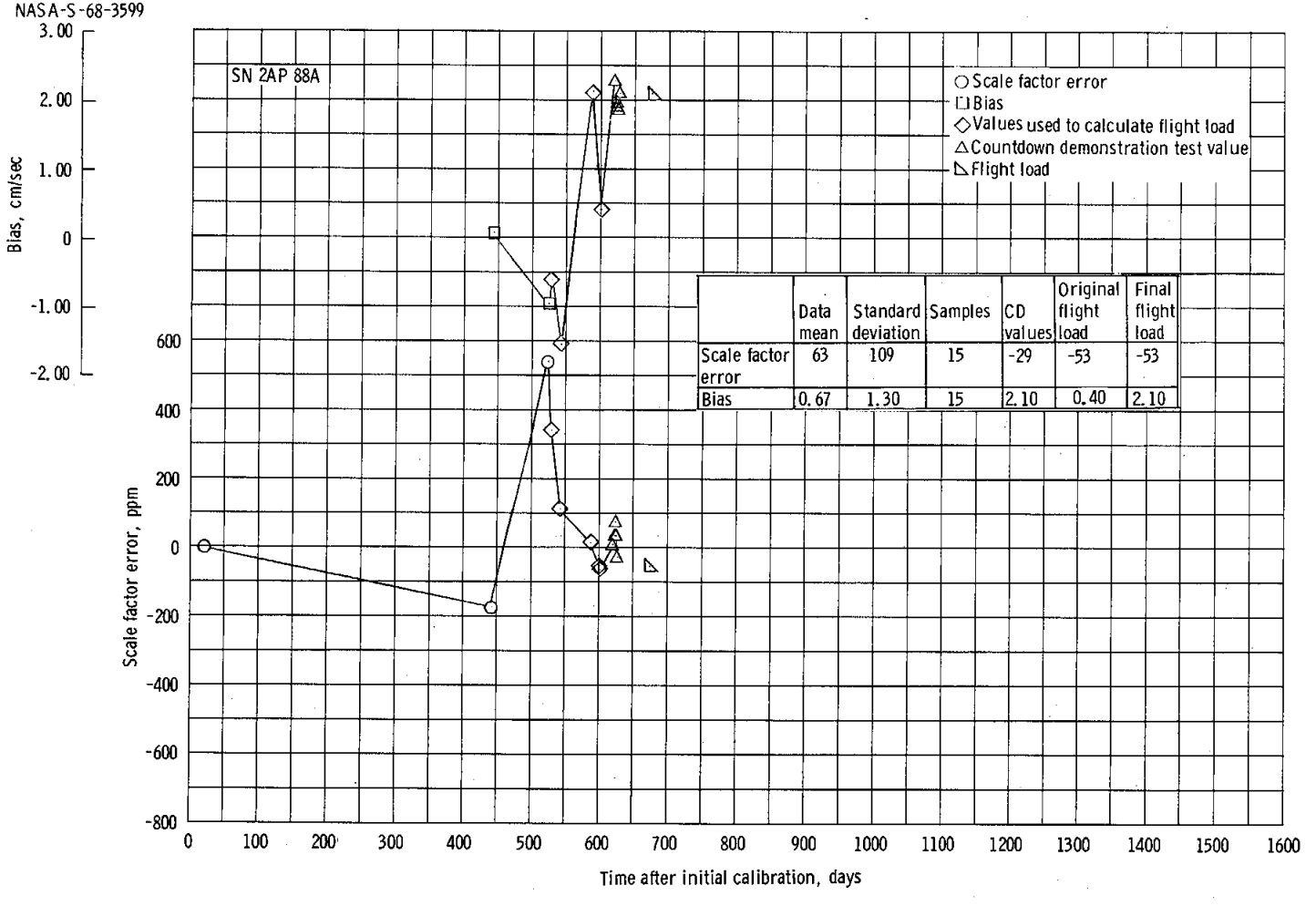

	Data mean	Standard deviation	Samples	CD values	Original flight load	Final flight load
Scale factor error	63	109	15	-29	-53	-53
Bias	0.67	1.30	15	2.10	0.40	2.10

(c) Z-axis accelerometer.

Figure 5.16-13. - Continued.

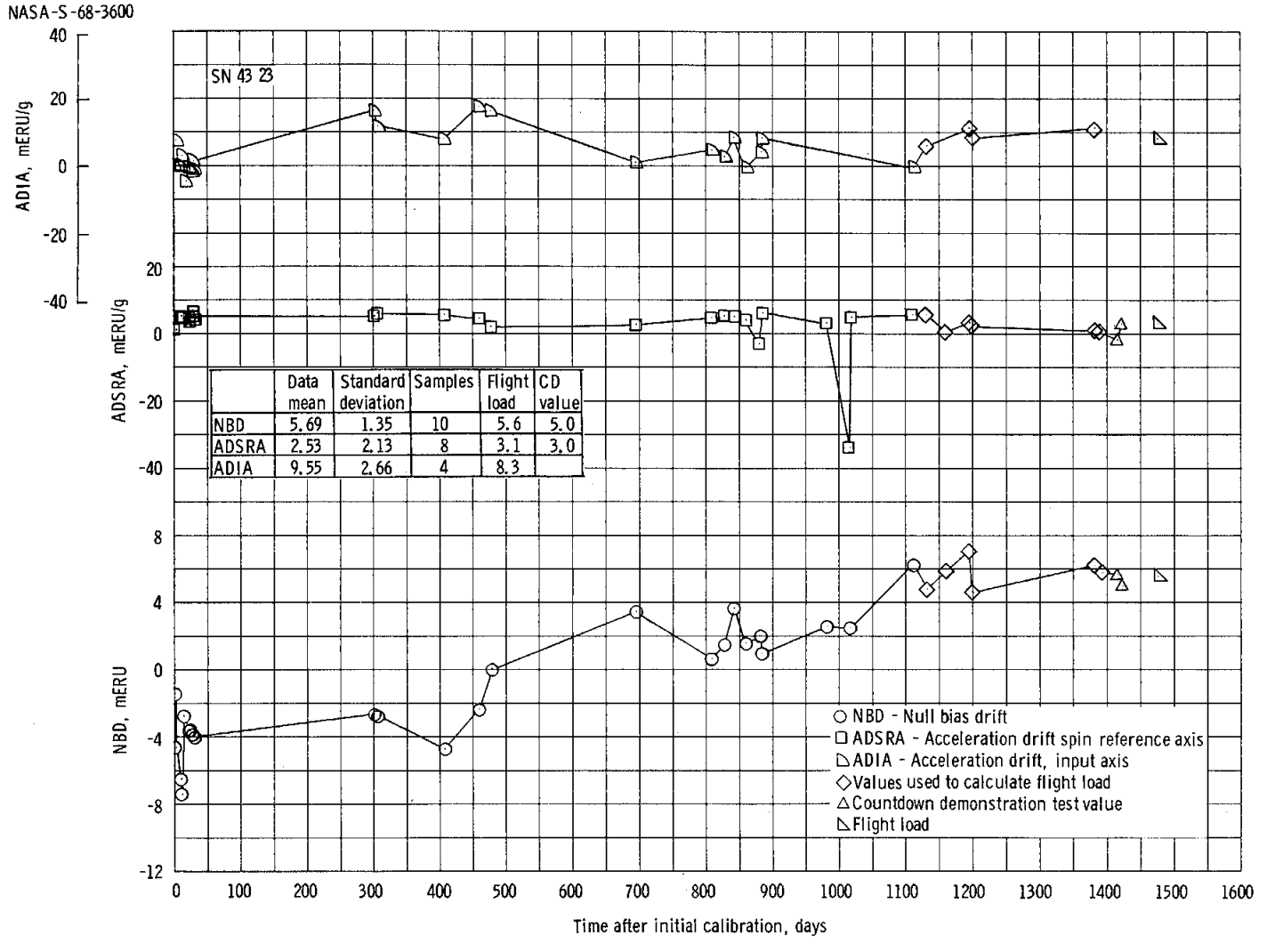

	Data mean	Standard deviation	Samples	Flight load	CD value
NBD	5.69	1.35	10	5.6	5.0
ADSRA	2.53	2.13	8	3.1	3.0
ADIA	9.55	2.66	4	8.3	

(d) X-axis gyro.

Figure 5.16-13. - Continued.

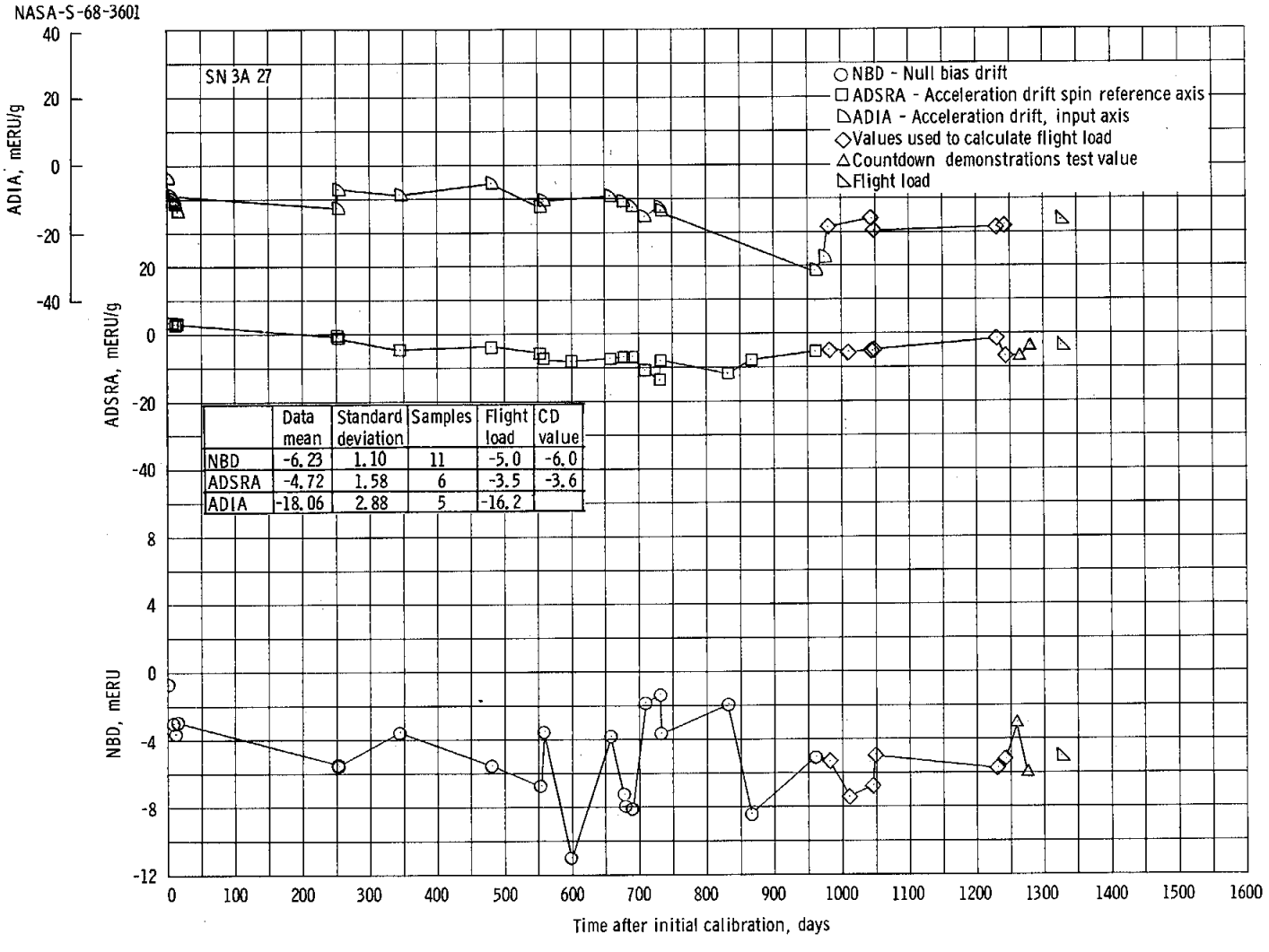

(e) Y-axis gyro.

Figure 5.16-13. - Continued.

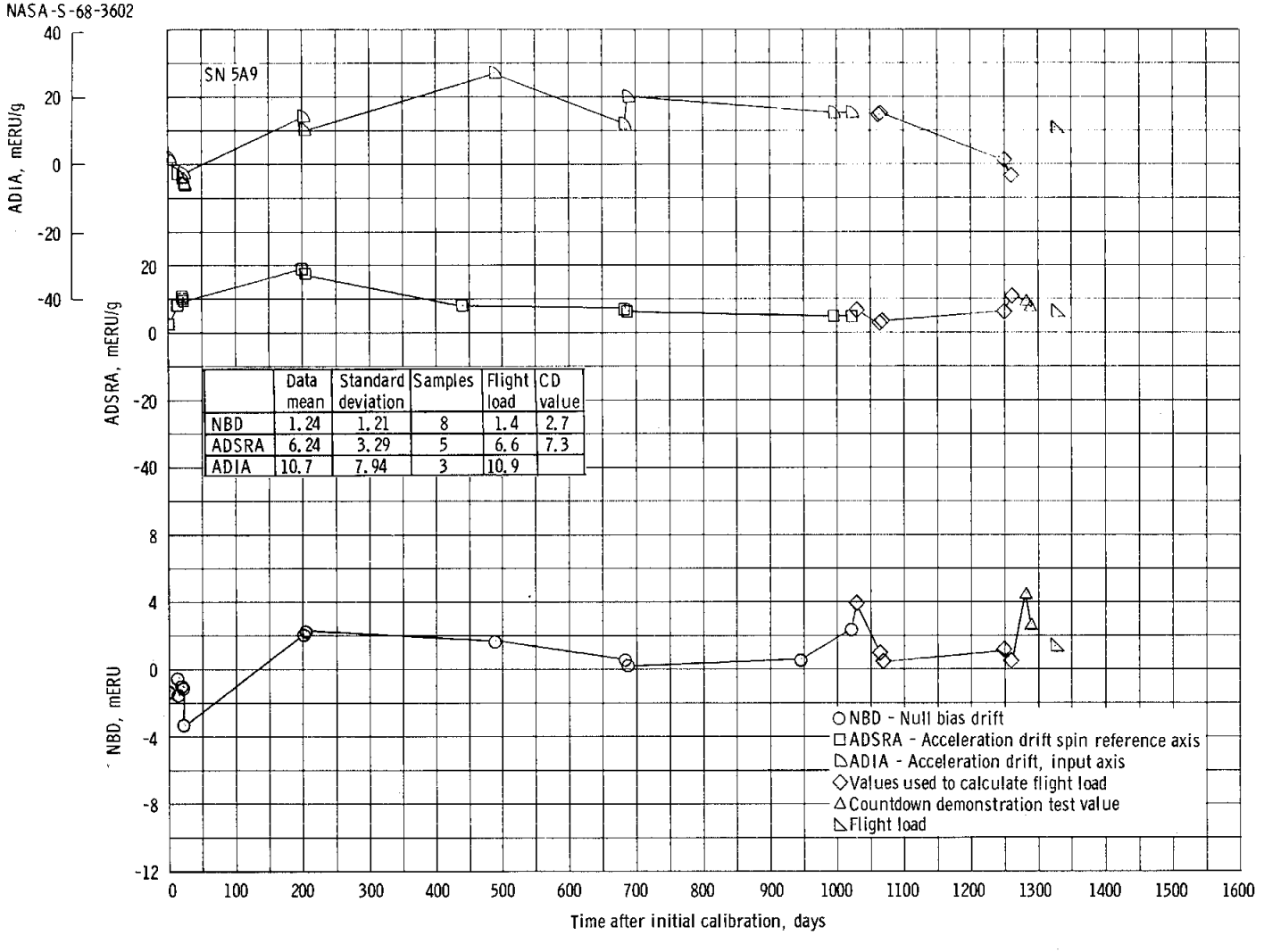

	Data mean	Standard deviation	Samples	Flight load	CD value
NBD	1.24	1.21	8	1.4	2.7
ADSRA	6.24	3.29	5	6.6	7.3
ADIA	10.7	7.94	3	10.9	

(f) Z-axis gyro.

Figure 5.16-13. - Concluded.

NASA-S-68-3603

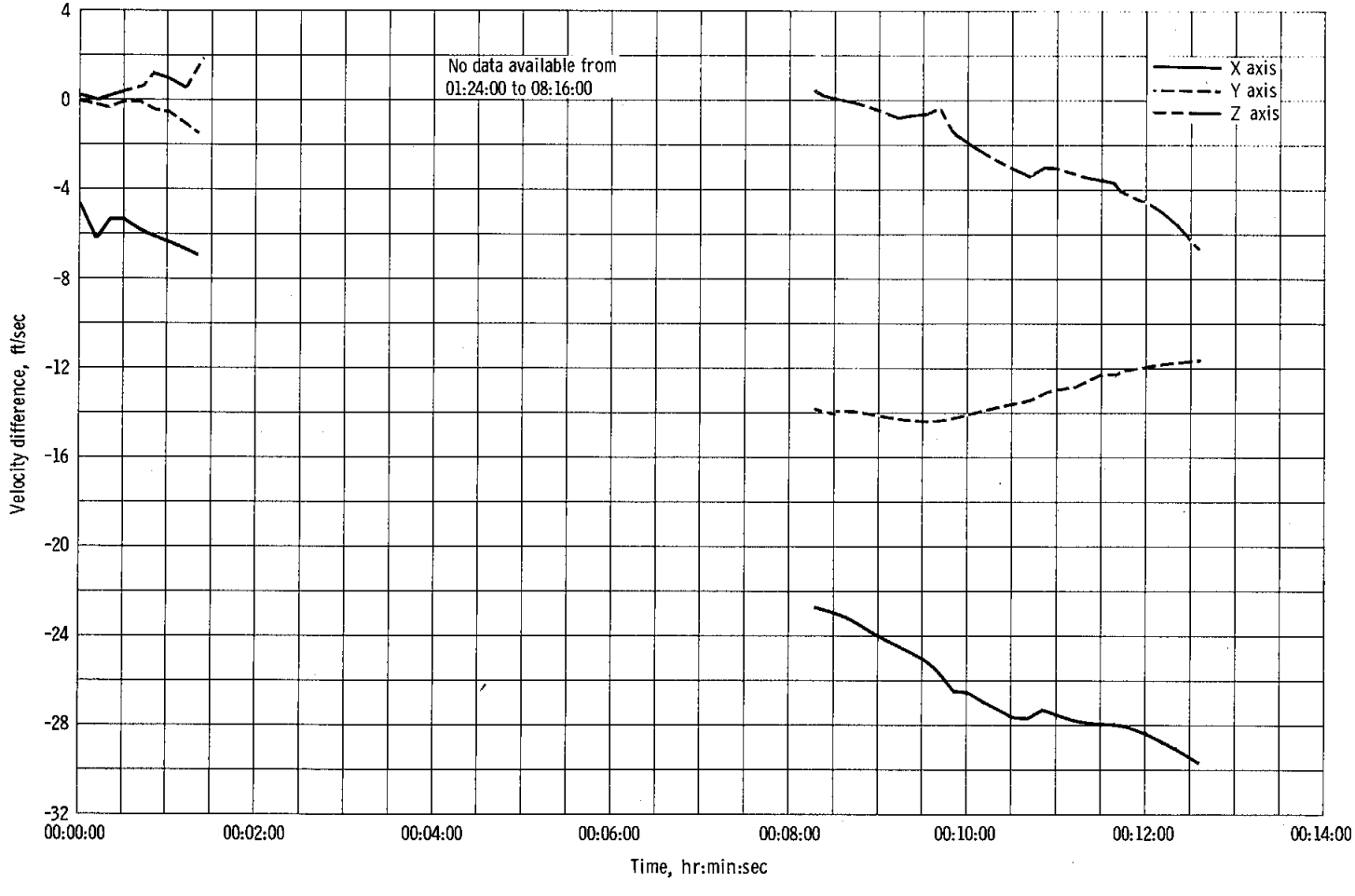

Figure 5.16-14. - Launch phase velocity comparison (guidance and navigation minus instrument unit).

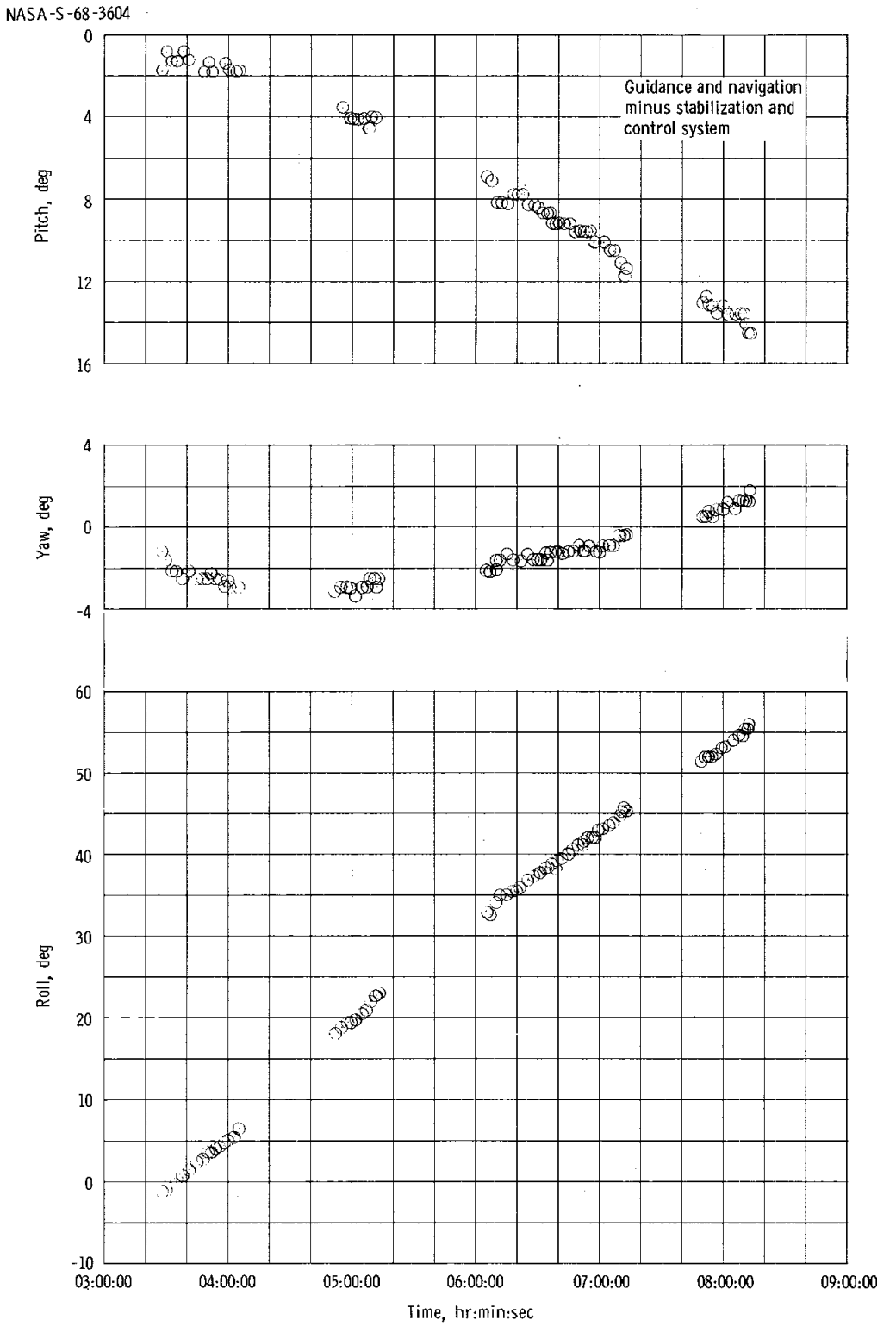

Figure 5.16-15. - Attitude reference drift instabilization and control system.

5.17 REACTION CONTROL

Both reaction control systems (command module and service module) performed nominally, except for the thermal control of one quad. All maneuvers using the reaction control system were completed satisfactorily. Normal maneuver rates, accelerations, and translation velocity changes were attained. Propellant usage by both systems was normal. The thermal control system for the service module reaction control system maintained the engine mounting structure and injector head temperatures at satisfactory levels for quads A, B, and D. Quad C displayed anomalous temperatures during the early portion of the cold-soak phase of the mission.

5.17.1 Service Module Reaction Control System

The service module reaction control system was similar to the one used for the Apollo 4 mission; some engines were block II configuration units with integral screens. No components were known to be malfunctioning or inoperative prior to lift-off.

Servicing and prelaunch activities.- Propellant servicing of the system was accomplished March 18 and 19, 1968. Helium servicing was accomplished April 2, 1968. The system was essentially activated during helium servicing because the helium isolation valves were open, and the propellant-tank pad pressure was at regulator lockup. Activation was completed when the propellant isolation valves were opened. The propellant isolation valves on quads A and B were inadvertently opened 14 hours before launch. The C and D valves were opened about 15 minutes before launch.

The propellant and helium loads were within the loading specification limits; propellant loads are given in table 5.17-I. The helium tank pressures remained within a ±30-psi band from the time of servicing until launch, indicating no helium leakage.

Performance.- Throughout the mission, performance of the system was nominal, except for the anomalous injector temperature discussed in the thermal control section.

Maneuvers: One direct ullage maneuver and two plus X translations were performed during the mission. The system also oriented the CSM for the service propulsion system engine firing, for the cold soak, for the inhibited second service propulsion system engine firing, and for the service module/command module separation. Additional functions included control of roll attitude and rates during the service propulsion system

engine firing, attitude control during the extended cold-soak period, and performance of the service module minus X translation and roll maneuver during service module/command module separation. The sequence of events is shown in table 5.17-II. The second plus X translation, which was an ullage firing for the planned second service propulsion system engine firing, lasted 50.1 seconds rather than the planned 30 seconds (section 5.16). The typical angular accelerations produced by reaction control engine firings during various phases of the mission are listed in table 5.17-III. The pitch angular acceleration was low for the first maneuver but soon recovered; this was most probably caused by trapped gas in the propellant lines. A similar occurrence was noted during the Apollo 4 mission. The velocity changes produced during the translation maneuvers are also shown in table 5.17-III; these velocity increments were taken from the guidance and navigation accelerometer data and were compared with the planned values and with values calculated from the engine duty cycle, assuming nominal thrust. The planned value for the second plus X translation was based on the planned 30-second firing time before the command for the second service propulsion system engine firing. The service module minus X translation following service module/command module separation was verified by the effects on the command module body rates, as noted from data of previous missions.

Engine activity: Engine activity during the cold-soak period was greater than planned, partly because of the decreased vehicle inertias resulting from the longer-than-planned service propulsion system engine firing. Overcontrol caused by four-engine roll control of a relatively light vehicle also increased the activity; two-engine control can be selected during manned flights. The estimated reaction control engine activity during the cold-soak period was based on data from 45 percent of the period (table 5.17-IV).

The effects of the propulsive venting caused by the water boiloff were noted in the bias between the number of commands to the opposing pitch engines. There was twice as much positive pitch as negative pitch activity. This bias was much less than had been noted during the Apollo 4 mission, when the positive pitch to negative pitch firing ratio was approximately 15:1.

Propellant consumption: The actual propellant consumption by the service module reaction control system has been compared with the expected consumption for the periods prior to cold soak, during cold soak, and after cold soak (figs. 5.17-1 through 5.17-3, respectively). The expected consumption during the service propulsion system engine firing has been adjusted for the increased duration, but not for changes in vehicle inertias. Also, the amount expended during the second plus X translation has been adjusted only for the longer duration. When the

16.9-lb/hr expected consumption during the cold-soak period is adjusted for vehicle inertias, a consumption rate of 23 to 26 lb/hr can be expected. The difference between this adjusted rate and the actual rate of 31.3 lb/hr may be attributed to overcorrection of the relatively light CSM by four-engine roll control. Greater than normal consumption because of overcontrol was also noted during the second plus X translation.

Thermal control.- The thermal control system on Apollo 6 was identical to that used for Apollo 4 with one exception. The Apollo 4 heaters were both bonded and mechanically clamped to the engine mounting structures. The Apollo 6 heaters were only bonded to the engine mounting structures. Mechanical clamps were incorporated on Apollo 4 because of uncertainties concerning heater-mounting structure bond strengths. Subsequent verification of bond quality permitted deletion of the mechanical clamps for Apollo 6. The heaters will only be bonded to the mounting structures on block II spacecraft. The primary and secondary thermal control systems were actuated at hatch closeout and remained active throughout the flight. The temperatures of the engine mounting structures of each of the four quads were monitored from launch through service module/command module separation. In addition, the temperatures of the injectors of the following engines were monitored during the same time period: negative pitch engine in quad A, positive yaw engine in quad B, clockwise roll engine in quad C, and counterclockwise roll engine in quad D.

The thermal control system maintained the engine mounting structures and the instrumented injectors of quads A, B, and D at satisfactory temperature levels during the flight. During the early portion of the cold-soak phase, the quad C engine mounting structure cooled excessively and anomalous temperature excursions occurred in the quad C clockwise roll engine injector (see section 12.0).

The maximum launch temperatures for the mounting structures and injectors of the four instrumented engines are shown in table 5.17-V. The maximum launch temperatures were comparable to, or slightly higher than, those encountered during the Apollo 4 mission. A comparison of trajectory parameters also indicated that the launch aerodynamic heating of the quads should have been slightly higher than the Apollo 4 flight.

The maximum temperature (226° F) of the positive yaw engine injector of quad B was higher than and occurred before the maximum temperatures of the other instrumented injectors because this engine was in the vertical up-firing position and received maximum aerodynamic launch heating. Conversely, the maximum temperature of the injector of the negative pitch engine of quad A was lower than and occurred later than for the other injectors because this engine was in the down-firing, or trailing, position during launch and received minimal launch aerodynamic heating. This

injector was primarily heated by conduction from the engine mounting structure. These data corroborate the conclusion based on Apollo 4 data that the launch heating for a lunar mission will probably not increase the temperature of the engine mounting structures to the level (205° F) required for actuation of the caution and warning light.

The reaction control engines were inactive during the two revolutions prior to S-IVB separation. The performance of the thermal control system during this time cannot be fully assessed because of periods when network station coverage was not complete. However, the available data indicate that the thermal switches and heaters operated in a nominal manner to maintain the engine mounting structures and injector heads within the temperature range of 110° to 140° F.

A summary of temperatures from CSM/S-IVB separation through service module/command module separation is shown in table 5.17-VI and figure 5.17-4. The operation of the thermal control system over this period is summarized in table 5.17-VII. As shown, all the mounting structure and injector temperatures increased as a result of the engine firing associated with S-IVB/CSM separation, the service propulsion system engine firing, and the orientation to cold-soak attitude. The injector temperature of the negative pitch engine of quad A was higher than the temperatures of the other injectors because of the steady-state firing performed during the CSM/S-IVB separation.

During the approximately 5.9-hour inertial cold soak, the CSM was oriented such that quads B and C were completely shaded and quads A and D had sun exposure at an oblique angle. During the cold-soak period, the quad A and D heaters underwent multiple cycles and maintained the engine mounting structures and the instrumented injector heads at satisfactory temperature levels.

After the engine activity associated with CSM/S-IVB separation and the CSM orientation to cold-soak attitude, the quad B mounting structure and the plus yaw engine injector cooled rapidly until the quad heaters were actuated ON at approximately 03:45:00. The heaters remained ON throughout the remainder of the cold-soak period. The mounting structure temperature quickly rose to 136.5° F and then underwent a gradual decline, reaching a minimum temperature of 104° F at the termination of the cold-soak period. The temperature of the plus yaw injector remained 20° to 25° F below the mounting structure temperature during this period, decreasing from 109° F at 03:45:00 when the heaters were actuated ON to 84.5° F at the termination of the cold soak.

The quad C heaters were actuated ON at approximately 03:50:00 at a mounting structure temperature of 114° F and remained ON throughout the entire cold-soak period. The mounting structure temperature quickly

increased to 122.5° F, then underwent a gradual decline, reaching 86.5° F at the termination of the cold-soak period. During this time, the temperature of the clockwise roll engine injector decreased from approximately 119° F, when the heaters were actuated ON, to 91.5° F at the termination of the cold soak. In general, the injector temperature remained 4° to 6° F above the mounting structure temperature. However, during several periods between 03:45:00 and 05:32:00, the indicated temperature of the clockwise roll engine injector (the only one instrumented in the quad) decreased sharply (several times going below 0° F), and then recovered to its original temperature at essentially the same rate. An example of this behavior between 04:55:00 and 05:05:00 is shown in figure 5.17-5. This problem is further discussed in section 12.0.

After the cold-soak period, the CSM was reoriented for the second plus X translation at 09:15:34. A 50.1-second plus X translation maneuver was initiated at 09:29:19.1, followed by orientation to service module/command module separation attitude, and subsequent separation. All mounting structure and injector temperatures increased sharply as a result of the thermal inputs of the engine firings during these maneuvers.

The effect of these maneuvers on the temperatures of the quad A engine mounting structure and the negative pitch engine injector are shown in figure 5.17-6. The injector was initially warmed by the engine firing activity during the attitude maneuver for the second plus X translation firing. The injector of the negative pitch engine used for the plus X translation reached a maximum soakback temperature of 200° F at the end of the firing. The injector temperature decreased sharply as a result of the firings associated with the attitude maneuver for service module/command module separation. This cooling effect resulted both from the convective cooling of the propellants flowing through the injector and the vaporization of the propellants remaining in the injector manifolds at the completion of each pulse.

5.17.2 Command Module Reaction Control System

The command module reaction control system was identical to the one used for the Apollo 4 command module. All system components were block I units. No components were known to have been malfunctioning or inoperative prior to lift-off.

Servicing.- Propellant servicing of the system was accomplished on March 18 and 19, 1968. Helium servicing was completed April 2, 1968. The propellant loads are listed in table 5.17-I.

Performance.- Performance of the system was entirely normal from activation until landing. The performance was verified as satisfactory for manned missions.

Maneuvers: During entry, the system performed a pitch maneuver and roll maneuvers, and provided attitude-hold control. The sequence of events is shown in table 5.17-II. Typical accelerations and crosscoupling, produced with dual system control, are shown in table 5.17-VIII. The crosscoupling noted was normal. The angular acceleration produced by the engines was typically low for the first pulse or pulses of an engine. This was most apparent in the positive pitch engine which was commanded ON within 1 second after system activation. At first, no effect was noted on the body rates of the vehicle, then rates implying reduced engine thrust and finally those of nominal engine thrust level (fig. 5.17-7) were noted. A similar effect was noted during the Apollo 4 mission and represented normal system activation. The slow buildup was noted in the chamber pressure of the first pulse of the A system counterclockwise roll engine and the associated roll body rate (fig. 5.17-8).

System pressures: System helium pressures from servicing through landing are shown in table 5.17-IX. The helium tank pressures and temperatures during entry are shown in figure 5.17-9. The constant pressure/temperature ratio prior to activation indicated that the system had not leaked. When the helium pressurization systems were activated, the source pressure of each system dropped 680 psi; this decrease, 240 psi greater than that seen during the Apollo 4 mission, was caused by the increased oxidizer tank ullage that resulted from loading 5 pounds less oxidizer in each system. At the time the helium purge was terminated, the A and B system source pressures were 273 psia and 253 psia (referenced to 70° F), respectively. Similar values had been noted during the Apollo 4 mission; the purge system will be modified for future command modules to permit a more rapid purging.

Control firing propellant consumption: Propellant consumption during the mission is compared with preflight expected values in figure 5.17-10. The expected values did not include the propellant required for service module/command module separation disturbances and the effect of service module reaction control plume impingement on the command module. The 84 pounds of propellant expended for control firings were 6 pounds less than were used for this purpose during the Apollo 4 mission.

Propellant depletion burn: The propellant depletion burn was accomplished successfully, burning approximately 152 pounds of propellant. The instrumented chamber pressures and the propellant manifold pressures during the propellant depletion burn and the subsequent helium purge

are shown in figure 5.17-11. The oxidizer tank pressure recovered several seconds before the fuel tank pressure, indicating that the usable oxidizer had been depleted before the fuel. Approximately 14.5 pounds of oxidizer remained trapped in the tank and lines of the two systems. The engine chamber pressure buildup during the helium purge indicated that at least part of this trapped oxidizer was burned. During the Apollo 4 mission, the fuel was depleted first, leaving 10.5 pounds of usable oxidizer in addition to the trapped quantity. To reduce the hazard of the unburned oxidizer damaging the parachutes during the Apollo 6 mission, 5 pounds less oxidizer were loaded in each system than had been loaded for previous missions. This oxidizer would have been in excess of that required for combustion of the usable fuel.

Thermal control.- The command module reaction control system was passively maintained within satisfactory temperature limits throughout the mission. The system adequately withstood the effects of a high heating load entry after having been subjected to an extended cold-soak period. A summary of the system thermal performance is given in table 5.17-X.

The temperatures of the A and B system helium tanks and of six of the engine oxidizer valves were monitored throughout the flight. During entry, the injector temperature and two engine outer-wall temperatures were monitored on each of four engines. To detect any leakage of hot combustion gas, the temperature of the interface seal between the ablative thrust chamber assembly and the ablative nozzle extension of the two positive pitch engines was monitored during entry.

During the two revolutions prior to CSM/S-IVB separation, the temperatures of the command module reaction control helium tank and oxidizer valve varied only slightly from the launch values. Temperature data for the engine injectors, outer walls, and chamber/nozzle interface seals were recorded by the onboard flight qualification tape recorder only during the launch and entry phases; however, during the first two revolutions, these temperatures should have varied only slightly from launch values.

During the coast-ellipse phase, the command module reaction control system was subjected to cold-soak conditions for approximately 6 hours. Because the system had received side sun exposure during the similar phase of the Apollo 4 mission, this flight represented the first opportunity to evaluate thermal response of the system after an extended cold-soak period. As expected, when the system was activated after the cold-soak period, the temperatures were well below ambient launch values. The system A and B helium tanks cooled 11° to 12° F, reaching temperatures of approximately 64° and 58° F, respectively, at service module/command module separation. These levels are considered to be normal for cold-soak operation and were well within design limits.

The engines were ported through, and bonded to, the heat shield and substantial conductive heat losses were experienced by the engines during the cold-soak period. At service module/command module separation, the engine outer-wall temperatures had decreased to the range of -25° to -2° F, the injectors to the range of 36° to 40° F, and the oxidizer valves to the range of 44° to 54° F. These values were well within design limits prior to activation; however, if Apollo 6 had been a manned mission, the crew would have had to apply current to the engine valves prior to entry to increase the injector temperatures to above 48° F.

From system activation through landing, the helium tank temperatures decreased normally as a result of gas withdrawal, while all of the engine component temperatures increased becuase of engine firing and aerodynamic entry thermal loads. During entry, the negative pitch engines were exposed to the airstream when the apex cover was jettisoned, and the subsequent cooling effect attenuated the temperature increase of the oxidizer valves for these engines. During entry, all measurement parameters remained well within design limits, and no chamber/nozzle interface seal leakage was detected on either of the positive pitch engines.

Postflight examinations: The postflight examination of the command module reaction control system revealed ruptured burst disks in the A-system oxidizer relief valve and in the B-system fuel relief valve; these ruptured burst disks have been characteristic of all previous missions and the ground-based test program. The ruptures are caused by a pressure surge or regulator overshoot at system pressurization. This problem has been eliminated on block II systems by relocating the relief valves to provide more volume between the regulators and relief valves.

Another problem was the crosswiring of the oxidizer and fuel valves of all four yaw engines, noted during system decontamination in Hawaii. The fuel lead wires and the oxidizer lead wires were reversed. This anomaly had no effect on engine performance in flight because the oxidizer and fuel valves are wired in parallel and receive a common command signal. Additional information on this anomaly is contained in section 12.0.

TABLE 5.17-I.- PROPELLANT SERVICING[a]

Reaction control system	Fuel,[b] lb	Oxidizer,[c] lb
Service module		
Quad A	67.4	138.3
Quad B	67.5	137.8
Quad C	67.3	137.6
Quad D	67.4	138.1
Command module		
System A	44.4	84.1
System B	44.5	84.3

[a]Loads are based on pressure-volume-temperature checks.

[b]Fuel tolerance is ±0.75 lb.

[c]Oxidizer tolerance is ±1.0 lb.

TABLE 5.17-II.- COMMAND AND SERVICE MODULE REACTION CONTROL SYSTEM SEQUENCE OF EVENTS

Event	Initiate, hr:min:sec	Complete, hr:min:sec
Direct mode firing	03:14:26.2	03:14:29.1
CSM/S-IVB separation		03:14:27.8
First automatic coil firing (roll)		03:14:28.6
Plus X translation (automatic coils)	03:14:29.1	03:14:36.3
Maneuver to first service propulsion system engine firing attitude	03:14:42.0	03:14:54.8
Service propulsion system engine firing	03:16:06.2	03:23:27.9
Pitch and yaw inhibit	03:16:07.2	03:23:28.9
Maneuver to cold-soak attitude	03:23:40.8	03:24:26.0
Cold-soak attitude hold	03:24:26.0	09:15:34.1
Maneuver to second plus X translation attitude	09:15:34.1	09:16:21.4
Second plus X translation	09:29:19.1	09:30:09.2
Maneuver to CM/SM separation attitude	09:35:05.8	09:36:09.9
CM reaction control system pressurization		09:36:55.6
CM/SM separation		09:36:56.6
Minus X translation (SM)	09:36:56.6	
CM reaction control system control firings	09:36:56.7	09:51:24.0
Maneuver to entry attitude	09:37:04.9	09:37:50.8
Main parachute deploy		09:52:13.4
Propellant depletion burn	09:52:33.4	09:53:16.6
Helium purge initiate	09:56:43.6	
Landing	09:57:19.9	
Helium purge complete		09:57:30.9

TABLE 5.17-III.- TYPICAL SERVICE MODULE REACTION CONTROL SYSTEM

ANGULAR ACCELERATIONS AND VELOCITY CHANGES

Event	Time, hr:min:sec		Acceleration, deg/sec^2						Firing time, sec	Translation		
			Pitch		Yaw		Roll			Change in velocity, ft/sec		
	From	To	Plus	Minus	Plus	Minus	Plus	Minus		Planned	ON time[a]	PIPA[b]
CSM/S-IVB separation[c]	03:14:27.8	03:14:36.3							8.47	1.93	1.48	1.49
First plus X translation	03:14:29.1	03:14:36.3	0.85	--	--	1.09	--	4.65				
Orientation to service propulsion system engine firing	03:14:42.0	03:14:54.8	1.21	1.17	0.85	0.87	5.46	5.37				
Maneuver to cold-soak attitude	03:23:40.8	03:24:26.0	1.77	1.77	1.37	1.26	--	9.15				
Second plus X translation	09:29:19.1	09:30:09.2							50.13	[d]15.04	23.76	23.76
Maneuver to CM/SM separation	09:35:05.8	09:36:09.9	1.31	1.57	1.49	1.73	9.57	9.62				

[a]Based on engine duty cycles and nominal thrust.

[b]Pulse integrating pendulous accelerometer.

[c]From physical separation to end of translation.

[d]Based on a 30-second maneuver.

TABLE 5.17-IV.- SERVICE MODULE REACTION CONTROL SYSTEM

ENGINE ACTIVITY DURING COLD-SOAK PERIOD

[Activity estimated using data from 45 percent of the period]

Activity	Number of pulses	ON time, sec
Pitch[a]		
Plus	485	8.4
Minus	260	4.4
Yaw[a]		
Plus	310	5.5
Minus	355	5.6
Roll[b]		
Plus	1975	38.4
Minus	2185	38.6

[a]Two-engine control.

[b]Four-engine control.

TABLE 5.17-V.- SERVICE MODULE REACTION CONTROL SYSTEM

LAUNCH HEATING SUMMARY

Parameter	Maximum temperature during launch, °F	Time of maximum temperature, hr:min:sec
Engine mounting structure		
Quad A	153	00:08:21
Quad B	158	00:10:00
Quad C	158	00:07:30
Quad D	154	00:11:06
Injector		
Negative pitch engine, quad A	132	00:15:00
Positive yaw engine, quad B	226	00:04:30
Clockwise roll engine, quad C	152	00:10:54
Counterclockwise roll engine, quad D	168	00:07:15

TABLE 5.17-VI.- SUMMARY OF SERVICE MODULE REACTION CONTROL SYSTEM TEMPERATURES FROM CSM/S-IVB SEPARATION THROUGH CM/SM SEPARATION

	Engine mounting structure				Injector			
	Quad A	Quad B	Quad C	Quad D	-P, quad A	+Y, quad B	CW, quad C	CCW, quad D
Temperature at initiation of S-IVB separation (03:14:26), °F	126.5	134	124.5	122	119.5	110	125.5	124.5
Maximum soakback temperature after S-IVB maneuver firing, °F	140	130	131	141.5	177.5	137.5	138	142.5
Time of occurrence, hr:min:sec	03:28:40	03:30:00	03:27:15	03:30:00	03:17:30	03:26:10	03:28:00	03:26:20
Maximum temperature during cold soak, °F	131	136.5	122.5	142.5	125.5	109	119	139
Minimum temperature during cold soak, °F (approx.)	119	104	86.5	122	121	84.5	-7	122.5
Temperature at initiation of reorientation maneuver prior to second +X translation (09:15:34), °F	132	104	86.5	135	121	84.5	91.5	122.5
Temperature at initiation of second +X translation (09:29:19), °F	125	124	100	128.5	131	110.5	105.5	124.5
Maximum soakback temperature after second +X translation, °F	151	141	115	150	200	118	131	154.5
Time of occurrence, hr:min:sec	09:36:56	09:36:56	09:36:56	09:36:56	09:33:18	09:36:56	09:36:56	09:33:30
Temperature at CM/SM separation (09:36:56), °F	151	141	115	150	179	118	131	148.5

TABLE 5.17-VII.- THERMAL CONTROL SYSTEM PERFORMANCE

SUMMARY DURING COLD-SOAK PERIOD

	Quad A	Quad B	Quad C	Quad D
No. of heater ON actuations[a]	31	1	1	12
No. of heater OFF actuations[a]	31	[b]0	[b]0	12
Actuation ON temperature, °F[a]	119 ± 2	121	114	122 ± 2
Actuation OFF temperature, °F[a]	131 ± 2	--	--	140 ± 3
Heater cycle rate,[c] minutes per cycle	8 to 11	--	--	25 to 30

[a]Estimated values based on available data coverage.

[b]Quads B and C experienced cold soak during this period and were never warmed sufficiently for the thermal switch to activate the heaters OFF.

[c]Time from actuation of the heater ON to the next actuation of the heater ON.

TABLE 5.17-VIII.- TYPICAL COMMAND MODULE REACTION CONTROL SYSTEM

CONTROL CROSSCOUPLING EFFECTS

Time, hr:min:sec		Commanded	Acceleration, deg/sec^2	Crosscoupling effects acceleration, deg/sec^2	
From	To			Pitch	Yaw
09:37:30.9	09:37:31.3	+ roll	+6.4	+1.2	-1.05
09:37:33.0	09:37:34.0	- roll	-7.2	+1.6	+0.97

TABLE 5.17-IX.- COMMAND MODULE REACTION CONTROL SYSTEM PRESSURE TRENDS

Event	Time, hr:min:sec	Helium source pressure, psia		Helium source temperature, °F		Pressure/temperature ratio	
		System A	System B	System A	System B	System A	System B
Helium servicing complete	10:00 p.m. e.s.t., April 2, 1968	4240	4250	82	79	7.8	7.9
Range zero		4200	4189	75	70	7.8	7.9
Adapter/SM separation	03:14:27.8	4200	4168	73	68	7.9	7.9
Apogee	06:28:58	4180	4147	70	64	7.9	7.9
Completion of maneuver to separation[a]	09:36:09.9	4138	4104	64	58	7.9	7.9
Start pitch to entry attitude[b]	09:37:04.9	3442	3440	61	58	6.6	6.6
Complete pitch to entry attitude	09:37:50.8	3400	3397	59	51	6.6	6.5
Start propellant depletion burn	09:52:33.4	2473	2412	32	28	5.0	4.9
Complete depletion burn	09:53:16.6	892	976	18	22	1.9	2.0
Start helium purge	09:56:43.6	765	933	11	22	1.6	1.9
Landing	09:57:19.9	260	234	7	16	0.5	0.5
Complete helium purge	09:57:30.9	239	226	3	12	0.5	0.5
Close engine valve	09:57:30.9	238	226	3	12	0.5	0.5

[a]Before system activation.

[b]After system activation.

TABLE 5.17-X.- COMMAND MODULE REACTION CONTROL SYSTEM THERMAL PERFORMANCE SUMMARY

Parameter	Measurement number	Engine	System	Launch	Completion of SPS firing	Apogee	CM/SM separation	Initiation of depletion burn	Landing	Design limit
				00:00:00	03:23:27.9	06:28:58	09:36:56.6	09:52:33.6	09:57:19.9	
Helium tank temperature, °F	CR0003T	--	A	74.6	73.4	70.5	63.8	32.7	6.5	--
Helium tank temperature, °F	CR0004T	--	B	69.6	68.4	65.5	57.7	28.5	16.9	--
Oxidizer valve temperature, °F	CR2201T	CCW	A	74.3	70.6	64.0	52.0	86.0	108.0	225° max.
Oxidizer valve temperature, °F	CR2202T	-Y	A	71.4	68.9	65.0	52.8	67.8	96.2	225° max.
Oxidizer valve temperature, °F	CR2203T	+Y	B	76.7	74.2	67.5	54.4	68.0	90.4	225° max.
Oxidizer valve temperature, °F	CR2204T	-P	B	67.7	64.0	57.5	44.2	47.1	78.9	225° max.
Oxidizer valve temperature, °F	CR2205T	-P	A	69.6	65.8	59.0	46.0	49.6	82.3	225° max.
Oxidizer valve temperature, °F	CR2206T	CW	B	75.5	69.3	63.0	52.0	78.9	97.8	225° max.
Injector temperature, °F	CR2103T	-Y	A	67.0	--	--	36.0	128.0	[b]	-10° min.
Injector temperature, °F	CR2114T	CCW	A	71.0	--	--	40.0	320.0	[b]	-10° min.
Injector temperature, °F	CR2115T	CCW	B	68.0	--	--	40.0	317.0	[b]	-10° min.
Injector temperature, °F	CR2116T	+Y	B	72.0	--	--	38.0	125.0	[b]	-10° min.
Engine outer wall temperature no. 1, °F	CR4553T	-Y	A	64.0	--	--	-11.0	20.0	[b]	850° max.
Engine outer wall temperature no. 2, °F	CR4554T	-Y	A	63.0	--	--	[a]-20.0	15.0	[b]	850° max.
Engine outer wall temperature no. 1, °F	CR4556T	+Y	B	68.0	--	--	[a]-22.0	10.0	[b]	850° max.
Engine outer wall temperature no. 2, °F	CR4557T	+Y	B	66.0	--	--	[a]-20.0	21.0	[b]	850° max.
Engine outer wall temperature no. 1, °F	CR4559T	CCW	A	72.0	--	--	-2.0	91.0	[b]	850° max.
Engine outer wall temperature no. 2, °F	CR4560T	CCW	A	66.0	--	--	[a]-20.0	59.0	[b]	850° max.
Engine outer wall temperature no. 1, °F	CR4580T	CCW	B	66.0	--	--	-5.0	76.0	[b]	850° max.
Engine outer wall temperature no. 2, °F	CR4581T	CCW	B	65.0	--	--	-25.0	89.0	[b]	850° max.
Chamber/nozzle interface temperature, °F	CR0570T	+P	A	55.0	--	--	-3.0	24.0	[b]	--
Chamber/nozzle interface temperature, °F	CR0571T	+P	B	75.0	--	--	5.0	33.0	[b]	--

[a] Estimated value.

[b] Data unavailable in time for inclusion.

NASA-S-68-3605

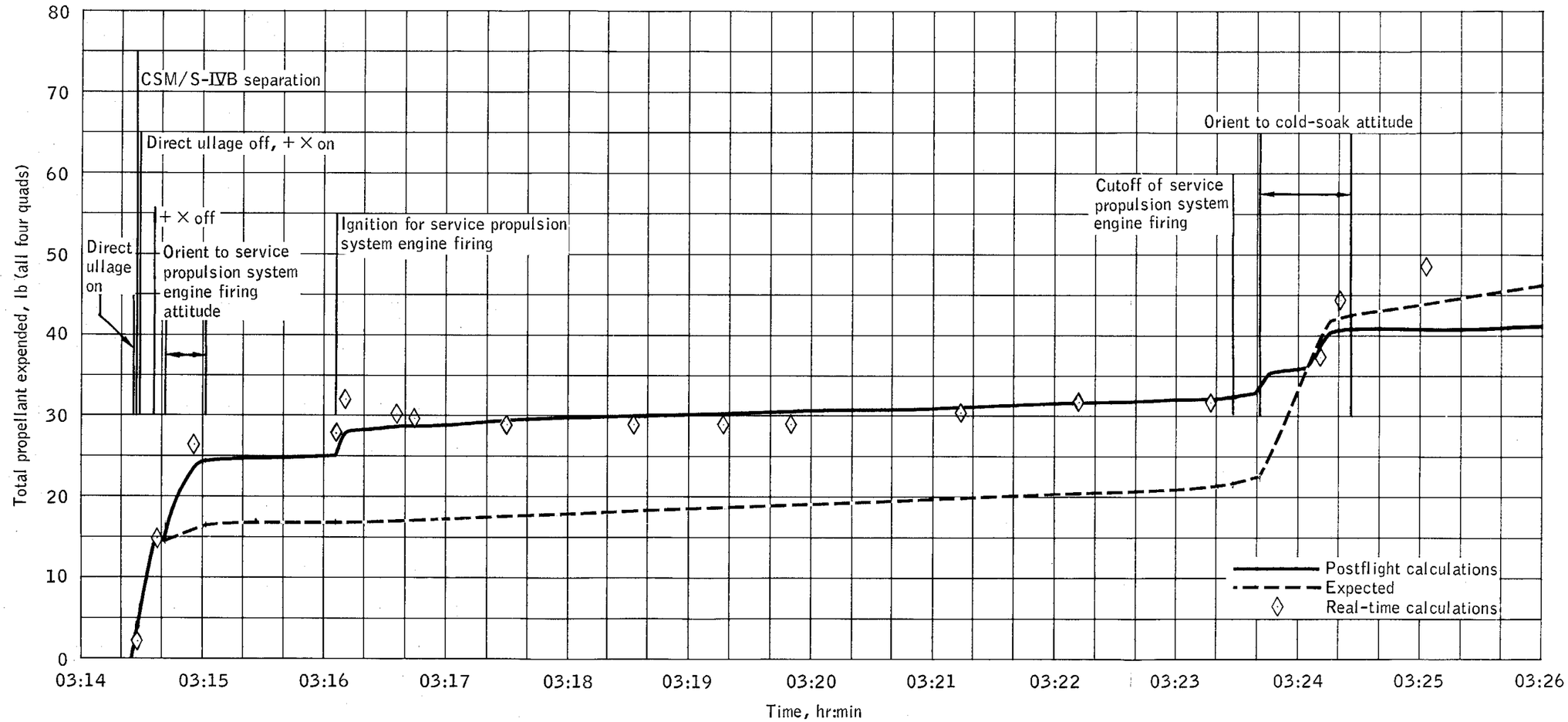

Figure 5.17-1.- Propellant consumption prior to cold soak.

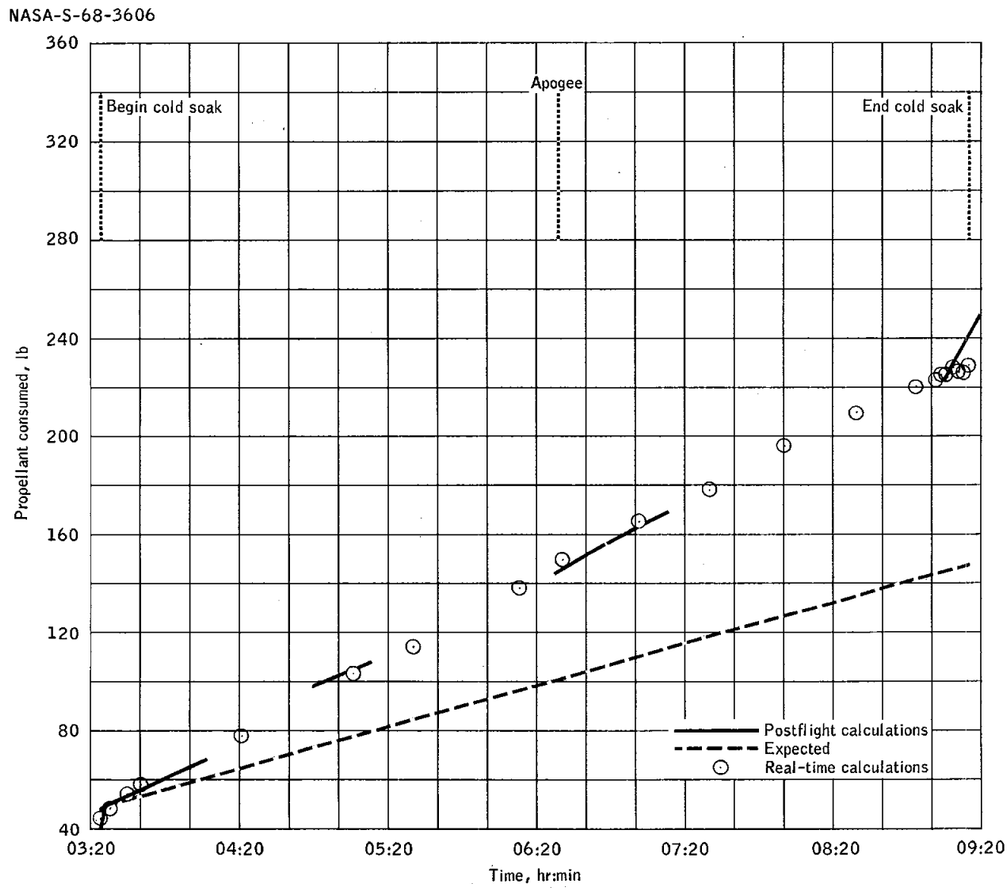

Figure 5.17-2.- Propellant consumption during cold soak.

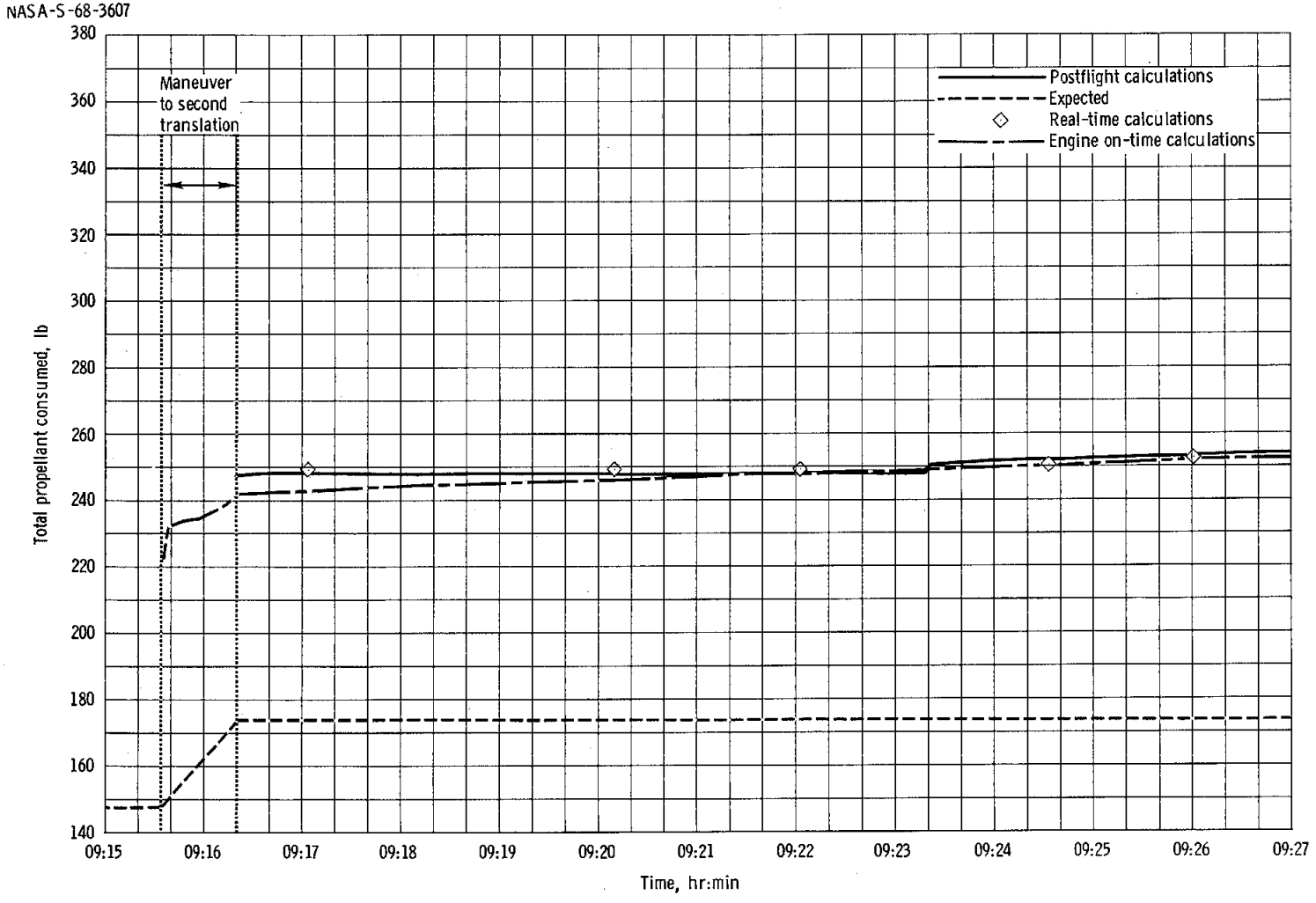

(a) 09:15:00 to 09:27:00

Figure 5.17-3. - Propellant consumption after cold soak.

NASA-S-68-3608

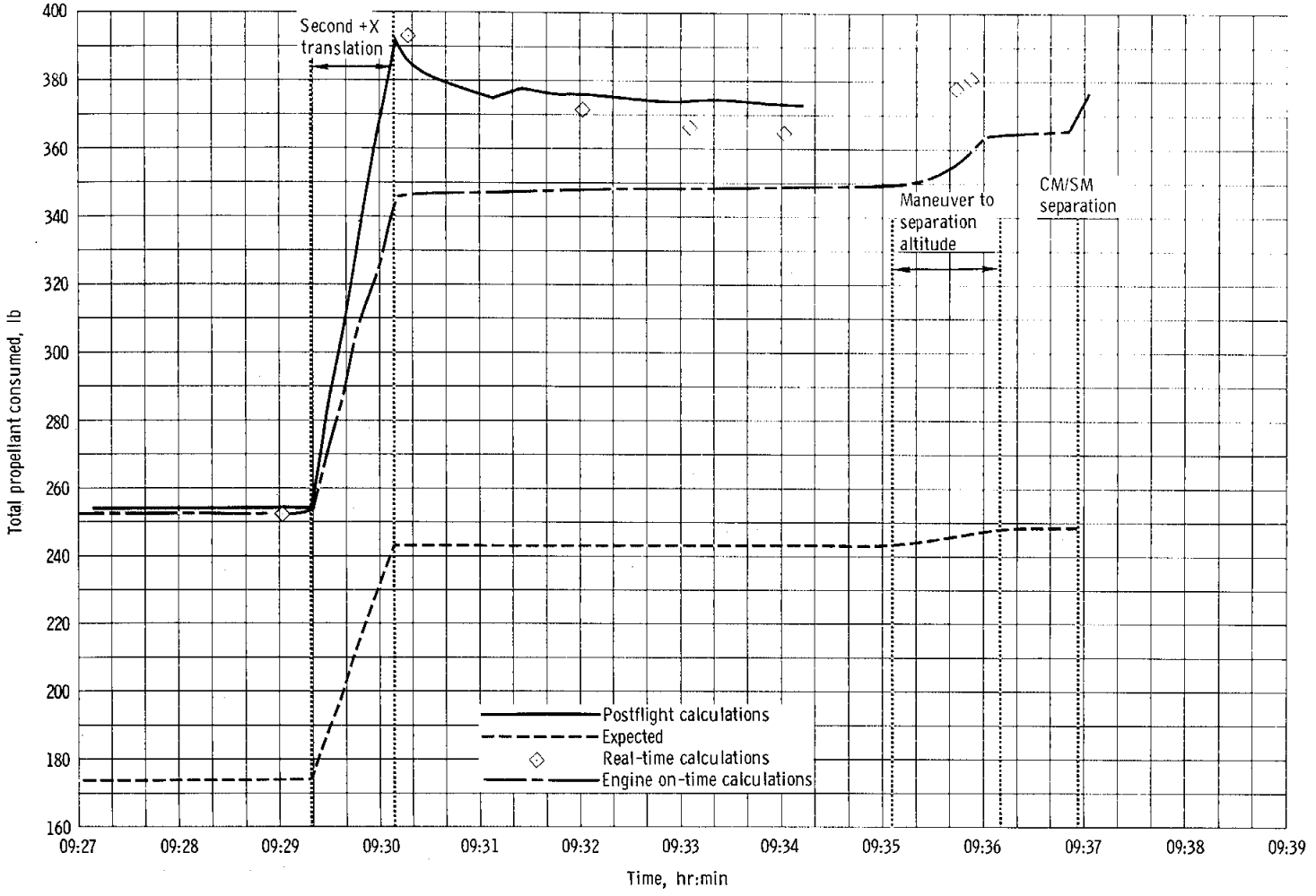

(b) 09:27:00 to 09:39:00.

Figure 5.17-3. - Concluded.

NASA-S-68-3609

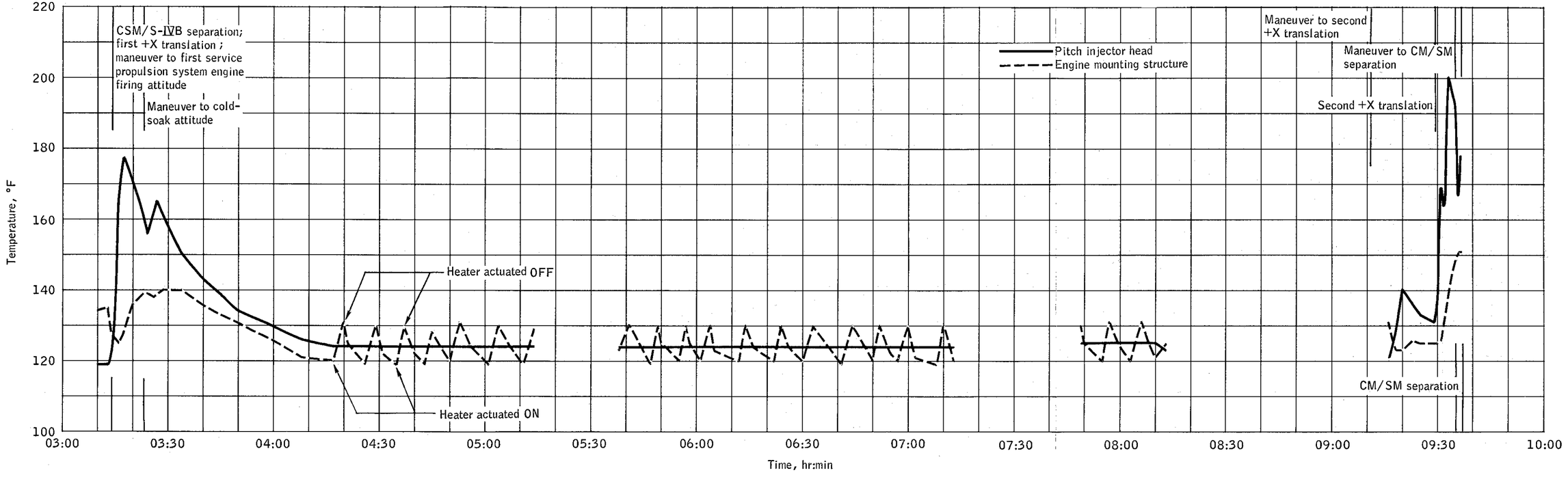

(a) Quad A.

Figure 5.17-4.- Service module reaction control system temperature from CSM/S-IVB separation through CM/SM separation.

NASA-S-68-3610

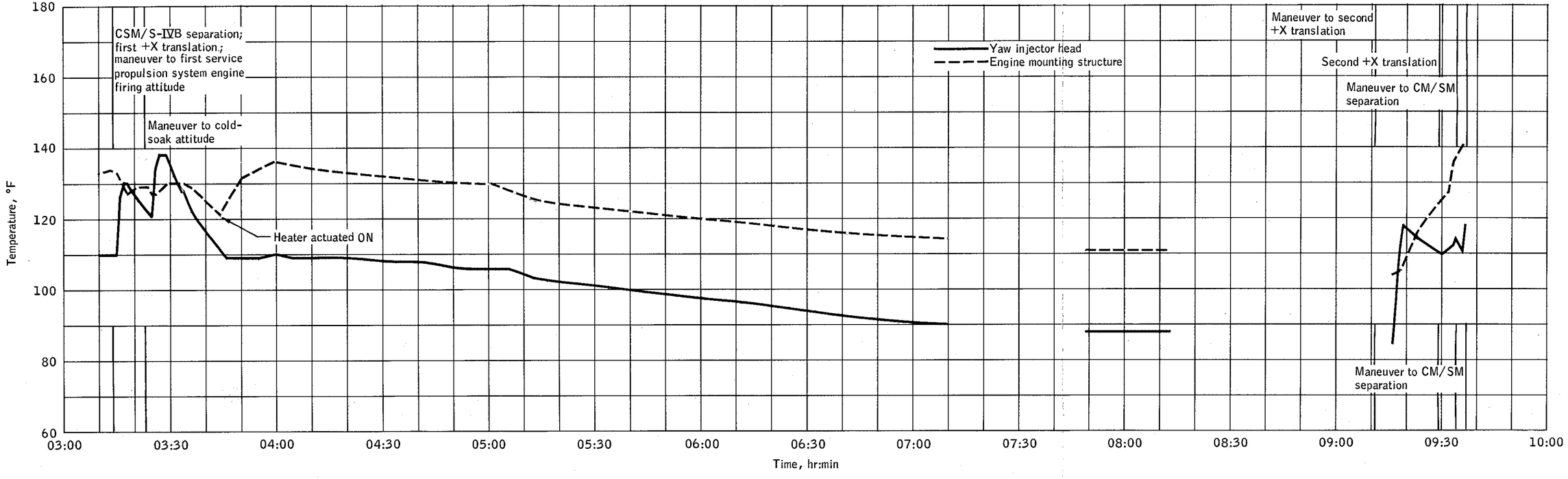

(b) Quad B.

Figure 5.17-4.- Continued.

NASA-S-68-3611

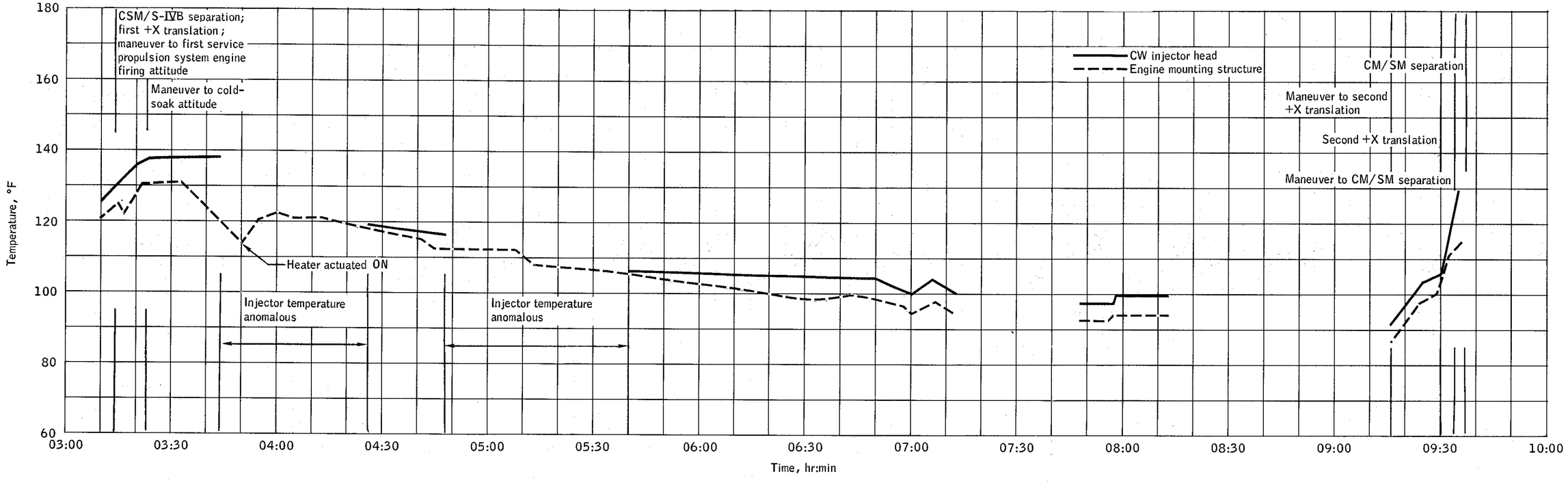

(c) Quad C.

Figure 5.17-4.- Continued.

NASA-S-68-3612

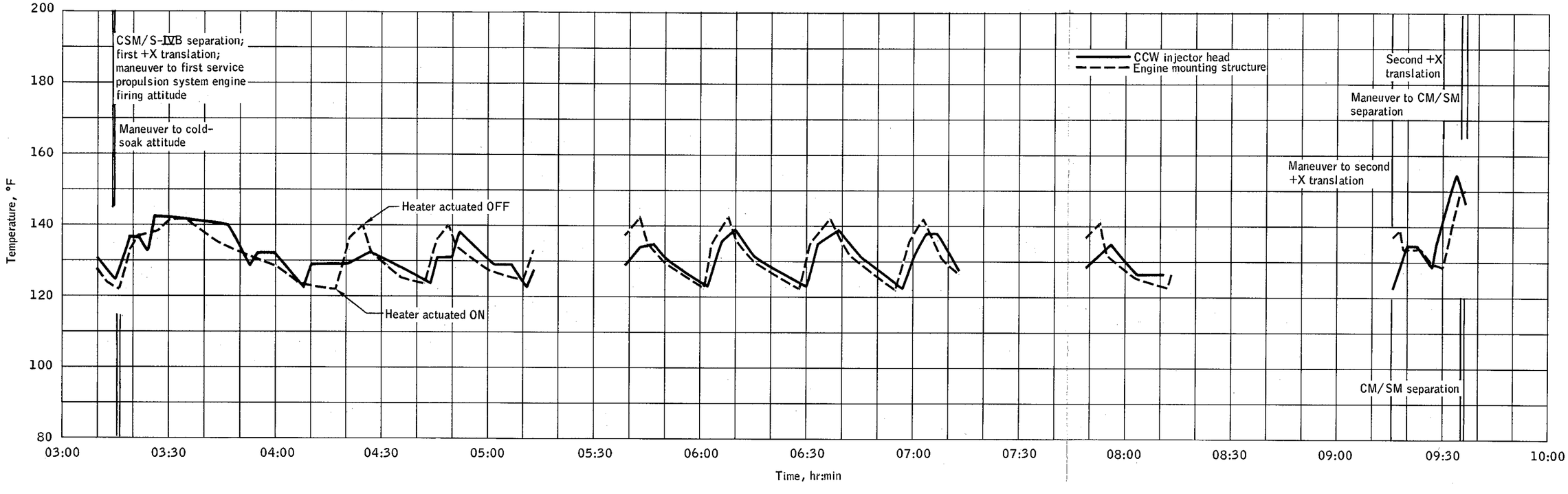

(d) Quad D.

Figure 5.17-4.- Concluded.

NASA-S-68-3613

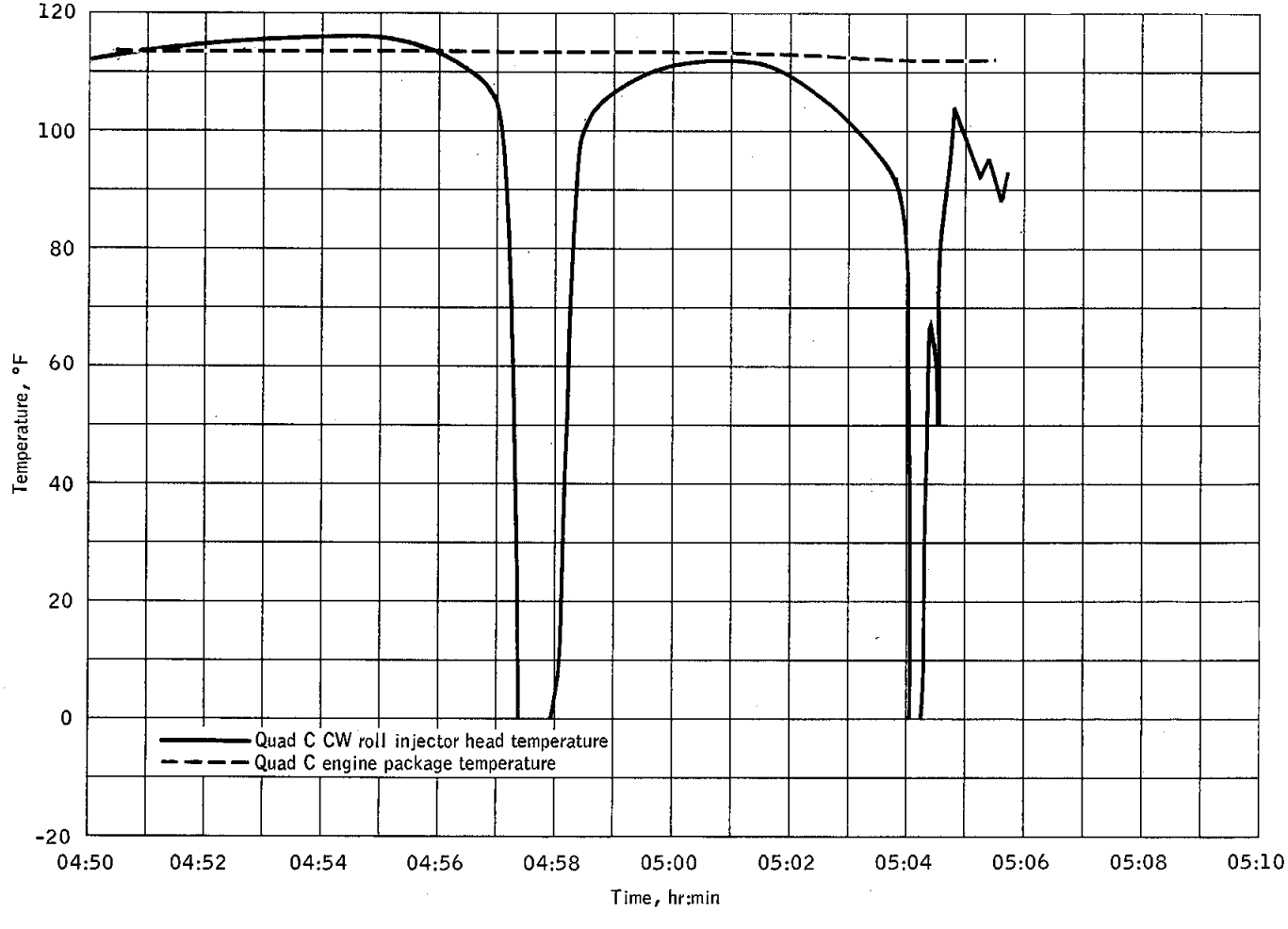

Figure 5.17-5.- Abnormal thermal behavior of quad C CW roll injector head during cold soak.

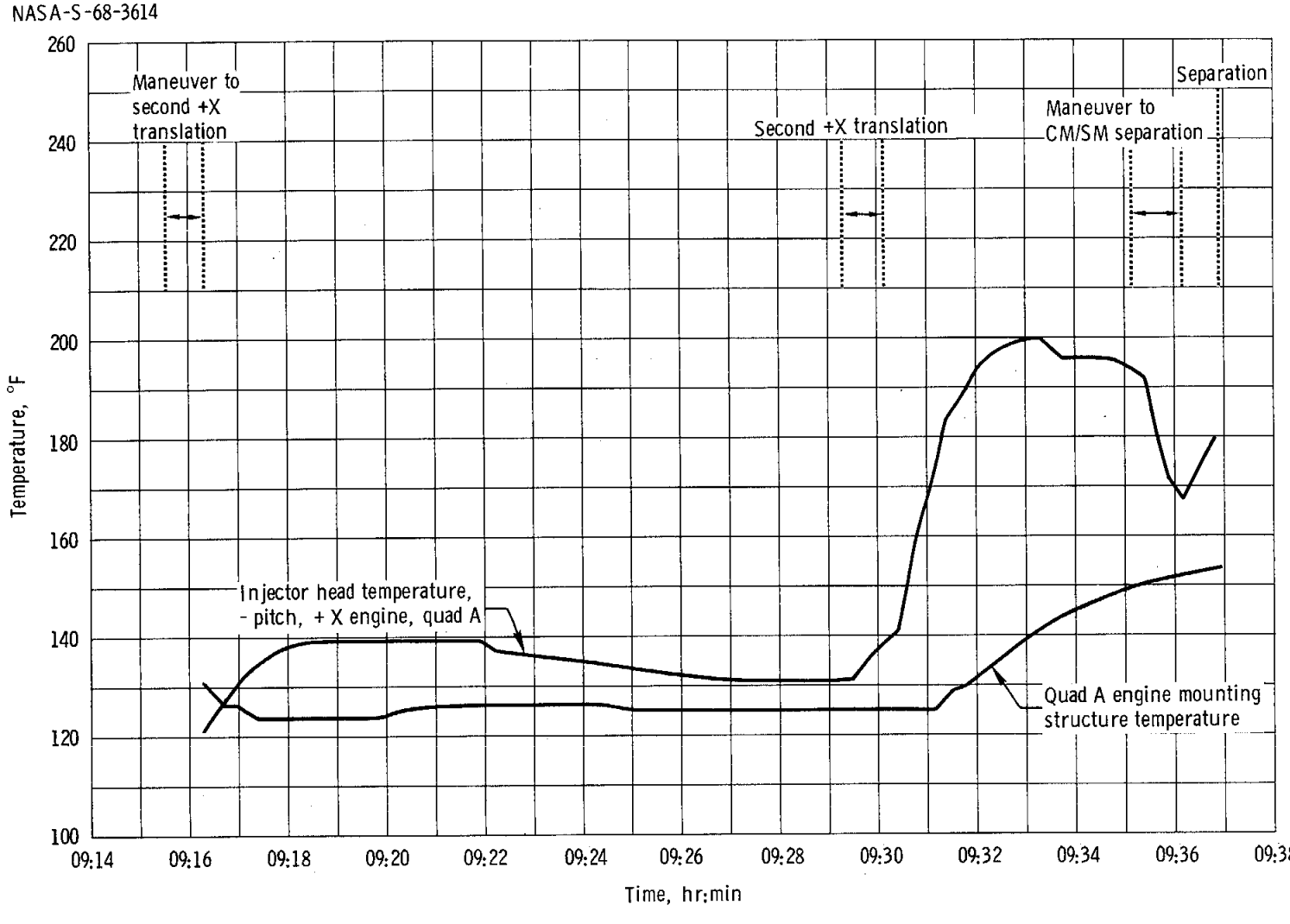

Figure 5.17-6. - Effect of engine firing on injector head and engine mounting structure temperatures.

NASA-S-68-3615

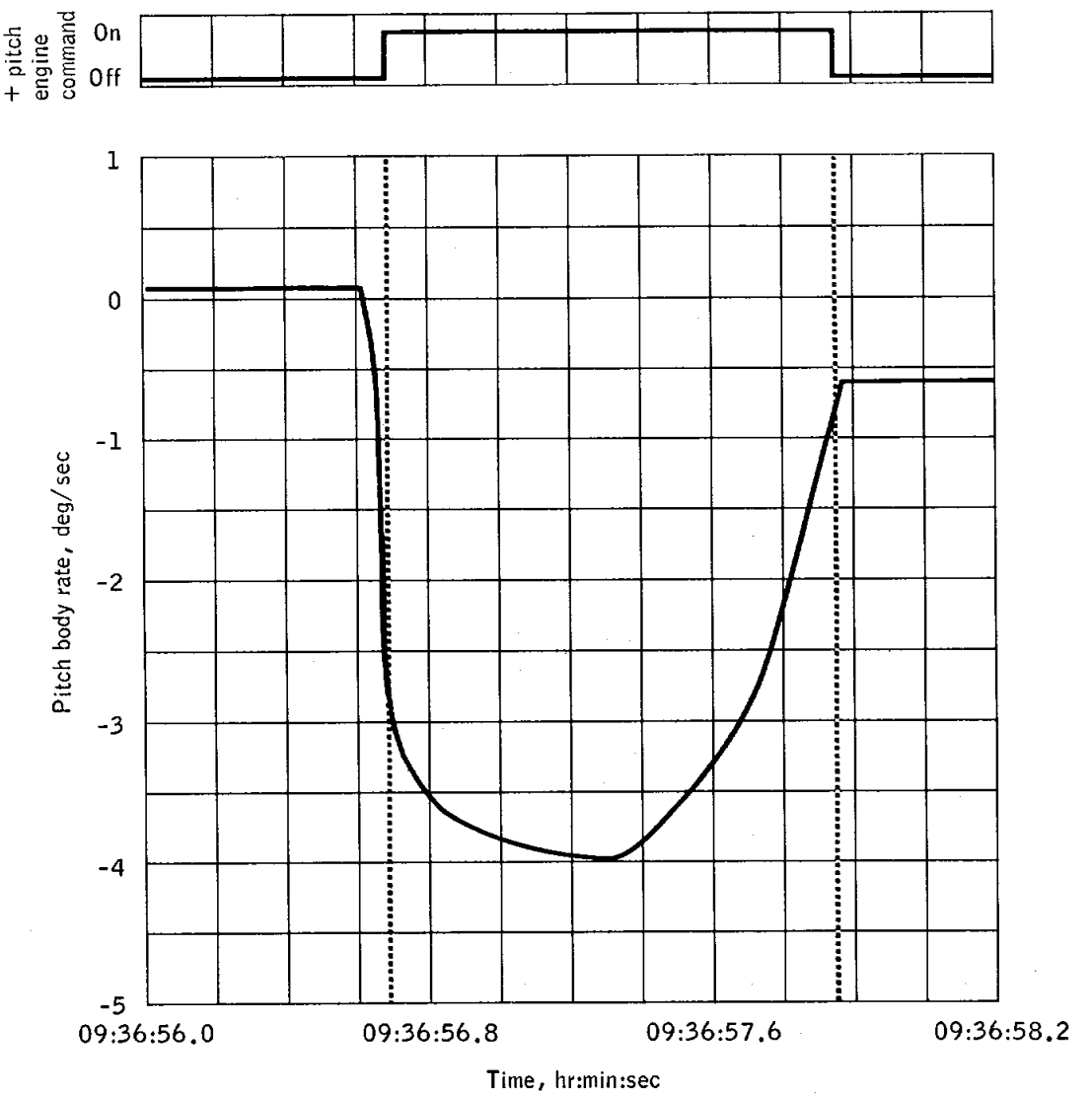

Figure 5.17-7.- CM/SM separation disturbances.

NASA-S-68-3616

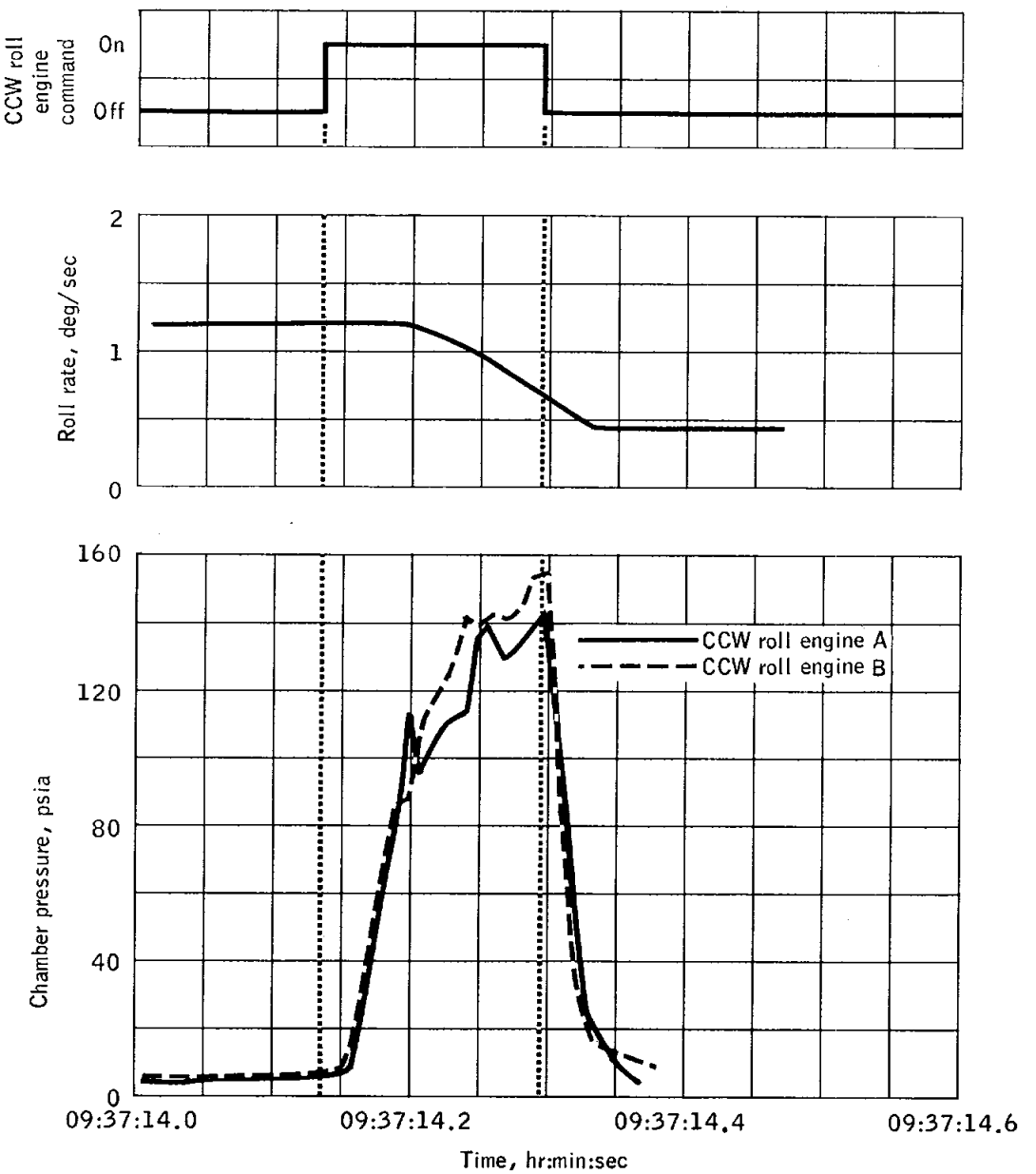

Figure 5.17-8.- First command module reaction control system CCW roll firing.

NASA-S-68-3617

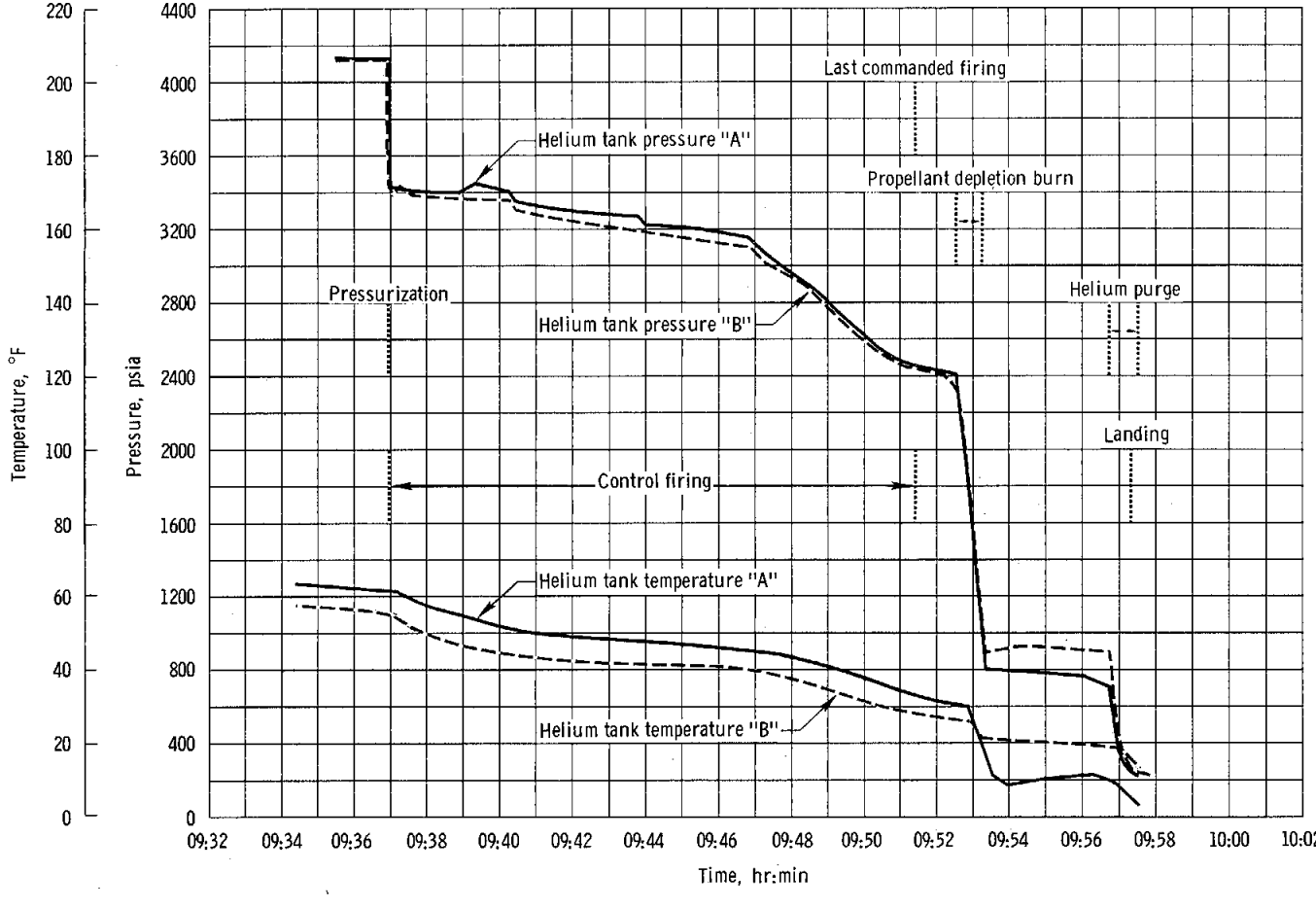

Figure 5.17-9. - Systems A and B helium tank pressure and temperature history for command module reaction control system.

NASA-S-68-3618

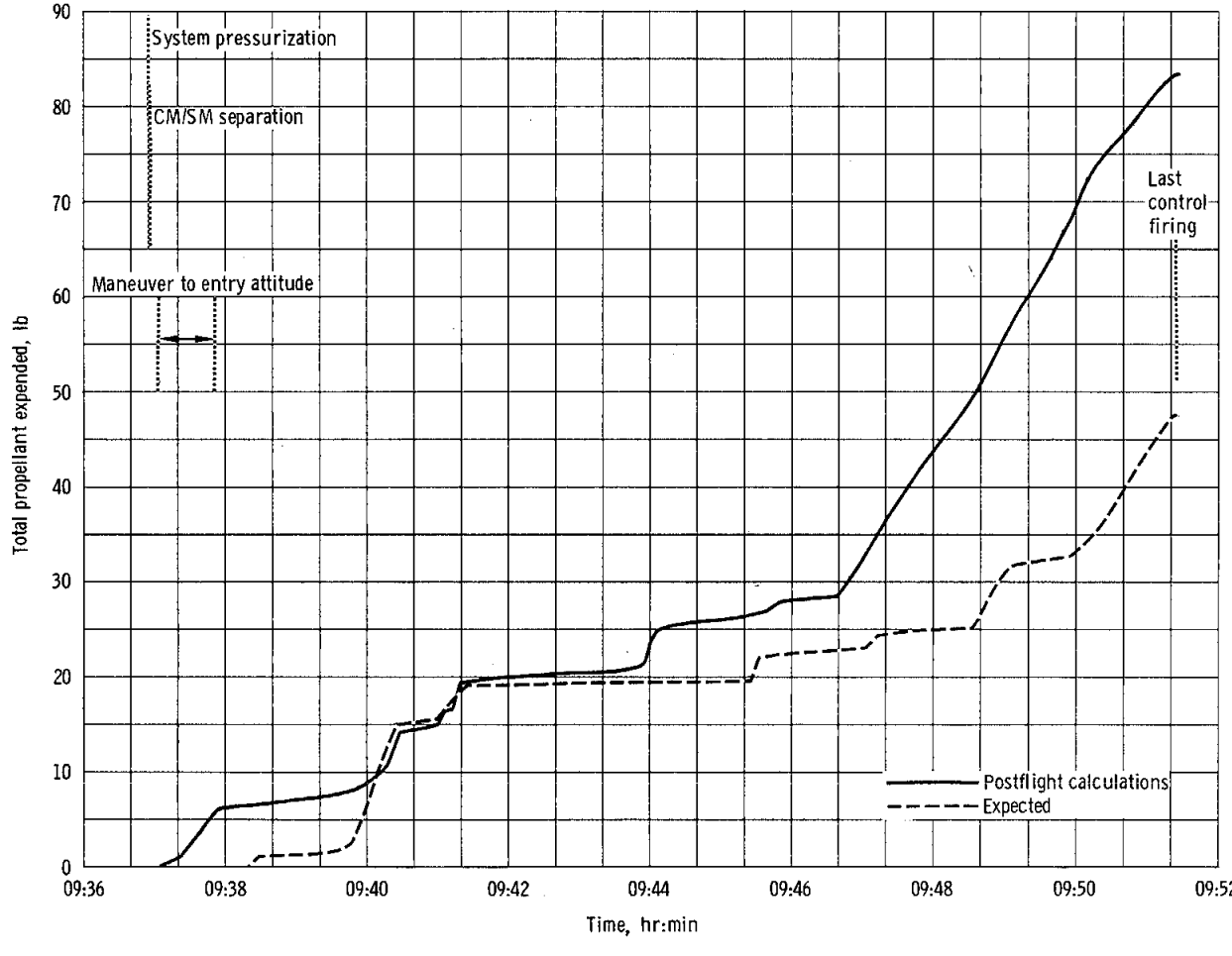

Figure 5.17-10. - Total command module reaction control system propellant usage for maneuvers.

NASA-S-68-3619

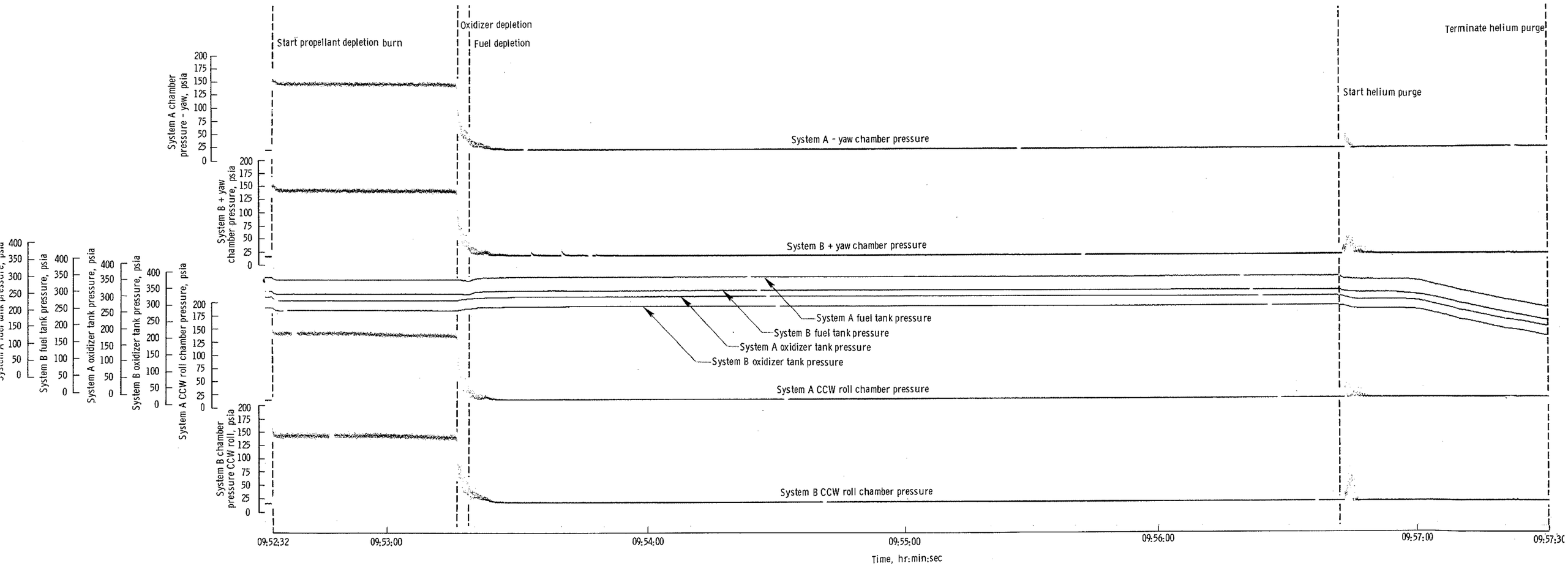

Figure 5.17-11.- Propellant depletion burn and helium purge.

5.18 SERVICE PROPULSION

The service propulsion system demonstrated a no-ullage start during a long-duration firing. The mission plan was for two service propulsion system engine firings — a 254-second firing to be followed after 6 hours by a 189-second firing. Because of malfunctions in the launch vehicle, the service propulsion system duty cycle was revised after lift-off and a single 441.71-second firing was obtained.

The performance of the service propulsion system was analyzed and found to be within the expected tolerances.

The service propulsion system hardware used on the Apollo 6 mission was identical to that used on the Apollo 4 mission. The propellant mass, however, was increased to fulfill a greater impulse requirement; the result was that the sump tanks were filled and the storage tanks were approximately 43 percent filled. The propellant gaging system operated in the primary mode.

Because of the inability to restart the S-IVB stage of the launch vehicle, an alternate mission plan was implemented. The alternate plan required the service propulsion system to provide the change in velocity necessary to transfer from an earth-parking orbit to the highly elliptical earth-intercepting orbit that was needed to satisfy the entry conditions of the heat shield test. The service propulsion system ignited at 03:16:06.20 and shut down 441.71 seconds later, at 03:23:27.91. The firing was not preceded by an ullage maneuver.

5.18.1 Propellant Loading

Oxidizer.- The service propulsion oxidizer tanks were loaded with nitrogen tetroxide on March 18, 1968. The oxidizer sump tank was filled to the top of the crossover line standpipe, and the sump tank primary gaging system probe was calibrated. The oxidizer storage tank was then loaded by overflowing the sump tank through the crossover line. The filling flow rate was maintained at approximately 15 gal/min to minimize the entrainment of helium from the sump tank ullage. This procedure thereby reduced the sump tank overfill from that observed during propellant loading of the Apollo 4 service propulsion tanks. The storage tank was filled to the top point sensor, and the primary gaging system probe was calibrated. Oxidizer then drained through the sump tank, until the required flight load was indicated on the storage tank primary gaging system probe. At that time, the storage tank gaging probe showed 6820 pounds, the sump tank probe showed 14 820 pounds, and the storage tank ullage pressure was 113 psia. The indicated sump tank overfill

(above top of standpipe) was approximately 80 pounds. When the storage tank ullage was test pressurized to 175 psia, the storage tank probe read 6520 pounds, and the sump tank probe showed a maximum reading of 15 000 pounds.

Fuel.- On March 19, the fuel tanks were loaded with Aerozine-50 in a manner similar to the oxidizer tanks. With the flight load onboard and a storage tank ullage pressure of 97 psia, the storage tank primary gaging system probe read 3320 pounds and the sump tank probe showed 7410 pounds. There was an indicated sump tank overfill of approximately 50 pounds. When the storage tank ullage pressure was raised to 175 psia, the storage tank probe read 3140 pounds, and the sump tank probe showed a maximum reading of 7500 pounds.

Propellant Density.- Density measurements were made of one oxidizer sample and of one fuel sample. The analysis indicated an oxidizer density of 90.252 lbm/ft^3 at the loaded temperature of 70° F and under a pressure of 113 psia. At 70° F and under a pressure of 97 psia, the fuel density was 56.638 lbm/ft^3.

The total propellant loads, as calculated from measured densities and gaging system readings during loading, were as follows:

Propellant	Total mass loaded, lb		
	Actual	Reported	Planned
Oxidizer[a]	22 185	22 015	21 980.2
Fuel[a]	11 038	10 964	10 940.5
Total	33 223	32 979	32 920.7

[a]Includes gageable, ungageable, and vapor-loaded quantities.

The differences between the actual and the reported loads result from use of the measured densities, the treatment of the vapor, and the inclusion of all the propellant in the standpipes.

5.18.2 Performance

The major analysis effort was concentrated on determining system performance for the service propulsion system engine firing. The performance was determined by use of the Apollo propulsion analysis program.

The results of the analysis program simulation of the service propulsion system engine firing are listed in table 5.18-I. The values shown in the table represent results midway between the ignition signal and storage tank depletion for the before-crossover values, and midway between storage tank depletion and engine cutoff for the after-crossover values. These data are representative of the values throughout these portions of the firing. Storage tank depletion (crossover) occurred at 138 seconds into the firing, with oxidizer crossover preceding fuel crossover by approximately 1.6 seconds. A time history of the propellant consumed is presented in figure 5.18-1. The total consumption was estimated to be 30 075 pounds.

The time history of the measured chamber pressure during the service propulsion system engine firing is shown in figure 5.18-2. The increase in chamber pressure noted at 03:18:25 was caused by storage tank depletion (crossover). Similar increases in inlet pressures are shown in table 5.18-I.

The following instrumentation errors were detected by performing a postflight simulation of the service propulsion system duty cycle. These errors were determined by calculating the values which would best correlate the data. Chamber pressure data calculated during the analysis program indicated that the measured chamber pressure was initially reading 3.5 psi low, and that the measured chamber pressure exhibited an increasing pressure drift of approximately 1.5 psi over the firing period. This is within the accuracy of the instrumentation. The increasing pressure drift was apparently thermally induced. A similar trend was observed during the Apollo 4 mission. Results of the program simulation indicated that the measured fuel inlet pressure was reading 1 to 2 psi low throughout the firing. The fuel check valve outlet pressure measurement was reading approximately 20.0 psi low during the major portion of the firing.

Engine acceptance tests are conducted to determine the performance of the engine segragated from the feed system. This makes a discrete evaluation of the engine possible, and provides a common basis for comparison of engines. The engine used for the Apollo 6 mission was known to be a low performance engine. It was determined from the analysis of this flight that the engine performance corrected to standard inlet conditions yielded a thrust of 21 357 pounds, a specific impulse of 309.8 seconds, and a propellant mixture ratio of 2.014. These values are 0.31 percent higher and 0.20 percent higher than the standard inlet condition values reported during the acceptance test of the engine. These differences are within the expected ranges. The operational trajectory was generated from the following acceptance test data: constant steady-state thrust 21 290 pounds, specific impulse 309.7 seconds, and propellant mixture ratio 2.01:1. The standard inlet condition performance values reported were calculated for the following nominal conditions.

Oxidizer interface pressure, psia . .	164
Fuel interface pressure, psia	170
Oxidizer interface temperature, °F .	70
Fuel interface temperature, °F . . .	70
Oxidizer density, lbm/ft^3	90.15
Fuel density, lbm/ft^3	56.31
Thrust acceleration, lbf/lbm	1.0
Throat area (initial value), in^2 . .	121.56

5.18.3 Propellant Utilization and Gaging

The propellant utilization and gaging system was operated in the primary mode. The storage and sump tank mass data were individually transmitted on separate measurements.

All gaging system signals were locked on preset values for 4.5 seconds following ignition to prevent excessive oscillations from propellant slosh.

Because of the 4.5-second lock-out period, both the fuel and oxidizer storage gages indicated an excessively high flow rate immediately after the lock-out period. After stabilization, the depletion rates indicated by the storage tank gages were within 0.9 and 0.21 percent of the computed oxidizer and fuel flow rate values, respectively. The oxidizer storage tank gage reading, when extrapolated to ignition, was not consistent with the preflight reading. The extrapolation showed an equivalent reading of approximately 6280 pounds, compared to a preflight reading (as noted in section 5.18.1) of 6520 pounds under 175 psia tank pressure. The oxidizer storage tank gage also showed a +100 pounds bias at depletion. This amount of bias was also noted during the Apollo 4 mission and could have been caused by improper zero point calibration of the storage probe.

Prior to storage tank depletion (crossover), both the oxidizer and fuel sump tank gages indicated a small continuous rise in level. A known bias exists in the sump tank gage readings, because of the difference in liquid levels in the sump tanks and inside the gaging system stillwells. The stillwell is a manometer that balances the pressure at the bottom of the stillwell with a fluid head. Under nonflow conditions, this fluid head would be equivalent to the level of propellant in the tank. However, when the propellant flowed, the fluid head in the stillwell would be reduced by the dynamic head of the propellant flowing by the bottom of the stillwell through the zero-gravity retention reservoir. Because

of the 4.5-second lock-out period and because the preflight levels at 175-psia tank pressure were above the sensing elements of the probes, it was difficult to determine the exact bias effect from flight data. Following the 4.5-second lock-out period, an apparent drop in the sump tank levels was caused by the decrease in levels inside the stillwells. The indicated continuous rise in sump tank levels immediately prior to crossover was caused by changes in the dynamic flow bias with acceleration and was expected.

The sump tanks levels began to decrease within 2.0 seconds of the crossover time as determined from the rise in engine inlet pressure and storage tank depletion. A high rate was indicated for 10 to 15 seconds after oxidizer and fuel crossover; a similar indication was observed during the Apollo 4 mission. A high flow rate was indicated because the initial sump tank levels were in the spherical portion of the tanks (that is, above the cylindrical section). The dynamic flow bias would cause the probe to sense a lower level that, as a function of the probe shape, was associated with a larger tank diameter; because the probe is actually sensing a change in height, the apparent flow rate would be high until the levels reach the cylindrical section of the tanks. After stabilization, the sump tank gages showed a normal depletion rate.

5.18.4 Pressurization

The service propulsion system pressurization operated nominally throughout the mission. There was no indication of leakage. Helium bottle pressure and temperature indicated a constant, nominal expulsion of helium.

Pressure oscillations were experienced in the helium pressurization system for the first 10 seconds of the firing. The oscillations were in the helium lines downstream from the regulators. However, propellant pressure measurements at the engine inlet indicated that the oscillations were completely damped in the ullages. The oscillations occurred because the initial fuel tank pressure was in excess of the regulation pressures. It is a characteristic of the regulator to oscillate when the demand is below the rated value.

5.18.5 Engine Transient Analysis

An analysis of the start and shutdown transients was performed to determine the transient impulse and time-variant performance characteristics during the Apollo 6 mission. The results of this analysis are summarized in table 5.18-II. Engine acceptance test data, specification requirements, and previous spacecraft flight data were used in the analysis of the flight test results.

As shown in table 5.18-II, all applicable transient specification criteria appeared to be satisfied, except for the chamber pressure overshoot during engine start. The favorable comparison of the data obtained during the Apollo 6 mission with those acquired from previous flights is also shown in table 5.18-II. The service propulsion system engine chamber-pressure start and stop transients are shown in figures 5.18-3 and 5.18-4, respectively.

The chamber pressure overshoot shown in figure 5.18-3 has also occurred during other flights. The flight chamber pressure measurement is sampled at the rate of 100 samples per second and has a nominal range of 0 to 150 psia. The maximum transducer output cannot be recorded because of telemetry limitations. For Apollo 4 and Apollo 6, the chamber pressure transducer was mounted on a 2-inch adapter. This change was made to correct thermally induced drifting of the transducer which was apparent on previous flights. The magnitude and the duration of the overshoot with the new mounting have shown a marked increase over that observed for the original mounting. A special series of ground tests will be conducted during the second week of June 1968 to determine whether the indicated overshoot is partially due to instrumentation errors.

A review of chamber pressure data indicated that five injector "pops" of unknown magnitude and duration, occurred during the service propulsion firing. These "pops" are random sharp chamber pressure spikes and are characteristic of the block I injector. "Pops" are caused by detonations in the combustion process. The "pops" during Apollo 6 represent the typical number for the block I engine performing a firing of this duration. Occurrences of this frequency do not significantly degrade the engine. "Popping" is much less frequent with block II engine.

TABLE 5.18-I.- SERVICE PROPULSION SYSTEM PERFORMANCE SUMMARY

Instrumented parameters	Nominal[a]	Before crossover		After crossover	
		Measured	Actual[b]	Measured	Actual[a]
Oxidizer storage tank pressure, psia	179	174	181.1	176	182.7
Fuel tank storage pressure, psia	179	168	182.3	162	183.5
Oxidizer inlet pressure, psia	154	154	154.8	161	161
Fuel inlet pressure, psia	154	147	152.3	152	157.5
Engine chamber pressure, psia	100	97	99.5	100	102.6
Calculated performance parameters					
Oxidizer flow rate, lbm/sec	45.8	-	44.67	-	45.89
Fuel flow rate, lbm/sec	22.9	-	22.51	-	22.95
Propellant mixture ratio	2.00(±1%)	-	1.984	-	2.000
Vacuum specific impulse, sec	311 minimum	-	310.2	-	310.3
Vacuum thrust, lbf	21 500(±1%)	-	20 840	-	21 360

[a]Based on standard inlet conditions.

[b]Not corrected to standard inlet conditions.

TABLE 5.18-II.- SERVICE PROPULSION SYSTEM FLIGHT SUMMARY OF TRANSIENT DATA

	Apollo 6 first firing	Apollo 6 service propulsion engine 032 acceptance test	Apollo 4 first firing	Apollo 4 second firing	AS-202 first firing	AS-202 second firing	AS-202 third firing	AS-202 fourth firing	Specification values
Start transient total vacuum impulse from ignition to 90 percent of steady-state thrust, lbf-sec	225.0	225	135.2	264.4	--	--	--	--	100-400
Time from ignition to 90 percent of steady-state thrust, sec	0.42	0.375	0.41	0.35	∿0.38	∿0.37	∿0.37	∿0.37	0.350-0.550
Time from ignition to steady-state thrust, sec	1.22	--	1.07	0.96	∿1.09	∿1.18	∿1.25	∿1.14	--
Chamber pressure overshoot during start, percent (based on nominal 100 psia chamber pressure)	56.0	--	48.6	34.2	36.5	22.0	24.5	11.0	20
Vacuum impulse from chamber pressure overshoot, lbf-sec	1908	--	1861	1040	--	--	--	--	--
Shutdown transient total vacuum impulse from cutoff to 10 percent of steady-state thrust, lbf-sec	11 626.5	8 282	10 083.8	11 910.8	--	--	--	--	8 000-13 000
Time from cutoff to 10 percent of steady-state thrust, sec	0.92	0.687	0.80	0.89	∿1.049	∿1.11	∿0.78	∿0.78	0.650-0.900
Shutdown transient total vacuum impulse from cutoff to 0 percent thrust, lbf-sec	11 905.4	--	11 122.3	12 275.7	10 700	--	--	10 000	8 830-14 200
Time from cutoff to 0 percent thrust, sec	1.44	--	1.82	1.50	--	--	∿1.23	∿1.13	--

NASA-S-68-3620

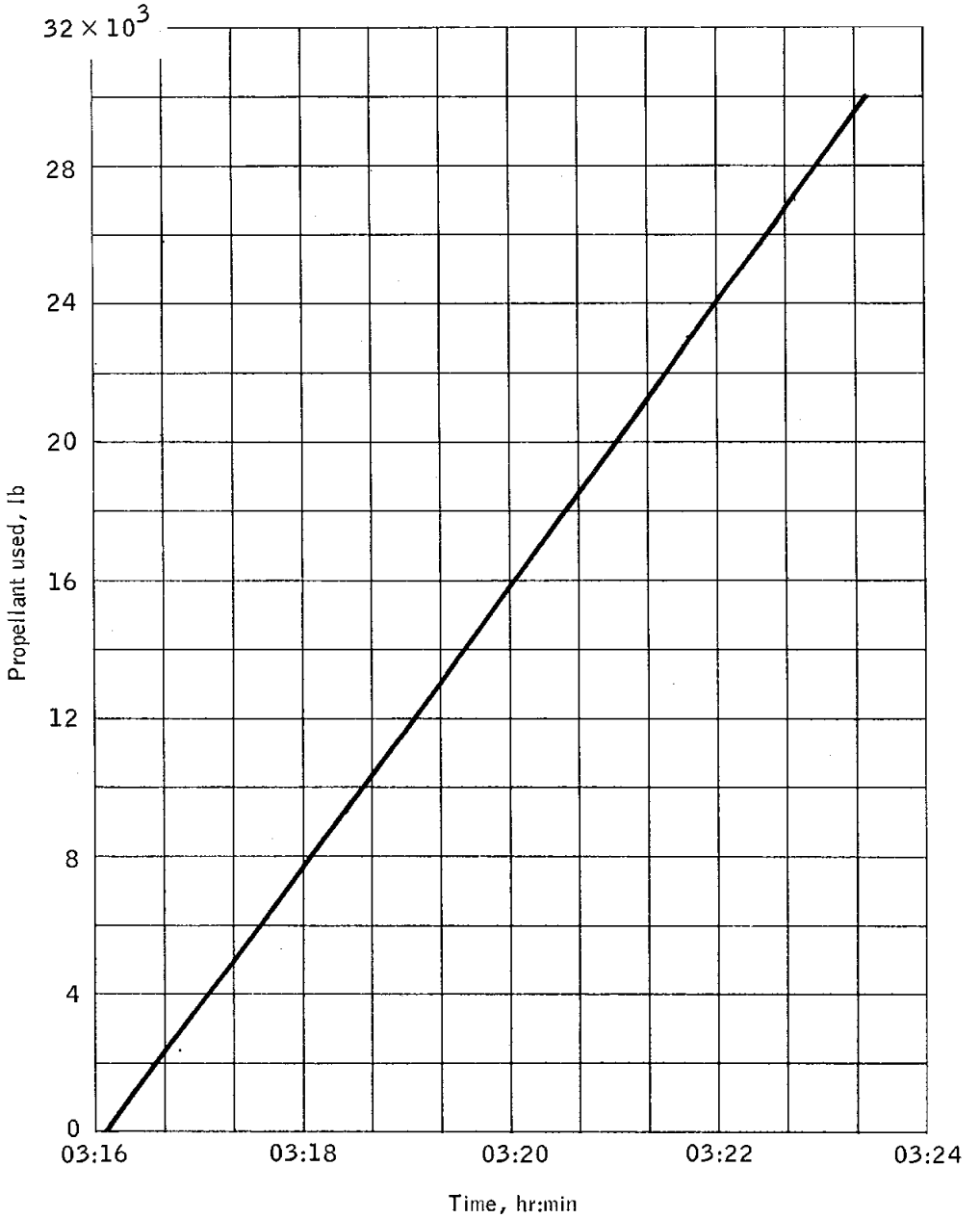

Figure 5.18-1.- Service propulsion system propellant usage.

NASA-S-68-3621

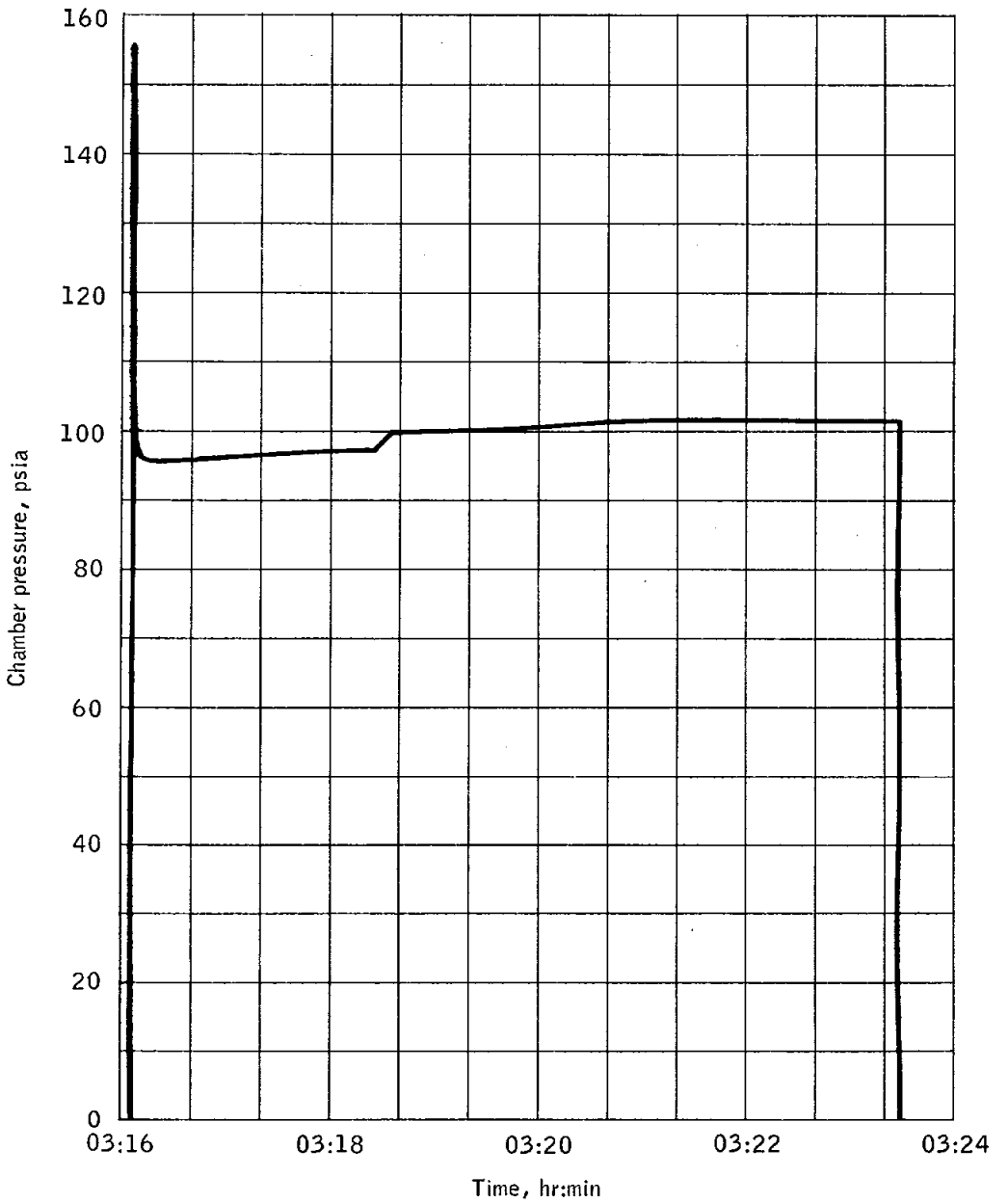

Figure 5.18-2.- Service propulsion system chamber pressure.

NASA-S-68-3622

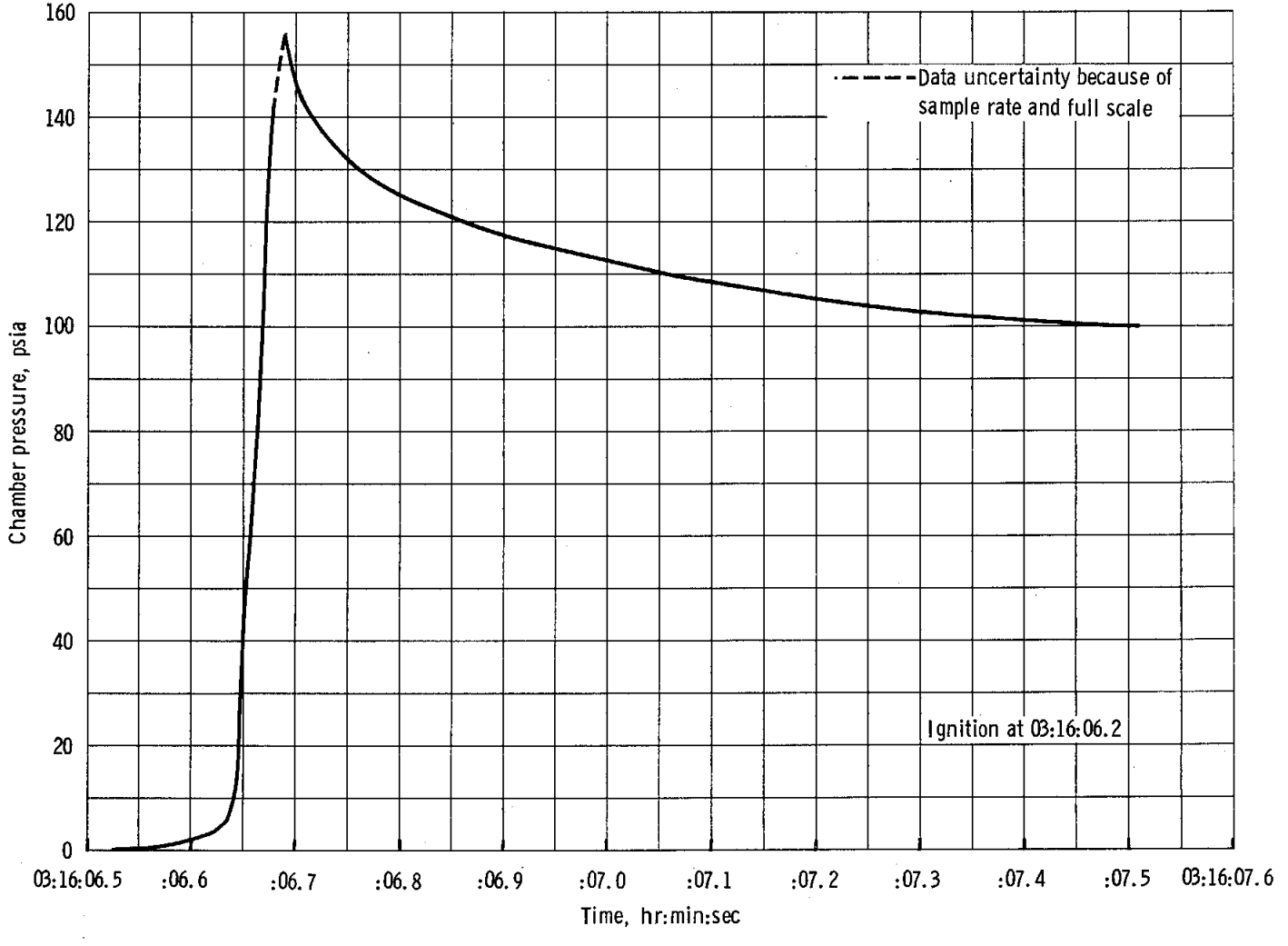

Figure 5.18-3. - Service propulsion system chamber pressure during start transient.

NASA-S-68-3623

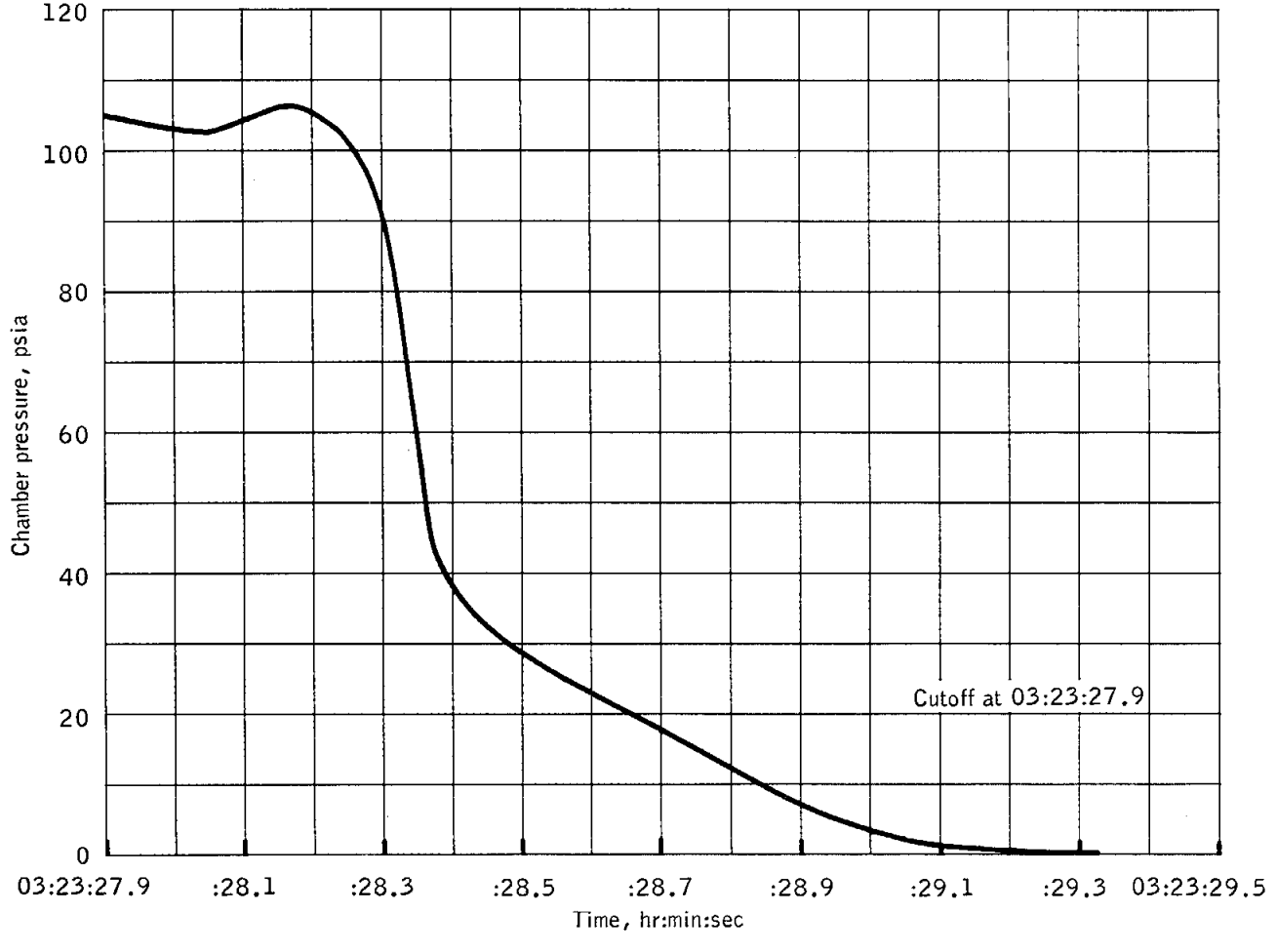

Figure 5.18-4.- Service propulsion system chamber pressure during shutdown transient.

5.19 ENVIRONMENTAL CONTROL

The environmental control system performed satisfactorily throughout the mission, except for a minor anomaly associated with the cabin-pressure launch profile.

5.19.1 Launch Phase

Prior to launch, the command module was pressurized to 15.68 psia with nitrogen gas. The cabin-pressure relief valve began relieving cabin pressure at approximately 00:00:52. During the launch phase, the differential between cabin pressure and ambient pressure reached 9.4 psia which exceeded the design limit of 8.6 psia (section 12.0). The expected differential pressure was 6.2. The cabin pressure stabilized at approximately 6.0 psia after the cabin-pressure relief valves had seated by 00:08:30. The cabin pressure decayed to 5.8 psia prior to entry. Considering temperature effects, the cabin leakage rate was computed to be approximately 0.02 lb/hr (the specification maximum leakage rate is 0.20 lb/hr). No significant oxygen usage rate was indicated during the mission; this confirms that cabin leakage was negligible. The cabin pressure did not bleed down to the pressure regulator control range of 5.0 (±0.2) psia; consequently the cabin-pressure regulator was not required to operate.

Thermal control of the command module equipment was provided by circulation of the heat transport fluid from the cabin heat exchanger and thermal coldplate network to the water/glycol evaporator. At 75 seconds before lift-off, the mission control programmer initiated the sequence for closing the motorized water/glycol isolation valve and placing the water/glycol circuit on the internal circulation mode. The evaporator outlet temperature was 51° F at lift-off and had increased to 62° F prior to loss of accurate data at 00:01:28. Because of a general telemetry problem during launch, it is not possible to determine when active cooling was initiated; however, normal evaporator operation was verified at 00:08:30, at which time the data was good. The backpressure control valve was preset at approximately 30-percent open. Active cooling by water boiloff occurred when the backpressure in the evaporator was less than 0.25 psia. The mission control programmer provided an enabling signal to the evaporator water inflow control valve at the time of tower jettison. This enable signal permitted automatic water-control valve operation in response to electrical signals from the temperature controller. Water boiloff in the glycol evaporator provided the only means of thermal control during the mission. The cabin temperature was approximately 66° F at lift-off and remained constant during the early ascent

phase. The expansion of the cabin gas caused the temperature to drop to approximately 60° F during cabin-pressure relief valve operation; the temperature stabilized at 64° F after active cooling was initiated by the glycol evaporator. The cabin was purged with gaseous nitrogen during prelaunch operations with the result that the cabin atmosphere contained 2 percent oxygen.

5.19.2 Orbital Phase

The glycol evaporator, the temperature controller, and the entire water/glycol coolant circuit performed satisfactorily. The evaporator outlet temperature stabilized between 48° and 49° F after the launch phase and decreased to between 46° and 47° F during the cold-soak period when the heat loads were lower. The computed heat rejection rate of the evaporator was approximately 5800 Btu/hr, initially. As a result of the extended command module cold-soak period, this rate decreased to approximately 4900 Btu/hr prior to entry. The evaporator steam backpressure was initially 0.15 psia and approached 0.13 psia when the heat loads were reduced. The evaporator performance data compared favorably with the data obtained during checkout of the glycol evaporator at the launch site. The average evaporator heat load was approximately 5400 Btu/hr, which resulted in a calculated average water-boiloff rate of 5.17 lb/hr. The average water/glycol flow rate produced by dual operation of the glycol pumps was approximately 240 lb/hr, based upon coldplate flow calibration curves utilizing the measurements of the main coldplate branch-2 differential pressure and average branch-2 coldplate temperatures.

The water/glycol pump discharge pressure readings were 8 to 10 psi higher than had been anticipated for 6.0-psia cabin operation and were similar to those that would be obtained in sea-level operation. Proper glycol pump operation was verified from flow calibration curves for the branch-2 coldplate network. This discrepancy is discussed in section 5.15.

The waste water tank quantity reading was 100.9 percent at launch. The reading, which fluctuated significantly with the other instrumentation during the boost phase, stabilized at approximately 40 percent at 00:08:30. The reading decreased slowly to 1 percent prior to entry. The sudden change in indicated quantity and the erroneous readings received during launch were attributed to an instrumentation data problem because four other measurements in the same telemetry sequencer gate were also in error. Based on the average water usage rate of 5.17 lb/hr, the total water used would have been approximately 50.6 pounds. Because this calculated usage was considerably in excess of the indicated usage (22 pounds) and because the potable water tank continued to fill during

the mission, it was concluded that the initial decrease of 60 percent in the indicated quantity was entirely an instrumentation error rather than actual water loss. Additional information is contained in section 5.15.

The pressure in the oxygen surge tank varied in phase with the pressure in cryogenic oxygen supply tank 2; this indicated that the 900-psi oxygen check valve failed to seat when the cryogenic tank 2 pressure decreased below the surge tank pressure during the cryogenic tank pressure cycles. This failure, which has been observed on similar check valves, has resulted in a design change in the valves for future spacecraft. Notwithstanding, postflight testing and failure analysis to detect possible contamination will be performed.

The cabin-temperature control valves were set in the full-cold position at cabin closeout, and no attempt was made to control cabin temperature during the mission. The average cabin temperature remained at 64° F until the start of the cold-soak period; the temperature then began decreasing until it reached 56° F just prior to entry.

The average evaporator-water usage rate was calculated to be 5.17 lb/hr, based on the average heat load of 5400 Btu/hr. The actual water usage rate is normally ascertained by measuring the water remaining in the waste water tank; however, through procedural error, both the waste and potable water tanks were inadvertently drained during postflight testing. Therefore, the best estimate of the total water supplied to the evaporator (50.6 pounds) was based on evaporator heat balance calculations. Similarly, the actual quantity of fuel cell water collected could not be measured because of the postflight testing error. On the basis of the readings from the potable water tank quantity transducer, it is estimated that there were 10.8 pounds of water in the potable tank at lift-off and that there were 30.9 pounds of water in the tank at landing; this indicates that a total of 20.1 pounds of water were produced by the fuel cells during the mission. This production compares favorably with the 19 pounds computed from the average fuel cell current production (fig. 5.19-1).

5.19.3 Entry Phase

At command module/service module separation, the mission control programmer initiated a command to close a shutoff valve that isolated the command module oxygen supply system from the service module system. The programmer also verified closure of the water/glycol shutoff valve. Water boiloff in the glycol evaporator provided cooling during entry until the increasing ambient pressure made water boiloff ineffective. Subsequent cooling was supplied by the glycol reservoir and system heat storage capacity only.

The evaporator outlet temperature began increasing at 09:49:48 as the ambient pressure increased; thus, additional cooling in the evaporator was ineffective. The cabin pressure began increasing at 09:51:36 and the cabin-pressure relief valve functioned normally during entry. The cabin temperature increased to 63° F as the cabin pressure increased during descent, but decreased to 59° F at landing.

5.19.4 Postrecovery Observations

Approximately 1-1/2 gallons of liquid were found in the cabin after spacecraft recovery. A chemical analysis indicated that the liquid was sea water and that the liquid did not contain any glycol. The sea water probably entered the spacecraft through the cabin-pressure relief valve. Salt water was also observed in the command modules recovered after the AS-201, AS-202, and Apollo 4 missions. The relief valve incorporates a sealing device that can be manually actuated during manned missions.

No vapor-sensitive tapes (used during Apollo 4 for detection of reaction control system fuel, oxidizer, and combustion products in the cabin) were installed in the Apollo 6 command module. However, two gas samples of the cabin atmosphere were taken aboard the recovery ship. The propellant contamination levels measured on Apollo 4 and 6 missions cannot be considered to be the expected levels for subsequent spacecraft because of differences in the amounts of fuel and oxidizer to be dumped and because of the relocation of the environmental control system steam duct on the block II spacecraft. Chemical analysis of the two gas samples indicated the presence of approximately 0.1 ppm oxidizer (nitrogen tetroxide) and less than 0.1 ppm fuel (monomethylhydrazine). Apollo 4 results indicated 0.3 ppm of oxidizer and no measurable quantity of fuel. A level of 1.0 ppm over an 8-hour period is considered to be acceptable. Procedures are being established either to close the cabin-pressure relief valve during the reaction control system propellant-depletion burn and reopen the valve after the propellants are depleted or to land with the propellants onboard and eliminate the depletion burn and inflight purge sequence.

The postlanding ventilation valves were tested aboard the recovery ship to determine the flight environment effect on valve operation. The inlet and outlet valves operated normally at a minimum voltage of 25 V dc. The average maximum current was 4.5 amperes, and the average opening time was 1.0 second; these values indicated satisfactory postflight operation of the valves.

A potable water sample taken while the command module was aboard the recovery ship was subsequently analyzed at the Manned Spacecraft Center for free hydrogen concentration. The analysis indicated a total of 14 micrograms hydrogen in the sample. This is considered insignificant.

NASA-S-68-3624

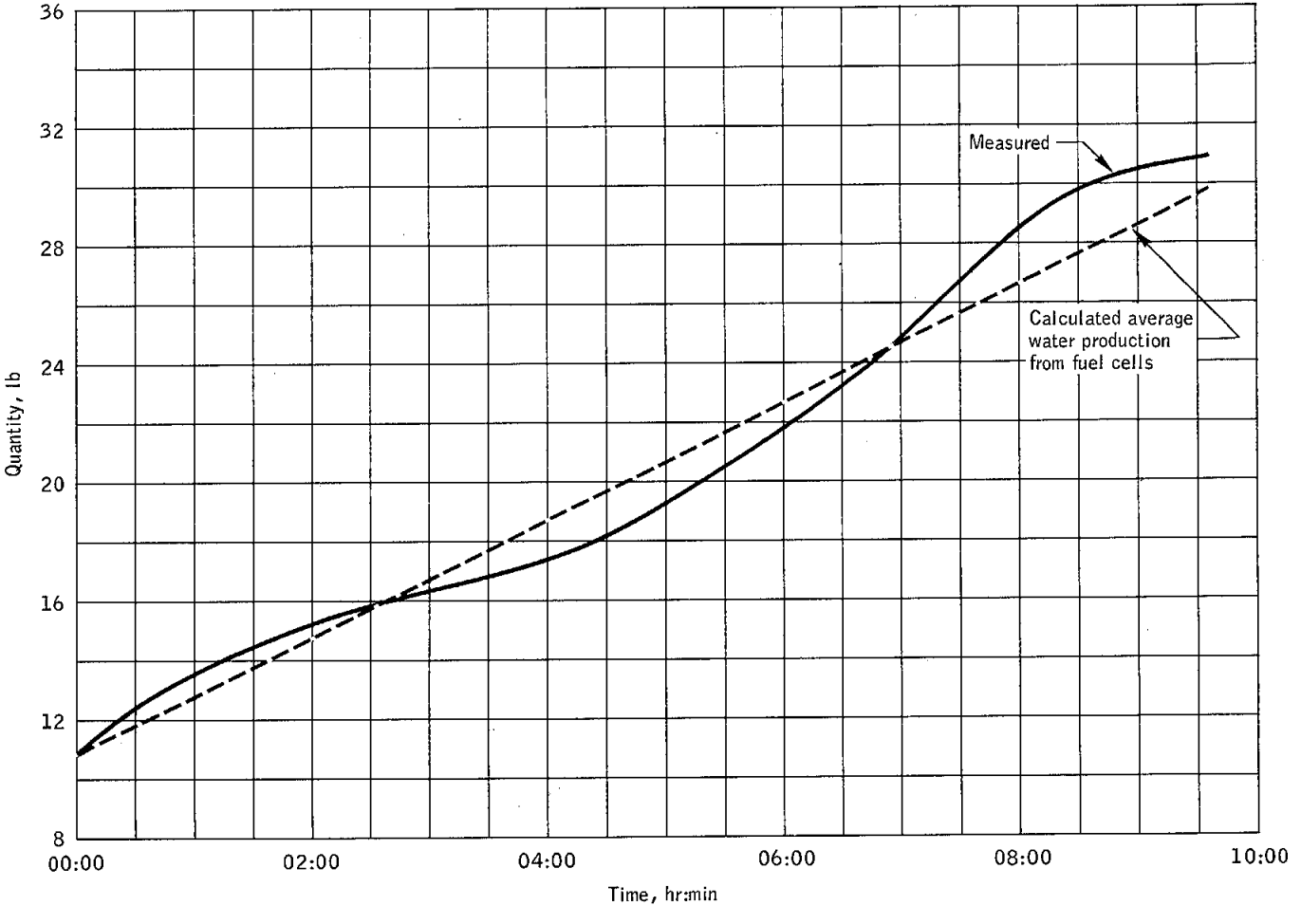

Figure 5.19-1.- Potable water tank quantity plotted against time.

5.20 CREW STATION

5.20.1 Crew Visibility

After the mission, all five of the command module windows had the same appearance with a very light gray film deposit. This film was deposited over the outer surface of each of the heat shield windows. The onboard camera film record indicates that the condition of the left rendezvous window during flight was considerably better than after entry and landing.

A postflight analysis has been conducted on the film obtained from a 16-mm movie camera which was mounted such that it obtained a view that approximated the command pilot's view through the left rendezvous window. The camera was mounted with the lens system at approximately the designated eye reference point for an 80-percentile crewman in the boost configuration. When the camera started, the boost protective cover was still on the command module. The area of the left rendezvous window not covered by the boost protective cover appeared dirty (fig. 5.20-1). At 00:02:00, this area began to clear up, becoming clear by 00:02:07.3. There was no evidence of contamination at S-IC cutoff or separation. At tower jettison a considerable number of droplets (similar to condensed water) became visible (fig. 5.20-2). These droplets, apparently frozen, remained on the window for the duration of the mission. Review of preflight photographs, taken 1 week before launch, indicated that some of the water droplets were present before launch. The lower two rows of droplets were also present in the preflight photograph. There was no evidence of increased contamination during S-II ignition or cutoff. The S-II retrorocket plume was observed through the window during S-II/S-IVB separation. The plume covered approximately two-thirds of the window area. Again, there was no evidence of the contaminant contacting the window surface. When the camera came on for the second time, it appeared that there had been no deterioration in window condition while the camera was off (fig. 5.20-3).

The first evidence of further window deterioration appeared approximately 2 minutes 10 seconds after the beginning of entry. The window surfaces appeared to be causing more optical diffusion than before entry. Subjective analysis of the window films indicated that there would be a moderate decrease in window resolution with the sun to the rear of the spacecraft. If sun shafting or glaring was present, light scatter through the window would be sufficient to destroy visual acuity, making out-the-window viewing very difficult (fig. 5.20-4).

Postflight direct light transmission analysis was performed on the spacecraft left rendezvous and right side windows. The general light transmission through both windows was 70 to 80 percent. The worst area on the rendezvous window had a light transmission of 60 to 65 percent in the visible wavelength of 450 to 650 millimicrons. The least contaminated area had a general transmission of 85 to 90 percent. The contamination on the right side window was more evenly distributed than that on the rendezvous window and a general direct transmission of approximately 85 percent from 550 to 600 millimicrons and 70 percent from 450 to 550 and 600 to 650 millimicrons (fig. 5.20-5).

These results indicate that the direct light transmission through CSM 020 windows was 50 percent better than CSM 009 and 37 percent better than CSM 011.

With respect to transmission and visual acuity, the inflight quality of the left rendezvous window was as good as, or (except for several large deposits of contaminant) better than that of the windows on the Gemini spacecraft. Analysis of the flight film indicated that considerable change occurred during the entry profile. The contamination became baked and burned on, thereby completely changing the characteristics of the window conditions.

During postflight tests, no water was found between the two inner window panes. The flight films indicate that the inflight condition of the windows will be as good as, if not better than, most of the Gemini spacecraft windows.

5.20.2 Crew Related Dynamics

The vibration levels measured on the crew compartment forward bulkhead and sway brace (kick ring) were assumed to represent the vibration environment to which crew members would be exposed. The predominant frequencies during these periods were the same as those noted for Apollo 4, but the amplitudes were between two and three times greater than those experienced on that flight. The frequencies were in the range of the natural resonant frequency of the upper torso. During these periods, the crew would have experienced gross body vibrations. Reduction of peripheral vision in monitoring cabin displays would have resulted, requiring greater crew concentration on critical displays. Crew members would also have experienced a loss of dexterity if multiple switching tasks had been required.

Acceleration measurements taken from the forward bulkhead of the crew compartment and from the sway brace were used to determine the vibration environment during the launch phase. The longitudinal vibration levels during the launch phase were greater than those noted for the

Apollo 4 mission. The resultant vibration reached 0.75g (peak-to-peak) at lift-off, decreased to 0.2g (peak-to-peak) within 60 seconds, and remained at that level until 00:01:15. Between 00:01:15 and 00:01:44, the vibration amplitude varied, increasing to 0.4g (peak-to-peak) and decreasing to 0.2g (peak-to-peak). At 00:01:44, the vibration became a steady sinusoidal oscillation, increasing in amplitude and reaching a maximum level of 1.4g (peak-to-peak) at 00:02:10.

The vibration amplitudes at inboard and outboard engine cutoff were 0.73g and 1.8g, respectively. The duration of each of these amplitudes was less than 1 second.

The lateral vibration levels (longitudinal related to the crew) were within acceptable range. At lift-off, the level was 0.2g (peak-to-peak) and remained at this amplitude through 00:01:15. At 00:01:15, the level started increasing, reaching a maximum of 0.5g (peak-to-peak) at 00:02:04, where it remained until 00:02:06 when it started decreasing, reaching 0.2g (peak-to-peak) by 00:02:24.

Spectral analysis of the significant periods of vibration indicated that the majority of the energy was contributed by a longitudinal component of 5.3 Hz. This vibration spectrum was the result of sustained longitudinal sinusoidal oscillations which were coupled to the first longitudinal mode of the S-IC stage. Other less significant frequencies were experienced during various phases of the launch. The natural resonant frequency of the human upper torso is 3 to 4.5 Hz. The vibrations observed were not of a sufficient magnitude or duration to have caused permanent physiological damage to the crew if properly strapped in.

NASA-S-68-3655

Figure 5.20-1. - Area of left rendezvous window through boost protective window.

NASA-S-68-3656

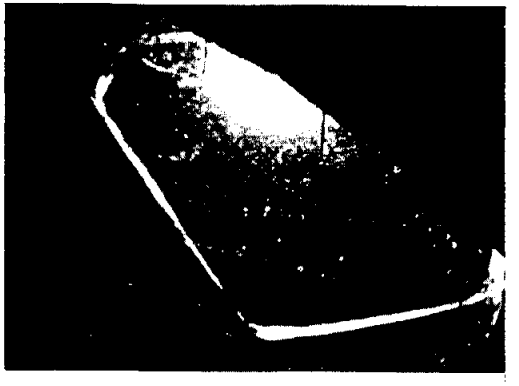

Figure 5.20-2. - First frame after boost protective cover jettison.

NASA-S-68-3657

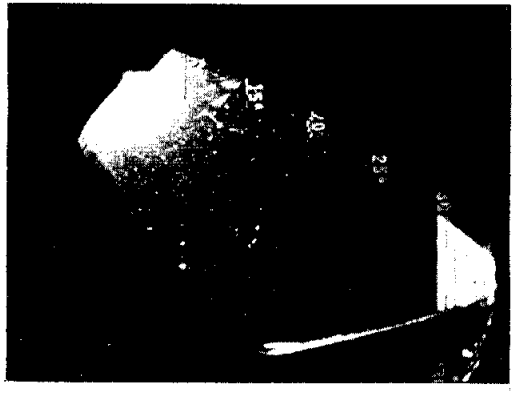

Figure 5.20-3. - Turnaround prior to command module/service module separation.

NASA-S-68-3658

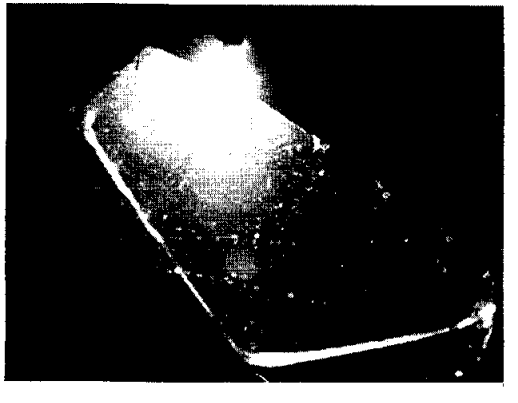

Figure 5.20-4. - Effects of sun shafting.

NASA-S-68-3654

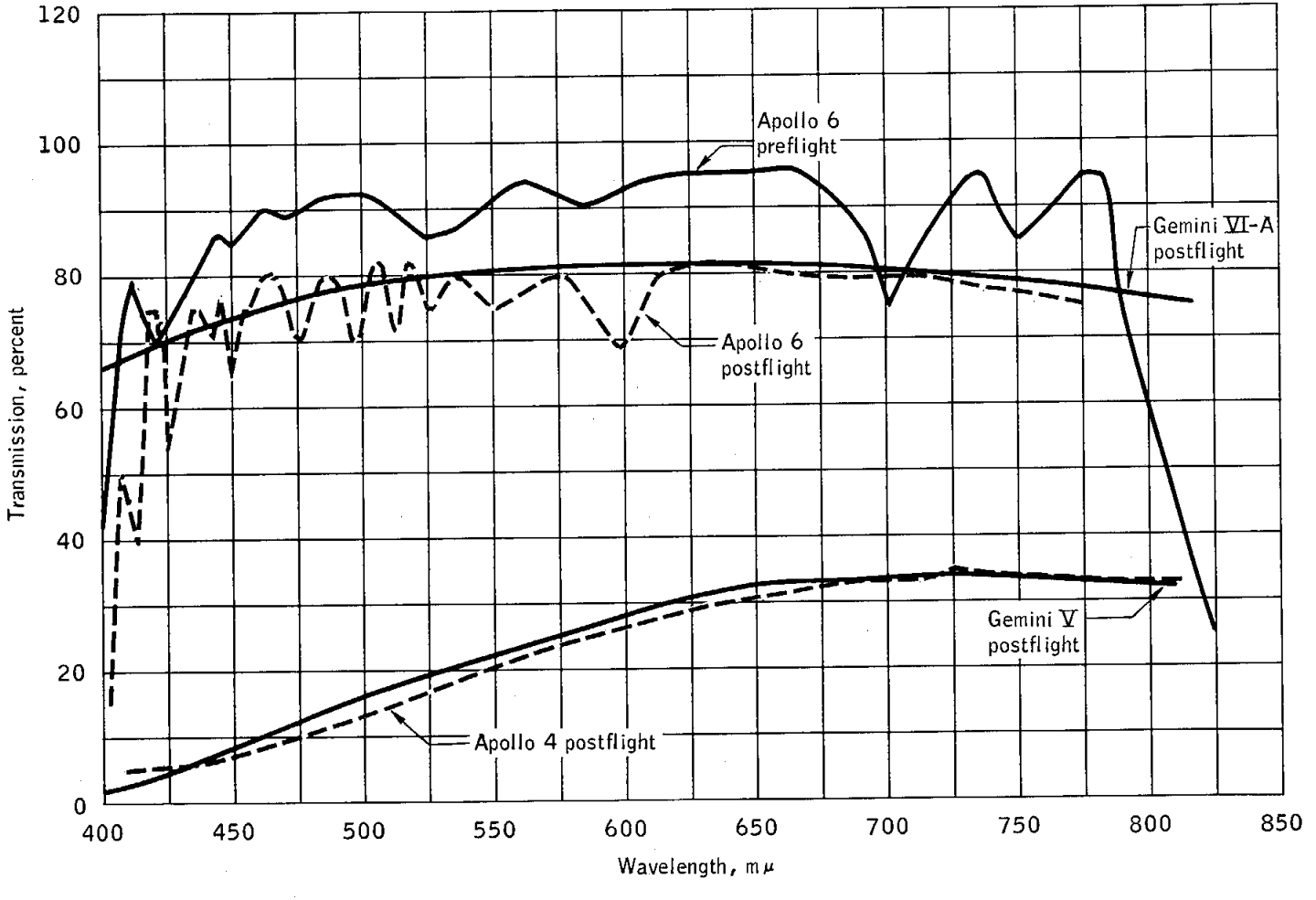

Figure 5.20-5.- Comparison of direct light transmission of Apollo 4 and 6 and Gemini V and VI-A windows.

5.21 CONSUMABLES

The usage of all liquid consumables, including cryogenics, is summarized in this section. Detailed derivation of these data appears in the applicable system performance analysis sections. Two other items sometimes considered as consumables, battery electrical power and ablator burn-off, are discussed in sections 5.7 and 13.5, respectively.

5.21.1 Service Propulsion System Propellants

The total service propulsion system propellant loadings calculated from gaging system readings and measured densities were as follows:

Loaded	Oxidizer, lb	Fuel, lb
In tanks	22 048	10 958
In lines	137	53
Total loaded	22 185	11 038
Total propellants loaded	33 223	

These figures include gageable, ungageable, and vapor-loaded quantities, and the propellants in the standpipes.

A best-estimate of propellant consumption during the service propulsion system engine firing (section 5.18) was derived from flight telemetry data; the total propellant consumed was 30 075 pounds, with a total of 3148 pounds remaining.

5.21.2 Reaction Control System Propellants

Service module.- The propellant loading utilization data for the service module reaction control system were as follows:

Propellant	Quad A	Quad B	Quad C	Quad D
Oxidizer loaded, lb	138.3	137.8	137.6	138.1
Fuel loaded, lb	67.4	67.5	67.3	67.4
Total propellant loaded, lb . . .	205.7	205.3	204.9	205.5

Consumption was calculated from telemetered helium bottle pressure histories using the relationships between pressure, volume, and temperature, assuming a constant temperature of 65° F; the total propellant consumed was 375 pounds, with a total of 446 pounds remaining.

Command module.- The propellant loading utilization data for the command module reaction control system were as follows:

Propellant	System A	System B
Oxidizer loaded, lb	84.1	84.3
Fuel loaded, lb	44.4	44.5
Total propellant loaded, lb	128.5	128.8
Oxidizer consumed, lb[a]	26.9	26.9
Fuel consumed, lb	15.1	15.1
Total propellant consumed, lb[a] . . .	42.0	42.0
Total propellant remaining, lb . . .	86.5	86.5

[a]Consumption was calculated by time integration of the engine valve autocoil electrical on/off event data, and the application of factors for event totals and integrated pulse widths.

5.21.3 Cryogenics

Hydrogen.- The hydrogen quantities at lift-off were 10.7 pounds in tank 1 and 13.5 pounds in tank 2; the usage as determined from telemetered tank quantity data was 0.9 pound from tank 1 and 1.2 pounds from tank 2.

Oxygen.- The tank 2 quantity measurement failed shortly after lift-off, and the tank 1 quantity time history was suspect because of the relatively small consumption indicated. It has been estimated that tank 1 should have supplied about 20 percent of the flow and tank 2 about 80 percent of the flow as indicated by pressure cycling, which showed the expected pattern with the tank 1 heaters disabled.

The fuel cell flowmeters showed an almost exact agreement with fuel cell theoretical performance; on this basis, the oxygen consumption can be estimated at eight times the hydrogen consumption (assuming that the cabin leakage was negligible). This calculation yielded an estimated total consumption of 18 pounds (proportioned as 4 pounds from tank 1 and 14 pounds from tank 2).

5.21.4 Water

The potable water quantity measurement history indicated unreasonable variations in slope, and the waste water quantity measurement became inoperative shortly after lift-off. Therefore, the waste water quantity changes have been computed rather than measured (see section 5.19). The waste water usage rate was assumed to be 5.17 lb/hr (equivalent to a heat load of 5400 Btu/hr). The potable water history data were fitted with a straight line, and the intercepts at lift-off and CM/SM separation then yielded the data tabulated below.

	Waste water, lb	Potable water, lb
Lift-off	55.0	10.8
Landing	4.4	30.8
Inflight change	-50.6 (consumed)	+20.0 (generated)
Net change	-30.6	

The 20.1 pounds of potable water generated agrees favorably with the 19.0 pounds predicted based on average fuel cell loads.

6.0 LUNAR MODULE PERFORMANCE

6.1 STRUCTURE

6.1.1 Loads

Structural interaction loads between the lunar module test article (LTA-2R) and the adapter were evaluated in the critical design regions of S-IC boost. Loads in these regions — lift-off, max $q\alpha$, and end of first-stage boost — when compared with lunar module design conditions, were less than those used for design (table 6.1-I). However, at approximately 00:01:50 (between max $q\alpha$ and the end of first-stage boost), axial and lateral accelerations of 5 Hz began in the LTA-2R, lasting until 00:02:13 when a major change in character occurred. The resultant accelerations exceeded the design values for the lunar module test article. These oscillations were also measured in the outrigger strut loads. The struts had peak-to-peak loads of approximately 7000 pounds. Oscillations of a similar nature were experienced during the Apollo 4 mission, but at lower amplitudes. The outrigger struts on Apollo 4 had peak-to-peak loads of 400 pounds. A detailed evaluation of the significance of these oscillations and loads will be presented in Anomaly Report number 6.

6.1.2 Low-Frequency Vibrations

Triaxial linear accelerometers were mounted on the LTA-2R ascent stage, and biaxial linear accelerometers, sensitive to X-axis and radial accelerations, were mounted on the plus Y apex fitting of the descent stage. Transient accelerations at lift-off are shown in table 6.1-II. The peak value for the X-axis accelerations exceeded the low-frequency vibration qualification criteria by a factor of approximately 1.5.

Low-amplitude accelerations were measured during the max $q\alpha$ portion of flight (table 6.1-II), but at 00:01:50, after max $q\alpha$, all acceleration measurements exhibited low-frequency oscillations (5.5 Hz) with motions primarily in the X and Z axes. These oscillations increased until 00:02:13, then decreased rapidly. The oscillations produced accelerations which exceeded the lunar module structure and systems criteria by a significant margin. The low-frequency oscillations are being analyzed and will be discussed in the anomaly report.

At first-stage inboard engine cutoff, significant vibrations occurred in the X and Z axes, but they did not exceed the low-frequency vibration qualification criteria in either axis. Significant vibrations were observed in all three axes at outboard engine cutoff, and the vibrations in

the X and Z axes substantially exceeded the low-frequency vibration qualification criteria.

6.1.3 High-Frequency Vibration

The LTA-2R was instrumented with six vibration transducers having the ranges and frequency responses shown in table 6.1-III. Three measurements were located on top of the plus Y descent-stage fuel tank and were sensitive in the X, Y, and Z axes. Three additional measurements were located on top of the minus Z descent-stage oxidizer tank and were sensitive in the X, Y, and Z axes.

During all phases of flight, the fuel tank vibrations were well below the mission-level vibration criteria. The mission-level vibration criteria reflect the qualification criteria reduced to mission levels, that is, qualification spectral density values divided by the safety factor of $(1.5)^2$.

At lift-off, in the transonic region, and in the maximum dynamic pressure region, the oxidizer tank vibration levels exceeded the mission-level vibration criteria by 16 dB and 11 dB at frequencies of 74 Hz and 95 Hz, respectively. Acceptance test values were also exceeded at 58 Hz and 85 Hz during lift-off but by only 3 dB, which is acceptable because of configuration differences between the flight tanks and the LTA-2R tanks. Acceleration spectral densities of the two measurements on top of the descent stage oxidizer tanks are shown in figures 6.1-1 and 6.1-2. Autocorrelation plots of these measurements are shown in figures 6.1-3 and 6.1-4. The presence of the slowly decaying oscillations at 74 Hz and 95 Hz indicate that the data at these frequencies are very narrow band and essentially periodic; therefore, they have no values definable by power spectral density analysis and should not be compared with the random vibration criteria, but with the sinusoidal qualification test levels. The peak value of the LTA-2R data, with all frequencies contributing, was 3.78g for the Y axis and 5.06g for the Z axis. The oxidizer tank sinusoidal qualification tests exposed the top of the tanks to 44g at 90 Hz. It was expected that frequencies of the qualification test and the flight measured peaks would not be identical because the oxidizer tanks on the LTA-2R were boilerplate construction and were not completely filled with fluid. Therefore, the qualification tests are considered adequate for demonstrating the ability of the oxidizer tanks to withstand the vibration levels measured on LTA-2R.

6.1.4 Acoustics

Acoustic pressures in the adapter/LTA-2R internal volume were measured with two microphones having the ranges and frequency responses shown in table 6.1-III. A microphone was located on a boom attached near the top of the plus Z face of the LTA-2R ascent stage. Another microphone was located on the minus Z face, diametrically opposite. Data from both measurements agreed within 1 dB overall and 2 dB within a 1/3 octave band during all phases of the flight except during the anomaly at 00:02:13. Overall levels were 141 dB at lift-off, 131 dB in the transonic flight region (00:00:57 to 00:01:00), and 126 dB in the maximum dynamic pressure region (00:01:14 to 00:01:16).

Figure 6.1-5 compares the Apollo 6 lift-off acoustic levels with those measured during the Apollo 4 mission and the LTA-3 ground tests. The discontinuity in the plus Z measurement at 845 Hz is due to electrical noise present prior to launch. The Apollo 6 overall level was approximately 2 dB higher than the Apollo 4 level and approximately 1 dB above the upper envelope of the LTA-3 levels. The variation between the two Apollo flights can be attributed to the differences in the first-stage engines and variations in the atmospheric conditions. The variation in acoustic absorption between the LTA-2R and a flight-type lunar module accounts for the differences between the Apollo 6 and the LTA-3 levels. During tests of the adapter/LTA-3 configuration, absorption measurements were made with an empty adapter, an adapter plus the LTA-3 without thermal shielding, and an adapter plus the LTA-3 with thermal shielding. The empty adapter showed 120 sabins of absorption, the adapter plus the LTA-3 showed 240 sabins, and the adapter plus the LTA-3 with thermal shielding showed 300 sabins. The LTA-2R should have absorption values between the empty adapter values and the adapter plus the LTA-3 without thermal shielding values. Assuming an average value of 180 sabins for the LTA-2R configuration, a 2-dB reduction in the Apollo 6 levels would be expected had it contained a flight-type lunar module. Therefore, it can be concluded that the acoustic levels measured during the Apollo 6 flight did not exceed the LTA-3 test levels when adjusted for variations in acoustic absorption.

TABLE 6.1-I.- LOADS DURING THE LAUNCH PHASE

[The LTA-2R weighed 26 000 pounds; the design criteria are based on a weight of 32 000 pounds.]

Acceleration	Lift-off		Max qα		End of first-stage boost	
	LTA-2R	Design	LTA-2R	Design	LTA-2R	Design
Lateral, g	0.300	0.650	0.15	0.30	4.9	4.9
Axial, g	1.60	1.60	2.00	2.07	0.1	0.1

TABLE 6.1-II.- LUNAR MODULE LOW-FREQUENCY VIBRATION DURING LAUNCH AND BOOST

Axis	Lift-off		Mid-boost[a]		Inboard engine cutoff		Outboard engine cutoff	
	Frequency, Hz	Amplitude, g	Frequency, Hz	Amplitude, g	Frequency, Hz	Amplitude, g	Frequency, Hz	Amplitude, g
X	4.75	±0.35	Not significant		5.7	±0.30	5.7	±0.9
Y	8.5	±0.30	18	±0.3	Not significant		5.7	±0.15
X	12.5	±0.12	5.5	±0.15	5.7	±0.20	5.7	±0.55

[a]Mid-boost is the time period from approximately 00:00:50 to 00:01:40.

TABLE 6.1-III.- LTA-2R STRUCTURAL DYNAMICS INSTRUMENTATION

Type of measurement	Measurement number	Sensitive axis	Location/description	Transmitter/ IRIG channel	Frequency response, Hz	Range
Linear accelerometer	GA2921D	X	-Y apex/electrically damped	D/9	60	-2.6, +10.0g
	GA2922D	Y	-Y apex/electrically damped	D/8	45	±2.0g
	GA7011A	X	Ascent stage/fluid damped	D/14	330	±11.0g
	GA7013A	Y	Ascent stage/fluid damped	D/13	220	-2.25, +2.2g
	GA7015A	Z	Ascent stage/fluid damped	D/12	160	-2.25, +2.2g
	GA7021A	X	Ascent stage/electrically damped	D/15	450	±10.0g
	GA7023A	Y	Ascent stage/electrically damped	A/2c	1000	±2.0g
	GA7025A	Z	Ascent stage/electrically damped	A/3c	1000	±2.0g
Vibration accelerometer	GA2651D	X	Top, +Y descent stage fuel tank	A/4c	1000	±10g
	GA2652D	Z	Top, +Y descent stage fuel tank	A/1c	1000	±10g
	GA2653D	Y	Top, +Y descent stage fuel tank	A/6c	1000	±10g
	GA2681D	X	Top, -Z descent stage oxidizer tank	A/7c	1000	±10g
	GA2682D	Y	Top, -Z descent stage oxidizer tank	A/8c	1000	±10g
	GA2683D	Z	Top, -Z descent stage oxidizer tank	A/9c	1000	±10g
Microphone	GA4021Y	omni	Ascent stage +Z axis	A/10c	2000	150 dB
	GA4022Y	omni	Ascent stage -Z axis	A/5c	2000	150 dB

NASA-S-68-3626

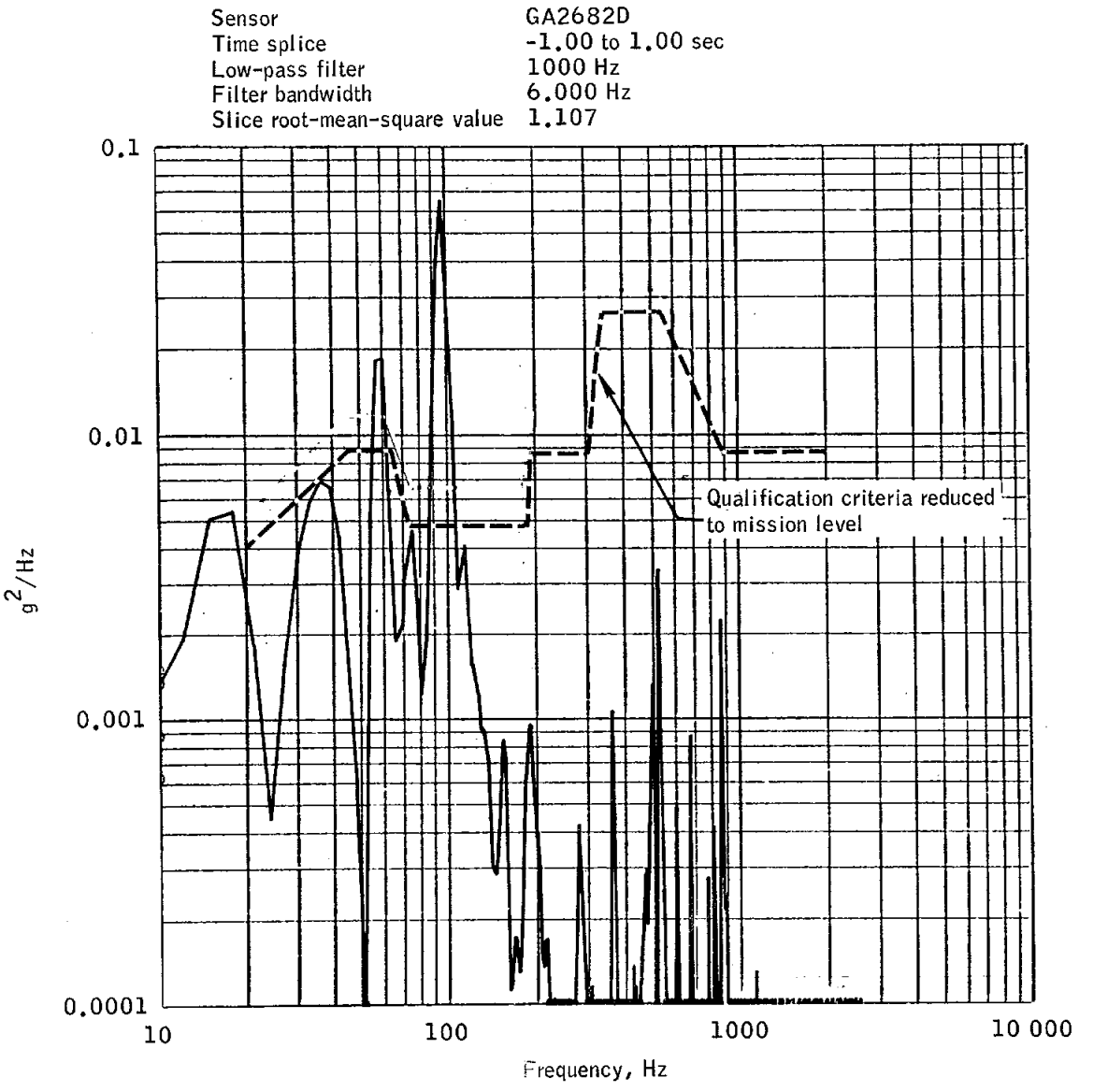

Figure 6.1-1.- Y axis vibration at lift-off, -Z oxidizer tank.

NASA-S-68-3625

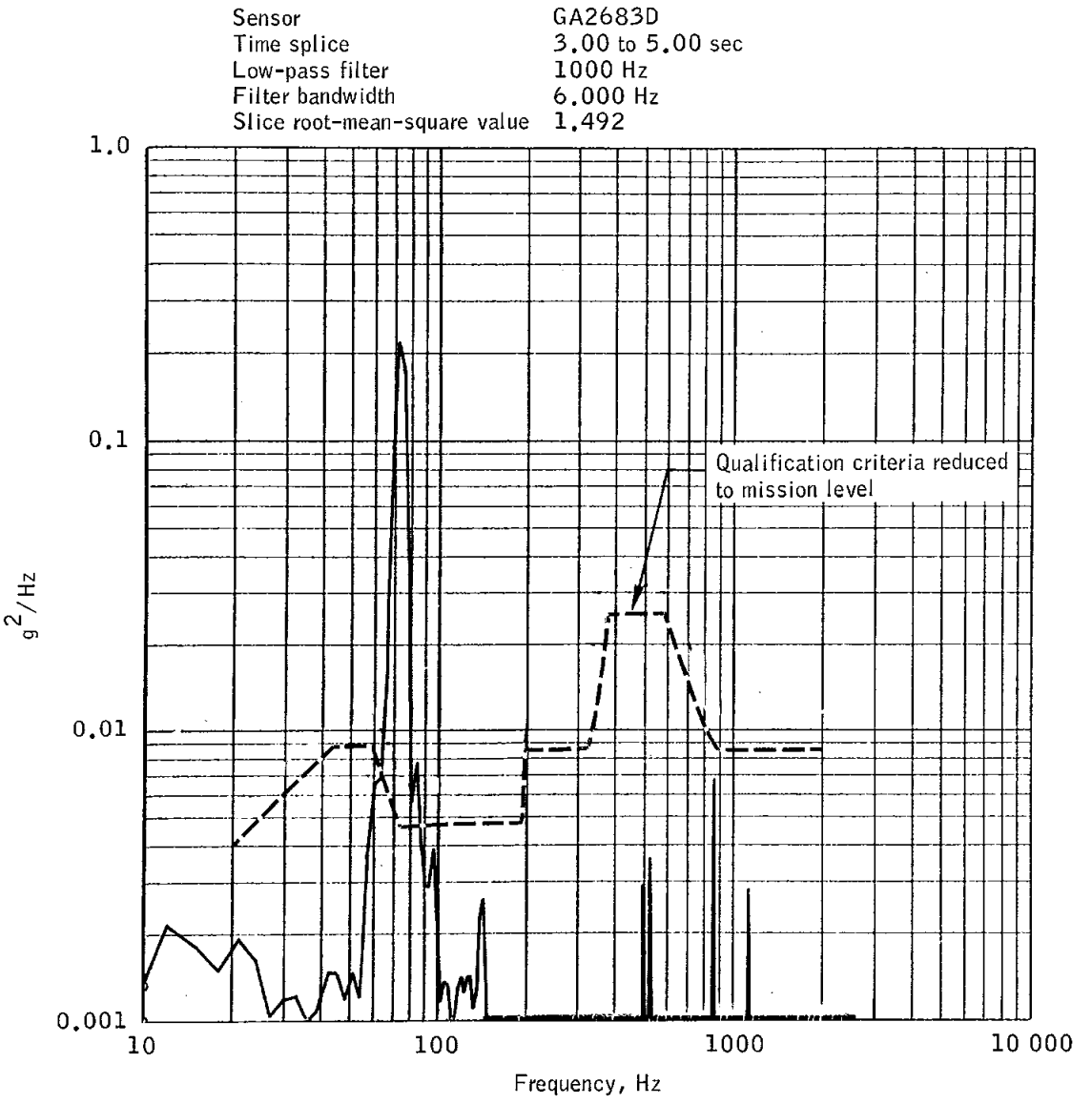

Figure 6.1-2.- Z axis vibration at lift-off, -Z oxidizer tank.

NASA-S-68-3627

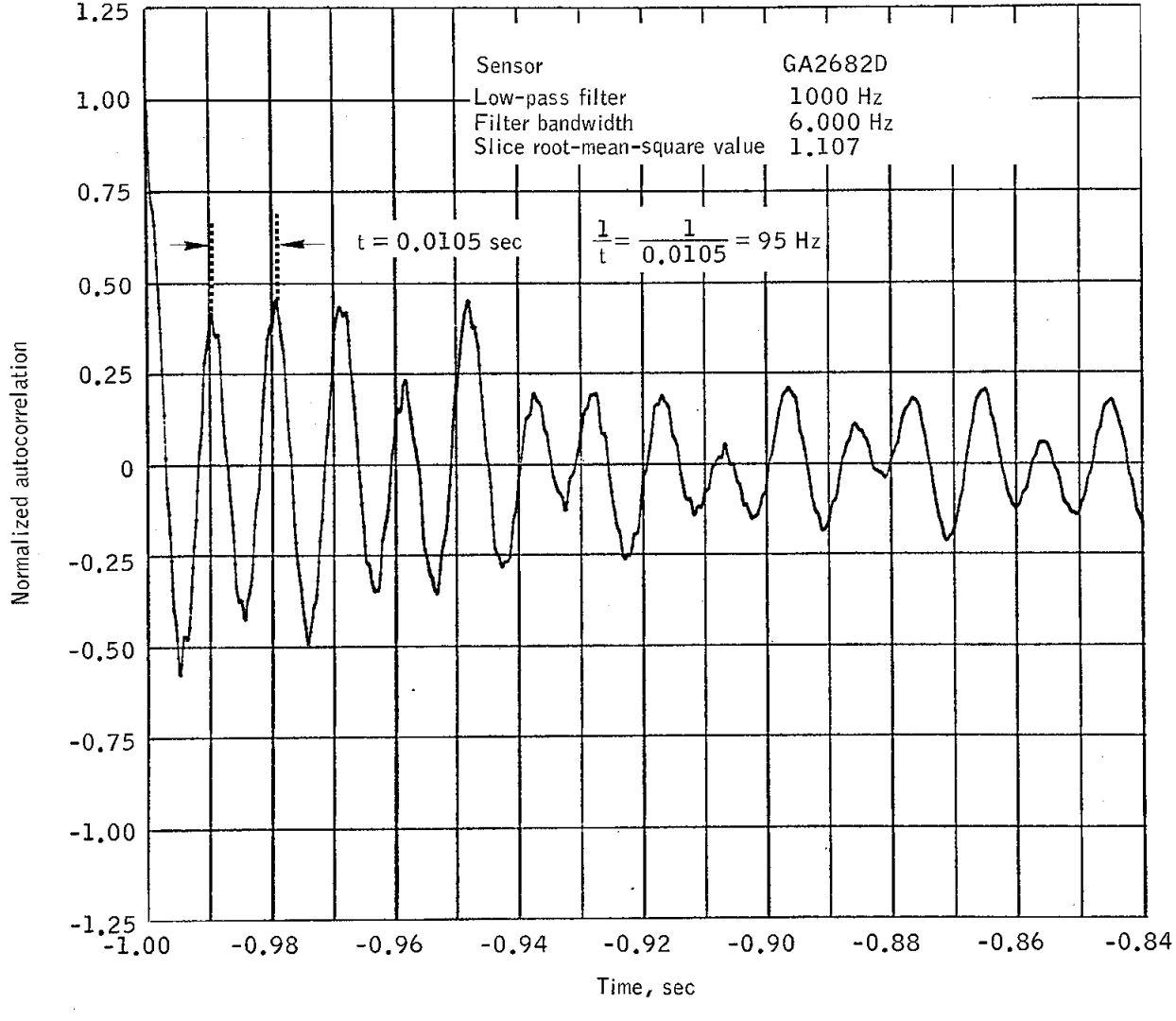

Figure 6.1-3.- Y axis autocorrelation at lift-off, -Z oxidizer tank.

NASA-S-68-3628

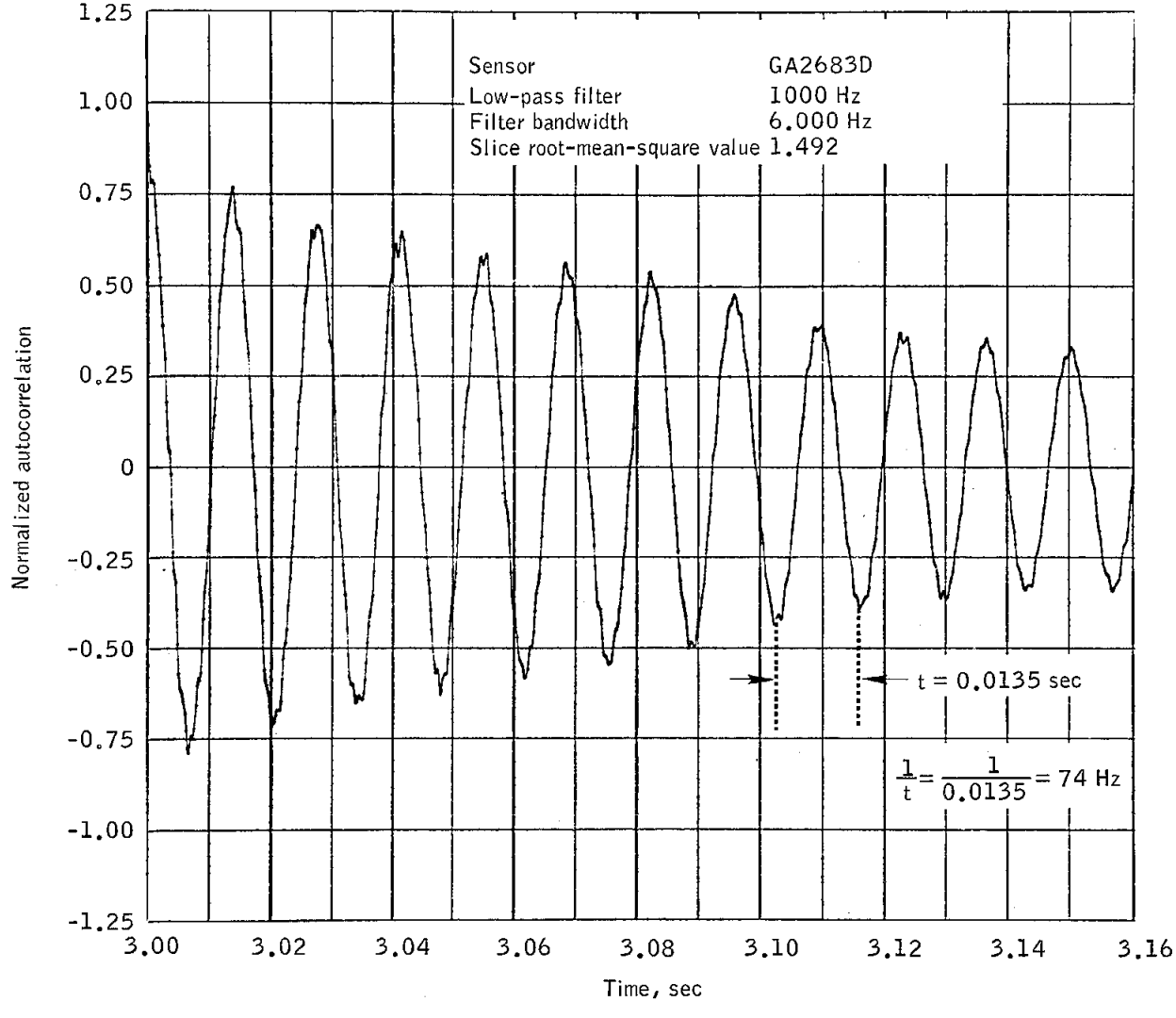

Figure 6.1-4.- Z axis autocorrelation at lift-off, -Z oxidizer tank.

NASA-S-68-3629

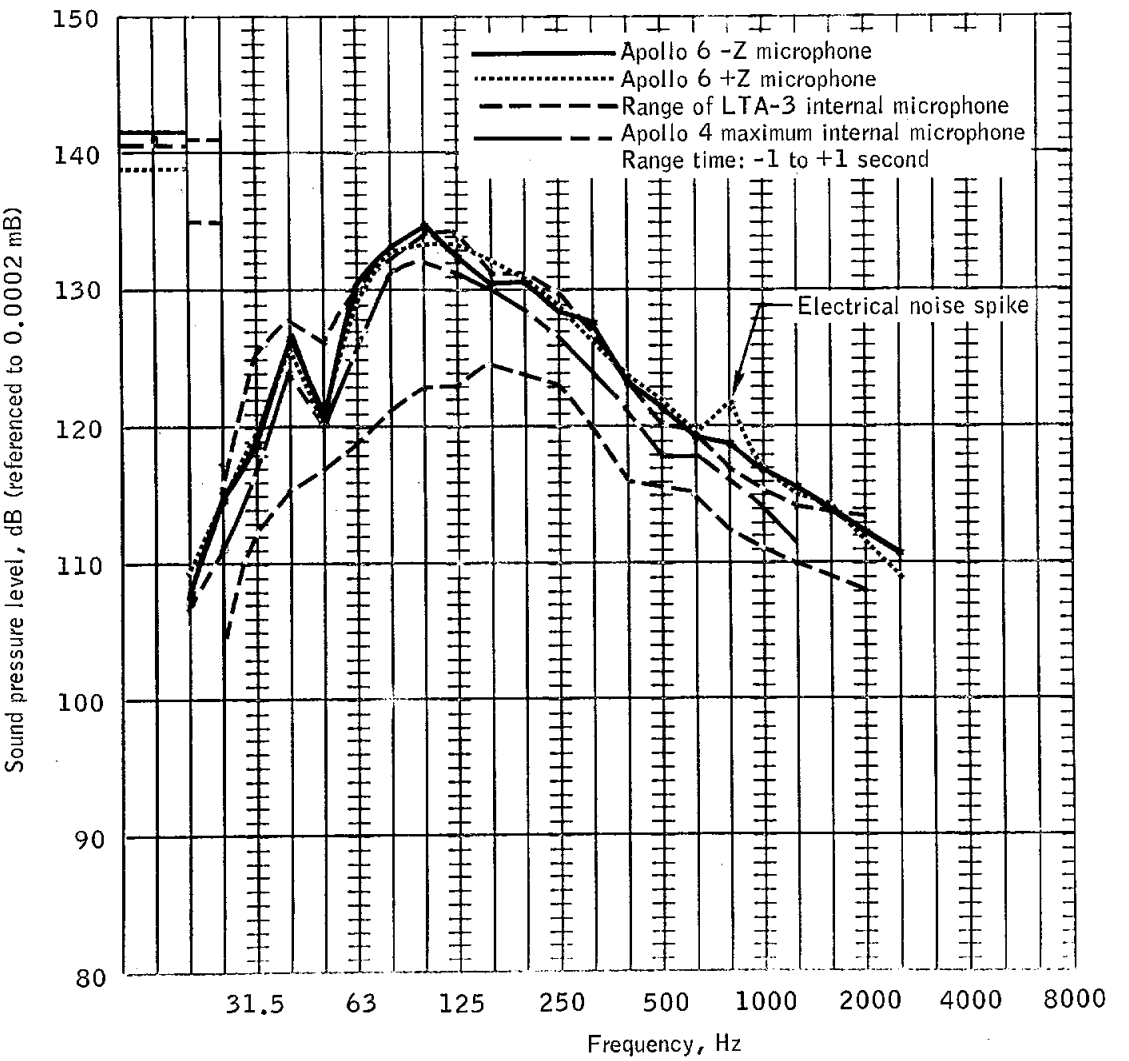

Figure 6.1-5.- Adapter/LTA-2R internal sound pressure levels compared with Apollo 4 and LTA-3.

6.2 INSTRUMENTATION

The LTA-2R development flight instrumentation performed satisfactorily except for minor problems associated with the vehicle structural anomaly at 00:02:13. Three of the 38 total measurements were lost at that time because an electrical short opened a fuse common to the three; these measurements were the acceleration 2 on the ascent stage Z axis, the load on the Z beam booster strut 3, and temperature 3 on the descent stage minus Z beam. Also, during this anomaly period, a loss of 16 milliseconds of data starting at 00:02:13.344 was caused by a momentary drop in radio frequency signal strength.

7.0 FLIGHT CREW

(This section is not applicable.)

8.0 BIOMEDICAL

(This section is not applicable.)

9.0 MISSION SUPPORT PERFORMANCE

This section of the report is based upon real-time observations, unless otherwise noted, and may not agree with the final analysis of the data in other sections of the report.

9.1 FLIGHT CONTROL

9.1.1 Prelaunch Operations

The Mission Control Center began flight control support of the terminal countdown at T minus 15 hours (15:00:00 G.m.t.) on April 3, 1968. Command module closeout was completed at T minus 9 hours 23 minutes.

The terminal count progressed as scheduled, with few problems, toward a planned lift-off time of 12:00:00 G.m.t. The Mission Control Center command checks to the space vehicle were completed nominally, except for two instances:

(a) At T minus 11 hours 51 minutes, the rate backup commands were transmitted and verified by the Mission Control Center. The launch complex personnel could not verify the cage function of the commands because the system was already in the rate backup configuration. The test checkout procedure should have called for the rate backup reset command to be sent prior to the rate backup commands. This presented no problem in the checkout, so the count proceeded.

(b) At T minus 10 hours 8 minutes, quad A and quad B propellant isolation valves were inadvertently opened. This activated the two systems earlier than desired but caused no serious problems to the count procedure. The Mission Control Center commanded quad C and quad D propellant isolation valves open at the nominal time of T minus 15 minutes.

Fuel cell activation and prelaunch activity were normal except for the manner in which the fuel cells were procedurally cycled ON and OFF the main buses. To maintain proper cryogenic tank pressure and to prevent the tanks from venting prior to lift-off, two fuel cells were used to supply main bus power. Two of the three fuel cells were placed online for a period of 6 hours, and then one of the two hot cells was replaced with the cold cell. This procedure appeared to result in unbalanced fuel cell operation at lift-off. As a result, fuel cell 2 supplied less power than either fuel cell 1 or 3, although during normal circumstances, it should have supplied more.

9.1.2 Power Flight

Lift-off occurred at 12:00:01 G.m.t. on April 4, 1968. During the S-IC burn, all functions and systems performance appeared to be nominal, except for the roll program. At the completion of the roll program, the launch vehicle stabilized with a roll offset of approximately 0.8 degree, probably because of engine misalignment. The trajectory was lofted (relative to the premission nominal) in the vicinity of maximum dynamic pressure (max q). The premission nominal trajectory was based on prelaunch wind data. S-IC inboard engine cutoff and outboard engine cutoff occurred at 00:02:24 and 00:02:28, respectively. At 00:01:27, the telemetry data (both VHF and S-band) became so erratic as to be unusable. This erratic condition continued until 00:08:20. The cause of the data problem was not determined; however, it is postulated that the PCM equipment was not correctly sequencing through the PCM format. When the data again became usable at 00:08:20, the following anomalies were noted:

a. Four telemetry parameters (battery B case temperature, fuel cell 2 radiator outlet temperature, waste water quantity, and oxygen tank 2 quantity) had failed. These parameters have a common input to one sequencer gate through four individual primary gates. It is postulated that one of these primary gates failed, clamping the remaining parameters to a common level.

b. The emergency detection system vote 1 and the adapter physical separation monitor B had changed state and were giving erroneous indications. (Editor's Note: In real time, these indications were believed to be erroneous; however, subsequent postflight analysis has shown that the emergency detection system vote 1 was valid as a result of the structural anomaly during first-stage boost.)

c. The central timing equipment output was erratic. The timing equipment performed until 00:01:27. At that time, it became erratic and remained so for the duration of the mission.

d. The guidance and navigation system was outputting ERROR DETECT, TELEMETRY FAIL, and K$\bar{K}$K BLOCK in the guidance computer. The K$\bar{K}$K BLOCK caused the TELEMETRY FAIL indication, which in turn caused the ERROR DETECT. There was a continuous problem throughout the mission with these three discretes.

S-II ignition was nominal, and all engines and systems operated satisfactorily during the main-stage operation. S-II engines 2 and 3 shut down at 00:06:52.9 and 00:06:54.2, respectively, and the inertial guidance mode began an abnormal amount of steering. The time was coincident with the nominal time of inertial guidance mode 2 and the Guidance Officer thought that this event had occurred even though the discrete was not set.

The engine failures could not be confirmed until 00:07:30 because the telemetry data from the launch vehicle were very noisy during this time period. The two-engines-out condition was verified by the thrust chamber pressures and the thrust not OK switches. One switch did not indicate properly for engine 2.

Mission rules required that a two-engines-out situation during this time period would require an early staging command. It was thought that the vehicle would go out of control and spin up in roll. However, the engines-out confirmation had been delayed and the vehicle was maintaining attitude control; consequently, the Booster Systems Engineer elected to continue the mission. The maximum angular rates observed during the engines-out period were 3 deg/sec in pitch, 1 deg/sec in yaw, and 0.8 deg/sec in roll. Attitude errors reached a maximum of plus 13.5 degrees in pitch, plus 1.6 degrees in yaw, and minus 2.7 degrees in roll at about 00:07:22. At approximately 00:08:37, inertial attitude hold (χ freeze) had been initiated. The exact time could not be determined in real time because there was no positive indication of this event. The flight-path angle, as well as the attitude, began to increase almost immediately. At S-II cutoff, the trajectory was 3 n. mi. too high.

The launch vehicle telemetry data continued to be intermittent and the problems were further compounded by failure of the Bermuda telemetry computer at 00:09:14. Because of this failure, the Booster Systems Engineer could not confirm S-IVB staging, which occurred about 00:09:36. The launch vehicle telemetry was restored at about 00:10:00 when Bermuda handed over communications coverage to U.S.N.S. Redstone.

During the S-IVB firing, all systems performed satisfactorily. However, because of the degraded S-II engine performance, the S-IVB was required to fire longer than the nominal time. At 00:09:48, after S-IVB ignition, the flight-path angle had increased to about 1.5 degrees greater than nominal but was beginning to decrease. The time to free fall, which had been lower than nominal at S-IVB ignition, began to rise at a higher-than-nominal rate, eventually crossing and then exceeding the nominal. A sudden decrease in time to free fall was noted at 00:10:50. The decrease lasted about 1 minute, resulting in reduction of time to free fall from 6 minutes to approximately 4 minutes. This reduction was accompanied by a drop in flight-path angle from plus 1.0 degree to minus 1.3 degrees with a velocity gain of less than 1000 ft/sec. Later analysis showed that the S-IVB pitched down about 50 degrees in this time period. At 00:11:20, the steering was reported to be converging, even though the vehicle was still maneuvering; the S-IVB cutoff was predicted to occur at 00:12:19. At 00:12:05, the S-IVB cutoff was predicted to be 00:12:33. During the last 20 seconds of powered flight, the S-IVB executed a rapid pitch-up maneuver from about 50 degrees below the local horizontal to about 65 degrees above the local horizontal. The S-IVB was attempting to

null out the negative flight-path angle with a minimal increase in forward velocity. S-IVB cutoff occurred at 00:12:27 with an overspeed of approximately 170 ft/sec. The ullage engines were confirmed ON for the proper interval, the continuous vent opened as scheduled, and a line pressure of about 27 psia was observed. The flight control computer was configured to the coast mode, and the auxiliary propulsion system maneuvered the vehicle to eliminate the attitude errors at insertion. At time base 5 plus 15 seconds, the orbital pitch rate was initiated, and the vehicle maneuvered to the local horizontal. The resulting orbit was 193.0 by 95.9 n. mi. (Editor's Note: These orbital values were those computed in real time; subsequent postflight trajectory reconstructions refined these values to those shown in section 2.0.)

9.1.3 Orbital Flight

The command and service module systems performed as expected during the orbit phase, with the following exceptions. The surge tank pressure was expected to remain stable at the highest pressure attained by either oxygen tank 1 or 2. However, the surge tank pressure followed oxygen tank 2 (which indicated the higher pressure) through each pressure excursion, indicating that an oxygen check valve had failed. The cryogenic temperature readouts were so noisy that cryogenic quantity calculations were erratic and, for hydrogen, unusable. The main bus voltage ranged between 29.3 V dc at 00:08:41 and 27.5 V dc at 05:21:11. In general, the main bus voltage was from 0.1 to 0.5 volt lower than predicted. The decreased voltage level was probably caused by the prelaunch procedure of cycling fuel cells ON and OFF to regulate the cryogenic tank pressures. The computer updata link block that occurred during launch was considered to be RF noise and was cleared at Carnarvon.

Concern was expressed as to whether the S-IVB restart equations and guidance equations were valid for the existing off-nominal orbit. The correct insertion weights and a continuous vent force of 24 pounds (roughly equal to the onboard value) were entered into the Real Time Computer Complex. A translunar injection maneuver was then generated in the Real Time Computer Complex, yielding an ignition time of 03:13:30.6, approximately 3 minutes later than the preflight-predicted time, but well within the tolerance for assuring a satisfactory onboard-computed ignition. The Huntsville Operation Support Center also confirmed that the perturbed orbit would cause no problem with the restart or guidance equations.

The insertion propellant weight was calculated to be 147 600 pounds, providing a time-to-depletion capability of 322 seconds for the second firing. The duration of the second firing was calculated to be 313 seconds, based on a first firing time of 166.5 seconds. The Huntsville

Operation Support Center determined these values to be 322 seconds for second firing capability and 309 seconds for the expected second firing duration. A guided cutoff on the second S-IVB firing was determined to offer the greatest probability of success, based on a 2.4 sigma (95 percent) probability of an oxidizer depletion cutoff; this was considered not to be catastrophic.

A cold helium leak rate of 3.5 psi/min and a tank pressure of 1269 psi were observed on the first revolution over Carnarvon. The cold helium continued to leak, and it was estimated that the tank pressure at restart would be 860 psi. It was confirmed that the second S-IVB firing could be completed with a cold helium tank pressure of 450 to 500 psi at ignition; the system was declared GO for restart.

Based on a guided cutoff for the second S-IVB firing, the following maneuver plan was developed:

Time for initiation of translunar injection start sequence, hr:min:sec	03:08:03.8
Time for ignition for translunar injection firing, hr:min:sec	03:13:31.6
Time for cutoff for translunar injection firing, hr:min:sec	03:18:41.0
Change in velocity, ft/sec	10 222
Firing time, min:sec	5:09.5
Time for CSM/S-IVB separation, hr:min:sec	03:21:41.0
Time for service propulsion system engine ignition, hr:min:sec	03:23:21.0
Time for service propulsion system engine cutoff, hr:min:sec	03:27:34.8
Change in velocity, ft/sec	3741
Firing time, min:sec	04:13.8

A navigation update was generated and was to be uplinked to the computer on the second revolution over Carnarvon. Navigation updates are normally generated by the Real Time Computer Complex and are confirmed by the Real Time Auxiliary Computing Facility. The computing facility was unable to confirm the update prior to Carnarvon loss of signal and the update was delayed until signal acquisition by Hawaii. It was determined that the Real Time Computer Complex was generating the navigation update referenced to the ground computer time frame instead of to the flight computer time frame. The lift-off time in the Real Time Computer Complex was changed so that the time reference was the same as that of the flight computer. The computer navigation update was again generated and subsequently verified by the Real Time Auxiliary Computing Facility.

When the computer update was attempted at Hawaii, a KK̄K FAIL signal was received. This was cleared by transmitting all zeros, ERROR RESET, and CLEAR. The update was then completed with no further problems. A KK̄K FAIL was received on the first keycode of every computer command sequence that was attempted. No problems were experienced with the updata link, and it was concluded that RF interference was being picked up between the receiver and the computer and was appearing in the computer uplink register.

9.1.4 Translunar Injection

During signal acquisition, Guaymas confirmed that the S-IVB auxiliary hydraulic pump was not providing system pressure; the hydraulic system pressure was 1337 psia, the oil level was 83 percent, the reservoir pressure was 65 psia, and the pump inlet temperature was 165° F. The current from the S-IVB aft battery 2 was 44 amperes compared with the predicted value of 88 amperes; this further confirmed the failure. Command loads for turning on the auxiliary hydraulic pump were not available at the Guaymas or Texas sites. The command computers at these sites were loaded with the preignition contingency commands. In addition, command action at this time was undesirable because operation of the auxiliary pump would have caused a high initial load on aft battery 2 and consequent damage the chilldown inverters. Moreover, hydraulic system pressure would be brought up to the normal operating level by the main pump at ignition.

The S-IVB low-g chilldown was in progress during Guaymas acquisition; the temperatures and pressures were as expected. Time base 6 was initiated at 03:08:09. The continuous vent valve closed properly and the ullage engines came ON as expected. The hydrogen and oxygen tanks were pressurized to 32.5 psia and 41 psia, respectively. The maneuver to the restart attitude was initiated on time at 03:11:29 and was satisfactorily completed. The liquid oxygen mass was observed to be off-scale high (100 percent), indicating the firing would be performed at a 5.5:1 engine mixture ratio. The prevalves opened, the fuel lead was initiated, the main fuel and liquid oxygen valves opened to 100 percent, the J-2 start bottle dumped, and the thrust chamber pressure increased from zero psi to a maximum of 35 psi. However, the S-IVB did not reignite; at 03:13:50, 14 seconds after the engine-start command had been sent, time base 7 was initiated by the launch vehicle digital computer. The reason for the failure to reignite could not be determined.

A real-time command through the mission control programmer initiated CSM/S-IVB separation at 03:14:25. The CSM separated immediately, and the service propulsion system engine ignited at 03:16:05. The guidance and navigation of the vehicle were excellent throughout the entire firing. The computer had to be used for a considerable amount of steering about

the Z axis during the firing. The desired coupling data unit readout in Z changed from 3 degrees to 11 degrees and then to 2 degrees in a smooth transition. The maximum change occurred during the middle of the firing. The computer commanded service propulsion system engine cutoff at 03:23:27, resulting in an orbit with the following parameters:

Apogee, n. mi.	11 987
Perigee, n. mi.	19.2
Inclination, deg	32.58
Longitude of the ascending node, deg/sec	83.59

After the first service propulsion system engine ignition, the fuel inlet pressure dropped to 147 psia. The inlet pressure was expected to drop to 154 ± 4 psia. The reason for this difference could not be determined but might have been transducer inaccuracy.

The essential loads on ac bus 1 were automatically transferred to ac bus 2 at 03:14:32. Telemetry data indicated that the voltages on phases A, B, and C were 49 volts, 0 volt, and 0 volt, respectively, for one wide-band data frame at the time the transfer occurred. The subsequent data frame at 03:14:33 indicated that the voltages for each phase on both buses were normal; the essential load transfer signal still indicated a load transfer. Subsequent inverter temperature shifts confirmed the transfer. The cause of the transfer was unknown but most probably was an excessive load transient on bus 1.

Based on Antigua C-band tracking and assuming no second service propulsion system engine firing, the initial entry interface time was determined to be 09:38:47; the comparable computer time was 09:38:31.5. Thus, the difference between the ground and computer times to free fall was less than 16 seconds. After about 30 minutes into the mission, change in time to free fall was only 6 seconds. Navigation by the computer, including time to free fall for the entry sequencing, was sufficiently accurate for entry without a second navigation update.

The second service propulsion system engine firing was inhibited by a real-time command at 04:14:00. This action resulted from the primary consideration of insufficient firing time remaining to obtain the desired heat shield test. After the long-duration first service propulsion system engine firing, propellant sufficient for only 23 seconds of firing time remained. This small quantity of propellants remaining would have provided only 22 percent of the desired additional entry velocity.

At 04:21:00, the Guidance Officer attempted to reset a TELEMETRY FAIL indication that had been set at approximately 03:16:00. A computer updata link block was received when ERROR RESET was commanded. The

Guidance Officer then proceeded to clear both the TELEMETRY FAIL and the updata link block. At 05:07:00, another updata link block occurred; however, there was no TELEMETRY FAIL indication. It is assumed that this block was caused by 16 noise bits that entered the uplink register. The updata link block was cleared on the second command attempt, but the block recurred at about 05:29:00. This updata link block was left on to prevent the possibility of noise bits getting into the computer. The second navigation update was started at 06:53:00 and was completed in approximately 30 minutes. Six updata link blocks occurred during the update; each block had to be reset before the update could be continued. After completion of the navigation update, an intentional updata link block was introduced (by commanding all zeros) to prevent the possibility of noise bits entering the computer.

During the high ellipse period, a drift developed in either the inertial measurement unit or in the attitude gyro coupling unit, particularly in the roll axis. At 03:28:26, the coupling unit was aligned to the cold-soak angles; the cold-soak angles, the inertial measurement unit, and the coupling unit were in agreement. At approximately 05:29:00, the two units showed a difference of 29 degrees in roll. At 09:13:32, the coupling unit was aligned a second time. The drift indicated by the coupling unit was as follows:

	Mission elapsed time, hr:min:sec	Pitch, deg	Yaw, deg	Roll, deg
Attitude gyro coupling unit at first alignment (coupling units agree)	03:28:26	160	0	58
Attitude gyro coupling unit prior to second alignment	09:13:32	177	356	351

It could not be determined whether the drift was in the inertial measurement unit or in the coupling unit; there was no third indication of attitude against which the two systems could be compared. However, the following information was known:

a. The inertial measurement unit was in good agreement with the instrument unit prior to CSM/S-IVB separation.

b. The inertial measurement unit performance during the first service propulsion system engine firing was excellent.

c. The body-mounted attitude gyros have previously exhibited a history of instability.

Consequently, the inertial measurement unit was accepted as the valid data system and the computer was permitted to control the entry.

9.1.5 Entry

The entry interface conditions (velocity of 32 813 ft/sec and flight-path angle of minus 5.94 degrees) resulting from the first service propulsion system engine firing were considerably off the nominal entry conditions that would have been achieved with a nominal second service propulsion system engine firing (velocity 36 500 ft/sec and flight-path angle minus 6.5 degrees). The computer program was not designed to fly entries with such off-nominal entry conditions nor with a target range of 1932 n. mi. Hence, two problems were encountered in using the computer to fly this entry.

a. The first problem was the nonoptimum UPCONTROL trajectory to be flown; UPCONTROL was the portion of the entry trajectory between the point that the command module started moving back up through the atmosphere and the skip-out point. Essentially, the computer determined the UPCONTROL trajectory by adjusting the velocity, flight-path angle, and the exit drag level Q_7 so that the range to the target would be within the capabilities of the system when the computer entered the FINAL phase (at Q_7 + 0.5 ft/sec^2). The problem was that the computer logic normally computes the drag level only once but iterates on the skip-out velocity and flight-path angle; as a result, a nonoptimum UPCONTROL trajectory could be generated and flown. In FINAL phase, the loss of lift resulting from a nonoptimum UPCONTROL trajectory cannot be compensated for in the computer logic, even though the command module flies a full-lift profile.

b. A second problem can also occur during the UPCONTROL trajectory. During UPCONTROL, the computer normally reverses the direction of the lift vector several times so that the magnitude and direction of the out-of-plane lift can be controlled and, at the same time, the required inplane lift can be achieved. The computer will allow a roll through the negative lift position if certain criteria are satisfied by the calculated UPCONTROL trajectory. If this roll reversal occurs at certain times during UPCONTROL, the lift lost by the "roll under" maneuver cannot be recovered during FINAL phase and the spacecraft will undershoot the target.

The lift-to-drag ratio at entry time was 0.343. The computer-determined landing point, based on entry weights and preflight aerodynamics, was at 28 degrees 50 minutes North latitude, 162 degrees 28 minutes West longitude. These coordinates indicated an undershoot of approximately 320 n. mi.; thus, the primary recovery ship was directed to move along the ground track in a westerly direction. The situation that existed is shown in figure 9.1-1. All ranges shown are referenced to entry interface. The cross-hatched area represents the entry ranges to which the computer could navigate with a miss distance of not more than 10 n. mi. The three sigma high and low lift-to-drag ratio landing

points are plotted, as well as the Retrofire Officer's best estimate of the landing point (based on the preflight prediction of the command module aerodynamics). The landing points, which were confirmed in the Real Time Computer Complex and in the Real Time Auxiliary Computing Facility, agreed to within 10 n. mi.

A decision had to be made as to whether or not an entry target point update was to be executed. Four alternatives were available, as follows:

Alternative A: Updating the target point to the zone of absolute landing predictability, thereby forcing the command module to miss the position of the primary recovery ship by approximately 400 n. mi. (based on a recovery ship speed of 20 knots for 6-1/2 hours).

Alternative B: Not updating the landing point and expecting an undershoot of as much as 380 n. mi. (for a three-sigma high lift-to-drag ratio, the end of mission target could be reached).

Alternative C: Updating the computer discrete recovery area coordinate locations with the predicted position of the primary recovery ship at the time of entry and sending the computer abort at Guam so that the command module would fly to these coordinates.

Alternative D: Sending guidance and navigation fail command and allowing a rolling entry.

Alternative B was chosen because, operationally, it was the simplest approach that could guarantee a safe entry. The primary disadvantage was that the landing point could not be predicted because the time of the "roll under the bottom" maneuver in the computer entry logic was extremely sensitive to very minor perturbations in the lift-to-drag ratio, entry velocity, and flight-path angle.

Alternative A was ruled out because excessive recovery ship access times would have resulted. In addition, updating would eliminate any chance of landing closer to the recovery ships.

Alternative C involved an attempt to update target point computer discrete recovery area coordinate locations. The updated coordinates would have been the predicted latitude and longitude of the primary recovery ship at entry. The computer abort would have been transmitted prior to loss of signal at Guam to force the computer to guide to the new coordinates in the discrete recovery area cores. If the computer abort command were to fail, then the computer would attempt to fly to the nominal end-of-mission target loaded in the manual cores. This procedure would have insured that the command module would not overshoot the primary recovery ship; however, it offered no protection against an undershoot. The procedure was brought to the attention of the Retrofire

Officer at 07:20:00. Although it was believed that Alternative C might be a workable procedure, it was discarded for several reasons: the brief time remaining before entry interface, the large amount of commanding required for implementation, and the fact that the procedure had not been practiced in simulations (that is, no operational confidence had been established).

Alternative D was discarded because the guidance and navigation had proven to be accurate and reliable prior to this time. In addition, a normally functioning guidance and navigation system offered the greatest probability of successful entry in all aspects (miss distance, operational simplicity, et cetera).

The computer started the entry program at 09:36:00. At 09:44:00, U.S.S. Carpenter reported both acquisition and loss of signal. The recovery forces successfuly recovered the command module and estimated the final landing coordinates as 27 degrees 40 minutes North latitude, 157 degrees 59 minutes West longitude.

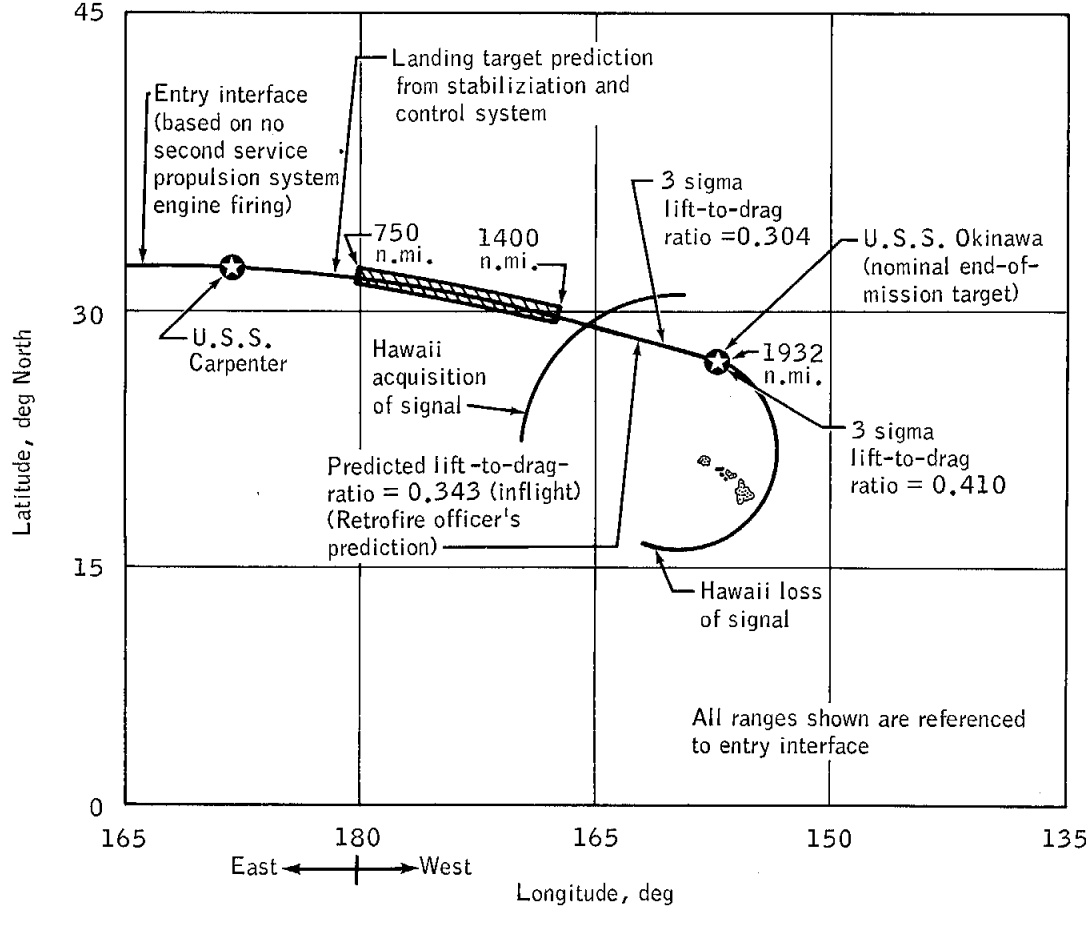

Figure 9.1-1.- Off-nominal entry-interface conditions resulting from first service propulsion system engine firing.

9.2 NETWORK PERFORMANCE

Lift-off for the Apollo 6 mission occurred on April 4, 1968, at 12:00:01.8 G.m.t. General support from the NASA and Department of Defense network stations was excellent. Those ground systems equipment anomalies that did occur had little or no effect on the mission support activities.

9.2.1 Apollo Range Instrumentation Aircraft

The Apollo range instrumentation aircraft at Bermuda supported the mission in excellent fashion, and data from the aircraft were dumped at Bermuda. The data were relayed to the Mission Control Center at Houston and, although noisy, were acceptable.

9.2.2 Telemetry

The Bermuda telemetry computer faulted at 00:09:00. Restarts were attempted, but the computer would only cycle for 10 to 20 seconds, then fault again. Although no problem could be discovered, the computer faulted again during the revolution 2 pass. There were no data lost as telemetry coverage had been handed over to U.S.N.S. Redstone. At the time of the preparation of this report, there has been no resolution of this problem; however, the Goddard Space Flight Center has formed a special team to investigate this problem.

9.2.3 Tracking

A marked improvement from the earlier missions was noted in the quality of the high-speed S-band tracking data. There were no significant S-band problems during this mission. The problems with acquisition messages, so much in evidence during the two previous missions, did not occur during the Apollo 6 mission. The radar at Tananarive did not acquire a valid track during the entire mission. This problem has been attributed to incorrect phasing as the result of a reversed diode.

9.2.4 Command

The Guam telemetry computer malfunctioned at 1 hour before the scheduled acquisition of signal for revolution 3. Efforts to identify the problem were not successful. Because telemetry had priority, the programs in the telemetry and command computers were switched. The

command computer faulted several times during the pass; however, there was no requirement for command transmission at this time.

9.2.5 Central Processor

Operation of the central processor at the Goddard Space Flight Center was satisfactory. The 494 mode of operation was used instead of the 490 mode used for the two preceding missions.

9.2.6 Real Time Computer Complex

The Real Time Computer Complex experienced no major problems in support of the mission. The following minor problems caused little or no degradation of support:

a. At 06:48:00, 09:59: 41, and 10:07:54 G.m.t. on April 4, the telemetry system received an arithmetic program interrupt while processing a low-speed telemetry message. No program problem has been identified, but evaluation of the data and the processor is continuing.

b. At 14:36:00 G.m.t., it was discovered that the command processor was erroneously using the Greenwich mean time at lift-off to process a computation of a navigation vector update time. To resolve the difference, the Greenwich mean time at lift-off in the command processor was set equal to the Greenwich mean time zero set in the flight computer.

c. At 15:19:42 G.m.t., the mission operations computer received a data check on the input data adapter from the command processor; this did not occur on the dynamic standby computer D. An immediate switchover of computers was performed to assure uninterrupted support during this period of the first service propulsion system engine firing. No problem developed and the Real Time Computer Complex remained in the exchanged configuration until the end of the mission.

d. At 16:54:00 G.m.t., the digital display used by the Flight Dynamics Officer indicated an incorrect initial revolution number for the trajectory resulting from the first service propulsion system engine firing. The condition was corrected by manually entering an anchor vector with the correct revolution number.

e. At 21:00:00 G.m.t., it was discovered that U.S.N.S. Watertown had not received a Department of Defense acquisition vector; the time for automatic acquisition data transmission occurred after the initiation of entry acquisition data processing. During the Apollo 6 mission, the Department of Defense messages were not part of entry acquisition processing.

f. During some periods when the input data rate was high, several central-processor sequence-count errors were noted. These occurrences indicate that the real-time operating system was in the disable mode for more than 20 milliseconds. The disable operating times should be substantially reduced in systems to be used for later missions.

9.2.7 Communications

The mission flight plan was not affected nor were any mission data lost as a result of the communications problem.

9.3 RECOVERY OPERATIONS

The responsibility of the Apollo 6 recovery forces was to recover the command module and the six launch vehicle camera capsules. The command module was successfully recovered approximately 6 hours after landing 400 n. mi. north of Honolulu, Hawaii. Two of the six camera capsules were recovered approximately 25 minutes after landing 400 n. mi. east of Cape Kennedy, Florida.

9.3.1 Landing Areas and Recovery Force Deployment

Potential landing areas were established to encompass both the end-of-mission target point and the predicted landing points that would follow an abort or alternate mission. The areas were defined as follows:

Launch site area.- The launch site area encompassed the potential landing points resulting from a mode I abort initiated prior to or during the early part of powered flight. This area included the terrain near launch complex 39A and extended downrange along the ground track for approximately 40 n. mi.

Continuous abort area.- The continuous abort area (fig. 9.3-1) encompassed the potential landing points resulting from a mode II abort. The area extended from the downrange extremity of the launch site area to 2250 n. mi. downrange of Cape Kennedy, Florida. The crossrange boundaries were 50 n. mi. either side of the ground track. The camera capsule recovery areas were located in the western portion of the continuous abort area.

Discrete abort area.- The discrete abort area (fig. 9.3-1) encompassed the potential landing points resulting from a mode III abort. The area was bounded by a 300 by 100 n. mi. ellipse centered on a point 50 n. mi. downrange of the abort target point, 28 degrees 18 minutes North latitude, 19 degrees 30 minutes West longitude.

Secondary landing area.- The secondary landing area encompassed potential landing points resulting from the majority of the possible aborts and alternate missions initiated after insertion. The area was an irregular ellipse approximately 3200 by 1700 n. mi. located in the western portion of the Pacific Ocean.

Primary landing area.- The primary landing area encompassed the planned end-of-mission target point, 27 degrees 19 minutes North latitude, 157 degrees 11 minutes West longitude, and the associated landing

point dispersion pattern. The area was a 200 by 100 n. mi. ellipse centered on a point 50 n. mi. uprange of the end-of-mission target point.

Contingency landing area.- The contingency landing area encompassed all the possible landing points not included in the preceding listed areas. This included the portion of the area between 32 degrees North and 32 degrees South latitude that was in the vicinity of the ground track.

The recovery force deployment in each area is listed in table 9.3-I.

9.3.2 Command Module Location and Retrieval

At lift-off, the predicted command module landing point and the location of the primary recovery ship were coincident with the end-of-mission target point contained in the command module guidance and navigation system. After the S-IVB engine failed to restart and the alternate sequence was performed, recovery forces began receiving updated landing information. Because the information predicted an uprange landing, the primary recovery ship, U.S.S. Okinawa, was directed west along the ground track. When recovery forces were given the final predicted landing point (28 degrees 50 minutes North latitude, 162 degrees 28 minutes West longitude) and time (21:56 G.m.t. on April 4), it was evident that U.S.S. Okinawa would be approximately 180 n. mi. downrange of this point at the time of landing. This consideration, and the fact that the entry trajectory had changed considerably, led to the decision to change the premission recovery force structure to that shown in figures 9.3-2 and 9.3-3.

After entry, the first contact with the command module by recovery forces was an S-band direction-finding signal received by the HC-130 aircraft, Hawaii Rescue 1. The signal was lost as the command module entered S-band blackout. During blackout, the only recovery force contact with the command module was an air search radar reception by the destroyer, U.S.S. Carpenter, located 1500 n. mi. uprange of the target point. After blackout, the rescue aircraft (Hawaii Rescue 4, 5, and 6) acquired the S-band signal and, using direction-finding equipment, were able to follow the command module during the final phase of entry. Aircraft (Hawaii Rescue 5 and 6) and helicopters (Recovery 3 and Search 1) acquired the VHF recovery beacon signal while the command module was descending on the main parachutes. Because VHF signal reception is limited to line-of-sight range, only the Hawaii Rescue 6 aircraft would have been expected to maintain continuous VHF contact through command module landing. The VHF signal was lost by the uprange aircraft as expected; however, it was also lost by the Hawaii Rescue 6 aircraft for a period of 2 minutes.

Using the VHF recovery beacon bearings reported by Search 1 helicopter and Hawaii Rescue 5 and 6 aircraft prior to command module landing, it was determined that the command module had landed past the predicted landing point and was downrange of the primary recovery ship. This distance was later calculated to be 70 n. mi. Hawaii Rescue 6 aircraft homed on the VHF signal and had visual contact with the command module 26 minutes after landing. At first sighting, the command module was floating in the stable I attitude (upright) with the uprighting bags deployed and partially inflated. The uprighting bag deployment, the 2-minute loss of the VHF recovery beacon signal by the Hawaii Rescue 6 aircraft, and the large amount of water later found to be trapped between the heat shield and pressure hull indicated that the command module had been in a stable II flotation attitude (inverted) for a brief period. The HF antenna was bent near the base and lying over the side of the command module. The command module appeared to be normal in all other aspects. A parachute was sighted on the first two passes over the command module but was not seen again. The apex cover was not sighted.

Because the Recovery 3 helicopter with swimmers was enroute to the landing point, pararescuemen were not deployed from the Hawaii Rescue 6 aircraft. The Recovery 3 helicopter deployed the swimmers 1 hour 46 minutes after command module landing. The swimmers installed the flotation collar in approximately 11 minutes and then made preparations to stay with the command module until retrieval. U.S.S. Okinawa retrieved the command module 4 hours 12 minutes later (figs. 9.3-4 to 9.3-6). The retrieval point was 27 degrees 38 minutes North latitude, 158 degrees West longitude, which is 48 n. mi. from the nominal premission target point on a bearing of 284 degrees true. This position was determined by U.S.S. Okinawa using two loran rates and two celestial observations of the lower limb of the sun.

The weather conditions reported by U.S.S. Okinawa at the time of retrieval were:

Wind direction, deg true	40
Wind velocity, knots	19
Air temperature, °F	68
Water temperature, °F	71

Sea state	Waves	Swells
Height, ft	7	4
Period, sec	8	12
Direction, deg true	50	340

The following is a chronological listing of significant events that occurred during the recovery operation:

G.m.t., hr:min	Mission elapsed time, hr:min	Event
21:38	9:38	Predicted time of entry interface; S-band contact by Hawaii Rescue 1
21:39	9:39	Predicted time of beginning of S-band blackout
21:40	9:40	Radar contact by U.S.S. Carpenter
21:44	9:44	Predicted time of end of S-band blackout
21:46	9:46	S-band contact by Hawaii Rescue 4 and 5
21:47	9:47	S-band contact by Hawaii Rescue 6
21:51	9:51	Predicted time of main parachute deployment
21:53	9:53	VHF recovery beacon contact by Hawaii Rescue 5, Hawaii Rescue 6, and Search 1
21:56	9:56	Predicted time of command module landing
22:23	10:23	Visual sighting of command module by Hawaii Rescue 6 at 27°40'N, 157°59'W
23:43	11:43	Swimmers and flotation collar deployed from Recovery 3 helicopter
23:54	11:54	Flotation collar installed
03:55	15:55	Command module retrieval by U.S.S. Okinawa at 27°38'N, 158°00'W

9.3.3 Communications

Recovery forces used the S-band equipment, the two VHF recovery beacons, and the HF beacon to locate the command module during the entry and postlanding portions of the mission. The following table summarizes the signal reception by the recovery forces.

S-band equipment

Aircraft	Aircraft location	G.m.t. of signal acquisition, hr:min:sec	G.m.t. of signal loss, hr:min:sec
Hawaii Rescue 1	30°50'N 170°15'E	21:38:06	21:38:50
Hawaii Rescue 4	28°01'N 166°50'W	21:46:20	21:47:24
Hawaii Rescue 5	28°01'N 162°45'W	21:46:08	21:51:18
Hawaii Rescue 6	26°04'N 159°32'W	21:47:20	21:53:36

VHF recovery beacons

Aircraft	Aircraft location at signal acquisition time	G.m.t. of signal acquisition, hr:min:sec	Range of reception, n. mi.
Hawaii Rescue 5	28°55'N 162°26'W	21:53:20	250
Hawaii Rescue 6	26°57'N 159°13'W	21:53:38 [a]21:59:38	80
Search 1	28°44'N 159°16'W	21:53	95
Recovery 3	27°22'N 159°48'W	21:55	100

[a]The signal was lost at 21:57:38 and was reacquired 2 minutes later.

Because Hawaii Rescue 5, Hawaii Rescue 6, and the two Apollo range instrumentation aircraft operating in the area reported receiving only one of the VHF beacons, it is apparent that one of the VHF beacons was not operating. An investigation to determine which beacon failed has been initiated.

HF beacon.- The HF antenna failed shortly after landing. This is the last time the HF equipment is scheduled to be flown on Apollo spacecraft.

9.3.4 Spacecraft Postrecovery Inspection

The following is a summary of the postlanding operations:

Command module gas sample.- The purge port plug was released by 200 in-lb torque and a slight positive pressure was noticed when the plug was removed. No fumes were noticed when the plug was removed, but a short time after the unified side hatch was opened, a slight odor of nitrogen tetroxide was detected.

Unified side hatch opening.- The clockwise torque necessary to retract the shear pin was 30 in-lb, and the counterclockwise torque necessary to retract the latches was 110 in-lb. The hatch automatically opened 30 degrees after which time a force of 25 pounds was necessary to bring the hatch to the full-open position. After the hatch was opened, the gaseous nitrogen pressure in the counterbalance was 750 psi compared with the prelaunch pressure of 100 psi.

Emulsion spectrometer and radiation dosimeter removal.- At 12:30 G.m.t. on April 5, the upper radiation dosimeter register readout was 057.67 rads and the lower dosimeter register readout was 108.01 rads.

Data storage equipment and flight qualification recorder removal.- The data recorders were removed on April 5.

Environmental control system inspection.- During inspection, approximately 1 gallon of water (which has been determined to be sea water) was found on the floor of the command module.

Command module exterior inspection.- As expected, the aft heat shield was considerably charred, but the general appearance of the char structure was good. The extravehicular handles except for a slight discoloration, were essentially in preflight condition. The sea anchor attach fitting was chipped by abrasion of the flotation collar attachment lines. The unified side hatch appeared to be in preflight condition except for a slight amount of discoloration. The hatch window was fogged and some brown spots were found on the exterior. The side windows

were heavily fogged on the inside surface of the outer pane. All upper deck pyrotechnics were fired. With the exception of the bent HF antenna, the only upper deck damage noticeable was that the drogue mortar cans had been dented as usual by the recovery loop.

Water samples.- Approximately 2100 milliliters of potable water, a free hydrogen sample, and approximately 1600 milliliters of waste water were removed and forwarded to the Manned Spacecraft Center for analyses.

Uprighting system inspection.- Because the uprighting bags were deployed and partially inflated, they were removed aboard the recovery ship.

Antenna inspection.- The root clamp of the HF antenna was not engaged and the antenna was folded over near the base. Both VHF antennas were erected and locked.

Flashing light inspection.- The flashing light was erected and locked. The flash rate at retrieval (6 hours after landing) was 18 flashes per minute with an occasional irregular time period between flashes.

Onboard camera inspection.- The filter on the 70-mm camera had condensation approximately 1/4 to 1/8 inch wide around the inner edge.

9.3.5 Command Module Deactivation

The command module arrived at Pearl Harbor, Hawaii, on April 5, 1968, aboard U.S.S. Okinawa. At the deactivation site, the landing and safing team made an evaluation of the pyrotechnics and safed the normally unfired pyrotechnics in the reaction control system. Safing caps were installed on the oxidizer and helium dump squib valves, and the initiators and electrical leads were tagged. The conditions noted during deactivation were as follows:

a. High residual helium pressures were found in the fuel and oxidizer systems.

b. The B system fuel helium relief valve diaphragm was ruptured; a cap was placed over the relief valve bleed port to stop leakage.

c. The A system oxidizer helium relief valve diaphragm was ruptured; a cap was placed over the relief valve bleed port to stop leakage.

d. The electrical wiring was crossed on all of the reaction control system yaw engines; that is, the electrical wiring to the direct coils

on the oxidizer valves was connected to the fuel valves, and the wiring to the fuel valves was connected to the oxidizer valves.

e. Only residual quantities of propellant vapors were found in the reaction control system.

Deactivation was completed on the morning of April 8, 1968, and the command module was transported to Long Beach, California, by a C-133B aircraft. It arrived at the contractor's facility on the morning of April 9, 1968.

9.3.6 S-IC/S-II Camera Capsule Recovery

In addition to providing command module recovery support in the western portion of the continuous abort area, U.S.S. Austin was responsible for recovering the four S-IC camera capsules and the two S-II camera capsules that were to be ejected from the launch vehicle. To accomplish this, four helicopters were launched from U.S.S. Austin prior to lift-off (fig. 9.3-7). Two of the four were stationed approximately 15 and 30 n. mi. uprange of the ship near the predicted S-IC camera capsule impact points. The third helicopter was approximately 15 n. mi. downrange of the ship near the predicted S-II camera capsule impact points. The fourth helicopter was stationed over the ship and later proceeded to the S-II camera capsule area.

An EC-121 radar aircraft provided multiple-target impact point information, and an EC-121 Terminal Radiation Program aircraft provided photographic coverage of the S-IC booster descent.

Only one of the four S-IC camera capsules was recovered. At this time, it is believed that only one of the four was ejected because frame-rate telemetry data from three cameras was being received 25 seconds after normal ejection time. S-IC camera capsule 1 was recovered at 30 degrees 18 minutes North latitude, 74 degrees 13 minutes West longitude, at 12:27 G.m.t. on April 4. Only S-II camera capsule 2 was recovered. It was retrieved at 30 degrees 18 minutes North latitude, 72 degrees 57 minutes West longitude at 12:36 G.m.t. on April 4. Indications are that S-II camera capsule 1 ejected normally but sank shortly after impact. Both recovered capsules were slightly damaged in that several shrouds had torn the restraining tunnels on the paraballoon. In addition to the torn shroud tunnels, the S-II camera capsule had a broken lens (fig. 9.3-8) and a torn paraballoon skirt. The capsules were flown from U.S.S. Austin by helicopter at 10:55 G.m.t. on April 5 to Patrick AFB, Florida, for transfer to the Marshall Space Flight Center, Alabama.

There was some launch vehicle debris sighted in the area, but it sank shortly after impact and none was recovered.

9.3.7 Recovery Equipment

Prior to the mission, extensive training and equipment checkout were performed by Department of Defense recovery units. During the mission, all recovery equipment performed normally except that the first flotation collar installed on the command module would not stay inflated because of small slits in both the primary and backup tubes. This collar was removed and a second collar was installed. The second collar deflated shortly before retrieval after coming into contact with a sharp object on the hull of the primary recovery ship.

TABLE 9.3-I.- DEPLOYMENT AND TYPES OF RECOVERY FORCES

Area	Maximum aircraft access time, hr	Maximum ship retrieval time, hr	Type and quantity of recovery units	Description of recovery units
Launch site	0.25		LCU (1)	Landing craft utility (landing craft with command module retrieval capabilities)
			LVTR (2)	Landing vehicle tracked retriever (tracked amphibious vehicles with command module retrieval capabilities)
			CH-3C (2)	Helicopters with 3-man swim team
			HH-53B (2)	Heavy lift helicopters
			FSK (2)	Fire suppression kits with 2 firemen.
Continuous abort area	4	21	LPD (1)	Landing platform dock (helicopter carrier) U.S.S. Austin
			SH-3A (4)	Helicopters, three with 3-man swim teams and one photographic (camera capsule recovery)
			EC-121 (2)	One radar aircraft. One photo aircraft (S-IC booster descent)
			HC-130 (2)	Search and rescue aircraft with 3-man para-rescue team
			DD (1)	Destroyer, U.S.S. DuPont
			LST (1)	Landing ship tank, U.S.S. York County
Discrete abort area	3	8	AO (1)	Fleet oiler, U.S.S. Chikaskia
			HC-130 (1)	Search and rescue aircraft with 3-man para-rescue team

TABLE 9.3-I.- DEPLOYMENT AND TYPES OF RECOVERY FORCES - Concluded

Area	Maximum aircraft access time, hr	Maximum ship retrieval time, hr	Type and quantity of recovery units	Description of recovery units
Secondary landing area	4	48	DD (1)	Destroyer, U.S.S. Carpenter
			HC-130 (6)	Search and rescue aircraft with 3-man para-rescue team
Primary landing area	1	5	LPH (1)	Primary recovery ship. Landing platform helicopter, U.S.S. Okinawa
			SH-3A (7)	Helicopters, three recovery with 3-man swim team, one photographic, two for air control, one for communications relay
Contingency landing area	18	-	HC-130 (10)	Search and rescue aircraft with 3-man para-rescue team. (Includes 3 from launch abort areas and 2 from secondary areas)

Total: Fixed-wing aircraft 16
Helicopters 15
Ships 7

NASA-S-68-3632

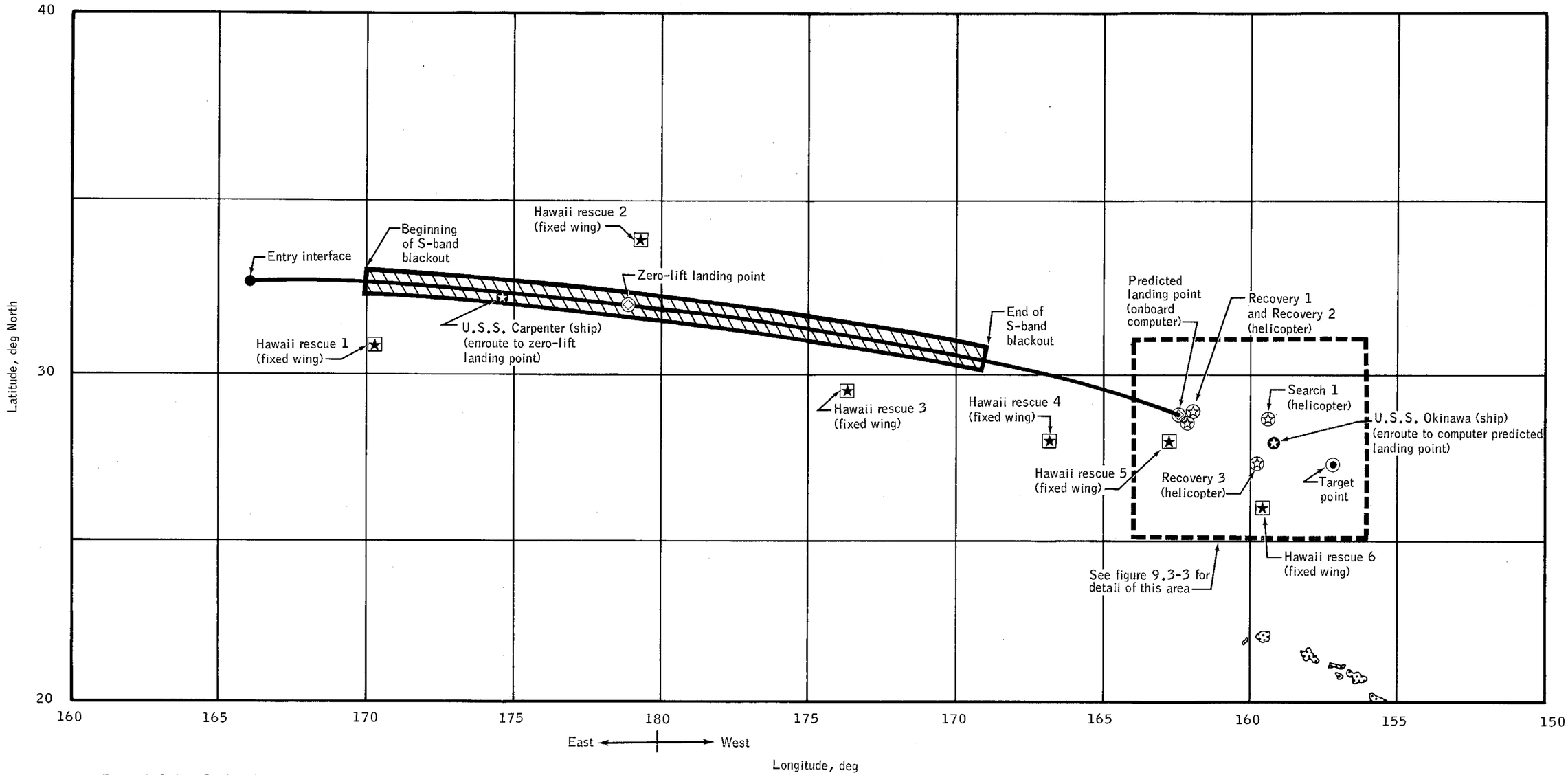

Figure 9.3-2.- Predicted entry trajectory and recovery force deployment.

Figure 9.3-2.- Predicted entry trajectory and recovery force deployment.

NASA-S-68-3631

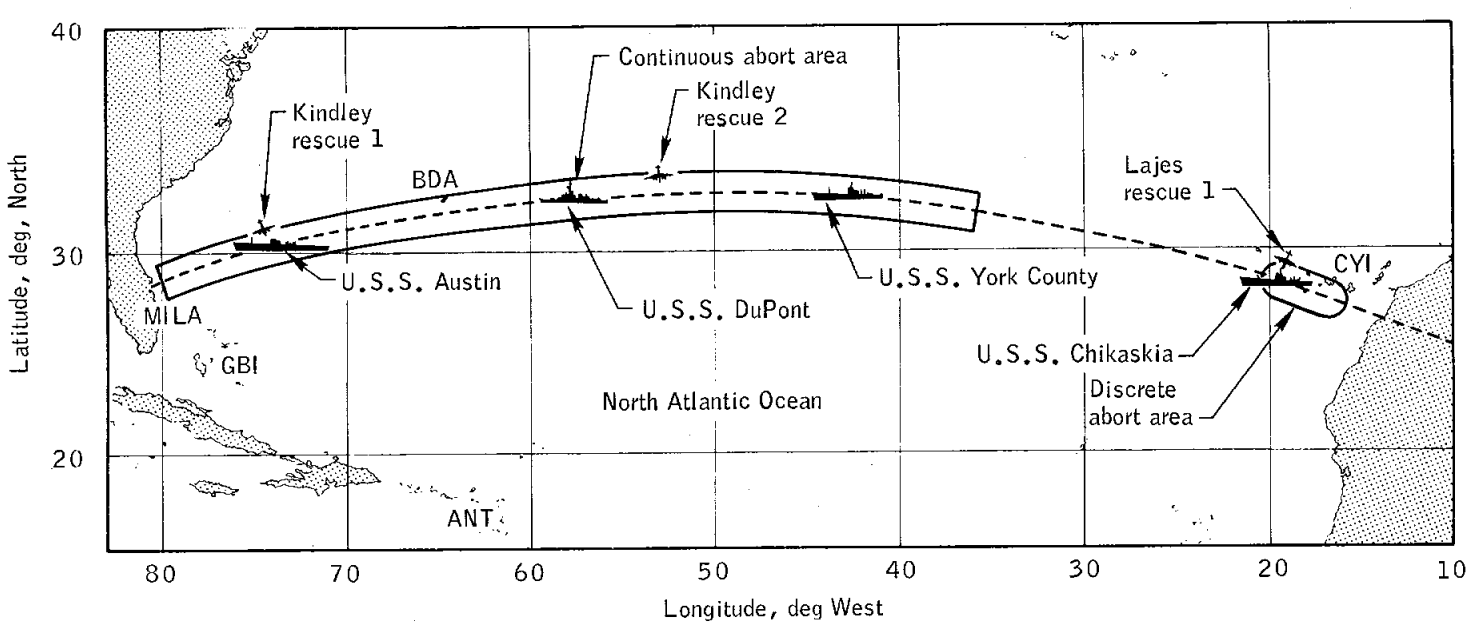

Figure 9.3-1.- Continuous and discrete abort areas and recovery force deployment.

NASA-S-68-3633

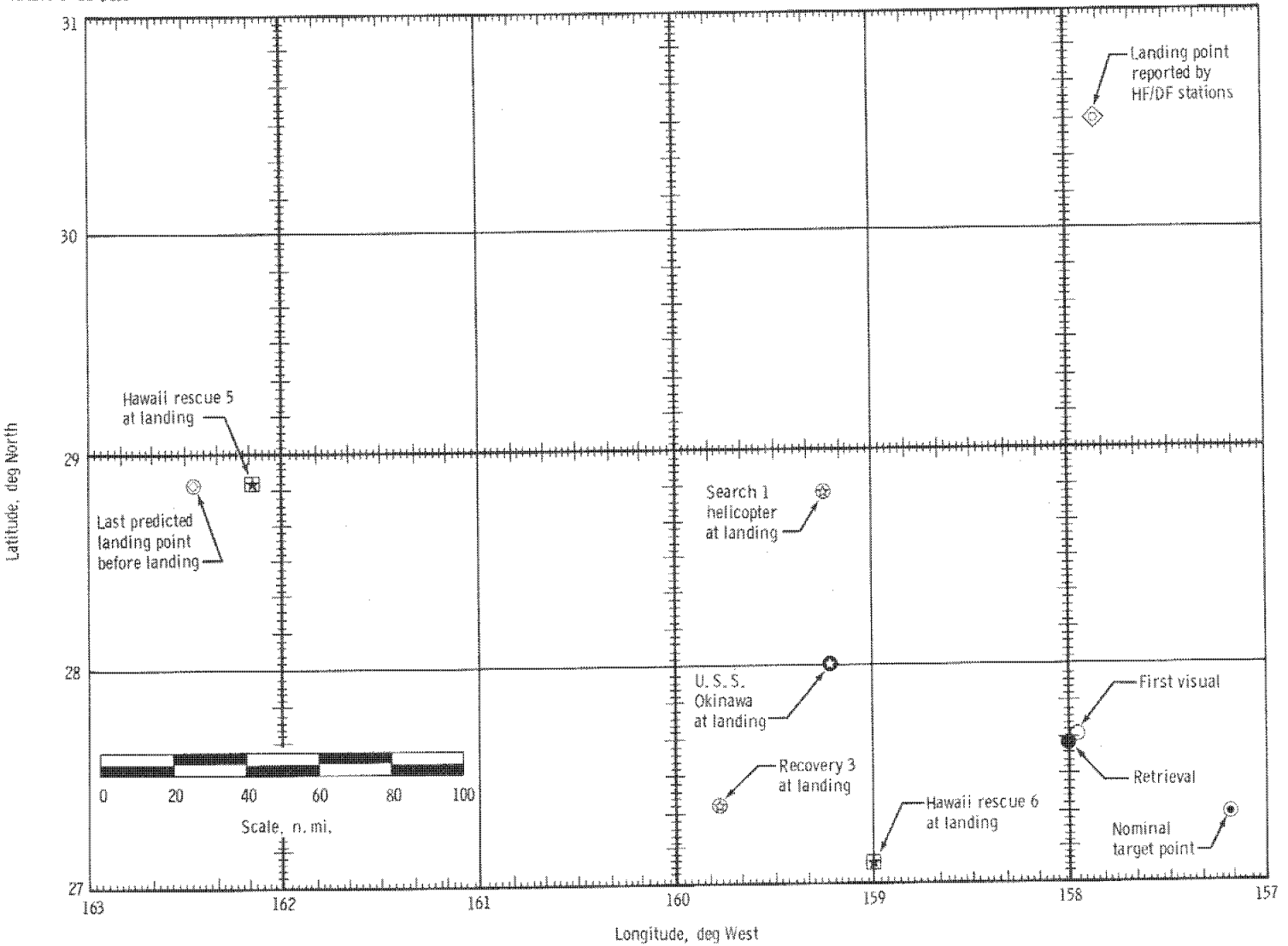

Figure 9.3-3. - Detail of landing area.

NASA-S-68-3634

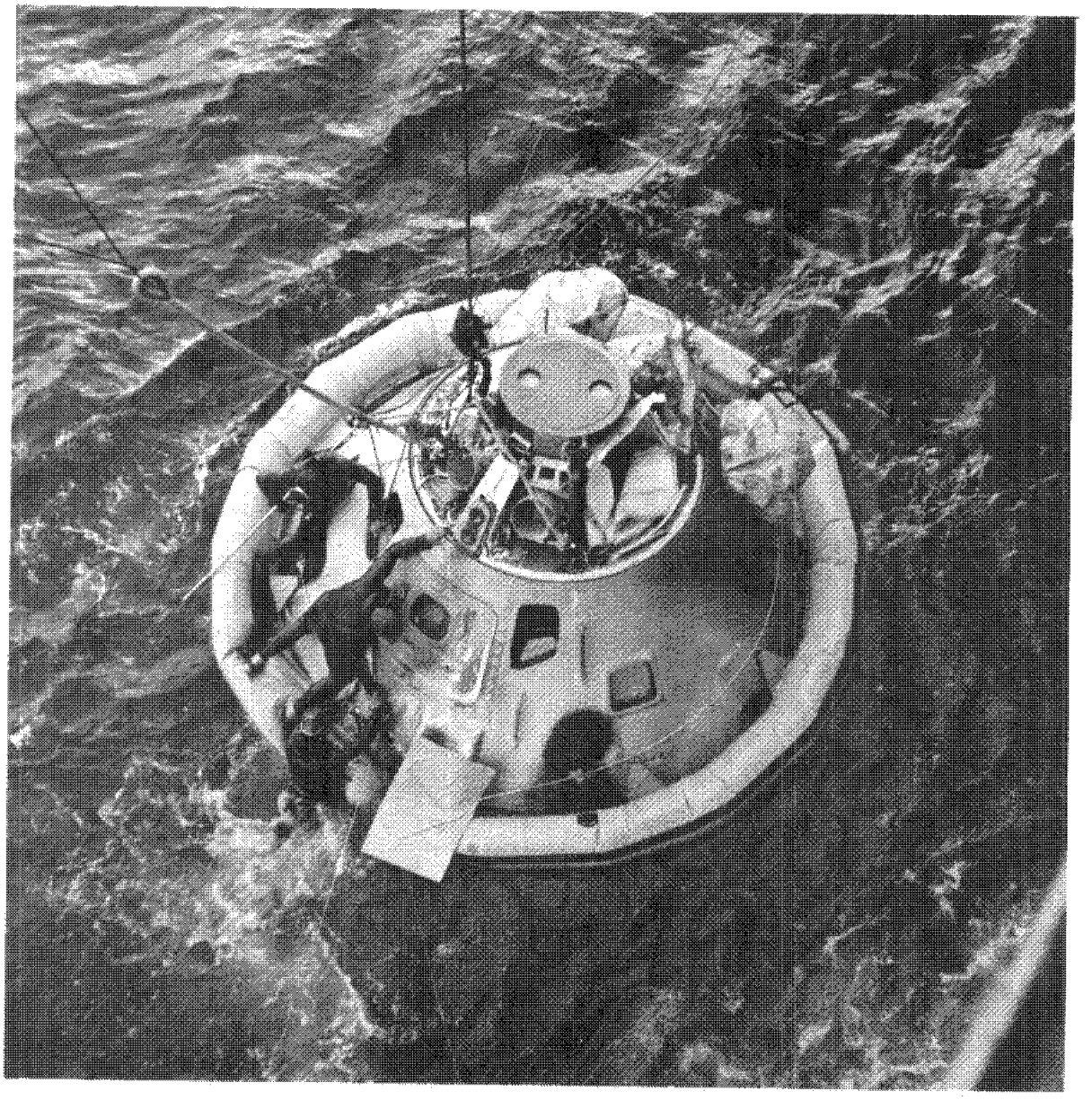

Figure 9.3-4.- Command module in flotation collar.

NASA-S-68-3635

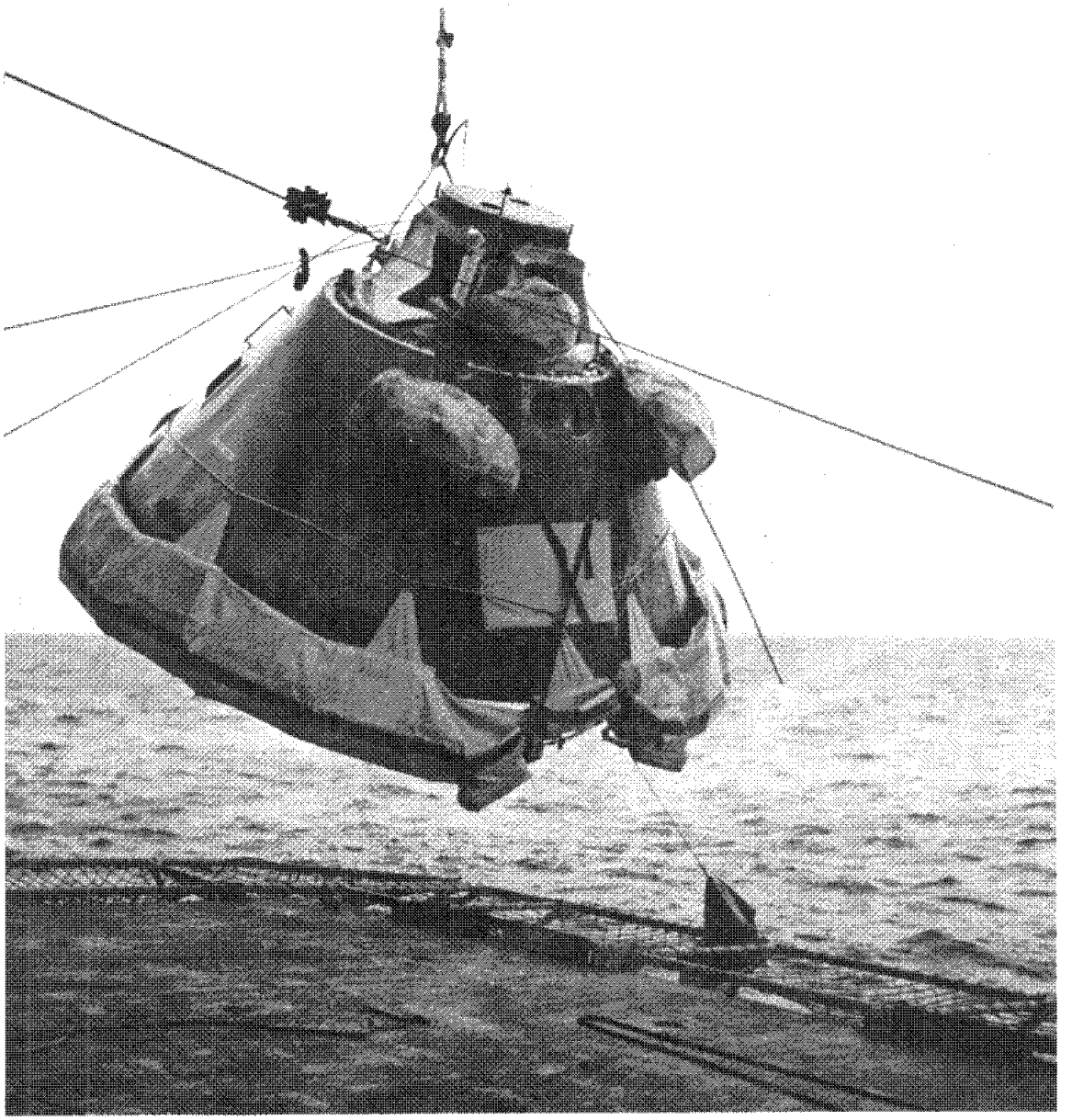

Figure 9.3-5.- Command module retrieval.

NASA-S-68-3636

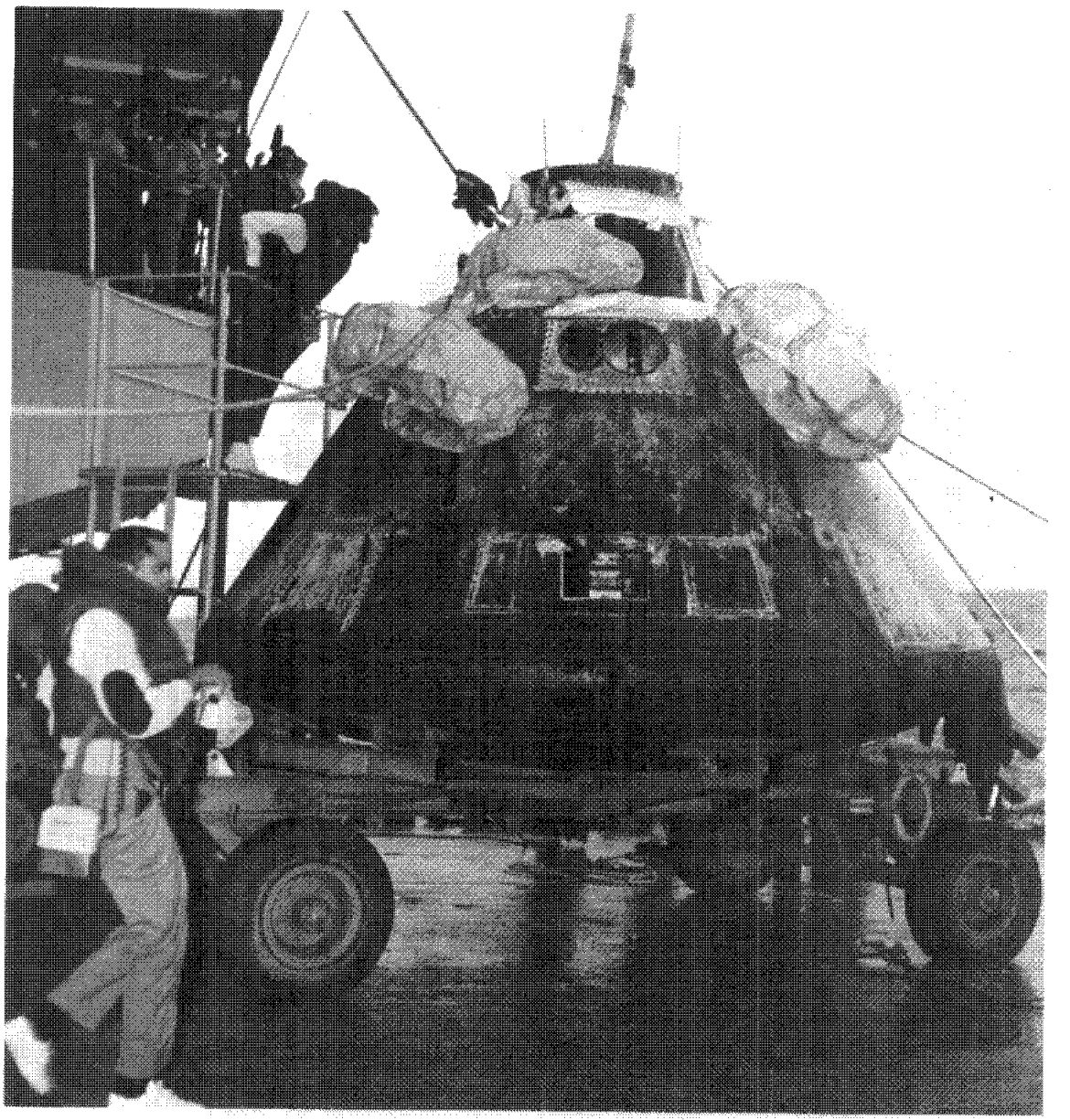

Figure 9.3-6.- Command module on dolly.

NASA-S-68-3637

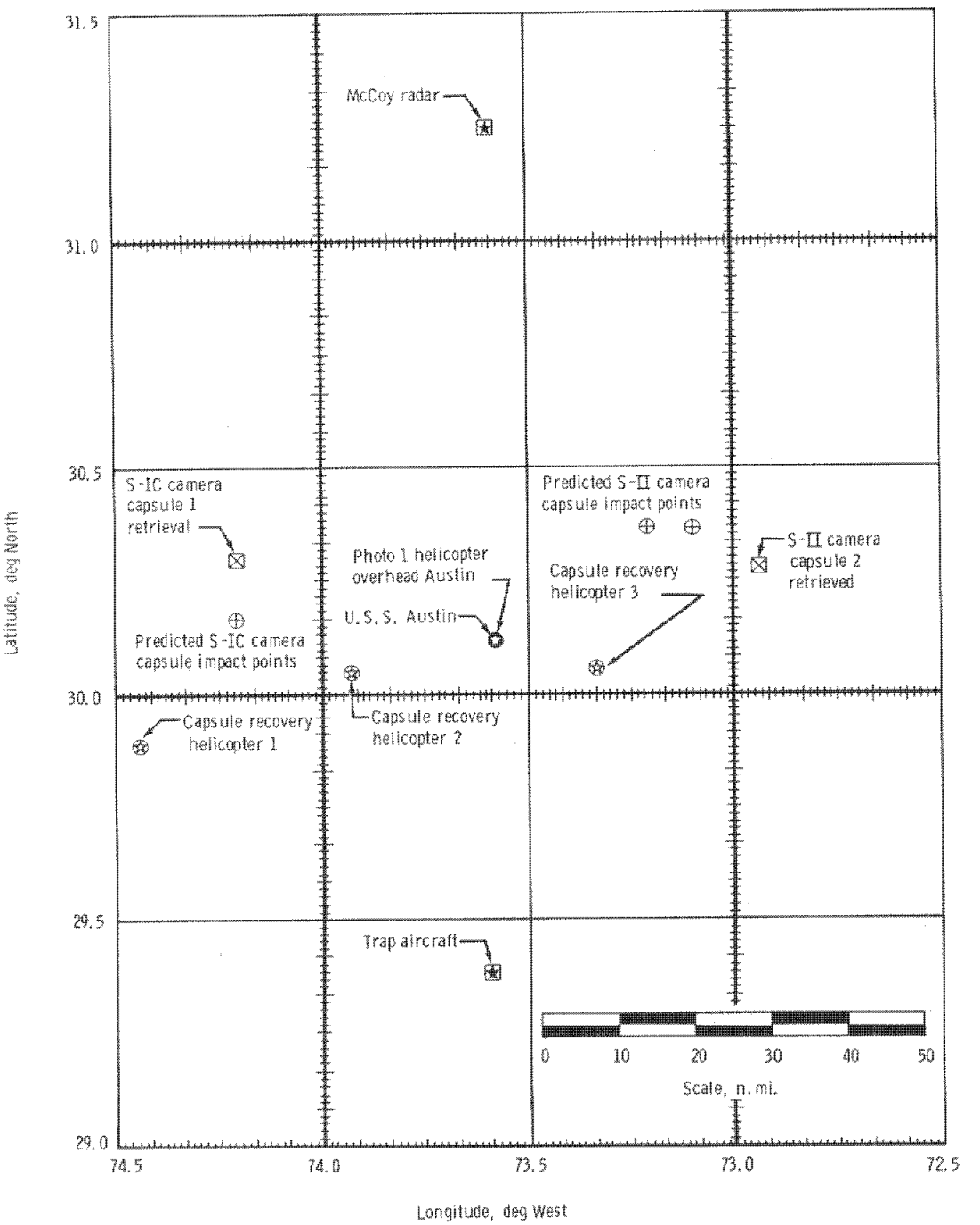

Figure 9.3-7. - Camera capsule landing area.

NASA-S-68-3638

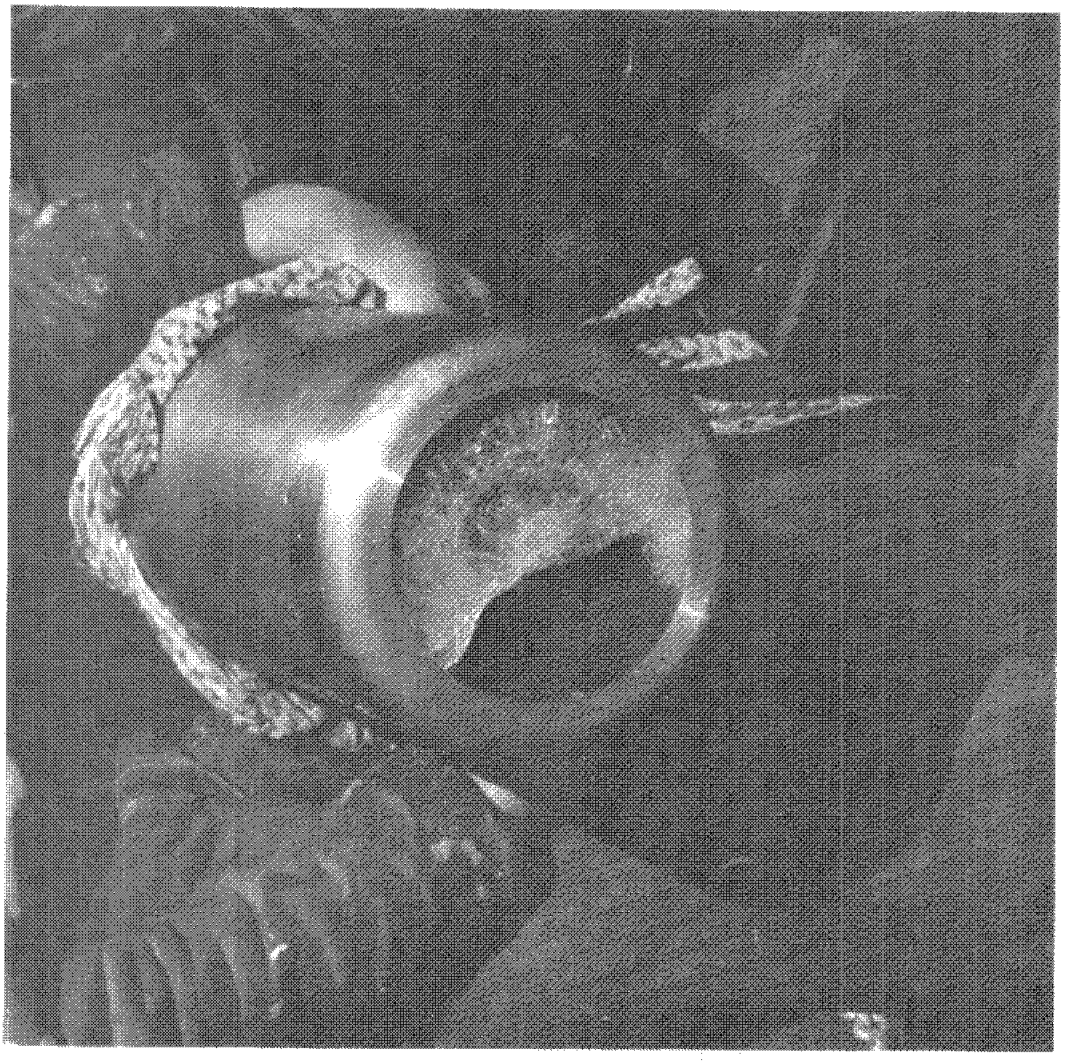

Figure 9.3-8.- S-II camera capsule showing damaged lens.

10.0 EXPERIMENTS

No experiments per se were assigned to this mission. However, for clarity, the earth photography and the radiation monitoring have been included in this section.

10.1 PHOTOGRAPHY

A 70-mm sequence camera was mounted onboard the Apollo 6 command module and took approximately 12 oblique and 358 vertical or near-vertical color photographs of the earth during daylight hours. The camera system was activated by a gravity switch set for 2.25g. The picture-taking sequence began at approximately 01:29:55, and the last photograph was taken at 03:18:27. An analysis of the camera operation from a system aspect is included in section 5.15. This photography was accomplished during the latter part of the first revolution, during the second revolution, and during the first part of the third revolution at altitudes ranging between 96 and 160 n. mi. The ground swath of the photographic coverage varied between 72 and 120 n. mi. with an exposure interval between frames of approximately 8.6 seconds. This interval produced a 54 to 75 percent forward overlap of individual frames, which is satisfactory for stereoscopic viewing. Photographs were taken across the United States, the Atlantic Ocean, Africa, and the western Pacific Ocean, and the scale ranged between 1:2 300 000 and 1:3 900 000. The haze-penetrating capability of the film-filter combination provided a better color balance and a higher resolution than those obtained on previous Mercury and Gemini missions.

10.2 RADIATION MONITORING

The principal radiation field measured during the mission was the inner high-intensity Van Allen radiation belt located at geodetic altitudes ranging between 500 and 6000 n. mi. at the equator and between 45 degrees North latitude and 45 degrees South latitude. This radiation field was measured by the radiation instrumentation during ascent to and descent from apogee. An interference problem during descent from apogee prevented real-time observation of the data; however, the information was recovered by postflight data reduction. The outer high-intensity Van Allen radiation belt was penetrated during the 12 000 n. mi. elliptic orbit; however, the dose contribution was not significant because of the shielding effect of the command module structure. The principal particles in the outer belt are high-energy electrons that do not exhibit the penetrative capabilities of the high-energy protons in the inner belt.

Four radiation monitoring instruments were included in the command module. These were two Van Allen belt dosimeters (located in a single unit), an integrating radiation dosimeter, and two nuclear emulsion spectrometers. The Van Allen belt dosimeters, mounted on the girth shelf under the right-hand window, were designed to measure skin and depth dose rates. The output (0 to 5 volts) of the two measurement systems represented five decades of dose-rate information in two overlapping ranges. A third measurement, the range sensor, had four dc levels to indicate the range (high or low) of each of the two dose-rate outputs. The integrating radiation dosimeter, mounted on top of the battery support, consisted of two personal radiation dosimeters for measuring integrated skin and depth dose. The nuclear emulsion spectrometers, which provided radiation spectrum and dose information, were located under the integration radiation dosimeter in the right-hand equipment bay.

A postflight evaluation of the four instruments indicated that the instruments were operating properly. The flight measurements closely correlated with the expected data. No definitive data are as yet available from the nuclear emulsion spectrometers. The integrating radiation dosimeter measured an integrated skin dose of 1.31 rads and an integrated depth dose of 0.9 rad.

During ascent to high apogee at a geodetic altitude of approximately 1300 n. mi., the Van Allen belt dosimeters measured peak dose rates of 3.8 rad/hr and 2.4 rad/hr for the skin and depth doses, respectively (fig. 10-1). During descent from high apogee, the skin and depth outputs switched range intermittently before the voltage outputs reached the preset switch points, and the data were questionable. The switching anomaly occurred in isolated instances during the ascent to apogee but not frequently enough to be a problem. This anomaly is discussed in section 12.0.

NASA-S-68-3639

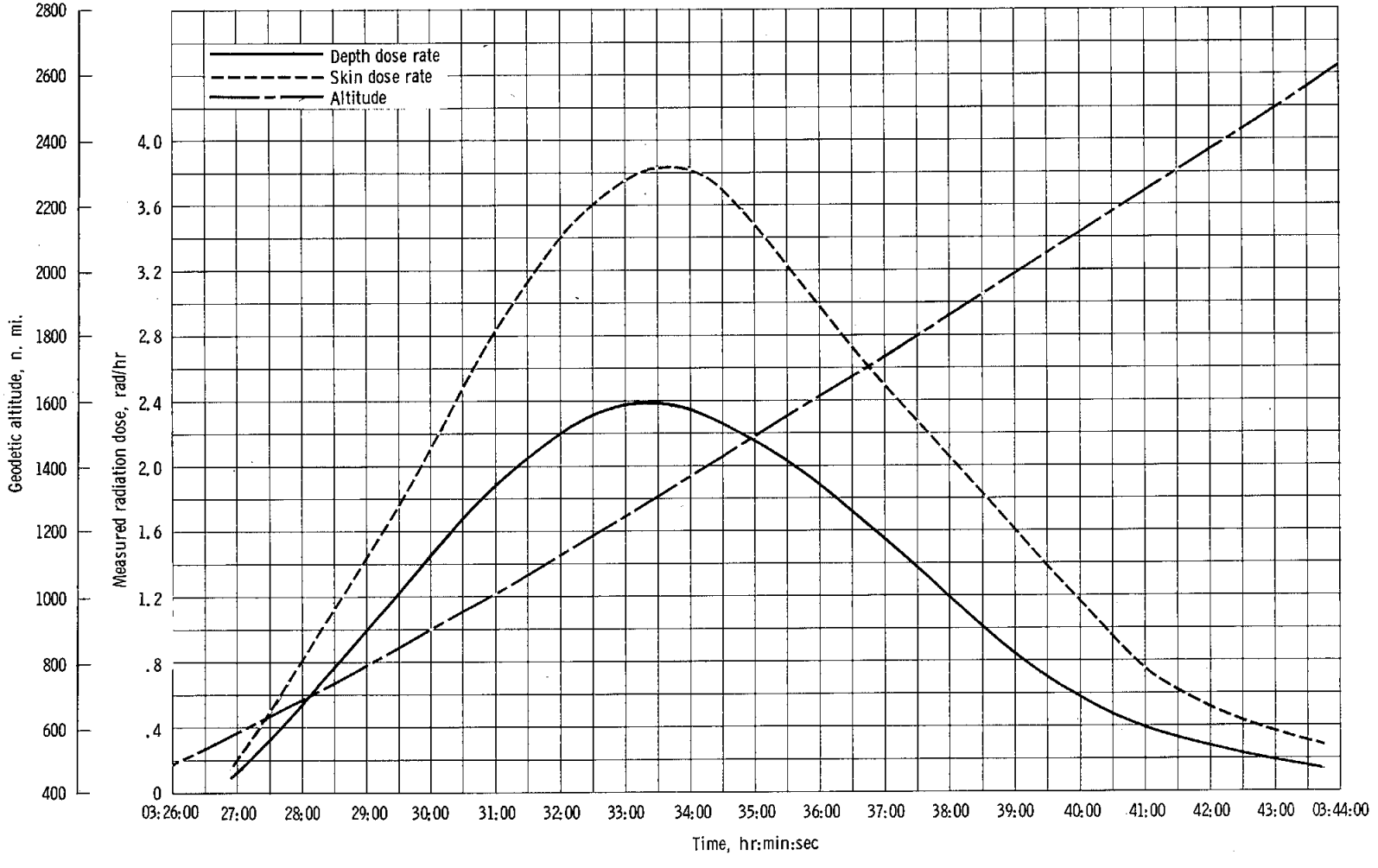

Figure 10-1. - Van Allen dosimeters measured dose rates compared with geodetic altitude during the ascent to apogee.

11.0 CONCLUSIONS

1. An as-yet-unexplained structural anomaly occurred during the boost phase of flight. This anomaly is attributed, at present, to larger-than-design launch-vehicle-induced oscillations.

2. Performance of the spacecraft systems was excellent. There was no evidence of any functional anomalies that affected the mission.

3. Performance of the emergency detection system, operating in a closed-loop mode, detected a single abort vote during the period of time (00:02:13) of the spacecraft structural problems. This one vote may have been caused by breaking one of the three wires between the instrument unit and the command module. Two votes would have been required before the abort sequence was initiated.

4. In the successful completion of the alternate mission, the command and service modules demonstrated the ability to withstand and adapt to adverse conditions and environments.

5. The service propulsion system engine firing duration of 442 seconds exceeded any known lunar mission requirements for this system, except for an abort after the translunar injection maneuver.

6. The block II unified side hatch on the command module withstood the launch, orbital, and entry environments and satisfactorily performed its functions. As a result, the unified side hatch is considered qualified for manned flights.

7. Large errors in the range data from the Ascension C-band radar caused large errors in the orbit determination of the vehicle. Similar range errors in these data were also noted during the Apollo 4 and Apollo 5 missions.

8. Vibration levels of the service module helium pressurization panel, the service module aft bulkhead, and the LTA-2R oxidizer tank exceeded the expected mission levels in narrow frequency bands.

9. The 49.2-n. mi. landing point miss distance resulted from off-nominal entry conditions which were beyond the design of the computer program.

10. The first demonstration of the uprighting system following space flight resulted in the command module properly returning to the stable I position from the stable II position.

11. There was no indication of interference between the apex cover and the negative pitch engine as occurred on the Apollo 4 mission when the cover was ejected.

12. The orbit during the coast ellipse was noticeably perturbed by the water boiler venting. This effect, but with greater magnitude, was also noticed during the Apollo 4 mission.

13. The actual cabin heat loads of 5400 Btu/hr compared favorably with the predicted values of 5350 Btu/hr.

14. The flight control operation and transfer of data were satisfactory, although this was the first mission in which the entire Manned Space Flight Network was remoted.

15. The frequency and amplitude of the vibration experienced during the Apollo 6 launch phase were much higher than the normally expected levels and were the most severe experienced on any Apollo flight.

12.0 ANOMALY SUMMARY AND POSTFLIGHT TESTING

12.1 ANOMALY SUMMARY

Analyses of the Apollo 6 mission results have disclosed 10 anomalies. There were no countdown anomalies. None of the anomalies discussed in the following paragraphs had any apparent effect on the mission. A separate report will be prepared for each anomaly.

12.1.1 Transfer of Essential AC Loads From Bus 1 to Bus 2

Statement.- The essential-load transfer circuit transferred essential nonredundant loads from ac bus 1 to ac bus 2.

Discussion.- The essential load transfer occurred at 03:14:31.4. Postrecovery checks of the command module showed that circuit breaker 100 on panel 22, which should have been closed, was open. This circuit breaker supplies phase A power from ac bus 1 to the oxygen and hydrogen cryogenic tank 1 fans in the service module. A short in this circuit would reduce the voltage and cause the ac bus 1 undervoltage sensor to trip, resulting in an essential-load transfer.

Conclusion.- Postflight tests have verified that no short exists in the circuit from the circuit breaker to the command module/service module umbilical circuit interrupter; therefore, it has been concluded that a short occurred in the cryogenic fan circuit in the service module. This short resulted in an undervoltage that initiated the switching of ac loads. The most probable cause was a single-phase short to ground in the fan motor.

Corrective action.- The block II cryogenic tank fans have been redesigned to ensure greater reliability. These fans have also been designed to operate on two out of three phases. In addition, for CSM 103, 104, 106, and subsequent vehicles, the fans in all four cryogenic tanks (eight fans) will have individual fuse protection in each phase of the motor. Consequently, failure of one fan motor will not cause an open circuit breaker for all four fans.

Mission effectivity.- Redesigned fans are to be used for all subsequent manned missions. Additional fuses will be used for each ac power phase in CSM 103, 104, 106, and subsequent vehicles.

Impact on next mission.- Because the redesigned fans will be used, this anomaly will have no impact on the next mission.

12.1.2 Erratic Data

Statement.- Data from PCM, certain flight qualification, and service module high-level commutator measurements were erratic. In addition, timing anomalies were noted in the central timing equipment and in the 4-second timer for the flight qualification tape recorder.

Discussion.- During the launch phase from 00:01:28 to 00:08:20, and during portions of the third revolution, the quality of the data from several sources was degraded. Listed are the equipment and data which were affected.

a. The PCM data cycled between good and bad at a 1-Hz rate during most of launch phase. Data were sporadically bad during the third revolution.

b. The operation of the 4-second timer for the flight qualification tape recorder became erratic at approximately 00:01:28 and remained so until recorder shutdown. Timer operation was normal during entry.

c. Operation of the high-level commutator 2 in the service module became erratic at approximately 00:01:28 and remained so until first recorder shutdown. After the recorder was turned on for the entry phase, the operation appeared normal for the approximate 1-second period until command module/service module separation.

d. Several analog measurements recorded by the flight qualification tape recorder became noisy between 00:01:28 and the time of recorder shutdown; however, the measurements appeared normal at the time of recorder restart.

e. The central timing equipment jumped 2 minutes at 00:02:25.6 and performed erratically thereafter.

Conclusion.- The cause of the erratic data is unknown. Postflight tests have failed to duplicate the problem.

Corrective action.- Any corrective action is pending completion of postflight tests and analyses.

Mission effectivity.- The mission effectivity is dependent on the corrective action to be implemented.

Impact on next mission.- The impact on the next mission is pending the results of the postflight tests and analyses.

12.1.3 Computer Update Rejections

Statement.- An excessive number of computer update alarms occurred during the mission; the alarms occurred with and without ground uplink activity in progress.

Discussion.- The computer uplink alarms indicated failure of the uplink word validity check (K$\bar{K}$K) that the computer makes before accepting data. The pattern of these alarms indicated that the problem became more severe as the flight progressed; however, no correlation with mission events that would explain this increase in severity has been found.

The fact that numerous CLEAR commands were processed indicated that the computer was performing as programmed. The alarms occurred with and without ground update activity, which indicated that extraneous bits were introduced into the computer input register.

Conclusion.- The available evidence suggests that noise pulses were being impressed on the input wires to the guidance computer. The specific conditions required to generate noise transients are under investigation. This investigation has included postflight testing of the command module with the computer powered-up alone and with other systems powered-up in a sequence to simulate flight conditions. S-band updates have then been sent, and real-time commands entered, but no update problems have occurred during these tests.

Corrective action.- Any corrective action is contingent upon the results of the investigation.

Mission effectivity.- The mission effectivity will be determined by the corrective action.

Impact on next mission.- The impact on the next mission is contingent upon results of the tests.

12.1.4 Excessive Cabin-to-Ambient Differential Pressure

Statement.- The differential between the cabin and ambient pressures reached approximately 9.4 psid; the maximum allowable is 8.6 psid.

Discussion.- The 15.7 psia cabin pressure began relieving at 00:00:52, as expected, and stabilized at 6.0 psia by 00:08:30. The expected maximum differential pressure between cabin and ambient was 6.2. This differential was exceeded between approximately 00:00:52 and 00:02:40, and reached a maximum value at approximately 00:01:30.

Conclusion.- Any conclusion is contingent upon results of the postflight test.

Corrective action.- The corrective action is contingent upon the results of the postflight test.

Mission effectivity.- Any required corrective action will be incorporated for all subsequent missions.

Impact on next mission.- The impact on the next mission is contingent upon the results of the postflight test.

12.1.5 Oxygen Check Valve Failure

Statement.- The command module oxygen surge tank pressure varied in phase with the oxygen storage tank pressure; however, because of check valve action, the surge tank pressure should have remained constant or indicated a slight decrease.

Discussion.- The two oxygen storage tanks in the service module were separated from the oxygen surge tank in the command module by check valves. The oxygen storage tank pressures and the surge tank pressure would cycle in phase if one of the oxygen check valves failed to seat properly. There is a history of this type of failure on block I check valves. Because there was no failure in any other portion of the system, this anomaly did not adversely affect the environmental control system performance.

Conclusion.- One or both of the oxygen check valves failed to seat properly. A postflight test will determine whether the failure is similar to those experienced with other valves of this type.

Corrective action.- The block I check valve seating is accomplished by a diaphragm operated by differential pressure. For block II valves, the diaphragm seating has been reinforced by the addition of a spring.

Postflight test results will be compared with block II redesign to ensure that failure will not recur.

Mission effectivity.- The corrective action is applicable to all subsequent missions.

Impact on next mission.- The impact of this anomaly on the next mission is contingent upon results of the tests.

12.1.6 Unexpected Structural Indications During Launch Phase

Statement.- At approximately 00:02:13, abrupt changes of strain, vibration, and acceleration measurements were indicated in the S-IVB, instrument unit, adapter, lunar module, and command and service module; photographs showed objects coming from the area of the adapter.

Discussion.- The instrumentation indications of this anomaly were supported by photographic coverage from cameras on the ground and in aircraft. Within 0.3 second, darkened areas appeared approximately 180 degrees around the adapter in the center third of the adapter surface. Strain gage measurements on the 16 lunar module support struts and on 8 of the S-IVB forward skirt stringers showed a shift in the inertial load balance. Coincident with the photographic and strain gage changes, other dynamic indications, such as vibrations, accelerations, and angular rates, were observed.

Conclusion.- A task team is analyzing data from all sources to determine the events and the cause of the events. No definite conclusion can be drawn from the analysis to date.

Corrective action.- Any corrective action is contingent on the results of the data analyses.

Mission effectivity.- Any corrective action will be applicable to all subsequent missions.

Impact on next mission.- The impact on the next mission is contingent upon the results of the analyses.

12.1.7 VHF Beacon Operations

Statement.- The recovery forces reported that either the VHF recovery beacon or the survival beacon was not operating.

Discussion.- The recovery helicopters reported that both VHF beacon signals were received, but the other monitoring aircraft reported only one beacon was operative; both beacons operate on the same frequency.

Conclusion.- During postflight tests, both beacons have operated.

Corrective action.- The corrective action is contingent on further data analysis and postflight tests.

Mission effectivity.- The mission effectivity will be determined by the required corrective action.

Impact on next mission.- The impact on the next mission is contingent upon results of the analysis and tests.

12.1.8 Erratic Dosimeter Measurements

Statement.- During passage through the Van Allen radiation belt, two dose-rate measurements of the Van Allen belt dosimeter randomly switched between low range and high range.

Discussion.- Range switching occurred infrequently during ascent to the high ellipse apogee, but occurred often during the descent from the apogee; range switching normally occurs when a dosimeter senses a radiation level in excess of the low range and the output exceeds the preset switching point of approximately 4.7 volts. This anomalous switching began when the minimum dosimeter output was 1.9 volts, indicating that electrical noise with a maximum positive amplitude of 2.8 volts was superimposed on the measurement output.

Postflight testing of the dosimeter equipment with other spacecraft systems revealed electrical noise present on the output signal of one of the dosimeter measurements with sufficient amplitude to cause the switching anomaly. This noise was not observed on the output of the other dosimeter measurement. The source of this noise was indicated to be a cross-coupling effect between the inertial measurement unit sine angle measurement and the dosimeter measurement, which are sampled by the same PCM data system sequencer gate. This noise was observed on the engine valve actuation tank pressure measurement but was not observed on the measurement inputs to the PCM data system.

Conclusion.- Additional postflight tests are being conducted to resolve this noise problem and to determine its relationship to the dosimeter switching anomaly.

Corrective action.- Any corrective action is contingent upon postflight testing of the PCM data system and the dosimeter.

Mission effectivity.- If the resulting corrective action is applicable to the dosimeters, it will be effective for any manned mission that penetrates the Van Allen radiation belts.

Impact on next mission.- This anomaly has no effect on the next (earth-orbital) mission.

12.1.9 Crosswiring of Command Module Reaction Control System

Statement.- The electrical wiring connections to the fuel valves and to the oxidizer valves of the plus and minus yaw engines of the command module reaction control system were crossed.

Discussion.- During the postflight deactivation procedures, the connector for wiring to the engine valves was removed from the reaction control system control box and reconnected to ground support equipment. When the minus yaw fuel valves, and subsequently the plus yaw fuel valves were opened, a brownish red vapor cloud and liquid droplets, indicative of oxidizer, were observed. Similarly, fuel was observed when the oxidizer valves were activated. No known changes had been made to the ground support equipment since the control system deactivation of the Apollo 4 command module.

Conclusion.- A postflight test has verified that the electrical wiring to the fuel and oxidizer valves of all yaw engines of the command module reaction control system were crossed.

Corrective action.- The corrective action is yet to be determined.

Mission effectivity.- Any corrective action will be effective for all subsequent missions.

Impact on next mission.- This anomaly will have no impact on the next mission.

12.1.10 Service Module Reaction Control System Quad C Temperature Decrease

Statement.- Low-temperature excursions of the clockwise roll engine injector head of quad C was indicated in the service module reaction control system.

Discussion.- During the cold-soak period, the service module reaction control system exhibited rapid, continuous excursions in the indicated temperature of the clockwise engine injector, quad C. During four intervals between 03:45:10 and 05:32:15, the indicated temperature decreased rapidly and several times dropped below the lower limit of the instrumentation (0° F).

The data indicated temperature decrease rates of as much as 20° F per second, and rise rates of as much as 10° F per second. Because of the rate of thermal fluctuation and the mass of the injector, this

phenomenon could not have resulted from an internal injector problem such as a propellant valve leak through the injector. The PCM data have been verified to be accurate.

Conclusion.- At this time, there is no conclusion relative to this anomaly.

Corrective action.- Any corrective action is pending the results of further analyses.

Mission effectivity.- The corrective action will be effective for all subsequent missions.

Impact on next mission.- The impact on the next mission is still to be determined.

12.1.11 CSM/S-IVB Separation Transient

Statement.- A pitch body rate transient equivalent to a disturbance torque of approximately 900 ft-lb occurred at separation of the CSM from the S-IVB.

Discussion.- The pitch transient at separation was 1.7 deg/sec over a 0.1-second period and contained a momentary reversal 0.04 second after initiation. The transients in roll and yaw were less than 0.5 deg/sec. The service module plus X control engines were operating at that time with attitude control inhibited. The pattern of disturbance torques appeared normal after the initial transient, thus indicating proper engine operation. A pitch excursion in phase with the CSM was also present in the S-IVB/instrument unit at that time. A sharp reversal occurred at 03:14:22.92, 0.07 second after separation, indicating that the motion of two vehicles was coupled at least until that time.

Conclusion.- The most likely cause of the transient appears to be a momentary physical hangup at the adapter/service module interface.

Corrective action.- The corrective action is contingent upon further analysis and a final conclusion.

Mission effectivity.- The mission effectivity will be determined by the required corrective action.

Impact on next mission.- Unknown at this time.

12.1.12 Internal Shorting of Entry and Postlanding Batteries

Statement.- During postflight tests, it was discovered that one auxiliary battery was completely discharged and that four other batteries appeared to have internal shorts.

Discussion.- One of the eight entry and postlanding batteries exhibited abnormal voltage during discharge of residual capacity. Four other batteries, when recharged, failed to achieve nominal-charge voltages or to maintain nominal open-circuit voltage after the recharging was concluded. These occurrences are indicative of shorted cells. Disassembly and inspection confirmed that each of the defective batteries contained several shorted cells; no manufacturing defects were noted. A heavy deposit of silver was observed in the separator material, as well as traces of zinc sludge between the separator layers; both these chemical changes would result from overcharging. A review of the preflight data revealed that the batteries had been overcharged.

Conclusion.- The battery failures were caused by shorted cells as a result of overcharging.

Corrective action.- The procedure for battery charging will be revised to limit the charge input.

Mission effectivity.- The corrective action is applicable to all subsequent missions.

Impact on next mission.- This anomaly will have no impact on the next mission.

12.2 POSTFLIGHT TESTING

The command module arrived at the contractor's facility in Downey, California, on April 9, 1968, after deactivation of the reaction control system and pyrotechnic safing in Hawaii. Postflight testing and inspection for evaluation of command module performance and the investigation of irregularities are being conducted at the contractor's and vendors' facilities and at the Manned Spacecraft Center. The anomaly testing is being conducted in accordance with the approved Apollo Spacecraft Hardware Utilization Requests (ASHUR's) listed in table 12-I. The testing and inspections are described in the following paragraphs and the results are discussed in the appropriate sections of this report.

12.2.1 Heat Protection

Ablator core samples were cut from selected areas of the aft heat shield for evaluation of entry effects. The core samples will be sectioned and the char depth and surface recession analyzed. The ablator test panels located at the simulated block II umbilical and left side window were removed and forwarded to the Manned Spacecraft Center for analysis. The astrosextant passive thermal protection observed during inspection of the heat shields:

a. Pieces of char had been broken off the aft heat shield in the stagnation area after the heating period. This was attributed to water impact and recovery operations.

b. In several locations on the aft heat shield, the char in the splice gaps was eroded to a depth of approximately 0.5 inch. Core samples will be analyzed.

c. One unfilled cell was found in the aft shield ablator. Individual cells and small repair plugs popped out to a depth of 0.5 inch, probably during or after landing.

d. The asymptotic calorimeter on the aft heat shield toroid at 180 degrees on the maximum diameter was missing and was possibly dislodged by the recovery flotation collar.

e. The outer ablator at the downstream side of the astrosextant was charred. The inner ablator and primary thermal seal were discolored.

f. The S-band antenna at 225 degrees was chipped.

g. The unified side hatch, extravehicular activity handholds, air and steam vents, sea anchor attach ring, urine dump nozzle, and windows showed little or no effects of heating.

h. The cavities between the aft heat shield tension-tie bolt insulators and holes in the compression pads were not completely filled with the RTV coating.

Approximately 20 gallons of sea water were drained from between the inner structure and the aft heat shield; however, additional water remained in the insulation. Also, about 57 gallons of water had been previously removed during the deactivation procedures.

12.2.2 Earth Landing

A visual examination showed that all earth landing system elements functioned as required. There were no marks on the vehicle or external equipment to indicate any abnormal operation. Minor powder marks were noted on the exterior of the main parachute retention flaps adjacent to the minus pitch reaction control engines. Neither the forward heat shield nor any of the parachutes were recovered.

12.2.3 Mechanical

A visual inspection of the uprighting system indicated that all functions were performed as required. Inspection of the deployed uprighting bags did not reveal any irregularities. The unified side hatch appeared to be in very good condition and showed little effect of heating. Seals were found intact with no damage. Gaps between the unified side hatch adapter frame and the basic structure were measured and in some cases, were found to exceed design tolerance limits. The hatch-latching mechanism operated smoothly and within specification limits. The force required to open the hatch was 40 to 45 pounds with 600 psig in the counterbalance. A force of 25 pounds was required following landing after the hatch had automatically opened 30 degrees. The hatch will be subjected to a functional test.

12.2.4 Electrical Power

The batteries were removed and subjected to load tests. Auxiliary battery 2 was completely discharged. The battery wiring was checked and was found to be normal.

The following observations were made during inspection of the electrical wiring:

a. At frame 7, on the right-hand side of the dummy umbilical, the coaxial cable (V16-717106-21) protective wrapping was cracked inside the clamp.

b. Four electrical connectors (C28AR35, C28AR36, C20AR300, and C28AR401) between aft compartment frames 12 and 13 were loose at the receptacle interface. The O-ring installation will be inspected.

c. Pyro connector P51 on the upper deck had a broken ceramic insert.

d. On the upper deck, the conformal coating on terminal board 13 was broken at the top of terminal 7.

e. There were approximately 25 damaged wires in the umbilical area, most of which had exposed conductors. There was no evidence that the damage had been caused by flight conditions.

f. On the inner face of the umbilical cover, the potting was scorched at the left side of the umbilical wire exit and discolored at the right side.

g. The edges were broken or corroded at the rear of connector shell J234.

h. Wire restraints were pulled loose throughout the aft heat shield instrumented area.

i. The black phenolic flange inside the shell at the connector face had pieces broken off at six electrical plugs (P419, P421, P422, P423, P425, and P428).

j. Corrosion, probably caused by sea water, appeared to have penetrated through connector shell P426.

k. There were blackened areas on multiconductor shielded non-jacketed cables throughout the heat shield instrumented area.

l. Salt deposits were found on all of the panel 25 circuit breaker stems, causing 17 breakers to stick in the closed position. Three were damaged when opened and three others were left closed.

12.2.5 Emergency Detection

The command module wiring associated with the emergency detection system abort logic was subjected to continuity and power-on tests as a result of the inflight one VOTE indication. No abnormal conditions were found.

Power was applied to the engine-status-indicate circuits to check out the command module portion of the system as a result of spurious EXCESSIVE RATE signals detected in the review of data. No abnormal conditions were found.

12.2.6 Communications

As a result of conflicting reports from the recovery forces regarding operation of the VHF recovery and survival beacons, the two beacons were tested. The beacons were found to function properly. Power-on tests were performed with the PCM and central timing equipment as a result of inflight difficulties experienced with this equipment. The cause of the difficulties has not been found. The equipment will be removed and returned to the vendors for further testing.

12.2.7 Instrumentation

Continuity checks will be performed on five measurement systems that showed excessive shift in values at 00:37:00.

The flight qualification tape recorder is being tested to determine whether it is generating the 80-Hz noise appearing on the direct record flight data.

The 90 by 10 high-level commutator will be removed and bench tested as a result of the shift in the entry flight data.

The PCM encoder and the central timing equipment will be tested to attempt to determine the cause of erratic operation during the mission.

12.2.8 Guidance and Control

Power-on tests of the command module systems were performed to determine the cause of the KK̄K alarm flight anomaly. This included the camera and dosimeter systems previously removed. As of this time, the anomaly has not been reproduced. After completion of the spacecraft tests, the computer and up-data link equipment will be removed for special tests.

12.2.9 Reaction Control

The following discrepancies were noted during the postflight inspection of the reaction control system:

a. A mismatch existed on the yaw engine outlet and nozzle extension interface (± yaw, systems A and B).

b. The negative-pitch, A-system engine nozzle extension had a blister and visible delamination.

12.2.10 Environmental Control

Analysis of cabin air samples taken before the hatch was opened in the recovery area revealed slight ingestion of reaction control contaminants (0.16 ppm oxidizer and less than 0.1 ppm fuel). A gallon of liquid found in the cabin at recovery was analyzed and found to be sea water (no glycol was present). An additional 3 pints of liquid were removed at the contractor's facility. Satisfactory operation of the postlanding vent valves was demonstrated aboard the recovery ship. Initial inspection of the environmental control system revealed a chip missing from the steam duct epoxy lining at the outside radius of the bend. The cabin-pressure relief valve was removed for analysis as a result of the high cabin pressure differential experienced during launch. A small foreign object found inside the screen of the valve during removal is being analyzed. Also being analyzed is a dark residue found inside the lower portion of the metering valve.

During the power-on testing for investigating the K$\bar{K}$K anomaly, a procedural error resulted in overboard dumping of the potable and waste water. Consequently, the actual amount of water in the tanks at the end of the mission cannot be determined. As a result of flight discrepancies, the high-pressure oxygen check valves, the water-glycol pump discharge pressure transducer (CF0016P) and the waste water tank quantity transducer (CF009Q) will be removed for analysis.

12.2.11 Crew Windows

The crew windows were subjected to grid photography. The heat shield panes were removed for spectral transmission, reflection, and light-scattering analysis and micrometeoroid examination. The unified side hatch window assembly will be inspected to determine the optical correction for analysis of the 70-mm photographic data obtained during the mission.

TABLE 12-I.- POSTFLIGHT ANOMALY TESTING

ASHUR Number	System	Purpose
020005	Environmental control	To investigate suspected leakage of the high pressure oxygen check valves
020006	Reaction control	To investigate crosswiring of the yaw engine fuel and oxidizer valves reported during deactivation
020007	Communications	To investigate the intermittent PCM data problem with the communications equipment powered up
020008	Instrumentation	To determine if the flight qualification tape recorder is generating the 80-Hz noise which appeared on the direct record flight data
020009	Environmental control	To determine if the waste water tank quantity transducer (CF0009Q) caused fluctuating water quantity readings during flight
020010	Communications	To investigate the possible failure of one of the VHF beacons during the postlanding phase
020012	Instrumentation	To determine if the 90 by 10 high-level commutator caused a shift in flight data during entry
020013	Thermal protection and instrumentation	To perform additional heat shield coring and analysis, and recalibrate selected calorimeters
020014	Instrumentation	To investigate the Van Allen belt dosimeter random switching problem
020016	Communications	To perform continuity checks of power and ground wiring for possible cause of the intermittent and noisy data
020017	Communications	To bench-test the VHF recovery and survival beacons for cause of possible failure during the postlanding phase
020018	Instrumentation	To identify the heat shield bondline thermocouple which were incorrectly wired
020019	Guidance and control	To perform equipment testing at the vendor's laboratory for investigating the cause of the KK̄K alarm indications experienced during flight
020020	Guidance and control	To determine whether the mission control programmer caused a possible failure of one of the VHF beacons during the postlanding phase
020021	Instrumentation	To determine the effect of the deposit of ablator products on the calibration of selected heat shield calorimeters
020501	Communications	To investigate the erratic operations of the time accumulator within the central timing equipment

TABLE 12-I.- POSTFLIGHT ANOMALY TESTING - Concluded

ASHUR Number	System	Purpose
020502	Emergency detection	To investigate the inflight loss of PCM signal abort logic 1 (CD0132X)
020503	Communications	To verify operations of the PCM telemetry equipment
020504	Environmental control	To investigate the excessive water-glycol pump discharge pressure (CF0016P) observed during the flight
020505	Electrical power	To perform wiring checks for possible cause of circuit breaker 100 opening during flight
020506	Guidance and control	To determine cause of the K$\bar{K}$K alarm indications experienced during flight
020509	Emergency detection	To investigate the spurious excessive rate signal (BS0020X) present during a portion of the launch
020510	Environmental control	To analyze the cabin pressure relief valve for the cause of the high cabin pressure during launch
020512	Reaction control	To determine the cause of apparent engine-nozzle extension interface dimensional differences and also a bubble formation in a nozzle extension
020515	Guidance and control	To determine why the astrosextant optics could not be rotated during postflight testing
020516	Environmental control	To determine whether the cabin pressure transducer incorrectly indicated the high cabin pressure observed during launch
020519	Environmental control	To determine whether the barometric pressure transducer caused an indication of high cabin pressure during launch
020520	Electrical power	To investigate the internally shorted cells of four of the spacecraft batteries, observed during postflight test

13.0 VEHICLE AND SYSTEMS DESCRIPTION

The combined space vehicle for the Apollo 6 mission consisted of Apollo spacecraft and a Saturn V launch vehicle (SA 502). The Apollo 6 spacecraft were a command module and service module (CSM 020), a spacecraft/lunar-module adapter (SLA 9), a lunar module test article (LTA-2R), and a launch escape system.

Since the launch vehicle and the spacecraft for the Apollo 6 mission were essentially of the same configuration as those used for the Apollo 4 mission, only the major differences will be presented. A more detailed description of the launch vehicle and spacecraft may be found in the Apollo 4 mission report (ref. 3).

13.1 COMMAND AND SERVICE MODULES

13.1.1 Structure

Significant structural changes between the command and service modules used for the Apollo 6 mission and those used for the Apollo 4 mission were as follows:

Command module.- A unified (incorporating the heat shield and crew compartment hatches into a single hatch) side hatch (fig. 13.1-1) of the block II spacecraft design was installed on CM 020, whereas CM 017 had separate heat shield and crew compartment hatches. The unified side hatch permits quick opening and improves ingress/egress capabilities. A simulated unified hatch seal was installed on CM 017 to obtain environmental data.

The nominal lift-to-drag ratio for CM 020 was changed from 0.35 to 0.343. This resulted from a shift in the Z axis center-of-gravity necessary to accommodate the unified side hatch within the ballast capability of the command module.

The number of extravehicular activity handrails (fig. 13.1-2) was increased from two to five to provide a more representative block II configuration.

The micrometeoroid windows (fig. 13.1-3) were not installed on CM 020 because the CM 017 flight data indicated that a lower-than-predicted heating environment existed around the windows, and removal of the windows permitted a weight reduction for block II spacecraft.

To obtain data on lightweight materials, after the Apollo 4 flight data had indicated a lower-than-predicted heating environment, ablator samples of low density material were installed on CM 020 at the left side window and at the simulated block II umbilical cavity (fig. 13.1-14).

The thermal control coating on CM 020 was gray paint having an emissivity of 0.90, while CM 017 had this paint on the plus Z side and aluminized plastic film with a 0.45 emissivity on the minus Z side. This difference resulted from the mission requirements for a minimum heat shield temperature (full cold soak) on CM 020 and maximum heat shield temperature gradient (cold and hot soak) on CM 017.

Service module.- The aft bulkhead on SM 020 was modified by filling the honeycomb cells with epoxy resin (fig. 13.1-5). This provided sufficient strength for the Apollo 6 loads at the time of S-IC engine cutoff when maximum acceleration was incurred. The Apollo 4 launch loads were lighter, so the SM 017 aft bulkhead did not require modification. The service propulsion system propellant tank support structure (tank skirt) was modified on all SM 020 tanks by replacing one-third of the original skirt with an increased thickness section (fig. 13.1-6). This modification was also the result of the higher launch loads predicted for Apollo 6.

The thermal coating on SM 020 was white paint, whereas SM 017 had aluminized paint.

13.1.2 Earth Landing System

There was no significant change in the earth landing systems.

13.1.3 Mechanical System

The only significant changes in the mechanical system were those related to the unified side hatch on CM 020. Mechanical components on the hatch included latches and linkage mechanism to provide the strength and seal forces necessary for pressure sealing of the crew compartment. A pneumatic counterbalance, which balanced the hatch weight and overcame seal drag, also enabled opening the hatch in a one-g environment.

The boost protective cover hatch was changed to accommodate the unified side hatch and also to permit the cover hatch to be opened during the unified side hatch opening sequence.

13.1.4 Electrical Power System

Significant electrical power system changes between CSM 020 and CSM 017 are as follows:

Cryogenic system.- The titanium hydrogen tanks on CSM 020 were equipped with stainless steel inlet lines. CSM 017 tanks had titanium lines, which were susceptible to spalling and were life-limited under hydrogen exposure.

Oxygen tank 2 on CSM 020 was a block II type and had a larger inlet line and higher fan power requirement (26 watts compared with 15 watts on block I tanks).

Batteries.- Two entry batteries, rated at 40 ampere-hours each, were added in parallel with entry batteries A and B to insure mission success in the event the normal entry batteries had remained connected to the main dc buses after the first service propulsion system engine firing. Had this occurred there would have been insufficient electrical energy for command module entry without the additional batteries.

13.1.5 Sequential Events Control System

There were no significant changes in the sequential events control system or in the mission control programmer. The same programmer (except for the attitude and deceleration sensor) was used on the Apollo 4 and Apollo 6 missions.

13.1.6 Pyrotechnic Devices

There were no significant changes in the pyrotechnic devices.

13.1.7 Emergency Detection System

The emergency detection system was configured for closed-loop operation on Apollo 6 compared with open-loop on Apollo 4. This provided the capability for automatic abort under the following conditions:

Parameter	Time effective
a. Vehicle dynamic rates exceed: a. ±4 deg/sec in pitch b. ±4 deg/sec in yaw c. ±20 deg/sec in roll	Lift-off to 0.4 second before S-IC inboard engine cutoff enable

Parameter	Time effective
b. Two engines out	Lift-off to 0.8 second before S-IC inboard engine cutoff enable
c. Loss of two out of three hot wire circuits Instrumentation unit/ command module—automatic abort	Lift-off to launch escape tower jettison

This capability was provided by placing the emergency detection system switch 2 on the main display console panel 16 to AUTO during the Apollo 6 missicn; this switch was OFF during the Apollo 4 mission.

13.1.8 Communications System

There were no significant changes in the communications system.

13.1.9 Instrumentation System

Significant instrumentation system changes in the Apollo 6 CSM were as follows:

A 16-mm motion picture camera was added to Apollo 6 command module to obtain photography through the left rendezvous window for determination of earth horizon cues for backup attitude reference during future manned missions. The camera was programmed to operate during the launch and entry phases of the mission.

A 70-mm sequence camera, like that used on the Apollo 4 command module, was relocated and reprogrammed in the Apollo 6 command module to acquire earth terrain and atmosphere photographs through the hatch window. The camera was programmed to operate during the second earth revolution.

Block diagrams of the developmental flight instrumentation and operational instrumentation systems are shown in figures 13.1-7 and 13.1-8, respectively.

A Van Allen belt dosimeter (fig. 13.1-9) was installed in the Apollo 6 command module to develop operational experience with the radiation dosimeter than will be used during future manned missions. The dosimeter is designed to provide a skin dose and body depth dose for determining the integrated radiation dosage to the crew.

The low-level commutators on the Apollo 6 CSM were of an improved solid-state type. The Apollo 4 had mechanical commutators, which had exhibited limited life capability.

13.1.10 Guidance and Control Systems

There were no significant changes in the guidance and navigation system or in the stabilization and control system.

13.1.11 Reaction Control System

There were no significant changes in the command module or service module reaction control systems.

13.1.12 Service Propulsion System

There were no significant changes in the service propulsion system.

13.1.13 Environmental Control System

Significant changes in the environmental control system were as follows:

The postlanding vent valves in the Apollo 6 command module were block II type, and differed from the Apollo 4 block I type in the mounting arrangement of the motor with respect to the valve blade. These valves on both the Apollo 4 and Apollo 6 command modules were not connected to the electrical system, but were operated postflight by ground personnel to evaluate functional capability.

The glycol evaporator temperature controller in the Apollo 6 command module was an improved unit incorporating softer potting for vibration isolation, and electrical circuitry changes for improved reliability.

Vapor-sensitive tapes were installed in the Apollo 4 crew compartment to detect ingestion of any reaction control fuel or oxidizer vapors through the cabin pressure relief valve during propellant dump. These tapes were not installed in the Apollo 6 command module because data obtained from Apollo 4 did indicate ingestion, and crew procedures have been established to preclude ingestion on manned flights.

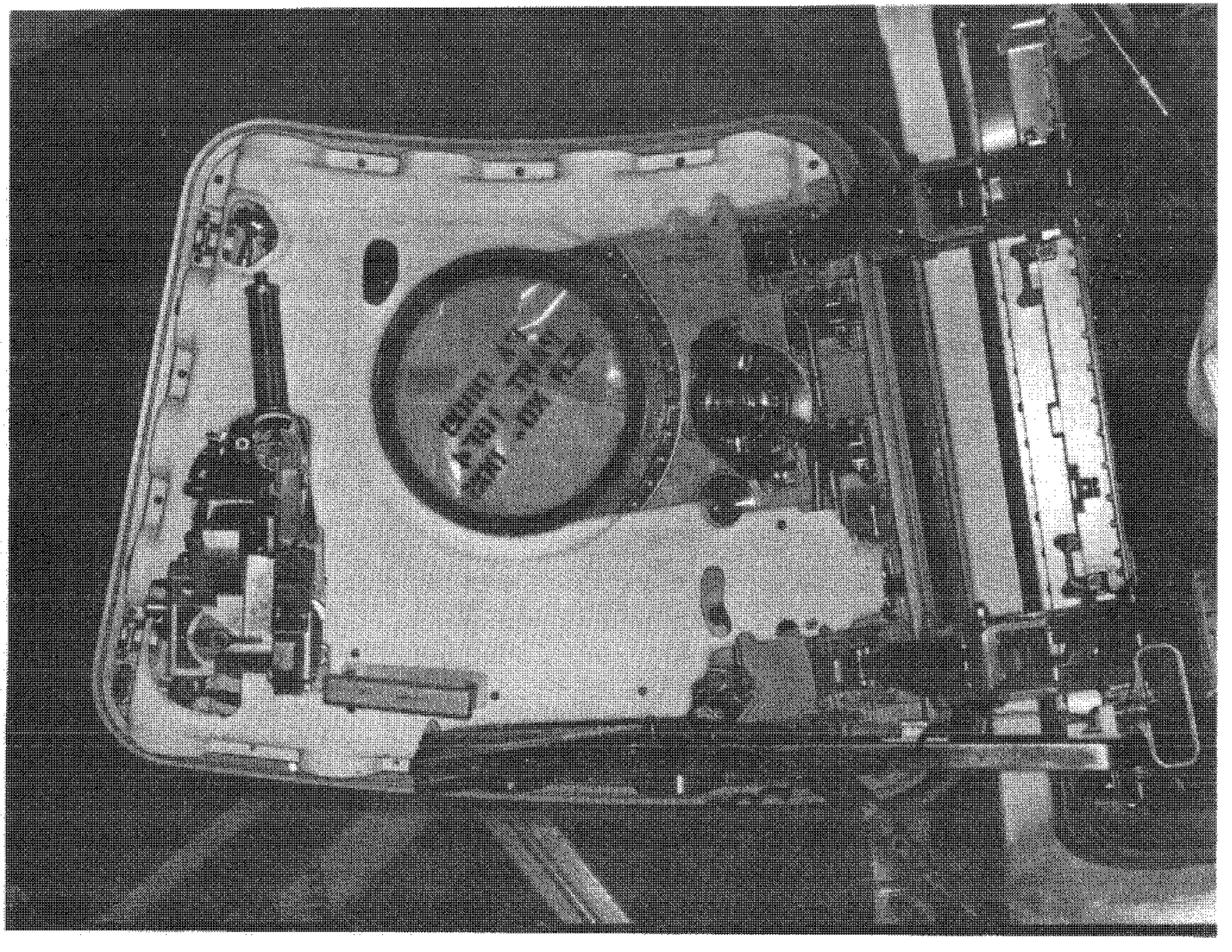

Figure 13.1-1.- Configuration of unified side hatch.

NASA-S-68-3641

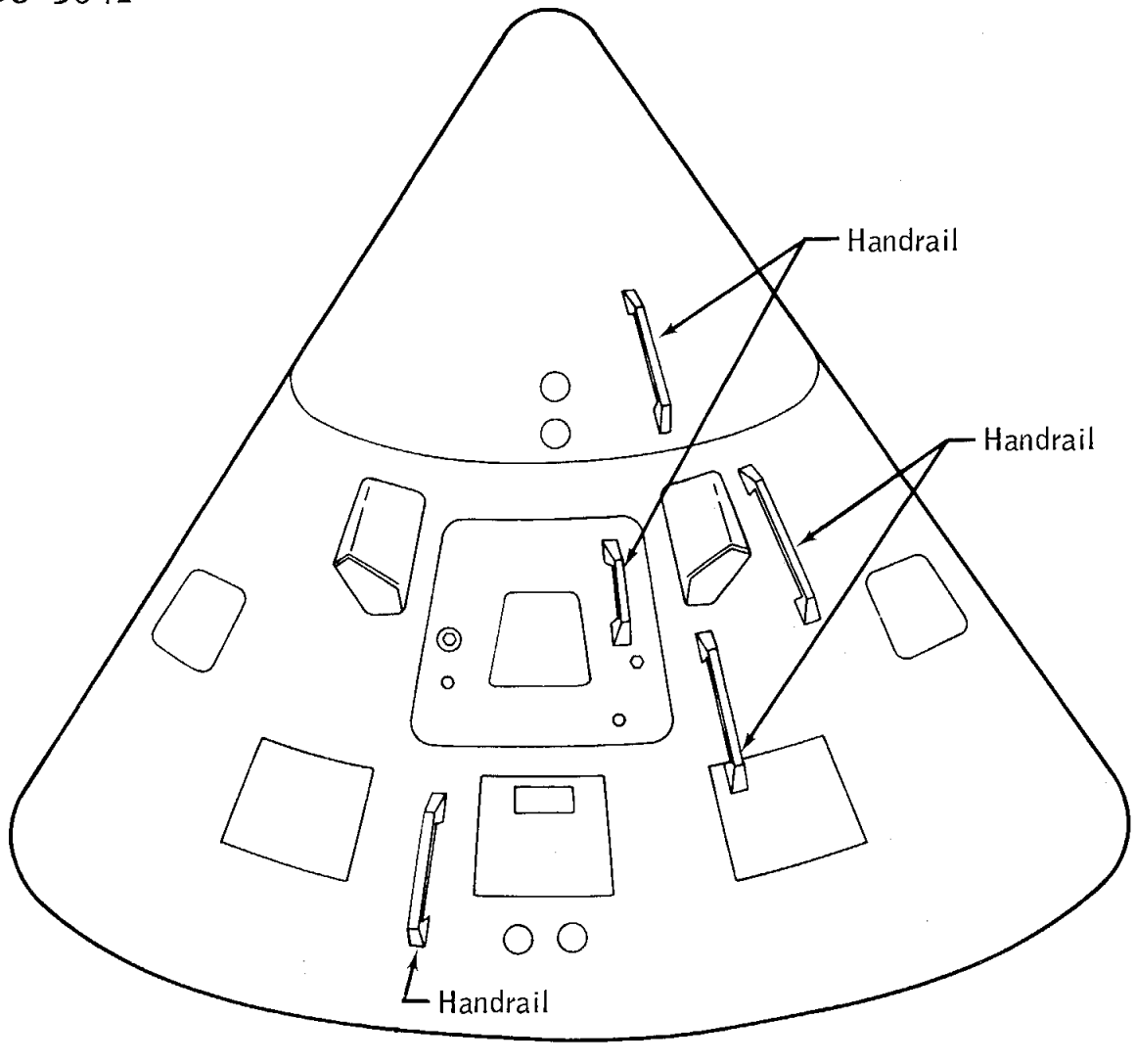

Figure 13.1-2.- Location of extravehicular activity handrails.

NASA-S-68-3642

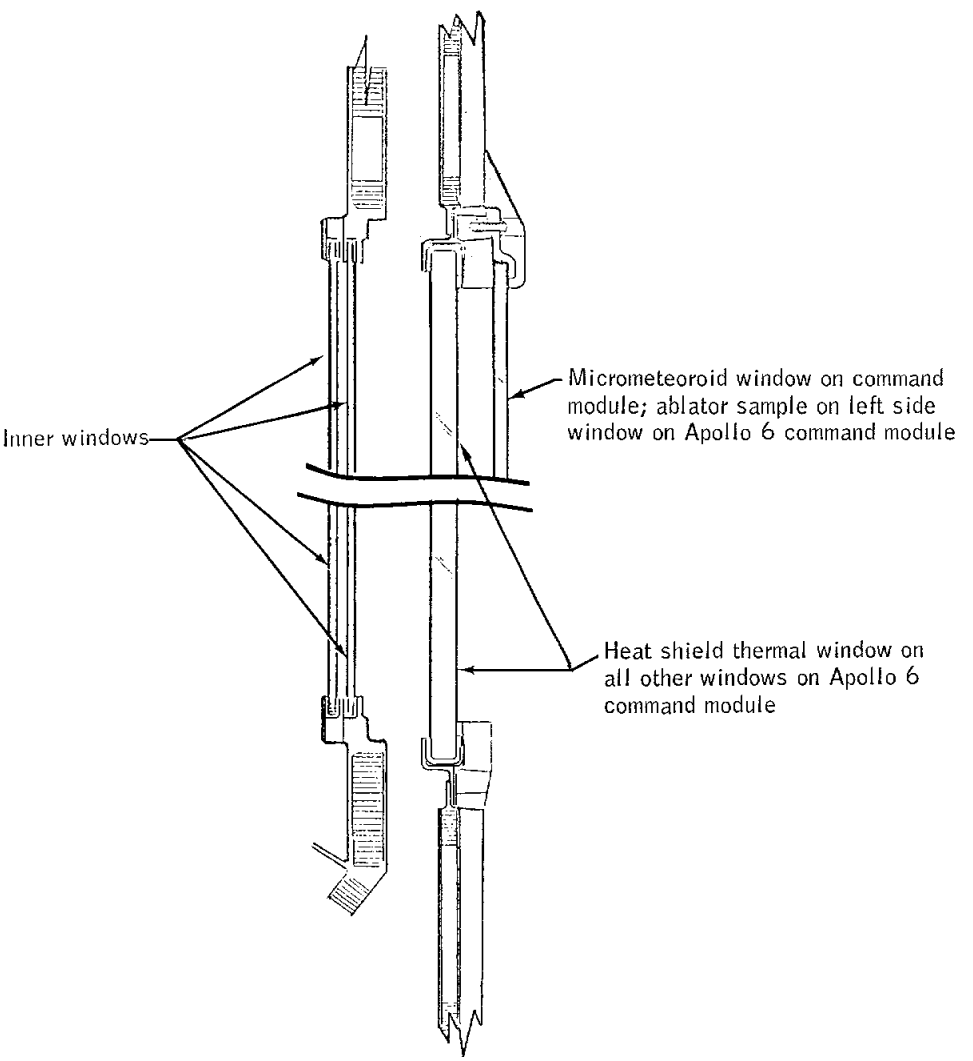

Figure 13.1-3.- Command module window configuration.

NASA-S-68-3643

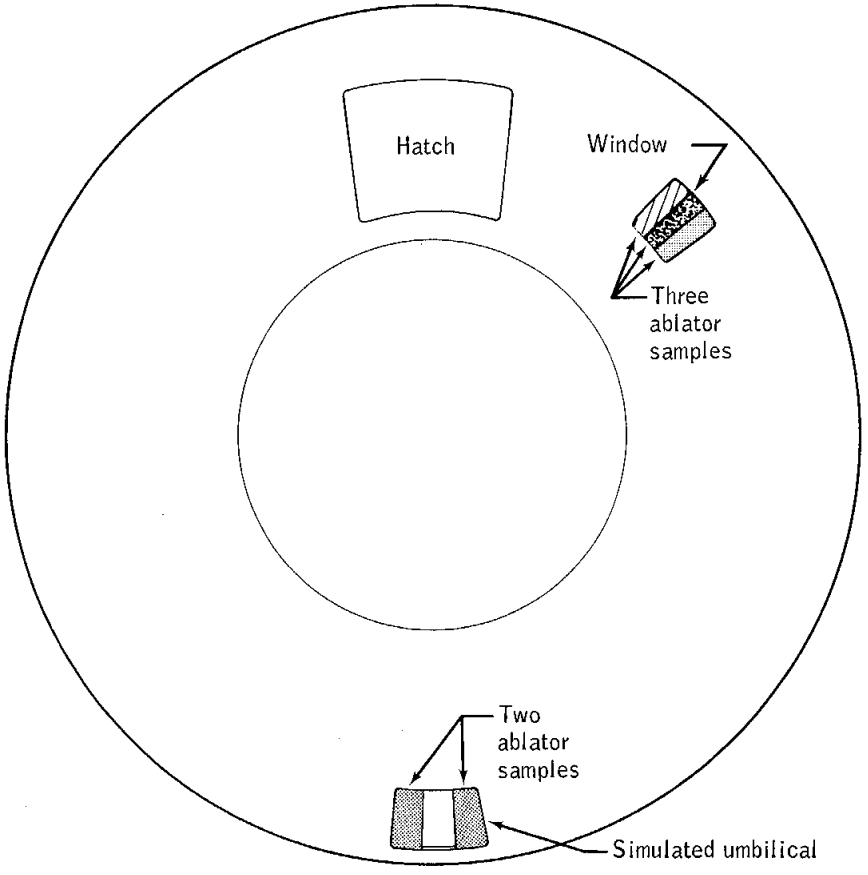

Figure 13.1-4.- Locations of ablator samples on command module.

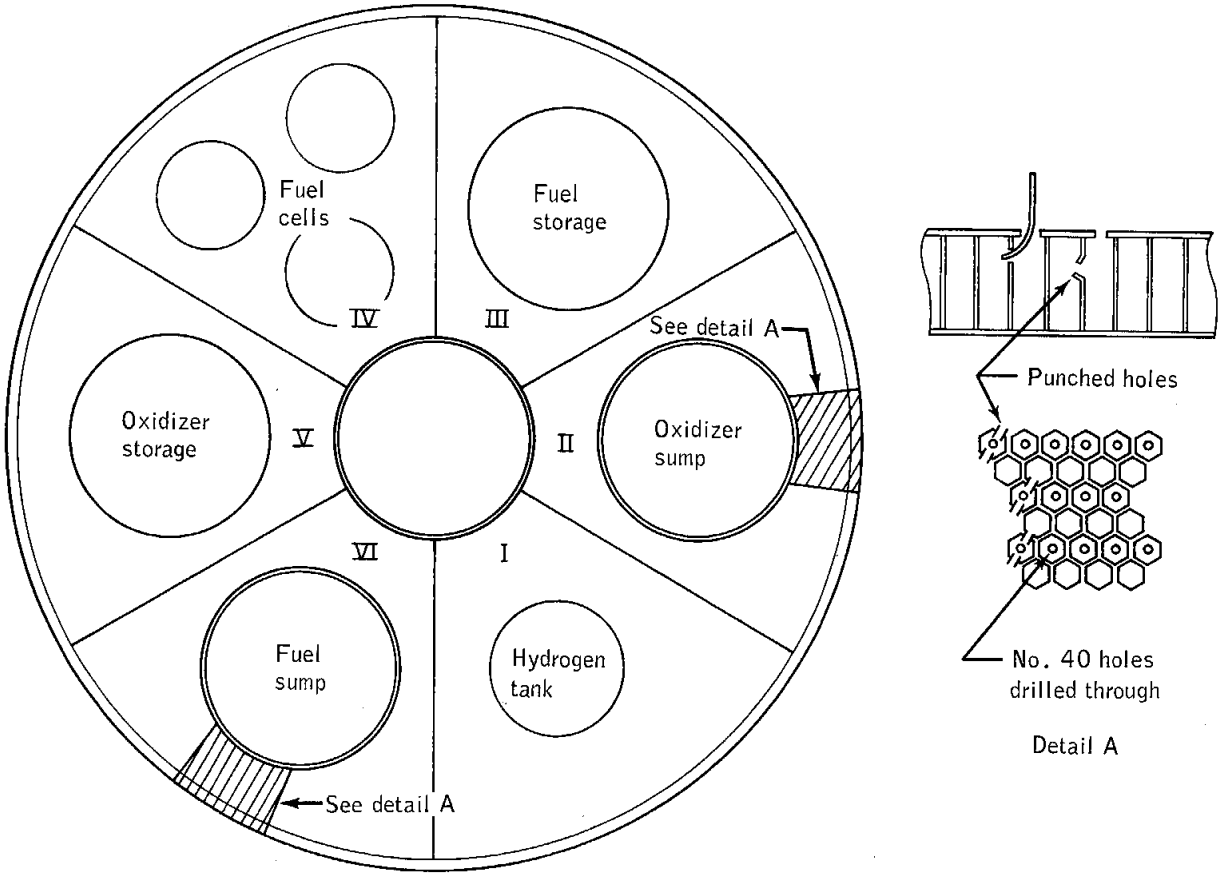

Figure 13.1-5.- Modification of service module aft bulkhead.

NASA-S-68-3645

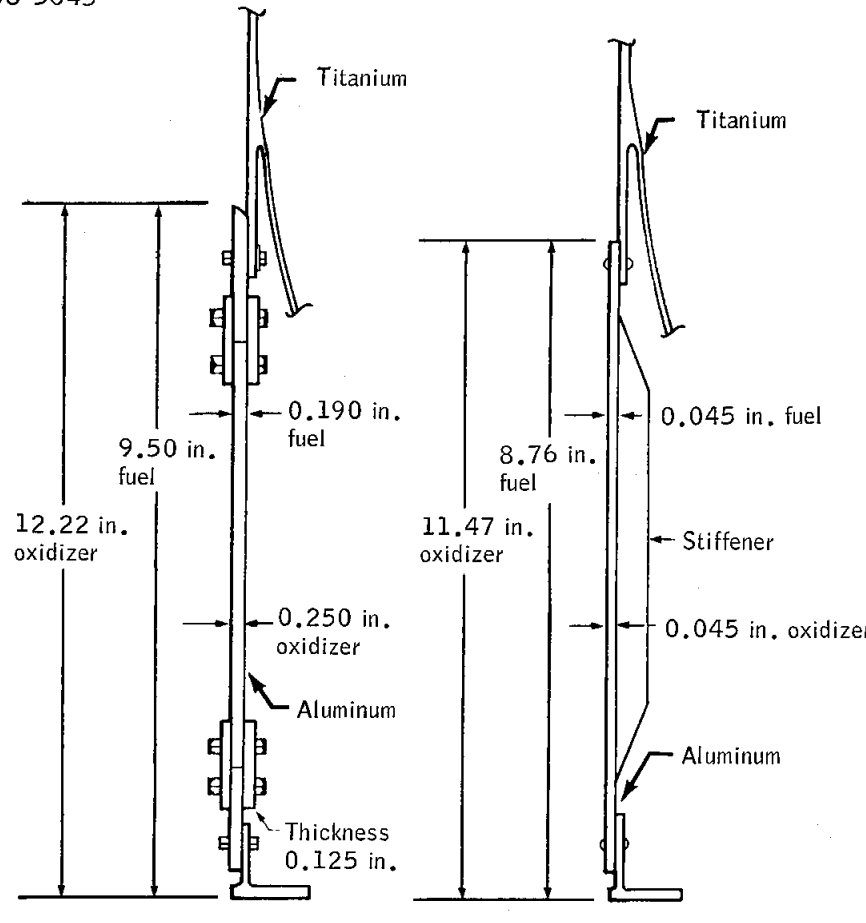

Partial view of service propulsion tank support assembly for Apollo 6 service module

Partial view of service propulsion tank support assembly for Apollo 4 service module

Figure 13.1-6.- Modification of service propulsion tank support assembly.

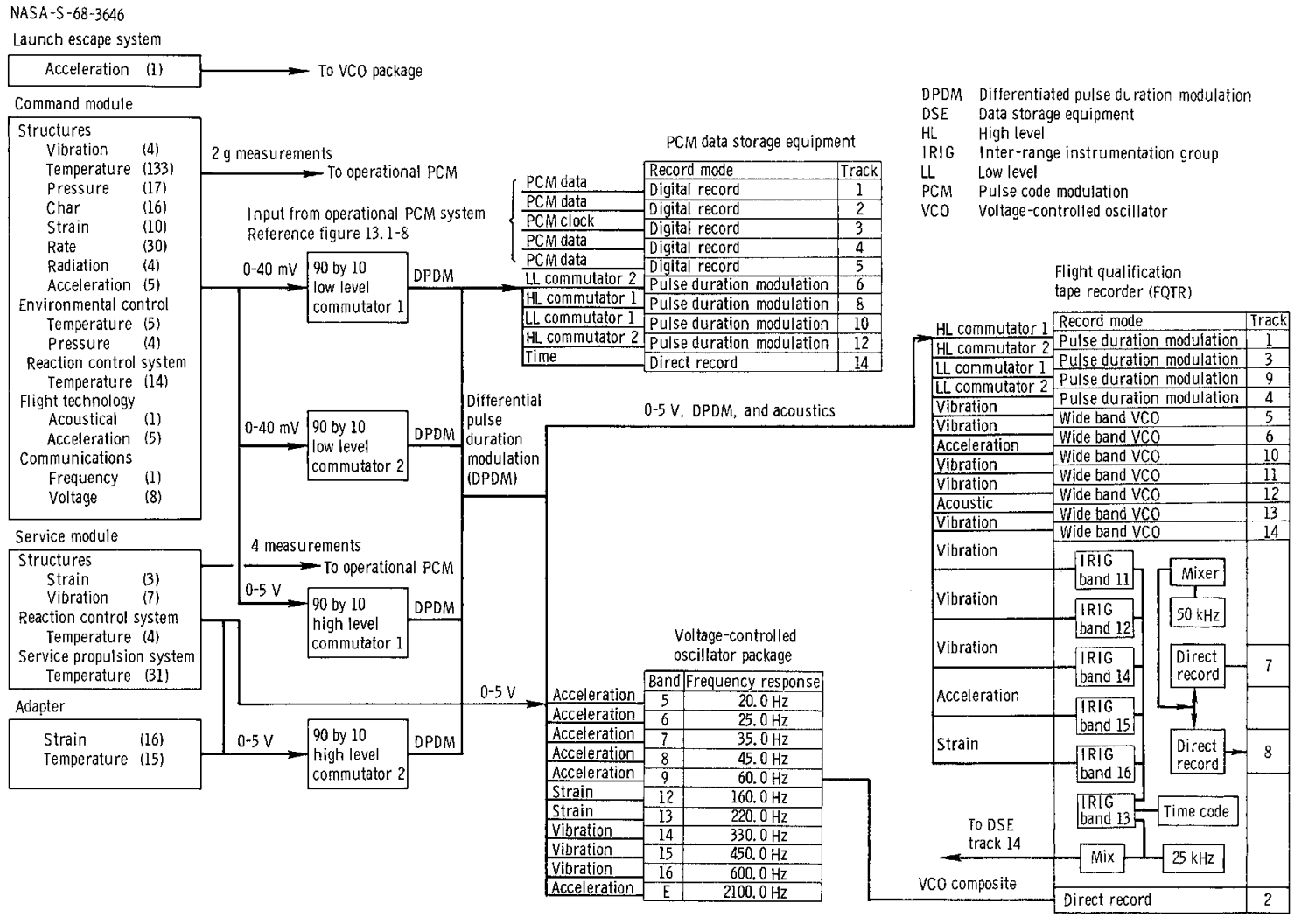

Figure 13.1-7. - Flight qualification instrumentation block diagram.

NASA-S-68-3647

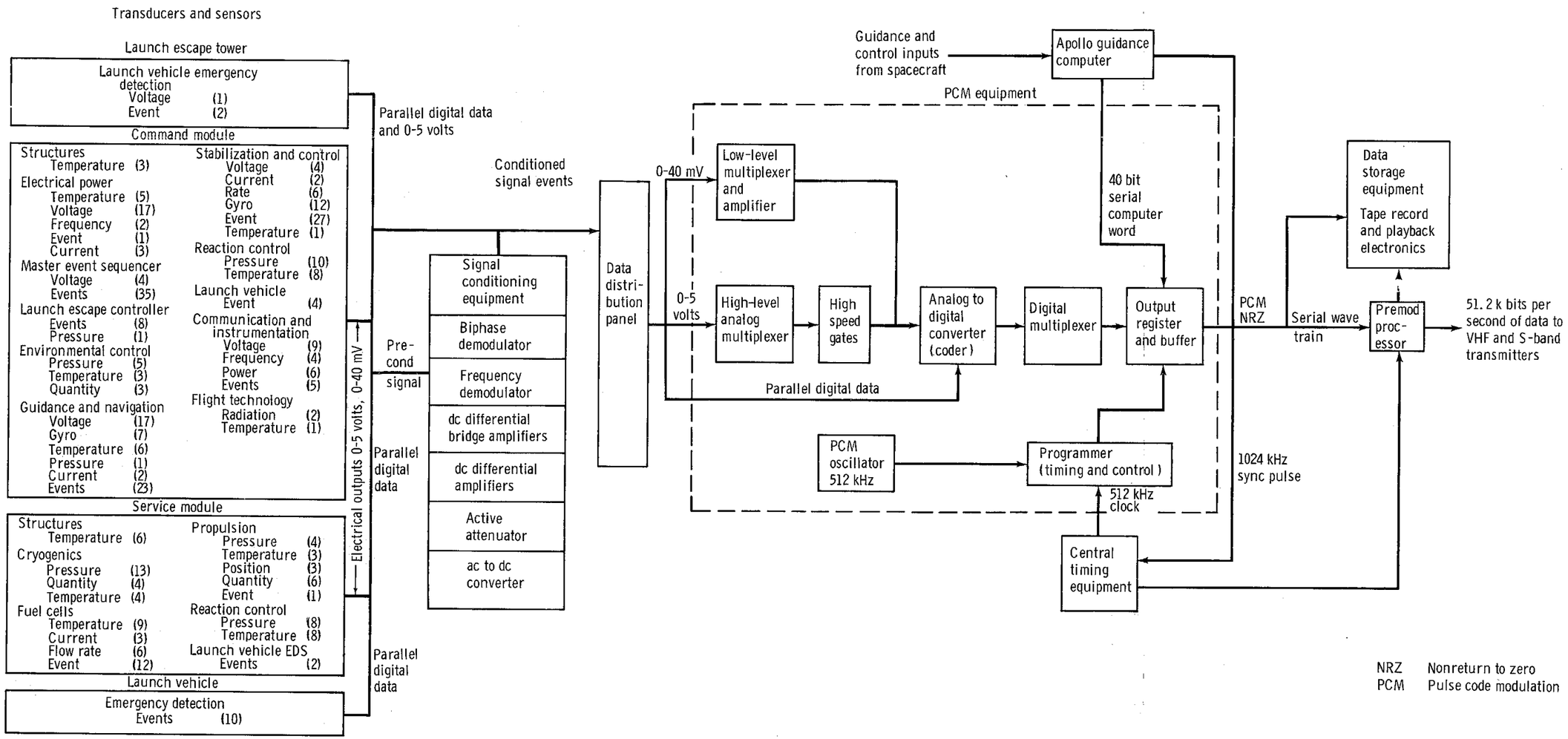

NRZ Nonreturn to zero
PCM Pulse code modulation

Figure 13.1-8. - Operational intrumentation block diagram.

NASA-S-68-3648

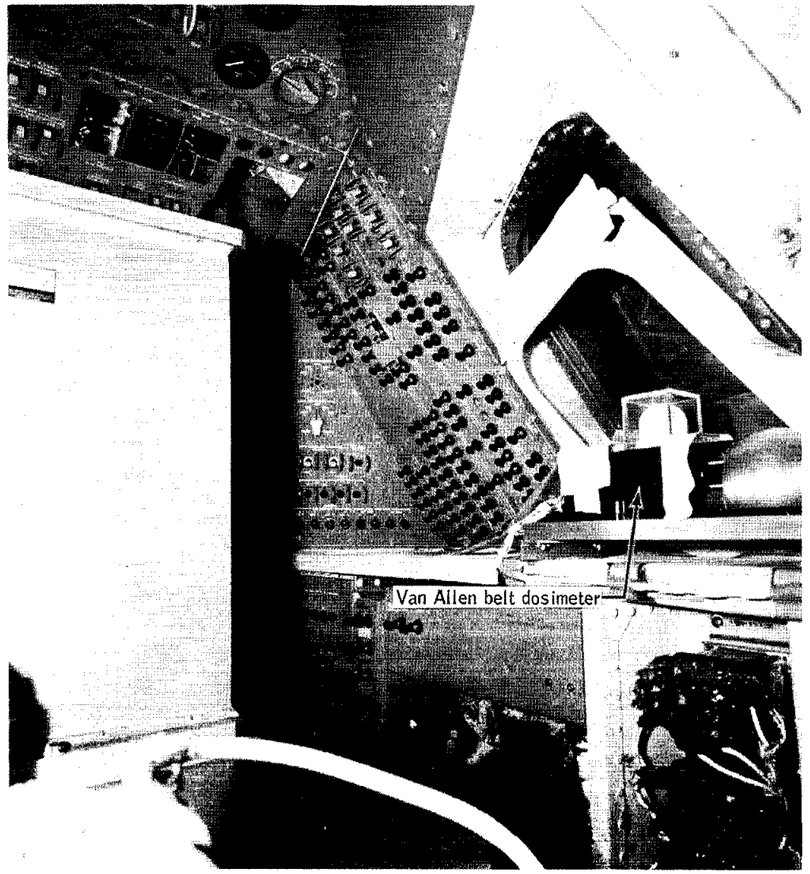

Figure 13.1-9.- Location of Van Allen belt dosimeter.

13.2 LUNAR MODULE TEST ARTICLE

13.2.1 General Description

The lunar module test article (LTA-2R) flown on the Apollo 6 mission was essentially the same as LTA-10R flown on Apollo 4. The major differences were as follows:

Vibration tests showed the need for increasing thickness of the descent-stage top deck from 0.008 to 0.040 inch. The LTA-2R ballast weight was 26 000 pounds compared with 29 500 pounds on LTA-10R. This reduction in ballast weight for LTA-2R was due to additional service propulsion system propellant loading requirements for Apollo 6. The descent-stage propellant ballast tanks were heavyweight aluminum tanks instead of the titanium tanks used for ballast in LTA-10R.

13.2.2 Instrumentation

The LTA-2R outrigger strut strain gages were calibrated in place by loading the struts to aid inflight data correlation. The LTA-10R struts were not load-calibrated. Three of the existing LTA-2R descent-stage linear accelerometers were relocated and three additional oil-damped linear accelerometers were installed on the ascent-stage lower diagonal strut. This change was made because Apollo 4 mission data showed that the mounting locations on LTA-10R caused high-frequency vibration to saturate the accelerometer.

13.3 LAUNCH VEHICLE DESCRIPTION

The Saturn V launch vehicle consisted of three propulsive stages (S-IC, S-II, S-IVB) and an instrument unit. The only significant difference between the launch vehicles used for the Apollo 4 and 6 missions was the inclusion of the S-IC standpipe ullage cutoff arrangement, which will be used on subsequent vehicles. This provision raised the 3 sigma high-g level to 4.58g for Apollo 6. The 3 sigma level for Apollo 4 was 3.93g.

13.4 COMMAND AND SERVICE MODULE/LUNAR MODULE ADAPTER

The command and service module/lunar module adapter used for the Apollo 6 mission was essentially of the same configuration as that used for the Apollo 4 mission.

13.5 WEIGHT AND BALANCE

The spacecraft mass properties for the Apollo 6 mission are summarized in tables 13.5-I and 13.5-II. These data represent the actual conditions as determined from postflight analyses of expendable loadings and usage during the flight.

The weights and centers of gravity for each module were measured prior to stacking. The inertia values were calculated for the actual weight data obtained. All changes after measurement and before launch were monitored and mass properties were revised as required.

The mass properties at launch, as shown in table 13.5-I, did not vary significantly from the predicted values used for the operational trajectory calculations. The final mission trajectory data were based on mass properties, which were adjusted for all changes including actual expendable loadings.

The command module mass properties during the entry phase are shown in table 13.5-II. Expendables usage shown were based on postflight data.

The mass properties variations have been determined for each significant mission phase from launch through command module landing. The expendables usage shown were based on reported postflight data.

TABLE 13.5-I.- SPACECRAFT MASS PROPERTIES AT LAUNCH AND DURING ORBITAL FLIGHT

	Weight, lb	Center of gravity[a], in.			Moment of inertia[b], slug-ft^2		
		X	Y	Z	I_{xx}	I_{yy}	I_{zz}
Launch							
Command module[c]	12 543.0	1039.2	0.3	6.7	6 572	6 008	4 850
Service module[d]	9 884.0	910.7	0.0	0.7	6 483	10 968	10 645
Service propulsion tanked propellants	32 993.0	900.8	11.3	-4.8	16 137	19 096	24 307
Spacecraft lunar module adapter (SLA)	3 886.0	644.5	1.2	-1.8	9.830	13 553	13 376
Launch escape system	8 886.0	1299.8	-0.3	1.3	745	30 008	29 988
Lunar module (LTA-2R)	26 001.0	588.4	0.1	0.0	17 269	19 890	20 914
Total spacecraft at launch	94 193.0	861.2	4.0	-0.8	57 920	1 030 510	1 035 344
Less: Launch escape system	-8 886.0	1299.8	-0.3	1.3	745	30 008	29 988
Insertion							
Total spacecraft	85 307.0	815.4	4.9	-0.9	57 141	591 769	596 593
Less: Adapter (less ring)	-3 795.0	639.9	1.2	-1.8	9 717	12 750	12 575
Lunar module	-26 001.0	588.4	0.1	0.0	17 269	19 890	20 914
Cryogenics -							
Hydrogen tank 1	-0.4	933.9	42.4	-42.4	0	0	0
Hydrogen tank 2	-0.6	858.4	42.4	-42.4	0	0	0
Oxygen tank 2	-5.2	896.0	23.0	-29.7	0	0	0
Service module reaction control propellants	-25.0	959.0	0.0	0.0	0	0	0
Waste water	-18.7	1022.6	-19.7	62.5	0	0	0
Plus: Potable water	+6.7	1022.6	-63.5	-16.4	0	0	0

[a]Referenced to the Apollo coordinate system.

[b]Inertia data are about the center of gravity of each item.

[c]Includes expendables and reaction control propellants.

[d]Includes expendables, reaction control propellants, and service propulsion system residuals of 229.7 pounds.

TABLE 13.5-I.- SPACECRAFT MASS PROPERTIES AT LAUNCH AND DURING ORBITAL FLIGHT - Continued

	Weight, lb	Center of gravity[a], in.			Moment of inertia[b], slug-ft^2		
		X	Y	Z	I_{xx}	I_{yy}	I_{zz}
Service Propulsion System Engine Ignition							
Total CSM	55 467.8	933.8	6.8	-1.2	29 923	75 558	79 383
Less: Service propulsion	30 075.0	905.6	9.9	-4.2	14 947	16 888	21 580
Cryogenics -							
Hydrogen tank 2	-0.1	858.4	42.4	-42.4	0	0	0
Oxygen tank 2	-0.1	896.0	23.0	-29.7	0	0	0
Service module reaction control propellants	-7.2	959.0	0.0	0.0	0	0	0
Waste water	-0.8	1022.6	-19.7	62.5	0	0	0
Plus: Potable water	+0.3	1022.6	-63.5	-16.4	0	0	0
Service Propulsion System Engine Cutoff							
Total CSM	25 384.9	967.3	3.2	2.4	14 720	47 385	46 262
Less: Service module reaction control system - orientation	-8.4	959.0	0.0	0.0	0	0	0
Total CSM - at coast	25 376.5	967.3	3.2	2.4	14 720	47 385	46 262
Less: Cryogenics -							
Hydrogen tank 1	-0.7	933.9	42.4	-42.4	0	0	0
Hydrogen tank 2	-0.5	858.4	42.4	-42.4	0	0	0
Oxygen tank 1	-3.0	971.5	23.0	-29.7	0	0	0
Oxygen tank 2	-7.8	896.0	23.0	-29.7	0	0	0
Service module reaction control propellants	-324.4	959.0	0.0	0.0	0	0	0
Waste water	-29.4	1022.6	-19.7	62.5	0	0	0

[a]Referenced to the Apollo coordinate system.

[b]Inertia data are about the center of gravity of each item.

TABLE 13.5-I.- SPACECRAFT MASS PROPERTIES AT LAUNCH AND DURING ORBITAL FLIGHT - Concluded

	Weight, lb	Center of gravity[a], in.			Moment of inertia[b], slug-ft^2		
		X	Y	Z	I_{xx}	I_{yy}	I_{zz}
Plus: Potable water	+13.1	1022.6	-63.5	-16.4	0	0	0
Total CSM at command module/service module separation	25 017.8	967.3	3.2	2.4	14 704	47 337	46 246

[a]Referenced to the Apollo coordinate system.

[b]Inertia data are about the center of gravity of each item.

TABLE 13.5-II.- COMMAND MODULE MASS PROPERTIES AT ENTRY

	Weight, lb	Center of gravity[a], in.			Moment of inertia[b], slug-ft^2		
		X	Y	Z	I_{xx}	I_{yy}	I_{zz}
Command module at launch[c]	12 543.0	1039.2	0.3	6.7	6572	6008	4850
Less: Waste water	-48.9	1022.6	-19.7	62.5	0	0	0
Plus: Potable water	+20.1	1022.6	-63.5	-16.4	0	0	0
Command module at command module/ service module separation	12 514.2	1039.2	0.3	6.4	6555	5976	4862
Less: Reaction control propellants - orientation	-6.0	1022.6	-5.7	57.0	0	0	0
Command module at entry	12 508.2	1039.2	0.3	6.4	6554	5975	4862
Less: Reaction control propellants	-77.5	1022.6	-5.7	57.0	17	2	15
Ablation	-95.0	1008.5	0.0	10.0	55	43	14
Forward heat shield	-413.0	1100.4	-0.2	0.4	59	57	55
Waste water	-1.7	1022.6	-19.7	62.5	0	0	0
Drogue chutes	-63.0	1090.3	0.0	-20.9	1	1	2
Command module main chute deploy	11 858.0	1037.2	0.3	6.4	6361	5408	4371
Less: Main chutes	-424.0	1090.5	-0.8	6.4			
Reaction control propellants	-173.9	1022.6	-5.7	57.0			
Command module at landing	11 260.1	1035.4	0.5	5.6			

[a]Referenced to the Apollo coordinate system.

[b]Inertia data are about the center of gravity of each item.

[c]Includes expendables and reaction control propellants.

14.0 SPACECRAFT HISTORIES

14.1 COMMAND MODULE AND SERVICE MODULE

The factory checkout flow history of the Apollo 6 command module and service module (CSM 020) at the contractor's facility in Downey, California, is shown in figure 14-1. The prelaunch checkout flow history of the combined space vehicle at Kennedy Space Center, Florida, is shown in figure 14-2.

14.2 LUNAR MODULE TEST ARTICLE

The factory refurbishment, modification, and checkout flow history of the lunar module test article (LTA-2R) at the contractor's facility at Bethpage, New York, is shown in figure 14-3. The prelaunch checkout flow history of the lunar module test article at Kennedy Space Center, Florida, is shown in figure 14-4.

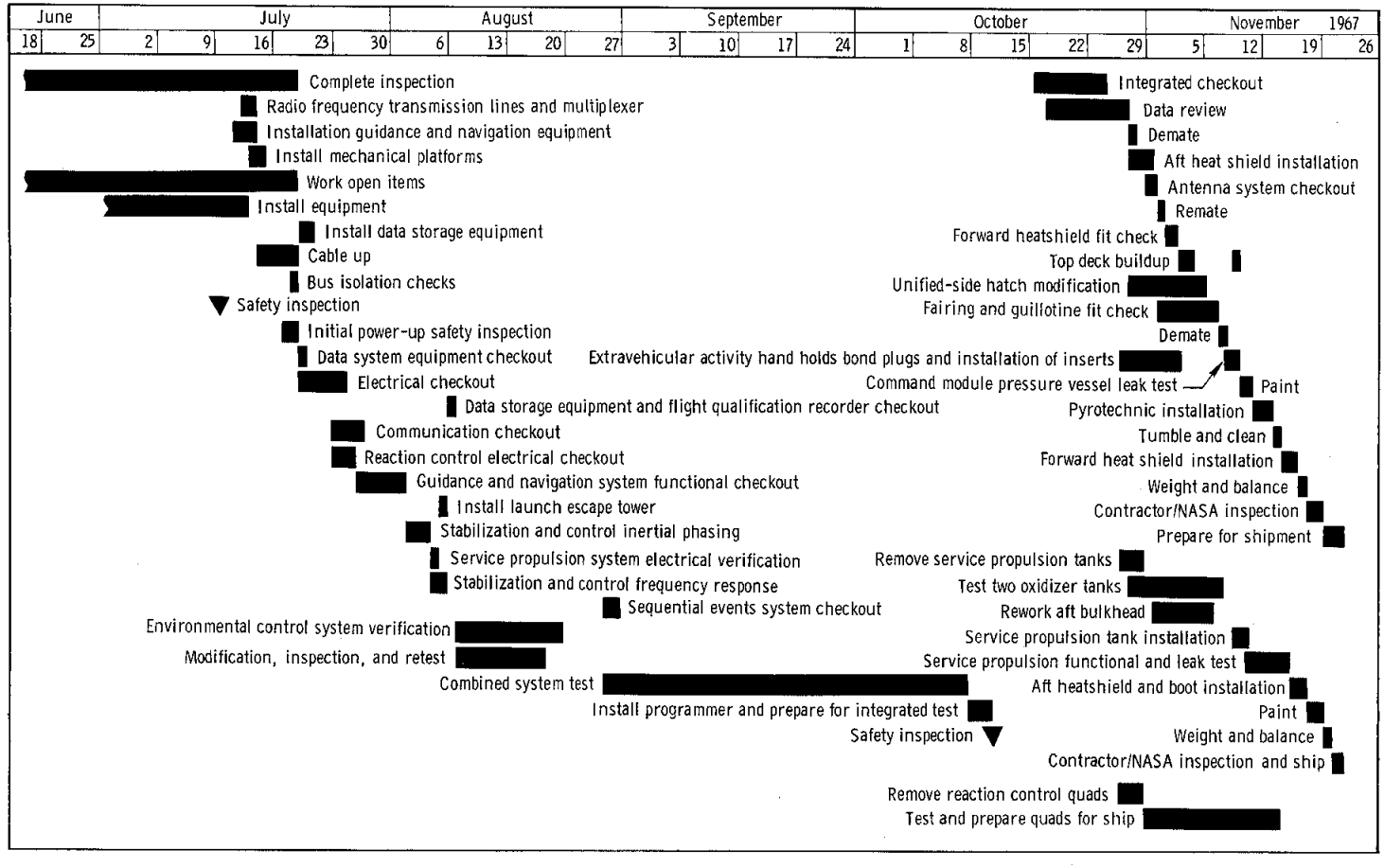

Figure 14-1. - Factory checkout flow for command module (020) and service module (020) at contractor's facility.

NASA-S-68-3650

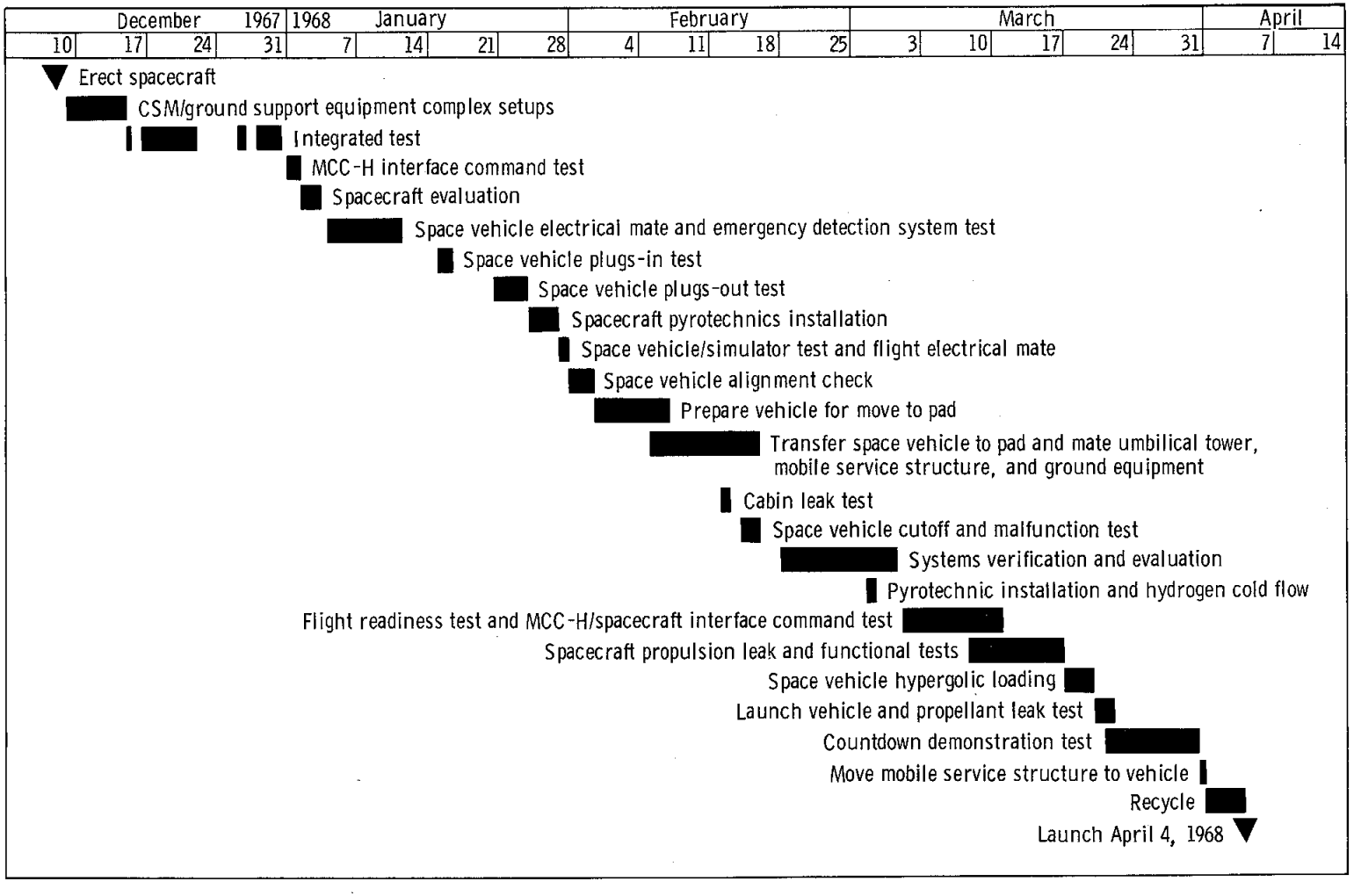

Figure 14-2. - Prelaunch checkout flow for command module (020) and service module (020) at Kennedy Space Center.

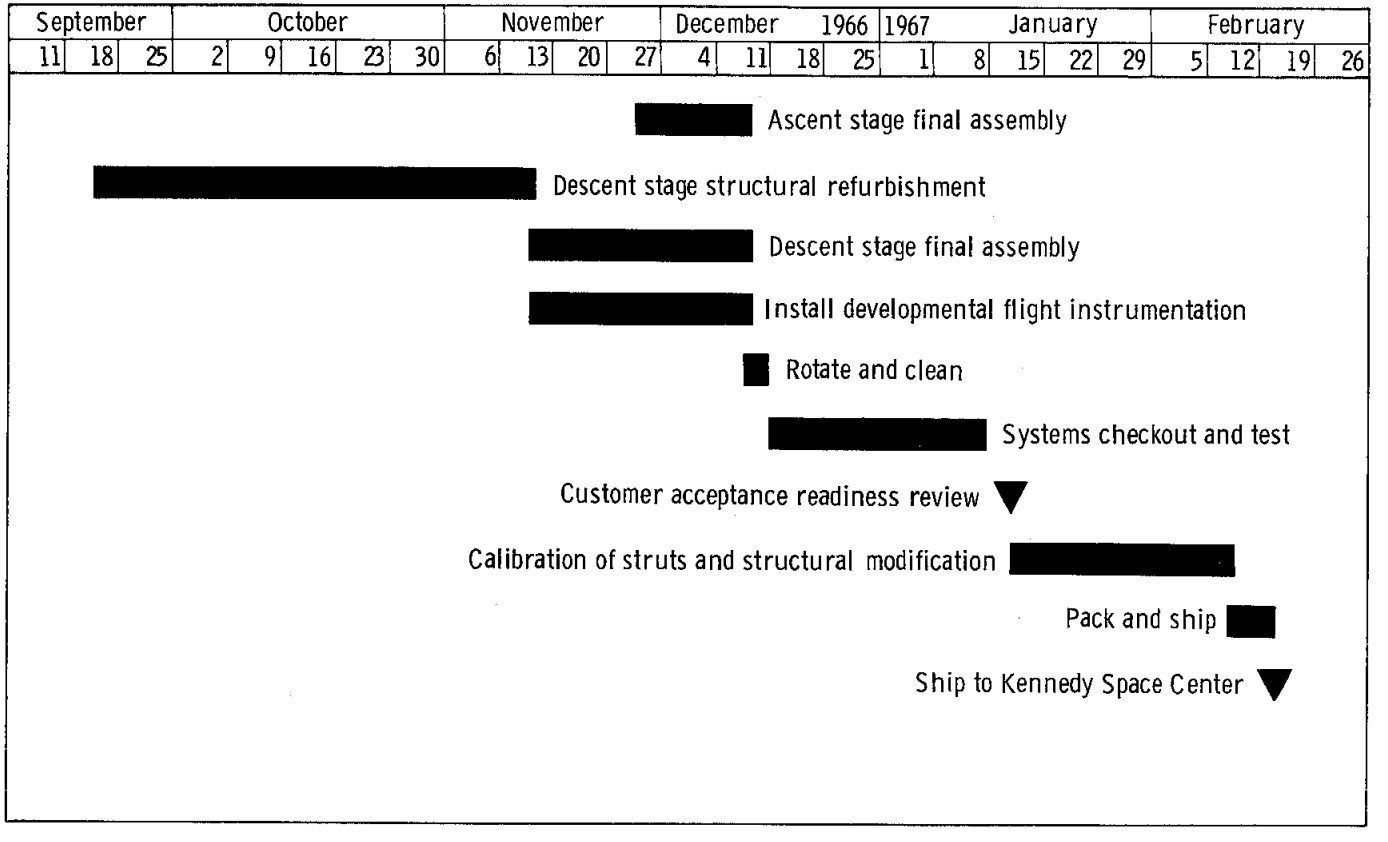

Figure 14-3. - Factory modification and checkout flow of lunar module test article at Bethpage.

NASA-S-68-3652

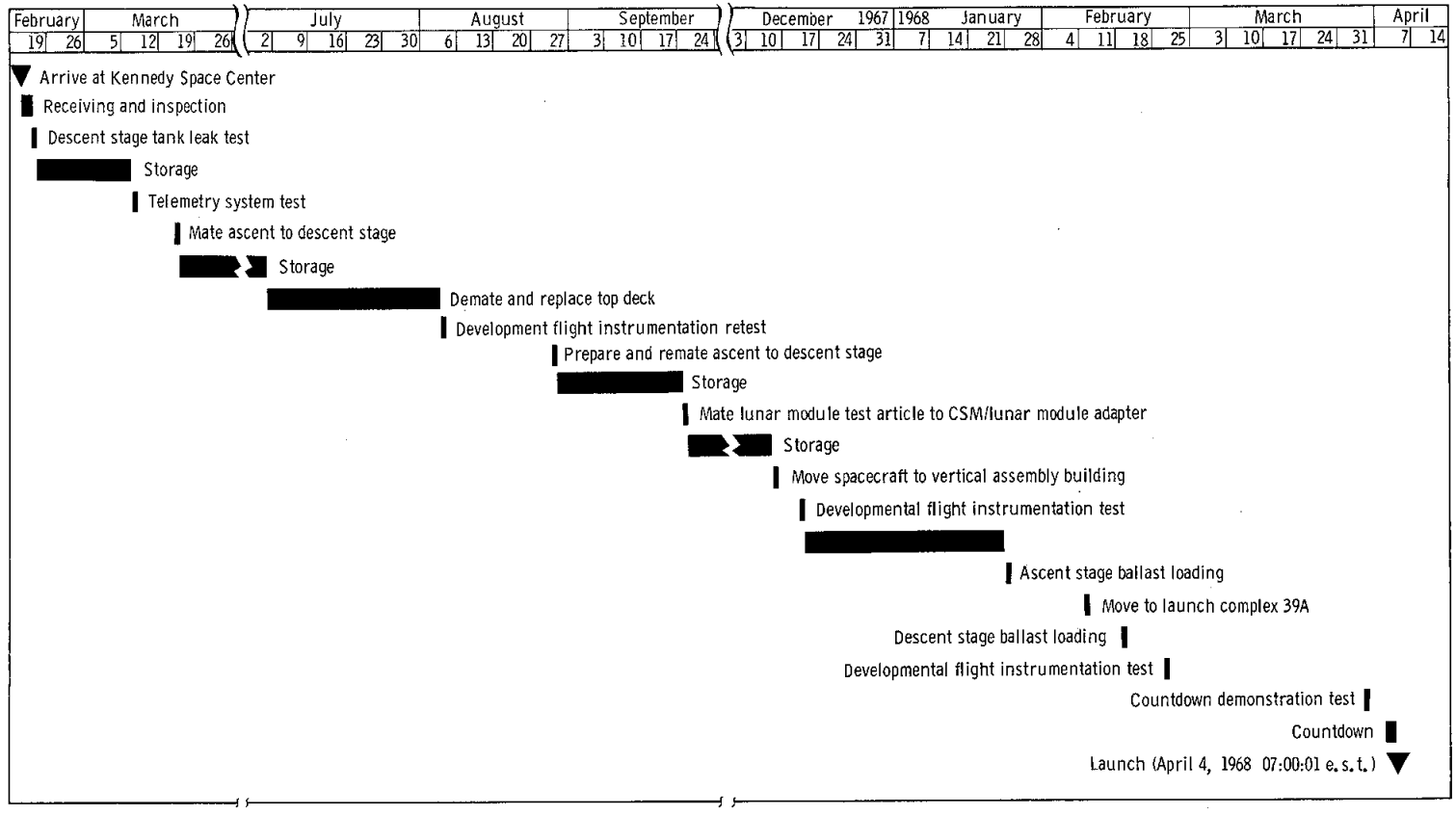

Figure 14-4. - Prelaunch checkout flow for lunar module test article at Kennedy Space Center.

15.0 SUPPLEMENTAL REPORTS

The following table lists the supplemental reports to be published for the Apollo 6 Mission Report:

Number	Subject	Responsible Analysis Manager	Expected publication date
1	Apollo 6 Postflight Trajectory Data	D. J. Incerto	June 27, 1968
2	Apollo 6 Guidance and Navigation Data	J. F. Hanaway	June 28, 1968
3	Detailed Evaluation of Heat Shield Performance	J. E. Pavlosky	July 10, 1968

16.0 REFERENCES

1. Boeing Company, Space Division: Saturn V AS-502 Launch Vehicle Operational Flight Trajectory. D5-15551(F)-2, December 12, 1967; and revised ephemeris S-93-10-H-4, March 27, 1968.

2. Marshall Space Flight Center: Apollo 6 Mission Report, Launch Vehicle. (This report has not yet been released; therefore, no report number can be cited.)

3. Manned Spacecraft Center: Apollo 4 Mission Report. MSC-PA-R-68-1, January 7, 1968.

17.0 DATA AVAILABILITY

The data reduction for the Apollo 6 mission evaluation was accomplished by processing only the data needed for analysis of anomalies and systems performance. The telemetry station coverage used to process data is shown in figure 17-1; the signal acquisition periods are listed in table 17-I. The total data reduction effort for the mission is presented in table 17-II.

TABLE 17-I.- TIME COVERAGE FOR DATA PROCESSING

Revolution	Station	Acquisition of signal, hr:min:sec	Loss of signal, hr:min:sec
1	Merritt Island	00:00:00	00:09:09
	Bermuda	00:03:54	00:13:06
	U.S.N.S. Redstone	00:09:20	00:16:05
	Canary Island	00:19:33	00:23:56
	Carnarvon	00:51:41	01:00:26
	Canberra	01:00:26	01:07:38
	Guaymas	01:29:20	01:37:45
	Texas	01:32:40	01:40:27
2	Merritt Island	01:36:46	01:44:05
	Bermuda	01:40:26	01:47:40
	U.S.N.S. Redstone	01:44:25	01:51:08
	Canary Island	01:51:54	01:58:14
	Carnarvon	02:26:22	02:36:23
	Canberra	02:36:19	02:40:41
	Hawaii	02:53:00	03:01:08
	Goldstone	03:04:24	03:10:17
	Guaymas	03:04:49	03:12:20
	Texas	03:08:03	03:15:21
3	Merritt Island	03:11:53	03:19:20
	Bermuda	03:15:34	03:22:53
	Antigua	03:18:39	03:27:34
	Canary $Island_1$	03:26:07	03:44:07
	$Ascension_1$	03:26:50	03:43:49
	Canary $Island_2$	03:44:40	04:07:05
	Canary $Island_3$	04:04:59	04:20:41
	$Ascension_2$	04:15:08	04:26:32
	$Carnarvon_1$	04:25:--	04:47:--
	$Ascension_3$	04:26:31	04:48:40
	$Carnarvon_2$	04:47:--	05:08:--
	$Ascension_4$	04:49:50	05:13:27
	$Carnarvon_3$	05:08:--	05:32:--

TABLE 17-II.- DATA PROCESSED FOR APOLLO 6 EVALUATION

Type of data processed (a)	Revolution 1								Revolution 2								Revolution 3																								
	MILA	BDA	RED	CNB	GYM	TEX	DSE	FQT	MILA	BDA	RED	CRO	HAW	GDS	GYM	TEX	MILA	BDA	ANT	CYI_1	CYI_2	CYI_3	ACN_1	ACN_2	ACN_3	ACN_4	CRO_4	ACN_6	ACN_7	ACN_8	ACN_9	ACN_{10}	CRO_{10}	CRO_{12}	CRO_{13}	GWM	WTN	DSE	FQT
Events	X	X	X	X	X	X	X		X	X		X	X	X	X	X	X	X	X	X	X		X	X	X	X	X	X	X	X		X	X	X	X	X	X	
Bandpass plots		X															X		X	X	X				X	X	X	X	X	X		X	X	X	X	X		
Bandpass tabs	X	X	X	X	X	X	X		X	X		X	X	X	X	X	X	X	X						X							X			X	X	X	
Bandpass tabs, special	X	X	X				X		X	X		X	X	X		X	X	X	X	X			X										X	X	X	X	X	
Computer word tabs	X	X	X	X		X	X		X	X		X	X	X		X	X	X	X	X	X				X	X	X	X	X	X	X		X	X	X	X	X	
Oscillograms																																						
1 and 3	X	X	X	X	X	X	X		X	X		X	X	X	X	X	X	X	X	X	X					X	X	X	X	X			X	X	X	X	X	
Special	X	X	X				X	X	X	X	X					X		X	X	X	X	X		X	X			X	X	X	X			X	X	X	X	X	X
Tel 4	X								X								X																					
LTA-2R	X	X							X																													
DPDM[b]							X																															X
Time history tabs																																						
LTA-2R	X																																					
CSM	X																																					
Special	X							X									X						X															
DPDM[b]																																						X
Time history plots																																						
LTA-2R PSD[c]	X																																					
CSM PSD[c]	X																																					
DPDM[b]							X	X																														X	
Special																				X			X														X	X
Special programs																																						
Fuel budget									X								X	X	X	X	X				X	X	X	X	X	X			X	X	X	X	X	X	
On time									X								X	X	X	X	X				X	X	X	X	X	X			X	X	X	X	X	X	
Propellant remaining									X								X	X	X	X	X					X	X	X	X	X			X	X	X	X	X	X	
Bit error, S-band	X																	X									X	X	X				X	X	X	X		
Bit error, VHF	X																	X									X	X							X	X		
Look angle																					X							X					X	X	X	X		
Gimbal angle	X	X	X	X						X		X	X	X			X	X	X	X	X					X	X	X	X	X			X	X	X	X	X	X	
Sun angle										X		X	X	X						X								X						X	X	X			
Rotation and translation								X																															
Quick-look quantity																																					X	
Angle of attack																																					X	
Coefficient tabs																																					X	
Stripcharts																									X	X	X	X	X	X	X	X	X	X	X			

[a] Synch and Data Qual Program was computer reduced for each station tape processed.

[b] Differentiated pulse duration modulation.

[c] Power spectral density.

X - Indicates data processed

TABLE 17-I.- TIME COVERAGE FOR DATA PROCESSING - Concluded

Revolution	Station	Acquisition of signal, hr:min:sec	Loss of signal, hr:min:sec
3	$Carnarvon_4$	05:31:--	05:54:--
	$Ascension_5$	05:38:20	06:02:00
	$Carnarvon_5$	05:53:--	06:17:--
	$Ascension_6$	06:01:50	06:25:09
	$Carnarvon_6$	06:16:--	06:39:--
	$Ascension_7$	06:25:10	06:48:55
	$Carnarvon_7$	06:38:--	07:02:--
	$Ascension_8$	06:49:50	07:13:06
	$Carnarvon_8$	07:01:--	07:24:--
	$Ascension_9$	07:12:51	07:37:01
	$Carnarvon_9$	07:24:--	07:48:--
	$Ascension_{10}$	07:36:50	08:00:29
	$Carnarvon_{10}$	07:49:29	08:13:10
	$Carnarvon_{11}$	No data	Bad tape
	$Carnarvon_{12}$	08:45:37	09:02:47
	$Carnarvon_{13}$	09:04:20	09:23:49
	Guam	09:16:20	09:34:30
	U.S.N.S. Watertown	09:34:29	09:38:53
Mission phase	Recorder		
Launch	Data storage equipment Flight qualification tape recorder	-00:01:00	00:03:06
Entry	Data storage equipment[a] Flight qualification tape recorder	09:36:58	09:57:31

[a]The dub time for the data storage equipment PCM tabulated data for entry was 24:00:00 (equivalent to 09:36:57.55 mission elapsed time).

NASA-S-68-3653

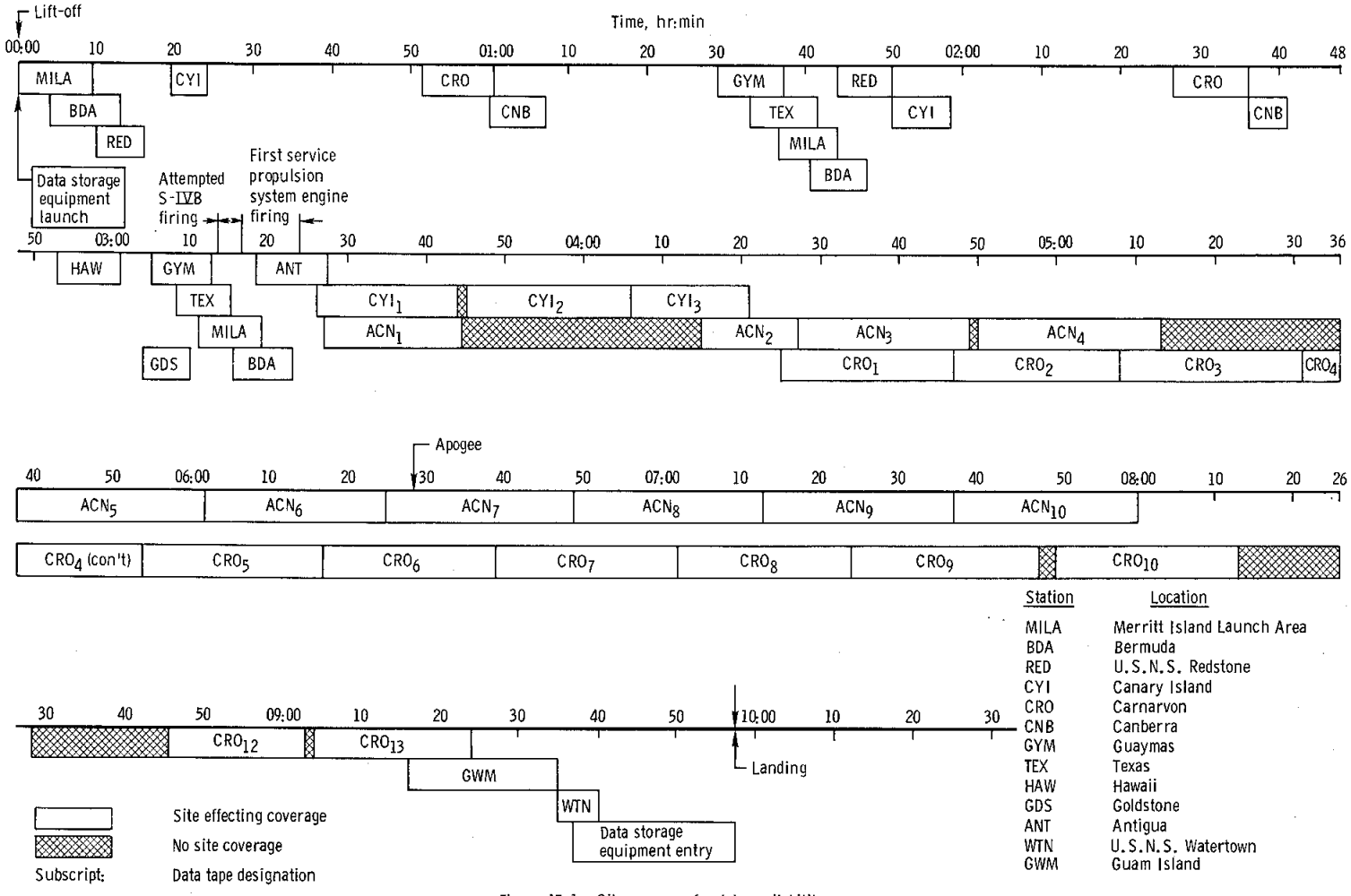

Figure 17-1. - Site coverage for data availability.

18.0 DISTRIBUTION

NATIONAL AERONAUTICS AND SPACE ADMINISTRATION

National Aeronautics and Space Administration
Washington, D.C. 20546
Attention: S. C. Phillips, MA 1
W. C. Schneider, MA 1
L. E. Day, MAT 8
M. C. Adams, R 1
J. E. Naugle, S 1
G. M. Truszynski, T 1
Library, USS-10 2

Manned Spacecraft Center
Houston, Texas 77058
Attention: Office of Director
R. R. Gilruth, AA 1
G. S. Trimble, AB 1
P. E. Purser, AC 1
D. R. Collins, AG 1
R. O. Piland, AH 1

Legal Office
M. P. Matthews, AL3 1

Public Affairs Office
P. Haney, AP 1
J. E. Riley, AP 1
Historical Office, AP6 3
Mission Planning and Operations Office, AP8 1

Director of Administration
P. H. Whitbeck, BA 1
Reproduction Services Branch, BF6 1
Distribution Operation Section, BF66
Security Branch, BM4 1
Technical Information Preparation Branch, BM5 4
Library Processes Office, BM6 6

Director of Flight Crew Operations
D. K. Slayton, CA 1
Chief, Astronaut Office, CB 10
Chief, Flight Crew Support Division, CF 10

Director of Medical Research and Operations
C. A. Berry, M.D., DA 4
Chief, Biomedical Research Office, DB 2
Chief, Medical Operations, DD 1

Director of Engineering and Development
M. A. Faget, EA 3
Chief, Information Systems Division, EB 7
Chief, Crew Systems Division, EC 6
Chief, Computation and Analysis Division, ED 2
Chief, Instrumentation and Electronic Systems Division, EE 10
Chief, Guidance and Control Division, EG 10

RASPO
Massachusetts Institute of Technology
75 Cambridge Parkway
Cambridge, Massachusetts 02142
Attention: Manager, EG442 1

RASPO
AC Electronics Division
Milwaukee, Wisconsin 53200
Attention: Manager, EG443 1

Chief, Propulsion and Power Division, EP 8
Chief, Structures and Mechanics Division, ES 10
Chief, Advanced Spacecraft Technology Division, ET 2

Director of Flight Operations
C. C. Kraft, Jr., FA 2
Chief, Flight Control Division, FC 10
Chief, Landing and Recovery Division, FL 5
Chief, Mission Planning and Analysis Division, FM 8
Chief, Flight Support Division, FL 3

Goddard Space Flight Center Liaison Office
W. B. Easter, GDF-L 1

Apollo Applications Program Office
R. F. Thompson, KA 1
J. E. Roberts/W. B. Mitchell, KA 1
Manager, Future Missions Project Office, KF 1
Manager, Mission Operations Office, KM 1
Manager, Program Control Office, KP 1
Manager, Systems Engineering Office, KS 1
Manager, Test Operations Office, KT 1
Manager, Orbital Workshop Project Office, KW 1

Reliability and Quality Assurance Office
A. C. Bond, NA 1
W. M. Bland, Jr., NA 8

Manned Spacecraft Center
Houston, Texas 77058
Attention: Apollo Spacecraft Program Office
G. M. Low, PA 1
E. F. M. Rees, PA 1
K. S. Kleinknecht, PA 1
C. R. Bolender, PA 1
S. E. Simpkinson, PA 1
G. W. S. Abbey, PA 1
H. W. Tindall, PA 1
Apollo Files, PA 2

RASPO
Grumman Aircraft Engineering Corporation
Bethpage, L.I., New York 11714
Attention: Manager, PS 3

RASPO
North American Rockwell Corporation
11214 Lakewood Boulevard
Downey, California 90240
Attention: Manager, PC 4

Chief, Systems Engineering Division, PD 9
Chief, LM Project Engineering Division, PE 2
Chief, CSM Project Engineering Division, PF 2
Chief, Program Control Division, PP 2

RASPO
Kennedy Space Center, Florida 32899
Attention: Manager, PSK 1

Chief, Test Division, PT 10

White Sands Missile Range
Office of the Manager
Post Office Drawer MM
Las Cruces, New Mexico 88001
Attention: M. L. Raines, RA 2

Langley Research Center Liaison Office
A. T. Mattson, RAA 1

Marshall Space Flight Center Resident Office
J. T. Hamilton, RL 1

Flight Safety Office
A. C. Bond, SA 1
J. C. French, SA 5

Director of Science and Applications
W. N. Hess, TA 1
Manager, Lunar Surface Project Office, TD 1
Manager, Applications Project Office, TE 1
Manager, Test and Operations, TF 2
Chief, Space Physics Division, TG 1
Chief, Lunar and Earth Science Division, TH 1

Air Force Systems Command Field Office (SAMSO Det.2)
Col. J. Green, ZR1 1

Department of Defense Representative
Cmdr. R. W. Colopy, ZR2 1

AFSC Scientific & Technical Liaison Office
Lt. Col. Thomas J. Borgstrom (STLO), ZR3 10

Ames Research Center
Moffett Field, California 94035
Attention: Dr. H. J. Allen, 200-1 1
Chief, Thermo and Gas-Dynamics Division, 229-3 1
Library, 202-3 2

Electronics Research Center
565 Technology Square
Cambridge, Massachusetts 02139
Attention: J. C. Elms, D 1
Library 2

Flight Research Center
Post Office Box 273
Edwards, California 93523
Attention: P. F. Bikle 1
Library 2

Goddard Space Flight Center
Greenbelt, Maryland 20771
Attention: John F. Clark, 100 1
M. F. Thompson, 506 1
W. P. Varson, 506 1
T. Roberts, 550 1
O. M. Covington, 800 1
H. F. Thompson, 801 1
Manned Flight Engineering Division, 810 5
Manned Flight Operations Division, 820 6
Manned Flight Planning and Analysis Division, 830 5
NASA Communications Division, 840 5
Library, 252 2

John F. Kennedy Space Center
Kennedy Space Center, Florida 32899
Attention: Dr. K. H. Debus, CD 1
R. C. Middleton, AP 1
S. T. Seddingfield, AP-SCO 3
G. M. Preston, DE 1
R. A. Petrone, LO 1
W. J. Kapryan, LO 1
J. J. Williams, LS 6
Library, IS-CAS-42 2

Lewis Research Center
2100 Brookpark Road
Cleveland, Ohio 44135
Attention: A. Silverstein, 3-2 1
I. A. Pinkle, 3-2 1
Library, 60-3 2

Langley Research Center
Langley Station
Hampton, Virginia 23365
Attention: Director, 106 1
Technical Library, 185 2

George C. Marshall Space Flight Center
Huntsville, Alabama 35812
Attention: Dr. W. von Braun, DIR 1
Gen. E. F. O'Connor, I-DIR 1
W. D. Brown, I-E-MGR 1
F. A. Speer, I-MO-MGR 1
L. F. Belew, I-S/AA-MGR 1
W. Teir, I-I/IB-MGR 1
Dr. A. Rudolph, I-V-MGR 1
J. P. Lindberg, R-AERO-F 2
Library, MS-I 2

U.S. GOVERNMENT

Air Force Eastern Test Range
Patrick Air Force Base, Florida 32925
Attention: Maj. Gen. V. S. Huston 1
Col. R. Olson, DOD Manager 3

MOI Systems Program Office
SAFSL-6
Air Force Unit Post Office
Los Angeles, California 90045 5

Chief, Army Field Office, SAMSO
Air Force Unit Post Office
Los Angeles, California 90045 2

SAMSO (SMTT)
Air Force Unit Post Office
Los Angeles, California 90045 1

SAMSO (SMAO)
Air Force Unit Post Office
Los Angeles, California 90045 1

SAMSO (SMAA)
Air Force Unit Post Office
Los Angeles, California 90045 1

Det 6, OAR (LOOAR)
Air Force Unit Post Office
Los Angeles, California 90045 1

Secretary of the Air Force
SAFSL (Maj. Gen. Stewart)
Washington, D.C. 20330 1

Commanding Office
Navy Space Systems Activity
Air Force Unit Post Office
Los Angeles, California 90045 1

CONTRACTORS

Jet Propulsion Laboratory
Pasadena, California 91103
Attention: Dr. W. H. Pickering, 180-905 1
Library, 111-113 2

Massachusetts Institute of Technology
75 Cambridge Parkway
Cambridge, Massachusetts 02142
Attention: D. C. Hoag 2

AC Electronics Division, General Motors Corporation
Milwaukee, Wisconsin 53200
Attention: H. Brudy 2

Bellcomm Inc.
1100 17th Street NW
Washington, D.C. 20036
Attention: Information System Analysis Department Head 1

Grumman Aircraft Engineering Corporation
Bethpage, L.I., New York 11714
Attention: J. G. Gavin, Jr. 25

Grumman Aircraft Engineering Corporation
Kennedy Space Center, Florida 32899
Attention: G. M. Szurla 5

Grumman Aircraft Engineering Corporation
1740 NASA Boulevard
Houston, Texas 77058
Attention: J. M. Buxton 12

North American Rockwell Corporation
12214 Lakewood Boulevard
Downey, California 90240
Attention: D. D. Myers 25

North American Rockwell Corporation
Kennedy Space Center, Florida 32899
Attention: B. Hello 5

North American Rockwell Corporation
1840 NASA Boulevard
Suite 201
Houston, Texas 77058
Attention: W. T. Short 12

TRW, Incorporated
Space Park Drive
Houston, Texas 77058
Attention: A. Rosenbloom, H1-2058 1
Library 1

The Boeing Company
Post Office Box 58747
Houston, Texas 77058
Attention: H. J. McClellan 3

General Electric Company
Post Office Box 58408
Houston, Texas 77058
Attention: L. W. Warwecha 3

Aerospace Corporation
Post Office Box 95085
Los Angeles, California 90045
Attention: W. C. Williams, A1/2082 1
B. A. Hohmann, 100/2507 1

Martin Marietta Corporation
Denver, Colorado 80201
Attention: C. B. Hurtt 1

Grumman Aircraft Engineering Corporation
Plant 35
Bethpage, L.I., New York 11714
Attention: Saul Ferdman 1

McDonnell Douglas Corporation
Post Office Box 516
St. Louis, Missouri 63166
Attention: J. M. Gardner 1

North American Rockwell Corporation
Space Division
11214 Lakewood Boulevard
Downey, California 90241
Attention: L. M. Tinnan 1

APOLLO SPACECRAFT FLIGHT HISTORY

(Continued from inside front cover)

Mission	Spacecraft	Description	Launch date	Launch site
Apollo 4	SC-017 LTA-10R	Supercircular entry at lunar return velocity	Nov. 9, 1967	Kennedy Space Center, Fla.
Apollo 5	LM-1	First lunar module flight	Jan. 22, 1968	Cape Kennedy, Fla.
Apollo 6	SC-020 LTA-2R	Verification of closed-loop emergency detection system	April 4, 1968	Kennedy Space Center, Fla.